BEILSTEIN JOURNAL OF ORGANIC CHEMISTRY

Green chemistry II

Edited by Luigi Vaccaro

Imprint

Beilstein Journal of Organic Chemistry
www.bjoc.org
ISSN 1860-5397
Email: journals-support@beilstein-institut.de

The *Beilstein Journal of Organic Chemistry* is published by the Beilstein-Institut zur Förderung der Chemischen Wissenschaften.

Beilstein-Institut zur Förderung der Chemischen Wissenschaften
Trakehner Straße 7–9
60487 Frankfurt am Main
Germany
www.beilstein-institut.de

BEILSTEIN JOURNAL OF ORGANIC CHEMISTRY

Safe and highly efficient adaptation of potentially explosive azide chemistry involved in the synthesis of Tamiflu using continuous-flow technology

Cloudius R. Sagandira and Paul Watts*

Full Research Paper

Open Access

Address:
Nelson Mandela University, University Way, Port Elizabeth, 6031, South Africa

Email:
Paul Watts* - Paul.Watts@mandela.ac.za

* Corresponding author

Keywords:
azide chemistry; continuous flow synthesis; hazardous; safe; Tamiflu

Beilstein J. Org. Chem. **2019,** *15,* 2577–2589.
doi:10.3762/bjoc.15.251

Received: 12 August 2019
Accepted: 08 October 2019
Published: 30 October 2019

This article is part of the thematic issue "Green chemistry II".

Guest Editor: L. Vaccaro

Abstract

Tamiflu is one of the most effective anti-influenza drugs, which is currently manufactured by Hoffmann-La Roche from shikimic acid. Owing to its importance, more than 60 synthetic routes have been developed to date, however, most of the synthetic routes utilise the potentially hazardous azide chemistry making them not green, thus not amenable to easy scale up. Consequently, this study exclusively demonstrated safe and efficient handling of potentially explosive azide chemistry involved in a proposed Tamiflu route by taking advantage of the continuous-flow technology. The azide intermediates were safely synthesised in full conversions and >89% isolated yields.

Introduction

Tamiflu is currently one of the most important drugs available to combat the influenza virus and this has seen immense research efforts by the scientific community to exclusively focus on the development of new, better and practical approaches to manufacture this drug [1,2]. More than 60 synthetic routes have been developed towards Tamiflu to date [1-3]. However, most of these synthetic approaches suffer from the use of potentially hazardous azide chemistry, thus raising safety concerns [4] and eventually ruled out for large scale synthesis in batch systems [1,2]. The importance and use of azide chemistry in organic chemistry synthesis is well documented [5]. However, there are potential hazards associated with its application thus posing safety concerns [6-8]. From the viewpoint of azide chemistry, the synthesis of Tamiflu is very interesting in many aspects, because azide chemistry is extensively utilised. Most reported synthetic routes towards Tamiflu employ the potentially explosive azide chemistry to introduce *N*-based substituents on the drug [5-8]. Furthermore, the current industrial production route by Hoffmann-La Roche is no exception. Hoffmann-La Roche worked closely with a firm that specialises in azide chemistry to develop its industrial process [1,2,6,9]. Numerous reported routes demonstrate amazing potential and inge-

nuity in the Tamiflu molecule assembly. However, most of them are not amenable to easy scale-up due to the safety concerns associated with azide chemistry [1,2]. Therefore, the development of alternative practical and safe processes for Tamiflu synthesis, which can be adapted at large scale is imperative. The safety concerns associated with the use of azide chemistry prompted the chemical community to develop azide-free synthetic routes [1,2,7,10,11]. However, routes involving azide chemistry proved to be more superior in most instances than azide free alternatives [2,12]. Hayashi's group developed highly efficient two 'one-pot' sequences towards Tamiflu at gram-scale, which proceeded in 10 steps with an outstanding 60% overall yield [1,13]. The approach required five isolations only. Unlike Magano [1], the authors could not avoid the use of the potentially explosive azide chemistry. The azide intermediate was not isolated to address the safety concerns posed by azides. Positively, their approach was characterised by low catalyst loading, no protecting group chemistry and absence of halogenated solvents [1,13]. Generally, this approach is attractive for large scale manufacturing, however, the safety concerns posed by the use of azide chemistry needs to be addressed especially at large scale where the risk is very high. In an effort to address the safety concerns raised by the potentially explosive acyl azide **1a** (Scheme 1), Hayashi and co-workers [14] demonstrated the handling of the Curtius rearrangement reaction (transformation from acyl azide **1a** to isocyanate **1b**) in a microreactor system (Scheme 1 and Figure 1). Acyl azide **1a** is a potentially explosive compound because of its nitro and azide moieties [14] and its safety concerns need to be dealt with for large scale synthesis. Safety in this reaction was achieved by in situ formation and consumption in flow of the hazardous intermediates (azide **1a** and isocyanate **1b**) (Scheme 1 and Figure 1).

Continuous-flow synthesis offers the generation and consumption of dangerous intermediates in situ preventing their accumulation, thus it represents a potential solution for dealing with hazardous reaction intermediates and products [15]. Additionally, microreactors can handle exothermic reactions extremely well, due to the inherent high surface area to volume ratio and rapid heat dissipation [16] unlike the conventional batch process. Continuous-flow production may certainly enhance the green metrics of synthesis in several ways [17] and their work clearly demonstrated the possibility of using continuous-flow systems as a way of solving the problems associated with handling hazardous intermediates and products in the synthesis of Tamiflu.

With this in mind, we investigated safe ways of handling this important but hazardous azide chemistry in Tamiflu synthesis by using continuous-flow technology. The two steps involving azide chemistry in flow are reported herein (Scheme 2), with the vision of further integrating the other steps towards continuous-flow total synthesis of this drug. To this effect, we have already reported continuous flow shikimic acid (**3**) esterification; the first step in the synthesis of Tamiflu [18].

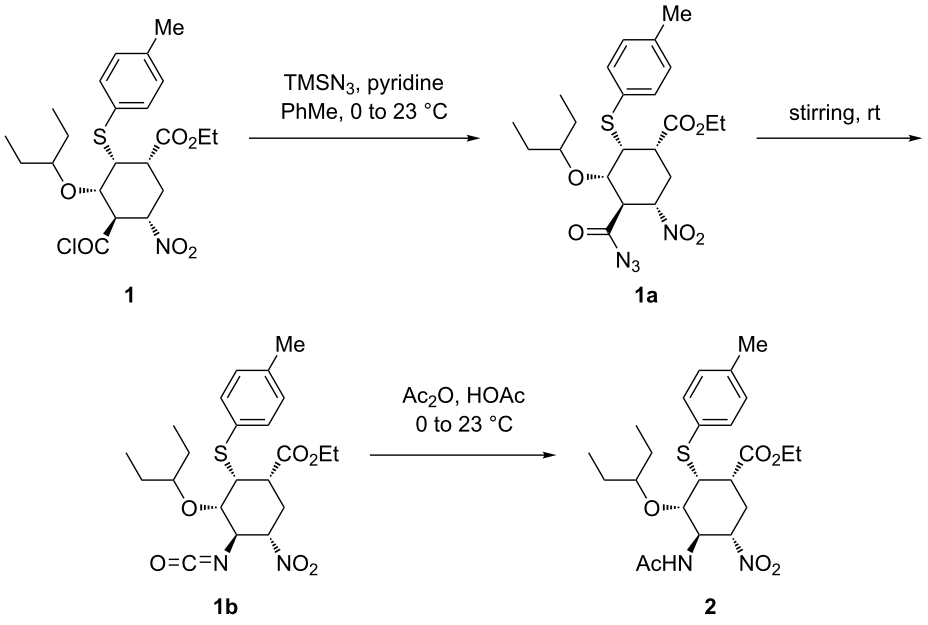

Scheme 1: Handling of azide chemistry in Tamiflu synthesis by Hayashi and co-workers [14].

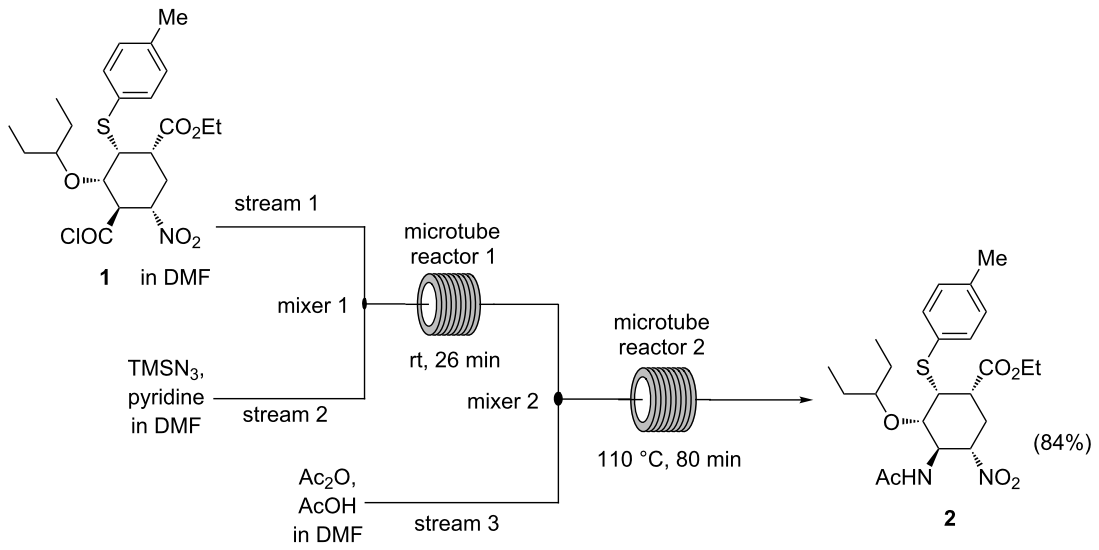

Figure 1: Synthesis of compound **2** from acyl chloride **1** via Curtius rearrangement using a continuous-flow system [14].

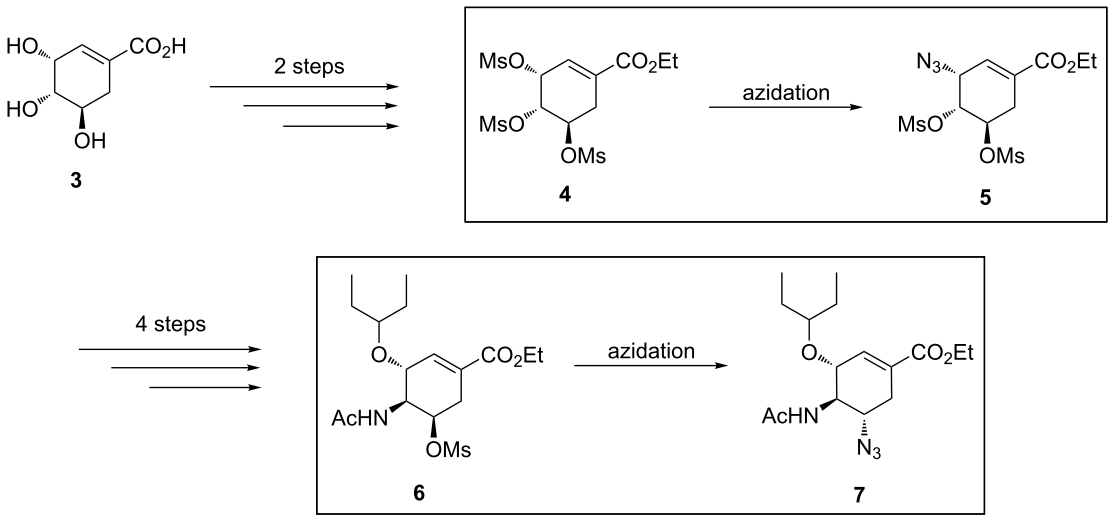

Scheme 2: Azide chemistry in the synthesis of Tamiflu.

Results and Discussion

Continuous-flow synthesis of ethyl (3*S*,4*R*,5*R*)-3-azido-4,5-bis(methanesulfonyloxy)cycohex-1-enecarboxylate (5). Mesyl shikimate azidation is a pivotal step in our proposed Tamiflu route. Mesyl shikimate **4** in the presence of a suitable azidating agent undergoes a highly regio- and stereoselective nucleophilic substitution of allylic *O*-mesylate at the C-3 position affording azide compound **5** (Scheme 3).

Nie and co-workers [19] reported the treatment of mesyl shikimate **4** with NaN_3 (4 equiv) in aqueous acetone (Me_2CO/H_2O 5:1) at 0 °C for 4 h in batch to afford azide **5** in 92% yield. The use of high temperatures was detrimental to azide **5** yield due to the formation of the side product ethyl 3-azidobenzoate (**5a**). For example, at room temperature for 3 h or at 50 °C for 2 h, the aromatic side product **5a** was obtained in 16% and 81% yield, respectively. Consequently, the reaction was strictly done at 0 °C and below. Therefore, the use of NaN_3 in high equivalence (4 equiv) was to probably improve reaction kinetics at low temperatures. Karpf and Trussardi [9] reported the synthesis of azide **5** from mesyl shikimate **4** and NaN_3 (1.1 equiv) in DMSO for 3 h at room temperature in batch. Unlike Nie et al. [19], they used only a slightly excess of NaN_3 (1.1 equiv) at room temperature to achieve good yields, however, the use of

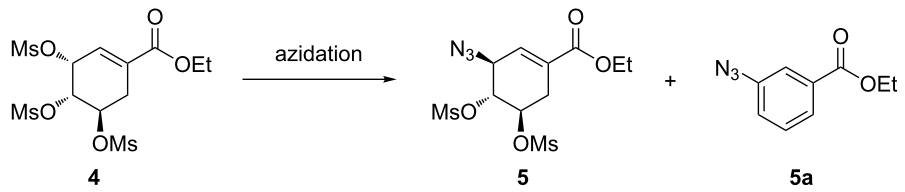

4 5 5a

Scheme 3: Azidation of mesyl shikimate **5**.

DMSO as solvent made the product isolation more difficult. Despite also acknowledging aromatisation side reactions, this communication did not report actual figures on yields for both desired azide **5** and side product **5a**. Kalashnikov et al. [20] observed that the slightly basic nature of NaN_3 also contributed to side reactions. To improve on Karpf and Trussardi's approach [9], they utilised less basic NH_4N_3 (1.5 equiv) generated in situ from NH_4Cl from NaN_3 in MeOH to azidate mesyl shikimate **4** for 5 h at room temperature in batch to afford desired azide **5** (95%) and side product **5a** was not quantified [20]. Ethyl 3-azidobenzoate (**5a**) is the common reported side product [19,20] for the mesyl shikimate **4** azidation reaction (Scheme 3).

We herein present a comprehensive study on various mesyl shikimate **4** azidation procedures; with goal of safely and selectively making azide **5** in flow.

Continuous flow C-3 mesyl shikimate azidation using sodium azide (NaN_3). A continuous flow system fitted with a 19 μL reactor (Chemtrix) was used to optimise the synthesis of azide compound **5** from mesyl shikimate **4** using aqueous NaN_3 (Figure 2). Initial studies had shown the same conversions in both acetone and acetonitrile as solvents. Although acetone is a greener solvent than acetonitrile [21,22], its use was accompanied with eventual microreactor blockage caused by a resulting precipitate from the acetone/aqueous NaN_3 mixture. Fortunately, acetonitrile is also an acceptable green solvent [21,22]. Furthermore, acetonitrile has a higher boiling point than acetone which is desirable for high temperature reaction interrogation. Consequently, acetonitrile was the preferred solvent for mesyl shikimate **4** for further optimisation in continuous-flow systems.

Mesyl shikimate **4** (0.1 M) in acetonitrile was treated with aqueous NaN_3 (0.11 M, 1.1 equiv) in a thermally controlled microreactor system (Figure 2). Generally, good mesyl shikimate conversions were obtained. As aforementioned, the reaction affords two products, the desired azide compound **5** and the side product **5a** (Scheme 3). The findings on the effect of various reaction conditions on conversion and selectivity are presented graphically (Figure 3 and Figure 4).

It is evident that mesyl shikimate conversion increases with increase in residence time and temperature (Figure 3). At 50 °C and above, full conversions were achieved at incredibly low residence times. Full conversion was achieved at 50 °C, 3 s residence time and 71% conversion at 0 ° C and 3 s residence time (Figure 3). Product selectivity to azide **5** is shown in Figure 4.

Generally, selectivity decreases with increase in residence time and temperature (Figure 4). However, there is 100% selectivity towards the desired azide **5** at 0 °C at all the investigated residence times with conversion ranging from 71% to 100%. There was full conversion at 150 °C with 67% and 0% azide **5** selectivity observed at 3 s and 300 s, respectively. At 50 °C, full conversion was achieved with 100% and 73% azide **5** selectivity at 3 s and 300 s, respectively (Figure 3 and Figure 4). It is

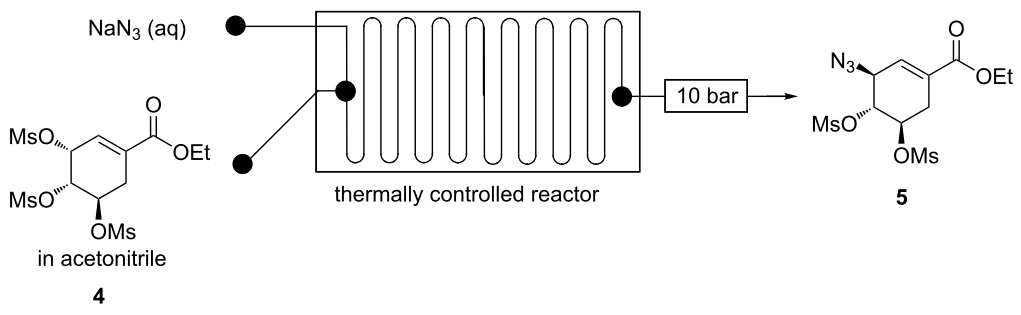

4 5

Figure 2: Continuous-flow system for C-3 azidation of mesyl shikimate using aqueous sodium azide.

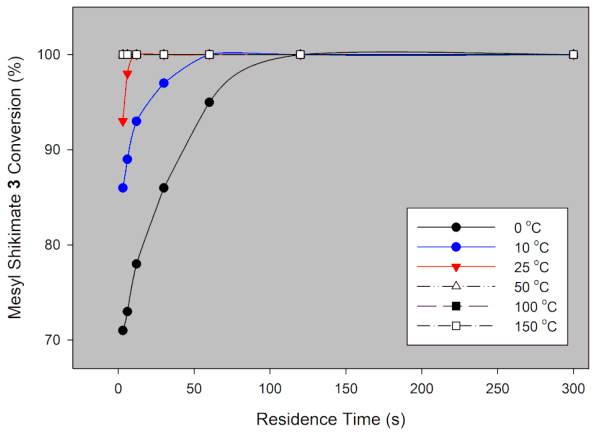

Figure 3: Mesyl shikimate azidation conversion in a continuous-flow system using NaN_3.

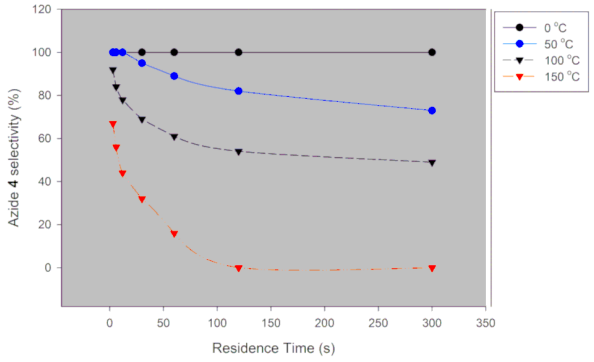

Figure 4: Desired azide **5** selectivity in a continuous-flow system using NaN_3.

evident that high temperatures favour the undesired aromatic azide compound **5a**. Nie et al. [19] obtained 16% yield of the aromatic compound **5a** at room temperature for 3 h and 81% at 50 °C for 2 h in batch. The undesired aromatic azide **5a** forms from the desired azide product **5** via elimination and aromatisation [19,20]. Kalashnikov and co-workers [20] further ascertained that the considerable basicity of NaN_3 caused the side reaction. Therefore, we investigated the effect of NaN_3 concentration on the reaction. Figure 5 illustrates the effect of NaN_3 molar equivalent on mesyl shikimate **4** conversion and selectivity of the desired azide **5** at 150 °C and 12 s residence time.

The selectivity towards azide **5** decreases with increase in NaN_3 concentration (Figure 5). Contrary, mesyl shikimate **4** conversion is improved with increased NaN_3 amounts (1 and 2 equivalents). The unexpected decrease in selectivity with increase in NaN_3 concentration can be understood by considering Kalash-

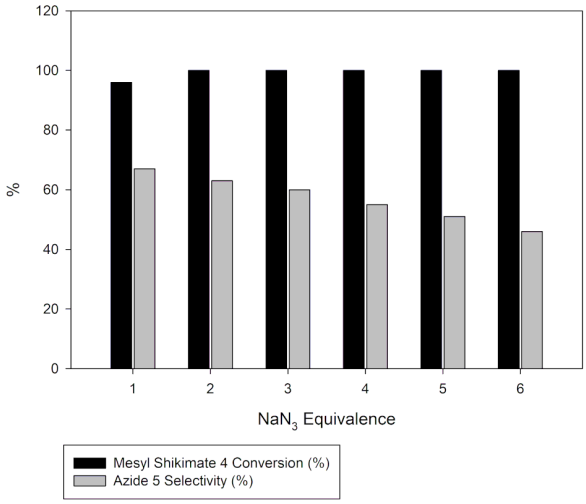

Figure 5: Effect of NaN_3 concentration on mesyl shikimate **4** conversion and azide **5** selectivity.

nikov and co-workers' [20] explanation on NaN_3 basicity-induced aromatisation resulting in undesired azide **5a**. Therefore, an excess of NaN_3 increases reaction basicity resulting in the undesired azide **5a** being favoured.

The continuous flow mesyl shikimate **4** azidation was highly regio- and stereoselective to the C-3 position [9,19,20,23]. The two OMs groups at C-4 and C-5 remaining intact as reported in batch [9,19,20]. The highly selective C-3 azidation is reasonable and easily understood because the C-3 position is much more reactive (allylic position) and less hindered (Figure 6).

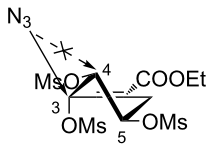

Figure 6: Regio- and stereospecific nucleophilic -N_3 group attack.

The optimum conditions in flow for this reaction were found to be 1.1 equivalents of NaN_3, 50 °C and 12 s residence time affording full conversion towards the desired azide **5**. Despite of high temperatures, long reaction times and basicity being detrimental to the selectivity of the desired azide **5** in batch, it is evident from our study that the use of a microreactor significantly improved the selectivity and massively reduced the reaction times. The production of azide **5** in 100% conversion simplified the purification procedure. Most importantly, microreactors improved safety as the potentially explosive azide chemistry was safely investigated even at very high temperatures thus making the process greener.

Although we successfully developed a safe and efficient continuous-flow procedure for the synthesis of azide **5** from mesyl shikimate **4** by using NaN_3 (aq), the vision, however, is further integrating all the steps in Tamiflu synthesis. We knew that the current step will not be compatible with the subsequent step when considering telescoping as it requires anhydrous conditions. This prompted us to investigate whether alternative azidating agents, which are soluble in organic solvents, such as diphenyl phosphoryl azide (DPPA), trimethylsilyl azide (TMSA) and tetrabutylammonium azide (TBAA) are suitable for the reaction.

Continuous flow C-3 mesyl shikimate azidation using either DPPA or TMSA. The use of either DPPA or TMSA as the azidating agent for mesyl shikimate **4** was investigated in a Chemtrix continuous-flow system (Figure 7).

Mesyl shikimate (0.1 M) was treated with a mixture of either DPPA or TMSA (0.11 M, 1.1 equiv) and TEA (0.12 M, 1.2 equiv) in a continuous-flow system (Figure 7). The reaction was quenched with aqueous HCl (0.05 M, 0.5 equiv) within the flow system.

Using DPPA as the azidating agent, an increase in both temperature and residence time resulted in the increase in mesyl shikimate conversion in microreactors (Figure 8). High temperatures easily gave full mesyl shikimate conversions. Generally, the trends found with the use of DPPA are comparable to NaN_3. Figure 9 illustrates the reaction selectivity at varying conditions.

Azide **5** selectivity decreases with increase in temperature and residence time (Figure 9). This trend was the same as observed with the use of NaN_3 as the azidating agent. However, azide **5** selectivity was better with NaN_3 than DPPA. At 50 °C and 30 s residence time, full conversion was achieved with 95% and 70% azide **5** selectivity using NaN_3 and DPPA as the azidating agent, respectively. The lower azide **5** selectivity associated with DPPA is a result of the base TEA used. Basic conditions are reportedly detrimental to the azide **5** selectivity [20]. The use of a base in the DPPA procedure was unavoidable as the

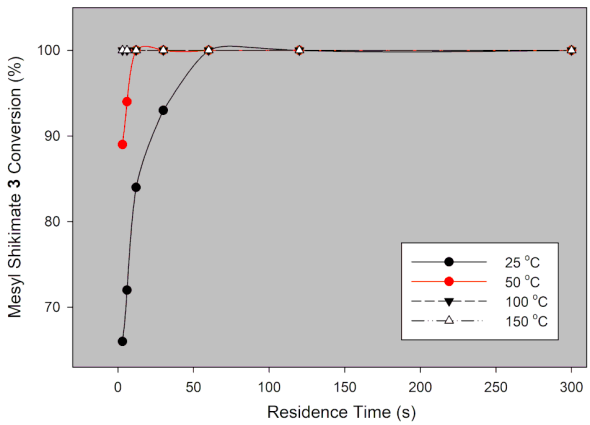

Figure 8: Mesyl shikimate azidation conversion in a continuous-flow system using DPPA.

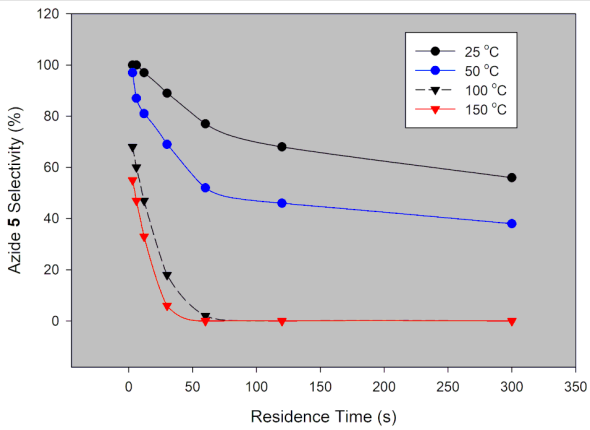

Figure 9: Desired azide **5** selectivity in a continuous-flow system using DPPA.

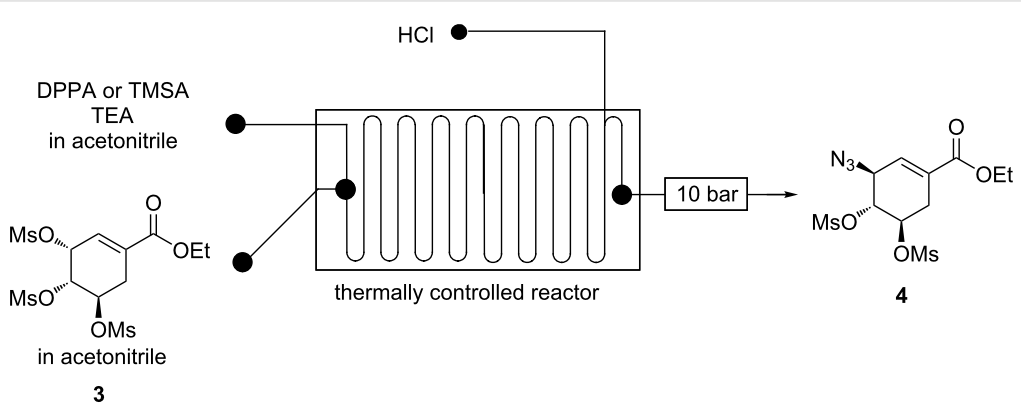

Figure 7: Continuous-flow system for C-3 azidation of mesyl shikimate using DPPA or TMSA.

reaction did not proceed in its absence. This can be understood by considering the DPPA azidating mechanism. The reaction takes place in two discrete steps, the first being phosphate formation followed by azide displacement (Scheme 4) [24].

We quenched the reaction within a microreactor using aqueous HCl. Since basic conditions were thought to be detrimental to azide **5** selectivity, investigation of the effect of TEA concentration on the selectivity was reasonable so as to further ascertain this. Therefore, the effect of base (TEA) concentration on azide **5** selectivity was investigated at room temperature and 6 s residence time to ascertain its role in the formation of the unwanted aromatic azide **5a**. Figure 10 illustrates the findings.

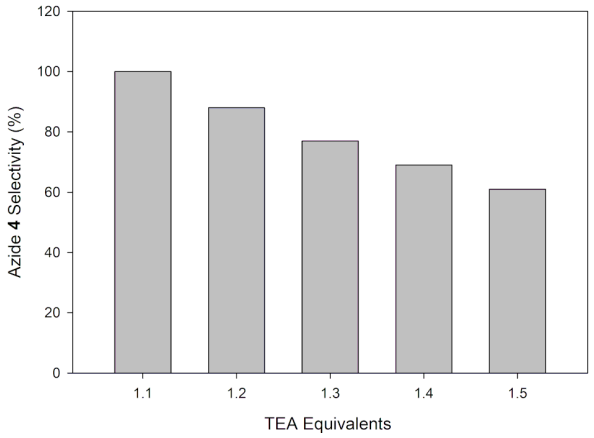

Figure 10: Effect of TEA concentration on the reaction selectivity.

The selectivity towards the desired azide **5** significantly decreased with increase in TEA concentration (Figure 10). The aromatization reaction becomes predominant with increasing reaction basicity thus indeed confirming the detrimental effect of basic conditions on the reaction. The use of 1 equiv TEA rather than 1.1 equiv is obviously more logical from the above selectivity study. However, it was accompanied by a 6% conversion loss.

TMSA was another azidating agent, which was investigated for mesyl shikimate azidation in a continuous-flow system (Figure 7). The reaction conversion and selectivity at varying conditions is presented graphically (Figure 11 and Figure 12).

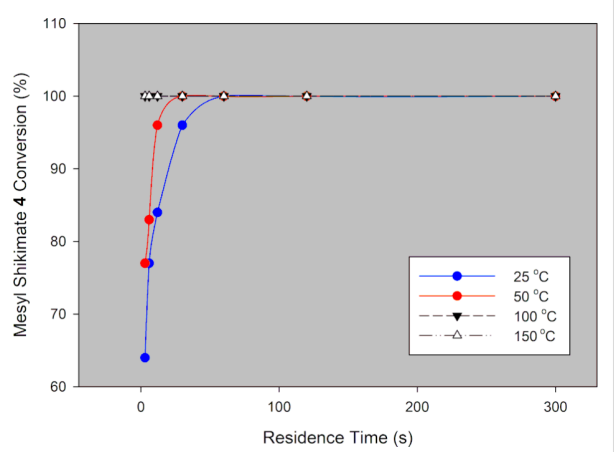

Figure 11: Mesyl shikimate azidation conversion in a continuous-flow system using TMSA.

Just as with the other investigated azidating agents, mesyl shikimate **4** conversion increased with increase in temperature and residence time (Figure 11). The conversions found with TMSA were comparable with both NaN_3 and DPPA. Mesyl shikimate conversions of 64%, 66% and 71% were obtained at 25 °C and 3 s residence time by using TMSA, DPPA and NaN_3 as azidating agents, respectively.

The azide **5** selectivity trend using TMSA was similar to DPPA and NaN_3 (Figures 4, 9 and 12). There is a general decrease in azide **5** selectivity with an increase in temperature and residence time (Figure 12). However, the use of NaN_3 gave better azide **5** selectivity than TMSA. Azide **5** selectivity of 95% (100% conversion) and 67% (100% conversion) were achieved at 25 °C and 30 s residence time using NaN_3 and TMSA, respectively. The lower selectivity was because of the basic reaction conditions as TEA was used as a base. The effect of the basic reaction conditions on the selectivity is explained in detail vide supra. Azide **5** selectivity was almost the same when DPPA (69%) and TMSA (67%) was used at 25 °C, 30 s residence time and 100% conversion. It is reasonable since both procedures utilised TEA (1.1 equiv).

We observed that DPPA and TMSA procedures can be used for mesyl shikimate **4** azidation in continuous-flow systems. From a green chemistry point of view, the use of TEA in both proce-

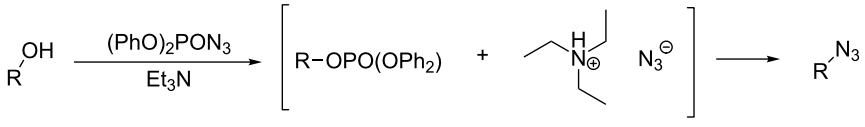

Scheme 4: DPPA azidating mechanism in the presence of a base.

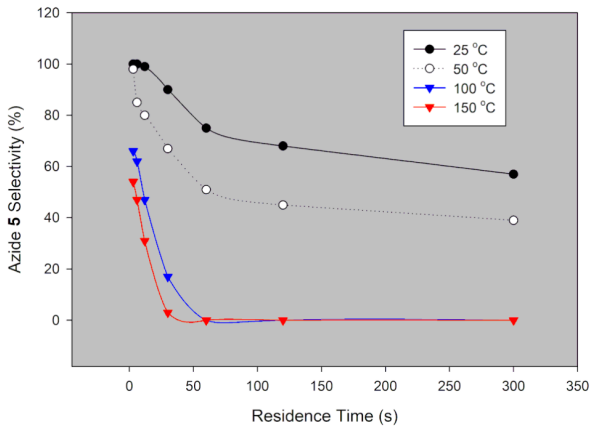

Figure 12: Desired azide **5** selectivity in a continuous-flow system using TMSA.

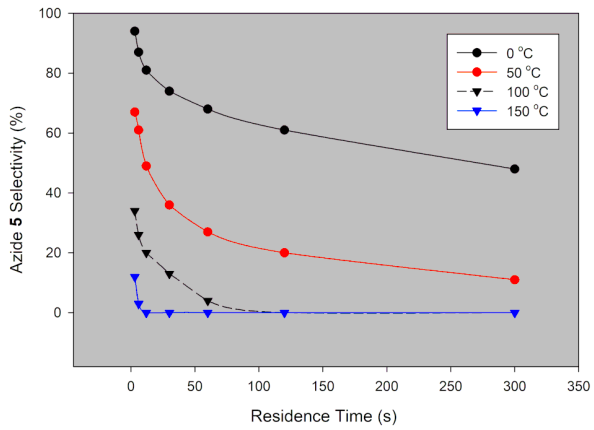

Figure 14: Continuous-flow system for C-3 azidation of mesyl shikimate using TBAA.

dures was found to be the bottleneck as it lowered azide **5** selectivity. Furthermore, TEA is classified as a non-green reagent, which is not ideal [21,22]. In an effort to resolve this, we investigated the use of TBAA for continuous-flow mesyl shikimate **4** azidation as it does not require a base.

Continuous flow C-3 mesyl shikimate azidation using tetrabutylammonium azide (TBAA). The use of TBAA as mesyl shikimate **4** azidating agent was investigated in a continuous-flow system (Figure 13).

Mesyl shikimate **4** (0.1 M) in acetonitrile was treated with TBAA (0.11 M, 1.1 equiv) in acetonitrile in a continuous-flow system (Figure 14). Interestingly, full mesyl shikimate **4** conversion was observed for all investigated reaction conditions, residence time (3–300 s) and temperature (0–150 °C). TBAA proved to be an effective azidating agent for mesyl shikimate **4**. However, there was a variation in azide **5** selectivity under the investigated conditions. The findings on reaction selectivity are presented graphically (Figure 14).

Generally, there is the same azide **5** selectivity trend as the others. Azide **5** selectivity decreased with increase in residence time and temperature (Figure 14). Despite initially promising to be the best azidating agent, this procedure generally gave poor selectivities towards our desired azide **5** compared to the others azidating agents under the same reaction conditions as a result of the basicity of TBAA, making it less green [12]. The optimum conditions are 3 s and 0 °C affording full conversion and 94% azide **5** selectivity. Using TBBA, it was important to quickly analyse the sample soon after collection as the reaction continues in the collection vial at room temperature. Azide **5** selectivity was reduced with time in the vial. Therefore, the development of a suitable quenching procedure may be helpful. The TBAA procedure seems to be a promising NaN_3 procedure replacement when considering the aforementioned anhydrous telescoping due to its superior azidating power.

Various safe and selective procedures for the synthesis of azide **5** from mesyl shikimate **4** in continuous-flow systems were suc-

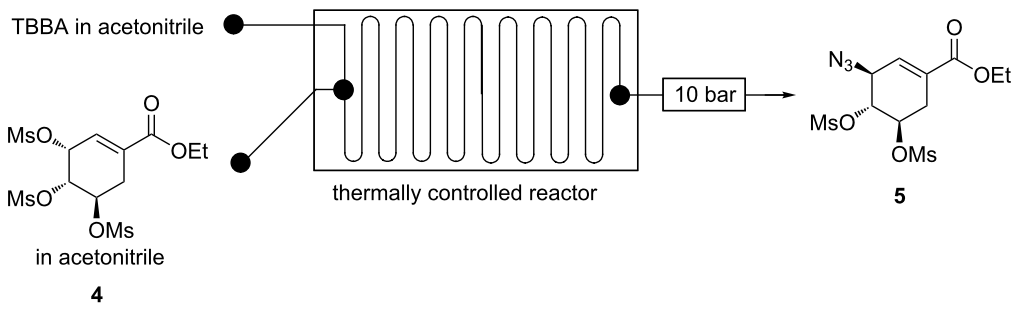

Figure 13: Continuous-flow system for C-3 azidation of mesyl shikimate using TBAA.

cessfully developed. NaN_3 (aq) is the best azidating agent for mesyl shikimate **4** towards the desired azide **5**. The optimum conditions are 1.1 equivalents of NaN_3, 50 °C and 12 s affording full conversion (HPLC) towards the desired azide **5** in 91% isolated yield. Unlike all literature procedures [9,19,20], side product **5a** was not detected using our procedure at 50 °C and 12 s residence time. The use of green solvents, excellent selectivities, safe handling of potentially explosive intermediates rendered the overall process green. The reported batch procedures afforded azide **5** in 91–93% yield over an average of 3 h [9,19,20] which evidently makes our continuous flow procedure more superior. Our procedure could have benefited from the 'fast and hot' strategy, which is exclusive to flow chemistry technology. In this strategy, reagents are passed through a heated zone under high temperature at very fast flow rates allowing for rapid reaction completion and is out of the heated zone before significant byproduct is formed [25]. NaN_3 is the cheapest and greenest azidating reagent of all the developed procedures, however, the drawback is that it is not possible to integrate with the next step, but if this is the case then that strategy will have to be implemented. Basic reaction conditions and high temperatures promote the unwanted aromatisation reaction. There was no aromatisation detected when pure azide **5** was heated. This means that basic conditions promoted OMs elimination and subsequent aromatisation of azide **5** at high temperatures. Our azidating procedures described herein are superior to the reported long batch procedures (2–4 h) [9,19,20].

Continuous-flow synthesis of ethyl (3*R*,4*S*,5*S*)-5-azido-4-acetylamino-3-(1-ethylpropyloxy)cyclohex-1-enecarboxylate (7): The azidation of acetamide **6** is another azidation step in our proposed Tamiflu synthesis route. Acetamide **6** is treated with a suitable azidating agent to afford azide **7**. The C-5 OMs group on acetamide **6** undergoes nucleophilic replacement by the N_3 group (Scheme 5).

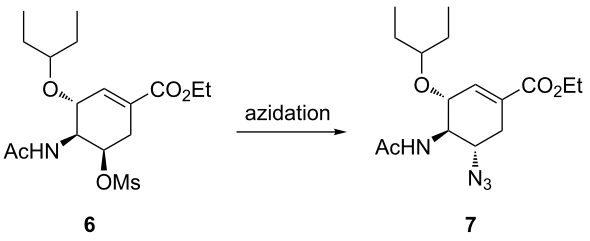

Scheme 5: C-5 azidation of acetamide **6** in our proposed route.

Karpf and Trussardi [9] reported acetamide **6** treatment with NaN_3 (2 equiv) in a solvent mixture of DMSO and EtOH at 90 °C for 20 h affording azide **6** in 66% yield in batch. Nie et al. [19] demonstrated batch azidation of acetamide **6** with NaN_3 (4 equiv) in EtOH/H_2O (5:1) under reflux for 8 h to afford azide **7** in 88% yield. Kalashnikov and co-workers [20] reported the treatment of acetamide **6** in batch with NaN_3 (3 equiv) by refluxing the reaction in 78% aqueous ethanol for 15 h to afford 95% of azide **7**. Nie and Shi [23] also reported a 3 h acetamide **6** azidating batch procedure using NaN_3 (4 equiv) in DMF/H_2O (5:1) affording 84% azide **7**.

Herein, we present acetamide **6** azidation using various azidating agents in a continuous-flow system.

Continuous flow acetamide 6 C-5 azidation using NaN_3. Acetamide **6** was treated with NaN_3 in a Chemtrix continuous-flow system affording azide **7** (Figure 15).

Guided by batch literature [9,19,20,23], preliminary experiments in flow were done using acetamide **6** (0.1 M) in DMF and aqueous NaN_3 (0.3 M, 3 equiv) in a 19.5 µL glass microreactor at 100 °C for 90 s affording azide **7** (63%). We achieved 59% of azide **7** when we replaced the hazardous DMF with acetonitrile. The amount of azide **7** produced decreased (44%)

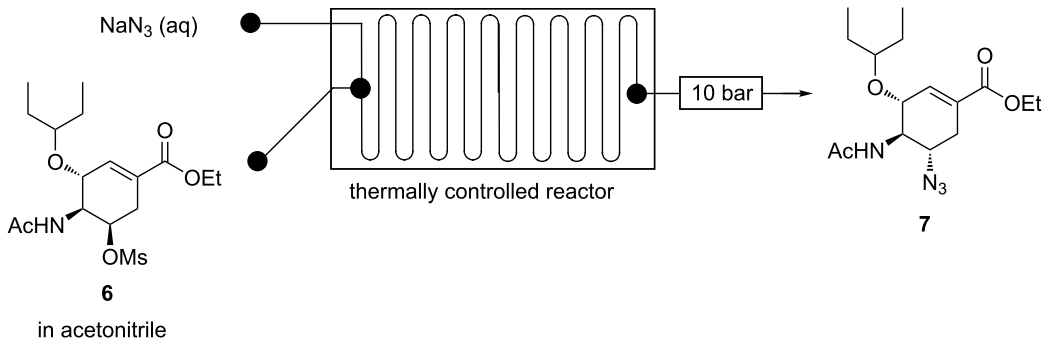

Figure 15: Continuous flow system for C-5 azidation of acetamide **6** using NaN_3.

when less NaN_3 (2 equiv) was used. The reaction was further optimised using acetonitrile as acetamide **6** (0.1 M) solvent and aqueous NaN_3 (0.1 M, 3 equiv) in the Chemtrix 19.5 µL glass reactor (Figure 15). The findings are graphically presented in Figure 16.

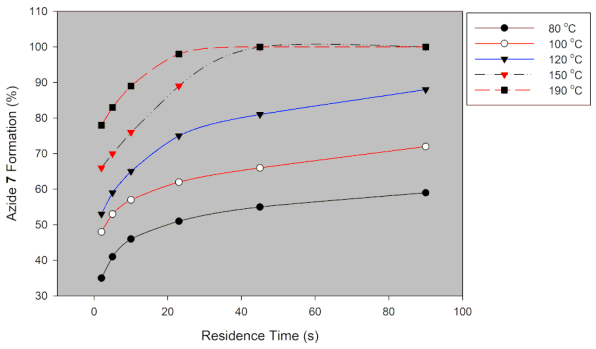

Figure 16: Continuous-flow C-5 azidation of acetamide **6** using NaN_3.

As expected azide **7** formation is a function of temperature and residence time (Figure 16). The conversion of acetamide **6** to azide **7** increased with increased temperature. Conversion towards azide **7** was 55% and 100% at 80 °C and 190 °C at 45 s residence time, respectively. At 80 °C, azide **7** was formed in 35% and 59% conversion, respectively (Figure 16). The hazardous DMF was successfully substituted with greener acetonitrile. The optimum conditions were found to be 190 °C and 45 s residence time to afford azide **7** in full conversion (HPLC) and 89% isolated yield. In batch, good yields (66–95%) were attained at reaction times between 3 h and 15 h at temperatures around 90 °C [9,19,20,23]. Our flow procedure was therefore more efficient than all the reported batch procedures. Continuous flow allowed for higher reaction temperatures than batch, which resulted in faster reactions.

Continuous flow acetamide 6 C-5 azidation using various azidating agents. The use of other azidating agents other than NaN_3 was also investigated in a continuous-flow system (Figure 17).

Optimum conditions found for NaN_3 (1 M, 3 equiv, 190 °C, and 45 s) were used to investigate the use of DPPA, TMSA and TBAA as azidating agents for acetamide **6** (0.03 M) in a 19.5 µL glass microreactor (Figure 17). These azidating agents were dissolved in acetonitrile, not in water as with NaN_3. Reagents flow rates were used to achieve the required reagents equivalents in flow. Experimental details for this study are outlined in the chapter Experimental. The findings of this study are graphically presented in Figure 18.

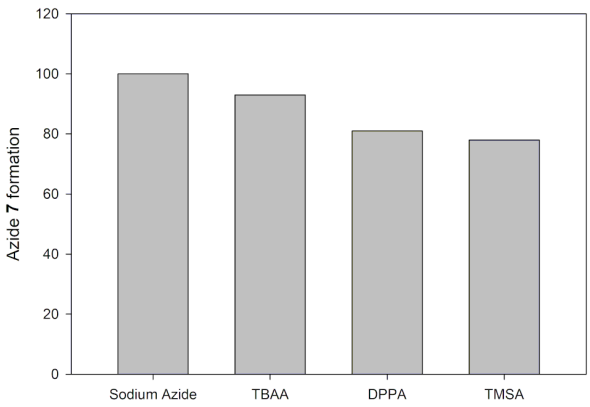

Figure 18: Continuous flow synthesis of azide **7** from acetamide **6** using various azidating agents.

We successfully azidated acetamide **6** affording azide **7** at varying conversions (%) using azidating agents (TBAA, DPPA and TMSA) other than NaN_3. NaN_3 proved to be the best azidating agent (Figure 18). It is evident that the application of ionic bonded azides (NaN_3 and TBAA) gave almost similar

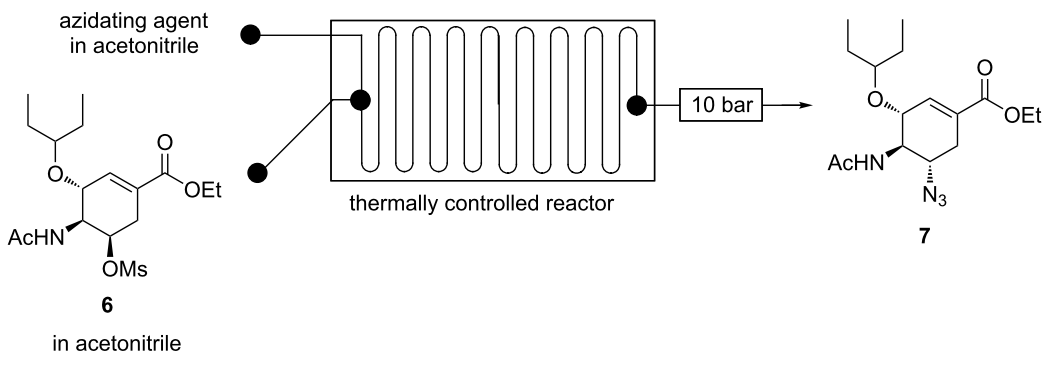

Figure 17: Continuous flow C-5 azidation of acetamide **6** using various azidating agents.

conversion, 100% and 93%, respectively. Whilst the use of covalently bonded azides (DPPA and TMSA) resulted in lower conversions, 84% and 81%, respectively (Figure 18). NaN_3 is the azidating agent of our choice on efficiency, affordability and availability viewpoint. TBAA can be used as azidating agent instead of NaN_3 when anhydrous conditions are required which are useful in multistep syntheses.

Azide **7** was successfully synthesised from acetamide **6** in a continuous-flow system using NaN_3 as the azidating agent. Optimum conditions for this reaction were found to be NaN_3 (3 equiv), 190 °C and 45 s residence time affording full conversion (HPLC) towards azide **7** in 89% isolated yield. The use of NaN_3 (2 equiv) was accompanied by a 15% decrease in conversion. However, full conversion (NaN_3 (2 equiv)) was achieved at a longer residence time (75 s) than using 3 equiv of NaN_3 (45 s). Our continuous-flow azidation procedure for acetamide **6** proved to be more efficient than all the literature procedures [9,19,20,23]. Furthermore, it is a green process as full conversion of potentially explosive azide **7** was achieved by using green solvents water and acetonitrile. The reaction temperatures for C-3 azidation (mesyl shikimate **4** azidation, 25 °C, vide supra) differed dramatically with the C-5 azidation (acetamide azidation, 190 °C). This is because the nucleophilic ($–N_3$) attack on C-3 (allylic position) is easier than that on C-5 (non-allylic position). Generally, we developed a safe and attractive continuous-flow procedure for the synthesis of azide **7** from acetamide **6**.

Conclusion

Continuous-flow technology allowed for safe handling of the potentially explosive azide chemistry is involved in our proposed Tamiflu synthesis. Highly efficient, green continuous-flow azide chemistry processes were successfully developed for this study. This useful technique can be utilised for good synthetic approaches towards Tamiflu, which were previously ruled out for large scale synthesis in batch systems on the basis of safety concerns poised by the use of the potentially explosive azide chemistry and other hazardous chemistry. Therefore, problems inherent in scale-up are effectively eliminated or reduced, making microreactor technology a viable tool in the synthesis of Tamiflu. The azide intermediates were safely synthesised in full conversions and >89% isolated yields.

Experimental

Chemicals were supplied by Sigma-Aldrich, Merck and Industrial Analytical and used as received. Anhydrous solvents were supplied by Sigma-Aldrich and maintained by drying over appropriate drying agents. Nuclear magnetic resonance (NMR) spectra were recorded at room temperature as solutions in deuterated chloroform ($CDCl_3$). A Bruker Avance-400 spectrometer (400 MHz) was used to record the spectra and the chemical shifts are reported in parts per million (ppm) with coupling constants in Hertz (Hz). Infrared spectra were recorded from 4000 to 500 cm^{-1} using a Bruker spectrometer and peaks (ν_{max}) reported in wavenumbers (cm^{-1}). Melting points of all compounds were determined using a Stuart® Melting Point Apparatus SMP30 and Agilent Zorbax C_{18}, 10 µm, 4.6 mm × 250 mm column. Continuous-flow reactions were performed on a Labtrix® Start system and a Uniquis FlowSyn system. Reactions were monitored by Agilent 1200 high-performance liquid chromatography (HPLC) fitted with a UV–vis detector. HPLC analysis was performed on Agilent Zorbax C_{18}-column (250 mm × 4.6 mm i.d, 5 µm) ambient temperature using an isocratic system. Analysis of collected samples was done using HPLC method (mobile phase consisted of 70% acetonitrile and 30% water. The sample injection volume was 5 µL, eluted at a flow rate of 1.5 mL/min and detected at 213 nm with a run time of 15 min).

Continuous-flow synthesis of ethyl (3*S*,4*R*,5*R*)-3-azido-4,5-bis(methanesulfonyloxy)cycohex-1-enecarboxylate (5). All the mesyl shikimate **4** azidation investigations were done in a continuous-flow system fitted with a 19.5 µL glass reactor for optimisation of the azidation of the OMs group at the allylic C-3 position of mesyl shikimate **4** in the presence of various azidating agents. Sodium azide (NaN_3), diphenylphosphoryl azide (DPPA), trimethylsilyl azide (TMSA) and tetrabutylammonium azide (TBAA) were the various azidating agents investigated in this system. Two syringe pumps were used to pump reagents from two 10 mL SGE Luer lock gas tight glass syringes into the thermally controlled microreactor system which was fitted with a 10 bar back pressure regulator. Mesyl shikimate was dissolved in acetonitrile (0.1 M) and azidating agent in appropriate solvent (0.11 M, 1.1 equiv) and pumped into the flow system separately. The reaction was quenched within the flow reactor using aqueous HCl (0.11 M, 1.1 equiv) when necessary. Samples were collected and analysed using HPLC resulting in 4.84 min retention time for azide **5**. For characterisation, **an** appropriate amount of toluene and water was added to the reaction mixture after acetonitrile was driven off in vacuo at room temperature. The organic layer was successively washed with water and brine. The organic phase was dried over anhydrous Mg_2SO_4 and concentrated in vacuo at room temperature. The crude product was purified by silica column chromatography using a 1:2 mixture of EtOAc and hexane to furnish azide compound **5** as a colourless oil. FTIR (cm^{-1}) ν: 2984, 2941, 2105, 1711, 1660, 1350, 1245, 1171, 1011, 823; ^{1}H NMR (400 MHz, $CDCl_3$) δ 1.25 (t, *J* = 7.0 Hz, 3H), 2.56–2.66 (m, 1H), 3.08 (s, 3H), 3.12 (dd, *J* = 6.2 Hz, 1H), 3.16 (s, 3H), 4.18 (q, *J* = 7.0 Hz, 2H), 4.23–4.31 (m, 1H), 4.64–4.74 (m, 1H), 4.77–4.88 (m, 1H), 6.69 (s, 1H) ppm; ^{13}C NMR (100 MHz,

$CDCl_3$) δ 14.1, 31.1, 39.0, 39.4, 61.1, 61.9, 73.8, 79.1, 130.3, 131.9, 164.17 ppm.

Continuous flow systhesis of ethyl (3*R*,4*S*,5*S*)-5-azido-4-acetylamino-3-(1-ethylpropyloxy)cyclohex-1-enecarboxylate (7). The continuous-flow system fitted with a 19.5 μL glass reactor was used to optimise the C-5 azidation of acetamide **6**. Acetamide **6** (0.1 M) in acetonitrile and azidating agent in appropriate solvent (0.3 M, 3 equiv) were pumped separately using two syringe pumps from two 10 mL SGE Luer lock gas tight glass syringes into the thermally controlled microreactor system which was fitted with a 10 bar back pressure regulator. NaN_3, DPPA, TMSA and TBAA were the various azidating agents investigated. Samples were collected and analysed using HPLC resulting in 4.84 min retention time for azide **5**. For characterisation, the reaction mixture was collected and ethyl acetate and water were added. The organic layer was separated, washed with brine and dried over anhydrous Mg_2SO_4. The residue was concentrated in vacuo to yield crude product **7** as a semi-crystalline oil. It was purified by silica column chromatography and the fractions were concentrated in vacuo to afford pure compound **7** as white crystals. Solid: mp 136.9–138.2 °C (Lit. value [9] mp. 136.6–137.7 °C); FTIR (cm^{-1}) ν: 3266, 2971, 2099, 1713, 1658, 1558, 1249, 1075; ^{1}H NMR (400 MHz, $CDCl_3$) δ 0.91 (m, 6H), 1.31 (t, *J* = 7.1 Hz, 3H), 1.42–1.63 (m, 4H), 2.10 (s, 3H), 2.18–2.33 (m, 1H), 2.88 (dd, *J* = 5.5, 17.6 Hz, 1H), 3.29–3.37 (m, 1H), 3.41–3.52 (m, 1H), 4.23 (q, *J* = 6.97 Hz, 3H), 4.49–4.63 (m, 1H), 6.45–6.70 (m, 1H), 6.80 (s, 1H) ppm; ^{13}C NMR (101 MHz, $CDCl_3$) δ 9.3, 9.5, 14.2, 23.2, 25.6, 26.3, 30.7, 57.3, 57.9, 61.1, 73.6, 77.2, 82.1, 128.1, 137.9, 165.7, 171.76 ppm.

Acknowledgements

We thank the National Research Foundation, Council for Scientific and Industrial Research and Nelson Mandela University for financial support.

ORCID® iDs

Cloudius R. Sagandira - https://orcid.org/0000-0002-6485-3606
Paul Watts - https://orcid.org/0000-0002-4156-5679

Preprint

A non-peer-reviewed version of this article has been previously published as a preprint doi:10.3762/bxiv.2019.84.v1

References

1. Magano, J. *Tetrahedron* **2011,** *67,* 7875–7899. doi:10.1016/j.tet.2011.07.010
2. Magano, J. *Chem. Rev.* **2009,** *109,* 4398–4438. doi:10.1021/cr800449m
3. Ogasawara, S.; Hayashi, Y. *Synthesis* **2017,** *49,* 424–428. doi:10.1055/s-2016-0036-1588899
4. Sagandira, C. R.; Watts, P. *J. Flow Chem.* **2018,** *8,* 69–79. doi:10.1007/s41981-018-0010-9
5. Abrecht, S.; Federspiel, M. C.; Estermann, H.; Fischer, R.; Karpf, M.; Mair, H.-J.; Oberhauser, T.; Rimmler, G.; Trussardi, R.; Zutter, U. *Chimia* **2007,** *61,* 93–99. doi:10.2533/chimia.2007.93
6. Karpf, M.; Trussardi, R. *J. Org. Chem.* **2001,** *66,* 2044–2051. doi:10.1021/jo005702l
7. Weng, J.; Li, Y.-B.; Wang, R.-B.; Li, F.-Q.; Liu, C.; Chan, A. S. C.; Lu, G. *J. Org. Chem.* **2010,** *75,* 3125–3128. doi:10.1021/jo100187m
8. Farina, V.; Brown, J. D. *Angew. Chem., Int. Ed.* **2006,** *45,* 7330–7334. doi:10.1002/anie.200602623
9. Karpf, M.; Trussardi, R. *Angew. Chem., Int. Ed.* **2009,** *48,* 5760–5762. doi:10.1002/anie.200901561
10. Oshitari, L.; Mandai, T. *Synlett* **2009,** 787–789. doi:10.1055/s-0028-1087940
11. Nie, L.-D.; Wang, F.-F.; Ding, W.; Shi, X.-X.; Lu, X. *Tetrahedron: Asymmetry* **2013,** *24,* 638–642. doi:10.1016/j.tetasy.2013.04.016
12. Bräse, S. *Organic Azides: Syntheses and Applications;* John Wiley & Sons: West Sussex, UK, 2010.
13. Ishikawa, H.; Suzuki, T.; Orita, H.; Uchimaru, T.; Hayashi, Y. *Chem. – Eur. J.* **2010,** *16,* 12616–12626. doi:10.1002/chem.201001108
14. Ishikawa, H.; Bondzic, B. P.; Hayashi, Y. *Eur. J. Org. Chem.* **2011,** 6020–6031. doi:10.1002/ejoc.201100074
15. Movsisyan, M.; Delbeke, E. I. P.; Berton, J. K. E. T.; Battilocchio, C.; Ley, S. V.; Stevens, C. V. *Chem. Soc. Rev.* **2016,** *45,* 4892–4928. doi:10.1039/c5cs00902b
16. Ehrfeld, W.; Hessel, V.; Löwe, H. *Microreactors: New Technology for Modern Chemistry;* Wiley-VCH: Weinheim, Germany, 2000. doi:10.1002/3527601953
17. Rogers, L.; Jensen, K. F. *Green Chem.* **2019,** *21,* 3481–3498. doi:10.1039/c9gc00773c
18. Sagandira, C. R.; Watts, P. *J. Flow Chem.* **2019,** *9,* 79–87. doi:10.1007/s41981-019-00037-w
19. Nie, L.-D.; Shi, X.-X.; Ko, K. H.; Lu, W.-D. *J. Org. Chem.* **2009,** *74,* 3970–3973. doi:10.1021/jo900218k
20. Kalashnikov, A. I.; Sysolyatin, S. V.; Sakovich, G. V.; Sonina, E. G.; Shchurova, I. A. *Russ. Chem. Bull.* **2013,** *62,* 163–170. doi:10.1007/s11172-013-0024-2
21. Prat, D.; Wells, A.; Hayler, J.; Sneddon, H.; McElroy, C. R.; Abou-Shehada, S.; Dunn, P. J. *Green Chem.* **2016,** *18,* 288–296. doi:10.1039/c5gc01008j
22. Byrne, F. P.; Jin, S.; Paggiola, G.; Petchey, T. H. M.; Clark, J. H.; Farmer, T. J.; Hunt, A. J.; McElroy, C. R.; Sherwood, J. *Sustainable Chem. Processes* **2016,** *4,* 7. doi:10.1186/s40508-016-0051-z
23. Nie, L.-D.; Shi, X.-X. *Tetrahedron: Asymmetry* **2009,** *20,* 124–129. doi:10.1016/j.tetasy.2008.11.027
24. Thompson, A. S.; Humphrey, G. R.; DeMarco, A. M.; Mathre, D. J.; Grabowski, E. J. J. *J. Org. Chem.* **1993,** *58,* 5886–5888. doi:10.1021/jo00074a008
25. Gernaey, K. V.; Cervera-Padrell, A. E.; Woodley, J. M. *Future Med. Chem.* **2012,** *4,* 1371–1374. doi:10.4155/fmc.12.77

BEILSTEIN JOURNAL OF ORGANIC CHEMISTRY

Palladium-catalyzed Sonogashira coupling reactions in γ-valerolactone-based ionic liquids

László Orha[1,2], József M. Tukacs[1], László Kollár[3] and László T. Mika[*1]

Full Research Paper

Open Access

Address:
[1]Department of Chemical and Environmental Process Engineering, Budapest University of Technology and Economics Műegyetem rkp. 3, Budapest, H-1111, Hungary, [2]Institute of Isotopes, Konkoly-Thege Miklós str. 29-33. Budapest, H-1121, Hungary and [3]Department of Inorganic Chemistry, University of Pécs and János Szentágothai Research Center and MTA-PTE Research Group for Selective Chemical Syntheses, Ifjúság u. 6.; Pécs, H-7624, Hungary

Email:
László T. Mika[*] - laszlo.t.mika@mail.bme.hu

* Corresponding author

Keywords:
catalysis; cross coupling; green chemistry; ionic liquids

Beilstein J. Org. Chem. **2019,** *15,* 2907–2913.
doi:10.3762/bjoc.15.284

Received: 07 October 2019
Accepted: 18 November 2019
Published: 03 December 2019

This article is part of the thematic issue "Green chemistry II".

Guest Editor: L. Vaccaro

Abstract

It was demonstrated that the γ-valerolactone-based ionic liquid, tetrabutylphosphonium 4-ethoxyvalerate as a partially bio-based solvent can be utilized as alternative reaction medium for copper- and auxiliary base-free Pd-catalyzed Sonogashira coupling reactions of aryl iodides and functionalized acetylenes under mild conditions. Twenty-two cross-coupling products were isolated with good to excellent yields (72–99%) and purity (>98%). These results represent an example which proves that biomass-derived safer solvents can be utilized efficiently in common, industrially important transformations exhibiting higher chemical and environmental efficiency.

Introduction

In the past few decades, the transition-metal-catalyzed coupling reaction has represented one of the most powerful and atom economical strategies for the efficient assembly of new carbon–carbon bonds. It has therefore become the most attractive approach to the synthesis of a wide range of functionalized organic molecules from laboratory to industrial scale [1-3]. Among these tools, the Pd-catalyzed coupling reactions have received substantial attention, due to the mild operation conditions, excellent functional group tolerance and chemoselectivity as well as wide applicability from syntheses of common building blocks to agrochemicals, just to name a few advantages [4-6]. From the series of palladium-assisted C–C bond formation, the Sonogashira coupling reaction has been identified as a viable synthetic method for the preparation of various alkenyl- and arylacetylenes [7,8] having great importance in organic synthetic schemes of the pharmaceutical industry.

From the environmental point of view, the Sonogashira reactions are usually performed in fossil-based common organic reaction media having high vapor pressure even at higher temperatures, toxicity, flammability, etc., which could result in several serious environmental concerns, especially when they are released into the atmosphere. According to the FDA guidelines [9], the typical solvents of Sonogashira reactions such as toluene [10], THF [11], DMF [12], NMP [13], DMA [14], or MeCN [15] are classified into Class 2, of which applications should be strictly limited, particularly in pharmaceutical industry. To develop an environmentally benign alternative of this useful method, the reaction has been extended to green solvents such as water [16], fluorous solvents [17], supercritical CO_2 [18], and very recently γ-valerolactone [19]. The series of these alternative media can implicitly be continued by ionic liquids (ILs) [20], which have attracted considerable attention, due to their extremely low vapor pressure, good solvating properties, reasonable thermal stability, and easily tuneable physical properties [21]. Accordingly, the Sonogashira reactions were also successfully performed in conventional ionic liquids such as [BMIM][PF_6] [22-25], [BMIM][BF_4] [23], [HMIM][BF_4] [24], [EMIM][NTf_2] [26], [nBuPy][X] (X = PF_6^-, BF_4^-, NO_3^-) [27], [DectBu_3P][BF_4] [28]. It was found that some of these systems could operate copper-free [25,27,29] and/or auxiliary base-free conditions [30]. Recently, some “designer" ionic liquids were also developed for this purpose [29-33] from which an imidazolium-based piperidine-appended one could act as task specific compound operating either as a solvent in itself [31] or as an additive to the common ionic liquids [30,33]. It should be noted; however, significant catalyst loadings (5–10 mol %) were necessary to obtain reasonable product yields for latter reactions.

Although the Sonogashira coupling is a well-studied transformation, it has not been carried out in γ-valerolactone-originated ILs, which can act as solvent, ligand and base. Thus, the preparation of various acetylenes in a partially or even biomass-based solvent without any auxiliary material could further control and reduce the environmental impacts of this industrially important transformation.

Herein we report a study on the palladium-catalyzed copper- and added base-free Sonogashira coupling reactions to synthesize various acetylenes in γ-valerolactone-based ionic liquids under mild conditions.

Results and Discussion

We recently demonstrated that copper-catalyzed Ullmann-type N–C coupling reactions could be performed in tetrabutylphosphonium 4-alkoxyvalerate-type ionic liquids, which can easily be synthesized from the renewable platform chemical γ-valerolactone and have negligible vapor pressures even at high temperatures [34]. In order to extend the applicability of valerate-based ionic liquids, the conventional imidazolium-type media and tetrabutylphosphonium 4-ethoxyvalerate ([TBP][4EtOV]) were compared in the coupling of iodobenzene (**1a**) and phenylacetylene (**2a**) as a model reaction (Scheme 1) under typically used “Sonogashira conditions” [7,35].

Because the role of ionic liquids as coordination agents for transition metal species was demonstrated [36,37] and palladium carboxylate complexes are well-known compounds, it can be proposed that the carboxylate group of the 4-ethoxyvalerate anion could stabilize the catalytically active species and therefore the ligand can be eliminated from the catalytic system.

Complete conversions of **1a** to diphenylacetylene (**3a**) were detected in the presence of Pd, Cu, and triethylamine (Et_3N) in all the ILs (Table 1, #1). It should be noted that the typically utilized base, Et_3N has a foul smell and could affect the product isolation procedure. In addition, it is well-established that

Table 1: Sonogashira coupling reaction of iodobenzene (**1a**) and phenylacetylene (**2a**) in different ionic liquids.[a]

Ionic liquid	Conversion of iodobenzene in the presence of Pd, Cu, and Et_3N (#1)	Pd and Cu (#2)	Pd (#3)
[BMIM][BF_4]	>99%	<1%	<1%
[EMIM][BF_4]	>99%	<1%	<1%
[BMIM][Octyls][b]	>99%	<1%	<1%
[BMIM][PF_6]	>99%	<1%	<1%
[TBP][4EtOV]	>99%	>99%	>99%

[a]Reaction conditions: 0.8 mL ionic liquid, 0.5 mol % $PdCl_2(PPh_3)_2$, 1 mol % CuI, 0.75 mmol phenylacetylene, 0.5 mmol iodobenzene, 0.75 mmol Et_3N, T = 55 °C, t = 3 h. [b]Octyls: octylsulfate anion.

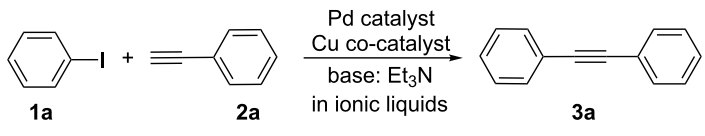

Scheme 1: Palladium-catalyzed Sonogashira cross-coupling of iodobenzene (**1a**) and phenylacetylene (**2a**) in ionic liquids.

the presence of Cu(I) salt can promote the in situ formation of some Cu(I) acetylides, which can readily undergo oxidative homocoupling of alkynes even in their slight excess in the reaction mixture [15,38,39]. Thus, the elimination of these auxiliary materials could result in an environmental benign alternative protocol. Hence, the scope of the reaction was investigated with a combination of palladium, copper co-catalyst and Et_3N as a base. By elimination of toxic Et_3N ($LD_{50(rat,\ oral)}$ = 560 mg/kg) [40], no reactions were detected in imidazolium-type ILs. However, complete conversion of **1a** was observed in [TBP][4EtOV], without Et_3N, proving that the solvent can act as a base in itself (Table 1, #2) as it was demonstrated for Cu-catalyzed C–N coupling reactions [34].

When, we attempted to couple **1a** and **2a** in the absence of any copper salt as cocatalyst, complete formation of **3a** was also detected after 3 h revealing that copper can be eliminated from the system without any decrease in the system's efficiency.

The source of palladium could also have a significant effect on the reaction's performance [23]. It was found that while $Pd(PPh_3)_4$, palladium acetate ($Pd(OAc)_2$), $PdCl_2(PPh_3)_2$, and tris(dibenzylideneacetone)dipalladium ($Pd_2(DBA)_3$) all catalyzed the Sonogashira reaction, the $PdCl_2(PPh_3)_2$ precursor turned out to have the best activity in the light of reaction rates (Figure 1). In the presence of 0.5 mol % of $PdCl_2(PPh_3)_2$ the treatment of 0.5 mmol **1a** with 0.75 mmol of **2a** afforded complete conversion of **1a** in 40 min. Similar performance of $PdCl_2(PPh_3)_2$ were reported by Ryu, when [BMIM][PF_6] was used as reaction medium [26]; however, by the use of 10 times higher catalyst loading.

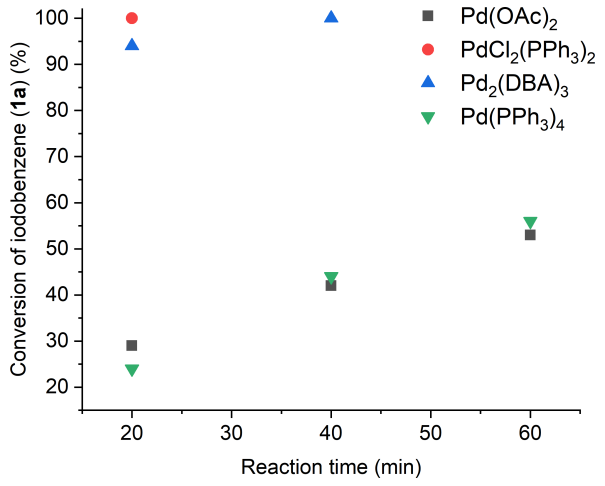

Figure 1: Effect of catalyst precursors used in Sonogashira coupling reaction of iodobenzene (**1a**, 0.5 mmol) and phenylacetylene (**2a**, 0.75 mmol). Reaction conditions: 0.8 mL [TBP][4EtOV], 0.5 mol % catalyst, T = 55 °C.

The moisture content of the reaction environment could have a significant effect on the efficiency of a transition-metal-catalyzed reaction. Because [TBP][4EtOV] was isolated from an aqueous solution, the investigation of possible influence of the residual water content on the reaction was highly desired. We found that no decrease in the formation of **3a** was detected when the moisture content was varied between 0.05 and 5.0 wt % (Table 2). Since the method is hardly sensitive to the residual moisture content, to exclude water from the reaction mixture no special pretreatment or handling of the solvent is necessary.

Table 2: Effect of water content on Sonogashira coupling of iodobenzene (**1a**) and phenylacetylene (**2a**).[a]

Entry	Water content (wt %)	Isolated yields of **3a** (%)
1	0.05	85
2	1.0	86
2	2.5	82
4	5.0	83

[a]Reaction conditions: 0.8 mL [TBP][4EtOV], 0.5 mol % $PdCl_2(PPh_3)_2$, 0.75 mmol phenylacetylene, 0.5 mmol iodobenzene, T = 55 °C, t = 3 h.

Hereafter, the air-stable and readily available $PdCl_2(PPh_3)_2$ was selected as a catalyst precursor to facilitate C–C bond couplings involving various iodoaromatic compounds (**1a–l**) and phenylacetylene (**2a**) in [TBP][4EtOV] in the absence of any additional ligands and auxiliary base at 55 °C for 3 h. In general, the catalytic system could be applied to various iodoarene substrates and the substrate reactivity was not influenced dramatically by the electronic parameters of the substituents. Both electron-withdrawing (chloro, fluoro and bromo) and electron-donating (methyl, methoxy) groups were tolerated on the aryl iodide (Table 3, entries 2–7). Under identical conditions, 2-iodothiophene, and iodopyridine derivatives could also easily be converted to the corresponding acetylene with good or even excellent isolated yields (**3i–n**). When 2-amino-3-iodopyridine (**1i**) was converted no C–N bond formation was detected excluding the copper impurities assisted Ullmann-coupling reactions. When 2-chloro-5-iodopyridine (**1l**) was reacted with 1 equiv of **2**, 2-chloro-5-(2-phenylethynyl)pyridine (**3l**) was isolated as product with a yield of 72%. By the use of 2.5 equiv of **2**, the chloro group also undergoes a coupling reaction to form 2,5-bis(2-phenylethynyl)pyridine (**3m**) under identical conditions (Table 3, entries 12 and 13).

By comparison with the conversion of 4-chloro-1-iodobenzene (**1g**), no formation of 1,4-bis(phenylethynyl)benzene was detected. It agrees with the activated substituents of 2-substituted pyridine derivatives. It can be concluded that by varying

Table 3: Palladium-catalyzed Sonogashira coupling of various iodoaromatic compounds (**1a–l**) with phenylacetylene (**2a**).[a]

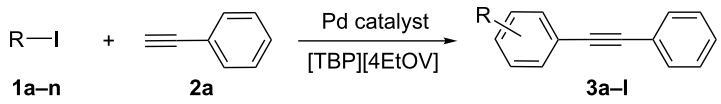

1a–n **2a** **3a–l**

#	Iodoaromatic compounds		Product	Yield (%)[b]
1	**1a**	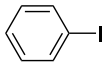	**3a**	85
2	**1b**	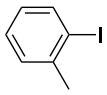	**3b**	96
3	**1c**	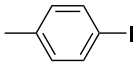	**3c**	95
4	**1d**	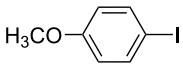	**3d**	82
5	**1e**	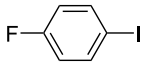	**3e**	80
6	**1f**	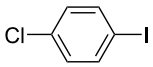	**3f**	87
7	**1g**	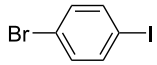	**3g**	52
8	**1h**		**3h**	80
9	**1i**	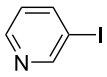	**3i**	75
10	**1j**	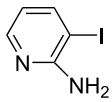	**3j**	93
11	**1k**	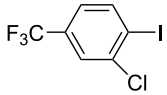	**3k**	79
12	**1l**	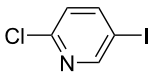	**3l**	72
13[c]	**1l**	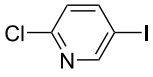	**3m**	69

[a]Reaction conditions: 0.8 mL [TBP][4EtOV], 0.5 mol % $PdCl_2(PPh_3)_2$, 0.75 mmol phenylacetylene, 0.5 mmol iodoaromatic compound, T = 55 °C, t = 3 h; [b]isolated yields; [c]1.25 mmol (2.5 equiv) of phenylacetylene, **3m**: 2,5-bis(2-phenylethynyl)pyridine.

electronic and steric properties of substituents of the iodoaromatic substrates at all *ortho*-, *meta*-, and *para*- positions, no significant changes in the product yields were achieved according to previous studies [26,41]. Regarding the negligible influence of the 4-substituents, i.e., no Hammett-plot can be obtained for the above reaction, it can be stated that the rate determining step of the Sonogashira coupling is not related to the formation of Pd-aryl species.

Subsequently, a series of different acetylenes, which can readily be dissolved in [TBP][4EtOV] were subjected to the coupling reaction under identical conditions. By comparison of the efficiency of conversion of iodobenzene and its electron-donating 4-methoxy (**1d**) and electron-withdrawing 4-nitro (**1m**) derivatives with different aliphatic acetylenes (**4**, **6**, and **8**), no significant differences in isolated yields were observed (Table 4, Table 5 and Table 6) verifying the wide range of func-

tional group tolerance by side of acetylenic substrates, as well. Same results were reported by Alper and co-workers, who perform this reaction in [BMIM][PF_6] as alternative solvent [22].

The possible reuse of the catalyst was subsequently investigated by the model reaction of 0.5 mmol of **1a** and 1.5 equiv of **2a** in the presence of 0.5 mol % $PdCl_2(PPh_3)_2$ at 55 °C for 2 h. After the first extraction of the product from the reaction mixture by the addition of 10 × 5 mL of pentane, **3a** was isolated with a yield of 88%. It should be noted that this reaction verified the reproducibility of the experiments (cf. Table 3, entry 1). Same amounts of substrates were added to the Pd catalyst contained in the ionic liquid phase followed by heating to 55 °C. In the second run 12% of decrease in the isolated yield was detected; however, after the 4th cycle, it became significant (Figure 2). The same tendency was reported by Toma for various acetylenes [24]. The ^{13}C NMR investigations of the $[4EtOV]^-$ anion throughout the reaction did not indicate any change in its composition. Nevertheless, a reaction of the alkoxyvalerate anion with HI that formed during the reaction could be assumed.

Table 4: Palladium-catalyzed Sonogashira coupling of various iodoaromatic compounds (**1a, d, m**) with propargyl alcohol (**4**).[a]

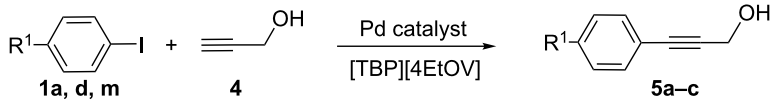

1a, d, m **4** **5a–c**

#		R	Product	Yield (%)[b]
1	**1a**	H	**5a**	80
2	**1m**	NO_2	**5b**	78
3	**1d**	OCH_3	**5c**	85

[a]Reaction conditions: 0.8 mL [TBP][4EtOV], 0.5 mol % $(PPh_3)_2PdCl_2$, 0.75 mmol propargyl alcohol, 0.5 mmol iodoaromatic compounds, T = 55 °C, t = 3 h; [b]isolated yields.

Table 5: Palladium-catalyzed Sonogashira coupling of various iodoaromatic compounds (**1a, d, m**) with 1-ethynyl-1-cyclohexanol (**6**).[a]

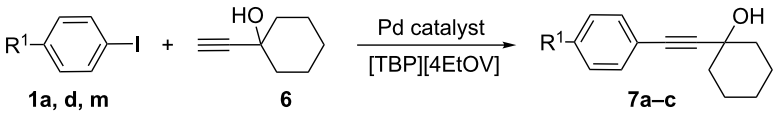

1a, d, m **6** **7a–c**

#		R	Product	Yield (%)[b]
1	**1a**	H	**7a**	85
2	**1m**	NO_2	**7b**	99
3	**1d**	OCH_3	**7c**	99

[a]Reaction conditions: 0.8 mL [TBP][4EtOV], 0.5 mol % $(PPh_3)_2PdCl_2$, 0.75 mmol 1-ethynyl-1-cyclohexanol, 0.5 mmol iodoaromatic compound, T = 55 °C, t = 3 h; [b]isolated yields.

Table 6: Palladium-catalyzed Sonogashira coupling of various iodoaromatic compounds (**1a, d, m**) with 3-ethyl-1-pentyn-3-ol (**8**).[a]

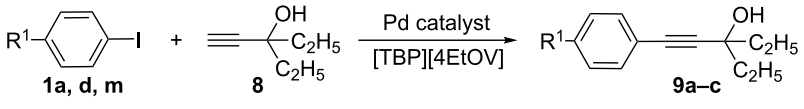

1a, d, m **8** **9a–c**

#		R	Product	Yield (%)[b]
1	**1a**	H	**9a**	87
2	**1m**	NO_2	**9b**	85
3	**1d**	OCH_3	**9c**	81

[a]Reaction conditions: 0.8 mL [TBP][4EtOV], 0.5 mol % $(PPh_3)_2PdCl_2$, 0.75 mmol 3-ethyl-1-pentyn-3-ol, 0.5 mmol iodoaromatic compound, T = 55 °C, t = 3 h; [b]isolated yields.

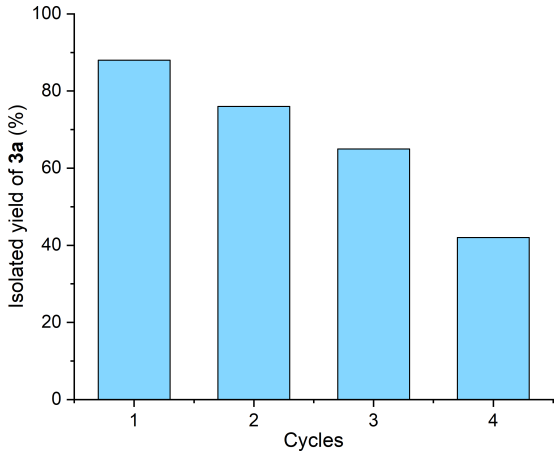

Figure 2: Re-use of Pd catalyst for Sonogashira coupling of iodobenzene (**1a**) and phenylacetylene (**2a**). Reaction conditions: 0.8 mL [TBP][4EtOV], 0.5 mol % catalyst, T = 55 °C, t = 3 h.

Conclusion

In conclusion, we have demonstrated that a γ-valerolactone-based ionic liquid, tetrabutylphosphonium 4-ethoxyvalerate can be utilized as an alternative solvent for Pd-catalyzed Sonogashira coupling reactions of aryl iodides and functionalized acetylenes under mild conditions. The reactions were performed by using 0.5 mol % catalyst loading and we pointed out that both copper and external base could be eliminated from the reaction mixture without any decrease in catalytic activity. The protocol was tested for a wide range of substrates and several products (**3a**–**n**, **5a–c**, **7a–c**, **9a–c**) were isolated in good to excellent yields. The Cu- and base-free reaction can be performed under air and are highly tolerant to moisture.

Experimental

The sources of chemicals are listed in Supporting Information File 1. The NMR spectra were recorded on a Brucker Avance 250 MHz spectrometer. The water contents of the ionic liquids were determined by Karl Fischer titration performed by HANNA Instruments 904.

The γ-valerolactone-based ionic liquid ([TBP][4EtOV]) was prepared as described in [34] with details presented in Supporting Information File 1.

Exact mass measurements were performed on a high-resolution Q-Exactive Focus hybrid quadrupole-orbitrap mass spectrometer (Thermo Fisher Scientific, Bremen, Germany) equipped with a heated electrospray ionization (ESI) source. Samples were dissolved in acetonitrile/water 1:1 (v/v) solvent mixture containing 0.1% (v/v) formic acid. Solutions were directly introduced into the ion source using a syringe pump. Under the applied conditions, the compounds form protonated molecules, $[M + H]^+$ in positive ionization mode (ESI).

Detailed experimental procedures, characterization data are reported in Supporting Information File 1.

General procedure for Sonogashira coupling reactions

In a 4 mL screw-cap vial, 0.5 mmol of corresponding iodoarene compound, 1.5 equiv of phenylacetylene or propargyl alcohol, 0.005 equiv $PdCl_2(PPh_3)_2$, and 0.8 mL of ionic liquid were mixed and stirred at 55 °C for 3 h. After cooling, the mixture was partitioned between 5 mL of water and 5 mL of pentane. After separation, the aqueous phase was extracted subsequently with 2 × 5 mL of pentane. The combined organic phase was washed with brine, dried over $MgSO_4$, filtered, and the solvent was evaporated under reduced pressure (ca. 10 mmHg). The oily residue was purified by chromatography on silica gel (Merck Silicagel 60 (0.063−0.200 mm) for column chromatography (70−230 mesh ASTM)) eluted with *n*-pentane/EtOAc. The purity of the isolated products was >98%. The detailed experimental procedure as well as the characterization of isolated compounds are provided in Supporting Information File 1.

Supporting Information

Supporting Information File 1

Source of chemicals, the detailed experimental procedure as well as characterization data of isolated compounds.
[https://www.beilstein-journals.org/bjoc/content/supplementary/1860-5397-15-284-S1.pdf]

Acknowledgements

This work was funded by the National Research, Development and Innovation Office – NKFIH (KH 129508 and K113177) and the Higher Education Excellence Program of the Ministry of Human Capacities in the frame of Biotechnology research area of Budapest University of Technology and Economics (BME FIKP-BIO). L.T. Mika is grateful for the support of a Scholarship of József Varga Foundation, Budapest University of Technology and Economics, Budapest, Hungary.

ORCID® iDs

László T. Mika - https://orcid.org/0000-0002-8520-0065

References

1. Yang, Y.; Lan, J.; You, J. *Chem. Rev.* **2017,** *117,* 8787–8863. doi:10.1021/acs.chemrev.6b00567
2. Shi, W.; Liu, C.; Lei, A. *Chem. Soc. Rev.* **2011,** *40,* 2761–2776. doi:10.1039/c0cs00125b

3. de Meijere, A.; Diederich, F., Eds. *Metal-Catalyzed Cross-Coupling Reactions;* Wiley-VCH: Weinheim, Germany, 2004. doi:10.1002/9783527619535
4. Johansson Seechurn, C. C. C.; Kitching, M. O.; Colacot, T. J.; Snieckus, V. *Angew. Chem., Int. Ed.* **2012,** *51,* 5062–5085. doi:10.1002/anie.201107017
5. Devendar, P.; Qu, R.-Y.; Kang, W.-M.; He, B.; Yang, G.-F. *J. Agric. Food Chem.* **2018,** *66,* 8914–8934. doi:10.1021/acs.jafc.8b03792
6. Jana, R.; Pathak, T. P.; Sigman, M. S. *Chem. Rev.* **2011,** *111,* 1417–1492. doi:10.1021/cr100327p
7. Chinchilla, R.; Nájera, C. *Chem. Rev.* **2007,** *107,* 874–922. doi:10.1021/cr050992x
8. Sonogashira, K. Palladium-Catalyzed Alkynylation: Sonogashira Alkyne Synthesis. In *Handbook of Organopalladium Chemistry for Organic Synthesis;* Negishi, E., Ed.; John Wiley & Sons: New York, NY, USA; pp 493–529. doi:10.1002/0471212466.ch22
9. https://www.fda.gov/media/71737/download (accessed Oct 2, 2019).
10. Severin, R.; Reimer, J.; Doye, S. *J. Org. Chem.* **2010,** *75,* 3518–3521. doi:10.1021/jo100460v
11. Karpov, A. S.; Müller, T. J. J. *Synthesis* **2003,** 2815–2826. doi:10.1055/s-2003-42480
12. Panda, B.; Sarkar, T. K. *Synthesis* **2013,** *45,* 817–829. doi:10.1055/s-0032-1318119
13. Moon, J.; Jeong, M.; Nam, H.; Ju, J.; Moon, J. H.; Jung, H. M.; Lee, S. *Org. Lett.* **2008,** *10,* 945–948. doi:10.1021/ol703130y
14. Nagy, A.; Novák, Z.; Kotschy, A. *J. Organomet. Chem.* **2005,** *690,* 4453–4461. doi:10.1016/j.jorganchem.2004.12.036
15. Gelman, D.; Buchwald, S. L. *Angew. Chem., Int. Ed.* **2003,** *42,* 5993–5996. doi:10.1002/anie.200353015
16. Bakherad, M. *Appl. Organomet. Chem.* **2013,** *27,* 125–140. doi:10.1002/aoc.2931
17. Markert, C.; Bannwarth, W. *Helv. Chim. Acta* **2002,** *85,* 1877–1882. doi:10.1002/1522-2675(200207)85:7<1877::aid-hlca1877>3.0.co;2-5
18. Akiyama, Y.; Meng, X.; Fujita, S.; Chen, Y.-C.; Lu, N.; Cheng, H.; Zhao, F.; Arai, M. *J. Supercrit. Fluids* **2009,** *51,* 209–216. doi:10.1016/j.supflu.2009.08.006
19. Strappaveccia, G.; Luciani, L.; Bartollini, E.; Marrocchi, A.; Pizzo, F.; Vaccaro, L. *Green Chem.* **2015,** *17,* 1071–1076. doi:10.1039/c4gc01728e
20. Li, J.; Yang, S.; Wu, W.; Jiang, H. *Eur. J. Org. Chem.* **2018,** 1284–1306. doi:10.1002/ejoc.201701509
21. Lei, Z.; Chen, B.; Koo, Y.-M.; MacFarlane, D. R. *Chem. Rev.* **2017,** *117,* 6633–6635. doi:10.1021/acs.chemrev.7b00246
22. Bong Park, S.; Alper, H. *Chem. Commun.* **2004,** 1306–1307. doi:10.1039/b402477j
23. Błaszczyk, I.; Trzeciak, A. M.; Ziółkowski, J. J. *Catal. Lett.* **2009,** *133,* 262–266. doi:10.1007/s10562-009-0181-y
24. Kmentová, I.; Gotov, B.; Gajda, V.; Toma, T. *Monatsh. Chem.* **2003,** *134,* 545–549. doi:10.1007/s00706-002-0558-8
25. Fukuyama, T.; Shinmen, M.; Nishitani, S.; Sato, M.; Ryu, I. *Org. Lett.* **2002,** *4,* 1691–1694. doi:10.1021/ol0257732
26. Fukuyama, T.; Rahman, M. T.; Sumino, Y.; Ryu, I. *Synlett* **2012,** *23,* 2279–2283. doi:10.1055/s-0031-1290456
27. de Lima, P. G.; Antunes, O. A. C. *Tetrahedron Lett.* **2008,** *49,* 2506–2509. doi:10.1016/j.tetlet.2008.02.110
28. Ermolaev, V.; Miluykov, V.; Arkhipova, D.; Zvereva, E.; Sinyashin, O. *Phosphorus, Sulfur Silicon Relat. Elem.* **2013,** *188,* 168–170. doi:10.1080/10426507.2012.744013
29. Harjani, J. R.; Abraham, T. J.; Gomez, A. T.; Garcia, M. T.; Singer, R. D.; Scammells, P. J. *Green Chem.* **2010,** *12,* 650–655. doi:10.1039/b919394d
30. Prabhala, P.; Savanur, H. M.; Kalkhambkar, R. G.; Laali, K. K. *Eur. J. Org. Chem.* **2019,** 2061–2064. doi:10.1002/ejoc.201900093
31. Savanur, H. M.; Kalkhambkar, R. G.; Laali, K. K. *Eur. J. Org. Chem.* **2018,** 5285–5288. doi:10.1002/ejoc.201800804
32. Iranpoor, N.; Firouzabadi, H.; Ahmadi, Y. *Eur. J. Org. Chem.* **2012,** 305–311. doi:10.1002/ejoc.201100701
33. Reddy, A. S.; Laali, K. K. *Tetrahedron Lett.* **2015,** *56,* 4807–4810. doi:10.1016/j.tetlet.2015.06.067
34. Orha, L.; Tukacs, J. M.; Gyarmati, B.; Szilágyi, A.; Kollár, L.; Mika, L. T. *ACS Sustainable Chem. Eng.* **2018,** *6,* 5097–5104. doi:10.1021/acssuschemeng.7b04775
35. Chinchilla, R.; Nájera, C. *Chem. Soc. Rev.* **2011,** *40,* 5084–5121. doi:10.1039/c1cs15071e
36. Hallett, J. P.; Welton, T. *Chem. Rev.* **2011,** *111,* 3508–3576. doi:10.1021/cr1003248
37. McLachlan, F.; Mathews, C. J.; Smith, P. J.; Welton, T. *Organometallics* **2003,** *22,* 5350–5357. doi:10.1021/om034075y
38. Siemsen, P.; Livingston, R. C.; Diederich, F. *Angew. Chem., Int. Ed.* **2000,** *39,* 2632–2657. doi:10.1002/1521-3773(20000804)39:15<2632::aid-anie2632>3.0.co;2-f
39. Li, J.-H.; Liang, Y.; Zhang, X.-D. *Tetrahedron* **2005,** *61,* 1903–1907. doi:10.1016/j.tet.2004.12.026
40. Triethylamine. https://onlinelibrary.wiley.com/doi/pdf/10.1002/3527600418.mb12144e0013 (accessed Oct 1, 2019). doi:10.22233/20412495.1019.1
41. Liang, Y.; Xie, Y.-X.; Li, J.-H. *J. Org. Chem.* **2006,** *71,* 379–381. doi:10.1021/jo051882t

License and Terms

BEILSTEIN JOURNAL OF ORGANIC CHEMISTRY

A green, economical synthesis of β-ketonitriles and trifunctionalized building blocks from esters and lactones

Daniel P. Pienaar*, Kamogelo R. Butsi, Amanda L. Rousseau and Dean Brady

Letter

Open Access

Address:
Molecular Sciences Institute, School of Chemistry, University of the Witwatersrand, PO Wits 2050, Johannesburg, South Africa

Email:
Daniel P. Pienaar* - Daniel.Pienaar@wits.ac.za

* Corresponding author

Keywords:
acylation; β-ketonitrile; enolizable; trifunctionalized; sustainable

Beilstein J. Org. Chem. **2019,** *15,* 2930–2935.
doi:10.3762/bjoc.15.287

Received: 16 September 2019
Accepted: 22 November 2019
Published: 06 December 2019

This article is part of the thematic issue "Green chemistry II".

Guest Editor: L. Vaccaro

Abstract

The acylation of the acetonitrile anion with lactones and esters in ethereal solvents was successfully exploited using inexpensive KO*t*-Bu to obtain a variety of β-ketonitriles and trifunctionalized building blocks, including useful *O*-unprotected diols. It was discovered that lactones react to produce the corresponding derivatized cyclic hemiketals. Furthermore, the addition of a catalytic amount of isopropanol, or 18-crown-6, was necessary to facilitate the reaction and to reduce side-product formation under ambient conditions.

Introduction

β-Ketonitriles represent highly versatile intermediates for the synthesis of heteroaromatic compounds and a wide variety of pharmaceuticals. A recent review by Kiyokawa et al. summarizes the applications of these valuable compounds and the abundant methods that have been developed over recent decades to prepare them [1], most of which still involve environmentally unfriendly transition-metal-based reactions. Acylations of in situ-generated nitrile anions with esters to produce β-ketonitriles were first reported long ago, for example by using sodium methoxide [2], sodium ethoxide [3] or sodium amide [4,5]. The reaction was found to proceed more efficiently when using sodium amide as the base [5], although the inherent risks of employing explosive sodium amide in synthesis are well known [6] and amidine side-product formation was observed at times through reaction of the nucleophilic amide base with nitrile. Furthermore, clearly two equivalents of base (and nitrile) were necessary to drive the reactions to completion as the acylated product is more acidic than the nitrile starting material. More recently, ester or Weinreb amide reactions with acetonitrile using lithium bases at low temperature [7], or similarly NaH at high temperatures [8], have been reported as feasible alternatives with varied success and usually a lack of general applicability (e.g., enolizable esters and ketone products may react undesirably under these highly basic reaction

conditions). Furthermore, these methods constitute either expensive, less scalable procedures employing an excess of reagents, hazardous, flammable, or toxic reagents and high temperatures are required, which, in turn, may be detrimental to more highly functionalized starting materials. Nevertheless, this reaction under milder conditions is a valuable C–C bond-forming reaction for the preparation of β-substituted carboxylic acid derivatives, in general, from cheap commercially available esters, and as such merited further investigation.

We required a green, safe and scalable process for the facile production of *O*-unprotected hydroxylated β-hydroxynitrile **1** via trifunctionalized β-ketonitrile **2** by a direct, atom-economical ring opening of enolizable δ-valerolactone (**3**, Scheme 1). Although a two-step (or four-step, should hydroxy group *O*-protection prove to be necessary prior to acylation) protocol could, in theory, be envisaged to produce β-ketonitrile **2** from **3** by ring-opening esterification to afford hydroxy ester **4** followed by reaction with acetonitrile (CH_3CN), a multistep approach would be less economical in industry (Scheme 1).

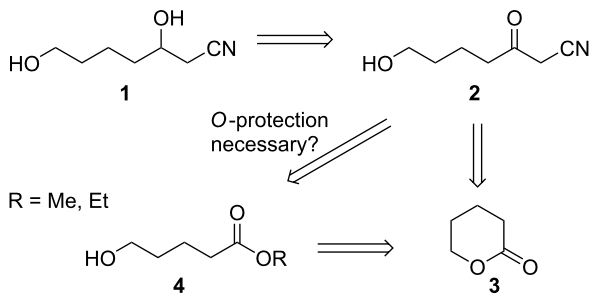

Scheme 1: Proposed retrosynthesis of the free diol **1**.

Results and Discussion

To date, the most economically appealing conditions from an environmentally friendly perspective entail relatively mild base-promoted (potassium *tert*-pentoxide or potassium *tert*-butoxide) acylation of substituted nitrile anions with esters under ambient conditions, as published by Ji et al. (2006) [9] and Kim et al. (2013) [10]. The large excess of ester and expensive base (potassium *tert*-pentoxide) required in the former method, in our opinion rendered it less economical and practical as a scalable option. Furthermore, when we applied Kim's (KO*t*-Bu) method to δ-valerolactone, we obtained a highly viscous oil made up of a mixture of inseparable compounds that were unidentifiable by crude ^{1}H NMR spectroscopy (see Supporting Information File 1). Similarly, using dry THF, 1 equiv CH_3CN and 1 equiv KO*t*-Bu at rt, we obtained within minutes a precipitated amorphous gum which, upon work-up (partitioning between EtOAc and water) and removal of the solvents in vacuo, afforded a complex mixture of undesirable products by ^{1}H NMR spectroscopy. However, to our delight, upon the addition of 20 mol % isopropanol (IPA) to the THF reaction mixture, we obtained a moderate amount of the desired product, albeit not as the open-chain β-ketonitrile **2**, but exclusively as the corresponding, cyclized hemiketal **5** (Scheme 2).

Furthermore, when using the green, sustainably produced solvent 2-methyltetrahydrofuran (2MeTHF) [11,12], in place of THF, we obtained a significantly higher yield of **5**. Remarkably,

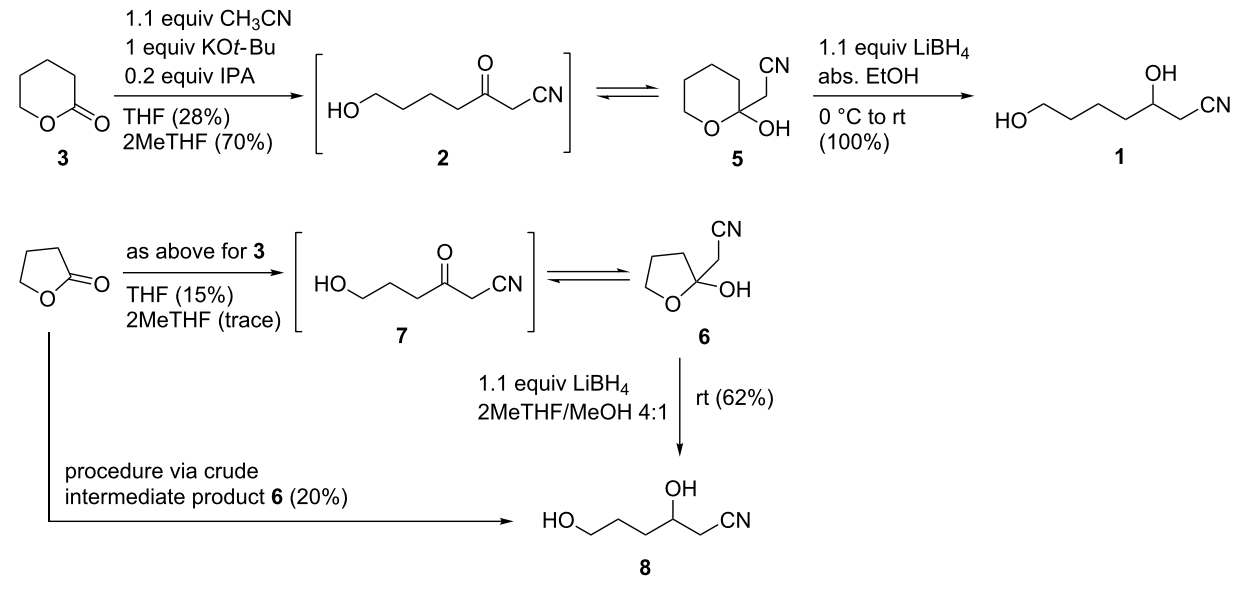

Scheme 2: Preparation of *O*-unprotected, trifunctionalized synthons from lactones.

a crude yield of 80% of the hemiketal was obtained from technical grade, solidified δ-valerolactone that had previously been stored at rt (a compound which is known to polymerize unavoidably upon storage, and the technical grade reagent contains up to 25% polymerized material). The crude product was shown to be almost pure by ^{1}H NMR and TLC. It can be seen in Supporting Information File 1 that the crude product obtained using 2MeTHF was significantly more enriched/purer in hemiketal **5** than that obtained using THF as the solvent. Pure product was readily obtained in 70% yield after purification by column chromatography. We reasoned that the lower aqueous miscibility of 2MeTHF, as compared to THF, resulted in a more efficient product extraction procedure, which further contributed to the increased yield of **5**. Varying the amount of IPA resulted in lower yields and more complex product mixtures. Substitution of IPA with *tert*-butanol or ethanol resulted in significantly lower product yields and a more complex product profile, as observed by crude product ^{1}H NMR spectroscopy.

The mechanism by which IPA facilitates the reaction towards the formation of the cyclic hemiketal and indeed, the desired β-ketonitrile scaffold, has not been conclusively determined in this work. It is well known that strong-base deprotonation of acetonitrile leads to the formation of a nitrile-stabilized carbanion, in resonance with a ketene iminate anion. It has been calculated that the latter CN double-bonded species is relatively unstable compared to the CN triple-bonded carbanion species, which has the negative charge localized on the α-carbon atom [13]. This carbanion is therefore an excellent nucleophile and is usually generated from nitriles using metal amides or other strong bases [14,15]. Under our reaction conditions at rt, we propose that the presence of a catalytic amount of IPA increases the dielectric constant of the solvent as a whole, thereby increasing the solubility of both the KO*t*-Bu base and the acetonitrile derived KCH_2CN salt. This effectively accelerates the generation of the latter and as such, its reaction with the lactone (or ester) carbonyl carbon. By increasing the solubility of the conjugate base salt, the pK_a of acetonitrile in the ethereal solvent is effectively lowered by adding a small amount of polar, protic IPA and this facilitates acetonitrile deprotonation. Alternatively, the addition of a crown ether is also known to enhance nucleophilic substitution reaction rates, but in this case through the suppression of ion-pairing [16]. We also investigated this option for the first time in the synthesis of β-ketonitriles from esters, as described later (see Table 1). Finally, it is probable that the presence of protic IPA suppresses enolization as the reaction progresses, by quenching KO*t*-Bu generated enolates and similarly, reactive alkoxide anions. This reduces the occurrence of undesirable side-reactions, e.g., intermolecular aldol reaction, lactone/ketonitrile product dimerization and ring-opening polymerization.

The application of this method to produce the analogous hemiketal **6** from γ-butyrolactone was not as efficient. Although the desired product **6** could indeed be isolated in 15% yield from γ-butyrolactone when the same reaction conditions were applied in THF, the use of 2MeTHF as solvent resulted in a complex mixture with only traces of the desired product, as revealed by crude product NMR spectroscopy. It is thought that the semivolatility of product **6** may have also resulted in lower yields compared to **5**.

It is well known that cyclic compounds often react differently dependent on their ring size, with 5-membered rings being generally more constrained and therefore more likely to ring-open than 6-membered rings. For example, in sugars, hemiacetal pyranoses (due to reduced bond angle strain) are energetically much more favored in solution compared to the corresponding 5-membered furanoses [17]. Significantly, ^{1}H (500 MHz) and ^{13}C NMR (126 MHz) of the purified product **6** (pure by TLC) indicated traces of what appears to be the uncyclized β-ketonitrile **7** (see Supporting Information File 1). This suggests that, in solution, the keto–hemiketal equilibrium for the butyrolactone product does not favor completely hemiketal **6**, as was observed for the 6-membered cycle **5**. The authors therefore propose that formation of the 6-membered hemiketal ring is more energetically favored under these reaction conditions, compared to the analogous 5-membered system. This effectively shields both the enolizable ketone and the sterically unhindered primary hydroxy functional groups in the valerolactone-derived product in situ, which reduces the occurrence of side-reactions and side-products, e.g., aldol reactions and polymerization, and results in a higher yield of the desired product compared to that obtained from γ-butyrolactone.

With compounds **5** and **6** in hand, simple and mild reduction protocols at rt satisfyingly afforded the desired diols **1** and **8**, thereby indicating that the hemiketals are still fully reducible under standard ketone reduction conditions. Purification of **6** afforded only a 10% overall yield of the diol **8**, but the direct conversion of crude intermediate product **6** resulted in a doubling of the overall yield of the diol from lactone to 20% (Scheme 2).

Due to the interest in the potential preparation of pyrimidines from β-ketonitriles and guanidine [18], we wanted to test the general applicability of this method for access to a variety of alkyl and aryl-substituted β-ketonitriles (as summarized in Table 1). When we applied this methodology to ethyl cyclopropane carboxylate in THF, we were delighted to obtain the desired (relatively volatile) product **9** in modest yield, because in our hands previous attempts to prepare **9** in sufficient

Table 1: Preparation of a variety of β-ketonitriles.

Entry	Product	R^1	R^2	CH_3CN (equiv)	KO*t*-Bu (equiv)	Additive (equiv)	Solvent (time at rt)	Yield (%)
1	**9**		Et	2	2	IPA (0.2)	2MeTHF (2 h)	48[a]
2	**10**	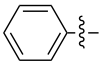	Me	2	2	IPA (0.2)	2MeTHF (2 h)	47
3	**11**	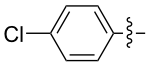	Me	2	2	IPA (0.2)	2MeTHF (1 h)	53
4	**12**		Me	2	2	IPA (0.2)	2MeTHF (2 h)	76[a]
5	**13**		Me	2	2	IPA (0.2)	2MeTHF (2 h)	47
6	**14**		Me	2	2	IPA (0.2)	2MeTHF (2 h)	43
7	**15**	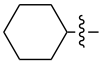	Me	2	2	IPA (0.2)	2MeTHF (2 h)	68
8	**16**		Me	2	2	IPA (0.2)	2MeTHF (2 h)	29[b]
9	**17**	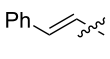	Et	1.5	1.1	IPA (0.2)	2MeTHF (30 min)	64
10	**18**		Me	1.2	1.2	IPA (0.1)	MTBE (2 h)	38
11	**18**		Me	1.2	1.2	18-crown-6 (0.1)	MTBE (30 min)	58
12	**18**		Me	1.2	1.2	18-crown-6 (0.1)	2MeTHF (30 min)	67

[a]Semivolatile products of which yield losses may have occurred upon solvent removal in vacuo. [b]A significant amount of the corresponding carboxylic acid was isolated as side-product. This suggests that base-catalyzed ester alcoholysis may be a competing side-reaction.

amounts by following a literature procedure using NaH (in refluxing THF) [8] had failed. The reaction, again with 20 mol % IPA added and under an inert N_2 atmosphere, afforded a similar product yield using 2MeTHF as solvent. Increasing the reaction time to 24 h did not increase the product yield, and residual starting material was observed throughout the reaction course, by TLC monitoring. Due to the persistent presence of unreacted starting materials in all examples given, it was decided to dose with second equivalents of base (KO*t*-Bu) and CH_3CN after 1 h of reaction, as seen in most examples in Table 1. Disappointingly, we were unable to further significantly increase product yields, for example for the phenyl-substituted fluoxetine (Prozac®) intermediate **10** [19], which remained at ca. 50%.

Other methods were explored in an attempt to increase product yields. Although a putative radical mechanism that may be promoted in the presence of oxygen had previously been postulated by Kim et al. [10], we did not obtain increased product yields when carrying out the reaction in air. Furthermore, heating the reaction mixtures above rt when using NaH as a base in refluxing THF was clearly detrimental to product yield according to our previous observations and was not attempted.

Significantly, no side-products were observed in the organic extract after work-up, and a series of β-ketonitriles (some of which are semivolatile compounds) was successfully prepared and isolated under standard, ambient conditions in modest yields. The best yields were obtained for the 2-propyl **12** (76%) and cyclohexyl **15** (68%) analogues. We were pleased to obtain

the highly versatile and synthetically useful cinnamoylacetonitrile **17** [20] from renewable ethyl cinnamate in 64% yield, as this yield was comparable to more expensive and hazardous lithiation protocols [7].

Finally, we attempted method optimization for the production of a commercially important pharmaceutical intermediate, thiophene-substituted β-ketonitrile precursor **18** of the antidepressant drug duloxetine (Cymbalta®) [21,22]. It was interesting to note that, although 38% of the thiophene product could be obtained using methyl *tert*-butyl ether (MTBE) with 0.1 equiv IPA as co-solvent/additive, a significantly higher yield of **18** was obtained when we used 10 mol % 18-crown-6 ether instead of IPA in a similarly catalytic amount. The yield was further improved to 67% using 2MeTHF as the solvent. It should be noted that the use of the crown ether resulted in recovery complications for some of the other compounds (e.g., when this methodology was applied to δ-valerolactone and γ-butyrolactone) and may therefore not be universally beneficial.

Conclusion

In conclusion, mild, environmentally friendly procedures were developed for the preparation of trifunctionalized building blocks (hydroxylated β-ketonitriles) and valuable β-ketonitriles (including enolizable compounds) in modest to good yields from lactones and esters. We are currently investigating novel applications of diols **1** and **8**, as well as the application of this methodology for the synthesis of glycomimetic products from sugar lactones, and for the synthesis of various pyrimidines.

Supporting Information

Supporting Information File 1

Experimental procedures, compound characterization data and NMR spectra.
[https://www.beilstein-journals.org/bjoc/content/supplementary/1860-5397-15-287-S1.pdf]

Acknowledgements

KRB thanks the National Research Foundation (South Africa) and the SABINA network for funding. DP and DB gratefully acknowledge the Department of Science and Technology Biocatalysis Initiative (Grant 0175/2013) and CHIETA (South Africa) for funding. The authors wish to thank Thapelo Mbhele, Tracy Lau and Vaughn Silversten for technical assistance.

ORCID® iDs

Daniel P. Pienaar - https://orcid.org/0000-0003-0609-1989
Kamogelo R. Butsi - https://orcid.org/0000-0003-4734-2465
Amanda L. Rousseau - https://orcid.org/0000-0002-9339-1797

References

1. Kiyokawa, K.; Nagata, T.; Minakata, S. *Synthesis* **2018,** *50,* 485–498. doi:10.1055/s-0036-1589128
2. Long, R. S. *J. Am. Chem. Soc.* **1947,** *69,* 990–995. doi:10.1021/ja01197a004
3. Dorsch, J. B.; McElvain, S. M. *J. Am. Chem. Soc.* **1932,** *54,* 2960–2964. doi:10.1021/ja01346a047
4. Levine, R.; Hauser, C. R. *J. Am. Chem. Soc.* **1946,** *68,* 760–761. doi:10.1021/ja01209a016
5. Eby, C. J.; Hauser, C. R. *J. Am. Chem. Soc.* **1957,** *79,* 723–725. doi:10.1021/ja01560a060
6. Urben, P. G.; Pitt, M. J., Eds. *Bretherick's Handbook of Reactive Chemical Hazards,* 7th ed.; Academic Press: Oxford, United Kingdom, 2007; pp 1686–1688.
7. Mamuye, A. D.; Castoldi, L.; Azzena, U.; Holzer, W.; Pace, V. *Org. Biomol. Chem.* **2015,** *13,* 1969–1973. doi:10.1039/c4ob02398f
8. Miyamoto, Y.; Banno, Y.; Yamashita, T.; Fujimoto, T.; Oi, S.; Moritoh, Y.; Asakawa, T.; Kataoka, O.; Yashiro, H.; Takeuchi, K.; Suzuki, N.; Ikedo, K.; Kosaka, T.; Tsubotani, S.; Tani, A.; Sasaki, M.; Funami, M.; Amano, M.; Yamamoto, Y.; Aertgeerts, K.; Yano, J.; Maezaki, H. *J. Med. Chem.* **2011,** *54,* 831–850. doi:10.1021/jm101236h
9. Ji, Y.; Trenkle, W. C.; Vowles, J. V. *Org. Lett.* **2006,** *8,* 1161–1163. doi:10.1021/ol053164z
10. Kim, B. R.; Lee, H.-G.; Kang, S.-B.; Jung, K.-J.; Sung, G. H.; Kim, J.-J.; Lee, S.-G.; Yoon, Y.-J. *Tetrahedron* **2013,** *69,* 10331–10336. doi:10.1016/j.tet.2013.10.007
11. Sheldon, R. A. *Green Chem.* **2017,** *19,* 18–43. doi:10.1039/c6gc02157c
12. Clarke, C. J.; Tu, W.-C.; Levers, O.; Bröhl, A.; Hallett, J. P. *Chem. Rev.* **2018,** *118,* 747–800. doi:10.1021/acs.chemrev.7b00571
13. Richard, J. P.; Williams, G.; Gao, J. *J. Am. Chem. Soc.* **1999,** *121,* 715–726. doi:10.1021/ja982692l
14. Fleming, F. F.; Zhang, Z.; Liu, W.; Knochel, P. *J. Org. Chem.* **2005,** *70,* 2200–2205. doi:10.1021/jo047877r
15. Fleming, F. F.; Shook, B. C. *Tetrahedron* **2002,** *58,* 1–23. doi:10.1016/s0040-4020(01)01134-6
16. Cook, F. L.; Bowers, C. W.; Liotta, C. L. *J. Org. Chem.* **1974,** *39,* 3416–3418. doi:10.1021/jo00937a026
17. Collins, P.; Ferrier, R. *Monosaccharides – Their Chemistry and Their Roles in Natural Products;* John Wiley & Sons Ltd.: Chichester, UK, 1995; 11 and 43.
18. Liu, B.; Liu, M.; Xin, Z.; Zhao, H.; Serby, M. D.; Kosogof, C.; Nelson, L. T. J.; Szczepankiewicz, B. G.; Kaszubska, W.; Schaefer, V. G.; Falls, H. D.; Lin, C. W.; Collins, C. A.; Sham, H. L.; Liu, G. *Bioorg. Med. Chem. Lett.* **2006,** *16,* 1864–1868. doi:10.1016/j.bmcl.2006.01.012
See for an example.
19. Hammond, R. J.; Poston, B. W.; Ghiviriga, I.; Feske, B. D. *Tetrahedron Lett.* **2007,** *48,* 1217–1219. doi:10.1016/j.tetlet.2006.12.057
20. Swellem, R. H.; Allam, Y. A.; Nawwar, G. A. M. *Z. Naturforsch., B: J. Chem. Sci.* **1999,** *54,* 1197–1201. doi:10.1515/znb-1999-0917
21. Rimoldi, I.; Facchetti, G.; Nava, D.; Contente, M. L.; Gandolfi, R. *Tetrahedron: Asymmetry* **2016,** *27,* 389–396. doi:10.1016/j.tetasy.2016.04.002
22. Wang, G.; Liu, X.; Zhao, G. *Tetrahedron: Asymmetry* **2005,** *16,* 1873–1879. doi:10.1016/j.tetasy.2005.04.002

BEILSTEIN JOURNAL OF ORGANIC CHEMISTRY

Oligomeric ricinoleic acid preparation promoted by an efficient and recoverable Brønsted acidic ionic liquid

Fei You[1], Xing He[1], Song Gao[1], Hong-Ru Li[*1,2] and Liang-Nian He[*1]

Full Research Paper

Open Access

Address:
[1]State Key Laboratory and Institute of Elemento-Organic Chemistry, College of Chemistry, Nankai University, Tianjin 300071, China and [2]College of Pharmacy, Nankai University, Tianjin 300353, China

Email:
Hong-Ru Li[*] - lihongru@nankai.edu.cn; Liang-Nian He[*] - heln@nankai.edu.cn

* Corresponding author

Keywords:
bio-lubricant; ionic liquids; oligomeric ricinoleic acid; ricinoleic acid; sustainable catalysis

Beilstein J. Org. Chem. **2020,** *16,* 351–361.
doi:10.3762/bjoc.16.34

Received: 07 January 2020
Accepted: 24 February 2020
Published: 10 March 2020

This article is part of the thematic issue "Green chemistry II".

Guest Editor: L. Vaccaro

Abstract

Raw material from biomass and green preparation processes are the two key features for the development of green products. As a bio-lubricant in metalworking fluids, estolides of ricinoleic acid are considered as the promising substitute to mineral oil with a favorable viscosity and viscosity index. Thus, an efficient and sustainable synthesis protocol is urgently needed to make the product really green. In this work, an environment-friendly Brønsted acidic ionic liquid (IL) 1-butanesulfonic acid diazabicyclo[5.4.0]undec-7-ene dihydrogen phosphate ([HSO_3-BDBU]H_2PO_4) was developed as the efficient catalyst for the production of oligomeric ricinoleic acid from ricinoleic acid under solvent-free conditions. The reaction parameters containing reaction temperature, vacuum degree, amount of catalyst and reaction time were optimized and it was found that the reaction under the conditions of 190 °C and 50 kPa with 15 wt % of the [HSO_3-BDBU]H_2PO_4 related to ricinoleic acid can afford a qualified product with an acid value of 51 mg KOH/g (which corresponds to the oligomerization degree of 4) after 6 h. Furthermore, the acid value of the product can be adjusted by regulating the reaction time, implying this protocol can serve as a versatile method to prepare the products with different oligomerization degree and different applications. The other merit of this protocol is the facile product separation by stratification and decantation ascribed to the immiscibility of the product and catalyst at room temperature. It is also worth mentioning that the IL catalyst can be used at least for five cycles with high catalytic activity. As a result, the protocol based on the IL catalyst, i.e. [HSO_3-BDBU]H_2PO_4 shows great potential in industrial production of oligomeric ricinoleic acid from ricinoleic acid.

Introduction

In recent years, the biomass has attracted much attention due to its abundance, renewability and potential of conversion to useful chemicals. It can't be denied that the diverse transformation and utilization of biomass provides an alternative avenue to liberate us from the reliance on petroleum resource [1]. Nowadays, fuels, fine chemicals and functional molecules/materials

can be derived from biomass such as lignocellulose and plant oils [2,3], wherein the plant oils play an important role in the polymer industry [4]. Especially, the characteristics of non-volatility and biodegradability make plant oil the most promising material to develop functional polymeric materials with superior performance [5-7].

Castor oil is one kind of nonedible oil and can be extracted from the seeds of the castor bean plant. Globally, around one million tons of castor seeds are produced every year and the leading producing areas are India, China, and Brazil [8]. The castor oil has long been used as purgative or laxative to counter constipation and nowadays it is used commercially as a highly renewable resource for the chemical industry [9,10]. Numerous platform chemicals such as ricinoleic acid and undecylenic acid can be prepared from castor oil, wherein ricinoleic acid is a crucial platform chemical for derivation of useful chemicals [11-14].

Ricinoleic acid can be easily prepared by hydrolysis of castor oil [15]. The presence of both hydroxy and carboxy groups in the molecule of ricinoleic acid enables it to undergo intermolecular esterification, thus resulting in the formation of the oligomeric ricinoleic acid. The oligomeric ricinoleic acid with different acid value (which is an indirect index for oligomerization degree) has different applications. For example, as an additive in shampoos, the oligomeric ricinoleic acid with an acid value of 60–90 mg KOH/g is required while for cosmetic formulations, an acid value of 20–40 mg KOH/g is suitable [16-19]. The oligomeric ricinoleic acid can also be used as lubricant for metal cutting oils due to its appropriate viscosity, good adsorptivity and film formation ability on metal surfaces. Furthermore, the biodegradability of these estolides in the environment makes them attractive as green products.

In parallel with the increasing demand for high-quality oligomeric ricinoleic acid, the synthetic method has kept on developing. Traditionally, *p*-toluenesulfonic or sulfuric acid are used as catalysts for the preparation of oligomeric ricinoleic acid. However, the equipment corrosion and the tedious workup process are inevitable, which reduce the process efficiency. Moreover, the byproduct formation and the resulting product coloration reduce the product quality. To address the above issues, the enzyme catalysis is proposed accordingly. Nevertheless, the high cost, low efficiency and operational unstability of enzymatic reaction make it difficult to industrial production [20-25]. Very recently, tin(II) 2-ethylhexanoate has been reported as an efficient catalyst for the synthesis of oligomeric ricinoleic acid [19]. Unfortunately, the separation of oligomeric ricinoleic acid and the recovery of the catalyst still encounters difficulties. Therefore, it is urgently desirable to develop an efficient, green and recyclable catalyst and design simple operating procedures for the preparation of estolides oligomeric ricinoleic acid.

Ionic liquids (ILs) have been proved to be efficient catalysts in various organic syntheses due to the designable structure, tunable properties as well as superior solubility [26,27]. Furthermore, the thermal stability and negligible vapor pressure of ILs can facilitate the product separation after reaction. To the best of our knowledge, the IL 1-butylsulfonic-3-methylimidazolium tosylate ([HSO_3-BMim]TS) can be used as catalyst in the synthesis of oligomeric ricinoleic acid, the estolide with an acid value of 48 ± 2.5 mg KOH/g was obtained after 14 h [28]. Nevertheless, the product separation and catalyst reusability have not yet been investigated until now.

Based on the fact that Brønsted acids present excellent catalytic activity for this intermolecular esterification reaction and Brønsted acidic ionic liquids have been successfully used as catalyst in organic syntheses [29-31], we designed a series of Brønsted acidic ionic liquids and applied them as catalysts for the preparation of oligomeric ricinoleic acid from ricinoleic acid to develop a facile synthesis and separation protocol. Gratifyingly, the IL [HSO_3-BDBU]H_2PO_4 showed to be efficient both in synthesis and product separation [32]. Through process parameter selection, it was found that a product with different acid value can be obtained by changing the reaction time at 190 °C and 50 kPa with 15 wt % IL as catalyst. The viscosity characterization showed the product derived from 6 h of reaction, whose acid value is 51 mg KOH/g and the corresponding average oligomerization degree is 4, meets the requirement of lubricant additive index. Notably, after reaction, the product and IL catalyst can be easily separated by phase separation and the recovered catalyst can be used at least for five cycles without obvious deactivation, which shows tremendous advantage for large-scale industrial application. The reaction and separation procedures are depicted in Scheme 1.

Results and Discussion

Considering protic acids have catalytic effects on the esterification reaction, we designed and synthesized a series of ILs containing protic anions as shown in Scheme 2. With the synthesized ILs as catalyst, the ricinoleic acid esterification was performed and the catalytic activity of these functional ILs was evaluated with the acid value of the product as it is a convenient index to monitor the degree of oligomerization by reflecting the concentration of carboxy groups in the system, which has been cross verified by HPLC method [19,28].

The results showed that the protic anion is necessary for the intermolecular esterification as no catalytic activity can be ob-

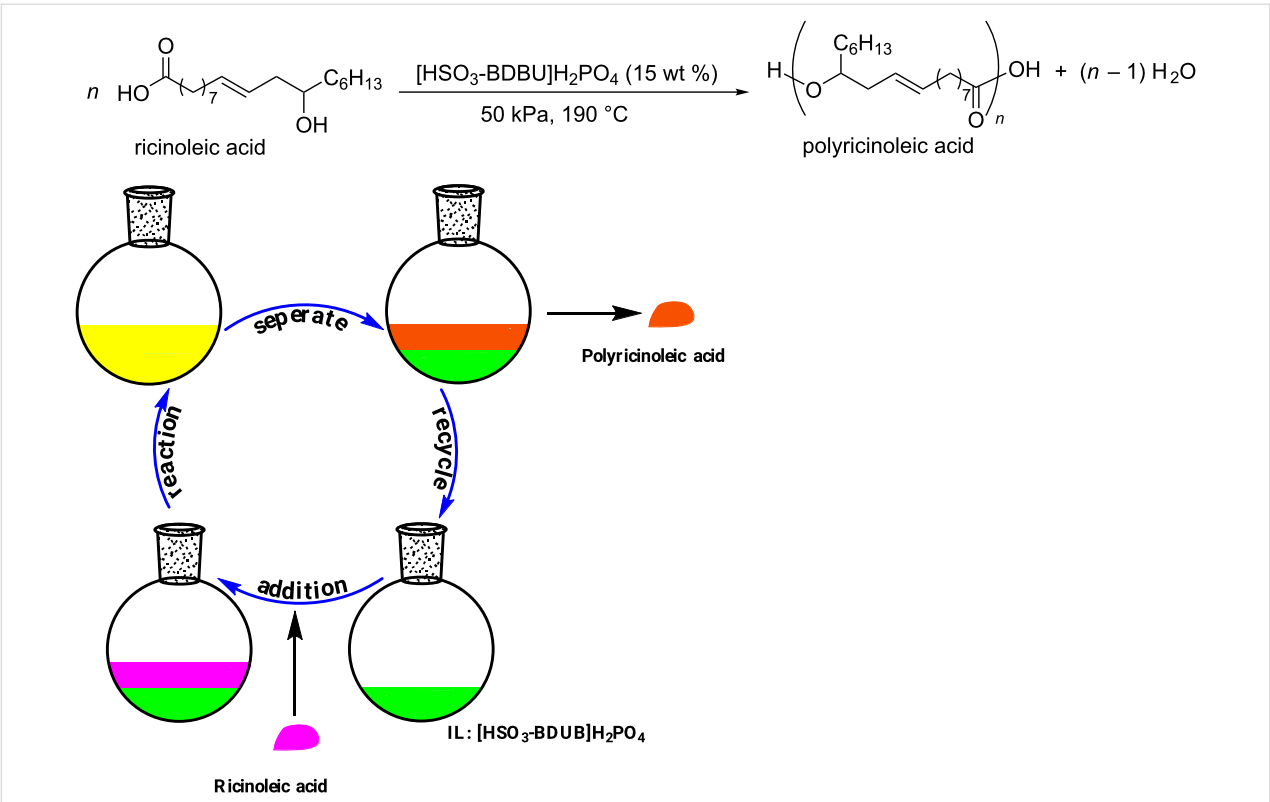

Scheme 1: [HSO_3-BDBU]H_2PO_4-promoted oligomerization and separation.

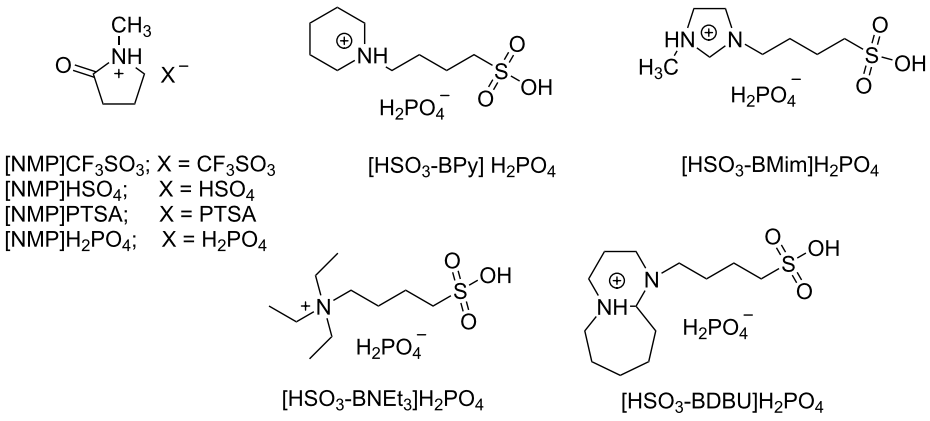

Scheme 2: Structures of ILs used in this work.

served for the IL with aprotic anion (Table 1, entries 1 and 2). For the ILs containing protic anions, the ILs containing polyprotic anions are more conducive to esterification (Table 1, entries 1–4 vs 5), which may originate from its higher proton concentration in the reaction system. With $H_2PO_4^-$ as anion, the ILs containing different cations were then synthesized and their catalytic activity on the esterification reaction was investigated. The results (Table 1, entries 5–9) revealed that the cation also affected the catalytic activity of the IL. Taking the decrease of acid value as catalytic activity index, the ionic liquid 1-butanesulfonic acid triethylamine dihydrogen phosphate ([HSO_3-$BNEt_3$]H_2PO_4) performed best among the tested ionic liquids in this study (Table 1, entry 8). However, the IL [HSO_3-BDBU]H_2PO_4 showed a much more attractive feature in product separation as stratification of product and catalyst was observed in the flask within a few minutes after reaction (Table 1, entry 9). Therefore, the IL [HSO_3-BDBU]H_2PO_4 not only acts as an efficient catalyst but also provides a facile protocol for

Table 1: Screening of ILs in the esterification of ricinoleic acid[a].

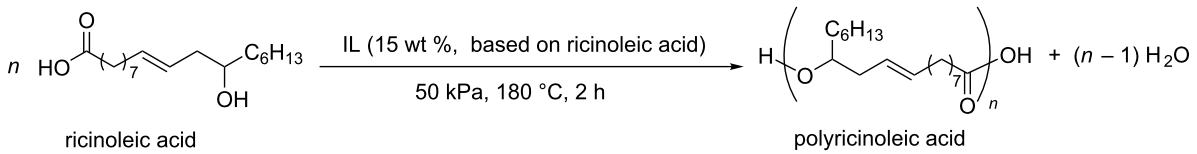

ricinoleic acid — polyricinoleic acid

Entry	IL	Acid value (mg KOH/g)
1	–	153
2	$[NMP]CF_3SO_3$	152
3	$[NMP]HSO_4$	83
4	[NMP]PTSA	90
5	$[NMP]H_2PO_4$	68
6	$[HSO_3\text{-BPy}]\ H_2PO_4$	63
7	$[HSO_3\text{-BMim}]\ H_2PO_4$	53
8	$[HSO_3\text{-BNEt}_3]H_2PO_4$	51
9	$[HSO_3\text{-BDBU}]H_2PO_4$	92

[a]Reactions were performed with ricinoleic acid (10 g, 30 mmol) and IL (15 wt %).

product and catalyst separation and thus avoids the workup procedure. In this context, $[HSO_3\text{-BDBU}]H_2PO_4$ was selected as the suitable catalyst for further investigations.

Having selected the IL $[HSO_3\text{-BDBU}]H_2PO_4$ as catalyst, the process optimization was performed to further promote the intermolecular dehydration esterification. The reaction temperature, catalyst loading, and vacuum degree on the reaction outcome were in detail investigated and the acid value of the product was used to evaluate the reaction results (Table 2). It was easily found that a higher temperature was favorable for the formation of oligomeric ricinoleic acid (Table 2, entries 1–5).

Table 2: Optimization of the key reaction parameters[a].

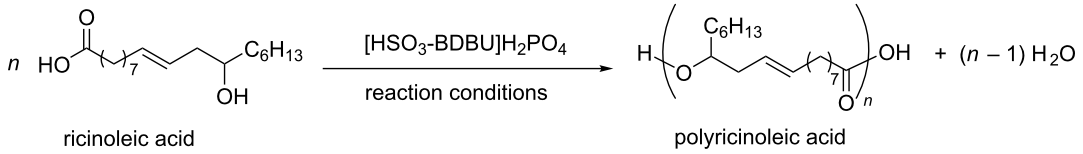

ricinoleic acid — polyricinoleic acid

Entry[b]	IL amount[c] (wt %)	Temp. (°C)	Vacuum degree (kPa)	Acid value (mg KOH/g)
1	10	160	50	123
2	10	170	50	106
3	10	180	50	92
4	10	190	50	88
5	10	200	50	86
6	0	190	50	148
7	5	190	50	117
8	15	190	50	73
9	20	190	50	69
10	15	190	0	101
11	15	190	10	63
12	15	190	30	52
13	15	190	50	44
14	15	190	70	43

[a]Standard reaction conditions: ricinoleic acid (10 g, 30 mmol) and different amount of IL at a variety of temperature and vacuum degree; [b]reaction time, 2 h (entries 1–9), 8 h (entries 10–14); [c]based on ricinoleic acid.

When the temperature was 190 °C, the acid value dropped to 88 mg KOH/g in 2 h. Further increasing the reaction temperature cannot lead to a significant drop of acid value. Thus, 190 °C was selected as the suitable reaction temperature. With the optimal reaction temperature, the amount of catalyst was studied at 190 °C and a vacuum degree of 50 kPa (Table 2, entries 6–9). As expected, the introduction of [HSO_3-BDBU]H_2PO_4 can improve the intramolecular esterification greatly compared with the scenario without catalyst and the catalyst loading has a positive effect on the oligomerization degree. When the amount of [HSO_3-BDBU]H_2PO_4 exceeded 15 wt % relative to ricinoleic acid, the catalytic efficiency was almost unchanged. Therefore, the optimum amount of catalyst was determined to be 15 wt % in the following investigation.

The vacuum degree is another factor to affect the intermolecular esterification as different vacuum degree can result in a different water removal rate, which may lead to a different equilibrium toward estolides product. Five different levels of vacuum degrees were applied to the reaction system, the results showed the oligomerization degree increased with increasing vacuum degree (Table 2, entries 10–14). A stable acid value was approached when the vacuum degree was higher than 50 kPa. Consequently, 50 kPa was select as a suitable vacuum degree.

According to the above results, the suitable conditions for the esterification of ricinoleic acid were set at 190 °C under a vacuum degree of 50 kPa and with 15 wt % [HSO_3-BDBU]H_2PO_4 as catalyst. Under the selected conditions, the acid value versus reaction time was inspected by sampling every 2 h (Table 3, entries 2–10). Simultaneously, the ^{1}H NMR spectra of the samples in $CDCl_3$ were also examined. In the ^{1}H NMR study, a peak found at 3.62 ppm gradually disappeared and a new peak at 4.88 ppm appeared (Figure 1). This is associated with the changes of the chemical environment for the C_{12}-H bond. That is, in ricinoleic acid (l_1, Figure 1), the C_{12} is attached to the hydroxy group while in the corresponding ester product ($l_{2–10}$, Figure 1), C_{12} is linked to the ester bond, thereby resulting in a change in the chemical shift of H connected with C_{12}. As the chemical shift of H in methyl at 0.87 ppm does not change before and after the reaction, it is used as reference and the peak integral ratio of C_{12}-H (A_n) to methyl-H (A_m) in the ^{1}H NMR spectra is used to determine the oligomerization degree. Theoretically, oligomeric ricinoleic acids with different oligomerization degree have their characteristic A_n/A_m values as listed in Table 3. For a specific sample, both the peaks for C_{12}-H and for methyl-H were integrated and the ratio of A_n/A_m was calculated. Then the resulting value was compared with the theoretical ones to determine the oligomerization degree of the product. It should be noted that this calculation is based on the assumption that the oligomerization degree of the product is monodisperse. Actually, the obtained oligomerization degree is the average oligomerization degree. By adopting the index A_n/A_m, the relationship of acid value and oligomerization degree can be constructed. According to the ^{1}H NMR results, the value A_n/A_m increased as the reaction proceeded (Table 3, entries 2–10 vs entry 1), which means that the average oligomerization degree of oligomeric ricinoleic acid can be adjusted by changing the reaction time.

For oligomeric ricinoleic acid, its physicochemical properties depend on the oligomerization degree. In order to be used as lubriant in metal-working fluid, the viscosity and the viscosity index of oligomeric ricinoleic acid should fall into the acceptable scope according to Hostagliss L4 oil soluble lubricant additive product index. To determine the suitable reaction time and obtain the qualified product, the viscosity and viscosity index of samples derived from 4 h, 6 h and 8 h of reaction (i.e. NK-A, NK-B and NK-C) were further measured and the results are compared with the commercial product Hostagliss L4 (Table 4).

Table 3: Acid value and the average oligomerization degree of oligomeric ricinoleic acid versus reaction time[a].

Entry	Reaction time (h)	Acid value (mg KOH/g)	Experimental A_n/A_m	Theoretical A_n/A_m	Average oligomerization degree
1	0	162	–	–	–
2	2	73	0.1682	0.1670	2
3	4	60	0.2219	0.2220	3
4	6	51	0.2530	0.2500	4
5	8	44	0.2680	0.2670	5
6	10	38	0.2781	0.2780	6
7	12	32	0.2861	0.2857	7
8	14	26	0.2915	0.2917	8
9	16	21	0.2963	0.2963	9
10	18	17	0.2999	0.3000	10

[a]The ricinoleic acid with an acid value of 162 mg KOH/g was used as raw material and interval sampling was performed every 2 h.

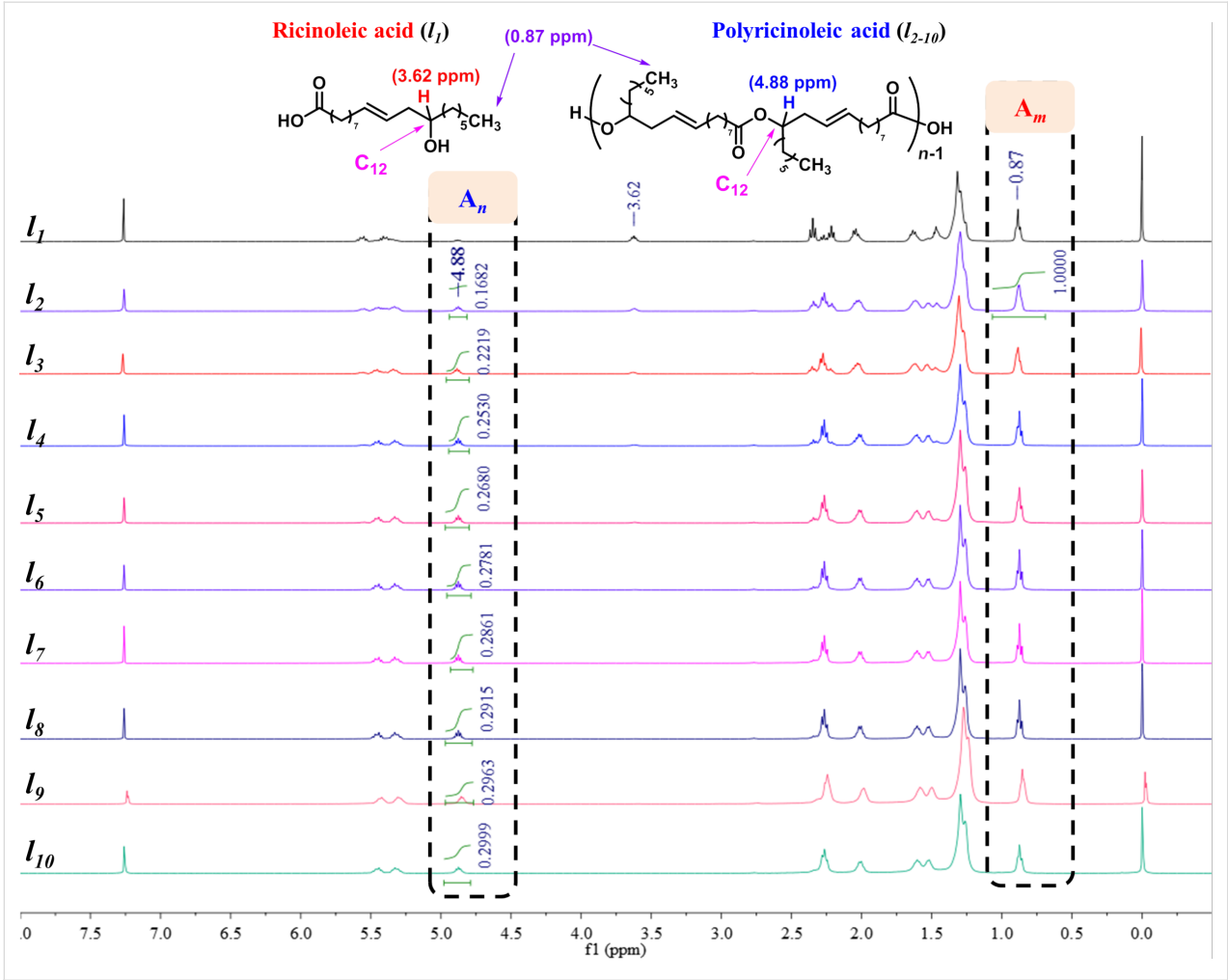

Figure 1: Monitoring oligomerization process by ^{1}H NMR (400 MHz, $CDCl_3$).

Table 4: Physicochemical properties of oligomeric ricinoleic acid compared to Hostagliss L4.

Entry	Sample	Acid value (mg KOH/g)	Viscosity (mm^2/s)		Viscosity index
			40 °C	100 °C	
1	Hostagliss L4	52	400	45	169
2	NK-A	60	373	39	154
3	NK-B	51	408	46	171
4	NK-C	44	514	53	167

As the results listed, NK-B meets the specifications of lubricant, which indicated that 6 h of reaction under the catalysis of $[HSO_3\text{-BDBU}]H_2PO_4$ can afford the standard-compliant bio-lubricant oligomeric ricinoleic acid.

Reusability of $[HSO_3\text{-BDBU}]H_2PO_4$

As the IL catalyst $[HSO_3\text{-BDBU}]H_2PO_4$ is immiscible with the product at room temperature, stratification occurs after reaction, thus renders an easy catalyst recyclability and product separation. After decanting the upper product and washing the remaining IL with a small amount of dichloromethane, the weight of $[HSO_3\text{-BDBU}]H_2PO_4$ was examined and then the fresh ricinoleic acid was added for the next cycle synthesis of oligomeric ricinoleic acid. The IL catalyst was used in five cycles of reaction and the resulting acid value of the product in each cycle was presented in Figure 2 along with the weight of

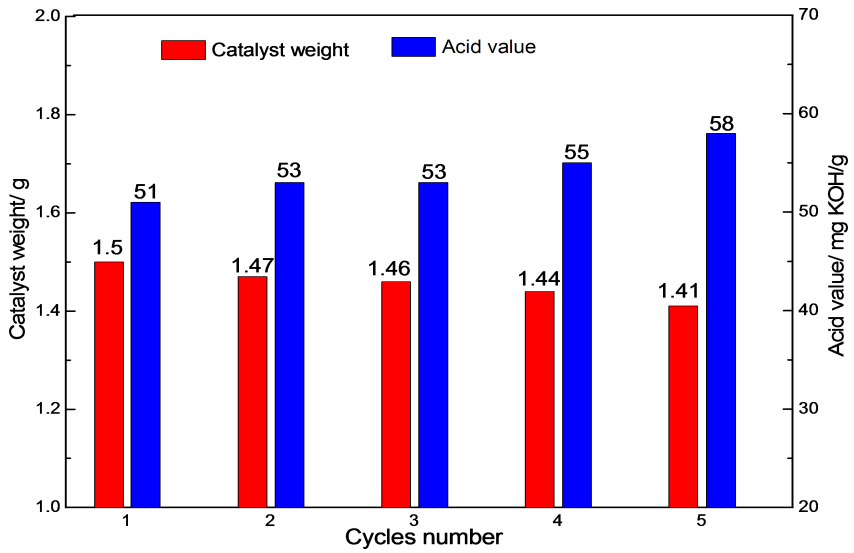

Figure 2: Reusability of the IL catalyst. Reaction conditions: 10 g (30 mmol) ricinoleic acid, 190 °C, 6 h, 50 kPa.

catalyst. It can be seen that $[HSO_3\text{-BDBU}]H_2PO_4$ can be utilized repeatedly for at least five times and only a slight decrease in catalytic activity was observed, which may be due to the weight loss of the recovered catalyst. To check the stability of the $[HSO_3\text{-BDBU}]H_2PO_4$ during reusability, the ^{1}H NMR of $[HSO_3\text{-BDBU}]H_2PO_4$ was examined after five cycles of reaction and the results were presented in Figure 3. It can be seen that the IL catalyst was stable during the reaction as the spectrum remained basically unchanged compared with the fresh catalyst.

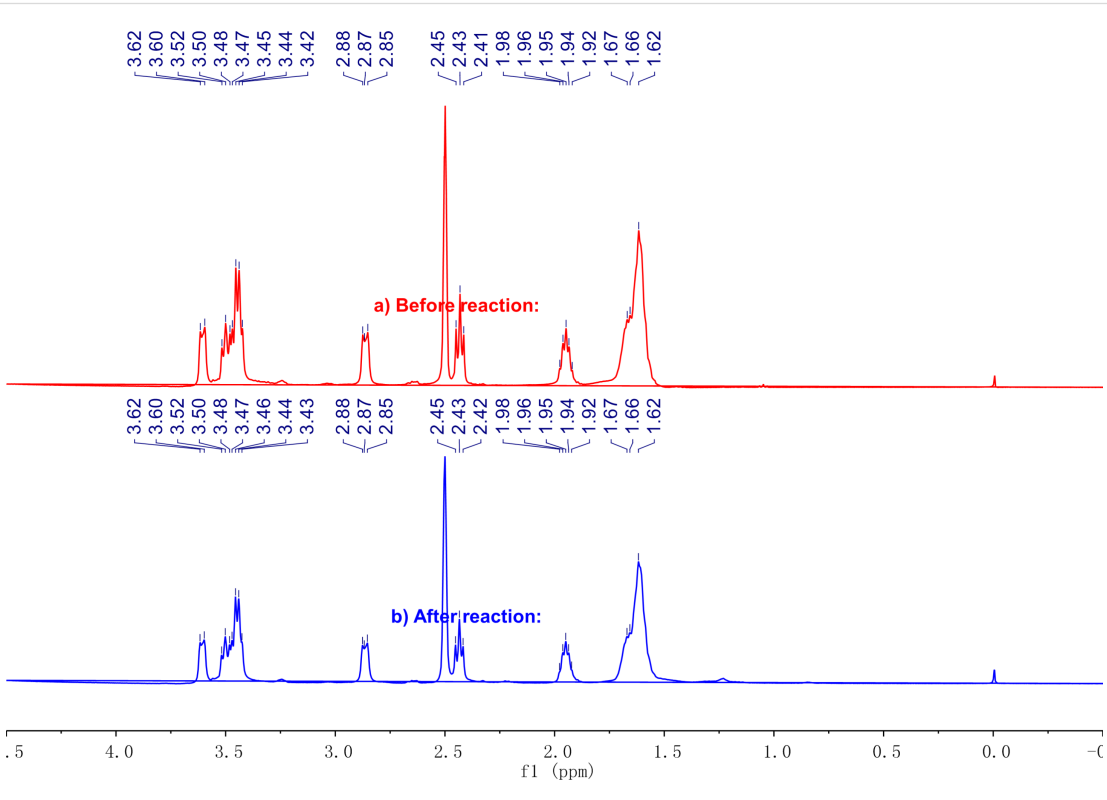

Figure 3: ^{1}H NMR (400 MHz, DMSO-d_6) spectra of $[HSO_3\text{-BDBU}]H_2PO_4$: a) Fresh one; b) used one after five cycles.

Proposed mechanism

According to our experimental results, the protic acid is crucial for the reaction. Therefore, it is inferred that the reaction undergoes proton-promoted intermolecular esterification and the reaction mechanism with catalyst $[HSO_3\text{-BDBU}]H_2PO_4$ is depicted in Scheme 3. Firstly, the Brønsted acidic IL $[HSO_3\text{-BDBU}]H_2PO_4$ activates the carbonyl group of ricinoleic acid, leading to the generation of intermediate **A**. Concurrently, the hydroxy group in another ricinoleic acid molecule may be activated by the cation of IL and attacks the intermediate **A** (step I), generating a tetrahedral intermediate **B**. Finally, dehydration and deprotonation of the tetrahedral intermediate occurs (step II), forming dimeric ricinoleic acid **C**. The carboxyl and hydroxy groups in the dimeric ricinoleic acid may further undergo esterification, providing the oligomeric ricinoleic acid with different oligomerization degree.

Conclusion

To conclude, a highly efficient Brønsted acidic IL catalyst $[HSO_3\text{-BDBU}]H_2PO_4$ was developed for the esterification of ricinoleic acid. The reaction performed well under solvent-free conditions, the qualified biolubricant oligomeric ricinoleic acid can be prepared at 190 °C and under vacuum degree of 50 kPa with 15 wt % IL as catalyst in 6 h. Both the acid value and average oligomerization degree of the product were determined and it was found the acid value was 51 mg KOH/g and the average

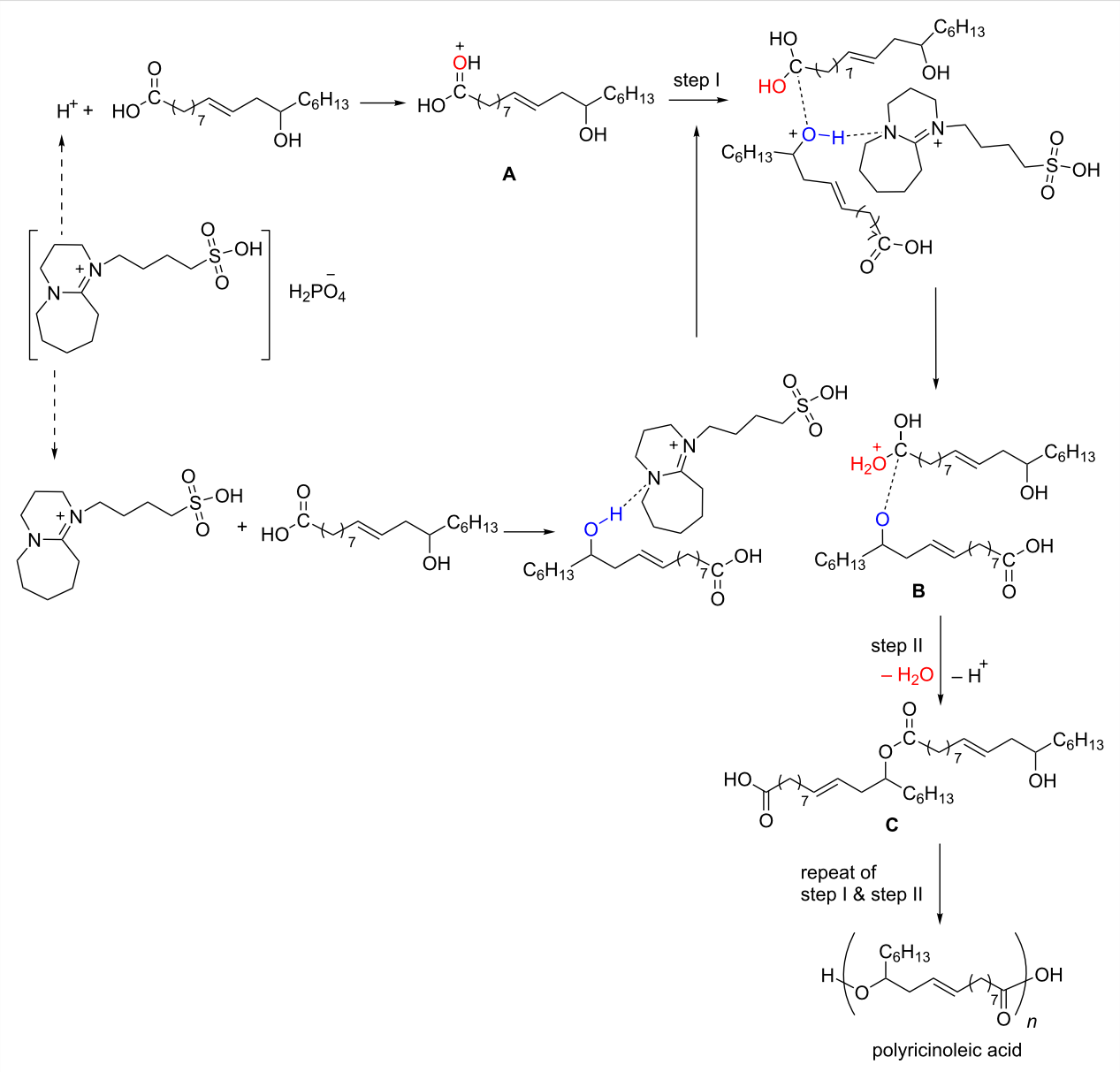

Scheme 3: Proposed mechanism for $[HSO_3\text{-BDBU}]H_2PO_4$ catalyzed oligomeric ricinoleic acid synthesis.

oligomerization degree was 4. The reaction has excellent selectivity and no other byproducts were detected except water. More remarkably, a simple stratifying at room temperature will cause the separation of catalyst and product, which means the additional solvent extraction or distillation separation employed in the traditional IL catalysis was unnecessary in this system. Besides, the catalyst can be reused at least for five cycles without significant activity lost. Therefore, this protocol employing the Brønsted acidic ionic liquid as catalyst represents a green synthesis method for oligomeric ricinoleic acid and can be run in environmentally manner. It is a promising candidate for the commercial production of oligomeric ricinoleic acid from ricinoleic acid.

Experimental

Preparation procedure of [HSO_3-BDBU]H_2PO_4

To prepare the IL [HSO_3-BDBU]H_2PO_4, 0.1 mol (13.6 g) 1,4-butane sultone was mixed with 0.1 mol (15.2 g) 1,8-diazobicyclo[5,4,0]undec-7-ene (DBU) in a flask containing 50 mL of acetonitrile. After 24 h reflux at 80 °C, the reaction mixture was cooled to room temperature. Then 30 mL diethyl ether was added to the reaction mixture to precipitate the product. After that, the precipitate was collected by filtration and washed twice with diethyl ether. The resulting light yellow precipitate was then dried in vacuum at 60 ºC for 4 h. Afterwards, the aqueous solution containing a stoichiometric amount of phosphoric acid was added dropwise to 50 mL CH_2Cl_2 containing 0.05 mol (14.4 g) [HSO_3-BDBU] and stirred at 60 °C for 4 h, forming a viscous liquid on the surface of CH_2Cl_2 which can be easily separated by centrifugation. Then the viscous liquid was washed twice with CH_2Cl_2 and dried at 100 ºC for 12 h, obtaining 18.6 g yellow viscous liquid with the yield of 96%. The resulting compound was identified to be IL [HSO_3-BDBU]H_2PO_4. ^{1}H NMR (400 MHz, DMSO-d_6) δ 1.62–1.67 (m, 10H), 1.92–1.98 (m, 2H), 2.41–2.45 (t, J = 6.8 Hz, 2H), 2.85–2.88 (t, J = 4.8, 2H), 3.42–3.62 (m, 8H) ppm; ^{13}C NMR (100 MHz, DMSO-d_6) δ 19.65, 22.13, 22.88, 25.55, 27.12, 27.22, 27.90, 46.58, 48.52, 50.65, 52.92, 53.98, 165.98 ppm; FTIR (KBr) ν_{max}/cm^{-1}: 3317.18, 2939.11, 2867.62, 1621.52, 1527.51, 1452.10, 1328.75, 1201.00, 998.74, 726.90, 600.28; ESIMS (+) m/z: 100.1, 102.1, 153.2, 289.3, 390.1.

For the preparation of other ILs in this paper and for full experimental data see Supporting Information File 1.

Catalytic dehydration esterification of ricinoleic acid and catalyst recycling

The dehydration esterification of ricinoleic acid was investigated using ILs as catalyst. In a typical run, 10 g (30 mmol) ricinoleic acid and 1 g (2.6 mmol) [HSO_3-BDBU]H_2PO_4 were added into a 100 mL glass flask equipped with magnetic stirrer, a reflux condenser and connected with vacuum line. Then, under a stirrer rate of 500 r/min, the temperature was increased to 190 °C to promote the esterification reaction. Simultaneously, the reaction run at 50 kPa to remove the generated water. After 2 h of reaction, the reaction mixture was cooled to room temperature for stratifying. The supernatant was oligomeric ricinoleic acid and it could be decanted directly for further treatment and acid value analysis. The IL catalyst deposited in the lower layer can be washed with a small amount of dichloromethane to remove the residual oligoester. After that, the fresh ricinoleic acid was added for the second run reaction and the recovered catalyst can be used repeatedly.

Product characterization

The oligomeric ricinoleic acid is a yellow oily liquid, and all experiments have yields greater than 90%, which are determined by weighing. The spectral results identified the product. ^{1}H NMR (400 MHz, $CDCl_3$) δ 0.85–0.88 (t, J = 3.9 Hz, 3H), 1.26–1.29 (m, 16H), 1.51–1.60 (m, 4H), 2.00–2.01 (m, 2H), 2.25–2.26 (m, 4H), 4.86–4.89 (m, 1H), 5.30–5.46 (m, 2H) ppm; ^{13}C NMR (100 MHz, $CDCl_3$) δ 14.08, 22.58, 25.11, 25.35, 27.20–27.35, 29.03–29.71, 31.75, 31.98, 33.62, 34.65, 73.69, 124.30, 132.51, 173.58 ppm; FTIR (KBr) ν_{max}/cm^{-1}: 3416.44, 3010.55, 2927.89, 2855.81, 1733.38, 1711.66, 1464.22, 1245.41, 1183.74, 725.11; ESIMS (+) m/z: 579.3, 876.6, 1139.7, 1437.8, 1716.9, 1997.1.

Acid value determination

The acid value of product was determined using a modified ASTM D664 method [33], in which about 1 g sample was dissolved in 30 mL CH_2Cl_2 and the resulting solution was titrated against standard 0.1 N isopropanol KOH. Acid value (mg KOH/g sample) was then calculated as follows:

$$\text{acid value} = \frac{56.11 \cdot V \cdot C}{W}$$

where V (mL) and C (mol/L) are the consumed volume and concentration of KOH solution, respectively, W (g) is the weight of the sample.

To exclude the presence of IL in supernatant and ensure the reliability of acid value in oligomerization degree determination, additional treatment was performed for the supernatant before acid value determination. That is, the supernatant was diluted with dichloromethane, and the putative IL in the sample was extracted three times with distilled water. Then the remaining organic phase was dried with Na_2SO_4 for 24 h followed by filtration. After that, the filtrate was collected and the dichloromethane solvent was removed by vacuum evaporation

to obtain oligomeric ricinoleic acid for acid value measurement (Table 5, entries 1, 3 and 5). On the other hand, the acid value of supernatant without any treatment was also determined for comparison (Table 5, entries 2, 4 and 6). The acid values of the two treatments were identical, indicating that IL settled well after the reaction and was absent in the product.

Table 5: Acid value measurement results of two different treatments for the supernatant.

Entry[a]	Reaction time (h)	Acid value (mg KOH/g)
1	1	108
2	1	108
3	2	74
4	2	73
5	4	60
6	4	60

[a]Reaction conditions: 10 g (30 mmol) ricinoleic acid, 1 g (2.6 mmol) [HSO_3-BDBU]H_2PO_4, 190 °C, 50 kPa.

Supporting Information

Supporting Information File 1

Experimental part and spectra of synthesized compounds.
[https://www.beilstein-journals.org/bjoc/content/supplementary/1860-5397-16-34-S1.pdf]

Funding

We thank the National Natural Science Foundation of China (21975135), Tianjin Nankai University Castor Engineering Science and Technology Co., Ltd. and Inner Mongolia Weiyu Biotech Co., Ltd. for financial support.

ORCID® iDs

Hong-Ru Li - https://orcid.org/0000-0002-4916-2815
Liang-Nian He - https://orcid.org/0000-0002-6067-5937

References

1. Ebata, H.; Yasuda, M.; Toshima, K.; Matsumura, S. *J. Oleo Sci.* **2008,** *57,* 315–320. doi:10.5650/jos.57.315
2. Alonso, D. M.; Bond, J. Q.; Dumesic, J. A. *Green Chem.* **2010,** *12,* 1493–1513. doi:10.1039/c004654j
3. Biermann, U.; Bornscheuer, U.; Meier, M. A. R.; Metzger, J. O.; Schäfer, H. J. *Angew. Chem., Int. Ed.* **2011,** *50,* 3854–3871. doi:10.1002/anie.201002767
4. Meier, M. A. R.; Metzger, J. O.; Schubert, U. S. *Chem. Soc. Rev.* **2007,** *36,* 1788–1802. doi:10.1039/b703294c
5. Miao, S.; Wang, P.; Su, Z.; Zhang, S. *Acta Biomater.* **2014,** *10,* 1692–1704. doi:10.1016/j.actbio.2013.08.040
6. Biermann, U.; Friedt, W.; Lang, S.; Lühs, W.; Machmüller, G.; Metzger, J. O.; Rüsch gen. Klaas, M.; Schäfer, H. J.; Schneider, M. P. *Angew. Chem., Int. Ed.* **2000,** *39,* 2206–2224. doi:10.1002/1521-3773(20000703)39:13<2206::aid-anie2206>3.0.co;2-p
7. Nayak, P. L. *J. Macromol. Sci., Rev. Macromol. Chem. Phys.* **2000,** *40,* 1–21. doi:10.1081/mc-100100576
8. Thomas, A.; Matthäus, B.; Fiebig, H.-J. *Ullmann's Encycl. Ind. Chem.* **2000,** 1–84. doi:10.1002/14356007.a10_173.pub2
9. Scarpa, A.; Guerci, A. *J. Ethnopharmacol.* **1982,** *5,* 117–137. doi:10.1016/0378-8741(82)90038-1
10. Mutlu, H.; Meier, M. A. R. *Eur. J. Lipid Sci. Technol.* **2010,** *112,* 10–30. doi:10.1002/ejlt.200900138
11. Ogunniyi, D. S. *Bioresour. Technol.* **2006,** *97,* 1086–1091. doi:10.1016/j.biortech.2005.03.028
12. Van der Steen, M.; Stevens, C. V. *ChemSusChem* **2009,** *2,* 692–713. doi:10.1002/cssc.200900075
13. Goodrum, J. W.; Geller, D. P. *Bioresour. Technol.* **2005,** *96,* 851–855. doi:10.1016/j.biortech.2004.07.006
14. Kim, H. T.; Baritugo, K.-A.; Oh, Y. H.; Hyun, S. M.; Khang, T. U.; Kang, K. H.; Jung, S. H.; Song, B. K.; Park, K.; Kim, I.-K.; Lee, M. O.; Kam, Y.; Hwang, Y. T.; Park, S. J.; Joo, J. C. *ACS Sustainable Chem. Eng.* **2018,** *6,* 5296–5305. doi:10.1021/acssuschemeng.8b00009
15. Borsotti, G.; Guglielmetti, G.; Spera, S.; Battistel, E. *Tetrahedron* **2001,** *57,* 10219–10227. doi:10.1016/s0040-4020(01)01057-2
16. Yoshida, Y.; Kawase, M.; Yamaguchi, C.; Yamane, T. *J. Am. Oil Chem. Soc.* **1997,** *74,* 261–267. doi:10.1007/s11746-997-0133-x
17. Hayes, D. G.; Kleiman, R. *J. Am. Oil Chem. Soc.* **1995,** *72,* 1309–1316. doi:10.1007/bf02546204
18. Zerkowski, J. A. *Lipid Technol.* **2008,** *20,* 253–256. doi:10.1002/lite.200800066
19. Vadgama, R. N.; Odaneth, A. A.; Lali, A. M. *Heliyon* **2019,** *5,* e01944. doi:10.1016/j.heliyon.2019.e01944
20. Bódalo-Santoyo, A.; Bastida-Rodríguez, J.; Máximo-Martín, M. F.; Montiel-Morte, M. C.; Murcia-Almagro, M. D. *Biochem. Eng. J.* **2005,** *26,* 155–158. doi:10.1016/j.bej.2005.04.012
21. Bódalo, A.; Bastida, J.; Máximo, M. F.; Montiel, M. C.; Gómez, M.; Murcia, M. D. *Biochem. Eng. J.* **2008,** *39,* 450–456. doi:10.1016/j.bej.2007.10.013
22. Bódalo, A.; Bastida, J.; Máximo, M. F.; Montiel, M. C.; Murcia, M. D.; Ortega, S. *Biochem. Eng. J.* **2009,** *44,* 214–219. doi:10.1016/j.bej.2008.12.007
23. Horchani, H.; Bouaziz, A.; Gargouri, Y.; Sayari, A. *J. Mol. Catal. B: Enzym.* **2012,** *75,* 35–42. doi:10.1016/j.molcatb.2011.11.007
24. Yoshida, Y.; Kawase, M.; Yamaguchi, C.; Yamane, T. *J. Jpn. Oil Chem. Soc.* **1995,** *44,* 328–333. doi:10.5650/jos1956.44.328
25. Erhan, S. M.; Kleiman, R.; Isbell, T. A. *J. Am. Oil Chem. Soc.* **1993,** *70,* 461–465. doi:10.1007/bf02542576
26. Zhang, Q.; Zhang, S.; Deng, Y. *Green Chem.* **2011,** *13,* 2619–2637. doi:10.1039/c1gc15334j
27. Petkovic, M.; Seddon, K. R.; Rebelo, L. P. N.; Silva Pereira, C. *Chem. Soc. Rev.* **2011,** *40,* 1383–1403. doi:10.1039/c004968a
28. Wang, G.; Sun, S. *J. Oleo Sci.* **2017,** *66,* 753–759. doi:10.5650/jos.ess17031
29. Li, M.; Wu, F.; Gu, Y. *Chin. J. Catal.* **2019,** *40,* 1135–1140. doi:10.1016/s1872-2067(19)63370-x

30. El-Harairy, A.; Yiliqi; Lai, B.; Vaccaro, L.; Li, M.; Gu, Y. *Adv. Synth. Catal.* **2019,** *361,* 3342–3350. doi:10.1002/adsc.201900246
31. El-Harairy, A.; Yiliqi; Yue, M.; Fan, W.; Popowycz, F.; Queneau, Y.; Li, M.; Gu, Y. *ChemCatChem* **2019,** *11,* 4403–4410. doi:10.1002/cctc.201900784
32. Ye, F.; He, L. N.; You, F.; Li, H. R.; Wang, Q. R.; Gao, S.; He, X.; Cui, X. Y. A protocol for oligomeric ricinoleic acid preparation and in-situ separation. Chin Patent CN202010124194.1, Feb 27, 2020.
33. *ASTM D664-17;* ASTM International: West Conshohocken, PA, 2017.

License and Terms

BEILSTEIN JOURNAL OF ORGANIC CHEMISTRY

Suzuki–Miyaura cross coupling is not an informative reaction to demonstrate the performance of new solvents

James Sherwood

Letter

Open Access

Address:
Green Chemistry Centre of Excellence, Department of Chemistry, University of York, Heslington, YO10 5DD, UK

Email:
James Sherwood - james.sherwood@york.ac.uk

Keywords:
cross coupling; green solvents; palladium; solvent selection; Suzuki reaction

Beilstein J. Org. Chem. **2020,** *16,* 1001–1005.
doi:10.3762/bjoc.16.89

Received: 03 March 2020
Accepted: 04 May 2020
Published: 13 May 2020

This article is part of the thematic issue "Green chemistry II".

Guest Editor: L. Vaccaro

Abstract

The development and study of new solvents has become important due to a proliferation of regulations preventing or limiting the use of many conventional solvents. In this work, the suitability of the Suzuki–Miyaura reaction to demonstrate the usefulness of new solvents was evaluated, including Cyrene™, dimethyl isosorbide, ethyl lactate, 2-methyltetrahydrofuran (2-MeTHF), propylene carbonate, and γ-valerolactone (GVL). It was found that the cross coupling is often unaffected by the choice of solvent, and therefore the Suzuki–Miyaura reaction provides limited information regarding the usefulness of any particular solvent for organic synthesis.

Findings

The objective of this work was to reveal if there is a relationship between the productivity of Suzuki–Miyaura cross couplings and the properties of the solvent, and whether this could be used to justify solvent selection. The choice of solvent is one variable that dictates reaction rate, selectivity, equilibria, solubility, and ultimately product yield. If there is an observable change in reaction performance correlating to one or more solvent properties (often polarity), then it is possible to identify and implement an optimum solvent. Suzuki–Miyaura cross coupling is the premier method of palladium catalysed carbon–carbon bond formation, making it an obvious case study to validate the performance of novel solvents [1-7]. The polarity of the solvent is known to determine the structure and activity of catalytic intermediates, the rate determining step, and stereochemistry (where applicable) of Suzuki–Miyaura cross couplings [8]. Despite this, the reaction is generally tolerant of a wide range of solvents (often an ether or amide solvent is used, and water is a common co-solvent). This calls into question the benefits of using Suzuki–Miyaura cross coupling as a test of new solvents, regardless of how vital the reaction is.

Three variations of the Suzuki–Miyaura cross-coupling protocol were performed. Each case study is a transformation of phenylboronic acid (1.2 molar equivalents) under different conditions (see Scheme 1), but all using 1 part water to 3 parts organic solvent (by volume) and 0.6 mmol (1 equivalent) of an aryl bro-

mide. The solvent screening included twelve solvents. The following eminent green and bio-based solvents were included in the study to assess their ability to substitute conventional solvents: Cyrene™ [3], and its alcohol equivalent levoglucosanol [9], ethyl lactate [10], 2-methyltetrahydrofuran (2-MeTHF) [11], γ-valerolactone (GVL) [12], dimethyl isosorbide (DMI) [6], and propylene carbonate [7]. This study compares solvents under the same conditions to offer a fair comparison. Additional solvents were included to ensure a range of polarities were investigated (see Supporting Information File 1). In each case study, conversion to the desired product was measured by ^{1}H NMR spectroscopy (see Supporting Information File 1, Figure S4). The results are summarised in Table 1. No evidence of significant hydrodehalogenation or other unintended reactions was observed throughout unless noted subsequently.

The first case study was adapted from that developed by Watson and co-workers [3,6]. The desired coupling is of 4-bromotoluene to produce 4-phenyltoluene, assisted by the inclusion of the bis(diphenylphosphino)ferrocene ligand and 3 equivalents of base (Scheme 1a). In this work the proportion of water added is less than that previously optimised for reactions in Cyrene™ [3], and more than that previously optimised for reactions in DMI [6]. In case study 1, the majority of sol-

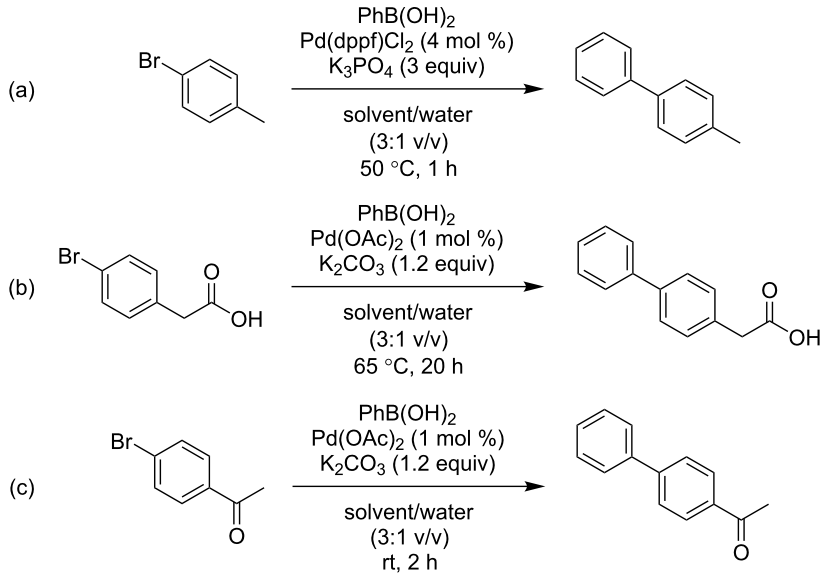

Scheme 1: (a) Case study 1, reaction of 4-bromotoluene; (b) case study 2, reaction of 4-bromophenylacetic acid; (c) case study 3, reaction of 4'-bromoacetophenone.

Table 1: Conversions in three Suzuki–Miyaura reactions.[a]

solvent	greenness ranking	case study 1	case study 2	case study 3
NMP	hazardous (reprotoxicity)	85%	98%	100%
toluene	problematic (health and safety issues)	94%	100%	42%
butanone	recommended	92%	92%	30%
2-propanol	recommended	81%	100%	100%
ethyl acetate	recommended	76%	100%	28%
ethyl lactate	problematic (causes serious eye damage)	75%	81%	73%
Cyrene™	problematic (low volatility)	83%	2%	5%
levoglucosanol	lacking data (low volatility)	77%	64%	82%
DMI	problematic (low volatility)	96%	63%	74%
propylene carbonate	problematic (low volatility)	81%	100%	98%
GVL	problematic (low volatility)	87%	98%	36%
2-MeTHF	problematic (health and safety issues)	79%	100%	16%

[a]Greenness ranking is taken from the CHEM21 solvent selection guide.

vents resulted in conversion to the product in the range of 75–85% after 1 hour. The highest conversion of 96% was obtained in DMI, but overall it is fair to conclude the reaction quickly reaches good conversions with little apparent influence from the solvent.

The second case study transformed 4-bromophenylacetic acid into felbinac, a nonsteroidal anti-inflammatory drug (Scheme 1b) [13]. Here, palladium acetate without an auxiliary ligand was used for a pre-catalyst and the base changed to potassium carbonate. Reaction conditions of 20 hours at 65 °C were decided after observing 11% conversion after 2 hours and 33% after 20 hours in NMP at room temperature. The majority of solvents provided conversions in excess of 90%. In the case of Cyrene™, its instability towards inorganic bases is presumably the reason for the very low conversion (2%). During one run the reaction mixture did solidify, as has been reported previously for various chemistries in Cyrene™ under basic conditions [14].

The third case study was a coupling of 4-bromoacetophenone (Scheme 1c) using the same pre-catalyst and base as in case study 2. In this example the reaction proceeds at room temperature, but now the conversion to the product varies considerably between solvents. Reactions in *N*-methyl-2-pyrrolidone (NMP) and 2-propanol (IPA) resulted in complete conversion, and the product could be isolated by crystallisation from diethyl ether. Propylene carbonate also provided excellent conversion to the product (98%). The alcohol functionalised solvents outperformed their aprotic analogues, while Cyrene™, GVL, and 2-MeTHF were poor solvents. Replacing potassium carbonate with triethylamine, the conversion in Cyrene™ rose slightly to 10%. Despite the variation between experiments no discernible correlation between any solvent properties and the observed conversions was found.

The results achieved in DMI across the three case studies typify the lack of an obvious solvent effect. In one instance DMI is the best performing solvent (case study 1), then the worst aside from the reactive Cyrene™ (case study 2), and then somewhere in between (case study 3). To demonstrate that not even case study 3 is robust enough to definitively establish a measurement of solvent performance in Suzuki–Miyaura cross couplings, a short optimisation study was conducted to improve the conversion to 4-phenylacetophenone in 2-MeTHF (originally 16%). Reducing the water content to an 18:1 v/v ratio and increasing the excess of base to 3 equivalents and catalyst to 5 mol % was found to be beneficial, as was a higher reaction temperature of 65 °C. These conditions produced a conversion of 79% after 4 hours in 2-MeTHF. This is an indication of the weak influence of the solvent compared to the impact of the reaction temperature, and the choice and quantity of catalyst and base.

Given the broad choice of solvents available, what is left to decide is the most benign solvent that should be preferred for conducting Suzuki–Miyaura reactions. Table 1 lists the greenness rating from the CHEM21 solvent selection guide (except for levoglucosanol which lacks the necessary data) [15]. The 'recommended' solvent with a high performance across the three case studies is IPA, known as a robust solvent for Suzuki–Miyaura type cross couplings [16-18]. However, it is also worth noting that the 'problematic' designation of Cyrene™, DMI, propylene carbonate, and GVL is due to their high boiling points placing a high energy demand on recovery by distillation. If recovery has been considered and deemed infeasible, then propylene carbonate in particular should also be considered given its superior hazard profile compared to IPA. However, caution is advised in the presence of nucleophilic reagents, as this has previously been reported to cause ring opening of propylene carbonate during Suzuki–Miyaura cross couplings [7]. In this work no decomposition of propylene carbonate was identified. Using only water as a solvent is also appealing from a green chemistry perspective if the water can be reused. To this end, micellar chemistry is appropriate for cross couplings [19]. Residual water also assists 'solvent-free' methods [20].

In summary, the Suzuki–Miyaura reaction is a fantastically versatile and industrially important reaction [21,22], and excels in a variety of reaction media. On the evidence of this study, it can be concluded that the Suzuki–Miyaura reaction is not an informative case study for solvent effects and cannot reliably validate the benefits of one particular solvent. This is because catalysts and conditions can be chosen to promote high conversions regardless of the properties of the solvent. Additionally, the diverse properties of high performance solvents across Suzuki–Miyaura reactions means it is hard to discern what are the requisite qualities of the reaction medium (if any) that encourage the desired cross coupling. Specific mechanistic studies whereby the rate limiting step or mechanism changes according to the solvent remain a valid pursuit, as does measuring the palladium contamination in products [23]. However, the works of Watson [24], Denmark [25], and others [26,27], have already elucidated many of the key fundamental principles of boron and palladium speciation and the role of the base in the Suzuki–Miyaura reaction.

For researchers developing safer solvents, the Mizoroki–Heck reaction is a more suitable cross-coupling methodology to demonstrate solvent performance [28]. The reaction kinetics of Mizoroki–Heck reactions have a strong dependence on the

dipolarity of the reaction medium, and the rate determining step can be controlled by the equivalents of ligand added, thereby eliminating one variable [8]. Reprotoxic solvents such as *N*,*N*-dimethylformamide (DMF) are routinely used in the Mizoroki–Heck reaction and hence there is also a motivation to investigate safer alternative solvents that the Suzuki–Miyaura reaction lacks.

If researchers are still compelled to study the utility of solvents in the Suzuki–Miyaura reaction, I encourage future studies to be directed at challenging substrates that correspond to commercially important products (e.g., enantiopure pharmaceuticals, polymeric materials) and if a substrate screening should follow, the protocol established by Collins and Glorius is effective [29]. For the development of new catalysts, it is preferable to work with a benign solvent such as aqueous IPA from the outset [30]. This is because late-stage solvent screens rarely reveal a superior solvent due to the catalyst having already been optimised to work in the original solvent, which may have been chosen only for ease of removal (e.g., the volatile but suspected carcinogen dichloromethane) or the high solubility of organic and inorganic reagents (e.g., the reprotoxic DMF).

Supporting Information

Supporting Information File 1

Synthetic procedures and calculation of reaction conversions and solvent polarity data.
[https://www.beilstein-journals.org/bjoc/content/supplementary/1860-5397-16-89-S1.pdf]

Funding

This research was funded by the Bio-Based Industries Joint Undertaking (JU) under the European Union's Horizon 2020 research and innovation programme (agreement No 745450). The publication reflects only the author's view and the JU is not responsible for any use that may be made of the information it contains.

ORCID® iDs

James Sherwood - https://orcid.org/0000-0001-5431-2032

References

1. Sarmah, M.; Mondal, M.; Bora, U. *ChemistrySelect* **2017,** *2,* 5180–5188. doi:10.1002/slct.201700580
2. Sherwood, J.; Parker, H. L.; Moonen, K.; Farmer, T. J.; Hunt, A. J. *Green Chem.* **2016,** *18,* 3990–3996. doi:10.1039/c6gc00932h
3. Wilson, K. L.; Murray, J.; Jamieson, C.; Watson, A. J. B. *Synlett* **2018,** *29,* 650–654. doi:10.1055/s-0036-1589143
4. Wolfson, A.; Dlugy, C. *Chem. Pap.* **2007,** *61,* 228–232. doi:10.2478/s11696-007-0026-3
5. Lei, P.; Ling, Y.; An, J.; Nolan, S. P.; Szostak, M. *Adv. Synth. Catal.* **2019,** *361,* 5654–5660. doi:10.1002/adsc.201901188
6. Wilson, K. L.; Murray, J.; Sneddon, H. F.; Jamieson, C.; Watson, A. J. B. *Synlett* **2018,** *29,* 2293–2297. doi:10.1055/s-0037-1611054
7. Czompa, A.; Pásztor, B. L.; Sahar, J. A.; Mucsi, Z.; Bogdán, D.; Ludányi, K.; Varga, Z.; Mándity, I. M. *RSC Adv.* **2019,** *9,* 37818–37824. doi:10.1039/c9ra07044c
8. Sherwood, J.; Clark, J. H.; Fairlamb, I. J. S.; Slattery, J. M. *Green Chem.* **2019,** *21,* 2164–2213. doi:10.1039/c9gc00617f
9. Sherwood, J.; Granelli, J.; McElroy, C. R.; Clark, J. H. *Molecules* **2019,** *24,* 2209. doi:10.3390/molecules24122209
10. Wan, J.-P.; Wang, C.; Zhou, R.; Liu, Y. *RSC Adv.* **2012,** *2,* 8789–8792. doi:10.1039/c2ra21632a
11. Ramgren, S. D.; Hie, L.; Ye, Y.; Garg, N. K. *Org. Lett.* **2013,** *15,* 3950–3953. doi:10.1021/ol401727y
12. Petricci, E.; Risi, C.; Ferlin, F.; Lanari, D.; Vaccaro, L. *Sci. Rep.* **2018,** *8,* 10571. doi:10.1038/s41598-018-28458-y
13. Del Zotto, A.; Amoroso, F.; Baratta, W.; Rigo, P. *Eur. J. Org. Chem.* **2009,** 110–116. doi:10.1002/ejoc.200800874
14. Wilson, K. L.; Kennedy, A. R.; Murray, J.; Greatrex, B.; Jamieson, C.; Watson, A. J. B. *Beilstein J. Org. Chem.* **2016,** *12,* 2005–2011. doi:10.3762/bjoc.12.187
15. Prat, D.; Wells, A.; Hayler, J.; Sneddon, H.; McElroy, C. R.; Abou-Shehada, S.; Dunn, P. J. *Green Chem.* **2016,** *18,* 288–296. doi:10.1039/c5gc01008j
16. Navarro, O.; Oonishi, Y.; Kelly, R. A.; Stevens, E. D.; Briel, O.; Nolan, S. P. *J. Organomet. Chem.* **2004,** *689,* 3722–3727. doi:10.1016/j.jorganchem.2004.04.001
17. Camp, J. E.; Dunsford, J. J.; Cannons, E. P.; Restorick, W. J.; Gadzhieva, A.; Fay, M. W.; Smith, R. J. *ACS Sustainable Chem. Eng.* **2014,** *2,* 500–505. doi:10.1021/sc400410v
18. Stewart, G. W.; Maligres, P. E.; Baxter, C. A.; Junker, E. M.; Krska, S. W.; Scott, J. P. *Tetrahedron* **2016,** *72,* 3701–3706. doi:10.1016/j.tet.2016.02.030
19. Isley, N. A.; Gallou, F.; Lipshutz, B. H. *J. Am. Chem. Soc.* **2013,** *135,* 17707–17710. doi:10.1021/ja409663q
20. Bernhardt, F.; Trotzki, R.; Szuppa, T.; Stolle, A.; Ondruschka, B. *Beilstein J. Org. Chem.* **2010,** *6,* No. 7. doi:10.3762/bjoc.6.7
21. Johansson Seechurn, C. C. C.; Kitching, M. O.; Colacot, T. J.; Snieckus, V. *Angew. Chem., Int. Ed.* **2012,** *51,* 5062–5085. doi:10.1002/anie.201107017
22. Magano, J.; Dunetz, J. R. *Chem. Rev.* **2011,** *111,* 2177–2250. doi:10.1021/cr100346g
23. Strappaveccia, G.; Ismalaj, E.; Petrucci, C.; Lanari, D.; Marrocchi, A.; Drees, M.; Facchetti, A.; Vaccaro, L. *Green Chem.* **2015,** *17,* 365–372. doi:10.1039/c4gc01677g
24. Molloy, J. J.; Seath, C. P.; West, M. J.; McLaughlin, C.; Fazakerley, N. J.; Kennedy, A. R.; Nelson, D. J.; Watson, A. J. B. *J. Am. Chem. Soc.* **2018,** *140,* 126–130. doi:10.1021/jacs.7b11180
25. Thomas, A. A.; Denmark, S. E. *Science* **2016,** *352,* 329–332. doi:10.1126/science.aad6981
26. Lennox, A. J. J.; Lloyd-Jones, G. C. *Angew. Chem., Int. Ed.* **2013,** *52,* 7362–7370. doi:10.1002/anie.201301737
27. Amatore, C.; Le Duc, G.; Jutand, A. *Chem. – Eur. J.* **2013,** *19,* 10082–10093. doi:10.1002/chem.201300177

28. Parker, H. L.; Sherwood, J.; Hunt, A. J.; Clark, J. H. *ACS Sustainable Chem. Eng.* **2014,** *2,* 1739–1742. doi:10.1021/sc5002287
29. Collins, K. D.; Glorius, F. *Nat. Chem.* **2013,** *5,* 597–601. doi:10.1038/nchem.1669
30. Dyson, P. J.; Jessop, P. G. *Catal. Sci. Technol.* **2016,** *6,* 3302–3316. doi:10.1039/c5cy02197a

License and Terms

BEILSTEIN JOURNAL OF ORGANIC CHEMISTRY

The charge-assisted hydrogen-bonded organic framework (CAHOF) self-assembled from the conjugated acid of tetrakis(4-aminophenyl)methane and 2,6-naphthalenedisulfonate as a new class of recyclable Brønsted acid catalysts

Svetlana A. Kuznetsova[1], Alexander S. Gak[2], Yulia V. Nelyubina[1], Vladimir A. Larionov[1,3], Han Li[4], Michael North[4], Vladimir P. Zhereb[5], Alexander F. Smol'yakov[1], Artem O. Dmitrienko[1], Michael G. Medvedev[1,6], Igor S. Gerasimov[1,6], Ashot S. Saghyan[7] and Yuri N. Belokon[*1]

Full Research Paper

Open Access

Address:
[1]Nesmeyanov Institute of Organoelement Compounds, Russian Academy of Sciences, Vavilov Street 28, 119991 Moscow, Russian Federation, [2]Moscow State University, Faculty of Material Science, Leninskie Gory 1/73, 119991 Moscow, Russian Federation, [3]Department of Inorganic Chemistry, People's Friendship University of Russia (RUDN University), Miklukho-Maklaya Street 6, 117198 Moscow, Russian Federation, [4]Green Chemistry Centre of Excellence, Department of Chemistry, University of York, Heslington, YO10 5DD, United Kingdom, [5]Siberian Federal University, School of Non-Ferrous Metals and Material Science, 95 Krasnoyarskiy Rabochiy pr., 660025 Krasnoyarsk, Russian Federation, [6]N. D. Zelinsky Institute of Organic Chemistry RAS, Leninsky Prospect, 47, 119991 Moscow, Russian Federation and [7]Institute of Pharmacy, Yerevan State University, 1 Alex Manoogian Str, Yerevan 0025, Armenia

Email:
Yuri N. Belokon[*] - yubel@ineos.ac.ru

* Corresponding author

Keywords:
Brønsted acid catalyst; charge-assisted hydrogen-bonded framework; Diels–Alder; epoxide ring opening; heterogeneous catalyst

Beilstein J. Org. Chem. **2020,** *16,* 1124–1134.
doi:10.3762/bjoc.16.99

Received: 19 February 2020
Accepted: 15 May 2020
Published: 26 May 2020

This article is part of the thematic issue "Green chemistry II".

Guest Editor: L. Vaccaro

Abstract

The acid–base neutralization reaction of commercially available disodium 2,6-naphthalenedisulfonate (NDS, 2 equivalents) and the tetrahydrochloride salt of tetrakis(4-aminophenyl)methane (TAPM, 1 equivalent) in water gave a novel three-dimensional charge-assisted hydrogen-bonded framework (CAHOF, **F-1**). The framework **F-1** was characterized by X-ray diffraction, TGA, elemental

analysis, and ^{1}H NMR spectroscopy. The framework was supported by hydrogen bonds between the sulfonate anions and the ammonium cations of NDS and protonated TAPM moieties, respectively. The CAHOF material functioned as a new type of catalytically active Brønsted acid in a series of reactions, including the ring opening of epoxides by water and alcohols. A Diels–Alder reaction between cyclopentadiene and methyl vinyl ketone was also catalyzed by **F-1** in heptane. Depending on the polarity of the solvent mixture, the CAHOF **F-1** could function as a purely heterogeneous catalyst or partly dissociate, providing some dissolved **F-1** as the real catalyst. In all cases, the catalyst could easily be recovered and recycled.

Introduction

Tremendous successes in homogeneous catalysis are well-known and documented [1-3]. However, problems associated with catalyst recovery limit the application of homogeneous catalysts in industry and sometimes make their heterogenization necessary. Unfortunately, the immobilization of a homogeneous catalyst onto supports, such as polystyrene, silica, glass, and others [4-12] generally leads to a deterioration of the catalytic properties of the initial homogeneous catalyst. This is due to factors including the nonhomogeneous structures of the catalytic centers on the surface of the carrier or inside the polymeric matrix and the low availability of the active sites to the substrates due to diffusion problems. Additionally, the self-association of catalytic centers on flexible polymeric chains may negatively influence the expected activity of the immobilized catalyst. Moreover, the degradation of cross-linked covalent polymeric matrixes or the destruction of catalytic centers during productive cycles can shorten the lives of the catalysts to an extent that makes the immobilization of homogeneous catalysts impractical [7].

In recent decades, novel classes of heterogeneous, porous, crystalline architectures have been discovered, which allow a rigid and uniform distribution of a single well-defined catalytic or precatalytic center within a solid matrix. Of these, metal–organic frameworks (MOFs) [13-18] and covalent organic frameworks (COFs) [19-22] have been the forerunners. The design of MOFs is based on metal nodes linked by organic ligands whilst COFs have ligands joined by organic nodes. Both displayed great catalytic properties, sometimes exceeding those of homogeneous analogs [23,24]. Unfortunately, stability problems, the cost of the initial materials, and the synthetic protocols for the matrix synthesis hamper the routine use of MOFs and COFs in industry, even for the production of high-added-value products.

Recently, new supramolecular porous materials named hydrogen-bonded organic frameworks (HOFs) or supramolecular organic frameworks (SOFs) have been developed [25-36]. Usually, a HOF is built from multitopic tectons that interact with their neighbors by directional hydrogen bonds, disfavoring close packing, and thus generating significant pore volumes within the crystal [25-28]. These heterogeneous, crystalline, supramolecular frameworks may be neutral, for example, those built by mutual interactions of multitopic carboxylic acids [25-29]. Alternatively, they can be constructed from components possessing oppositely charged multitopic tectons, in which case the framework becomes a charge-assisted hydrogen-bonded framework (CAHOF), as was the case when multitopic guanidinium or amidinium cations were combined with polycarboxylates, polysulfonates, or polyphosphonates [30-33]. The synthesis of a HOF or CAHOF consists of simply mixing the two components together [29]. An additional advantage of HOFs and CAHOFs is their self-healing property, as the frameworks can easily self-reassemble after the disassembly induced by an external stimulus [26,27,37].

Although the field of HOF and CAHOF applications is still in its infancy, there are some promising advances in proton conductivity [30,31], gas separation and absorption [28,29], enzyme encapsulation [36], and even asymmetric synthesis (albeit with a framework that contained a transition metal ion) [37]. However, for the HOF and CAHOF catalysts to have a similar appeal to other regular active site distribution materials, such as zeolites, MOFs, or COFs, a broader scope of applications has to be investigated. We thought that the CAHOFs present a very promising material, as they can be considered as heterogeneous ionic liquids with a great potential for becoming efficient heterogeneous, purely organic catalysts. In particular, salts that are insoluble in organic solvents and derived from the neutralization of polyacidic and polybasic tectones could be good candidates for becoming efficient heterogeneous Brønsted acids.

Herein, we report the synthesis of a novel, purely organic, charge-assisted hydrogen-bonded self-assembled organic framework **F-1**. The structure of **F-1** was established by single crystal and powder X-ray diffraction, NMR spectroscopy, and elemental analysis. The morphology of **F-1** was assessed by SEM, and its stability was determined by TGA. We report the use of **F-1** as a heterogeneous, robust, and recoverable catalyst for the Brønsted acid-catalyzed ring opening reactions of epoxides with alcohols and water, with the latter reaction occurring in a three-phase medium. In addition, a Diels–Alder reaction was promoted by **F-1** in heptane.

Results and Discussion

Mixing together aqueous solutions of two equivalents of NDS and of one equivalent of TAPM at ambient temperature immediately produced **F-1** as a white precipitate (Scheme 1). The pK_a (in water) of NDS is expected to be −11 to −10, by analogy with the pK_a of polystyrene sulfonic acids [12]. The four pK_as of the conjugated acids of TAPM were calculated (see Supporting Information File 1) to be 4.94, 4.46, 4.04, and 3.79. Thus, the difference in the acidity of the NDS and TAPM components was large enough to ensure a complete salt formation.

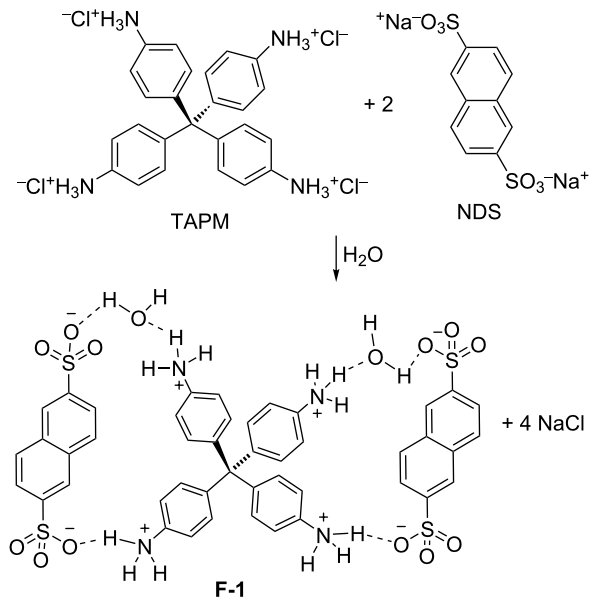

Scheme 1: The synthesis of **F-1**.

Solid **F-1** was practically insoluble in organic solvents with the exception of DMSO. The analytical data supported its structure as depicted in Scheme 1. A crystal of the compound was grown by diffusion of water into a solution of **F-1** in DMSO. The results of the X-ray diffraction analysis are shown in Figure 1. The single crystal material of **F-1** (**F-1a** phase) was in the monoclinic space group $P2_1/c$, with the lattice parameters a = 20.6034(8) Å, b = 20.1330(8) Å, c = 22.4357(8) Å, β = 91.989(1)°, and cell volume = 9300.9(6) Å^3 at 120 K. An asymmetric part of the unit cell contained two ammonium cations, four sulfonate anions, and nine water molecules, held together by numerous hydrogen bonds (Table S2, Supporting Information File 1), so that the resulting three-dimensional network had no macro- or mesopores (Figure S1, Supporting Information File 1). The volume of the unit cell that was potentially accessible to a solvent was only 29.0 Å^3, as calculated by PLATON [38].

The same crystal phase (**F-1a**) was present in **F-1** before the crystallization, as confirmed by powder diffraction data

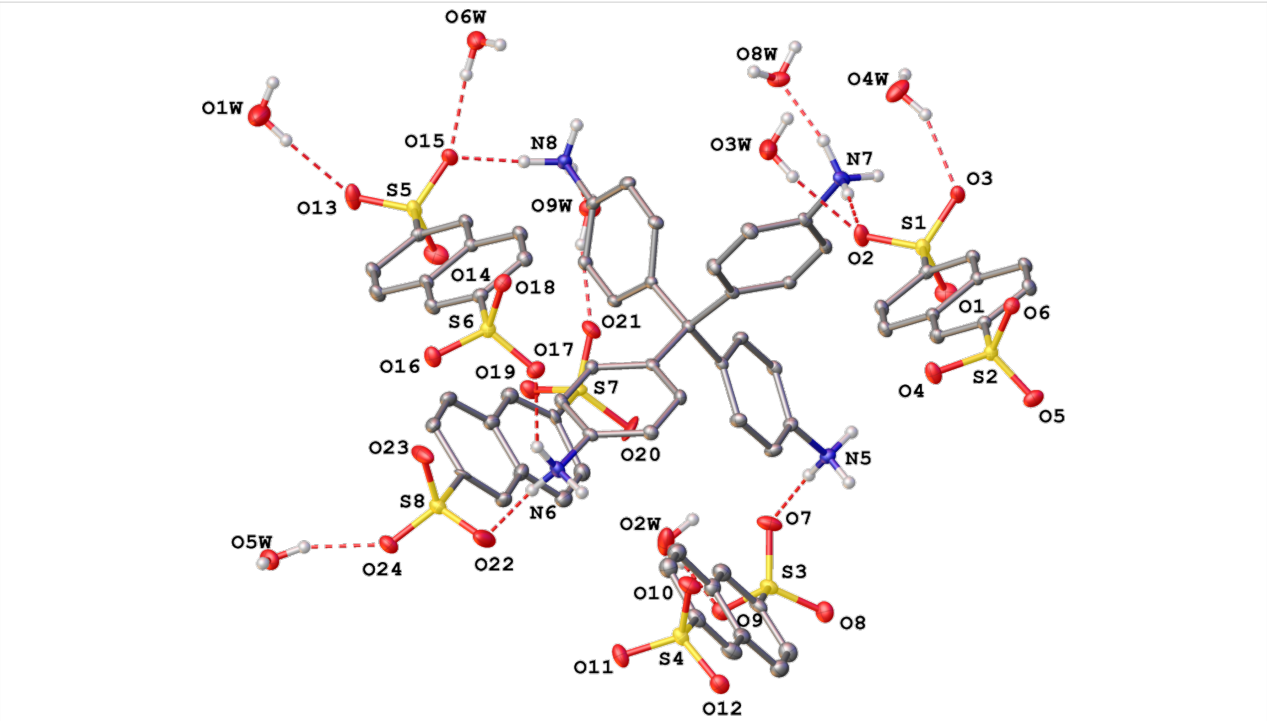

Figure 1: View of the crystal structure of **F-1** (**F-1a** phase), with representation of atoms by thermal ellipsoids at a 30% probability level. The hydrogen atoms, except for those in NH groups and solvate water molecules, were omitted for clarity. Only the labels of symmetry-independent heteroatoms are shown.

collected at room temperature for the white precipitate obtained from the mixed water solutions of TAPM and NDS. Space group $P2_1/c$, a = 20.9609(10) Å, b = 19.7563(9) Å, c = 22.6642(10) Å, β = 92.694(3)°, cell volume = 9375.1(8) Å^3.

When **F-1** was submitted to vacuum drying at 100 °C for several hours, a sample **F-1b** was obtained. X-ray powder diffraction showed that **F-1b** contained a mixture of unknown phases (Figure S3, Supporting Information File 1). However, after a few hours of being exposed to air, it reverted into the phase **F-1a**, the same phase it had before the drying. Space group $P2_1/c$, a = 20.8677(13) Å, b = 20.0951(13) Å, c = 22.6324(15) Å, β = 92.432(5)°, cell volume = 9482.1(11)Å^3 (Figures S4 and S5, Supporting Information File 1). The different powder patterns obtained for the initially formed **F-1** and for **F-1b** immediately after vacuum drying suggested that some structural parameters, such as the water content, varied in the two analyses.

The final proof that the phase change was due to some water molecules escaping the crystal, and this proof came from the X-ray diffraction analysis of heated crystals of **F-1** (with **F-1a** phase) that were immediately put into silicon grease and cooled to 120 K at the diffractometer. The data collection revealed a triclinic P-1 phase, with the lattice parameters a = 13.416(7) Å, b = 13.887(7) Å, c = 22.730(12) Å, α = 88.564(8)°, β = 87.351(8)°, γ = 89.836(9)°, cell volume = 4229(4) Å^3. The resulting structure designated as **F-1** (**F-1a'** phase, Figure 2) had two ammonium cations and four sulfonate dianions in the asymmetric part of the unit cell, with no traces of water molecules. Its three-dimensional network is built by charge-assisted hydrogen bonds between the ions (Table S3, Supporting Information File 1), with small voids occurring near the sulfonate and ammonium groups (Figure S2, Supporting Information File 1). The solvent-accessible volume of the unit cell was 105.8 Å^3, as calculated by PLATON [38]. The dried sample with the **F-1a'** phase readily absorbed water, reverting to the **F-1a** phase with nine molecules of water for every two residues of TAPM within 10–20 minutes of atmospheric exposure.

In addition, **F-1** reversibly took up methanol (1.5 molecules per TAPM moiety), benzene (4–5 molecules per TAPM), and propylene oxide (1.5 molecules per TAPM) in a closed vessel saturated with the vapors of these compounds. The absorbed material changed its PRXD reversibly, returning to its original structure after the absorbed solvent was allowed to evaporate from the sample.

The morphology of uncrystallized **F-1** was studied by scanning electron microscopy (SEM) analysis. It had a "tangerine wedge" morphology (Figure 3 and Figures S9 and S10, Supporting Information File 1), with evident macropores present on the surface of the particles. The size distribution of the **F-1** particles was in the range of 3–5 to 45–50 µm, and most of the particles had a size within a range of 15–30 µm.

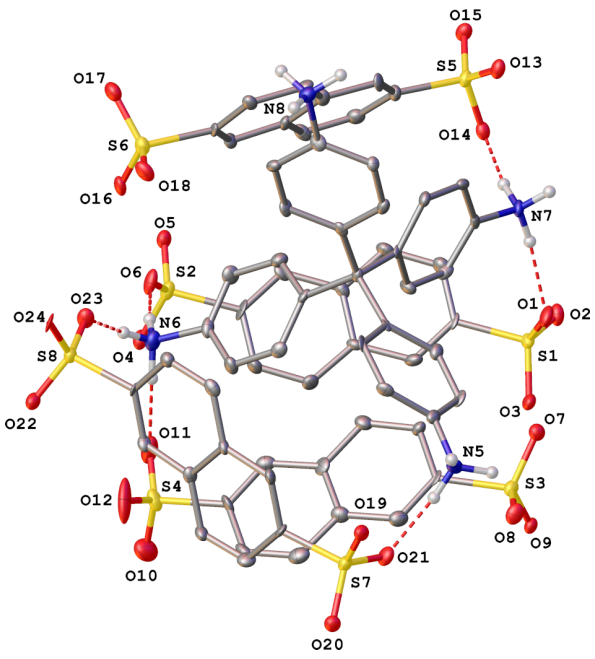

Figure 2: View of the crystal structure of **F-1** (**F-1a'** phase), with representation of the atoms via thermal ellipsoids at a 30% probability level. The hydrogen atoms, except for those in NH groups, were omitted for clarity. Only the labels of symmetry-independent heteroatoms are shown.

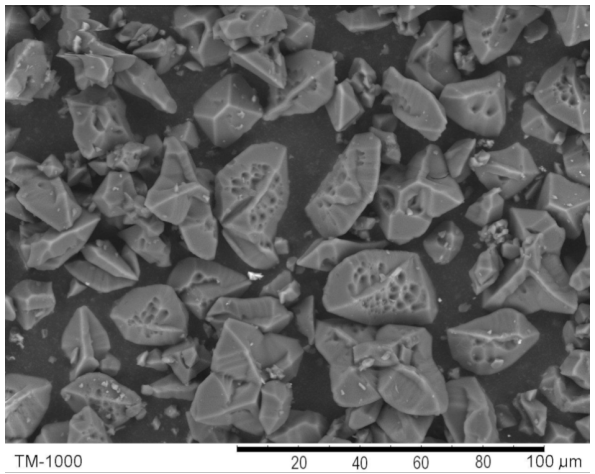

Figure 3: SEM image of **F-1**.

SEM imaging of crystals of **F-1** in the **F-1a** phase formed from a DMSO/water system indicated the existence of two types of crystals (Figure 4). Type 1 was a set of platelets with heights of

0.7–1 mm, grown from a common planar base with a diameter of 0.1–0.3 mm. In other words, the crystals were a typical druse setup. Type 2 were well-formed, nonisotropic crystals with two parallel planes in varying sizes (0.3 × 0.4 × 1 mm).

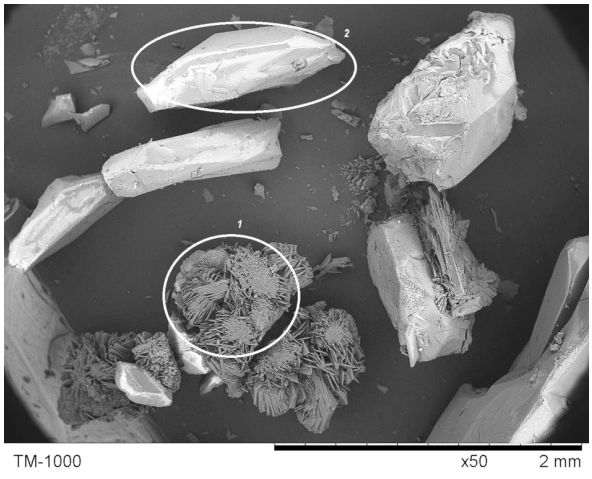

Figure 4: SEM image of **F-1** with an **F-1a** phase.

The thermogravimetric analysis and differential scanning calorimetry (TGA-DSC) of **F-1** was conducted to examine its thermal properties. The TGA curve of the bulk crystals (Figure 5) reached a plateau at 160 °C after 5.9% of the mass was removed as water. The plateau was maintained until 340 °C, when the sample underwent an endothermic decomposition. The decomposition produced sulfur dioxide, naphthalene, and aniline, according to the infrared spectra of the produced gases (Figures S11 and S12, Supporting Information File 1).

The CAHOF **F-1** was also analyzed by nitrogen porosimetry (see Supporting Information File 1). It was found to contain mesopores and macropores with an adsorption average pore width of 5.2 nm, a BET surface area of 2.606 $m^2 \cdot g^{-1}$, a mesopore volume of 0.00093 $cm^3 \cdot g^{-1}$, a macropore volume of 0.00168 $cm^3 \cdot g^{-1}$, and a total pore volume of 0.00336 $cm^3 \cdot g^{-1}$. The porosimetry data could not be directly relevant to the catalytic activity of the composite as the framework as the porosimetry sample needed to be thoroughly degassed prior to the analysis. However, the framework **F-1** underwent "breathing" in organic solvent solutions (see below), which allowed catalytic sites to become available without the need for a pore structure in the desolvated material. The calculated acidity of the components of **F-1** (see above) indicated possible catalytic applications of the material. Thus, the catalytic properties of uncrystallized **F-1** and **F-1** with an **F-1a** phase were explored in a series of reactions typically promoted by Brønsted acids, such as epoxide ring openings with methanol and water (Scheme 2). The reactions were conducted at room temperature,

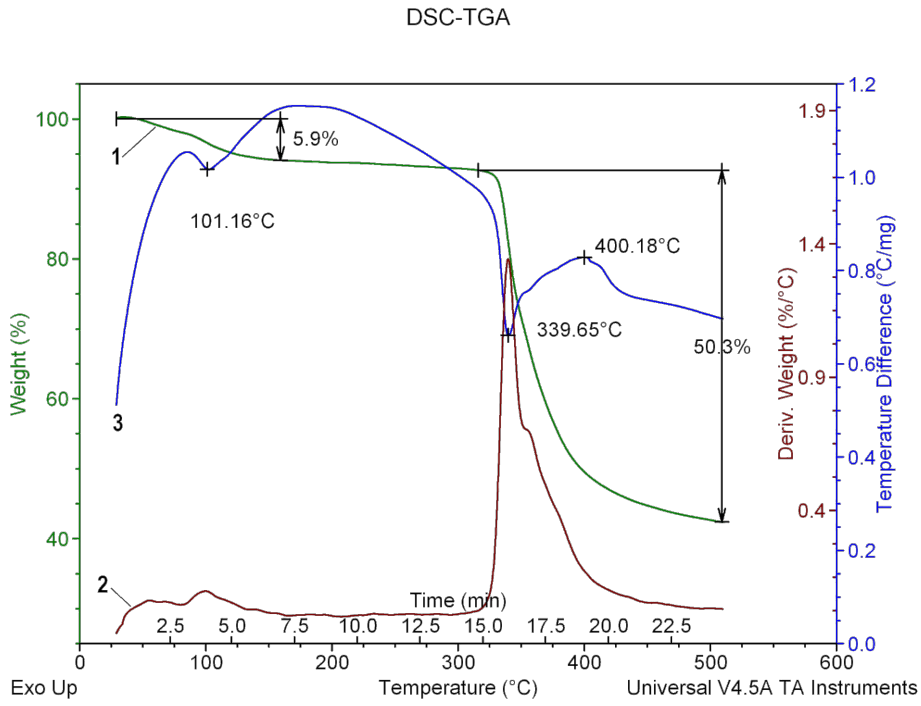

Figure 5: TGA-DSC analysis of a sample of **F-1**. The TGA plot is shown in green, the DSC curve is shown in blue, and the first differential of the DSC curve is shown in red.

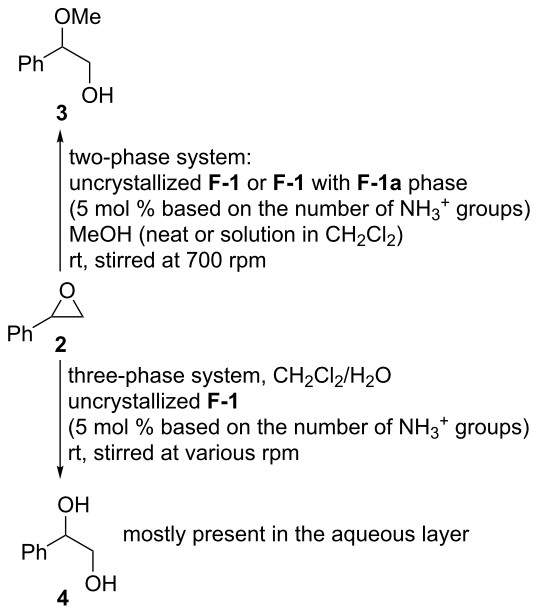

Scheme 2: Uncrystallized **F-1** or **F-1** with an **F-1a** phase promoted the two- and three-phase reactions of styrene oxide (**2**).

and after several hours, the catalyst was removed by centrifugation or filtration through a dense paper filter. The filtrates were evaporated, and the residue was weighed and analyzed by ^{1}H NMR spectroscopy. The experimental results are summarized in Table 1.

Uncrystallized **F-1** promoted the ring opening of styrene oxide (**2**) with methanol. Within 1 hour at room temperature, the alcohol **3** was obtained in a quantitative yield and as a single regioisomer (Table 1, run 2). The CAHOF **F-1** was robust and retained the catalytic activity after being recovered from the reaction mixture five times (Table 1, run 3). In addition, its ^{1}H NMR spectrum was unchanged after being used in five catalytic cycles (Figure S17, Supporting Information File 1). In the absence of a catalyst, no reaction occurred under the experimental conditions (Table 1, run 1). To determine if the reaction was being catalyzed by a homogeneous or heterogeneous species, the CAHOF **F-1** and methanol were mixed together and stirred for 15 minutes. Then, the remaining solid **F-1** was removed by filtration, and the filtrate was tested as a catalyst for the ring opening reaction. The alcohol **3** was obtained in 67% yield (Table 1, run 4), proving that some soluble components of **F-1** were catalytically active, and hence that the reaction was partly catalyzed heterogeneously and partly promoted by the leached catalyst under the experimental conditions. To investigate this in more detail, studies on the solubility of **F-1** in MeOH were conducted by UV–vis spectroscopy at 275 nm (ε = 5670), and it was found that **F-1** had a solubility of 0.25 g/L in MeOH.

Table 1: The ring opening of styrene oxide (**2**) by MeOH or H_2O, promoted by uncrystallized **F-1** or **F-1** with an **F-1a** phase at room temperature.

run	catalyst	nucleophile	*t* (h)	conversion (%)	yield (%)
1	none	MeOH (neat)	24	0	0
2[a]	**F-1**	MeOH (neat)	1	100	>98
3[b]	**F-1**	MeOH (neat)	1	100	>98
4[a,c]	**F-1** filtrate	MeOH (neat)	1	67	67
5[d]	**F-1**	MeOH in CH_2Cl_2	24	56	53–56
6[c,d]	**F-1** filtrate	MeOH in CH_2Cl_2	24	<1	<1
7[d]	**F-1a**	MeOH in CH_2Cl_2	24	24	22
8[e,f]	**F-1**	H_2O/CH_2Cl_2	3	3	3
9[e,g]	**F-1**	H_2O/CH_2Cl_2	3	3	3
10[e,h]	**F-1**	H_2O/CH_2Cl_2	3	40	40
11[e,i]	**F-1**	H_2O/CH_2Cl_2	3	52	52
12[e,j]	**F-1**	H_2O/CH_2Cl_2	3	55	55
13[e,h,k]	**F-1** filtrate	H_2O/CH_2Cl_2	3	45	45
14[e,h]	**F-1**	H_2O/CH_2Cl_2	24	100	95
15[l]	IR-120	H_2O/CH_2Cl_2	3	0	0

[a]Reaction conditions: **2** (0.2 mL, 1.83 mmol), MeOH (10 mL), uncrystallized **F-1** or **F-1** with an **F-1a** phase (0.023 g, 9.61×10^{-5} mol of $^+NH_3$ groups, 5.3 mol %), stirred at 700 rpm (unless indicated otherwise). [b]**F-1** was recovered, and reused five times in pure MeOH. Each of these reactions gave a full conversion after 1 hour, and the yield given is that from the 5th use of the catalyst. [c]**2** (0.2 mL, 1.83 mmol), MeOH (1.5 mL, 36.6 mmol), CH_2Cl_2 (10 mL), uncrystallized **F-1** (or **F-1** with an **F-1a** phase, 0.023 g, 9.61×10^{-5} mol of $^+NH_3$ groups). [d]The same reaction conditions as in the runs 2 or 5, but the catalyst was filtered before the start of the reaction, and the filtrate was used as the catalyst. [e]**2** (1 mL, 9.17 mmol), CH_2Cl_2 (25 mL), and H_2O (50 mL), uncrystallized **F-1** (0.11 g, 0.46 mmol of $^+NH_3$ groups). [f]The reaction was not stirred. [g]The reaction was stirred at 200 rpm. [h]The reaction was stirred at 700 rpm. [i]The reaction was stirred at 1000 rpm. [j]The reaction was stirred at 1400 rpm. [k]The same reaction conditions as in run 10, but the catalyst **F-1** was filtered 15 minutes after the reaction had started, and the filtrate was used as the catalyst. [l]The same conditions as in run 5, but instead of **F-1**, IR-120 in an H^+ form (0.15 g, 0.485 mmol) mixed with $PhNH_2$ (0.485 mmol) was used as a catalyst.

Hence, under the reaction conditions, 10% of **F-1** would be dissolved in the reaction mixture. Table 1, run 4 shows that the activity of the dissolved part of **F-1** was sufficient to bring the reaction to 67% completion but not to obtain the full conversion seen in Table 1, run 2 and run 3 where both the dissolved and undissolved parts of **F-1** coexisted. This indicated that both the dissolved and the heterogeneous parts of the catalyst were catalytically active. Once these reactions were complete, the filtrate was evaporated, and **F-1** was recovered from the residue by sedimentation by addition of dichloromethane. The structure of the recovered **F-1** was the same as that of the undissolved **F-1**, illustrating the self-healing properties of the framework.

The catalyst could be made completely heterogeneous by performing the same CAHOF **F-1**-catalyzed reaction in a less polar medium. For this purpose, the reaction was conducted in a mixture of methanol and dichloromethane (1.5/10 by volume), and the yield of the alcohol **3** was 53–56% after 24 hours (Table 1, run 5). The filtrate derived from the stirred **F-1** in this solvent mixture was catalytically inactive, and after 24 hours, the reaction contained the epoxide **2** and traces of **3** (less than 1% yield, Table 1, run 6). This observation clearly showed that dissolved (leached) parts of **F-1**, even if present, could not be responsible for the catalytic performance. To investigate if any leaching did occur, a sample of the filtrate was evaporated and then dissolved in DMSO-d_6. No resonances corresponding to **F-1** were present in the ^{1}H NMR spectrum of this sample, which supported the absence of any leaching of the catalyst into the reaction medium. The morphology of uncrystallized **F-1** and **F-1** with an **F-1a** phase (Figure 3 and Figure 4) had an influence on the performance of the catalysts. A ground sample of **F-1** with an **F-1a** phase was less active than uncrystallized **F-1** (Table 1, runs 5 and 7).

It is notable that the framework **F-1** (uncrystallized or with an **F-1a** phase), although possessing few or almost no pores, was still catalytically active. An explanation for this involves the potential capacity of the frameworks to react to external stimuli by increasing the distances between the crystal components by, for example, "breathing" in polar solvents. This may disrupt the nondirectional forces in the crystal whilst leaving the directional hydrogen bonds still present so that the framework remained heterogeneous. Notably, simple organic cages that exhibit guest-induced "breathing" and selective gas separation have been reported [29,39-41]. The reversible rearrangement of the crystal framework of a CAHOF derived from the salt of terephthalic acid and tetrakis(4-amidiniumphenyl)methane, in response to the addition of water or the application of heat, also suggested that this "breathing" was feasible [32]. Closely similar behavior was also detected in "flexible" MOFs, which contracted and expanded their pores in the presence of guest gases [42]. In the limiting case, the framework may even become partially dissolved in a polar solvent.

The CAHOF **F-1** was also catalytically active for the conversion of styrene oxide (**2**) into the diol **4** (Table 1, runs 8–14). This reaction was a three-phase system, including two immiscible liquid phases (dichloromethane and water) and solid **F-1**. As the CAHOF **F-1** was insoluble in dichloromethane and poorly soluble in water, the solid catalyst resided between the dichloromethane and water phases. The epoxide **2** was added to this mixture, and the reaction was stirred. After 3 (or 24) hours, the solid catalyst was filtered, the layers were separated, evaporated, and analyzed. The aqueous layer contained only the diol **4** and some dissolved **F-1**. The organic mixture contained a mixture of the epoxide **2** and the diol **4**. Therein, the catalyst was a homogeneous, water-soluble part of **F-1**. The filtered solution was catalytically active to the same extent as the initial heterogeneous one (Table 1, run 13). Thus, in this case, solid **F-1** served mostly as a reservoir for the production of the soluble catalyst, although the dissolved part could easily be recovered by evaporating the aqueous layer, adding dichloromethane to the residue and filtering the insoluble catalyst.

The efficiency of the multiphase reactions should depend on the rate of stirring the reaction. The runs 8–12 in Table 1 illustrated the dependence of the yield of the diol **4** on the stirring velocity over a three-hour reaction period. Expectedly, without any stirring, the hydrolysis did not proceed (Table 1, run 8), and the same poor performance occurred at a stirring rate of 200 rpm (Table 1, run 9). When the stirring rate was increased to 700 rpm, the yield of diol **4** increased to 40% (Table 1, run 10). There was little dependence of the product yield (40–55%) on the stirring rate above the threshold of 700 rpm (Table 1, runs 10–12). A complete conversion of the epoxide **2** into the diol **4** was observed after a reaction time of 24 hours at a stirring rate of 700 rpm (Table 1, entry 14).

Both the pH of the medium (specific acid catalysis) and general acid catalysis by the ammonium groups of **F-1** were potentially important for the ring opening reactions. The ring openings were conducted in three different media: neat methanol, a mixture of methanol and dichloromethane, and a mixture of water and dichloromethane. The methanol and dichloromethane mixture did not need to be considered as **F-1** was not soluble in this mixture. For the other two solvent mixtures, the four ammonium groups of the protonated form of TAPM had pK_a values in water (according to the calculations discussed above) ranging from 5.0 to 3.8. The solubility of **F-1** in water was determined by UV–vis spectroscopy to be 0.9 g/L. This corresponded to approximately 50% of the catalyst **F-1** being dissolved in the water phase of the reactions reported in Table 1, runs 12–14.

The concentration of the ammonium groups was then 4.0×10^{-2} M in water. Assuming that the average pK_a value of the ammonium groups of the protonated form of TAPM was around 4.0, the pH value of the solution would be between 4 and 5. It is therefore most likely that **F-1** operated via the general acid catalysis mechanism in this solvent mixture. As the pK_a value of anilinium cations will only change to a small extent when the solvent is changed from water to methanol, the same general acid catalysis mechanism would be expected to occur in reactions carried out in methanol.

For comparison, the commercially available (and most often used heterogeneous Brønsted acid catalyst) cation exchange resin IR-120, which contains sulfonic acid functionalities, was mixed in its hydrogen form with aniline to give a model of **F-1**. An attempted use of the resulting compound with the same amount of ammonium groups as in **F-1** for the conversion of the epoxide **2** into the alcohol **3** was unsuccessful (Table 1, run 15). Evidently, the catalytic properties of the CAHOF **F-1** were superior to those of standard ion exchange materials under these reaction conditions.

The CAHOF **F-1** could also promote the ring opening of cyclohexene oxide (**5**) by alcohols (Scheme 3), with the efficiency of the reaction dropping as the size of the alcohol was increased and its polarity decreased (Table 2, runs 1–3). Water could also be used as the nucleophile (Table 2, runs 4 and 5) and led to the *trans*-cyclohexane diol **6** under the same experimental conditions used for the styrene oxide ring opening. Other epoxides were also studied as substrates for the three-phase ring-opening with water (Table 2, runs 6–9). Propylene oxide and butylene oxide were good substrates for the reaction (Table 2, runs 6 and 7), but hex-1-ene oxide was almost unreactive (Table 2, runs 8 and 9), indicating that some partitioning of the epoxide into the aqueous phase was necessary for reaction to occur. Cyclohexene oxide (**5**) is, however, a good substrate under the same reaction conditions (Table 2, entry 5), possibly due to the greater reactivity of its fused bicyclic ring system.

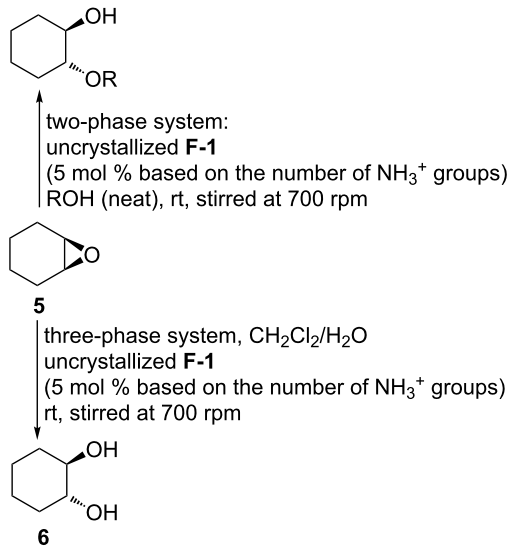

Scheme 3: CAHOF **F-1**-promoted reactions of cyclohexene oxide (**5**) with alcohols and water.

The Diels–Alder reaction of methyl vinyl ketone with cyclopentadiene was also efficiently promoted by the CAHOF **F-1** in heptane at room temperature (Scheme 4). After three hours, the catalyst was filtered, and the filtrate was evaporated to give a mixture of the *endo* and *exo* adducts in a 3.5:1 ratio and a yield of 52%. A reaction carried out under the same conditions in the absence of **F-1** produced the Diels–Alder adduct in a yield of just 10%.

Table 2: Ring opening of epoxides by water or alcohols promoted by **F-1** at room temperature.[a]

run	epoxide	nucleophile	*t* (h)	yield (%) (by ^{1}H NMR)
1	**5**	MeOH	4	98
2	**5**	EtOH	4	20
3	**5**	iPrOH	4	<1
4	**5**	H_2O/CH_2Cl_2	3	20
5	**5**	H_2O/CH_2Cl_2	24	80
6	propylene oxide	H_2O/CH_2Cl_2	24	82
7[b]	butylene oxide	H_2O/CH_2Cl_2	24	60
8[b]	hex-1-ene oxide	H_2O/CH_2Cl_2	24	2
9[b]	hex-1-ene oxide	H_2O/CH_2Cl_2	144	10

[a]The epoxide (1.83×10^{-3} mol) in 10 mL of alcohol or in a mixture of 5 mL CH_2Cl_2 and 10 mL H_2O was stirred at 700 rpm with **F-1** (0.023 g, 9.61×10^{-5} mol of $^+NH_3$ groups, 5.3 mol %). [b]The yields were determined by ^{1}H NMR spectroscopy, directly from the reaction mixture, by running the experiments in D_2O.

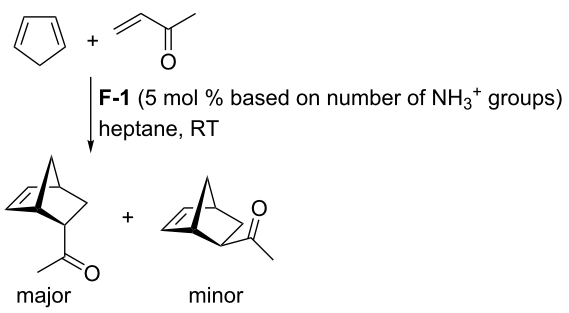

Scheme 4: F-1-promoted Diels–Alder reaction.

Conclusion

In summary, by utilizing the acid–base neutralization reaction between two equivalents of NDS and one equivalent of the tetrahydrochloride salt of TAPM in water, a novel three-dimensional material **F-1** was prepared and characterized by X-ray diffraction, TGA-DSC, elemental analysis, and ^{1}H NMR spectroscopy. One important role played by NDS was that the crystalline three-dimensional CAHOF **F-1** was supported by hydrogen bonds between the sulfonate anions and the ammonium cations of NDS and TAPM, respectively. By virtue of the three oxygen atoms of each sulfonate of NDS, through which the negative charge was distributed, NDS could support different crystalline arrangements, as shown in Figure 1 and Figure 2.

The framework **F-1** was able to reversibly absorb solvents and water in a process called "breathing". The material served as a new type of Brønsted acid catalyst in a series of reactions, including epoxide ring opening reactions and a Diels–Alder reaction. A second role for NDS was that one of its sulfonate oxygen atoms could form hydrogen bonds with water whilst leaving the other two oxygen atoms to engage the ammonium groups of TAPM (see the crystal structure of the **F-1a** phase). This structure was thermodynamically stable and hinted at a possible activation of water or methanol as nucleophiles by the sulfate anions during the ring opening of epoxides. When the coordinated water was removed by drying at higher temperatures, another phase, **F-1a'**, was formed (Figure 2). A greater amount of vacant space appeared in the crystal, and the structure became thermodynamically unstable. It reverted to the original **F-1a** phase over a few hours when water was present in the surrounding atmosphere.

Depending on the polarity of the solvent mixture, **F-1** could function as a purely heterogeneous catalyst or as a reservoir, providing some soluble **F-1** as the real catalyst. In all cases the catalyst could easily be recovered and recycled. The system has the potential for future elaboration, for example, by incorporating multitopic tectons with a greater number of negatively charged sulfonate groups mutually rigidly fixed in space. Such arrangement should produce large pores within the framework and further reduce the framework's solubility in water and organic solvents. Additionally, the acidity of these frameworks could be tuned by varying the ratio of anion/cation multitopic components and the basicity of the cation component.

Supporting Information

Supporting Information File 1

Experimental, characterization, and pK_a calculation details as well as SEM and TGA analyses.
[https://www.beilstein-journals.org/bjoc/content/supplementary/1860-5397-16-99-S1.pdf]

Supporting Information File 2

X-ray details for **F-1** (**F-1a** phase).
[https://www.beilstein-journals.org/bjoc/content/supplementary/1860-5397-16-99-S2.cif]

Supporting Information File 3

X-ray details for **F-1** (**F-1a'** phase).
[https://www.beilstein-journals.org/bjoc/content/supplementary/1860-5397-16-99-S3.cif]

Acknowledgements

The Siberian branch of the Russian Academy of Sciences (SB RAS) Siberian Supercomputer Center is gratefully acknowledged for providing supercomputer facilities.

Funding

The X-ray diffraction data were collected with financial support from the Ministry of Science and Higher Education of the Russian Federation using the equipment of the Center for Molecular Composition Studies of INEOS RAS. Quantum chemical calculations were performed with financial support from RFBR (#17-03-00907). The publication has been prepared with the support of the "RUDN University Program 5-100" (V.A.L., PXRD investigation). The authors gratefully acknowledge financial support from a RFBR research grant No 18–53-05004 Arm-a.

ORCID® iDs

Vladimir A. Larionov - https://orcid.org/0000-0003-3535-1292
Michael North - https://orcid.org/0000-0002-6668-5503
Vladimir P. Zhereb - https://orcid.org/0000-0002-0013-4282
Michael G. Medvedev - https://orcid.org/0000-0001-7070-4052
Yuri N. Belokon - https://orcid.org/0000-0002-9859-2512

References

1. Busacca, C. A.; Fandrick, D. R.; Song, J. J.; Senanayake, C. H. *Adv. Synth. Catal.* **2011,** *353,* 1825–1864. doi:10.1002/adsc.201100488
2. Schlögl, R. *ChemCatChem* **2017,** *9,* 533–541. doi:10.1002/cctc.201700026
3. Hayler, J. D.; Leahy, D. K.; Simmons, E. M. *Organometallics* **2019,** *38,* 36–46. doi:10.1021/acs.organomet.8b00566
4. Sartori, G.; Maggi, R. *Chem. Rev.* **2011,** *111,* PR181–PR214. doi:10.1021/cr100375z
5. Climent, M. J.; Corma, A.; Iborra, S. *Chem. Rev.* **2011,** *111,* 1072–1133. doi:10.1021/cr1002084
6. Clot-Almenara, L.; Rodríguez-Escrich, C.; Osorio-Planes, L.; Pericàs, M. A. *ACS Catal.* **2016,** *6,* 7647–7651. doi:10.1021/acscatal.6b02621
7. Jones, C. W. *Top. Catal.* **2010,** *53,* 942–952. doi:10.1007/s11244-010-9513-9
8. Mayani, V. J.; Abdi, S. H. R.; Kureshy, R. I.; Khan, N.-u. H.; Das, A.; Bajaj, H. C. *J. Org. Chem.* **2010,** *75,* 6191–6195. doi:10.1021/jo1010679
9. Kohrt, C.; Werner, T. *ChemSusChem* **2015,** *8,* 2031–2034. doi:10.1002/cssc.201500128
10. Wegener, S. L.; Marks, T. J.; Stair, P. C. *Acc. Chem. Res.* **2012,** *45,* 206–214. doi:10.1021/ar2001342
11. Copéret, C.; Comas-Vives, A.; Conley, M. P.; Estes, D. P.; Fedorov, A.; Mougel, V.; Nagae, H.; Núñez-Zarur, F.; Zhizhko, P. A. *Chem. Rev.* **2016,** *116,* 323–421. doi:10.1021/acs.chemrev.5b00373
12. Konwar, L. J.; Mäki-Arvela, P.; Mikkola, J.-P. *Chem. Rev.* **2019,** *119,* 11576–11630. doi:10.1021/acs.chemrev.9b00199
13. Cook, T. R.; Zheng, Y.-R.; Stang, P. J. *Chem. Rev.* **2013,** *113,* 734–777. doi:10.1021/cr3002824
14. Diercks, C. S.; Kalmutzki, M. J.; Diercks, N. J.; Yaghi, O. M. *ACS Cent. Sci.* **2018,** *4,* 1457–1464. doi:10.1021/acscentsci.8b00677
15. Gascon, J.; Corma, A.; Kapteijn, F.; Llabrés i Xamena, F. X. *ACS Catal.* **2014,** *4,* 361–378. doi:10.1021/cs400959k
16. Li, X.; Wu, J.; He, C.; Meng, Q.; Duan, C. *Small* **2019,** *15,* 1804770. doi:10.1002/smll.201804770
17. Yuan, G.; Jiang, H.; Zhang, L.; Liu, Y.; Cui, Y. *Coord. Chem. Rev.* **2019,** *378,* 483–499. doi:10.1016/j.ccr.2017.10.032
18. Zhai, Q.-G.; Bu, X.; Zhao, X.; Li, D.-S.; Feng, P. *Acc. Chem. Res.* **2017,** *50,* 407–417. doi:10.1021/acs.accounts.6b00526
19. Waller, P. J.; Gándara, F.; Yaghi, O. M. *Acc. Chem. Res.* **2015,** *48,* 3053–3063. doi:10.1021/acs.accounts.5b00369
20. Li, H.; Pan, Q.; Ma, Y.; Guan, X.; Xue, M.; Fang, Q.; Yan, Y.; Valtchev, V.; Qiu, S. *J. Am. Chem. Soc.* **2016,** *138,* 14783–14788. doi:10.1021/jacs.6b09563
21. Xu, H.-S.; Ding, S.-Y.; An, W.-K.; Wu, H.; Wang, W. *J. Am. Chem. Soc.* **2016,** *138,* 11489–11492. doi:10.1021/jacs.6b07516
22. Zhang, J.; Han, X.; Wu, X.; Liu, Y.; Cui, Y. *J. Am. Chem. Soc.* **2017,** *139,* 8277–8285. doi:10.1021/jacs.7b03352
23. Wu, X.; Han, X.; Xu, Q.; Liu, Y.; Yuan, C.; Yang, S.; Liu, Y.; Jiang, J.; Cui, Y. *J. Am. Chem. Soc.* **2019,** *141,* 7081–7089. doi:10.1021/jacs.9b02153
24. Tan, C.; Jiao, J.; Li, Z.; Liu, Y.; Han, X.; Cui, Y. *Angew. Chem., Int. Ed.* **2018,** *57,* 2085–2090. doi:10.1002/anie.201711310
25. Fournier, J.-H.; Maris, T.; Wuest, J. D. *J. Org. Chem.* **2004,** *69,* 1762–1775. doi:10.1021/jo0348118
26. Hu, F.; Liu, C.; Wu, M.; Pang, J.; Jiang, F.; Yuan, D.; Hong, M. *Angew. Chem., Int. Ed.* **2017,** *56,* 2101–2104. doi:10.1002/anie.201610901
27. Yin, Q.; Zhao, P.; Sa, R.-J.; Chen, G.-C.; Lü, J.; Liu, T.-F.; Cao, R. *Angew. Chem., Int. Ed.* **2018,** *57,* 7691–7696. doi:10.1002/anie.201800354
28. Zhou, Y.; Kan, L.; Eubank, J. F.; Li, G.; Zhang, L.; Liu, Y. *Chem. Sci.* **2019,** *10,* 6565–6571. doi:10.1039/c9sc00290a
29. Wang, H.; Li, B.; Wu, H.; Hu, T.-L.; Yao, Z.; Zhou, W.; Xiang, S.; Chen, B. *J. Am. Chem. Soc.* **2015,** *137,* 9963–9970. doi:10.1021/jacs.5b05644
30. Xing, G.; Yan, T.; Das, S.; Ben, T.; Qiu, S. *Angew. Chem., Int. Ed.* **2018,** *57,* 5345–5349. doi:10.1002/anie.201800423
31. Karmakar, A.; Illathvalappil, R.; Anothumakkool, B.; Sen, A.; Samanta, P.; Desai, A. V.; Kurungot, S.; Ghosh, S. K. *Angew. Chem., Int. Ed.* **2016,** *55,* 10667–10671. doi:10.1002/anie.201604534
32. Morshedi, M.; Thomas, M.; Tarzia, A.; Doonan, C. J.; White, N. G. *Chem. Sci.* **2017,** *8,* 3019–3025. doi:10.1039/c7sc00201g
33. Boer, S. A.; Morshedi, M.; Tarzia, A.; Doonan, C. J.; White, N. G. *Chem. – Eur. J.* **2019,** *25,* 10006–10012. doi:10.1002/chem.201902117
34. Zaręba, J. K.; Białek, M. J.; Janczak, J.; Zoń, J.; Dobosz, A. *Cryst. Growth Des.* **2014,** *14,* 6143–6153. doi:10.1021/cg501348g
35. Liu, Y.; Hu, C.; Comotti, A.; Ward, M. D. *Science* **2011,** *333,* 436–440. doi:10.1126/science.1204369
36. Liang, W.; Carraro, F.; Solomon, M. B.; Bell, S. G.; Amenitsch, H.; Sumby, C. J.; White, N. G.; Falcaro, P.; Doonan, C. J. *J. Am. Chem. Soc.* **2019,** *141,* 14298–14305. doi:10.1021/jacs.9b06589
37. Gong, W.; Chu, D.; Jiang, H.; Chen, X.; Cui, Y.; Liu, Y. *Nat. Commun.* **2019,** *10,* 600. doi:10.1038/s41467-019-08416-6
38. Spek, A. L. *Acta Crystallogr., Sect. D: Biol. Crystallogr.* **2009,** *65,* 148–155. doi:10.1107/s090744490804362x
39. Wang, Z.; Sikdar, N.; Wang, S.-Q.; Li, X.; Yu, M.; Bu, X.-H.; Chang, Z.; Zou, X.; Chen, Y.; Cheng, P.; Yu, K.; Zaworotko, M. J.; Zhang, Z. *J. Am. Chem. Soc.* **2019,** *141,* 9408–9414. doi:10.1021/jacs.9b04319
40. Bao, Z.; Xie, D.; Chang, G.; Wu, H.; Li, L.; Zhou, W.; Wang, H.; Zhang, Z.; Xing, H.; Yang, Q.; Zaworotko, M. J.; Ren, Q.; Chen, B. *J. Am. Chem. Soc.* **2018,** *140,* 4596–4603. doi:10.1021/jacs.7b13706
41. Zhu, A.-X.; Yang, Q.-Y.; Kumar, A.; Crowley, C.; Mukherjee, S.; Chen, K.-J.; Wang, S.-Q.; O'Nolan, D.; Shivanna, M.; Zaworotko, M. J. *J. Am. Chem. Soc.* **2018,** *140,* 15572–15576. doi:10.1021/jacs.8b08642
42. Taylor, M. K.; Runčevski, T.; Oktawiec, J.; Bachman, J. E.; Siegelman, R. L.; Jiang, H.; Mason, J. A.; Tarver, J. D.; Long, J. R. *J. Am. Chem. Soc.* **2018,** *140,* 10324–10331. doi:10.1021/jacs.8b06062

BEILSTEIN JOURNAL OF ORGANIC CHEMISTRY

Synthesis of pyrrolidinedione-fused hexahydropyrrolo[2,1-*a*]isoquinolines via three-component [3 + 2] cycloaddition followed by one-pot *N*-allylation and intramolecular Heck reactions

Xiaoming Ma[*1], Suzhi Meng[1], Xiaofeng Zhang[2,3], Qiang Zhang[4], Shenghu Yan[1], Yue Zhang[1] and Wei Zhang[*2]

Full Research Paper

Open Access

Address:
[1]School of Pharmaceutical Engineering and Life Science, Changzhou University, Changzhou 213164, China, [2]Center for Green Chemistry and Department of Chemistry, University of Massachusetts Boston, 100 Morrissey Boulevard, Boston, MA 02125, USA, [3]Department of Cancer Biology, Dana-Farber Cancer Institute, Department of Medicine, Harvard Medical School, Boston, MA 02215, USA and [4]School of Chemistry, Biology and Materials Engineering, Suzhou University of Science and Technology, Suzhou 215009, China

Email:
Xiaoming Ma[*] - mxm.wuxi@cczu.edu.cn; Wei Zhang[*] - wei2.zhang@umb.edu

* Corresponding author

Keywords:
[3 + 2] cycloaddition; Heck reaction; hexahydropyrrolo[2,1-*a*]isoquinoline; one-pot reactions

Beilstein J. Org. Chem. **2020,** *16,* 1225–1233.
doi:10.3762/bjoc.16.106

Received: 15 March 2020
Accepted: 26 May 2020
Published: 04 June 2020

This article is part of the thematic issue "Green chemistry II".

Guest Editor: L. Vaccaro

Abstract

Two kinds of [3 + 2] cycloaddition intermediates generated from the three-component reactions of 2-bromobenzaldehydes and maleimides with amino esters or amino acids were used for a one-pot *N*-allylation and intramolecular Heck reactions to form pyrrolidinedione-fused hexahydropyrrolo[2,1-*a*]isoquinolines. The multicomponent reaction was combined with one-pot reactions to make a synthetic method with good pot, atom and step economy. MeCN was used as a preferable green solvent for the reactions.

Introduction

Pyrrolo[2,1-*a*]isoquinoline and hexahydropyrrolo[2,1-*a*]isoquinoline are privileged heterocyclic rings existing in many natural products and synthetic compounds possessing antitumor, antibacterial, antiviral, antioxidizing, and other biological activities (Figure 1) [1,2]. For example, the alkaloid crispine A isolated from *Carduus crispus L* has antitumor activity [3]. Erythrina alkaloids have curare-like neuromuscular blocking activities [4], and also antioxidant activity against

DPPH free radicals [5]. Lamellarins isolated from marine invertebrates [6] are inhibitors for HIV-1 integrase and also have immuno modulatory activity [7,8]. Trolline has inhibitory activity against Gram-negative and Gram-positive bacteria [9], also as free radical scavenger in rat brain [10]. Organic chemists have been continuously interested in the development of methods for the synthesis of pyrrolo[2,1-*a*]isoquinolines and related ring systems [11-15], while medicinal chemists have also been interested in making related compounds for biological screening and drug development [16,17].

Multicomponent reactions (MCRs) have been developed as highly efficient tools for assembling heterocyclic scaffolds related to natural products [18-20]. Among the well-established MCRs, three-component 1,3-dipolar cycloadditions of benzaldehydes, maleimides, and amino esters have been developed for making *N*-containing 5-membered heterocycles (Scheme 1) [21,22]. The [3 + 2] cycloadditions of maleimides with stabilized azomethine ylides **I-a** generated from the condensation of aldehydes and amino esters for making pyrrolidines **II-a** have been well-reported [23-26], while the [3 + 2] cycloaddition of the less stable azomethine ylides **I-b** generated from the reaction of aldehydes and amino acids for pyrrolidines **II-b** was less explored [27-29].

In recent years, our lab has reported a series of 1,3-dipolar cycloaddition-initiated methods for the synthesis of diverse heterocycles **A**–**J** bearing fused polycyclic rings such as tetrahydroepiminobenzo[*b*]azocines, tetrahydropyrrolobenzodiazepinones, triazolobenzodiazepines and tetrahydrochromeno[3,4-*b*]pyrrolizine (Scheme 2) [30-39]. Many of these scaffolds were synthesized through the combination of MCR and one-pot synthesis. A literature search indicated that a [3 + 2] cycloaddition-initiated method has also been used for the synthesis of hexahydropyrrolo[2,1-*a*]isoquinolines by employing stable 1,3-dilpolar compounds generated from amino

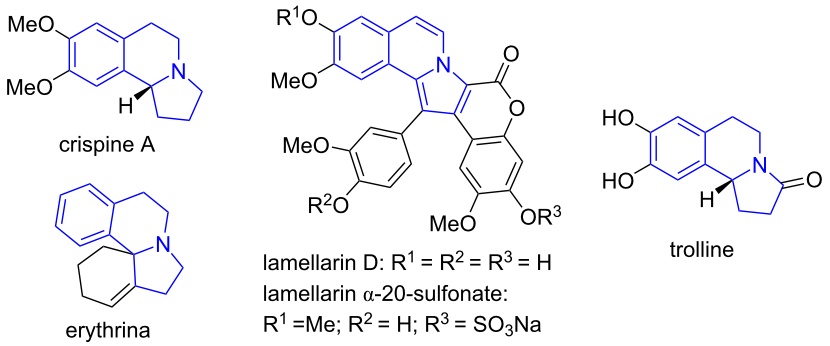

Figure 1: Bioactive pyrrolo[2,1-*a*]isoquinolines and hexahydropyrrolo[2,1-*a*]isoquinolines.

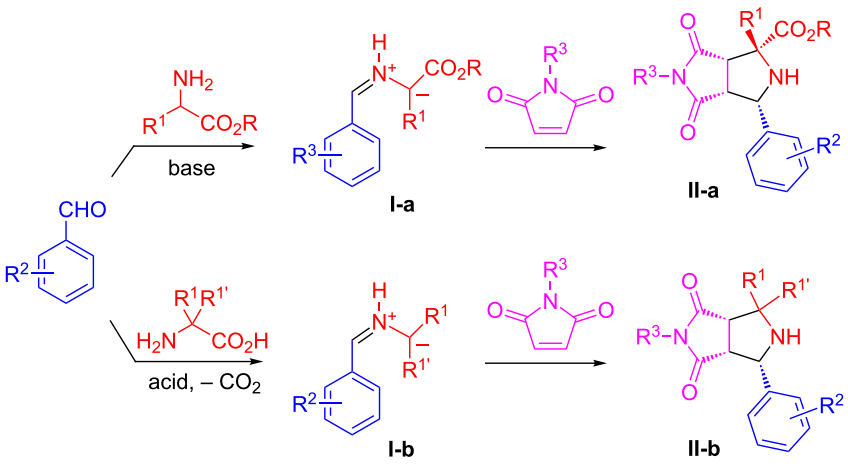

Scheme 1: [3 + 2] Cycloaddition with amino esters or amino acids.

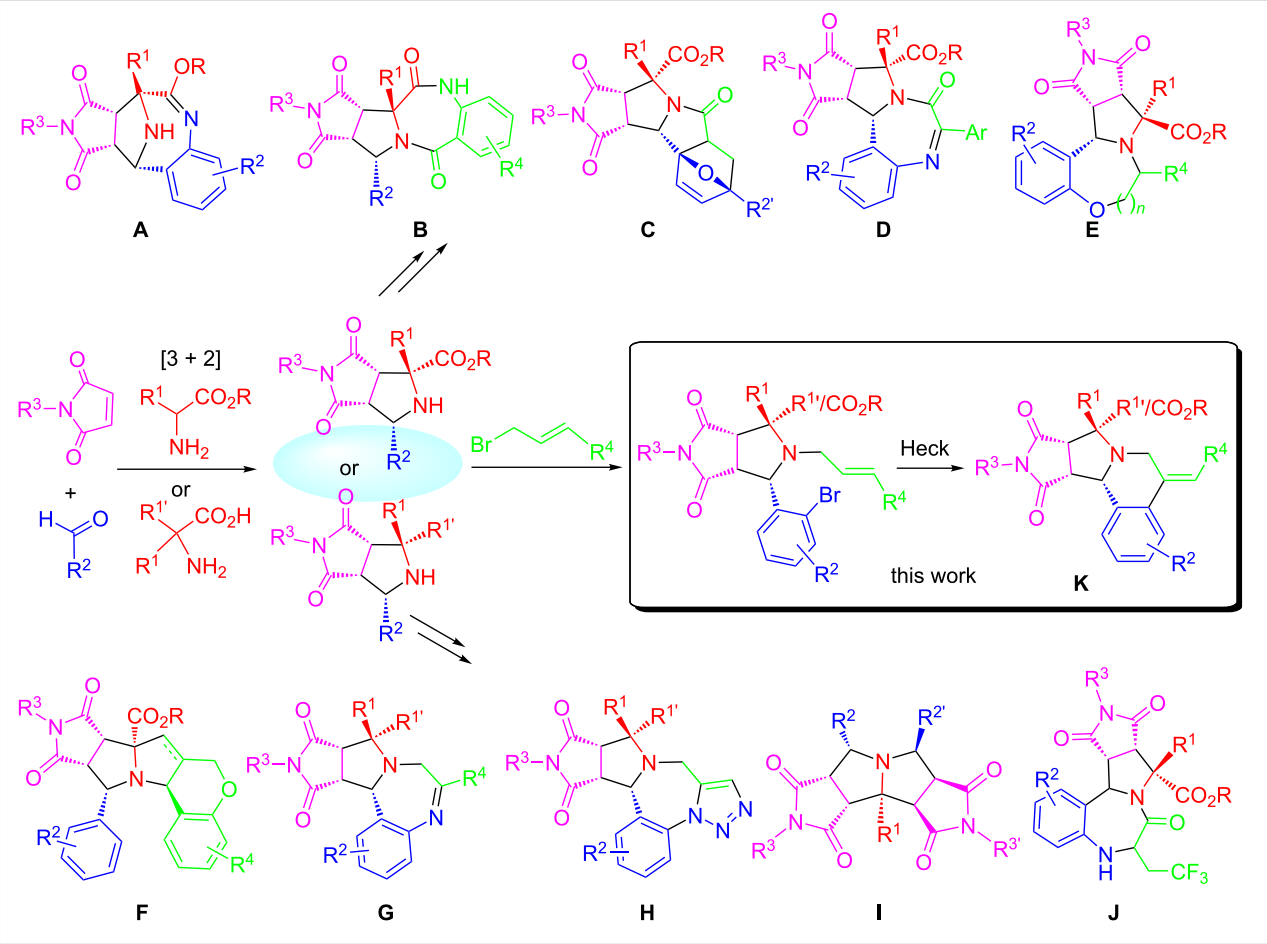

Scheme 2: Scaffolds derived from the initial [3 + 2] adducts.

esters [15,40] or isoquinolines [41-49]. We like to report in this paper our effort on the synthesis of pyrrolidinedione-fused hexahydropyrrolo[2,1-*a*]isoquinolines via sequential 1,3-dipolar cycloaddition, *N*-allylation, and intramolecular Heck cyclization reactions [50-54] (Scheme 2, **K**). Both stabilized and non-stabilized azomethine ylides could be used for the initial [3 + 2] cycloaddition. A multicomponent reaction was combined with one-pot reactions to make it a green synthetic method with pot, atom and step economy (PASE) [55,56].

Results and Discussion

Following the reported procedures for amino ester- and amino acid-based [3 + 2] cycloaddition reactions, pyrrolidine adducts **5** and **6** were synthesized by a three-component reaction of **1** or **2** with 2-bromobenzaldehydes **3** and maleimides **4** (Scheme 3) [30,37]. The cycloaddition reactions were diastereoselective (>20:1 dr for adducts **5** and >6:1 dr for adducts **6**). The major diastereomers of **5** and **6** were isolated for following *N*-allylation and intramolecular Heck reactions.

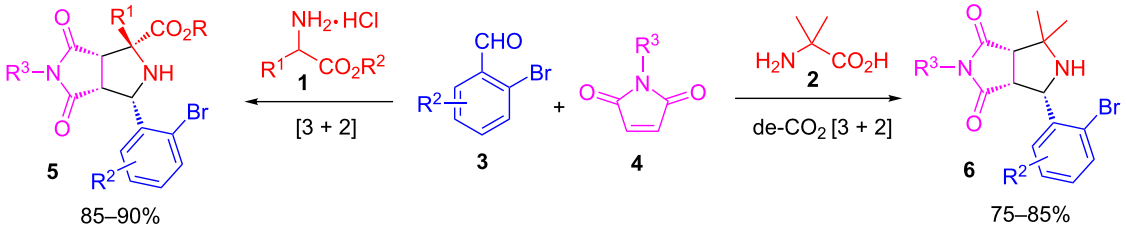

Scheme 3: [3 + 2] Cycloaddition with amino esters or amino acids. Conditions: **1**:**3**:**4** (1.2:1:1.1), Et_3N (1.5 equiv), EtOH (3 mL), 110 °C for 6 h; **2**:**3**:**4** (1.2:1:1), AcOH (0.3 equiv), MeCN (3 mL), 110 °C for 6 h.

Adduct **5a** generated from [3 + 2] cycloaddition was used as a model compound to develop the reaction conditions for the one-pot *N*-allylation and intramolecular Heck reactions (Table 1). *N*-Allylation of **5a** with 3-bromopropene (**7**) for **8a** was accomplished by heating the reaction mixtures in MeCN at 105 °C for 4 h. After evaporating unreacted 3-bromopropene (**7**) from the reaction mixture, crude product **8a** was used for developing the intramolecular Heck reaction by screening Pd(II) catalysts, ligands, bases, additives, solvents, temperatures and reaction time (Table 1). The initial intramolecular Heck reactions were carried out using 10 mol % of $Pd(OAc)_2$ or 10 mol % of $PdCl_2$ with 20 mol % of PPh_3 as a ligand and 2 equiv of K_2CO_3 in MeCN at 80 °C for 10 h without additive to give 6-*exo*-cyclized product **9a** in 32% and 18% yields, respectively (Table 1, entries 1 and 2). Addition of NaOAc increased the yield of **9a** to 71% (Table 1, entry 3). Other attempts to improve the Heck reaction using different ligands, such as ($P(o\text{-tol})_3$, PCy_3 and dppm, were not successful (Table 1, entries 4–6). The reaction at 105 °C in MeCN gave **9a** in 78% yield (Table 1, entry 7), while at 120 °C in DMF gave **9a** in 77% yield (Table 1, entry 11). Reducing the amount of $Pd(OAc)_2$ to 5 mol % or the reaction temperature to 40 °C gave lower product yields (Table 1, entries 8 and 10). Double the amount of $Pd(OAc)_2$ to 20 mol% gave **9a** in 79% yield, just 1% increase than that of using 10 mol % of catalyst (Table 1, entry 9). Besides K_2CO_3, other bases including Na_2CO_3, Cs_2CO_3 and Et_3N were also used for the Heck reaction, but none of them improved the product yield (Table 1, entries 12–14). A base-free control reaction gave **9a** in 10% yield (Table 1, entry 15). Thus, the optimized conditions for the Heck reaction was to use 10 mol % of $Pd(OAc)_2$, 20 mol % of PPh_3, 2 equiv of K_2CO_3 and 1 equiv of NaOAc in 3 mL of MeCN at 105 °C for 3 h which give **9a** in 78% yield (Table 1, entry 7). It is worth noting that there was no **9ab** observed as a byproduct because 6-*exo* cyclization is more favorable [50,51].

The optimized reaction conditions were then employed for the synthesis of analogs of **9** (Scheme 4). A variety of [3 + 2] cycloaddition adducts **5** bearing different R, R^1, R^2 and R^3 groups, derived from amino esters **1**, 2-bromobenzaldehydes **3** and maleimides **4**, were subjected to *N*-allylation followed by intramolecular Heck reaction to pyrrolidinedione-fused hexahy-

Table 1: Optimization of the one-pot reaction conditions.[a]

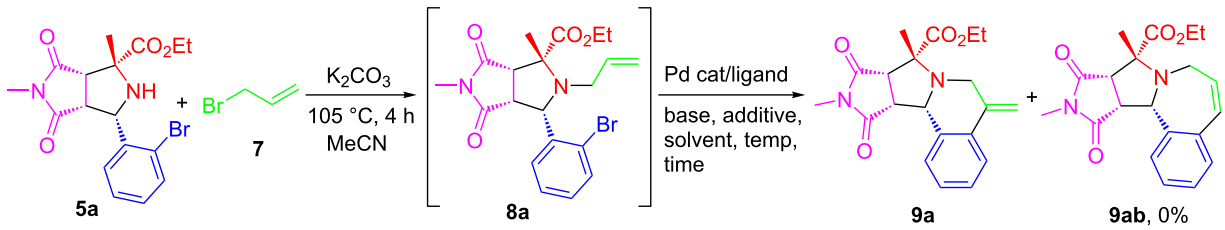

entry	Pd Cat.	ligand	base	additive	solvent	temp [°C]	time [h]	yield [%][b]
1	$Pd(OAc)_2$	PPh_3	K_2CO_3	–	MeCN	80	10	32
2	$PdCl_2$	PPh_3	K_2CO_3	–	MeCN	80	10	18
3	$Pd(OAc)_2$	PPh_3	K_2CO_3	NaOAc	MeCN	80	6	71
4	$Pd(OAc)_2$	$P(o\text{-tol})_3$	K_2CO_3	NaOAc	MeCN	80	6	61
5	$Pd(OAc)_2$	PCy_3	K_2CO_3	NaOAc	MeCN	80	6	45
6	$Pd(OAc)_2$	dppm	K_2CO_3	NaOAc	MeCN	80	6	58
7	**$Pd(OAc)_2$**	**PPh_3**	**K_2CO_3**	**NaOAc**	**MeCN**	**105**	**3**	**78**
8[c]	$Pd(OAc)_2$	PPh_3	K_2CO_3	NaOAc	MeCN	105	3	28
9[d]	$Pd(OAc)_2$	PPh_3	K_2CO_3	NaOAc	MeCN	105	3	79
10	$Pd(OAc)_2$	PPh_3	K_2CO_3	NaOAc	MeCN	40	12	13
11	$Pd(OAc)_2$	PPh_3	K_2CO_3	NaOAc	DMF	120	3	77
12	$Pd(OAc)_2$	PPh_3	Na_2CO_3	NaOAc	MeCN	105	6	19
13	$Pd(OAc)_2$	PPh_3	Cs_2CO_3	NaOAc	MeCN	105	6	34
14	$Pd(OAc)_2$	PPh_3	Et_3N	NaOAc	MeCN	105	6	11
15	$Pd(OAc)_2$	PPh_3	–	NaOAc	MeCN	105	6	10

[a]Reaction conditions: 0.5 mmol **5a** in 3 mL MeCN, **7** (3 equiv), K_2CO_3 (2 equiv) for *N*-allylation; Pd catalyst (10 mol %), ligand (20 mol %), base (2 equiv) and NaOAc (1 equiv) in 3 mL solvent under nitrogen for the Heck reaction; $P(o\text{-tol})_3$ = tri(*o*-tolyl)phosphine, dppm = 1,1-bis(diphenylphosphino)methane. [b]Isolated yield. [c]$Pd(OAc)_2$ 5 mol %, PPh_3 10 mol %. [d]$Pd(OAc)_2$ 20 mol %, PPh_3 40 mol %.

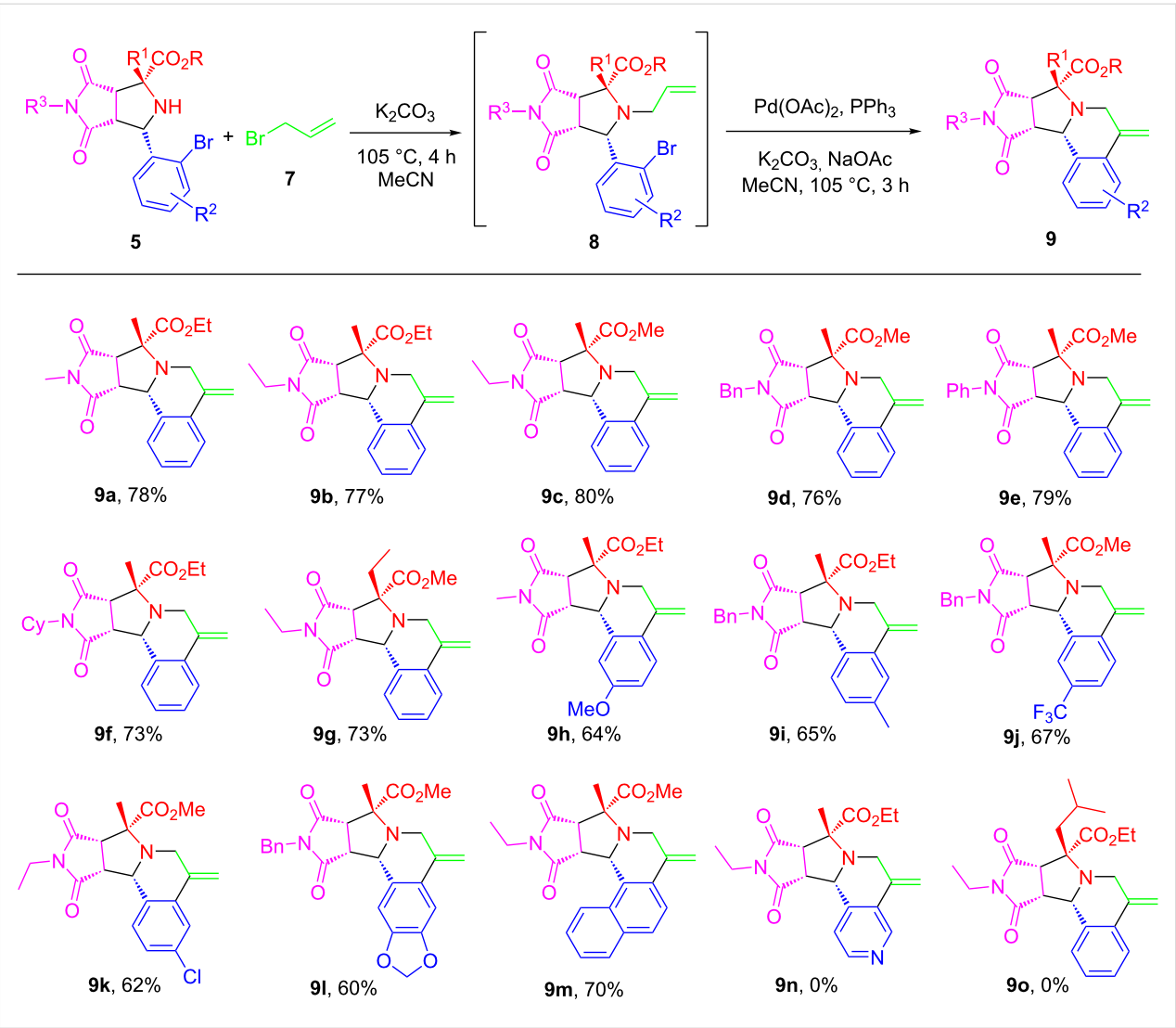

Scheme 4: Synthesis of pyrrolo[2,1-*a*]isoquinolines **9**. Reaction conditions: **5** (0.5 mmol, 1 equiv), **7** (3 equiv) and K_2CO_3 (2 equiv) in MeCN (3 mL) for *N*-allylation; then $Pd(OAc)_2$ (10 mol %), PPh_3 (20 mol %), K_2CO_3 (2 equiv) and NaOAc (1 equiv) in MeCN (3 mL) under nitrogen for the Heck reaction. Isolated yield.

dropyrrolo[2,1-*a*]isoquinoline compounds **9a**–**o** in moderate to good yields as a single isomers which were confirmed by ^{1}H NMR analysis of the crude reaction mixtures. The substitution groups R^3 (Me, Et, Ph, Bn, *c*-C_6H_{11}) on maleimide have no significant influence on the product yields to afford **9a**–**f** in 73–80% yields. The substituent groups R^2 including electron-donating (Me, OMe, -OCH_2O) or -withdrawing groups (CF_3, Cl) on the benzene ring have a little effect on the yield of products **9h**–**l**. Product **9m** bearing a naphthyl group was produced in 70% yield. Product **9n** containing a pyridine ring was not obtained due to the low yield at the *N*-allylation step. Same result happened to **9o** in which hindered iBu blocked the *N*-allylation.

We next employed intermediated **6** prepared from the decarboxylative [3+2] cycloaddition of amino acids for one-pot *N*-allylation and intramolecular Heck reactions under the same optimized conditions developed in Table 1. Pyrrolidinedione-fused hexahydropyrrolo[2,1-*a*]isoquinoline **11a**–**i** were produced in 65–78% yields also as single isomers (Scheme 5).

Allylation of [3 + 2] adducts **5** or **6** with cinnamyl bromide were also conducted and the intermediates were used for the Heck reaction for making products **12a–d** (Scheme 6). Even the allylated intermediates were not terminal alkenes, the Heck reaction gave the *Z*-products exclusively [52].

A general mechanism for Pd-catalyzed intramolecular Heck reaction of **8a** for the synthesis of pyrrolo[2,1-*a*]isoquinoline **9a** is shown in Scheme 7. The oxidative addition of the Pd(0) species to alkene intermediate **8a** leads to Pd-complex **I**. Intra-

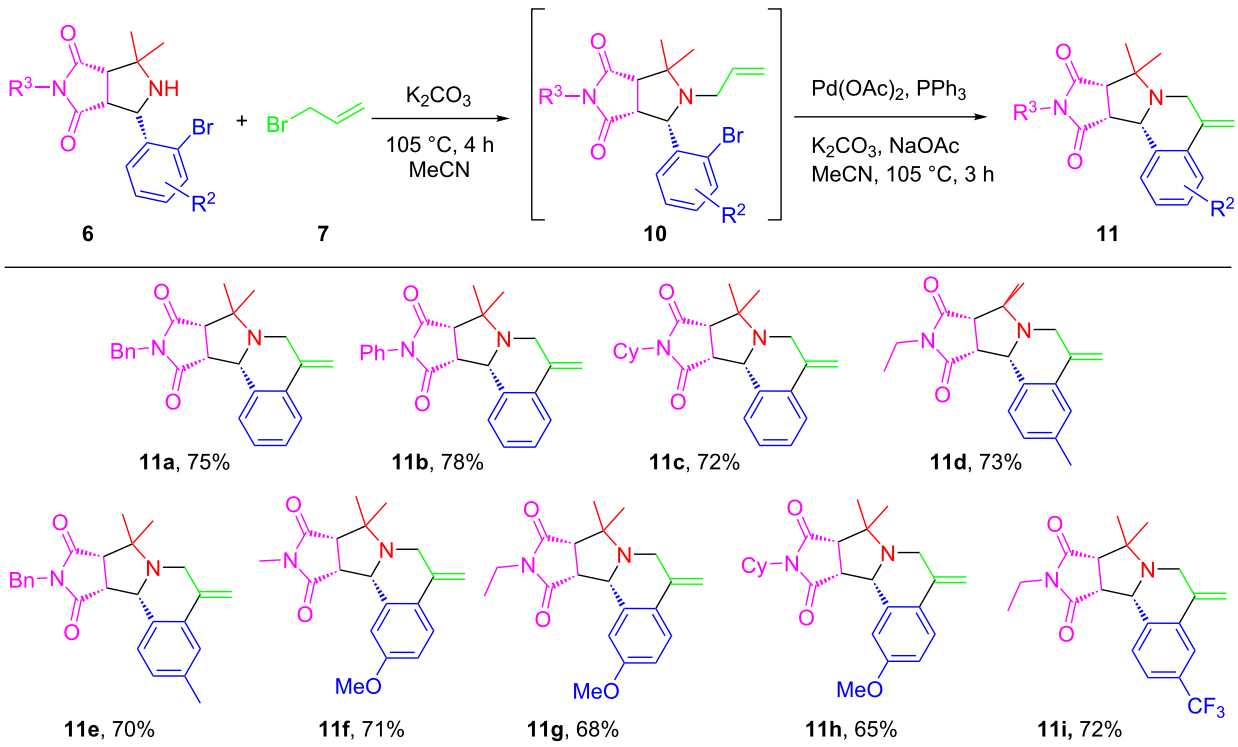

Scheme 5: Synthesis of pyrrolo[2,1-*a*]isoquinolines **11**. Reaction conditions: **6** (0.5 mmol, 1 equiv), **7** (3 equiv) and K_2CO_3 (2 equiv) in MeCN (3 mL) for the *N*-allylation; then $Pd(OAc)_2$ (10 mol %), PPh_3 (20 mol %), K_2CO_3 (2 equiv) and NaOAc (1 equiv) in MeCN (3 mL) under nitrogen for the Heck reaction. Isolated yield.

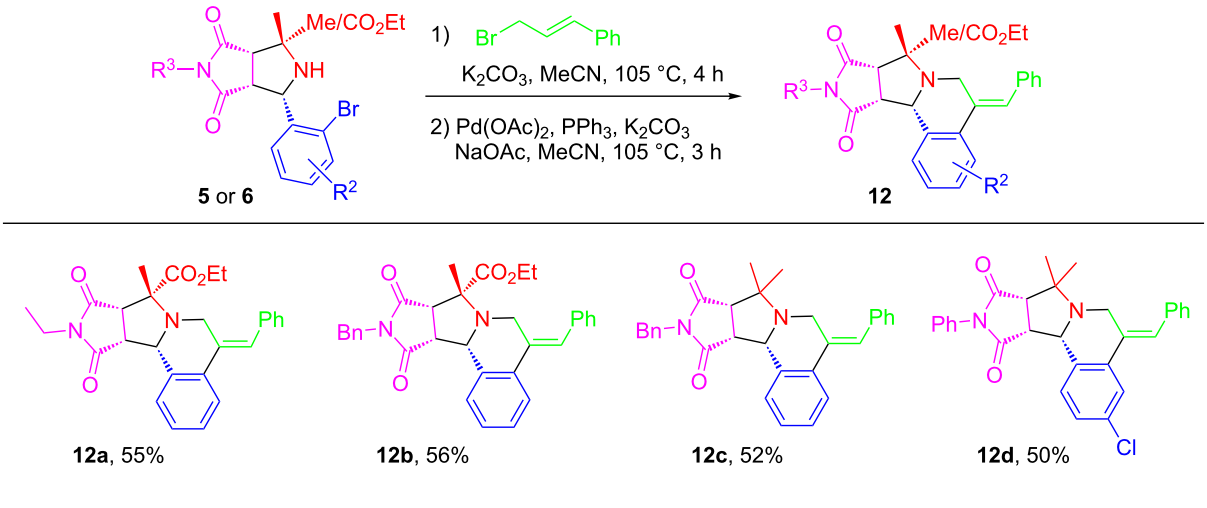

Scheme 6: Synthesis of pyrrolo[2,1-*a*]isoquinolines **12**. Reaction conditions: **5** or **6** (0.5 mmol, 1 equiv), cinnamyl bromide (3 equiv) and K_2CO_3 (2 equiv) in MeCN (3 mL) for the *N*-allylation; then $Pd(OAc)_2$ (10 mol %), PPh_3 (20 mol %), K_2CO_3 (2 equiv) and NaOAc (1 equiv) in MeCN (3 mL) under nitrogen for the Heck reaction. Isolated yield.

molecular coordination of Pd-complex **I** with the C–C double bond forms complex **II** which is followed by the *syn* insertion of alkene to give complex **III** [50,51]. Subsequent β-hydride elimination of **III** gives complex **IV** which undergoes dissociation to afford product **9a**. The hydridopalladium(II) halide is converted to the catalytically active Pd(0) with a base.

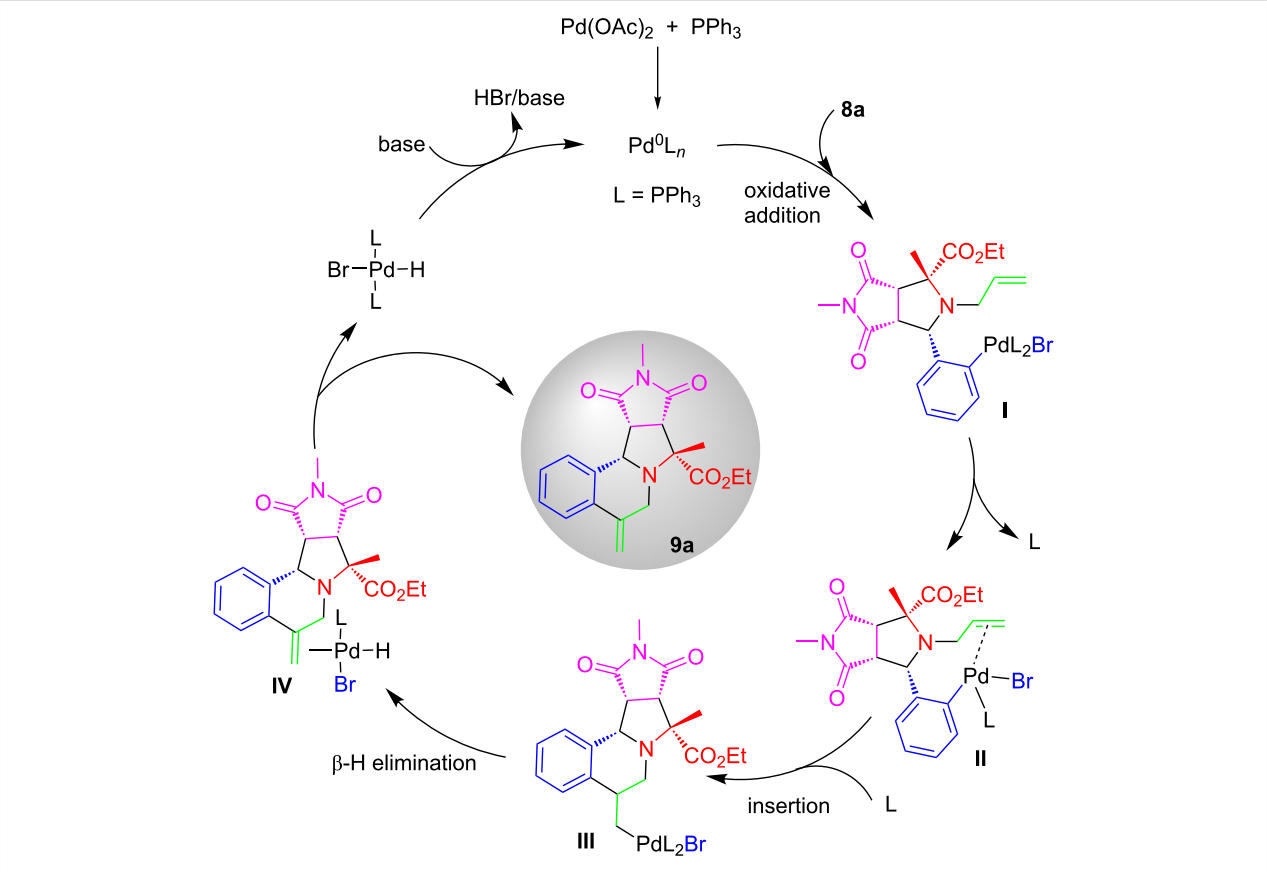

Scheme 7: Plausible mechanism for the synthesis of **9a**.

Conclusion

In summary, we have developed an efficient method through a three-component [3 + 2] cycloaddition followed by a one-pot *N*-allylation and an intramolecular Heck reaction for the synthesis of pyrrolidinedione-fused hexahydropyrrolo[2,1-*a*]isoquinolines. Two different kinds of [3 + 2] adducts generated from the reactions of amino esters or amino acids were used as the key intermediates for sequential transformations. A high synthetic efficiency was achieved by the combination of a three-component reaction with one-pot reactions. This synthetic sequence is a new addition of our [3 + 2] cycloaddition-initiated reactions for making diverse cyclic scaffolds.

Experimental

General procedure for the synthesis of pyrrolidine adducts **5**

A solution of amino ester **1** (1.2 mmol), 2-bromobenzaldehyde **3** (1 mmol) and maleimide **4** (1.1 mmol) in EtOH (3 mL) with Et_3N (1.5 mmol) was heated at 110 °C for 6 h in a sealed vial. The concentrated reaction mixture was isolated by column chromatography on silica gel to afford adduct **5** in 85–90% yield.

General procedure for the synthesis of pyrrolidine adducts **6**

A solution of 2-aminoisobutyric acid (**2**, 1.2 mmol), 2-bromobenzaldehyde **3** (1 mmol) and maleimide **4** (1 mmol) in MeCN (3 mL) with AcOH (0.3 mmol) was heated at 110 °C for 6 h in a sealed vial. The concentrated reaction mixture was isolated by column chromatography on silica gel to afford adduct **6** in 75–85% yield.

General procedure for the synthesis of pyrrolo[2,1-*a*]isoquinolines **9** or **11**

To a solution of pyrrolidine adduct **5** or **6** (0.5 mmol), 3-bromopropene (**7**, 1.5 mmol) in MeCN (3 mL) was added K_2CO_3 (1 mmol), the mixture was heated at 105 °C for 4 h in a sealed vial. Upon the completion of reaction as monitored by HPLC or LC–MS, the mixture was evaporated under vacuum to remove unreacted 3-bromopropene to give crude *N*-allylation intermediate **8** or **10**. Without further purification, it was used for the Heck reaction with $Pd(OAc)_2$ (0.05 mmol), PPh_3 (0.1 mmol), K_2CO_3 (1 mmol) and NaOAc (0.5 mmol) in MeCN (3 mL) at 105 °C for 3 h under nitrogen atmosphere. After aqueous work up, the crude product was purified by flash chromatography to afford product **9** or **11**.

General procedure for the synthesis of pyrrolo[2,1-*a*]isoquinolines **12**

To a solution of pyrrolidine adduct **5** or **6** (0.5 mmol), cinnamyl bromide (1.5 mmol) in MeCN (3 mL) was added K_2CO_3 (1 mmol), the mixture was heated at 105 °C for 4 h in a sealed vial. Upon the completion of reaction as monitored by HPLC or LC–MS, the mixture was evaporated and the unreacted cinnamyl bromide was isolated to give *N*-allylation intermediate which was then used for the Heck reaction with $Pd(OAc)_2$ (10 mol %), PPh_3 (20 mol %), K_2CO_3 (2 equiv) and NaOAc (1 equiv) in MeCN (3 mL) at 105 °C for 3 h under nitrogen atmosphere. After aqueous work-up, the crude product was purified by flash chromatography to afford product **12**.

Supporting Information

Supporting Information File 1

General reaction procedures, compound characterization data, and copies of NMR spectra.
[https://www.beilstein-journals.org/bjoc/content/supplementary/1860-5397-16-106-S1.pdf]

Acknowledgements

We thank Prof. Jian Li for the discussion of this paper. We also thank Huimin Zhang's early work for this project.

ORCID® iDs

Xiaoming Ma - https://orcid.org/0000-0003-1358-428X
Wei Zhang - https://orcid.org/0000-0002-6097-2763

Preprint

A non-peer-reviewed version of this article has been previously published as a preprint doi:10.3762/bxiv.2020.28.v1

References

1. Pässler, U.; Knöller, H. J. The pyrrolo[2,1-*a*]isoquinoline alkaloids. In *The Alkaloids: Chemistry and Biology;* Knöller, H. J., Ed.; Elsevier: Amsterdam, The Netherlands, 2011; Vol. 70, pp 79–151. doi:10.1016/b978-0-12-391426-2.00002-5
2. Fan, H.; Peng, J.; Hamann, M. T.; Hu, J.-F. *Chem. Rev.* **2008,** *108,* 264–287. doi:10.1021/cr078199m
3. Zhang, Q.; Tu, G.; Zhao, Y.; Cheng, T. *Tetrahedron* **2002,** *58,* 6795–6798. doi:10.1016/s0040-4020(02)00792-5
4. Zhang, F.; Simpkins, N. S.; Blake, A. J. *Org. Biomol. Chem.* **2009,** *7,* 1963–1979. doi:10.1039/b900189a
5. Parsons, A. F.; Palframan, M. J. Erythrina and related alkaloids. In *The Alkaloids: Chemistry and Biology;* Cordell, G. A., Ed.; Academic Press: London, UK, 2010; Vol. 68, pp 39–81. doi:10.1016/s1099-4831(10)06802-1
6. Andersen, R. J.; Faulkner, D. J.; He, C. H.; Van Duyne, G. D.; Clardy, J. *J. Am. Chem. Soc.* **1985,** *107,* 5492–5495. doi:10.1021/ja00305a027
7. Reddy, M. V. R.; Rao, M. R.; Rhodes, D.; Hansen, M. S. T.; Rubins, K.; Bushman, F. D.; Venkateswarlu, Y.; Faulkner, D. J. *J. Med. Chem.* **1999,** *42,* 1901–1907. doi:10.1021/jm9806650
8. Malla Reddy, S.; Srinivasulu, M.; Satyanarayana, N.; Kondapi, A. K.; Venkateswarlu, Y. *Tetrahedron* **2005,** *61,* 9242–9247. doi:10.1016/j.tet.2005.07.067
9. Wang, R.-F.; Yang, X.-W.; Ma, C. M.; Cai, S.-Q.; Li, J.-N.; Shoyama, Y. *Heterocycles* **2004,** *63,* 1443–1448. doi:10.3987/com-04-10062
10. Yang, Z.; Liu, C.; Xiang, L.; Zheng, Y. *Phytother. Res.* **2009,** *23,* 1032–1035. doi:10.1002/ptr.2742
11. Lin, W.; Ma, S. *Org. Chem. Front.* **2017,** *4,* 958–966. doi:10.1039/c7qo00062f
12. Umihara, H.; Yoshino, T.; Shimokawa, J.; Kitamura, M.; Fukuyama, T. *Angew. Chem., Int. Ed.* **2016,** *55,* 6915–6918. doi:10.1002/anie.201602650
13. Komatsubara, M.; Umeki, T.; Fukuda, T.; Iwao, M. *J. Org. Chem.* **2014,** *79,* 529–537. doi:10.1021/jo402181w
14. Kapat, A.; Kumar, P. S.; Baskaran, S. *Beilstein J. Org. Chem.* **2007,** *3,* No. 49. doi:10.1186/1860-5397-3-49
15. Dondas, H. A.; Fishwick, C. W. G.; Gai, X.; Grigg, R.; Kilner, C.; Dumrongchai, N.; Kongkathip, B.; Kongkathip, N.; Polysuk, C.; Sridharan, V. *Angew. Chem., Int. Ed.* **2005,** *44,* 7570–7574. doi:10.1002/anie.200502066
16. Sun, H.; Tawa, G.; Wallqvist, A. *Drug Discovery Today* **2012,** *17,* 310–324. doi:10.1016/j.drudis.2011.10.024
17. Hu, Y.; Stumpfe, D.; Bajorath, J. *J. Med. Chem.* **2017,** *60,* 1238–1246. doi:10.1021/acs.jmedchem.6b01437
18. Zhi, S.; Ma, X.; Zhang, W. *Org. Biomol. Chem.* **2019,** *17,* 7632–7650. doi:10.1039/c9ob00772e
19. Haji, M. *Beilstein J. Org. Chem.* **2016,** *12,* 1269–1301. doi:10.3762/bjoc.12.121
20. Dömling, A.; Wang, W.; Wang, K. *Chem. Rev.* **2012,** *112,* 3083–3135. doi:10.1021/cr100233r
21. Pandey, G.; Banerjee, P.; Gadre, S. R. *Chem. Rev.* **2006,** *106,* 4484–4517. doi:10.1021/cr050011g
22. Hashimoto, T.; Maruoka, K. *Chem. Rev.* **2015,** *115,* 5366–5412. doi:10.1021/cr5007182
23. Amornraksa, K.; Grigg, R.; Gunaratne, H. Q. N.; Kemp, J.; Sridharan, V. *J. Chem. Soc., Perkin Trans. 1* **1987,** 2285–2296. doi:10.1039/p19870002285
24. Coldham, I.; Hufton, R. *Chem. Rev.* **2005,** *105,* 2765–2810. doi:10.1021/cr040004c
25. Harju, K.; Yli-Kauhaluoma, J. *Mol. Diversity* **2005,** *9,* 187–207. doi:10.1007/s11030-005-1339-1
26. Zhang, W.; Zhang, X.; Ma, X.; Zhang, W. *Tetrahedron Lett.* **2018,** *59,* 3845–3847. doi:10.1016/j.tetlet.2018.09.023
27. Tsuge, O.; Kanemasa, S.; Ohe, M.; Takenaka, S. *Bull. Chem. Soc. Jpn.* **1987,** *60,* 4079–4089. doi:10.1246/bcsj.60.4079
28. Grigg, R.; Idle, J.; McMeekin, P.; Vipond, D. *J. Chem. Soc., Chem. Commun.* **1987,** 49–51. doi:10.1039/c39870000049
29. Grigg, R.; Surendrakumar, S.; Thianpatanagul, S.; Vipond, D. *J. Chem. Soc., Perkin Trans. 1* **1988,** 2693–2701. doi:10.1039/p19880002693
30. Ma, X.; Zhang, X.; Xie, G.; Awad, J. M.; Zhang, W. *Tetrahedron Lett.* **2019,** *60,* 151127. doi:10.1016/j.tetlet.2019.151127

31. Zhang, W.; Lu, Y.; Hiu-Tung Chen, C.; Zeng, L.; Kassel, D. B. *J. Comb. Chem.* **2006,** *8,* 687–695. doi:10.1021/cc060061e
32. Lu, Q.; Huang, X.; Song, G.; Sun, C.-M.; Jasinski, J. P.; Keeley, A. C.; Zhang, W. *ACS Comb. Sci.* **2013,** *15,* 350–355. doi:10.1021/co400026s
33. Ma, X.; Zhang, X.; Awad, J. M.; Xie, G.; Qiu, W.; Zhang, W. *Green Chem.* **2019,** *21,* 4489–4494. doi:10.1039/c9gc01642b
34. Muthengi, A.; Zhang, X.; Dhawan, G.; Zhang, W.; Corsini, F.; Zhang, W. *Green Chem.* **2018,** *20,* 3134–3139. doi:10.1039/c8gc01099d
35. Zhang, X.; Qiu, W.; Ma, X.; Evans, J.; Kaur, M.; Jasinski, J. P.; Zhang, W. *J. Org. Chem.* **2018,** *83,* 13536–13542. doi:10.1021/acs.joc.8b02046
36. Ma, X.; Zhang, X.; Awad, J. M.; Xie, G.; Qiu, W.; Muriph, R. E.; Zhang, W. *Tetrahedron Lett.* **2020,** *61,* 151392. doi:10.1016/j.tetlet.2019.151392
37. Ma, X.; Zhang, X.; Qiu, W.; Zhang, W.; Wan, B.; Evans, J.; Zhang, W. *Molecules* **2019,** *24,* 601. doi:10.3390/molecules24030601
38. Zhang, X.; Qiu, W.; Evans, J.; Kaur, M.; Jasinski, J. P.; Zhang, W. *Org. Lett.* **2019,** *21,* 2176–2179. doi:10.1021/acs.orglett.9b00487
39. Muthengi, A.; Erickson, J.; Muriph, R. E.; Zhang, W. *J. Org. Chem.* **2019,** *84,* 5927–5935. doi:10.1021/acs.joc.9b00448
40. Grigg, R.; Coulter, T. *Tetrahedron Lett.* **1991,** *32,* 1359–1362. doi:10.1016/s0040-4039(00)79667-5
41. Dumitrascu, F.; Caira, M. R.; Georgescu, E.; Georgescu, F.; Draghici, C.; Popa, M. M. *Heteroat. Chem.* **2011,** *22,* 723–729. doi:10.1002/hc.20740
42. Boudriga, S.; Haddad, S.; Askri, M.; Soldera, A.; Knorr, M.; Strohmann, C.; Golz, C. *RSC Adv.* **2019,** *9,* 11082–11091. doi:10.1039/c8ra09884k
43. Peng, W.; Zhu, S. *J. Chem. Soc., Perkin Trans. 1* **2001,** 3204–3210. doi:10.1039/b103586j
44. An, J.; Yang, Q.-Q.; Wang, Q.; Xiao, W.-J. *Tetrahedron Lett.* **2013,** *54,* 3834–3837. doi:10.1016/j.tetlet.2013.05.053
45. Bastrakov, M. A.; Starosotnikov, A. M. *Russ. Chem. Bull.* **2019,** *68,* 1729–1734. doi:10.1007/s11172-019-2617-x
46. Shang, Y.; Wang, L.; He, X.; Zhang, M. *RSC Adv.* **2012,** *2,* 7681–7688. doi:10.1039/c2ra21116e
47. Dumitrascu, F.; Georgescu, E.; Georgescu, F.; Popa, M. M.; Dumitrescu, D. *Molecules* **2013,** *18,* 2635–2645. doi:10.3390/molecules18032635
48. Wu, L.; Sun, J.; Yan, C.-G. *Org. Biomol. Chem.* **2012,** *10,* 9452–9463. doi:10.1039/c2ob26849c
49. Muthusaravanan, S.; Perumal, S.; Yogeeswari, P.; Sriram, D. *Tetrahedron Lett.* **2010,** *51,* 6439–6443. doi:10.1016/j.tetlet.2010.09.128
50. Link, J. T. The intramolecular heck reaction. In *Organic Reactions;* Overman, L. E., Ed.; John Wiley & Sons: New York, NY, USA, 2002; Vol. 60, pp 157–213. doi:10.1002/0471264180.or060.02
51. Bharath Kumar Reddy, P.; Ravi, K.; Mahesh, K.; Leelavathi, P. *Tetrahedron Lett.* **2018,** *59,* 4039–4043. doi:10.1016/j.tetlet.2018.09.068
52. Wang, G.; Liu, C.; Li, B.; Wang, Y.; Van Hecke, K.; Van der Eycken, E. V.; Pereshivko, O. P.; Peshkov, V. A. *Tetrahedron* **2017,** *73,* 6372–6380. doi:10.1016/j.tet.2017.09.034
53. Murru, S.; McGough, B.; Srivastava, R. S. *Org. Biomol. Chem.* **2014,** *12,* 9133–9138. doi:10.1039/c4ob01614a
54. Hou, C.; Chen, H.; Xu, X.; Zhu, F.; Guo, L.; Jiang, M.; Yang, C.; Deng, L. *Eur. J. Org. Chem.* **2015,** 3040–3043. doi:10.1002/ejoc.201500180
55. Zhang, W.; Yi, W.-B. *Pot, atom, and Step Economy (PASE) Synthesis;* Springer: Cham, Switzerland, 2019. doi:10.1007/978-3-030-22596-4_1
56. Clarke, P. A.; Santos, S.; Martin, W. H. C. *Green Chem.* **2007,** *9,* 438–440. doi:10.1039/b700923b

License and Terms

The definitive version of this article is the electronic one which can be found at: doi:10.3762/bjoc.16.106

BEILSTEIN JOURNAL OF ORGANIC CHEMISTRY

In silico rationalisation of selectivity and reactivity in Pd-catalysed C–H activation reactions

Liwei Cao[1,2], Mikhail Kabeshov[3,4], Steven V. Ley[3] and Alexei A. Lapkin[*1,2]

Full Research Paper

Open Access

Address:
[1]Department of Chemical Engineering and Biotechnology, University of Cambridge, Cambridge CB3 0AS, UK, [2]Cambridge Centre for Advanced Research and Education in Singapore, CARES Ltd., CREATE Way, CREATE Tower #05-05, 138602 Singapore, [3]Department of Chemistry, University of Cambridge, Lensfield Rd, Cambridge CB2 1EW, UK and [4]Benevolent AI, Minerva Building, Babraham Research Campus, Cambridge CB22 3AT, UK

Email:
Alexei A. Lapkin[*] - aal35@cam.ac.uk

* Corresponding author

Keywords:
C–H activation; density functional theory; reaction prediction

Beilstein J. Org. Chem. **2020,** *16,* 1465–1475.
doi:10.3762/bjoc.16.122

Received: 09 March 2020
Accepted: 02 June 2020
Published: 25 June 2020

This article is part of the thematic issue "Green chemistry II".

Guest Editor: L. Vaccaro

Abstract

A computational approach has been developed to automatically generate and analyse the structures of the intermediates of palladium-catalysed carbon–hydrogen (C–H) activation reactions as well as to predict the final products. Implemented as a high-performance computing cluster tool, it has been shown to correctly choose the mechanism and rationalise regioselectivity of chosen examples from open literature reports. The developed methodology is capable of predicting reactivity of various substrates by differentiation between two major mechanisms – proton abstraction and electrophilic aromatic substitution. An attempt has been made to predict new C–H activation reactions. This methodology can also be used for the automated reaction planning, as well as a starting point for microkinetic modelling.

Introduction

Periodically, our knowledge of chemistry is enriched with new transformations that provide significant breakthroughs by enabling new synthetic strategies. Such examples in recent years include olefin metathesis [1] as well as C–C and C–N coupling reactions [2], among the most obvious examples. While these reactions undoubtedly had very significant impacts on the development of much cleaner and efficient chemical synthesis strategies, the early days of all new transformations are invariably challenging, with very slow and protracted paths from the initial discoveries to the demonstrations of broad substrate applicability and robustness, that are expected of industrial catalytic processes. Today, there exist a number of fairly recently (re)discovered transformations, that are of potential high industrial significance, and where one can observe the

same problem of a lack of robustness. Thus, any approach that may speed-up the transition from a discovery of a new transformation to it becoming a robust synthetic strategy, is highly desired.

Recent years have seen the emergence of new methods of research in chemistry and process development, which include high-throughput experiments [3], autonomous self-optimising reactors [4-6], as well as predictions of reaction outcomes and of reaction conditions based on machine learning (ML) and artificial intelligence (AI) tools [7-9]. Especially the methods of ML/AI for prediction of reaction outcomes are attracting a lot of attention. Prediction accuracies in the order of 70–80% for the reaction outcomes [9], and around 60–70% for reaction conditions [10], were recently demonstrated. While machine learning methods are showing great promise and continue to be improved upon, it is also clear that a ML model is unlikely to ever be able to compete in accuracy and interpretability with fully predictive mechanistic models, were it not for the prohibitively high cost of developing the mechanistic models based on accurate quantum chemical methods, such as the density functional theory (DFT) methods, decreases. Automation of DFT, as well as using results of DFT to develop less expensive predictive models, are the two approaches that may offer the alternatives to the fully data-driven statistical methods.

Here we demonstrate an approach that was developed to automate the DFT-level calculations of energies of the auto-generated reaction intermediates. These results were further used to generalize mechanistic knowledge of a class of reactions, and the developed models were used for in silico prediction of reaction outcomes. This approach was tested on the for green chemistry important class of C–H activation reactions. Whilst this study does not completely solve the problem of developing a robust chemical reaction, it offers an approach that is complementary to efforts of developing machine learning models for predicting reaction outcomes.

C–H activation reactions allow conversion of relatively inexpensive and abundant hydrocarbons into the more sophisticated value-added molecules [11]. With the notion of step-economical and environmentally friendly synthesis, direct functionalization of C–H bonds is a powerful strategy for the synthesis and derivatization of organic molecules [12]. Homogeneous catalysis employing transition metal complexes has been widely accepted as one of the most efficient ways to perform C–H activation-based synthesis with high selectivity under relatively mild conditions [13]. In particular, reactions involving palladium-catalysed activation of sp^2 or sp^3 C–H bonds of arenes or alkanes have been extensively investigated due to their wide scope and functional group tolerance [14].

A number of different mechanisms are proposed in the literature, explaining the experimental observations for C–H activation reactions, depending on the nature of a ligand (L_n) and transition metal (M) in the catalytically active species (L_nM). These mechanisms include four elementary steps: oxidative addition, σ-bond metathesis, electrophilic substitution and 1,2-addition, respectively [15]. Even though the mechanisms are inherently different, three most important aspects should be primarily taken into account when classifying and rationalising C–H activation reactions:

1. the proximity of C–H bond to the transition metal;
2. the energy of C–H bond cleavage within the transition metal coordination sphere;
3. the energy of a new M–C bond formed and the thermodynamic stability of organometallic product.

With new developments in computational chemistry, mechanistic studies using density functional theory (DFT) provide valuable insights into the reactivity of organometallic complexes in C–H activation reactions. Along with the huge increase in computing power, this method becomes practically feasible to build model systems that provide parameters of the actual experimental systems with acceptable accuracy [16]. Recently, a predictive tool using quantum mechanics descriptors was proposed for classifying whether the carbon atoms are active or inactive toward electrophilic aromatic substitution [17]. Also, a quantum mechanical approach was introduced to compute *ortho*-directing groups (DGs) in palladium-catalysed aromatic C–H activation reactions [18]. However, there is a big challenge remaining which is to apply the computational analysis to a large number of mechanistically different transformations, both described and novel, in order to start generating accurate in silico reaction predictions. Here, we report an algorithm with high-performance computing (HPC) implementation, which has been developed to automatically generate and analyse the structures of the intermediates, and which allows prediction of the final products. The application of the developed methodology is in predicting reactivity for various substrates within a class of reactions. Using analysis of the computational data, a threshold to distinguish between two possible reaction mechanisms was established.

Computational Methods

The NWChem, an open source software package, was used for the DFT calculations. It is easily scalable and designed to solve large scientific computational problems efficiently employing modern supercomputer clusters [19]. The structures were generated by the Python module developed in house and explained in detail elsewhere [20]. Electronic energies were evaluated using Becke's three-parameter hybrid B3LYP functional, while the

molecular orbitals are expanded in triple-zeta all electron 6-31 set with added polarization and diffuse functions [6-31g(d,p)] [21]. B3LYP functional was proven to give accurate description of geometries, frequencies, relative stabilities of different conformers and the energy profile calculation [22]. Implementation of the tools is available at GitHub: https://github.com/sustainable-processes/Pd-catalysed_C-H_activation_reaction_prediction.

Results and Discussion

Computational approach to rationalise reactivity in Pd-catalysed C–H bond activation reactions

Chemical reactivity is simultaneously influenced by many factors including catalysts, reactants, reaction conditions, and so on [23]. In order to achieve accurate and efficient reaction prediction, a mechanism-based method was chosen to direct quantum chemistry calculations and predictions, see Figure 1.

For the Pd(II)-catalysed C–H activation reactions, there are two main commonly accepted mechanisms: a) electrophilic aromatic substitution (S_EAr) mechanism and b) proton abstraction (PA) mechanism. The key step for the electrophilic aromatic substitution is an electrophilic attack by Pd(II) onto the aromatic substrate that also defines the regioselectivity of the overall process [24]. The key feature of the proton abstraction (PA) mechanism [25] is that the formation of the metal–carbon bond (M–C) occurs simultaneously with the cleavage of the carbon–hydrogen (C–H) bond, while the hydrogen is being transferred to a basic centre, Scheme 1.

Assuming the reaction proceeds through the formation of a relatively unstable intermediate (Figure 1) [26], the Hammond postulate can be applied to the electrophilic substitution reactions. The Hammond postulate states that a transition state will be structurally and energetically similar to the species (reactant, intermediate or product) nearest to it on the reaction path. In this case, the intermediates are likely to be close to, and resemble, transition states. Due to that, their relative energy of formation can be translated to relative reaction kinetic barriers and thus be used, as the first approximation, to predict distributions of the final products, as well as the relative reactivity of the substrates [27]. For the PA mechanism, it has not been shown that the Hammond postulate can also be employed. Nevertheless, it is still reasonable to propose that the Hammond postulate can similarly be applied as a first approximation to produce in silico predictions.

Employing the Python module [20] and OpenBabel executables [28], the 3D structures of the most stable conformers were generated from the 2D structure of a substrate. Subsequently, structures of all possible palladium intermediates representing both mechanisms (PA and S_EAr) were built for each conformer. A quick geometry optimization (maximum number of iteration steps was set to 5) was then applied to refine the intermediates and discard the ones with high energy (energy cut off of 10 kcal·mol^{-1}). Full geometry optimisation followed by the frequency and thermochemistry analysis was then performed for the selected intermediates to obtain electronic energies. Multiple error handlers were implemented in order to automatically reprocess computational analysis for the intermediates when initial geometry optimisation failed. These include:

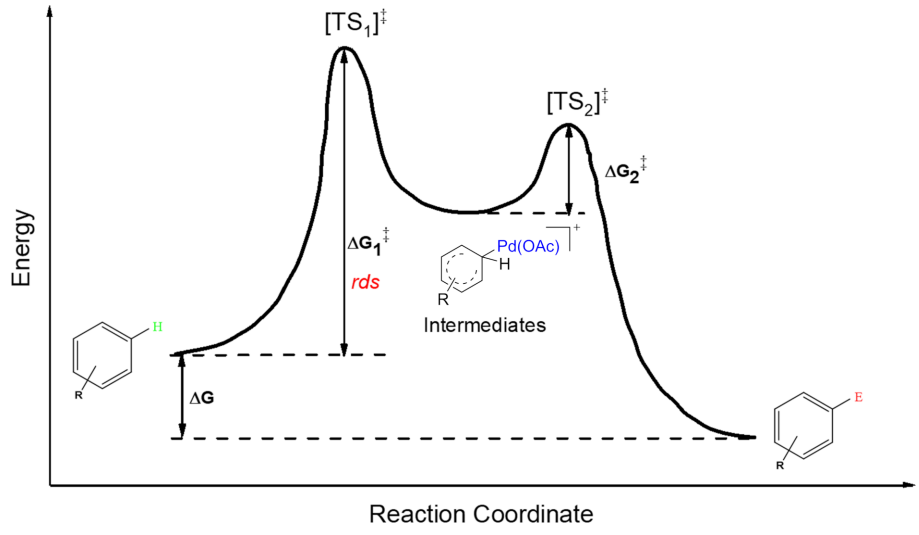

Figure 1: An approximate energy map for the electrophilic aromatic substitution mechanism.

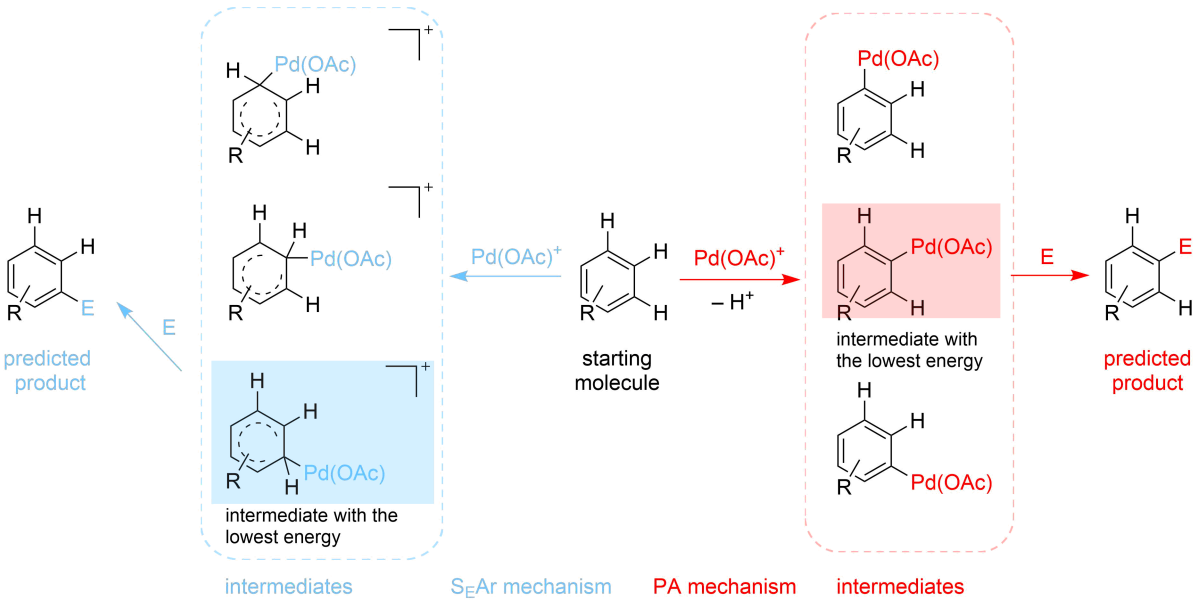

Scheme 1: Schematic representation of the two mechanisms of Pd-catalysed C–H activation reaction considered in this study.

(i) erroneous optimisation to a saddle point where the final structure is changed by applying a move along imaginary coordinate followed by standard geometry optimisation, (ii) failed optimisation due to the need of updating Hessian in cases where significant geometry change occurred – standard resubmission starting from the last coordinate, (iii) failure to perform initial guess due to particularly bad initial geometry – discard the conformer/intermediate, (iv) decomposed intermediate (no Pd–C bond determined by interatomic distance analysis) – discard intermediate.

Literature validation

In order to test the developed algorithm, a representative literature data selection of Pd-catalysed C–H activation reactions, consisting of reactant, reagents, and product structures as well as reaction conditions, was taken and analysed. Thus, twelve substrates shown in Table 1 were submitted to the algorithm, assuming that both mechanisms are possible. Using the relative energies of the intermediates obtained, the theoretically expected regioselectivity of the selected reactions was devised and then compared against the previously reported experimental data.

For all the examples regioselectivity predicted by at least one mechanism matched the previously reported experimental results, see Table 1. In the cases where only one product was predicted it is expected to be isolated in high yield without the need of further purification from any other regioisomer. For the examples where formation of multiple products was expected due to the close energies of the respective reaction intermediates, the ratio of products was calculated from the relative energies of these intermediates using the Boltzmann distribution equation.

Establishing the threshold between the two mechanisms

Although both, the proton-abstraction and the electrophilic aromatic-substitution, mechanisms are well established and described in the literature, it is not trivial to suggest the preferred mechanism for a given substrate based on a simple computational analysis. Through analysis of the results described above, the two-step evaluation algorithm was suggested.

Firstly, the optimised geometries were manually examined to ensure they represent the intermediates according to the particular mechanism. In particular, the bond length between the palladium atom and the corresponding carbon atom was given a maximum value of 2.4 Å to filter out inappropriate intermediates where there is no stable Pd–C bond [40].

Secondly, among the intermediates refined at the previous step, their relative Gibbs energies can be used to set a threshold establishing the likeliness of electrophilic aromatic substitution mechanism for C–H activation of a particular substrate. The more stable the ipso-complex between palladium acetate and the substrate is, the more likely the substrate is to follow the

electrophilic mechanism. After performing the computational analysis of 12 examples which include five structures following the electrophilic mechanism, a threshold has been developed by choosing the example 6 as the reference, Table 1, and introducing the ipso-complex stability parameter. We define this parameter to be the energy difference between the most stable intermediate of the S_EAr mechanism and the one of the PA mechanism.

Table 1: Comparison of the published experimental results with the computational predictions for the $Pd(OAc)_2$-catalysed reactions.[a]

No [ref]	Starting molecule	Exp. cond.	Predicted active centre		Experimentally isolated product
			Via acidity mechanism	Via electrophilic mechanism	
1 [29]	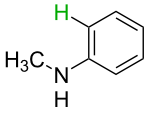	CO, EtOH, $Pd(OAc)_2$, $Cu(OAc)_2$, KOAc, DMF, KI, 100 °C, 13 h	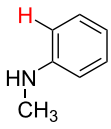	no stable intermediate	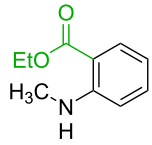
2 [30]	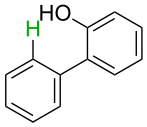	CO, $Pd(OAc)_2$, $Cu(OAc)_2$, PivOH, mesitylene, 120 °C, 6 h	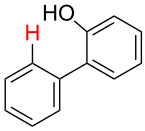	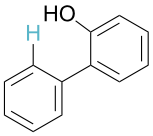	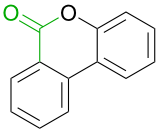
3 [31]	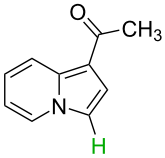	$Cu(OAc)_2$, $Pd(OAc)_2$, K_2CO_3, DMF, 60 °C, 0.6 h	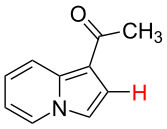	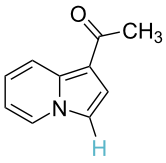	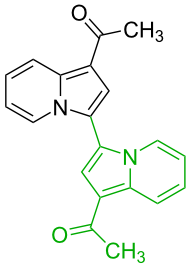
4 [32]	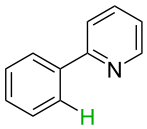	$PhCOCO_2H$ $Pd(OAc)_2$, $K_2S_2O_8$, MeCN, 25 °C, 16 h	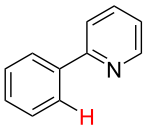	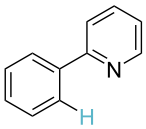	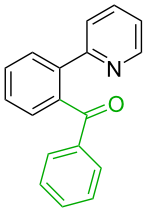
5 [33]	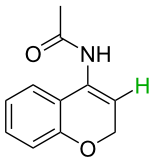	$PhSi(OMe)_3$, $Pd(OAc)_2$, AgF, dioxane, 80 °C, 16 h	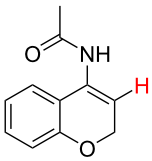	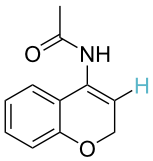	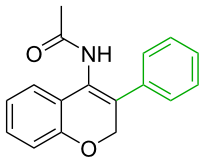
6 [32]	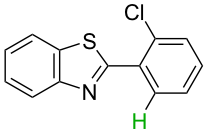	Ph-CHO, $Pd(OAc)_2$, TBHP, toluene, 110 °C, 5 h	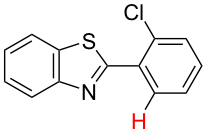	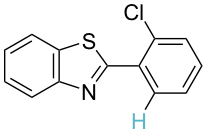	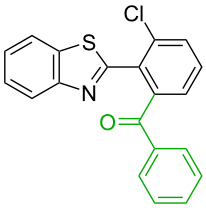
7 [34]	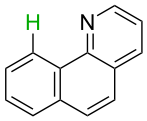	Ph-CHO, $Pd(OAc)_2$, xylene, O_2 120 °C, 24 h	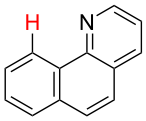	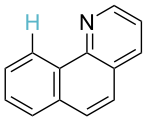	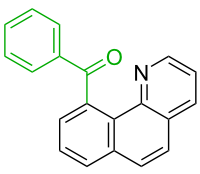

Table 1: Comparison of the published experimental results with the computational predictions for the $Pd(OAc)_2$-catalysed reactions.[a] (continued)

8 [35]	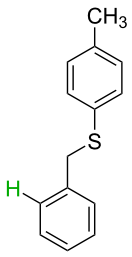	$PhCOCO_2H$, $Pd(OAc)_2$, Ag_2CO_3, DMF, 120 °C, 24 h	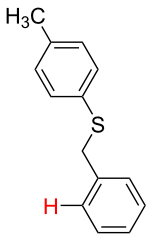	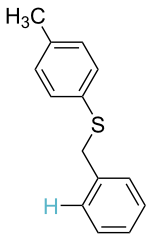	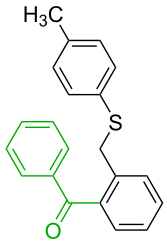
9 [36]	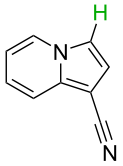	H-COOPh, $Pd(OAc)_2$, I_2, K_2CO_3, DMF, 100 °C, 12 h	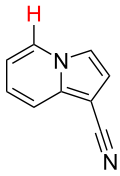	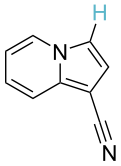	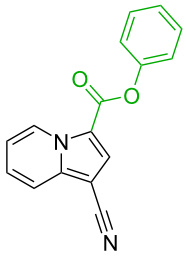
10 [37]	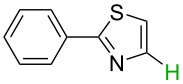	$PhB(OH)_2$, $Pd(OAc)_2$, TEMPO, phen, DMAc, O_2, 100 °C, 48 h	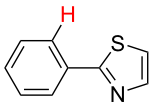	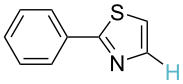	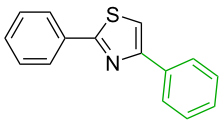
11 [38]	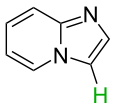	benzene, $Pd(OAc)_2$, O_2, HOAc, DMA, 130 °C, 20 h	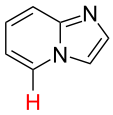	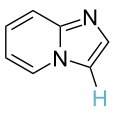	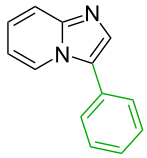
12 [39]	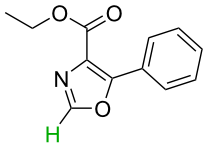	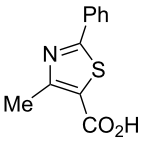 $Pd(OAc)_2$, $CuCO_3$, dioxane, DMSO, 140 °C, 16 h	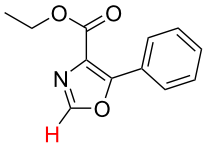	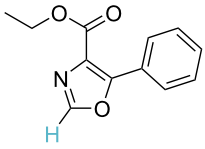	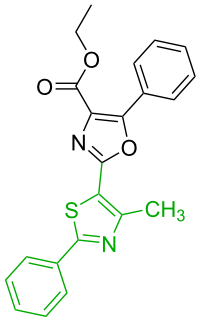

[a]Protons marked green are those that react under the conditions reported in the literature. Protons marked red and blue are the predicted active centres via the acidity and the electrophilic mechanisms, respectively.

By comparing the computational results obtained to the literature experimental data, the two mechanisms can be segregated based on the following rules:

1. If the relative stability is below zero, the starting molecule will follow the proton abstraction mechanism.
2. If the relative stability is above five, the starting molecule will follow the electrophilic aromatic substitution mechanism.
3. If the relative stability is between zero and five, both mechanisms are regarded as plausible.

Although the rules set above seem rather approximate, they are consistent with the given examples, and further work aimed at increasing the accuracy and the scope of the algorithm is on-going. Based on the suggested rules, the predicted reactive centres for eight commercially available aromatic and heteroaromatic substrates as well as the most likely mechanisms are shown in Table 2.

In order to test the algorithm and the value of the threshold, an additional set of six examples was analysed, and the results are shown in Table 3. Both selectivity and mechanism were

Table 2: Predicting C–H activation bond for heteroaromatic compounds.[a]

No.	Starting molecule	Pred. mec.	Computational prediction			
			Acidity mechanism		Electrophilic mechanism	
1	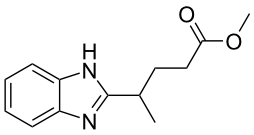	S_EAr	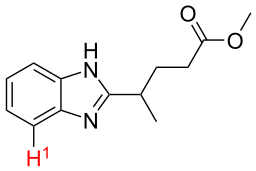	**H1:0.0**	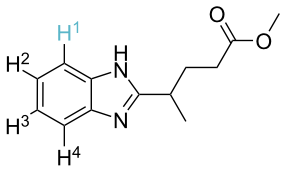	**H1:0.0**
2	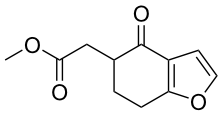	S_EAr	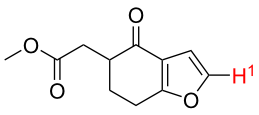	**H1:0.0**	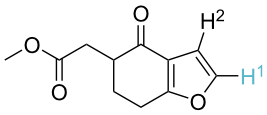	**H1:0.0** H2:0.5
3	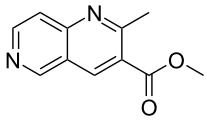	PA	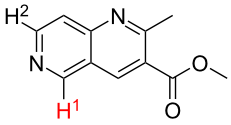	**H1:0.0** H2:0.7	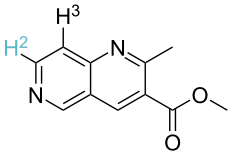	**H2:0.0** H3:0.9
4	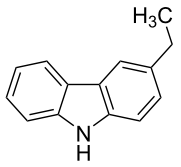	PA	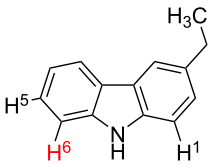	H1:1.9 H5:9.8 **H6:0.0**	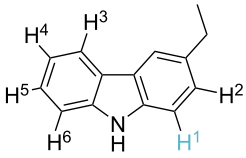	**H1:0.0** H2:3.9 H3:2.9 H4:2.9 H5:4.2
5	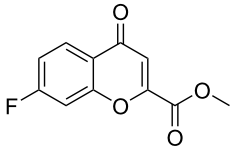	PA	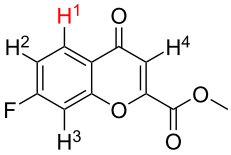	**H1:0.0** H2:2.7 H3:9.7 H4:6.2	no stable intermediate	
6	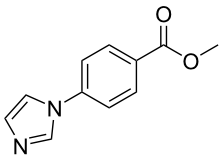	PA/S_EAr	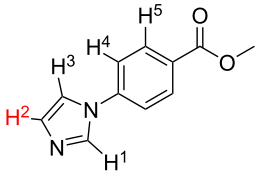	H1:0.2 **H2: 0.0** H3: 0.3 H4:0.9 H5:2.6	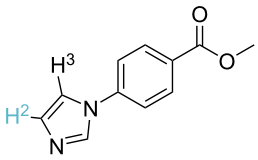	**H2:0.0** H3:2.7
7	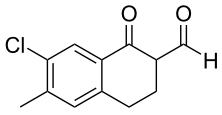	PA	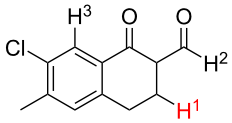	**H1:0.0** H2:2.8 H3:10.0	no stable intermediate	
8	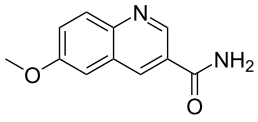	PA	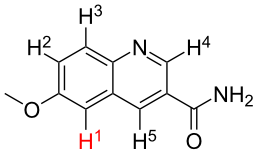	**H1:0.0** H2:0.8 H3:5.5 H4:4.3 H5:6.0	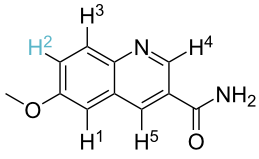	H1:0.1 **H2:0.0** H3:14.9 H4:15.0 H5:15.8

[a]Most probable intermediates for each mechanism are shown, and relative Gibbs free energy are given in kcal mol^{-1}. If only one possible intermediate is given, it means that either the other intermediates are unstable or the other intermediates have 10 more kcal mol^{-1} Gibbs free energy than the most probable one. 'no stable intermediate' means instead of sitting on the corresponding carbon, the palladium sits on alternative atom. The predicted mechanism is given based on the threshold described in the previous section.

correctly identified by the algorithm applying the previously set threshold to the SnAr intermediate stability (intermediates 5), which is shown in Table 4.

Conclusion

A computational algorithm rationalising the existing palladium catalysed C–H activation reactions has been developed. Compu-

Table 3: A comparison of the published experimental results with the computational predictions for the $Pd(OAc)_2$-catalysed reactions.[a]

No [ref]	Starting molecule	Exp. cond.	Predicted active center		Experimentally isolated product
			Via acidity mechanism	Via electrophilic mechanism	
1 [41]	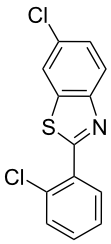	$Pd(OAc)_2$, TBHP, toluene, 120 °C, 6 h	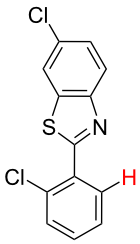	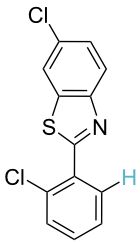	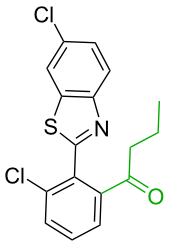
2 [42]	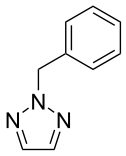	$Pd(OAc)_2$, TBHP, DCE 80 °C, 16 h	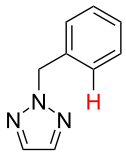	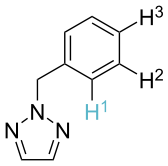 **H1:0.0** H2:26.0 H3:27.5	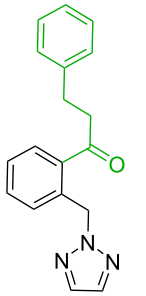
3 [43]	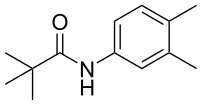	$Pd(OAc)_2$, TBHP, toluene, TFA, 40 °C, 3 h	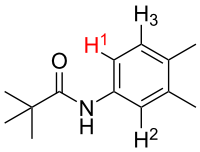 **H1:0.0** H2:1.9 H3:7.6	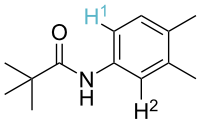 **H1:0.0** H2:3.2	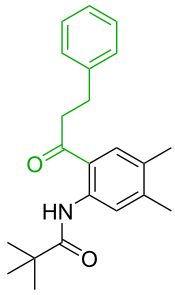
4 [44]	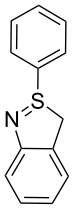	$Pd(OAc)_2$, toluene, TBHP, 110 °C, 5 h	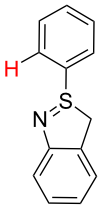	no stable intermediate	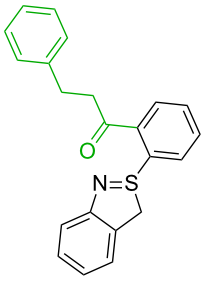
5 [45]	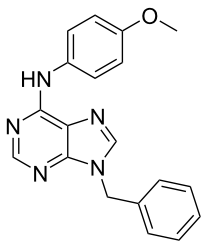	$Pd(OAc)_2$, 1,4-dioxane, AcOH, DMSO, TBHP, 110 °C, 24 h	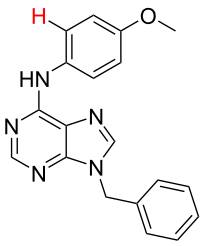	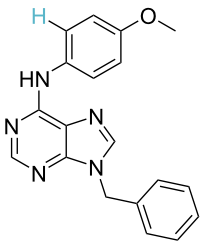	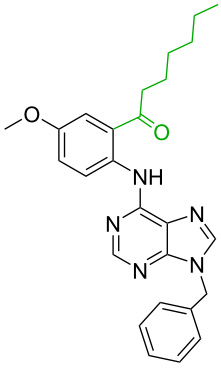

Table 3: A comparison of the published experimental results with the computational predictions for the $Pd(OAc)_2$-catalysed reactions.[a] (continued)

6 [46]	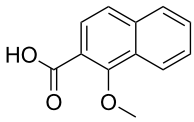	Ag_2CO_3, $Pd(OAc)_2$, NaOAc, CO, 1,4-dioxane, 130 °C, 18 h	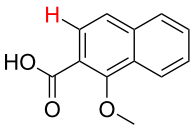	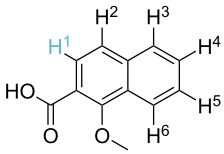 **H1:0.0** H2:2.6 H3: 2.2 H4:2.5 H5:2.2 H6:2.8	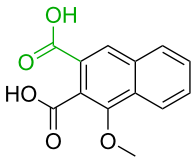

[a]Protons marked red and blue are the predicted active centres via the acidity and the electrophilic mechanisms, respectively.

Table 4: A mechanism threshold tested based on the literature examples.[a]

Entry	Gibbs free energy of Pd–substrate [Hartree]	d(Pd–C) [Å]	Relative stability	Predicted mechanism	Reported mechanism
1	−355.5652	2.3005	3.0777	PA/S_EAr	PA/S_EAr
2	−355.5577	2.3778	−1.6369	PA	PA
3	−355.5626	2.1345	1.4558	PA S_EAr	PA/S_EAr
4	no stable intermediate	–	–	PA	PA
5	355.5717	7.1781	2.2326	S_EAr	S_EAr
6	−355.5254	2.1680	−21.9298	PA	PA

[a]Gibbs free energy of Pd-substrate is obtained by calculating the Gibbs free energy difference between starting molecule and the most probable intermediate in Hartree. The distance between the palladium atom and the corresponding carbon are measured based on the web-based molecular structure virtualization, which can be accessed through https://leyscigateway.ch.cam.ac.uk/index.php.

tational threshold to distinguish between the two main mechanisms, proton abstraction (PA) and electrophilic aromatic substitution (S_EAr) mechanism, has been proposed and tested against literature experimental data. This model can give not only the most probable reactive site and the appropriate mechanism, but also provides information for further kinetic studies and process development, thus contributing to the development of robust new chemical transformations.

Supporting Information

Supporting Information File 1

Comutational details, comparison of data, mechanistic threshold, Cartesian coordinates and energies.
[https://www.beilstein-journals.org/bjoc/content/supplementary/1860-5397-16-122-S1.pdf]

Funding

This project was in part supported by EPSRC grant EP/K009494/1 (MK and SL) and the National Research Foundation, Prime Minister's Office, Singapore under its CREATE programme, project "Cambridge Centre for Carbon Reduction in Chemical Technology" (LC and AL).

ORCID® iDs

Liwei Cao - https://orcid.org/0000-0002-7639-8022
Steven V. Ley - https://orcid.org/0000-0002-7816-0042
Alexei A. Lapkin - https://orcid.org/0000-0001-7621-0889

References

1. Grubbs, R. H.; Chang, S. *Tetrahedron* **1998,** *54,* 4413–4450. doi:10.1016/s0040-4020(97)10427-6
2. Buchwald, S. L.; Mauger, C.; Mignani, G.; Scholz, U. *Adv. Synth. Catal.* **2006,** *348,* 23–39. doi:10.1002/adsc.200505158

3. Buitrago Santanilla, A.; Regalado, E. L.; Pereira, T.; Shevlin, M.; Bateman, K.; Campeau, L.-C.; Schneeweis, J.; Berritt, S.; Shi, Z.-C.; Nantermet, P.; Liu, Y.; Helmy, R.; Welch, C. J.; Vachal, P.; Davies, I. W.; Cernak, T.; Dreher, S. D. *Science* **2015,** *347,* 49–53. doi:10.1126/science.1259203
4. Echtermeyer, A.; Amar, Y.; Zakrzewski, J.; Lapkin, A. *Beilstein J. Org. Chem.* **2017,** *13,* 150–163. doi:10.3762/bjoc.13.18
5. Holmes, N.; Akien, G. R.; Blacker, A. J.; Woodward, R. L.; Meadows, R. E.; Bourne, R. A. *React. Chem. Eng.* **2016,** *1,* 366–371. doi:10.1039/c6re00059b
6. Fitzpatrick, D. E.; Battilocchio, C.; Ley, S. V. *Org. Process Res. Dev.* **2016,** *20,* 386–394. doi:10.1021/acs.oprd.5b00313
7. Segler, M. H. S.; Waller, M. P. *Chem. – Eur. J.* **2017,** *23,* 6118–6128. doi:10.1002/chem.201604556
8. Coley, C. W.; Jin, W.; Rogers, L.; Jamison, T. F.; Jaakkola, T. S.; Green, W. H.; Barzilay, R.; Jensen, K. F. *Chem. Sci.* **2019,** *10,* 370–377. doi:10.1039/c8sc04228d
9. Schwaller, P.; Gaudin, T.; Lányi, D.; Bekas, C.; Laino, T. *Chem. Sci.* **2018,** *9,* 6091–6098. doi:10.1039/c8sc02339e
10. Gao, H.; Struble, T. J.; Coley, C. W.; Wang, Y.; Green, W. H.; Jensen, K. F. *ACS Cent. Sci.* **2018,** *4,* 1465–1476. doi:10.1021/acscentsci.8b00357
11. Korwar, S.; Burkholder, M.; Gilliland, S. E.; Brinkley, K.; Gupton, B. F.; Ellis, K. C. *Chem. Commun.* **2017,** *53,* 7022–7025. doi:10.1039/c7cc02122d
12. Roudesly, F.; Oble, J.; Poli, G. *J. Mol. Catal. A: Chem.* **2017,** *426,* 275–296. doi:10.1016/j.molcata.2016.06.020
13. Chen, X.; Engle, K. M.; Wang, D.-H.; Yu, J.-Q. *Angew. Chem., Int. Ed.* **2009,** *48,* 5094–5115. doi:10.1002/anie.200806273
14. McNally, A.; Haffemayer, B.; Collins, B. S. L.; Gaunt, M. J. *Nature* **2014,** *510,* 129–133. doi:10.1038/nature13389
15. Balcells, D.; Clot, E.; Eisenstein, O. *Chem. Rev.* **2010,** *110,* 749–823. doi:10.1021/cr900315k
16. Dedieu, A. *Chem. Rev.* **2000,** *100,* 543–600. doi:10.1021/cr980407a
17. Tomberg, A.; Muratore, M. É.; Johansson, M. J.; Terstiege, I.; Sköld, C.; Norrby, P.-O. *iScience* **2019,** *20,* 373–391. doi:10.1016/j.isci.2019.09.035
18. Tomberg, A.; Johansson, M. J.; Norrby, P. O. *J. Org. Chem.* **2018,** *84,* 4695–4703. doi:10.1021/acs.joc.8b02270
19. Valiev, M.; Bylaska, E. J.; Govind, N.; Kowalski, K.; Straatsma, T. P.; Van Dam, H. J. J.; Wang, D.; Nieplocha, J.; Apra, E.; Windus, T. L.; de Jong, W. A. *Comput. Phys. Commun.* **2010,** *181,* 1477–1489. doi:10.1016/j.cpc.2010.04.018
20. Kabeshov, M. A.; Śliwiński, É.; Fitzpatrick, D. E.; Musio, B.; Newby, J. A.; Blaylock, W. D. W.; Ley, S. V. *Chem. Commun.* **2015,** *51,* 7172–7175. doi:10.1039/c5cc00782h
21. Krishnan, R.; Binkley, J. S.; Seeger, R.; Pople, J. A. *J. Chem. Phys.* **1980,** *72,* 650–654. doi:10.1063/1.438955
22. Van Speybroeck, V.; Van Neck, D.; Waroquier, M.; Wauters, S.; Saeys, M.; Marin, G. B. *J. Phys. Chem. A* **2000,** *104,* 10939–10950. doi:10.1021/jp002172o
23. Seregin, I. V.; Gevorgyan, V. *Chem. Soc. Rev.* **2007,** *36,* 1173–1193. doi:10.1039/b606984n
24. Sommai, P.-A.; Tetsuya, S.; Yoshiki, K.; Masahiro, M.; Masakatsu, N. *Bull. Chem. Soc. Jpn.* **1998,** *71,* 467–473.
25. García-Cuadrado, D.; de Mendoza, P.; Braga, A. A. C.; Maseras, F.; Echavarren, A. M. *J. Am. Chem. Soc.* **2007,** *129,* 6880–6886. doi:10.1021/ja071034a
26. Hardinger, S. *Chemistry 14D thinkbook;* 2005.
27. Hammond, G. S. *J. Am. Chem. Soc.* **1955,** *77,* 334–338. doi:10.1021/ja01607a027
28. O'Boyle, N. M.; Banck, M.; James, C. A.; Morley, C.; Vandermeersch, T.; Hutchison, G. R. *J. Cheminf.* **2011,** *3,* 33. doi:10.1186/1758-2946-3-33
29. Chen, M.; Ren, Z.-H.; Wang, Y.-Y.; Guan, Z.-H. *J. Org. Chem.* **2015,** *80,* 1258–1263. doi:10.1021/jo502581p
30. Luo, S.; Luo, F.-X.; Zhang, X.-S.; Shi, Z.-J. *Angew. Chem., Int. Ed.* **2013,** *52,* 10598–10601. doi:10.1002/anie.201304295
31. Xia, J.-B.; Wang, X.-Q.; You, S.-L. *J. Org. Chem.* **2009,** *74,* 456–458. doi:10.1021/jo802227u
32. Hossian, A.; Manna, M. K.; Manna, K.; Jana, R. *Org. Biomol. Chem.* **2017,** *15,* 6592–6603. doi:10.1039/c7ob01466j
33. Zhou, H.; Xu, Y.-H.; Chung, W.-J.; Loh, T.-P. *Angew. Chem., Int. Ed.* **2009,** *48,* 5355–5357. doi:10.1002/anie.200901884
34. Jia, X.; Zhang, S.; Wang, W.; Luo, F.; Cheng, J. *Org. Lett.* **2009,** *11,* 3120–3123. doi:10.1021/ol900934g
35. Xu, B.; Liu, W.; Kuang, C. *Eur. J. Org. Chem.* **2014,** 2576–2583. doi:10.1002/ejoc.201400096
36. Wu, J.; Lan, J.; Guo, S.; You, J. *Org. Lett.* **2014,** *16,* 5862–5865. doi:10.1021/ol502749b
37. Tani, S.; Uehara, T. N.; Yamaguchi, J.; Itami, K. *Chem. Sci.* **2014,** *5,* 123–135. doi:10.1039/c3sc52199k
38. Wang, S.; Liu, W.; Cen, J.; Liao, J.; Huang, J.; Zhan, H. *Tetrahedron Lett.* **2014,** *55,* 1589–1592. doi:10.1016/j.tetlet.2014.01.069
39. Zhang, F.; Greaney, M. F. *Angew. Chem., Int. Ed.* **2010,** *49,* 2768–2771. doi:10.1002/anie.200906921
40. Orpen, A. G.; Brammer, L.; Allen, F. H.; Watson, D. G.; Taylor, R. Typical interatomic distances: organometallic compounds and coordination complexes of the d- and f-block metals. In *International Tables for Crystallography Volume C: Mathematical, physical and chemical tables;* Prince, E., Ed.; Springer Netherlands: Dordrecht, 2004; pp 812–896. doi:10.1107/9780955360206000622
41. Wang, J.; Nie, Z.; Li, Y.; Tan, S.; Jiang, J.; Jiang, P.; Ding, Q. *J. Chem. Res.* **2013,** 263–267. doi:10.3184/174751913x13639769724276
42. Tian, Q.; He, P.; Kuang, C. *Org. Biomol. Chem.* **2014,** *12,* 7474–7477. doi:10.1039/c4ob01406e
43. Chan, C.-W.; Zhou, Z.; Yu, W.-Y. *Adv. Synth. Catal.* **2011,** *353,* 2999–3006. doi:10.1002/adsc.201100472
44. Banerjee, A.; Santra, S. K.; Guin, S.; Rout, S. K.; Patel, B. K. *Eur. J. Org. Chem.* **2013,** 1367–1376. doi:10.1002/ejoc.201201503
45. Allu, S.; Swamy, K. C. K. *RSC Adv.* **2015,** *5,* 92045–92054. doi:10.1039/c5ra18447a
46. Giri, R.; Yu, J.-Q. *J. Am. Chem. Soc.* **2008,** *130,* 14082–14083. doi:10.1021/ja8063827

BEILSTEIN JOURNAL OF ORGANIC CHEMISTRY

Mechanochemical green synthesis of hyper-crosslinked cyclodextrin polymers

Alberto Rubin Pedrazzo*, Fabrizio Caldera, Marco Zanetti, Silvia Lucia Appleton, Nilesh Kumar Dhakar and Francesco Trotta

Full Research Paper

Open Access

Address:
Dipartimento di Chimica, Università degli Studi di Torino, Via Giuria 7, Torino 10125, Italy

Email:
Alberto Rubin Pedrazzo* - alberto.rubinpedrazzo@unito.it

* Corresponding author

Keywords:
β-cyclodextrin; ball-milling; crosslinking; green chemistry; mechanochemistry; nanosponges

Beilstein J. Org. Chem. **2020,** *16,* 1554–1563.
doi:10.3762/bjoc.16.127

Received: 04 March 2020
Accepted: 17 June 2020
Published: 29 June 2020

This article is part of the thematic issue "Green chemistry II".

Guest Editor: L. Vaccaro

Abstract

Cyclodextrin nanosponges (CD-NS) are nanostructured crosslinked polymers made up of cyclodextrins. The reactive hydroxy groups of CDs allow them to act as multifunctional monomers capable of crosslinking to bi- or multifunctional chemicals. The most common NS synthetic pathway consists in dissolving the chosen CD and an appropriate crosslinker in organic polar aprotic liquids (e.g., *N*,*N*-dimethylformamide or dimethyl sulfoxide), which affect the final result, especially for potential biomedical applications. This article describes a new, green synthetic pathway through mechanochemistry, in particular via ball milling and using 1,1-carbonyldiimidazole as the crosslinker. The polymer obtained exhibited the same characteristics as a CD-based carbonate NS synthesized in a solvent. Moreover, after the synthesis, the polymer was easily functionalized through the reaction of the nucleophilic carboxylic group with three different organic dyes (fluorescein, methyl red, and rhodamine B) and the still reactive imidazoyl carbonyl group of the NS.

Introduction

The research in the fields of nanomedicine and nanotechnology has nowadays become predominant. Polysaccharides and, among them, starch derivatives such as cyclodextrins (CD), have recently emerged as they are safe, of low cost and biodegradable. Cyclodextrin nanosponges (CD-NS) are crosslinked cyclodextrin polymers characterized by a nanosized three-dimensional network. The reactive hydroxy groups of CDs allow them to act as polyfunctional monomers, permitting the crosslinking with bi- or multifunctional chemicals, such as dianhydrides, diisocyanates, diepoxides, and dicarboxylic acids, etc. The polarity and size of the polymer network can be easily tuned by varying the type of the crosslinker and degree of crosslinking, thus influencing the final properties [1,2].

Among the various bifunctional compounds that could be used as crosslinking agents, active carbonyl compounds, such as carbonyldiimidazole (CDI) and diphenyl carbonate have given interesting results in the last 20 years. The produced CD

nanosponges, after crosslinking, comprise carbonate bonds between the cyclodextrin monomers. If this reaction is carried out under classical conditions in a *N*,*N*-dimethylformamide (DMF) solution, an amorphous crosslinked insoluble polymer is obtained. In general, carbonate nanosponges are insoluble in water and organic solvents and, unlike other types of NS, do not swell appreciably. In addition, they are nontoxic [1,3], stable up to 300 °C, and their structure allows modification through different functional groups before and/or after the synthesis. Carbonate nanosponges demonstrated promising results in removing organic compounds from wastewater and could therefore be suited for purifying water contaminated by persistent organic pollutants (POPs), such as chlorobenzenes and chlorotoluenes [2]. Moreover, CD nanosponges have found many applications in the pharmaceutical field, as for example, drug-delivery systems [3-5]: together with their capability of hosting drugs, they are biocompatible and nontoxic. In the last few years nanosponges were employed to encapsulate and release a wide variety of drugs [6,7], associated with an improvement in bioavailability and release kinetics. Nanosponges, as a powder, could be used as excipients in tablets, capsules, suspensions and dispersions, and topical formulations [8].

The most common NS synthetic pathway consists in dissolving the chosen CD in a suitable solvent, under continuous stirring, and then adding the crosslinker followed by a catalyst, if necessary. The solvents of choice were usually organic polar aprotic liquids, for example, *N*,*N*-dimethylformamide or dimethyl sulfoxide (DMSO). An alternative synthetic route relied on interfacial polymerization, where two immiscible solutions, one consisting of CDs dissolved in an alkaline aqueous solution and the other one containing the crosslinker in a chlorinated immiscible solvent, were mixed and stirred. At the interface between the solutions, crosslinking occurred [9].

In both cases the preparation of nanosponges, especially carbonate nanosponges, required the use of organic and often toxic solvents. The presence of these solvents affected the whole synthesis as the final material required rigorous purification extraction procedures with excess of water or volatile solvents to remove residual solvent inside the material's structure. The removal of any synthetic contamination is essential for the use of nanosponges in the biomedical field. In addition, these synthetic procedures may also not be convenient for a possible future scale up of the reaction, as huge amounts of solvent have to be disposed of. Moreover, organic solvents are expensive and DMSO and DMF are difficult to recycle because of their high boiling points.

According to the Green Chemistry Principles, published in 1998 [10], processes have to be designed in order to "minimize the quantity of final waste and to avoid hazardous or toxic solvents". Nanosponges themselves, nevertheless, are synthesized from starch derivatives and are biodegradable, so they are a very promising material from this point of view.

In this article a new, green synthesis of nanosponges through a mechanochemical approach is proposed.

Mechanochemistry relies on the application of mechanical forces (such as compression, shear, or friction) to drive and control chemical reactions, for example, using grinding or milling to transfer energy to chemical bonds [11]. Mechanochemical transformations are well established in inorganic chemistry and they are easily transferable to an industrial scale [12,13]. Mechanochemistry in organic chemistry, applied to organic syntheses and polymers has gained growing interest in recent years [14-18]. Mechanochemical syntheses are safe and represent efficient activation methods for greener processes, avoiding the use of solvents and reducing energy consumption. Recently, many examples for modifications of starch using ball milling have been reported. These included esterifications and etherifications of starch [19] and cellulose [20]. In 2017, Jicsinszky et al. obtained CD derivatives through a solid-state reaction, using a planetary ball mill [21,22] and by other green processes [23]. The main goal of this work was to obtain cyclodextrin nanosponges via a ball-milling-driven synthesis, having the same physicochemical characteristics as the material synthesized through the solvent-based approach.

Among the various types of cyclodextrin nanosponges, we chose carbonate NS, synthesized with 1,1-carbonyldiimidazole as the crosslinker, for the following reasons: the reaction was usually performed at 90 °C, therefore, the heating of the system related to the ball friction is not only acceptable but also useful for the kinetics of the reaction, and the solvent for solubilizing the reactants was DMF.

We herein present a new green synthesis of biodegradable polymers through a solvent-free procedure, displaying high potential of applications in various fields. After the synthesis, a significant amount of still reactive imidazoyl carbonyl groups within the NS structure were detected. These could be easily removed by washing with water at 40 °C leading to carbonate NS. On the other hand, the presence of a "tunable" quantity of remaining reactive groups could be used for further functionalization. In the present work this was demonstrated by a straightforward covalent coupling of the synthesized cyclodextrin nanosponges with selected organic dyes that are used as probe molecules with different structures (methyl red, rhodamine B, and fluorescein). The simple functionalization of the cyclodextrin NS, in this case via reactive imidazole moieties, is par-

ticularly interesting for a variety of applications. For instance, dye-modified cyclodextrins and CD derivatives have found wide use for the preparation of chemical sensors [24,25]. As CDs and consequently CD nanosponges can be easily coupled with fluorophores, they could find applications in the pharmacological area, for example, as biological markers, in image-guided therapies [26-28], and in conjugated drug delivery. This simple procedure also enables other active molecules to be grafted on the NS, to obtain conjugated nanocarriers, with reducing or in certain cases eliminating the need to use organic solvents.

Results and Discussion

We performed various syntheses using different cyclodextrins with varying molar ratios of the cyclodextrin and crosslinker. Details of all polymers synthetized are collected in Table 1. The abbreviation βNS-CDI bm refers to a crosslinked β-cyclodextrin-based polymer (NS), obtained by crosslinking with CDI in a ball mill (bm). The same abbreviation was used for α and γ-cyclodextrins. The number following the crosslinker in the abbreviation refers to the molar ratio between the cyclodextrin and the crosslinker.

Three different ratios (1:2, 1:4, and 1:8) were tested using β-cyclodextrin. As usual for mechanochemistry [21,29], the synthetic procedure was easy to carry out and gave a high yield (>90%). Good mass balances (68%) were also achieved. The yield was calculated by considering the weight of the dried polymer with respect to the theoretical weight, equal to the sum of β-CD and C=O bridge between β-CDs. The solubility in various common solvents (water, acetone, ethanol, *N*,*N*-dimethylformamide or dimethyl sulfoxide, diethyl ether, and petroleum ether) of the new nanosponges was tested.

Like nanosponges obtained from batch experiments, also the ones from ball-mill synthesis, as expected, were insoluble in the tested solvents, in accordance with the formation of a cross-linked network and with data from previous literature [9].

Table 1: Elemental analysis of NS-CDI polymers synthesized in a ball mill, after PSE and 2, 4 and 8 h in water at 40 °C. The presence of nitrogen was tested starting from t_0 on plain NS after a simple wash with water and acetone at rt, after PSE extraction in acetone (high temperature and pressure, which efficiently removed imidazole, IMH), and after 2, 4 and 8 h of hydrolysis in water at 40 °C in order to remove the residual covalently bonded imidazolyl carbonyl group.

type of nanosponge	weight % of nitrogen		STD
αNS-CDI 1:4 bm	t_0 (plain NS)	1.33	0.07
	after 2 h in H_2O 40 °C	0.53	0.02
	after 4 h in H_2O 40 °C	0.25	0.00
	after 8 h in H_2O 40 °C	0.20	0.01
βNS-CDI 1:4 bm	t_0 (plain NS)	2.69	0.12
	after 2 h in H_2O 40 °C	0.63	0.01
	after 4 h in H_2O 40 °C	0.31	0.01
	after 8 h in H_2O 40 °C	0.23	0.02
γNS-CDI 1:4 bm	t_0 (plain NS)	2.21	0.16
	after 2 h in H_2O 40 °C	0.61	0.02
	after 4 h in H_2O 40 °C	0.11	0.10
	after 8 h in H_2O 40 °C	0.00	0.00
βNS-CDI 1:8 bm	t_0 (plain NS)	6.39	0.05
	after 2 h in H_2O 40 °C	2.56	0.03
	after 4 h in H_2O 40 °C	1.31	0.03
	after 8 h in H_2O 40 °C	0.40	0.03
βNS-CDI 1:2 bm	t_0 (plain NS)	1.27	0.01
	after 2 h in H_2O 40 °C	0.77	0.01
	after 4 h in H_2O 40 °C	0.52	0.01
	after 8 h in H_2O 40 °C	0.17	0.01
after pressurized solvent extraction			
βNS-CDI 1:2 bm	after PSE (acetone)	0.79	0.02
βNS-CDI 1:4 bm	after PSE (acetone)	1.19	0.07
βNS-CDI 1:8 bm	after PSE (acetone)	3.28	0.09

Figure 1 reports FTIR spectra of the cyclodextrin NS, with a comparison between βNS-CDI 1:4 obtained through ball-mill synthesis and βNS-CDI 1:4 from synthesis in DMF and a comparison of the FTIR spectra after 4 h treatment in water at 40 °C. The FTIR spectra of βNS-CDI 1:4 obtained through different synthetic approaches, with and without solvent, exhibited a band at around 1750 cm^{-1} due to the carbonyl group of the carbonate bond. Even after hours of treatment in H_2O at 40 °C the band was still present confirming the stability of the system. The spectra were almost superimposable, confirming the structure and the formation of carbonate bonds.

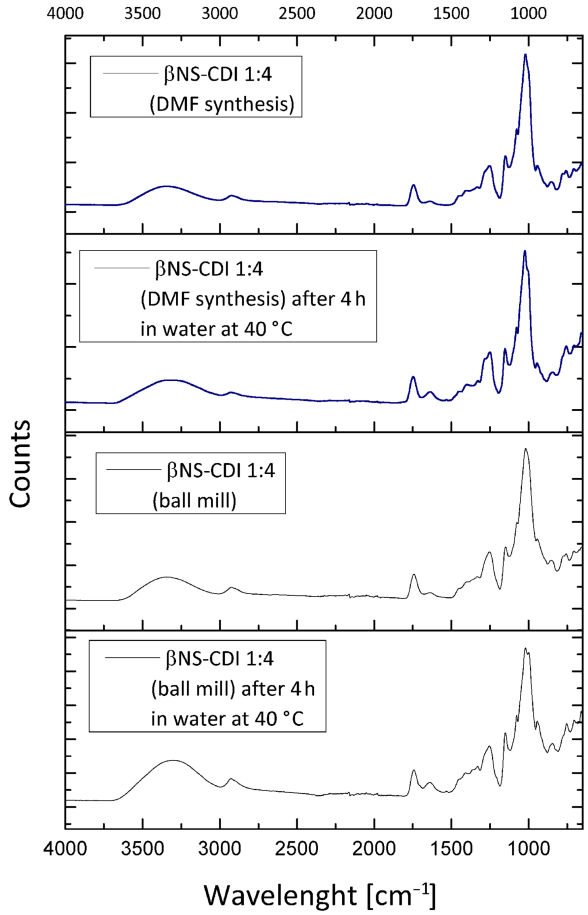

Figure 1: FTIR analysis of βNS-CDI 1:4, before and after treatment for 4 h in H_2O at 40 °C, synthesized with and without solvent. The band of interest at around 1750 cm^{-1} assignable to the carbonyl group of the carbonate bond, was visible in all samples, even after treating for hours in H_2O at 40 °C.

It was evident from the TG mass-loss curves and the corresponding derivate curves of the β-CD-based carbonate nanosponges (Figure 2), used for all further characterizations, that the crosslinked polymers synthesized by both methods exhibited a very close degradation path and, consequently, the same molecular structure was expected. The largest mass loss started above 300 °C for both βNS and the relative maximum rate peak was located at around 345 °C for both the βNS-CDI 1:4 from DMF and for the βNS-CDI 1:4 from ball mill. The initial mass loss present in both βNS-CDI 1:4 was due to adsorbed environmental water, always present when dealing with hygroscopic cyclodextrin-based nanoparticles. In addition to this, the particle size played a key role: the smaller the particles were the more the extended surface was exposed to the environmental humidity. In Figure 3, a direct comparison of the thermograms of αNS, βNS, and γNS synthesized through the ball-mill approach are shown.

As can be seen from Figure 3, the degradation paths were similar, however, with an interesting difference in the initial loss of water, which was due to the different water affinity of the CDs, resulting in different hygroscopy of the final materials.

In Figure 4, a test on the ability of the β-CD-based carbonate nanosponge obtained through ball-mill synthesis to remove organic compounds from aqueous solutions is shown. As can be seen methyl red was completely removed from its solution by adding a small amount of the bm carbonate nanosponge (50 mg for 10 mL of an aqueous solution of methyl red, 50 ppm).

As determined by DLS, the particle sizes of the βNS-CDI obtained through ball milling, were less than a micron (800–900 nm) immediately after the synthesis. Moreover, stable suspensions (also in time) with a particle size of around 200 nm for all βNS-CDI were obtained after a short cycle of ball milling with smaller spheres (for details, see Supporting Information File 1).

The zeta-potential, Figure 5, of colloidal suspensions of bm βNS-CDI was tested for all of the nanomaterials. In general, the stronger the charge, the better the colloidal stability of the particles: βNS-CDI synthesized by ball-milling showed an interesting negative ζ-potential, which explained the stability of the dispersion.

As shown in Figure 5, all CD nanosponges exhibited a negative ζ-potential and this was in line with previous literature [2,9,30]. The negative charge seemed to be related to the amount of crosslinker: the larger the amount, the more negative the ζ-potential detected. The elemental analyses showed the presence of nitrogen even after pressurized solvent extraction (PSE) and this was attributed to the presence of reactive imidazolyl carbonyl groups (IM). In an ideal reaction, the carbonyl diimidazole should react completely with two hydroxy groups of CDs, forming a carbonate bond between two monomers and therefore releasing two imidazole molecules that are soluble in water and could be removed after synthesis.

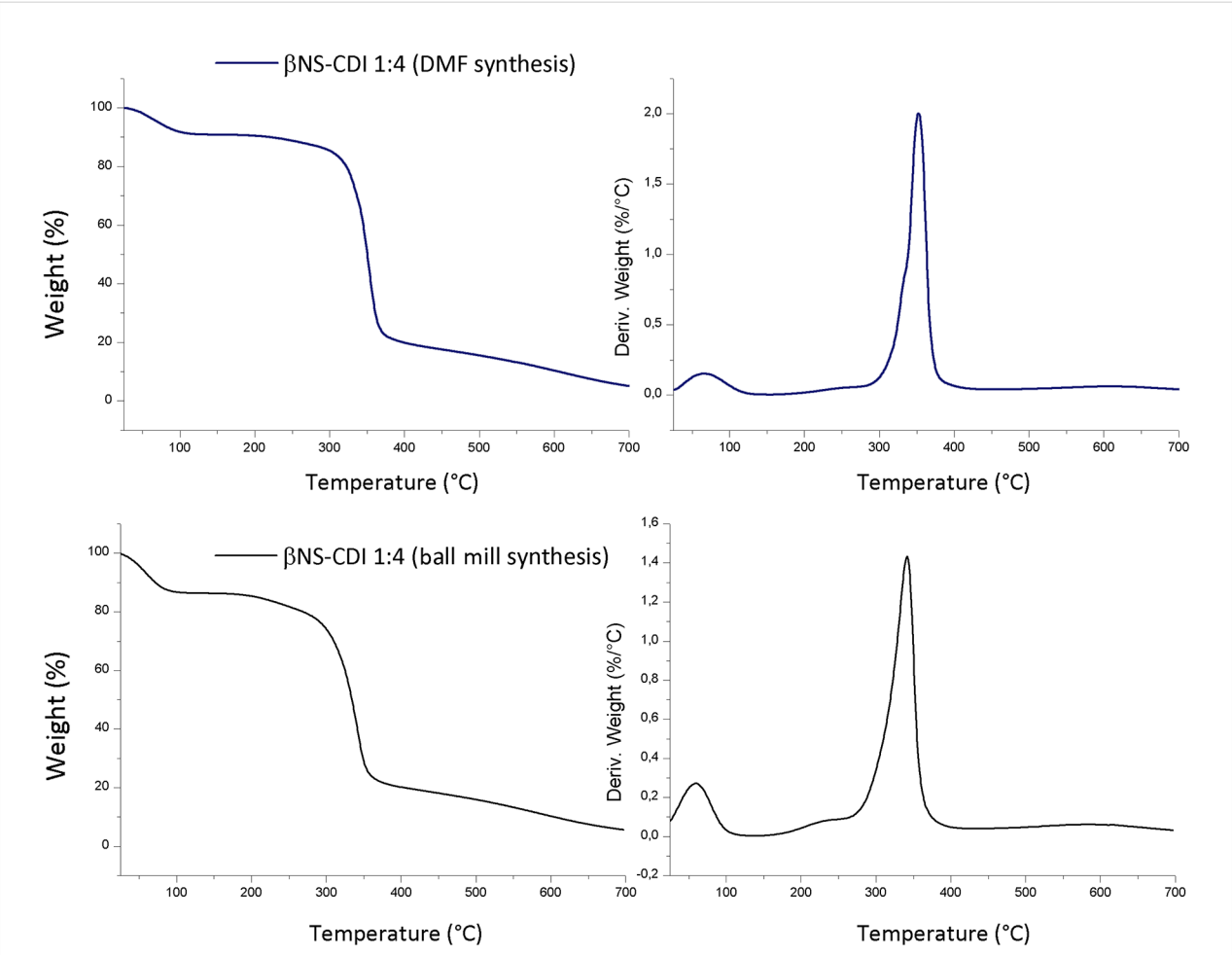

Figure 2: Thermogravimetric analysis of β-CD-based carbonate nanosponges, obtained through solution (DMF) and mechanochemical (ball mill) synthesis. Conditions: nitrogen flow, ramp rate 10 °C/min, rt to 700 °C.

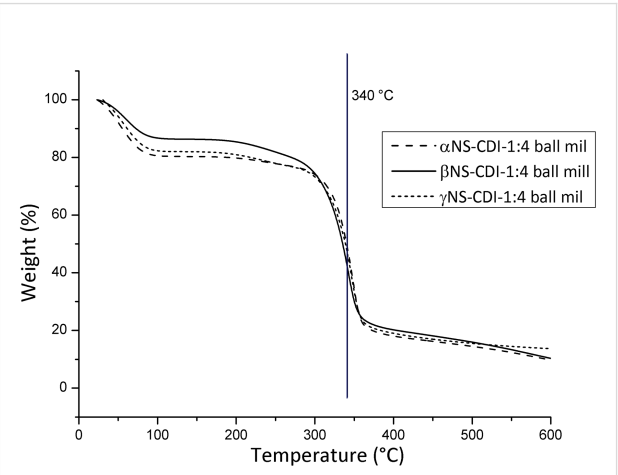

Figure 3: Thermogravimetric analysis of α, β and γ-CD-based carbonate nanosponges, obtained through ball-mill synthesis. Conditions: nitrogen flow, ramp rate 10 °C/min.

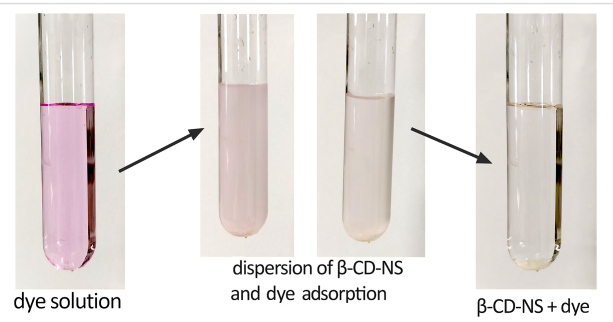

Figure 4: Adsorption of organic dyes by ball-mill synthesized β-CD-based carbonate nanosponges. Conditions: a small amount of NS (50 mg) was added to a clear solution containing the dye (10 mL). After the adsorption and the deposition of the NSs powder containing the organic dye, a clear solution was obtained.

CDI, however, may react asymmetrically forming only one bond with cyclodextrin leaving one of the two moieties reactive. This is consistent with what was reported in the literature: the

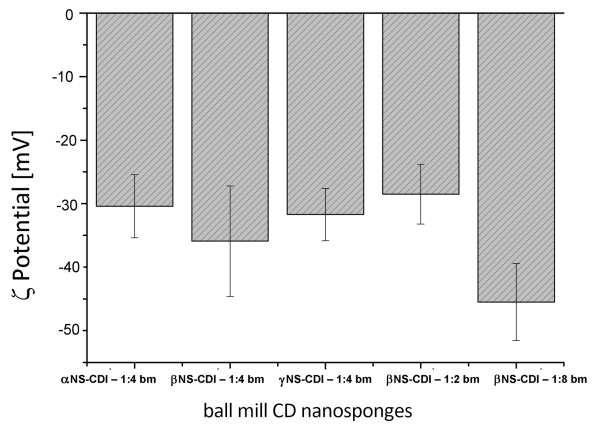

Figure 5: ζ-Potential of bm cyclodextrin nanosponges with relative STDev (mV).

first activation of an alcohol by carbonyl imidazole showed faster kinetics than the second one, which needed longer reaction times and/or a higher temperature (from 60 °C to 80 °C) to obtain a significant yield [31,32].

To distinguish between the free imidazole (IMH) as byproduct and IM still able to form bonds (for example, with nucleophilic groups of active molecules) βNS-CDI was treated in two different ways: the first one entailed "hard" washing of the samples using acetone and PSE. Since acetone does not react by hydrolyzing the bond between the NS and the IM, the high pressure (120 bar) in PSE allowed the removal of the encapsulated IMH. The second treatment was longer and involved maintaining a small amount of material in water at 40 °C for 8 h, in order to effect hydrolysis (Figure 6):

Every 2 h, aliquots were withdrawn, washed with water to remove IMH, freeze-dried, and subjected to elemental analysis. The results were summarized in Table 1 and in Figure 7, nitrogen contents determined for different CD monomers reacted at the same CD/CDI ratio and for β-CD crosslinked with CDI at different ratios are shown. In Figure 1, the comparison between DMF and βNS-CDI 1:4 bm after 4 h treatment in water, confirmed what was stated in the previous paragraphs, such as the solubility and especially the consistency as far as the properties are concerned between the βNS-CDI obtained through the two different kinds of synthesis.

The results of the elemental analysis, reported in detail in Table 1 and Figure 7 agreed with what was expected from the reaction conditions and applied molar ratios: the βNS-CDI 1:8 exhibited the highest nitrogen content (around 6 wt %), before any further steps of purification. This result was consistent with the quantity of CDI involved in this nanosponge as it was 2–4 times higher as for the other βNS-CDI, assuming that the kinetics and reactivity were the same in all experiments. As a consequence, the IMH and unreacted IM contents were higher. Noteworthy was that most of the CDI reacted in the crosslinking step, as the amount of nitrogen after PSE using acetone dramatically decreased due to release of the IMH byproduct entrapped in the NS network. Furthermore, it could be stated that after about 8 hours, it was possible to eliminate almost completely both IMH and IM, using only water, from all nanomaterials.

The solubility and physicochemical properties of the NS-CDI were not depleted by these two different processes: all NS-CDI, with different molar ratios and different CDs, were still not soluble in any of the solvents tested previously (therefore, as shown in Figure 1, for βNS-CDI 1:4 the FTIR spectra were comparable). Hydrolysis, in fact, affected only the imidazolyl carbonyl groups and not the carbonate bond of the CD-NSs.

In order to confirm the presence of reactive imidazolyl carbonyl groups, which would make the functionalization of NS

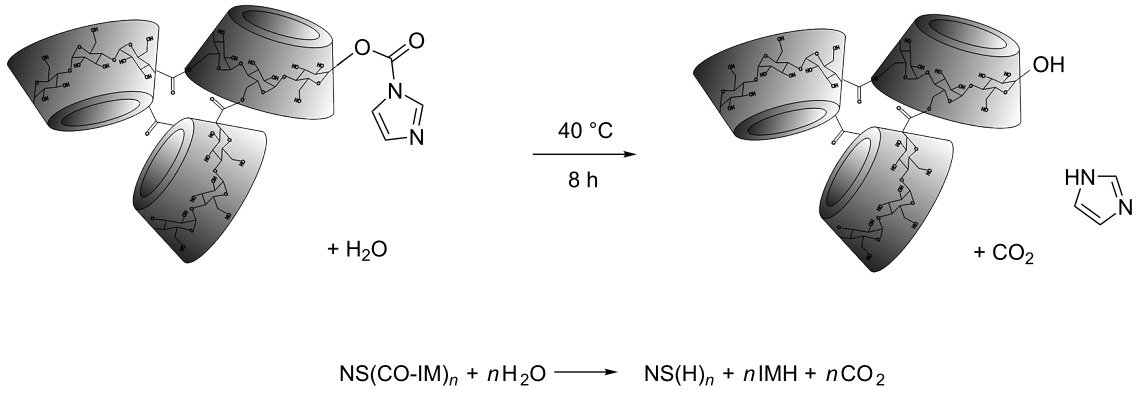

Figure 6: Hydrolysis of the imidazoyl carbonyl group in water at 40 °C.

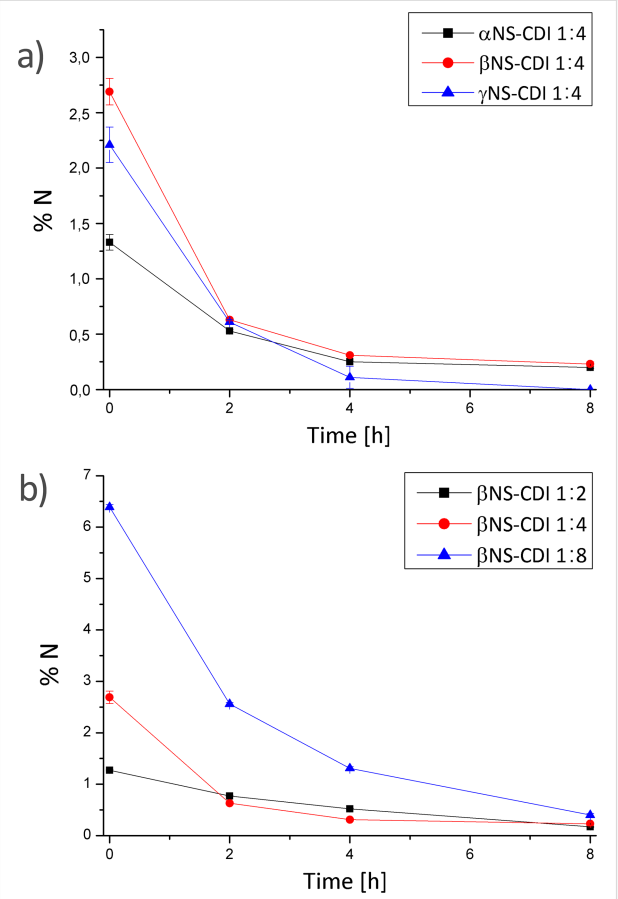

Figure 7: Nitrogen content in weight % in cyclodextrins NS-CDI from ball mill synthesis. a) comparison between different monomers with the same CD/CDI ratio and b) between the same CD crosslinked with different ratios.

possible, an attempt was made on βNS-CDI 1:8 by using different organic dyes. First, βNS-CDI 1:8 was purified by PSE (and so, with only reactive IM left) and accurately milled. The functionalization, as described in the experimental section, was performed in DMSO, an organic solvent in which the material was insoluble but which was suitable for reactions in an anhydrous environment as in this case with organic dyes.

The choice fell on three common, well known and widely investigated organic dyes, i.e., fluorescein, methyl red, and rhodamine B. They have a slightly different structures (and color), and also different surface charges but share a reactive nucleophilic carboxylic group. The simplified schematic reaction (previously reported by Staab [31] and more recently by Jadhav et al. [33]), with the relative ζ-pot of nanoparticles after functionalization, is presented in Figure 8. Through a simple reaction in closed vials with an excess (dye/CD ratio) of the organic dye, a covalent bond formation with the still reactive NS was achieved. As shown by elemental analysis, after PS extraction, the amount of nitrogen and therefore of reactive IM was very low. The experiment was conducted on nanosponges having 1:2, 1:4, 1:8 βCD/CDI ratios, and good results were obtained only with βNS-CDI 1:8. Even in case of βNS-CDI 1:8, if treated for 8 h in H_2O at 40 °C (0.40% N), presented a low amount (≈0) of reactive IM, therefore the reaction did not occur at all, leading only to an inclusion complex with the dyes, which could be easily removed through a PS extraction with acetone). Moreover, this could be also explained since not all the reactive groups are freely accessible within the NS structure.

Carbonyl diimidazole can react with carboxylic acids at room temperature in many aprotic solvents (such as tetrahydrofuran, DMSO, or DMF) to form imidazolides in nearly quantitative yields, with the release of carbon dioxide and formation of IMH. The reaction kinetics of alcohols with *N*,*N*'-carbonyldiimidazole were generally slower, so the presence of

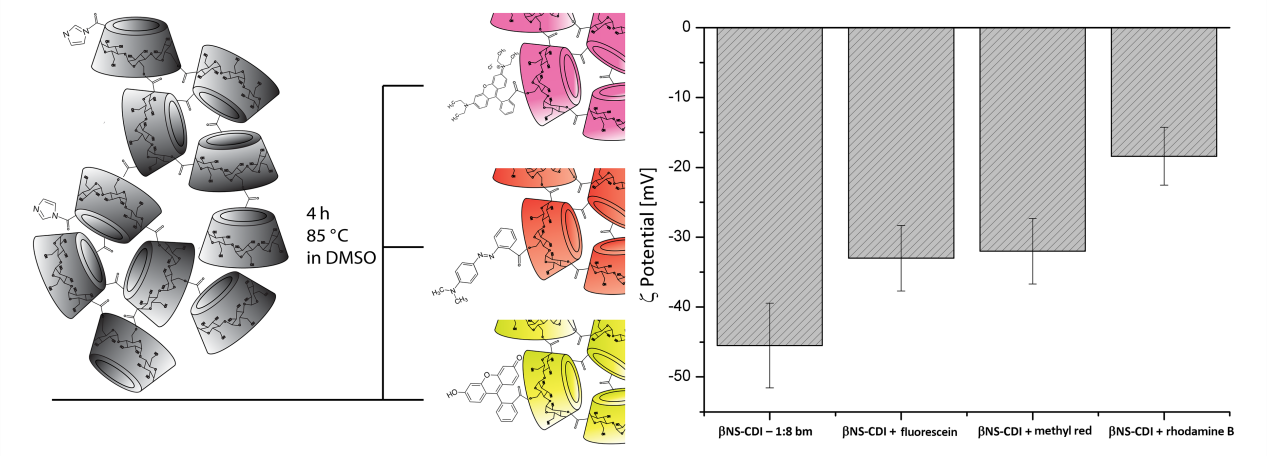

Figure 8: Simplified schematic reaction and procedure for obtaining the dye-functionalized βNS-CDI. Surface zeta potential of the plain and functionalized βNS-CDI 1:8.

reactive IM moieties may be particularly interesting for an easy functionalization via reaction with nucleophilic carboxy groups [31].

Additionally, the reaction with fluorescein was tested on both βNS-CDI 1:4 and βNS-CDI 1:2, which exhibited a considerably lower amount of nitrogen and consequently of reactive IM (nitrogen content: 0.79 wt % and 1.19 wt % for βNS-CDI 1:2 and 1:4, respectively, and 3.28 wt % for βNS-CDI 1:8 based on elemental analysis; see Table 1 for details). No appreciable differences in color or in ζ potential were observed. The presence of reactive imidazole was therefore crucial for this type of easy functionalization under mild conditions. The βNS-CDI 1:8 samples after reaction with the organic dyes and after two extractions with PSE using acetone, were colored. The functionalized materials were still insoluble in the tested solvents with no release of the dyes in any of them.

Of particular interest was the difference in the surface ζ-potential. It ranged from a very negative ζ-potential of around −45 mV (due to carbonate bonds and IM groups) to −33 mV, −32 mV, and −18,4 mV, after reaction with fluorescein, methyl red, and rhodamine B, respectively. The variation of the ζ-potential was consistent with the rhodamine B structure, exhibiting a positive charge. The elemental analyses of the samples containing rhodamine B, confirmed the presence of the organic compound within the structure (≈1 wt % N).

Conclusion

Crosslinked cyclodextrin polymers, also called nanosponges (NS), were prepared via a new synthetic route based on mechanochemistry. The green synthetic route proposed here afforded a biodegradable polymer, displaying the same characteristics as cyclodextrin-based polymers synthesized in a solvent-based approach. The CD-based carbonate NSs were synthesized using an active carbonyl compound as a crosslinker, 1,1-carbonyldiimidazole, leading to an insoluble crosslinked polymer after 3 hours of ball milling. The synthesis was carried out using different cyclodextrins (α, β, and γ) and adopting the following molar ratios between cyclodextrin and the crosslinker, 1:2, 1:4 and 1:8.

The polymer obtained using the ball-mill method exhibited the same characteristics as a CD-based carbonate NS synthesized in a solvent and displayed insolubility in water and organic solvents. FTIR and TG analyses were performed on the new material, confirming the structure with a carbonate bond.

Nanoparticles, after cycles of ball milling and high-pressure homogenization had a mean diameter of less than 200 nm, as determined by DLS, and exhibited a negative ζ-potential (the most negative being at around −45 mV, measured for βNS at a 1:8 ratio of β-cyclodextrin/carbonyldiimidazole). Elemental analyses were conducted on all synthesized nanosponges in order to detect the presence of nitrogen derived from reactive imidazole moieties originating, in turn, from carbonyl diimidazole. This was confirmed by the reaction between the nanoparticles obtained and the nucleophilic carboxylic group of three different organic dyes, fluorescein, methyl red, and rhodamine B, leading to a colored (even after a PS extraction) functionalized material, with a less negative ζ potential.

Experimental

Materials

β-Cyclodextrin (β-CD), α-cyclodextrin (α-CD), and γ-cyclodextrin (γ-CD) were kindly provided by Roquette Italia SpA and Wacker Chemie. Carbonyldiimidazole (CDI, ≥97.0% (T)), 1,4-diazabicyclo[2.2.2]octane (DABCO, ReagentPlus® grade, ≥99%), methyl red, rhodamine B, and fluorescein (for all dyes, declared dye content 95%), *N*,*N*-dimethylformamide (DMF, anhydrous, 99.8%), acetone (ACS reagent, ≥99.5%), and ethanol (ACS reagent, 96%) were purchased from Sigma-Aldrich (Munich, Germany) and used without further purification. The cyclodextrins were dried before use in an oven at 100 °C until constant weight. Elemental analyses were performed on a Thermo Scientific FlashEA 1112, using vanadium pentoxide purchased from Sigma. As planetary ball mill, a Retsch PM200 High Speed Planetary Ball Mill was used, with 20 sintered zirconium oxide balls of 10 mm diameter in 2 jars of 50 mL (10 balls per jar), also made from zirconium oxide. Rotation speed: sun wheel speed 600 rpm, changing rotation direction from clockwise to anticlockwise every 15 min. Thermogravimetric analyses were carried out on a Hi-res TGA 2050 Thermogravimetric Analyzer from TA Instruments. Parameters for all TG analyses were as the following: nitrogen flow, ramp rate 10 °C/min, rt to 700 °C. IR spectra of dried powders were recorded on a PerkinElmer Spectrum 100 FT-IR Spectrometer with 16 scans. Zeta potential and DLS measurements were performed on Zetasizer Nano ZS from Malvern Panalytical. All measurements were performed in triplicate. Solvent extraction for purifying samples was carried out with a pressurized solvent extractor (PSE) SpeedExtractor E-914 from Büchi.

Solvent synthesis of cyclodextrin nanosponges

The synthesis of α, β, γ carbonate nanosponges in a solvent is widely described in the literature [2,3]. The CDI crosslinked nanosponges synthesized for comparison with the ball-mill NS were prepared at different molar ratios of the respective anhydrous cyclodextrin and carbonyl diimidazole. For the 1:4 molar ratio, for example, the procedure was as follows: 3.00 g of α-cyclodextrin, 3.33 g of β-cyclodextrins and 4.05 g of

γ-cyclodextrins (3.30 mmol) were dissolved in 10 mL of DMF (in three different round-bottomed flasks). After complete dissolution of the cyclodextrins, 2.00 g (13 mmol) of CDI as cross linker were added to each batch. The three flasks were heated at 90 °C for 3 h under stirring in an oil bath. Once the reaction was complete, the solid bulk obtained was crushed in a mortar, then extracted by PSE to remove the solvent, and unreacted crosslinker and CD. Finally, the polymers were ball-milled for 45 min.

Ball-mill synthesis of cyclodextrin nanosponges

The three CD crosslinked polymers were prepared using a ball mill in a one-step reaction without a solvent. The α, β, γ carbonate nanosponges were synthesized in the ball mill at 1:2, 1:4 and 1:8 molar ratios of the respective anhydrous cyclodextrin and carbonyldiimidazole. For example, for the 1:4 ratio synthesis, 3.38 g of α-cyclodextrin, 3.75 g of β-cyclodextrins and 4.56 g of γ-cyclodextrins were placed inside a 50 mL jar containing 10 zirconia balls. The amount of CDI added in each batch to maintain the 1:4 molar ratio was 2.25 g.

After 3 h of sun wheel rotation at 600 rpm, the reaction was completed and the external temperature was between 50–60 °C (the temperature according to previous studies reported in the literature was always indicated as lower than 72 °C under various conditions [22]). The finely ground powder was then dispersed in water and washed several times with deionized water and acetone. The samples were then extracted by pressurized solvent extraction (PSE), using acetone, to remove the residual imidazole in the NS structures.

Functionalization of cyclodextrin nanosponges

The functionalization was done following the same procedure for all samples: 500 mg of carbonate βNS 1:2, 1:4, 1:8 (molar ratio between β-CD and crosslinker, as mentioned previously) were dispersed in anhydrous DMSO. An excess of the organic dye (50 mg of dye, 10 wt % of the NS), methyl red, rhodamine B, and fluorescein, respectively, was then added to the dispersion, followed by heating at 85 °C in an oil bath for 4 h. The final product was washed with an excess of water and then extracted with acetone using PSE to remove the unreacted dyes.

Supporting Information

Supporting Information File 1

Additional experimental data.
[https://www.beilstein-journals.org/bjoc/content/supplementary/1860-5397-16-127-S1.pdf]

Acknowledgements

We thank Roquette Frères and Wacker Chemie AG.

ORCID® iDs

Marco Zanetti - https://orcid.org/0000-0001-7074-9859

References

1. Caldera, F.; Tannous, M.; Cavalli, R.; Zanetti, M.; Trotta, F. *Int. J. Pharm.* **2017,** *531,* 470–479. doi:10.1016/j.ijpharm.2017.06.072
2. Trotta, F. Cyclodextrin Nanosponges and their Applications. In *Cyclodextrins in Pharmaceutics, Cosmetics and Biomedicine: Current and Future Industral Applications;* Bilensoy, E., Ed.; John Wiley & Sons, Inc.: Hoboken, NJ, USA, 2011; pp 323–342. doi:10.1002/9780470926819.ch17
3. Trotta, F.; Zanetti, M.; Cavalli, R. *Beilstein J. Org. Chem.* **2012,** *8,* 2091–2099. doi:10.3762/bjoc.8.235
4. Trotta, F.; Caldera, F.; Cavalli, R.; Soster, M.; Riedo, C.; Biasizzo, M.; Uccello Barretta, G.; Balzano, F.; Brunella, V. *Expert Opin. Drug Delivery* **2016,** *13,* 1671–1680. doi:10.1080/17425247.2017.1248398
5. Trotta, F.; Dianzani, C.; Caldera, F.; Mognetti, B.; Cavalli, R. *Expert Opin. Drug Delivery* **2014,** *11,* 931–941. doi:10.1517/17425247.2014.911729
6. Swaminathan, S.; Cavalli, R.; Trotta, F. *Wiley Interdiscip. Rev.: Nanomed. Nanobiotechnol.* **2016,** *8,* 579–601. doi:10.1002/wnan.1384
7. Cavalli, R.; Trotta, F.; Tumiatti, W. *J. Inclusion Phenom. Macrocyclic Chem.* **2006,** *56,* 209–213. doi:10.1007/s10847-006-9085-2
8. Krabicová, I.; Appleton, S. L.; Tannous, M.; Hoti, G.; Caldera, F.; Rubin Pedrazzo, A.; Cecone, C.; Cavalli, R.; Trotta, F. *Polymers (Basel, Switz.)* **2020,** *12,* 1122. doi:10.3390/polym12051122
9. Trotta, F.; Shende, P.; Biasizzo, M. Method for Preparing Dextrin Nanosponges. PCT Pat. Appl. WO2012/147069 A1, Nov 1, 2012.
10. Anastas, P. T.; Warner, J. C. *Green Chemistry: Theory and Practice;* Oxford University Press: Oxford, UK, 1998.
11. Takacs, L. *Chem. Soc. Rev.* **2013,** *42,* 7649–7659. doi:10.1039/c2cs35442j
12. Burmeister, C. F.; Kwade, A. *Chem. Soc. Rev.* **2013,** *42,* 7660–7667. doi:10.1039/c3cs35455e
13. Wang, X.; Sun, F.; Huang, Y.; Duan, Y.; Yin, Z. *Chem. Commun.* **2015,** *51,* 3117–3120. doi:10.1039/c4cc08876j
14. Willis-Fox, N.; Rognin, E.; Aljohani, T. A.; Daly, R. *Chem* **2018,** *4,* 2499–2537. doi:10.1016/j.chempr.2018.08.001
15. Lanzillotto, M.; Konnert, L.; Lamaty, F.; Martinez, J.; Colacino, E. *ACS Sustainable Chem. Eng.* **2015,** *3,* 2882–2889. doi:10.1021/acssuschemeng.5b00819
16. Tan, D.; Friščić, T. *Eur. J. Org. Chem.* **2018,** 18–33. doi:10.1002/ejoc.201700961
17. Andersen, J.; Mack, J. *Green Chem.* **2018,** *20,* 1435–1443. doi:10.1039/c7gc03797j
18. Bose, A.; Mal, P. *Beilstein J. Org. Chem.* **2019,** *15,* 881–900. doi:10.3762/bjoc.15.86
19. Gilet, A.; Quettier, C.; Wiatz, V.; Bricout, H.; Ferreira, M.; Rousseau, C.; Monflier, E.; Tilloy, S. *Green Chem.* **2018,** *20,* 1152–1168. doi:10.1039/c7gc03135a

20. Gan, T.; Zhang, Y.; Su, Y.; Hu, H.; Huang, A.; Huang, Z.; Chen, D.; Yang, M.; Wu, J. *Cellulose* **2017,** *24,* 5371–5387. doi:10.1007/s10570-017-1524-2
21. Jicsinszky, L.; Caporaso, M.; Calcio Gaudino, E.; Giovannoli, C.; Cravotto, G. *Molecules* **2017,** *22,* 485. doi:10.3390/molecules22030485
22. Jicsinszky, L.; Tuza, K.; Cravotto, G.; Porcheddu, A.; Delogu, F.; Colacino, E. *Beilstein J. Org. Chem.* **2017,** *13,* 1893–1899. doi:10.3762/bjoc.13.184
23. Cravotto, G.; Caporaso, M.; Jicsinszky, L.; Martina, K. *Beilstein J. Org. Chem.* **2016,** *12,* 278–294. doi:10.3762/bjoc.12.30
24. Ogoshi, T.; Harada, A. *Sensors* **2008,** *8,* 4961–4982. doi:10.3390/s8084961
25. Kuwabara, T.; Nakajima, H.; Nanasawa, M.; Ueno, A. *Anal. Chem. (Washington, DC, U. S.)* **1999,** *71,* 2844–2849. doi:10.1021/ac9814041
26. Mieszawska, A. J.; Kim, Y.; Gianella, A.; van Rooy, I.; Priem, B.; Labarre, M. P.; Ozcan, C.; Cormode, D. P.; Petrov, A.; Langer, R.; Farokhzad, O. C.; Fayad, Z. A.; Mulder, W. J. M. *Bioconjugate Chem.* **2013,** *24,* 1429–1434. doi:10.1021/bc400166j
27. Becuwe, M.; Landy, D.; Delattre, F.; Cazier, F.; Fourmentin, S. *Sensors* **2008,** *8,* 3689–3705. doi:10.3390/s8063689
28. Huang, J.; Weinfurter, S.; Pinto, P. C.; Pretze, M.; Kränzlin, B.; Pill, J.; Federica, R.; Perciaccante, R.; Ciana, L. D.; Masereeuw, R.; Gretz, N. *Bioconjugate Chem.* **2016,** *27,* 2513–2526. doi:10.1021/acs.bioconjchem.6b00452
29. Wang, G. W. *Chem. Soc. Rev.* **2013,** *42,* 7668–7700. doi:10.1039/c3cs35526h
30. Dhakar, N. K.; Caldera, F.; Bessone, F.; Cecone, C.; Pedrazzo, A. R.; Cavalli, R.; Dianzani, C.; Trotta, F. *Carbohydr. Polym.* **2019,** *224,* 115168. doi:10.1016/j.carbpol.2019.115168
31. Staab, H. A. *Angew. Chem., Int. Ed. Engl.* **1962,** *1,* 351–367. doi:10.1002/anie.196203511
32. Trotta, F.; Moraglio, G.; Marzona, M.; Maritano, S. *Gazz. Chim. Ital.* **1993,** *123,* 559.
33. Jadhav, S. A.; Karande, S. D.; Burungale, S. H. *Mater. Des. Process. Commun.* **2019,** *1,* e75. doi:10.1002/mdp2.75

License and Terms

BEILSTEIN JOURNAL OF ORGANIC CHEMISTRY

One-pot synthesis of isosorbide from cellulose or lignocellulosic biomass: a challenge?

Isaline Bonnin[1,2], Raphaël Mereau[2], Thierry Tassaing[2] and Karine De Oliveira Vigier[*1]

Review

Open Access

Address:
[1]Université de Poitiers, IC2MP, UMR CNRS 7285, 1 rue Marcel Doré, 86073 Poitiers Cedex 9, France and [2]Institut des Sciences Moléculaires, UMR 5255 CNRS-Université de Bordeaux, 351 Cours de la Libération, 33405 Talence Cedex, France

Email:
Karine De Oliveira Vigier[*] - karine.vigier@univ-poitiers.fr

* Corresponding author

Keywords:
catalysis; cellulose; isosorbide; lignocellulosic biomass

Beilstein J. Org. Chem. **2020,** *16,* 1713–1721.
doi:10.3762/bjoc.16.143

Received: 15 April 2020
Accepted: 02 July 2020
Published: 16 July 2020

This article is part of the thematic issue "Green chemistry II".

Guest Editor: L. Vaccaro

Abstract

The catalytic conversion of (ligno)cellulose is currently subject of intense research. Isosorbide is one of the interesting products that can be produced from (ligno)cellulose as it can be used for the synthesis of a wide range of pharmaceuticals, chemicals, and polymers. Isosorbide is obtained after the hydrolysis of cellulose to glucose, followed by the hydrogenation of glucose to sorbitol that is then dehydrated to isosorbide. The one-pot process requires an acid and a hydrogenation catalyst. Several parameters are of importance during the direct conversion of (ligno)cellulose such as the acidity, the crystallinity and the particle size of cellulose as well as the nature of the feedstocks. This review highlights all these parameters and all the strategies employed to produce isosorbide from (ligno)cellulose in a one-pot process.

Introduction

Cellulose, a homopolymer of D-glucose, is the most abundant component of lignocellulosic biomass. Cellulose is a crystalline polymer due to its intra- and intermolecular hydrogen bond network. The conversion of cellulose to added value chemicals has received a lot of interest due to the rarefaction of fossil oil and environmental concerns. One of the interesting reactions is the conversion of cellulose to isosorbide, a 1,4:3,6-dianhydrohexitol [1]. This reaction occurs in several steps: 1) hydrolysis of cellulose to glucose 2) hydrogenation of glucose to sorbitol and 3) dehydration of sorbitol to isosorbide (Scheme 1).

Isosorbide, a molecule obtained from biomass can find many applications such as additives, pharmaceuticals [2,3] and monomers for polymer industries [4-6]. For instance, one polymer obtained from isosorbide, poly(ethylene-*co*-isosorbide) terephthalate, can replace polyethylene terephthalate (PET) [7]. In the production of polycarbonate and epoxy resins, the physicochemical properties of isosorbide allow the replacement of bisphenol A by this bio-based molecule [8,9]. At an industrial level, isosorbide is produced from the double dehydration of D-sorbitol using a strong acid catalyst [10,11]. D-Sorbitol is pro-

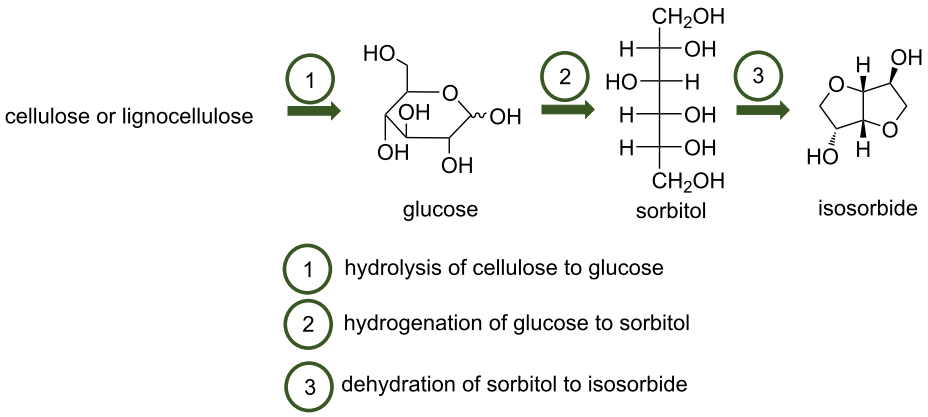

Scheme 1: Conversion of cellulose to isosorbide.

duced from the hydrogenation of glucose obtained mostly from the hydrolysis of starch, but also from sucrose or cellulose. Consequently, the cellulose valorization can be realized from the one-pot conversion of cellulose to isosorbide. The hydrolysis of cellulose to glucose, the first step, is reported using acid catalysts such as H_3PO_4, H_2SO_4 and HCl as well as heterogeneous catalysts tungstolitic acid ($H_4SiW_{12}O_{40}$), niobium phosphate, Amberlyst-70 and Dowex-H [1,12]. For the second step (hydrogenation of glucose to sorbitol), the common catalysts used are Ru- and Ni-based ones [13-16]. Then sorbitol is dehydrated trough an acid-catalyzed process leading to isosorbide with the formation of 1,4- and 3,6-sorbitan intermediates in the third step [17]. The synthesis of isosorbide is performed under high hydrogen pressures and high temperatures to allow efficient hydrogenation of glucose and dehydration of sorbitol and sorbitans [12,18]. In 2010, Almeida et al. studied each step for the synthesis of isosorbide from cellulose using molten $ZnCl_2$ associated with different catalysts [19]. Based on the study of each step reported in the literature, several researchers investigated the direct conversion of cellulose or lignocellulosic biomass to isosorbide. Several strategies were employed such as a combination of homogeneous acid and supported metal catalyst, or a combination of supported metal catalyst and solid acid or a metal on an acid support. Here, we will report all these strategies to perform the one-pot conversion of (ligno)cellulose to isosorbide and the key parameters of this reaction (acidity, nature of the feedstocks, poisoning of the catalyst).

Review

Combination of an acidic homogeneous catalyst and a supported metal catalyst

The conversion of cellulose or lignocellulosic biomass to isosorbide was studied by combining a homogeneous acid catalyst to promote the hydrolysis of cellulose to glucose and the dehydration of sorbitol to isosorbide and a supported metal catalyst to hydrogenate glucose to sorbitol. Several homogeneous catalysts were used such as mineral acids, boron phosphate and heteropolyacids (Scheme 2).

Palkovits et al. studied the combination of supported noble metal catalysts based on Pt, Pd and Ru with dilute mineral acids such as phosphoric or sulfuric acid for the conversion of cellulose and even spruce in a one-step hydrogenolysis reactions to form C4 to C6 sugar alcohols [20]. For the C6 sugar alcohols including the isosorbide formation, the yield was below 6% whatever catalyst was used at 160 °C, under 50 bar of H_2 in a 36 mL stainless steel autoclave equipped with Teflon inserts for a reaction time between 1 h to 5 h. Another study was performed using sulfuric or hydrochloric acid in the presence of

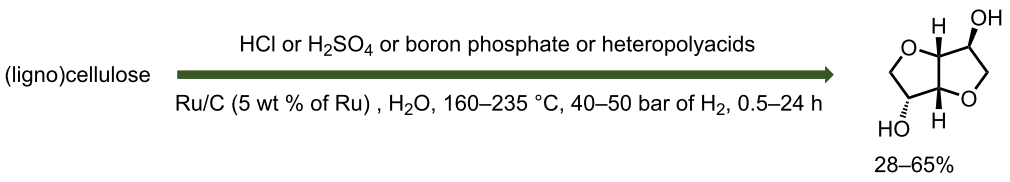

Scheme 2: Combination of mineral acids or heteropolyacids and a supported metal catalyst to produce isosorbide from (ligno)cellulose.

Pt/C, Pd/C or Ru/C catalysts [21]. In the presence of Pt/C and Pd/C associated to HCl or H_2SO_4 the isosorbide yield was very low (below 4%) for a total conversion of cellulose in agreement with the results obtained by Palkovits et al. [20]. In the presence of Ru/C (5 wt % of Ru, 20 mg) associated with HCl (235 °C, 6.0 MPa of H_2, 60 min, 10 mL of acidified water, 0.01 M of HCl, in a 50 mL Teflon-lined stainless steel autoclave), 41% of isosorbide was obtained for a full conversion of cellulose. If the Ru/C catalyst was associated with H_2SO_4 only 14% of isosorbide was produced under similar conditions. This study showed that the nature of the mineral acid and thus the acidity is of importance to produce isosorbide from cellulose. The most active metal catalyst is Ru/C among the metal-supported solids studied. One can mention, that by decreasing the reaction temperature from 235 °C to 215 °C, 50% of isosorbide was obtained after 30 min of reaction under 6.0 MPa of H_2 in the presence of 20 mg of Ru/C (5 wt % of Ru) and HCl in 10 mL of water with a concentration of 0.01 M. A similar strategy was employed but starting from lignocellulosic biomass [22] such as bagasse pulp (BP) containing 95 wt % of cellulose and 5 wt % of lignin and the results were compared to glucose and microcrystalline cellulose (MCC). Commercial Ru/C combined with H_2SO_4 led to higher isosorbide yield (50% under optimized conditions, 220 °C under 40 bar of H_2 for 2 h and 0.5 M H_2SO_4 (aq) 30 mL, 40 mg of Ru/C (5 wt % of Ru) in a glass insert in an autoclave) than Pt/C, Pd/C and Rh/C catalysts for the one-pot one step conversion of BP to isosorbide. The nature of the acids to catalyze the hydrolysis of cellulose and dehydration of sorbitol and sorbitans was studied and their efficiency decreased in the order of H_2SO_4 > triflic acid (HOTf) > trifluoroacetic acid (TFA) > Amberlyst-38 > HCl > HNO_3. It was shown that when MCC was used as starting material, in the presence of Ru/C and H_2SO_4, 50% yield of isosorbide was obtained. These results are in contradiction with the results observed by Liang et al. [21]. Hence, a isosorbide yield of 14% was obtained. The reasons could be the different conditions used. In the work of Liang et al. [21], 0.2 g of cellulose was added in 10 mL of acidified water with a concentration of H_2SO_4 of 0.05 M in the presence of 20 mg of Ru/C at 235 °C whereas 0.19 g of cellulose was added in 30 mL of acidified water (H_2SO_4 concentration of 0.5 M, 10 times higher than in the other work) in the presence of 40 mg of Ru/C at 220 °C. All these parameters can explain the difference observed and again it confirms that the pH is a key parameter in the conversion of cellulose or lignocellulosic biomass to isosorbide.

The main bottlenecks of this one-step process are the deactivation of the commercial Ru/C catalyst and the degradation of isosorbide upon prolonged reaction time. Keskivali et al. studied the two-step reaction [22]. The first step included the hydrolysis of cellulose to glucose, hydrogenation of glucose into sorbitol and partial dehydration of sorbitol to sorbitans. The second step was the dehydration of sorbitol and 1,4-sorbitan to isosorbide (Scheme 3). Optimal reaction conditions for the first step are middle temperatures to enhance the recyclability of Ru/C catalyst. 59% of sorbitol was obtained at 170 °C with 0.5 M of H_2SO_4, 20 bar of H_2 for 2 h and in the presence of 0.02 mmol of Ru. The second step was performed starting from

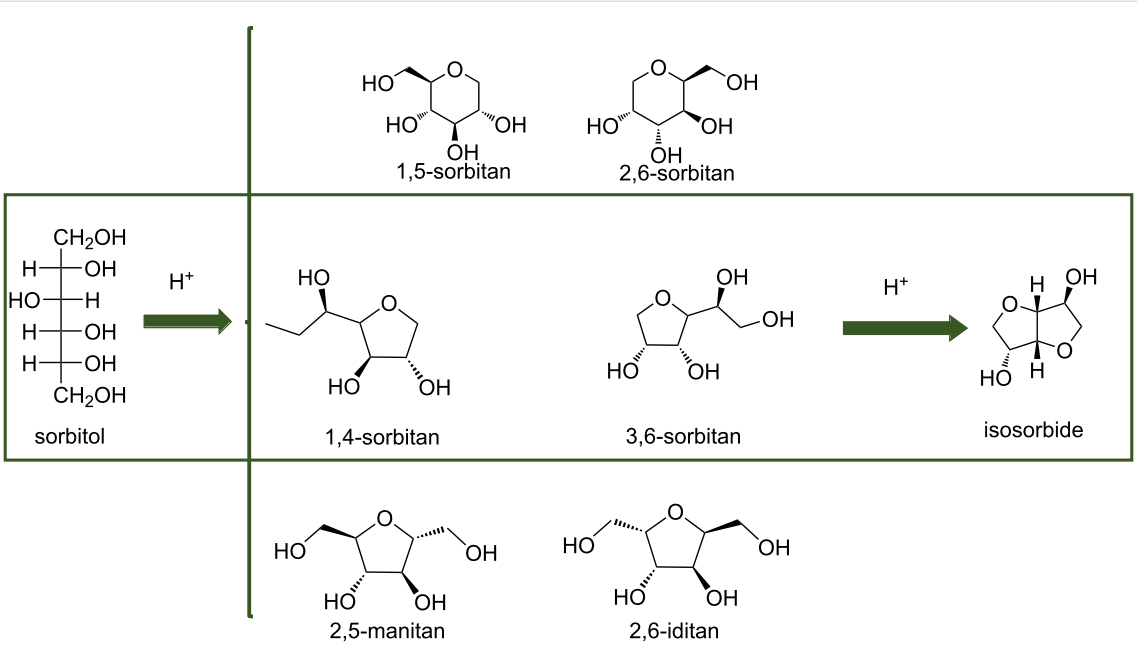

Scheme 3: Conversion of sorbitol to isosorbide via the formation of sorbitans.

the first step hydrogenation solution after the removal of the Ru/C catalyst by filtration. A temperature higher than 200 °C was used in order to obtain a high isosorbide yield. A reaction temperature of 240 °C and 270 °C led to an isosorbide yield of 43% and 47%, respectively, after 1 h of reaction. A prolonged reaction time led to a decrease of the isosorbide yield due to side reactions. A decrease of the temperature from 240 °C to 170 °C led to an increase of the isosorbide yield (58%) after 24 h of reaction showing that a lower temperature can be used for this reaction but a prolonged reaction time is required.

The authors observed a deactivation of the Ru-catalyst in the presence of substrates containing lignin that was probably due to fouling and poisoning. Moreover, the presence of sulfuric acid could have been modified the Ru/C catalyst. With the increase of strong acid sites on the catalyst surface, the activity and recyclability of the catalyst was improved. A modification of the Ru/C hydrogenation catalyst's surface by sulfonation and oxidative treatment was performed and had a significant effect on the catalyst properties in the isosorbide synthesis. Hence, strong acid sites are generated on the surface of the catalyst support leading to an increase of its hydrophilicity. The catalyst treated with a solution of 10 M of sulfuric acid during 3 h was recycled at least for four consecutive runs starting from bagasse pulp. Under optimized conditions (30 mL of aqueous solution of 0.5 M H_2SO_4; first step reaction conditions: 170 °C, 20 bar H_2, 2 h and 0.02 mmol of modified Ru/C catalyst, 3 h; second step reaction conditions: 200 °C, 40 bar H_2, 6 h after the removal of Ru/C catalyst) isosorbide was generated in high yields of 56–57% (49–50 wt %) from different cellulosic substrates. This study showed that the acidity is important in the conversion of lignocellulosic biomass to isosorbide and that the acid can react with the metal-supported catalyst.

Another study was devoted to the use of boron phosphate for the conversion of cellulose into liquid hydrocarbon C_1–C_6 over Ru/C [23]. A mixture of MCC (0.8 g) and Ru/C catalyst (5 wt % of Ru, 0.2 g) in 40 mL of water under 60 bar of H_2 at 230 °C for 24 h in a 100 mL stainless-steel autoclave was used in the one-pot conversion of cellulose. C_1–C_4 compounds were obtained predominantly. However, with the addition of 4 mmol boric acid (H_3BO_3), which is a weak acid, sorbitol was observed with 5% yield along with 1% of sorbitan and 10% of isosorbide. The authors showed that a complex of borate-polyol and sorbitol or sorbitan as polyols was formed leading to an increase of their stabilities and thus their yields. When boric acid is replaced by phosphoric acid (which is a strong acid) for the conversion of cellulose, an isosorbide yield of 29% is reached indicating that double cyclodehydration is favored under these conditions. On the contrary, the addition of equimolar amounts of boric acid and phosphoric acid decreases the yield of isosorbide and sorbitan from 29% to 22% and from 5% to 3%, respectively. A similar tendency was observed in the presence of boron phosphate. This was due to the slow dissolution of boron phosphate in aqueous solution implying a release of H^+ according to reaction time. They also observe an increase of isosorbide production from 18% to 28% with the increase of boron phosphate amount from 1 to 4 mmol due to the increase of the media acidity at 230 °C under 6.0 MPa of H_2 in the presence of 0.2 g of Ru/C in 40 mL of water.

An interesting family of acids was used in combination with metal-supported heteropolyacids as catalyst. Heteropolyacids were chosen since they are nontoxic or noncorrosive chemicals (Scheme 4).

Palkovits et al. showed that heteropolyacids (tungstosilic $H_4SiW_{12}O_{40}$ or phosphotungstic acid and $H_3PW_{12}O_{40}$) can be used in association with a Ru/C catalyst to produce isosorbide from α-cellulose [24]. The experiments were made in a batch reactor containing 500 mg of α-cellulose, 100 mg of 5 wt % Ru/C catalyst and 10 mL of water with an acid concentration

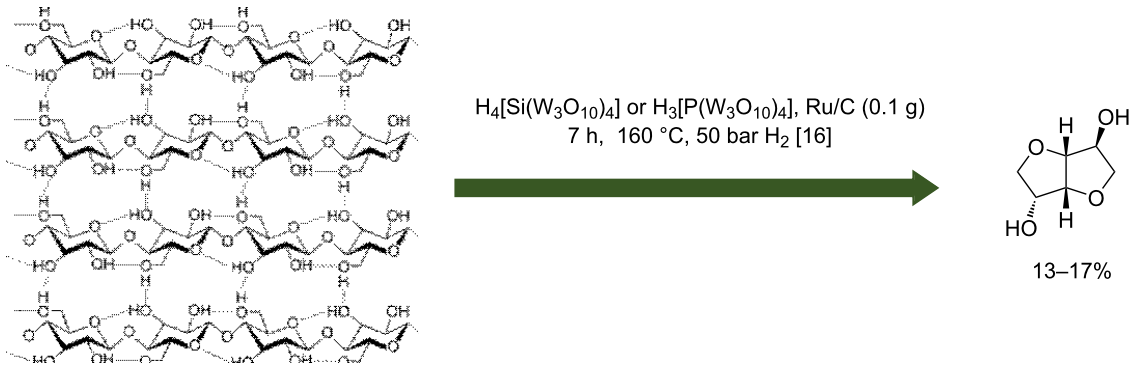

Scheme 4: Conversion of cellulose to isosorbide in the presence of heteropolyacids and metal-supported catalyst [24].

from 3.47 to 55.1 mmol·L^{-1} at 160 °C under 50 bar of H_2 (25 °C). It was reported that the rate of cellulose hydrogenolysis reaction depends on the acid concentration and reaction time. Indeed, an increase of isosorbide and sorbitan yields was observed after 7 h of reaction at 160 °C and 50 bar H_2 with an acid concentration of 55.1 mmol·L^{-1}. The isosorbide yield was 17% and 13% for a cellulose conversion above 90% for respectively $H_4[Si(W_3O_{10})_4]$ and $H_3[P(W_3O_{10})_4]$.

Later, Op de Beeck et al. explored a combination of Ru/C and tungstosilic acid ($H_4SiW_{12}O_{40}$) for the one-pot conversion of cellulose into isosorbide [25]. They studied the different steps of the reaction. They have shown that for the last step (dehydration of sorbitol to isosorbide) the increase of the temperature from 190 to 230 °C and the acid concentration from 0 to 61 mM of H^+ allows the dehydration of sorbitol to isosorbide (60% yield). However in this reaction, if the acid concentration is too high (over 61 mM of H^+), polymeric compounds were formed limiting the yield to isosorbide. Based on these results, it is clear that a control of the acidity is required for the dehydration of sorbitol to isosorbide. Another important parameter is the control of the sorbitol concentration. Indeed, polymeric compounds were also observed with the fivefold increase in the sorbitol concentration (from 22.4 g·L^{-1} to 112 g·L^{-1}). This is an advantage for the one-pot conversion of cellulose, because the concentration of sorbitol produced from cellulose is usually low. The one-pot conversion of cellulose was investigated first using a MCC Avicel PH-101 cellulose (0.8 g), Ru/C (200 mg), water (40 mL), under 5 MPa of initial H_2 pressure at room temperature. It was shown that fast and selective hydrogenation of glucose is required to increase the isosorbide yield and that at elevated temperatures, there is a selectivity loss through degradation of glucose to insoluble byproducts. Side reactions can be minimized by decreasing the reaction temperature to 210 °C, improving the hydrogenation capacity by optimization of the concentration of Ru/C and decreasing the solvent volume to 40 mL. A formation of isomerization products of isohexides was observed as the isomerization of glucose is acid-catalyzed, and the isomerization of alditols is catalyzed by Ru/C. An isosorbide yield of 52% was obtained after 1 h at 210 °C and 50 bar of H_2 from 10 wt % of cellulose and a catalyst/cellulose ratio of 1:4 in the presence of 1 g of Ru/C (5 wt % of Ru). It was also shown that a longer reaction time led to an increased production of insoluble byproducts. The productivity of isosorbide can reach 40.2 g·L^{-1}·h^{-1}with a purity of 73%. The recycling of the metal-supported catalyst (Ru/C) was studied and a high catalytic activity decrease was observed after the first run, showing that the catalyst was not recyclable. Despite their effort to regenerate the catalyst, the loss of activity and yield was always observed. The scope of biomass used was investigated and experiments were performed using hardwood (42% cellulose, 4% hemicellulose and 18% lignin), soft wood (35% cellulose, 23% hemicellulose and 27% lignin), nonpretreated wheat straw (35% cellulose, 1% hemicellulose and 18%lignin) and pretreated wheat straw as raw materials in order to investigate the influence of the delignification on the cellulose conversion. Two pretreatments were used: i) The ethanosolv method that consists in the treatment of wheat straw for 1.5 h in an ethanol/water (50:50) mixture at 210 °C, and ii) CIMV (Compagnie Industrielle de la Matière Végétale) technology, where wheat straw was treated during 3.5 h of acetic acid/formic acid/water (50:30:15 m/m/m) extraction at 105 °C and then in the presence of H_2O_2 and organic acids (peracetic and performic acids) for further delignification. After the pretreatment, the cellulose content is 69% and 82% and the lignin content 16% and 8%, respectively. The results obtained from the nontreated biomass showed that nontreated softwood, containing a higher hemicellulose amount compared to hardwood and wheat straw led to the highest isosorbide yield of 7%. This can be due to a higher carbohydrate content and a lower amount of impurities than in the other raw materials. Based on this, the pretreatment of the delignified biomass will promote the synthesis of isosorbide. Hence, CIMV-delignified wheat straw pulp led to 63% of isosorbide, corresponding to a productivity of 40 g·L^{-1}·h^{-1} with 72% of purity. This high yield can be ascribed to several parameters such as small particle diameter, large surface area/porosity and lower crystallinity. For the particle size, cellulose fiber diameters are 2 μm and 50 μm of respectively pre-treated wheat straw and microcrystalline Avicel PH-101, that can explain the higher yield of isosorbide from CIMV-delignified wheat straw pulp. The crystallinity and the particle size effects were confirmed by starting from a ball-milled Avicel PH-101 cellulose. A higher yield of isosorbide (around 65%) was observed than from non treated Avicel PH-101 cellulose (52%).

A one-pot conversion of cellulose to isosorbide has been reported using a combination of supported metal catalyst and a homogeneous acid such as mineral acids and heteropolyacids (Scheme 5). The maximum isosorbide yield observed is 65% under optimal conditions. In these processes, a neutralization procedure is essential to remove homogeneous acid catalysts and also separation processes of the products from the salt solutions are required. Regarding an industrial application, if heteropolyacids are used with low concentration, a reduced salt will be formed after the neutralization step. Moreover, heteropolyacids can be precipitated via ion exchange with larger cations, e.g., K^+, Cs^+ and NH_4^+, or in certain cases even extracted to allow direct recycling. Thus, the usage of heterogeneous acid catalysts is desirable for easy separation of the products. Thus, from a sustainable point of view, it is of interest to study heterogeneous catalysts for the direct conversion of cellulose or lignocellulosic biomass to isosorbide.

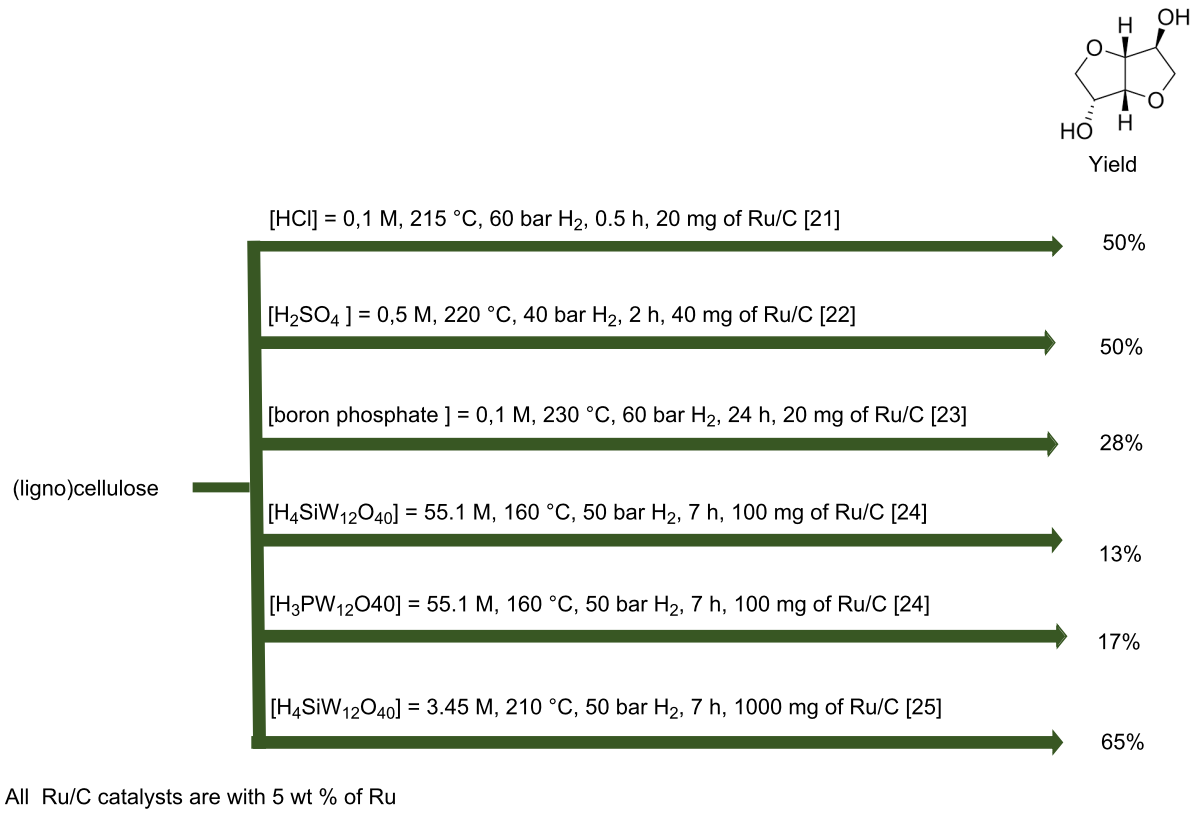

Scheme 5: Summary of the results obtained in one-pot one step processes [21-25].

Heterogeneous catalysts for the conversion of (ligno)cellulose to isosorbide

Solid acid catalysts such as ion exchange resins exhibiting sulfonic groups on their external surface resembling to some extent *p*-toluenesulfonic acid (*p*-TSA) can be used in combination with supported metal catalyst (Scheme 6).

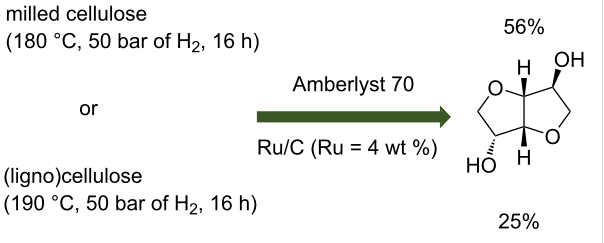

Scheme 6: Conversion of (ligno)cellulose to isosorbide in the presence of Amberlyt 70 and a Ru/C catalyst [26,27].

Yamaguchi et al. used a combination of Ru/C and Pt/C with Amberlyst 70, an ion-exchange resin containing sulfonic acid sites in the one-pot conversion of ball-milled cellulose to isosorbide [26]. A yield of 8% of isosorbide was obtained at 190 °C in the presence of Pt/C (Pt = 2 wt %) catalyst (0.2 g), 1 g of Amberlyst 70 from 0.324 g of milled cellulose diluted in 40 g of water under 50 bar of H_2 during 16 h in a batch reactor of 100 mL. This yield was lower than the expected one (38%) using a sequential process. They have shown that the amount of Amberlyst 70 is important and under optimized conditions (0.2 g of 2 wt % Pt/C and 3 g of Amberlyst 70) 16% of isosorbide were obtained. When the loading of Pt was increased from 2 wt % to 4 wt %, 30% of isosorbide was observed at 453 K with 5 MPa H_2 for 16 h in the presence of 0.3 g of Amberlyst 70. The same approach and reaction conditions were used replacing the Pt/C catalyst by Ru/C (Ru = 4 wt %) catalytic material. Higher isosorbide yields were observed in the presence of the Ru/C catalyst compared to those obtained in the presence of the Pt/C catalyst suggesting that Ru/C is more active for the production of isosorbide from cellulose with Amberlyst 70. Best results are obtained under the following conditions: 0.2 g of 4 wt % Ru/C, 3 g of Amberlyst 70, isosorbide yield of 56% at 180 °C under 50 bar of H_2 after 16 h of reaction. A comparison between these results and sequential reactions leading in the first step (hydrogenolysis of cellulose) to 51% of sorbitol and in the second step (dehydration of sorbitol) to 63% of isosorbide showed that the activity of the Ru/C catalyst was enhanced by the presence of Amberlyst 70 in the one-pot reaction. On the opposite, the Pt/C activity was inhibited by the presence of

Amberlyst 70. The effects of the Ru loadings and catalyst amounts on the isosorbide yield from cellulose were also investigated. An optimum amount of 0.2 g of 4 wt % Ru/C led to 56% of isosorbide whereas 0.4 g of 2% Ru/C led to a lower isosorbide yield (24%) despite the same amount of Ru atoms on these catalysts. The metal dispersion of these two catalysts was almost identical but the particle size differs (2.6 nm for 2% Ru/C and 5.3 nm for 4% Ru/C) suggesting that the Ru species formed in the 4 w. % Ru/C catalyst are more active for conversion of cellulose into isosorbide. The recycling of 4 wt % Ru/C and Amberlyst 70 catalysts was studied at different temperatures. At all the temperatures studied, the isosorbide yield decreased due to carbon deposition on the metal.

Amberlyst 70 was also used in the conversion of lignocellulosic feedstocks to isosorbide in the presence of supported metal catalysts [27]. Japanese cedar, eucalyptus and bagasse are used and they contain between 37% and 41% of cellulose and a glucose content between 40.1% and 46.5%. The biomass feedstock was crushed by a simple ball milling procedure without further treatment. The one-pot conversion of Japanese cedar was carried out by combining Pt/C or Ru/C with 4 wt % of metal and Amberlyst 70 catalysts in a batch reactor of 100 mL. Ru/C catalyst was more active than Pt/C catalyst. Indeed, in the presence of Ru/C (0.2 g) and Pt/C (0.3 g) catalysts, an isosorbide yield of 25% and 2% was obtained, respectively, at 190 °C under 50 bar of H_2 after 16 h in the presence of 3 g of Amberlyst 70. They supposed that the Ru/C catalyst exhibits a better activity owing to Amberlyst 70 as shown in their previous work [22]. A one-pot conversion with Amberlyst 70 and Ru/C is thereafter tested in eucalyptus and bagasse feedstocks. Interestingly, 8% and 13% of isosorbide were observed from eucalyptus and bagasse respectively at 190 °C under 50 bar of H_2 after 16 h in the presence of 3 g of Amberlyst 70 and 0.2 g of Ru/C. They suggest that lignin or an inorganic component contained in eucalyptus and bagasse can affect the acidity of Amberlyst 70 which implies the lower yield of isosorbide and the higher yield of 1,4-sorbitan.

Xi et al. studied a combination of a Ru/C catalyst with mesoporous niobium phosphate and Ru support over mesoporous niobium phosphate in the conversion of cellulose to isosorbide [28]. Different preparation methods of $NbOPO_4$ were performed depending on the final pH (2, 7 and 10) of the solution at the end of the solid synthesis. Based on the results obtained in the dehydration of sorbitol to isosorbide, the $NbOPO_4$-pH_2 catalyst was chosen for the production of isosorbide from cellulose. Two strategies were employed: a one-step and a two-step process. The one-step conversion of cellulose to isosorbide consists in using the same reaction conditions and the same catalyst for the hydrolysis/hydrogenation and dehydration reactions. An isosorbide yield of 13% was obtained in the presence of 5% Ru/$NbOPO_4$-pH_2 (0.2 g) at 230 °C and 24 h of reaction in a 100 mL stainless steel reactor starting from cellulose (0.24 g) in 15 mL of water. In the case of an association of Ru/C and $NbOPO_4$-pH_2, the yield of isosorbide was around 20%. The one-step strategy seems to be not efficient for the conversion of cellulose to isosorbide due to the temperature of the reaction that is different for the two reactions (hydrolysis/hydrogenation and dehydration). To overcome this temperature issue a two-step process was studied. In the first step, 0.24 g of cellulose was added in 15 g of water at 170 °C for 24 h in the presence of 0.1 g of Ru/$NbOPO_4$-pH_2. Ru/$NbOPO_4$-pH_2 was then removed and the aqueous solution containing sorbitol and sorbitans was dehydrated at 230 °C during 18 h in the presence of 0.1 g of $NbOPO_4$-pH_2 for the second step. After the first step, an aqueous mixture of 59% of sorbitol, 20% of 1,4- and 3,6-sorbitans, respectively, 4% of 2,5-sorbitan and 4% of isosorbide was obtained. The second step led to an isosorbide yield of 56% which is higher than the yield obtained after the one-step strategy. The two-step reaction was also performed using a similar Ru/$NbOPO_4$-pH_2 catalyst in both steps and the yield of isosorbide was 33%. This decrease was due to a different acidity. Hence, the ruthenium species occupied the strong and medium acid site of $NbOPO_4$-pH_2 after its impregnation. The recyclability of $NbOPO_4$-pH_2 was performed for the two-step conversion of cellulose to isosorbide as the Ru/$NbOPO_4$-pH_2 recyclability was proved in a previous study in the conversion of cellulose to isosorbide [29]. A decrease of approximately 10% in isosorbide yield is reported after four runs due to carbon deposition (confirmed by thermogravimetry analysis) or during the recycling procedure. However, the carbon deposition was removed by calcination of the catalyst at 400 °C and a similar isosorbide yield as the one obtained at the first run was observed.

A sustainable method for the isosorbide production from cellulose is the use of a bifunctional catalyst (Scheme 7). A series of Ru catalysts on acid support were prepared by the adsorption of colloidal Ru nanoparticles on mesoporous and bulk niobium phosphate, mesoporous and bulk niobium oxide hydrate, phosphoric acid-treated mesoporous and bulk niobium oxide hydrate [30]. These catalysts were compared to Ru@HZMS5, Ru@NaY, Ru@γ-Al_2O_3 solids. Cellulose was converted over all niobia-based catalysts with 25–43% yield of isosorbide starting from 0.6 g cellulose using 0.06 g catalyst (5.0 wt % Ru, Ru nanoparticles (NPs): 0.9 nm) in 30 mL H_2O after 1 h of reaction at 220 °C under 60 bar of H_2. Trace amounts or even no isosorbide was obtained over microporous HZSM-5, NaY, and γ-Al_2O_3-supported Ru catalysts. A bifunctional Ru catalyst supported on mesoporous niobium phosphate with a mean size of Ru NPs of 5.5 nm was used for the direct conversion of

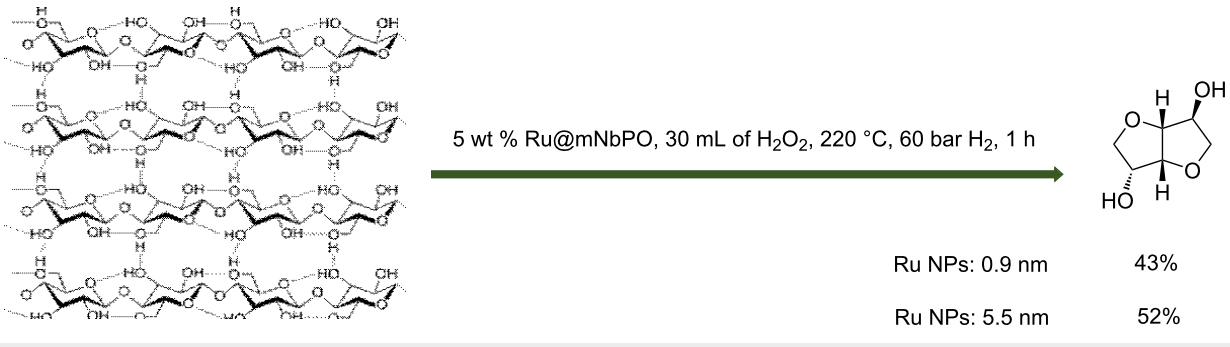

Scheme 7: Use of Ru-supported on mesoporous nobium phosphate (mNbPO) for the synthesis of isosorbide from cellulose [30].

cellulose to isosorbide and 52% yield of isosorbide was observed with almost 100% cellulose conversion. The large surface area, pore size, and strong acidity of mesoporous niobium phosphate are key parameters for the hydrolysis of cellulose and dehydration of sorbitol. An appropriate size of the supported Ru nanoparticles avoids unnecessary hydrogenolysis of sorbitol. The recyclability was investigated and up to 6 cycles could be performed without significant loss in catalytic properties. Moreover, no leaching of Ru was observed. This study shows that a bifunctional catalyst can be a more sustainable solution to produce isosorbide from (ligno)cellulose.

Conclusion

The isosorbide synthesis from cellulose is performed via acid-catalyzed hydrolysis of cellulose, followed by hydrogenation of glucose to sorbitol and further dehydration to sorbitans. The dehydration of sorbitol to isosorbide required temperatures around 200 °C exposing hydrogenation catalysts to the harsh reaction conditions in the one-pot process. Unfortunately, one-step conditions seem to facilitate the deactivation of the hydrogenation catalysts, thus preventing their efficient recycling due to the production of insoluble byproducts, metal particle sintering and leaching. From all the studies, it is clear that Ru/C was the most active catalyst in the hydrogenation reaction. Based on the stability of the hydrogenated catalyst, some studies used a two-step process to increase the isosorbide yield. One important parameter is also the acidity strengths of the acid catalyst used. An appropriate acidity is required to depolymerize cellulose to glucose and to dehydrate sorbitol to isosorbide. If the acidity is too high, byproducts are formed decreasing the yield of isosorbide. Another important factor is the nature of the feedstocks used. Hence, most of the isosorbide syntheses are from pure cellulose and sugars as substrates, such as microcrystalline cellulose and glucose, while studies describing an isosorbide synthesis from lignin-containing cellulosic substrates are scarce. The presence of lignin can be detrimental for the activity of the catalysts. Hence, investigations of reaction conditions and the development of the hydrogenation catalysts to tolerate the presence of lignin should be further investigated.

For the one-pot conversion of lignocellulose to isosorbide, a sustainable and interesting route should be the design of a heterogeneous catalyst composed of a metal supported on an acid support. These catalysts should be designed in order to be stable in water and tolerant to the presence of lignin. Otherwise, the solution should be to realize this reaction under continuous flow using two catalytic beds.

Finally, we emphasize that mechanistic insights on the catalytic conversion of biomass-derived platform molecules are required to make this value chain competitive with respect to the traditional synthesis of chemicals from fossil fuels. In particular, in situ kinetic studies by spectroscopic methods [31] correlated to computational chemistry approaches [32] might reveal specific interaction between reactants and catalysts as well as solvent effects at work in such a complex system that should provide an understanding of the underlying reason for the observed unique kinetics, yields and selectivity in these one-pot reactions. In addition, such in-depth fundamental mechanistic and kinetic studies should enable determining the key structural parameters of the catalytic platform that govern its efficiency hence supporting the design of novel highly active and selective catalysts for the valorization of cellulose as a sustainable feedstock.

Funding

The authors acknowledge the Region Nouvelle Aquitaine and the University of Poitiers for their financial support for the Ph.D. of I. Bonnin. They are grateful to the region Nouvelle Aquitaine for the CPER and EU-FEDER support and to INCREASE Federation.

ORCID® iDs

Raphaël Mereau - https://orcid.org/0000-0002-0357-4654
Thierry Tassaing - https://orcid.org/0000-0003-4114-170X
Karine De Oliveira Vigier - https://orcid.org/0000-0003-3613-7992

References

1. Dussenne, C.; Delaunay, T.; Wiatz, V.; Wyart, H.; Suisse, I.; Sauthier, M. *Green Chem.* **2017,** *19,* 5332–5344. doi:10.1039/c7gc01912b
2. Kobayashi, H.; Fukuoka, A. *Green Chem.* **2013,** *15,* 1740–1763. doi:10.1039/c3gc00060e
3. Parker, J. D.; Parker, J. O. *N. Engl. J. Med.* **1998,** *338,* 520–531. doi:10.1056/nejm199802193380807
4. Zhu, Y.; Durand, M.; Molinier, V.; Aubry, J.-M. *Green Chem.* **2008,** *10,* 532–540. doi:10.1039/b717203f
5. Tundo, P.; Aricò, F.; Gauthier, G.; Rossi, L.; Rosamilia, A. E.; Bevinakatti, H. S.; Sievert, R. L.; Newman, C. P. *ChemSusChem* **2010,** *3,* 566–570. doi:10.1002/cssc.201000011
6. Flèche, G.; Huchette, M. *Starch/Staerke* **1986,** *38,* 26–30. doi:10.1002/star.19860380107
7. Gohil, R. M. *Polym. Eng. Sci.* **2009,** *49,* 544–553. doi:10.1002/pen.20840
8. Chatti, S.; Schwarz, G.; Kricheldorf, H. R. *Macromolecules* **2006,** *39,* 9064–9070. doi:10.1021/ma0606051
9. Feng, X.; East, A. J.; Hammond, W. B.; Zhang, Y.; Jaffe, M. *Polym. Adv. Technol.* **2011,** *22,* 139–150. doi:10.1002/pat.1859
10. Schreck, D. J.; Bradford, M. M.; Clinton, N. A.; Aubry, P. Dianhydrosugar Production Process. U.S. Pat. Appl. US20090259057A1, Oct 15, 2009.
11. Holladay, J. E.; Hu, J.; Wang, Y.; Werpy, T. A. Two-stage dehydration of sugars. U.S. Pat. Appl. US20070173651A1, July 26, 2007.
12. Barbaro, P.; Liguori, F.; Moreno-Marrodan, C. *Green Chem.* **2016,** *18,* 2935–2940. doi:10.1039/c6gc00128a
13. Kusserow, B.; Schimpf, S.; Claus, P. *Adv. Synth. Catal.* **2003,** *345,* 289–299. doi:10.1002/adsc.200390024
14. Komanoya, T.; Kobayashi, H.; Hara, K.; Chun, W.-J.; Fukuoka, A. *Appl. Catal., A* **2011,** *407,* 188–194. doi:10.1016/j.apcata.2011.08.039
15. Crezee, E.; Hoffer, B. W.; Berger, R. J.; Makkee, M.; Kapteijn, F.; Moulijn, J. A. *Appl. Catal., A* **2003,** *251,* 1–17. doi:10.1016/s0926-860x(03)00587-8
16. Almeida, J. M. A. R.; Da Vià, L.; Demma Carà, P.; Carvalho, Y.; Romano, P. N.; Peña, J. A. O.; Smith, L.; Sousa-Aguiar, E. F.; Lopez-Sanchez, J. A. *Catal. Today* **2017,** *279,* 187–193. doi:10.1016/j.cattod.2016.06.017
17. Rose, M.; Palkovits, R. *ChemSusChem* **2012,** *5,* 167–176. doi:10.1002/cssc.201100580
18. Geboers, J.; Van de Vyver, S.; Carpentier, K.; de Blochouse, K.; Jacobs, P.; Sels, B. *Chem. Commun.* **2010,** *46,* 3577–3579. doi:10.1039/c001096k
19. de Almeida, R. M.; Li, J.; Nederlof, C.; O'Connor, P.; Makkee, M.; Moulijn, J. A. *ChemSusChem* **2010,** *3,* 325–328. doi:10.1002/cssc.200900260
20. Palkovits, R.; Tajvidi, K.; Procelewska, J.; Rinaldi, R.; Ruppert, A. *Green Chem.* **2010,** *12,* 972–978. doi:10.1039/c000075b
21. Liang, G.; Wu, C.; He, L.; Ming, J.; Cheng, H.; Zhuo, L.; Zhao, F. *Green Chem.* **2011,** *13,* 839–842. doi:10.1039/c1gc15098g
22. Keskiväli, J.; Rautiainen, S.; Heikkilä, M.; Myllymäki, T. T. T.; Karjalainen, J.-P.; Lagerblom, K.; Kemell, M.; Vehkamäki, M.; Meinander, K.; Repo, T. *Green Chem.* **2017,** *19,* 4563–4570. doi:10.1039/c7gc01821e
23. Chen, L.; Li, Y.; Zhang, X.; Liu, Y.; Zhang, Q.; Wang, C.; Ma, L. *Energy Procedia* **2019,** *158,* 160–166. doi:10.1016/j.egypro.2019.01.064
24. Palkovits, R.; Tajvidi, K.; Ruppert, A. M.; Procelewska, J. *Chem. Commun.* **2011,** *47,* 576–578. doi:10.1039/c0cc02263b
25. Op de Beeck, B.; Geboers, J.; Van de Vyver, S.; Van Lishout, J.; Snelders, J.; Huijgen, W. J. J.; Courtin, C. M.; Jacobs, P. A.; Sels, B. F. *ChemSusChem* **2013,** *6,* 199–208. doi:10.1002/cssc.201200610
26. Yamaguchi, A.; Sato, O.; Mimura, N.; Shirai, M. *Catal. Commun.* **2015,** *67,* 59–63. doi:10.1016/j.catcom.2015.04.009
27. Yamaguchi, A.; Mimura, N.; Shirai, M.; Sato, O. *J. Jpn. Pet. Inst.* **2016,** *59,* 155–159. doi:10.1627/jpi.59.155
28. Xi, J.; Zhang, Y.; Ding, D.; Xia, Q.; Wang, J.; Liu, X.; Lu, G.; Wang, Y. *Appl. Catal., A* **2014,** *469,* 108–115. doi:10.1016/j.apcata.2013.08.049
29. Zhang, Y.; Wang, J.; Ren, J.; Liu, X.; Li, X.; Xia, Y.; Lu, G.; Wang, Y. *Catal. Sci. Technol.* **2012,** *2,* 2485–2491. doi:10.1039/c2cy20204b
30. Sun, P.; Long, X.; He, H.; Xia, C.; Li, F. *ChemSusChem* **2013,** *6,* 2190–2197. doi:10.1002/cssc.201300701
31. Weckhuysen, B. M. *Chem. Soc. Rev.* **2010,** *39,* 4557–4559. doi:10.1039/c0cs90031a
32. Réocreux, R.; Michel, C. *Curr. Opin. Green Sustainable Chem.* **2018,** *10,* 51–59. doi:10.1016/j.cogsc.2018.02.004

License and Terms

BEILSTEIN JOURNAL OF ORGANIC CHEMISTRY

Natural dolomitic limestone-catalyzed synthesis of benzimidazoles, dihydropyrimidinones, and highly substituted pyridines under ultrasound irradiation

Kumar Godugu[‡1], Venkata Divya Sri Yadala[‡1], Mohammad Khaja Mohinuddin Pinjari[‡1], Trivikram Reddy Gundala[‡1], Lakshmi Reddy Sanapareddy[2] and Chinna Gangi Reddy Nallagondu[*1]

Full Research Paper

Open Access

Address:
[1]Department of Chemistry, Green and Sustainable Synthetic Organic Chemistry Laboratory, Yogi Vemana University, Kadapa-516 005, Andhra Pradesh, India and [2]Department of Physics, S.V.D. College, Kadapa-516003, Andhra Pradesh, India

Email:
Chinna Gangi Reddy Nallagondu[*] - ncgreddy@yogivemanauniversity.ac.in

* Corresponding author ‡ Equal contributors

Keywords:
benzimidazoles; dihydropyrimidinones; highly substituted pyridines; natural dolomitic limestone; ultrasound irradiation

Beilstein J. Org. Chem. **2020,** *16,* 1881–1900.
doi:10.3762/bjoc.16.156

Received: 02 April 2020
Accepted: 23 July 2020
Published: 03 August 2020

This article is part of the thematic issue "Green chemistry II".

Guest Editor: L. Vaccaro

Abstract

Natural dolomitic limestone (NDL) is employed as a heterogeneous green catalyst for the synthesis of medicinally valuable benzimidazoles, dihydropyrimidinones, and highly functionalized pyridines via C–N, C–C, and C–S bond formations in a mixture of ethanol and H_2O under ultrasound irradiation. The catalyst is characterized by XRD, FTIR, Raman spectroscopy, SEM, and EDAX analysis. The main advantages of this methodology include the wide substrate scope, cleaner reaction profile, short reaction times, and excellent isolated yields. The products do not require chromatographic purification, and the catalyst can be reused seven times. Therefore, the catalyst is a greener alternative for the synthesis of the above N-heterocycles compared to the existing reported catalysts.

Introduction

Nitrogen heterocycles are recognized as “privileged medicinal scaffolds” because these compounds are found in a wide variety of bioactive natural products and pharmaceuticals [1-3]. Among them, benzimidazoles, dihydropyrimidinones, and pyridines have emerged as promising and valuable structural units in many pharmaceutical lead compounds (Figure 1) [4-9]. Hence, there is a great need for the development of a green and sustainable synthetic route to the aforesaid nitrogen-containing heterocycles.

Benzimidazoles are an important class of N-heterocycles due to their potential applications in both biology and medicinal chem-

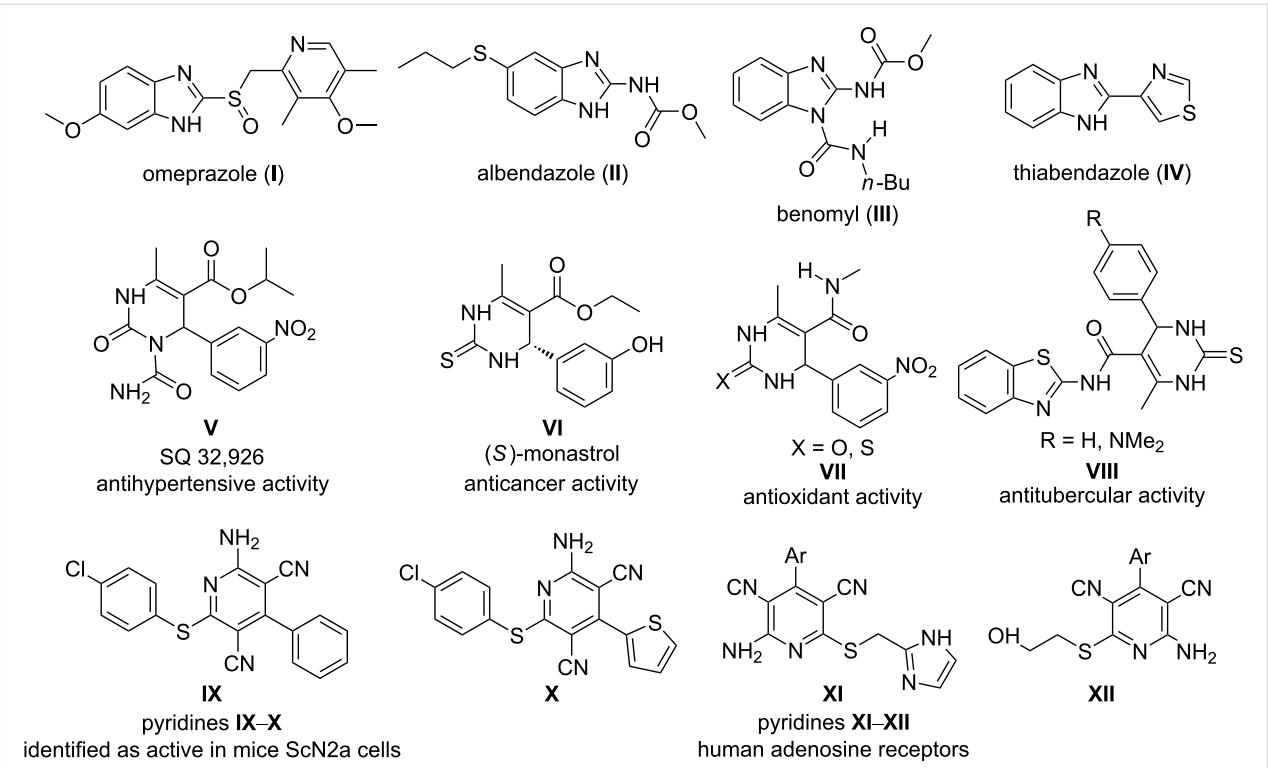

Figure 1: The benzimidazoles **I–IV**, dihydropyrimidinones/-thiones **V–VIII**, and 2-amino-4-aryl-3,5-dicarbonitrile-6-sulfanylpyridines **IX–XII** as medicinally privileged structures.

istry [10-13]. These compounds are used in the treatment of diseases, such as obesity, ischemia-reperfusion injury, hypertension, etc. [14-16]. In addition, these compounds are important intermediates in a variety of organic reactions and key elements in many functional materials [17-19]. Because of their potential utility, a huge number of synthetic protocols has been developed for the preparation of benzimidazole derivatives. The most common method for the preparation of benzimidazoles is the reaction between *o*-phenylenediamines and carboxylic acids [20,21]. Another general synthetic route reported is the condensation reaction of *o*-phenylenediamine with aldehydes in the presence of various catalysts, such as Zn–proline, trimethylsilyl chloride (TMSCl), Amberlite® IR-120, indion 190, trifluoroethanol, YCl_3, $HClO_4$–SiO_2, MMZ_Y zeolite, $Er(OTf)_3$, etc. [22-30].

Developments in already established multicomponent reactions (MCRs) are interesting topics in organic synthesis. For instance, the Biginelli reaction is a renowned and tunable MCR to synthesize the pharmacologically active 3,4-dihydropyrimidin-2-(1*H*)-ones (DHPMs, Biginelli products) [31]. These compounds occupy an important position in the fields of natural products and synthetic organic chemistry owing to their potential pharmacological properties [32-37]. A wide variety of Brønsted acids and Lewis acids are employed as efficient catalysts for the Biginelli reaction [38-47]. In addition, some transition metal-based catalysts and a few nonacidic inorganic salts are also utilized as catalysts for the above reaction [48-58]. Only few basic catalysts, such as *t*-BuOK, Ph_3P, and L-proline are reported for the Biginelli reaction [59-61].

2-Amino-4-aryl-3,5-dicarbonitrile-6-sulfanylpyridines have gained considerable attention due to their wide-ranging biological activities [62,63]. The most common synthetic route for the preparation of 2-amino-4-aryl-3,5-dicarbonitrile-6-thiopyridines is the condensation reaction of aldehydes, malononitrile, and thiols in the presence of a variety of catalysts [64-72]. Though the reported methods are efficient to provide the desired 1,2-disubstituted benzimidazoles, dihydropyrimidinones/-thiones and 2-amino-4-aryl-3,5-dicarbonitrile-6-sulfanylpyridines, there are still some drawbacks, which include the use of expensive catalysts, the preparation of the catalyst, long reaction times, the limited substrate scope, and complicated work-up processes; further, the products require chromatographic purification.

The mineral NDL is an irregular combination of calcium and magnesium carbonate. It is water-insoluble, environmentally benevolent, inexpensive, nontoxic, and abundant in nature. Further, dolomite is used as a heterogeneous green catalyst in

very few organic transformations, such as Knoevenagel, Michael–Henry, and transesterification reactions [73,74]. To the best of our knowledge, there are no reports on the NDL-catalyzed synthesis of aforesaid N-heterocycles under ultrasonic irradiation (USI).

In this paper, we wish to report the use of NDL as a heterogeneous green catalyst for the synthesis of the 1,2-disubstituted benzimidazoles **3**, the dihydropyrimidinones/-thiones **7**, and the 2-amino-4-(hetero)aryl-3,5-dicarbonitrile-6-sulfanylpyridines **11** via C–N, C–C, and C–S bond-forming reactions, respectively, in a mixture of EtOH and H_2O 1:1 under ultrasonic irradiation (Scheme 1).

Results and Discussion

Geological background of the NDL catalyst

The NDL catalyst was collected from V. Kothapalli village (N 14°31'54", E 78° 02'58"), Vemula Mandal of the Cuddapah district, Rayalaseema, Andhra Pradesh, India. The rock formation in the mineralized area of this village belongs to the Vempalli Formation (VF) of the Papaghni group of the lower Cuddapah Supergroup in the Cuddapah Basin (CB). The carbonate minerals, such as limestone and dolomite, are the most abundant ones and common sedimentary rocks present in this area.

Catalyst characterization

The NDL catalyst was ground into a fine powder and then sieved in a 200-mesh sieve. The chemical composition of the catalyst was determined by standard quantitative analysis. The basic strength of the catalyst was analyzed by using Hammett indicators. The catalyst was characterized by XRD, IR, Raman, SEM, and EDAX analysis.

The chemical composition of the NDL was determined by adopting a standard quantitative analysis [75]. The obtained results are summarized in Table 1.

The basic strength of the NDL catalyst (H_) was measured using Hammett indicators, namely bromothymol blue (H_ = 7.2), phenolphthalein (H_ = 9.8), 2,4-dinitroaniline (H_ = 15.0), and nitroaniline (H_ = 18.4) as Hammett indicators. In each case, 5 mL of a methanolic solution of the Hammett indicator was added to 50 mg of the catalyst, shaken

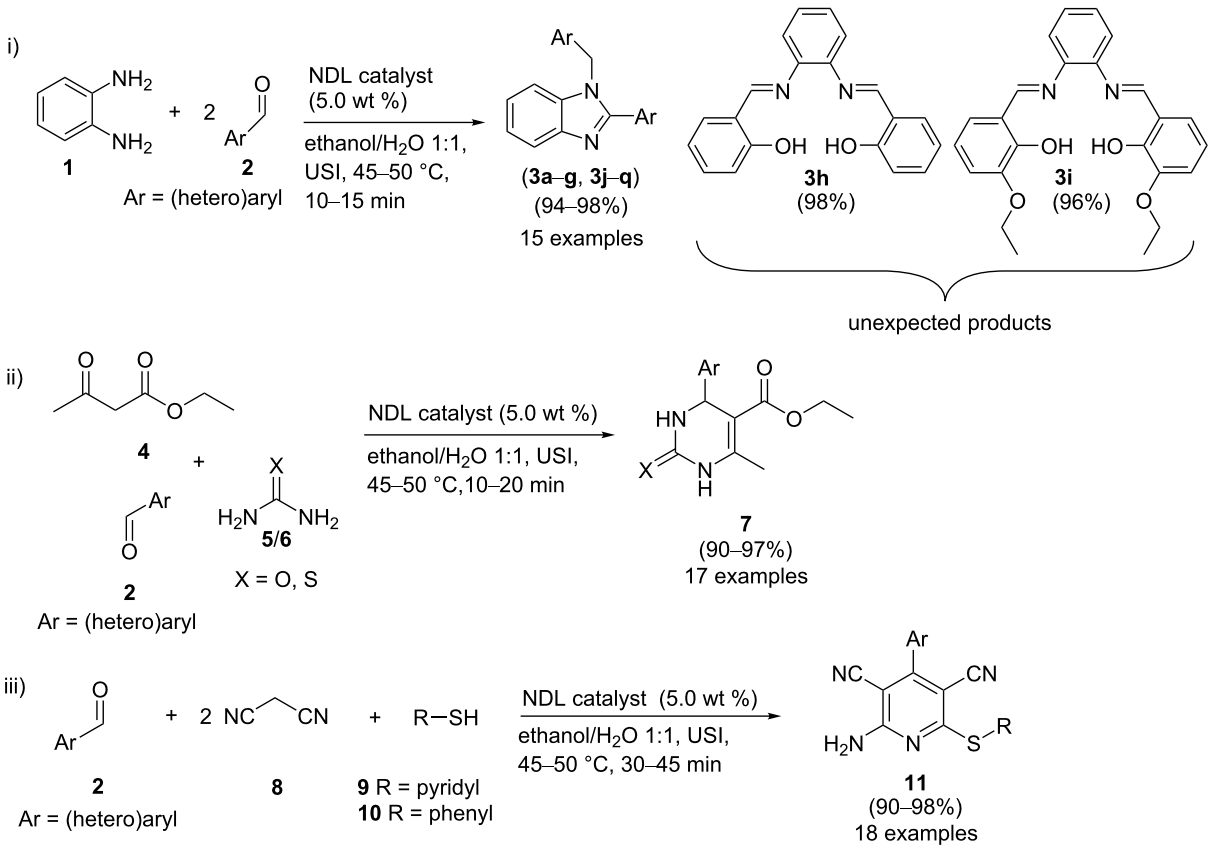

Scheme 1: NDL-catalyzed synthesis of i) 1,2-disubstituted benzimidazoles **3**, ii) dihydropyrimidinones/-thiones **7**, and iii) 2-amino-4-(hetero)aryl-3,5-dicarbonitrile-6-sulfanylpyridines **11** under ultrasound irradiation.

Table 1: Chemical composition of the NDL catalyst. LOI: loss of ignition.

component	LOI	CaO	MgO	SiO_2	Al_2O_3	Fe_2O_3	SO_3	Na_2O	K_2O
%	38.90	41.84	9.90	7.3	0.94	0.30	0.24	0.28	0.05

well, and then allowed to equilibrate for 2 h. No color variation of the indicators was observed. The study revealed that the basic strength of the NDL catalyst was weaker than the bromothymol blue indicator, i.e., H_ < 7.2. Hence, the NDL catalyst is a mild base, and it can activate both nucleophilic and electrophilic groups [73]. Further, the amount of basic sites on the catalyst was estimated by titration using a standard benzoic acid solution and bromothymol blue indicator. Initially, the catalyst (50 mg) was stirred with the methanolic solution of the indicator (5 mL) for 30–40 min, and then, the mixture was titrated with a 0.02 M benzoic acid solution. From the titer values of the benzoic acid solution, the amount of the basic sites was found to be 0.033 mmol/g.

The powder XRD pattern of the NDL catalyst is shown in Figure 2. The diffraction peaks at 2θ = 23.16, 29.51, 31.05, 36.02, 38.07, 39.40, 43.0, 47.2, 47.5, 48.5, 56.6, 57.6, 60.9, and 64.8° were attributed to the (012), (104), (006), (015), (110), (113), (021), (024), (018), (116), (211), (122), (214), and (030) plane, respectively, of the NDL catalyst (JCPDS card file 5–586: calcite and 11–78: dolomite) [76,77]. Small quantities of aluminium silicates (kaolinite) and iron oxides were also confirmed by the XRD pattern. The less intense diffraction peaks at 2θ = 12.3, 24.8, and 37.4 were assigned to the 001, 002, and 003 plane, respectively, of kaolinite (JCPDS card file 14-0164) [78]. The low-intense peaks at 2θ = 18.6, 26.1, 44.7, 54.6, 58.4, and 63.0 were ascribed to the 111, 211, 400, 422, 511, and 440 plane, respectively, of iron oxides (JCPDS card file 39-1346 and JCPDS card file 19-629) [79,80]. The above results were supported by FTIR and Raman characterization studies of the catalyst (vide infra).

The FTIR spectrum of the catalyst is shown in Figure 3. In the IR spectrum, two distinct vibrational modes of the carbonates, i.e., out-of-plane bending and in-plane bending, were observed at 875 cm^{-1} (ν_2) and 720 cm^{-1} (ν_4), respectively. The bands at 1086 cm^{-1} and 1424 cm^{-1} were ascribed to a symmetric stretching vibration (ν_1) and an asymmetric stretching vibration (ν_3) of the carbonate group, respectively. The combined bands of the carbonate group, i.e., $\nu_1 + \nu_4$ and $\nu_1 + \nu_3$ were observed at

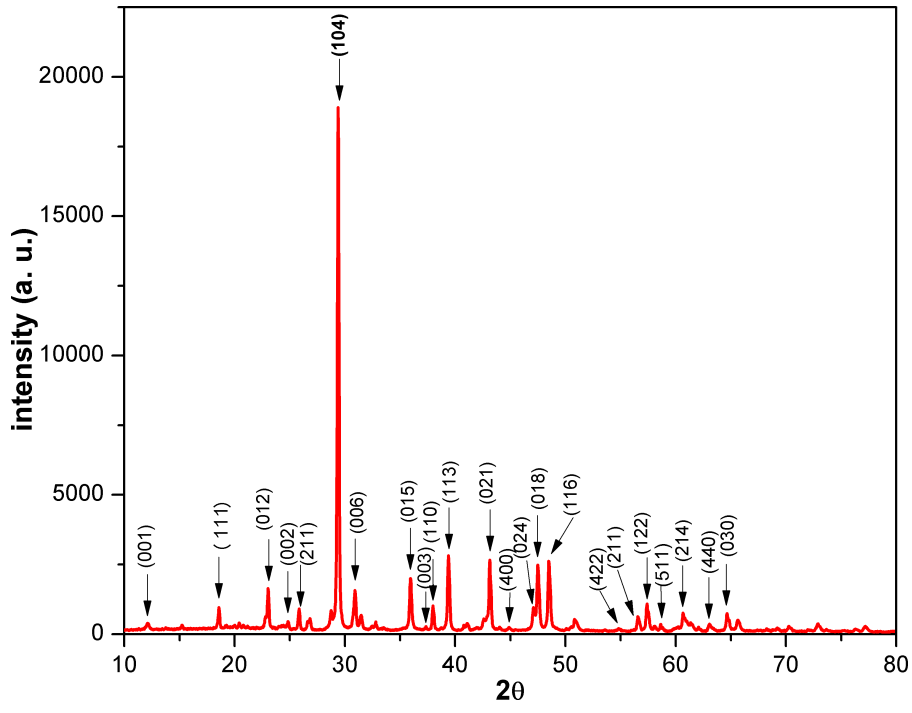

Figure 2: XRD pattern of the NDL catalyst.

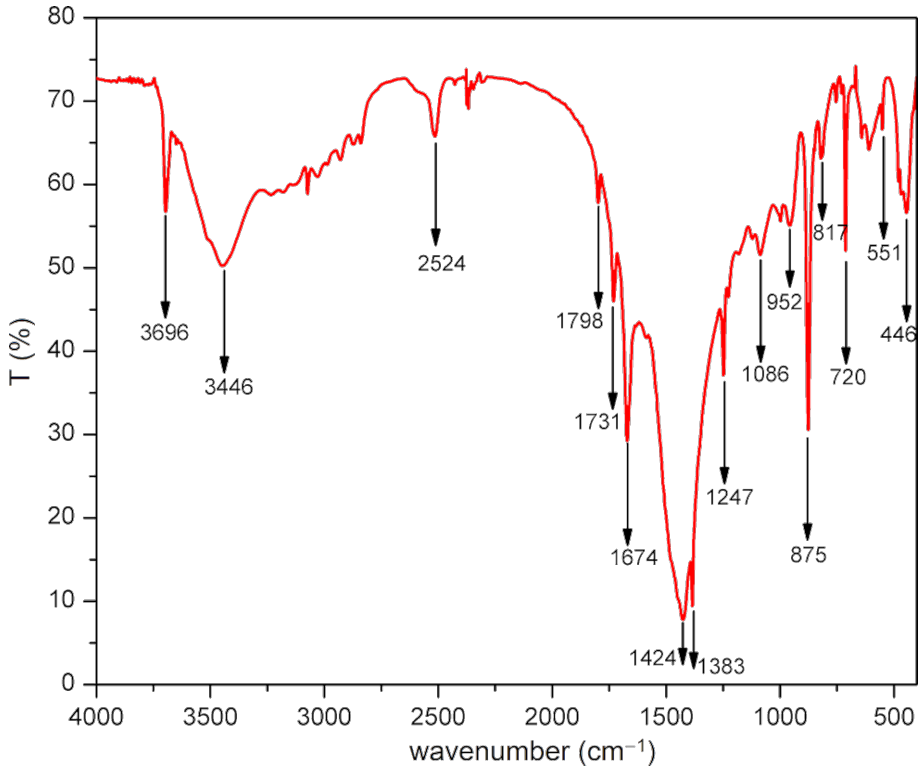

Figure 3: FTIR spectrum of the NDL catalyst.

1798 and 2524 cm^{-1}, respectively [76,77,81]. The IR bands at 3446 cm^{-1} (broad) and 1674 cm^{-1} (sharp) indicated the presence of stretching and bending vibrations of water [82]. The impurities aluminium silicate and iron oxides in the NDL were confirmed by IR spectroscopy. The peaks located at 446, 551, 817, 952, 1247, and 1383 cm^{-1} were attributed to the Si–O bending, Fe–O stretching, Al–O–Si stretching, Si–OH bending, Si–O stretching, and Al–O bending, respectively [83,84]. Further, the sharp band at 3696 cm^{-1} indicated the presence of a well-ordered kaolinite structure [76].

The Raman spectrum of the NDL catalyst is shown in Figure 4. The band at 1092 cm^{-1} was attributed to the symmetric stretching vibration (ν_1) of the carbonate group. The peaks at 714 and 1435 cm^{-1} were assigned to a symmetric bending (ν_4) and an asymmetric stretching vibration (ν_3) of carbonate. The weak peak at 1750 cm^{-1} was due to the combined band $\nu_1 + \nu_4$. The bands at 152 and 278 cm^{-1} were ascribed to the external vibrations of the carbonate group [76,77]. The presence of aluminium silicates and iron oxides present in the sample were confirmed by Raman spectroscopy. The bands at 418, 578, 753, and 985 cm^{-1} were assigned to Al–O bending, Si–O rocking, Al–O stretching, and Si–OH stretching vibrations, respectively [85]. Further, a very weak peak at 618 cm^{-1} was attributed to iron oxide, and a very broad peak at 1312 cm^{-1} (magnon) indicated the presence of magnetically ordered ferromagnetic or antiferromagnetic iron oxides [86]. The observed Raman and infrared vibrational bands of the NDL were in good agreement with the reported values. The minor shift in the band positions might be due to the presence of trace metal contents and impurities.

The morphology of the NDL catalyst was analyzed by scanning electron microscopy (Figure 5). The SEM images revealed that the morphology of the NDL catalyst consists of irregular shapes and sizes with a random dispersion. Further, the elemental composition of the NDL catalyst was determined by EDAX analysis (Figure 6).

The catalytic activity of the NDL for the synthesis of the 1,2-disubstituted benzimidazoles **3**, the dihydropyrimidinones/-thiones **7**, and the 2-amino-4-(hetero)aryl-3,5-dicarbonitrile-6-sulfanylpyridines **11** was investigated, along with other, commercially available catalysts.

NDL-catalyzed synthesis of 1,2-disubtituted benzimidazoles **3**

To check the catalytic activity of the NDL, initially, *o*-phenylenediamine (**1**) and benzaldehyde (**2a**) were chosen as model substrates to optimize the reaction conditions for the syn-

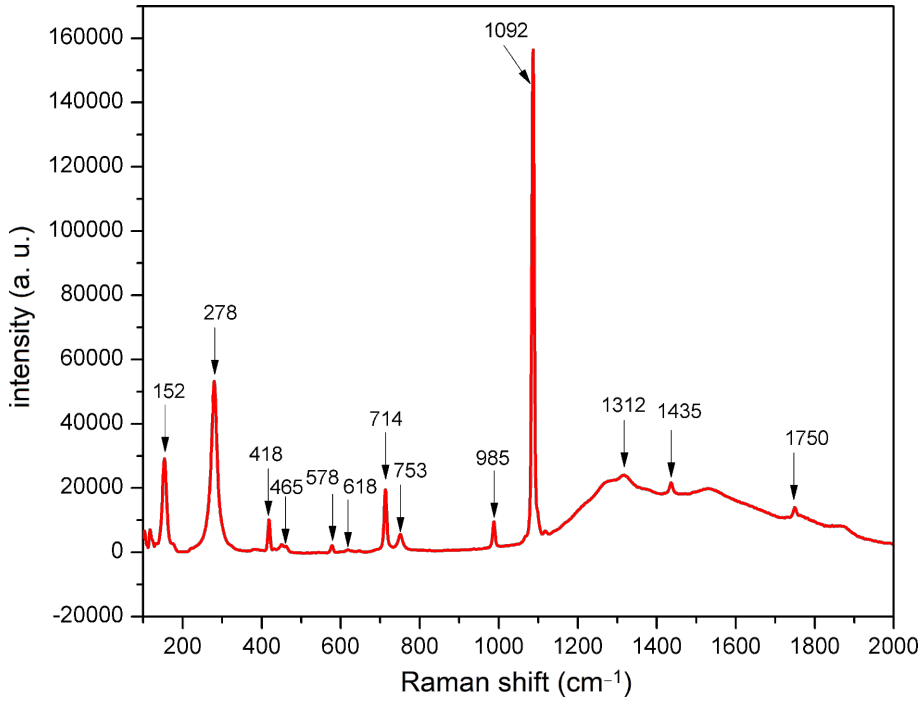

Figure 4: Raman spectrum of the NDL catalyst.

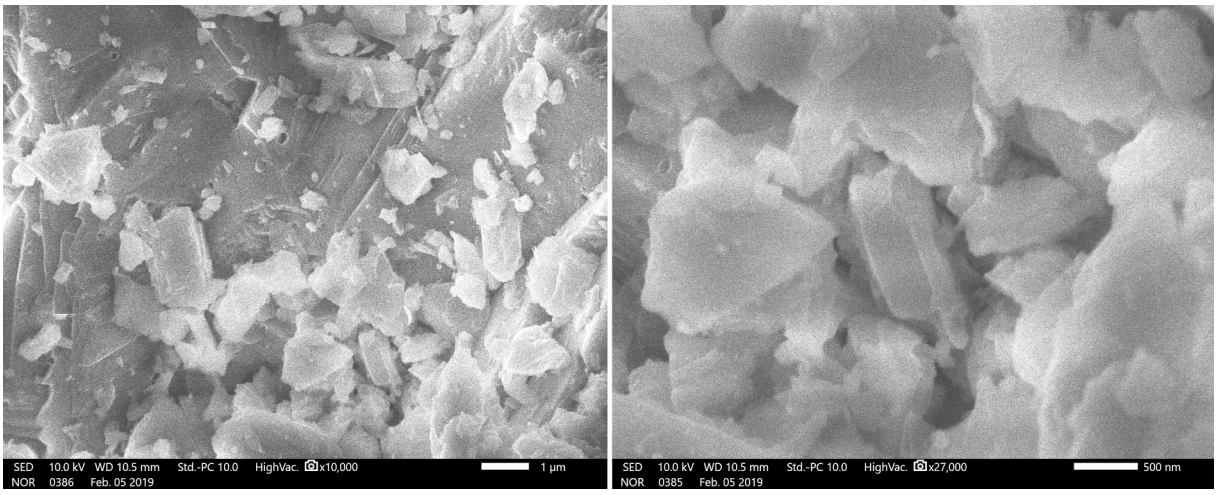

Figure 5: SEM images of the NDL catalyst.

thesis of 1-benzyl-2-phenyl-1*H*-benzo[*d*]imidazole (**3a**). At first, a control experiment was conducted by using model substrates, **1** and **2a**, in H_2O in the absence of catalyst under ultrasound irradiation for 60 min at 45–50 °C. It was found that the reaction did not proceed in the absence of a catalyst (Table 2, entry 1). To achieve the target compound **3a**, the same reaction was repeated by employing various catalysts (2.5 wt %), such as Fe_2O_3, Al_2O_3, KF–alumina, dolomitic limestone, triethylamine, pyridine, and DABCO in different solvents, such as water, acetone, iPrOH, EtOH, and EtOH/H_2O 1:1 (Table 2, entries 2–8) under ultrasound irradiation at 45–50 °C. From this study, it was observed that the NDL (2.5 wt %) was the best option, which gave the target compound **3a** in a high yield (85%) in a mixture of EtOH and H_2O 1:1 under ultrasound irradiation for 30 min at 45–50 °C (Table 2, entry 5). The other catalysts, Fe_2O_3, Al_2O_3, KF–alumina, triethylamine, pyridine, and

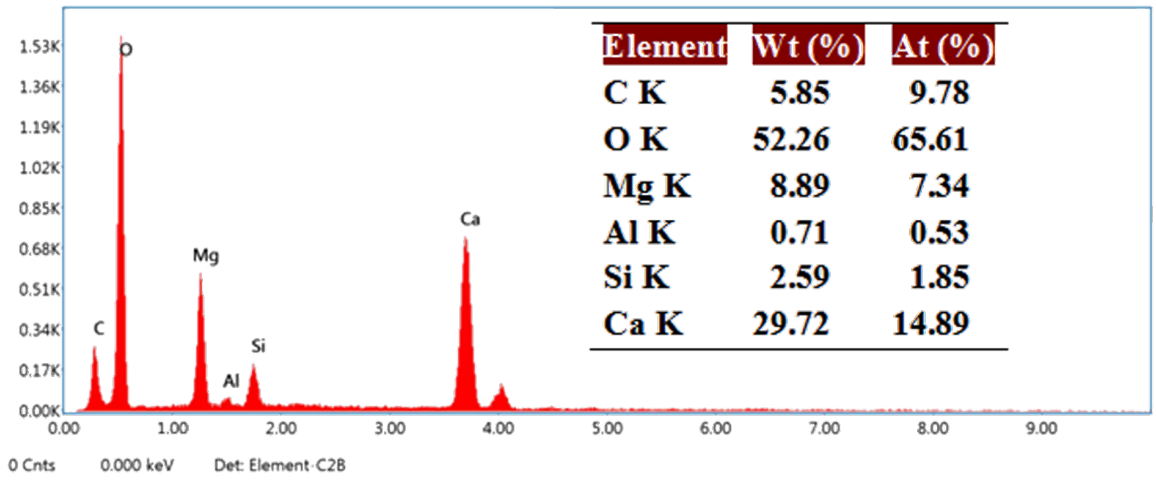

Figure 6: EDAX analysis of the NDL catalyst.

Table 2: Optimization of the reaction conditions.[a]

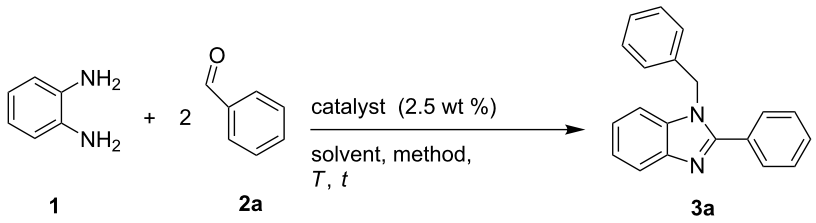

entry	catalyst (2.5 wt %)	solvent	product	conventional method[b]		USI[c]	
				t (min)	yield[d] (%)	*t* (min)	yield[d] (%)
1[e]	no catalyst	H_2O	**3a**	180	–	60	–
2	Fe_2O_3	H_2O	**3a**	60	10	30	15
		acetone		60	–	30	–
		iPrOH		60	10	30	20
		EtOH		60	15	30	20
		EtOH/H_2O 1:1		60	20	30	25
3	Al_2O_3	H_2O	**3a**	60	20	30	20
		acetone		60	–	30	–
		iPrOH		60	15	30	20
		EtOH		60	25	30	25
		EtOH/H_2O 1:1		60	30	30	40
4	KF–alumina	H_2O	**3a**	60	30	30	30
		acetone		60	–	30	–
		iPrOH		60	25	30	30
		EtOH		60	40	30	35
		EtOH/H_2O 1:1		60	50	30	40
5	NDL	H_2O	**3a**	60	55	30	65
		acetone		60	–	30	–
		iPrOH		60	35	30	45
		EtOH		60	60	30	75
		EtOH/H_2O 1:1		60	70	30	85

Table 2: Optimization of the reaction conditions.[a] (continued)

6	Et_3N	H_2O	**3a**	60	10	30	10
		acetone		60	–	30	–
		iPrOH		60	10	30	10
		EtOH		60	15	30	20
		EtOH/H_2O 1:1		60	10	30	10
7	pyridine	H_2O	**3a**	60	–	30	–
		acetone		60	–	30	–
		iPrOH		60	5	30	5
		EtOH		60	10	30	10
		EtOH/H_2O 1:1		60	5	30	5
8	DABCO	H_2O	**3a**	60	10	30	5
		acetone		60	–	30	–
		iPrOH		60	15	30	5
		EtOH		60	15	30	15
		EtOH/H_2O 1:1		60	10	30	10

[a]Reaction conditions: *o*-phenylenediamine (**1**, 1.0 mmol), benzaldehyde (**2a**, 2.0 mmol), catalyst (2.5 wt %), solvent (3.0 mL). [b]Performed by stirring at reflux (entries 2–8). [c]USI method performed at 45–50 °C. [d]Isolated yield. [e]Conventional method performed by stirring at 45–50 °C.

DABCO, provided a moderate to low yield of the product **3a** (Table 2, entries 2–4 and 6–8). The aforesaid reaction was performed under conventional stirring of the model substrates **1** and **2a** in H_2O in the absence of catalyst for 180 min at 45–50 °C. It was observed that the reaction did not proceed in the absence of a catalyst (Table 2, entry 1). Further, when the reaction temperature was raised from 45–50 °C to reflux, a very low yield (10%) of the product **3a** was obtained after 120 min. Next, the reaction was repeated in the presence of different catalysts and solvents at reflux under conventional reaction conditions as mentioned in Table 2. The study revealed that the NDL in a mixture of EtOH and H_2O 1:1 afforded a moderate yield (70%) of the product **3a** (Table 2, entry 5), whereas the other catalysts, in various solvents, provided lower yields under similar reaction conditions (Table 2, entries 2–4 and 6–8). From the above observations, it was concluded that the ultrasound irradiation method is better than the conventional method in giving the maximum yield of **3a**.

Next, the amount of catalyst was varied (using 2.5, 5.0, 7.5, 10.0, and 12.5 wt %, respectively,) to improve the yield of **3a** (Table 3). The study revealed that 5.0 wt % of the NDL was the best option to get the highest yield of the product **3a** (98%) in a short reaction time (10 min, Table 3, entry 3). It was also noticed that the same yield was obtained with an increasing amount of the catalyst, i.e., 7.5, 10.0, and 12.5 wt % (Table 3, entries 4–6).

In order to demonstrate the effect of the temperature on the course of the model reaction, the control experiment was performed at different temperature ranges (30–35, 35–40, 40–45, and 45–50 °C) by using the model substrates **1** and **2a** in the

Table 3: Effect of the catalyst loading.[a]

entry	NDL (wt %)	solvent	*t* (min)	product	yield[b] (%)
1	2.5	EtOH/H_2O 1:1	30	**3a**	85
2	2.5	EtOH/H_2O 1:1	10	**3a**	75
3	5.0	EtOH/H_2O 1:1	10	**3a**	98
4	7.5	EtOH/H_2O 1:1	10	**3a**	98
5	10.0	EtOH/H_2O 1:1	10	**3a**	98
6	12.5	EtOH/H_2O 1:1	10	**3a**	98

[a]Reaction conditions: *o*-phenylenediamine (**1**, 1.0 mmol), benzaldehyde (**2a**, 2.0 mmol), NDL (2.5 to 12.5 wt %), EtOH/H_2O 1:1 (3.0 mL), ultrasound irradiation at 45–50 °C. [b]Isolated yield.

presence of 5.0 wt % of the NDL in a mixture of ethanol and water 1:1 for 10 min under both conventional stirring and ultrasound irradiation. The obtained results are presented in Table 4. It was observed that the reaction proceeded with an improved yield of **3a** (70–98%) by increasing the temperature range from 30–35 to 45–50 °C with an ultrasound irradiation method (Table 4, entries 1–4). Under conventional stirring, the yield of the product **3a** increased from low to moderate when the reaction temperature was raised from 30–35 °C to reflux (Table 4, entries 1–5). From the results, it was concluded that a temperature of 45–50 °C is the optimum temperature to obtain the maximum yield of the desired product **3a** within a short reaction time (10 min) under ultrasound irradiation (Table 4, entry 4).

To demonstrate the generality and substrate scope of the present method, a variety of (hetero)aromatic aldehydes was investigated. The obtained results are presented in Table 5. *o*-Phenylenediamine (**1**) reacted well with benzaldehyde (**2a**) to obtain the corresponding product **3a** with 98% yield (Table 5, entry 1). The reactions of *o*-phenylenediamine (**1**) with substituted benzaldehydes having activating groups (4-Me: **2b**, 4-*t*-Bu: **2c**, 2,4-dimethyl: **2d**, 4-OMe: **2e**, 3,4-dimethoxy: **2f**, 3,4,5-trimethoxy: **2g**, 4-OH-3-OMe: **2j**, and 4-OH-3-OC_2H_5: **2k**, Table 5, entries 2–7, 10 and 11), a deactivating group (4-NO_2: **2l**, Table 5, entry 12), or a halo group (4-F: **2m**, 4-Cl: **2n**, and 4-Br: **2o**, Table 5, entries 13–15) in different positions provided good to excellent isolated yields of the corresponding products **3b**–**g** and **3j**–**o** that ranged from 94 to 98% in a stipulated period of time, as specified in Table 5. Further, heteroaromatic aldehydes, such as furan-2-aldehyde (**2p**) and thiophene-2-aldehyde (**2q**) produced the corresponding products **3p** and **3q** in good isolated yields within a short period of time (15 min and 13 min, respectively, Table 5, entries 16 and 17).

However, salicylaldehyde (**2h**) afforded the unexpected product 2,2'-((1*E*,1'*E*)-(1,2-phenylenebis(azanylylidene))bis(methanylylidene))diphenol (**3h**, bisimine I) within 10 min (Table 5, entry 8). The reaction was expected to proceed through the activation of the carbonyl group of **2h** (of which 2.0 mmol were used) by the cations (Ca^{2+} and Mg^{2+}, respectively) of the NDL. This was followed by a nucleophilic attack of the NH_2 groups of *o*-phenylenediamine (**1**, of which 1.0 mmol was used), which are activated by the carbonate part of the NDL, followed by dehydration to obtain **3h** (Scheme 2). Due to the mild basic nature of the NDL catalyst, it acts as a dual activator of the electrophilic carbonyl and the nucleophilic NH_2 groups. The formation of the bisimine I was confirmed by ^{1}H NMR spectral studies (Figure 7). In the ^{1}H NMR spectrum (DMSO-d_6), the two hydroxy protons of the bisimine I appeared as a broad, strongly downfield-shifted singlet at δ 13.19. The sharp singlet at δ 8.66 indicated the two imine protons (–N=C**H**) of the bisimine I. From this result, it was confirmed that the reaction stopped at the bisimine I stage. This was due to the intramolecular hydrogen bonding between the hydrogen atom of the *ortho*-hydroxy group and the nitrogen atom of the imine group in a six-membered ring transition state [87]. Similarly, the reaction between 3-ethoxysalicylaldehyde (**2i**) and *o*-phenylenediamine (**1**) also ended with the intermediate 6,6'-((1*E*,1'*E*)-(1,2-phenylenebis(azanylylidene))bis(methanylylidene))bis(2-ethoxyphenol) (**3i**) stage (Table 4, entry 9 and Supporting Information File 1, Figure S13). Most of the synthesized compounds are known and were identified easily by comparison of the melting point and spectroscopic data with those reported.

NDL-catalyzed synthesis of dihydropyrimidinones/-thiones **7**

The results encouraged us to further investigate the catalytic activity of the NDL in the Biginelli reaction. To check the feasibility, a control experiment was performed by using the model substrates benzaldehyde (**2a**, 1.0 mmol), ethyl acetoacetate (**4**, 1.0 mmol), and urea (**5**, 1.0 mmol) in H_2O (3.0 mL) in the absence of a catalyst under ultrasound irradiation at 45–50 °C for 60 min. It was observed that the reaction proceeded with a

Table 4: Effect of the temperature.[a]

entry	*T* (°C)	product	*t* (min)	conventional method[b] yield[d] (%)	USI[c] yield[d] (%)
1	30–35	**3a**	10	10	70
2	35–40	**3a**	10	14	79
3	40–45	**3a**	10	20	87
4	45–50	**3a**	10	26	98
5[e]	reflux	**3a**	10/60	35/70	–

[a]Reaction conditions: *o*-phenylenediamine (**1**, 1.0 mmol), benzaldehyde (**2a**, 2.0 mmol), NDL (5.0 wt %), EtOH/H_2O 1:1 (3.0 mL). [b]Conventional stirring and heating with a silicone oil bath. [c]Ultrasound irradiation in a water bath. [d]Isolated yield. [e]Conventional stirring at reflux.

Table 5: NDL-catalyzed synthesis of 2-aryl-1-arylmethyl-1*H*-benzo[*d*]imidazoles 3.[a]

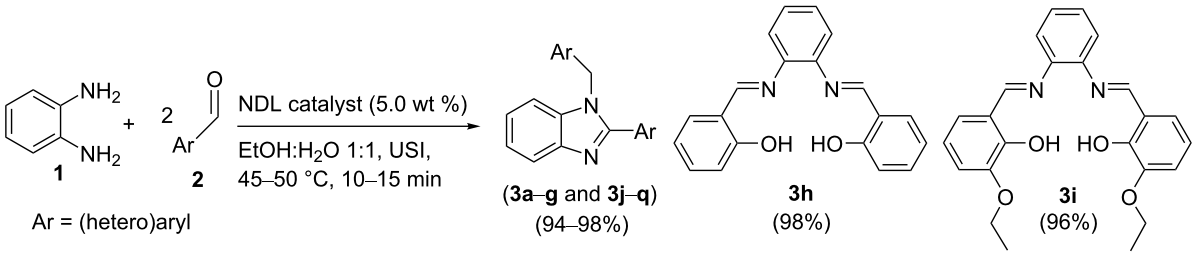

entry	Ar	product	*t* (min)	yield[c] (%)	mp (°C)	
					found	reported
1	phenyl: **2a**	**3a**	10	98	128–131	133–134 [23]
2	4-methylphenyl: **2b**	**3b**	10	98	127–128	128–129 [23]
3	4-*tert*-butylphenyl: **2c**	**3c**	15	94	124–125	122–126 [25]
4	2,4-dimethylphenyl: **2d**	**3d**	12	96	120–122	119–123 [25]
5	4-methoxyphenyl: **2e**	**3e**	11	98	157–159	158–160 [23]
6	3,4-dimethoxyphenyl: **2f**	**3f**	12	95	167–169	171–173 [24]
7	3,4,5-trimethoxyphenyl: **2g**	**3g**	15	94	261–262	262–263 [22]
8[b]	2-hydroxyphenyl: **2h**	**3h**	10	98	167–168	160–162 [23]
9[b]	2-hydroxy-3-ethoxyphenyl: **2i**	**3i**	12	96	285–287	–
10	4-hydroxy-3-methoxyphenyl: **2j**	**3j**	12	96	181–183	184–186 [24]
11	4-hydroxy-3-ethoxyphenyl: **2k**	**3k**	10	97	205–207	200–201 [26]
12	4-nitrophenyl: **2l**	**3l**	10	98	190–192	189–191 [23]
13	4-fluorophenyl: **2m**	**3m**	10	98	108–109	110–112 [23]
14	4-chlorophenyl: **2n**	**3n**	10	98	138–140	137–139 [23]
15	4-bromophenyl: **2o**	**3o**	12	96	158–160	160–162 [23]
16	2-furanyl: **2p**	**3p**	15	95	90–92	88–89 [23]
17	2-thienyl: **2q**	**3q**	13	96	149–150	150–152 [23]

[a]Reaction conditions: *o*-phenylenediamine (**1**, 1.0 mmol), aldehyde (**2**, 2.0 mmol), NDL (5.0 wt %), EtOH/H_2O 1:1 (3.0 mL), USI, 45–50 °C. [b]The reaction stopped at the bisimine I, i.e., **3h**/**i** stage. [c]Isolated yield.

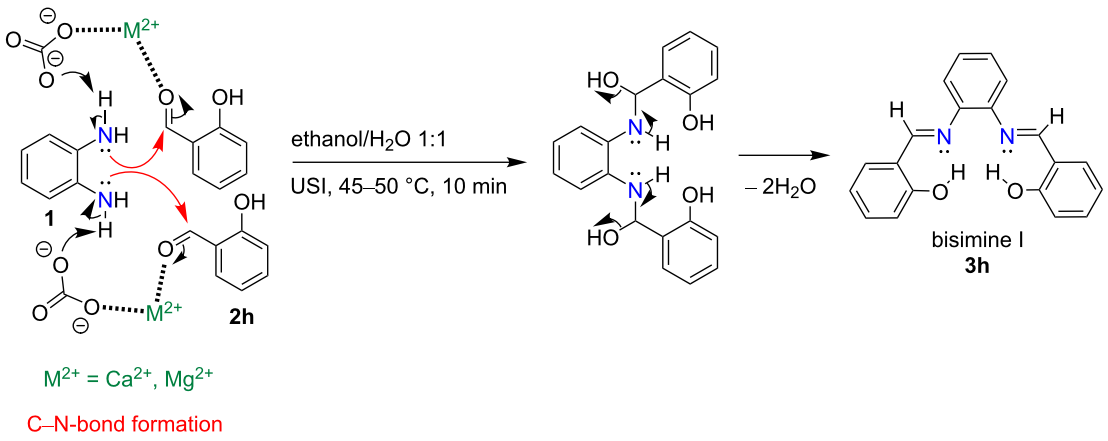

Scheme 2: Unexpected formation of the bisimine I, **3h**, from *o*-phenylenediamine (**1**) and salicylaldehyde (**2h**).

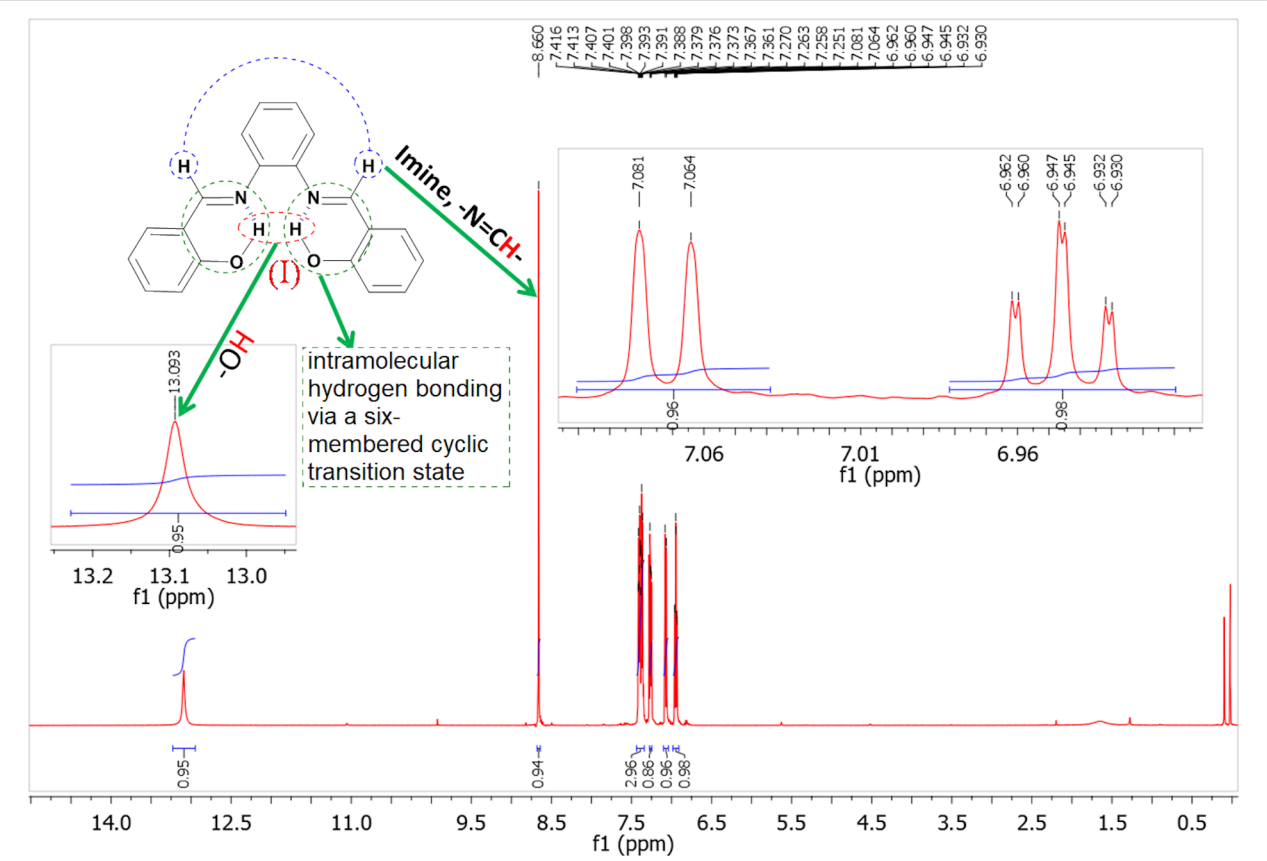

Figure 7: ^{1}H NMR spectrum of 2,2'-((1*E*,1'*E*)-(1,2-phenylenebis(azanylylidene))bis (methanylylidene))diphenol (bisimine I, **3h**).

very low yield (20%) of product **7a**. The same reaction was repeated in the presence of the NDL catalyst (5.0 wt %) in EtOH/H_2O 1:1 under ultrasound irradiation at 45–50 °C for 15 min, which resulted in 97 % yield of **7a**.

To exploit the substrate scope and generality of the method, various (hetero)aromatic aldehydes **2** were examined. The obtained results are summarized in Table 6. Benzaldehyde (**2a**) underwent the reaction with ethyl acetoacetate (**4**) and urea (**5**) to obtain the corresponding dihydropyrimidinone **7a** in 97% yield (Table 6, entry 1). Benzaldehyde derivatives bearing electron-donating groups, such as 4-Me (**2b**), 4-OMe (**2e**), 3,4-dimethoxy (**2f**), 3-OH (**2r**), and 2-OH (**2h**), respectively, at different positions on the ring reacted well with ethyl acetoacetate (**4**) and urea (**5**) to produce the products, **7b–f** in good isolated yields that ranged from 92–96% (Table 6, entries 2–6). A benzaldehyde derivative with an electron-accepting nitro group (**2l**) at the *para* position on the ring showed a good reactivity with ethyl acetoacetate (**4**) and urea (**5**) to afford the product **7g** in an excellent isolated yield (94%, Table 6, entry 7). Halogen atoms at different positions on the ring of benzaldehyde derivatives (4-F: **2m**, 4-Cl; **2n**, and 3-Br: **2s**) underwent the reaction with ethyl acetoacetate (**4**) and urea (**5**) to form the corresponding products (**7h–j**) in good isolated yields that ranged from 93–96% (Table 6, entries 8–10). Heteroaromatic aldehydes, such as furan-2-aldehyde (**2p**) and thiophene-2-aldehyde (**2q**) showed a good reactivity, with good yields of **7k** (90%) and **7l** (92%), respectively (Table 6, entries 11 and 12). From this study, it was concluded that the optimized reaction conditions are suitable for monosubstituted (both electron-rich and electron-deficient) and disubstituted benzaldehyde derivatives as well as heteroaromatic aldehydes. To expand the scope of this method, thiourea (**6**) was also investigated (Table 6, entries 13–17). Benzaldehyde (**2a**) reacted with ethyl acetoacetate (**4**) and thiourea (**6**) to give the product **7m** in an excellent isolated yield (96%, Table 6, entry 13). Benzaldehyde derivatives bearing electron-donating groups, such as 4-Me (**2b**) and 4-OMe (**2c**) exhibited a good reactivity with ethyl acetoacetate (**4**) and thiourea (**6**) to produce the products **7n** (95%) and **7o** (95%) in excellent yields, respectively (Table 6, entries 14 and 15). Benzaldehyde with electron-withdrawing groups, such as 4-NO_2 (**2f**) and 4-Cl (**2i**) at the *para* position reacted well with ethyl acetoacetate (**4**) and thiourea (**6**) to afford the corresponding products **7p** and **7q** in good isolated yields (94 and 95%) (Table 6, entries 16 and 17). Most of the synthesized compounds are known and were identified easily by compari-

Table 6: NDL-catalyzed synthesis of dihydropyrimidinone/-thione derivatives **7**.[a]

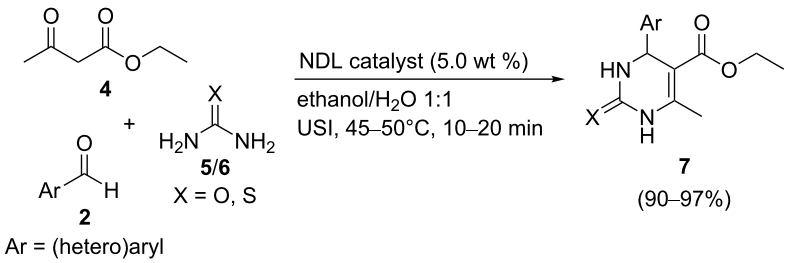

entry	Ar	X	product	*t* (min)	yield[b] (%)	mp (°C)	
						found	reported
1	phenyl: **2a**	O	**7a**	15	97	207–209	209–210 [50]
2	4-methylphenyl: **2b**	O	**7b**	15	96	213–214	215–216 [38]
3	4-methoxyphenyl: **2e**	O	**7c**	17	96	200–201	199–202 [48]
4	3,4-dimethoxyphenyl: **2f**	O	**7d**	18	94	213–215	212–214 [52]
5	3-hydroxyphenyl: **2r**	O	**7e**	17	95	162–164	163–165 [38]
6	2-hydroxyphenyl: **2h**	O	**7f**	15	92	198–200	199–201 [49]
7	4-nitrophenyl: **2l**	O	**7g**	12	94	210–211	209–212 [48]
8	4-fluorophenyl: **2m**	O	**7h**	13	95	176–179	175–177 [37]
9	4-chlorophenyl: **2n**	O	**7i**	12	96	208–210	209–211 [48]
10	3-bromophenyl: **2s**	O	**7j**	18	93	184–185	185–186 [47]
11	2-furanyl: **2p**	O	**7k**	20	90	204–206	203–205 [48]
12	2-thienyl: **2q**	O	**7l**	20	92	216–218	215–217 [38]
13	phenyl: **2a**	S	**7m**	15	96	211–212	208–210 [38]
14	4-methylphenyl: **2b**	S	**7n**	15	95	189–190	192–194 [38]
15	4-methoxyphenyl: **2e**	S	**7o**	17	95	148–150	150–152 [38]
16	4-nitrophenyl: **2l**	S	**7p**	10	94	113–114	109–111 [38]
17	4-chlorophenyl: **2n**	S	**7q**	11	95	190–191	192–194 [38]

[a]Reaction conditions: aldehyde (**2**, 1.0 mmol), ethyl acetoacetate (**4**, 1.0 mmol), urea/thiourea (**5**/**6**, 1.0 mmol), NDL (5.0 wt %), ethanol/H_2O 1:1 (3.0 mL), USI at 45–50 °C. [b]Isolated yield.

son of the melting point and spectroscopic data with those reported.

NDL-catalyzed synthesis of 2-amino-4-(hetero)aryl-3,5-dicarbonitrile-6-sulfanylpyridines **11**

We further examined the catalytic efficacy of the NDL catalyst in the synthesis of the medicinally privileged highly functionalized pyridines **11**. For this purpose, a control experiment in the absence of a catalyst was conducted by using the model substrates benzaldehyde (**2a**, 1.0 mmol), malononitrile (**8**, 2.0 mmol), and 2-mercaptopyridine (**9**, 1.0 mmol) in H_2O (3.0 mL) under ultrasound irradiation at 45–50 °C for 60 min. It was observed that the reaction did not afford any product in the absence of a catalyst. The above reaction was carried out in the presence of the NDL (5.0 wt %) in EtOH/H_2O 1:1 (3.0 mL) under ultrasound irradiation for 10 min, which resulted in 70% yield of **11a**. To improve the yield of **11a**, the same reaction was repeated at different time intervals; 15, 20, 25, 30, 35, and 40 min, respectively, at 45–50 °C, and the yields of **11a** obtained were 75, 83, 89, 96%, 96, and 96%, respectively. From this study, it was found that the maximum yield of **11a** (96%) was obtained in 30 min, and the yields remained the same when the reaction time was increased from 30 to 40 min.

The optimized procedure was successfully applied for the synthesis of a series of highly substituted pyridines (**11b**–**r**, Table 7) by utilizing a range of (hetero)aromatic aldehydes **2**, malononitrile (**8**), and the thiols **9** and **10**, respectively, as starting materials. Benzaldehyde (**2a**) underwent the reaction with malononitrile (**8**) and 2-mercaptopyridine (**9**) to form product **11a** in 96% yield (Table 7, entry 1). Benzaldehyde deriva-

Table 7: NDL-catalyzed synthesis of 2-amino-4-(hetero)aryl-3,5-dicarbonitrile-6-sulfanylpyridines **11**.[a]

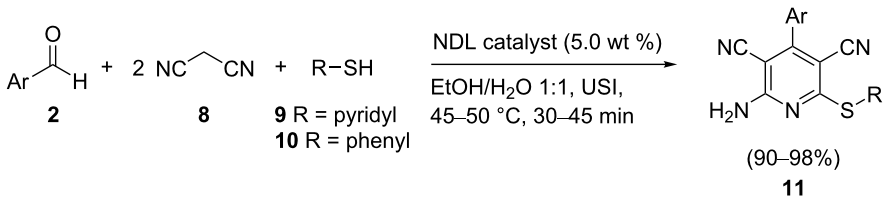

2 **8** **9** R = pyridyl **10** R = phenyl **11**

entry	Ar	R	product	*t* (min)	yield[b] (%)	mp (°C)	
						found	reported
1	phenyl: **2a**	pyridyl **9**	**11a**	30	96	222–223	224–227 [70]
2	4-methoxyphenyl: **2e**	pyridyl **9**	**11b**	35	96	248–249	250–253 [70]
3	3,4,5-trimethoxyphenyl: **2g**	pyridyl **9**	**11c**	40	92	267–269	265–268 [70]
4	3-hydroxyphenyl: **2r**	pyridyl **9**	**11d**	35	94	223–224	222–226 [70]
5	4-nitrophenyl: **2l**	pyridyl **9**	**11e**	32	96	241–243	245–248 [70]
6	4-fluorophenyl: **2m**	pyridyl: **9**	**11f**	32	95	248–250	246–249 [70]
7	4-bromophenyl: **2o**	pyridyl: **9**	**11g**	30	94	257–258	260–263 [70]
8	3,4-difluorophenyl: **2t**	pyridyl: **9**	**11h**	37	90	252–253	251–254 [70]
9	pyridyl: **2u**	pyridyl: **9**	**11i**	45	93	230–231	233–235 [70]
10	phenyl: **2a**	phenyl: **10**	**11j**	30	98	210–212	215–216 [63]
11	4-methylphenyl: **2b**	phenyl: **10**	**11k**	30	98	206–207	208–210 [69]
12	4-methoxyphenyl: **2e**	phenyl: **10**	**11l**	35	97	234–235	236–238 [64]
13	3,4,5-trimethoxyphenyl: **2g**	phenyl: **10**	**11m**	38	94	240–241	238–239 [63]
14	4-nitrophenyl: **2l**	phenyl: **10**	**11n**	30	95	280–282	286–287 [63]
15	4-fluorophenyl: **2m**	phenyl: **10**	**11o**	30	96	127–128	224–225 [69]
16	4-chlorophenyl: **2n**	phenyl: **10**	**11p**	30	96	220–221	222–223 [69]
17	3-bromophenyl: **2s**	phenyl: **10**	**11q**	34	94	250–253	256–258 [65]
18	pyridyl: **2u**	phenyl: **10**	**11r**	42	94	300–302	305–306 [63]

[a]Reaction conditions: aldehyde (**2**, 1.0 mmol), malononitrile (**8**, 2.0 mmol), thiol **9** or **10** (1.0 mmol), NDL (5.0 wt %), EtOH/H_2O 1:1 (3.0 mL), USI at 45–50 °C. [b]Isolated yield.

tives containing a range of functional groups, such as electron-donating groups (4-OMe: **2e**, 3,4,5-trimethoxy: **2g**, and 3-OH: **2r**), an electron-withdrawing group (4-NO_2: **2l**), and halogen atoms (4-F: **2m**, 4-Cl: **2n**, and 3,4-difluoro: **2t**), respectively, at different positions on the aromatic ring showed a good reactivity with the said reactants and afforded the corresponding products **11b**–**h** that ranged from 90 to 96% (Table 7, entries 2–8). Further, the use of pyridine-2-aldehyde (**2u**) resulted in a good isolated yield of **11i** (93%, Table 7, entry 9). In a similar way, the reaction of benzaldehyde (**2a**) with malononitrile (**8**) and thiophenol (**10**) gave the product **11j** in 98% yield (Table 7, entry 10). Benzaldehyde derivatives bearing various functional groups, such as electron-donating groups (4-Me: **2b**, 4-OMe: **2e**, and 3,4,5-trimethoxy: **2g**), an electron-accepting group (4-NO_2: **2l**), and halogen atoms (4-F: **2m**, 4-Cl: **2n**, and 3-Br: **2s**), respectively, at different positions on the aromatic ring displayed a good reactivity with malononitrile (**8**) and thiophenol (**10**) to give the corresponding products (**11k**–**q**) in good yields, ranging from 94 to 98% (Table 7, entries 11–17). Pyridine-2-aldehyde (**2u**) also provided the product **11r** in a good yield (94%, Table 7, entry 18). It was observed from the above results that all reactions proceeded well irrespective of the substituents present on the (hetero)aromatic aldehyde and afforded the highly substituted pyridines **11** in good isolated yields that ranged from 90 to 98%. Most of the synthesized compounds are known and were identified easily by comparison of the melting point and spectroscopic data with those reported.

Evaluation of the green chemistry metrics for the synthesis of benzimidazoles **3**, dihydropyrimidinones **7**, and highly functionalized pyridines **11**

In order to evaluate the "greenness" of the proposed methodologies, the green chemistry metrics, such as the atom economy (AE), E-factor, process mass intensity (PMI), Curzon's reac-

tion mass efficiency (RME), and generalized or global reaction mass efficiency (gRME) were evaluated by adopting established standard empirical formulae [88,89]. The obtained results are summarized in Tables 8–10. This study revealed that the reactions displayed a good to excellent AE (88–95%) and Curzon's RME (78–93%) as well as a low to moderate E-factor (26.202–50.760) and PMI (27.202–51.760). The detailed calculations of the green chemistry metrics (AE, E-factor, PMI, Curzon's RME, and gRME) for the synthesis of the compounds **3a**, **7a**, and **11a** (Table 8, entry 1, Table 9, entry 1, and Table 10, entry 1) are presented in Supporting Information File 1 (see Reaction-S1–Reaction-S3).

Catalyst reusability experiments

Catalyst reusability tests were performed showcasing the synthesis of the compounds **3k**, **7a**, and **11e** under the optimized reaction conditions.

Catalyst reusability experiments in the synthesis of compounds **3k**, **7a**, and **11e**

The catalyst was tested for reusability in the preparation of **3k** using *o*-phenylenediamine (**1**) and 3-ethoxy-4-hydroxybenzaldehyde (**2k**) under USI for 10 min. After completion of the first reaction cycle, the reaction mass was allowed to cool to rt, and ethyl acetate (4.0 mL) was added. Then, the catalyst was

Table 8: Green chemistry metrics for the synthesis of 2-aryl-1-arylmethyl-1*H*-benzo[*d*]imidazoles **3**.

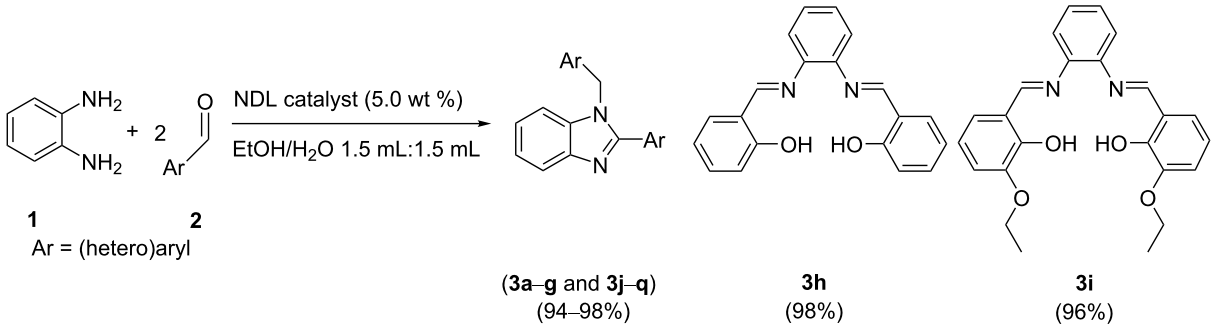

1 **2**
Ar = (hetero)aryl

(**3a**–**g** and **3j**–**q**) (94–98%) **3h** (98%) **3i** (96%)

entry	Ar	product	AE[a] (%)	E-factor[b]	PMI[c]	Curzon's RME[d] (%)	gRME[e] (%)
1	phenyl: **2a**	**3a**	89	40.864	41.864	87	2.4
2	4-methylphenyl: **2b**	**3b**	90	37.261	38.261	88	2.6
3	4-*tert*-butylphenyl: **2c**	**3c**	92	30.614	31.614	86	3.2
4	2,4-dimethylphenyl: **2d**	**3d**	90	35.044	36.044	86	2.8
5	4-methoxyphenyl: **2e**	**3e**	91	33.837	34.837	89	2.9
6	3,4-dimethoxyphenyl: **2f**	**3f**	92	29.729	30.729	87	3.3
7	3,4,5-trimethoxyphenyl: **2g**	**3g**	93	26.202	27.202	87	3.7
8	2-hydroxyphenyl: **2h**	**3h**	90	36.781	37.781	88	2.6
9	2-hydroxy-3-ethoxyphenyl: **2i**	**3i**	92	29.412	30.412	88	3.3
10	4-hydroxy-3-methoxyphenyl: **2j**	**3j**	91	31.609	32.609	88	3.1
11	4-hydroxy-3-ethoxyphenyl: **2k**	**3k**	92	29.102	30.102	89	3.3
12	4-nitrophenyl: **2l**	**3l**	91	31.017	32.017	89	3.1
13	4-fluorophenyl: **2m**	**3m**	90	36.312	37.312	88	2.7
14	4-chlorophenyl: **2n**	**3n**	91	33.052	34.052	89	2.9
15	4-bromophenyl: **2o**	**3o**	93	26.920	27.920	89	3.6
16	2-furanyl: **2p**	**3p**	88	45.454	46.454	84	2.2
17	2-thienyl: **2q**	**3q**	89	40.169	41.169	85	2.4

[a]AE = 100·(GMW of the product/sum of the GMWs of the reactants); GMW = gram molecular weight. [b]E-factor = total input mass (^{m}inputs)[f] – mass of the target product (^{m}**3**) – mass of the recovered materials/^{m}**3**. [c]PMI = (^{m}inputs – mass of the recovered materials)/^{m}**3** or 1 + E-factor.
[d]Curzon's RME = ^{m}**3**/ ^{m}**1** + ^{m}**2** or yield × AE × 1/stoichiometric factor (SF); SF = 1. [e]gRME = 100·(^{m}**3**/(^{m}inputs – mass of the recovered materials)) or 100·(1/(1 + E-factor)). [f]Total input mass, including water (^{m}inputs) = ^{m}**1** + ^{m}**2** + ^{m}solvent (S) + ^{m}catalyst (C) + ^{m}work-up materials (WPM) + mpurification materials (PM).

Table 9: Green chemistry metrics for the synthesis of dihydropyrimidinones/-thiones **7**.

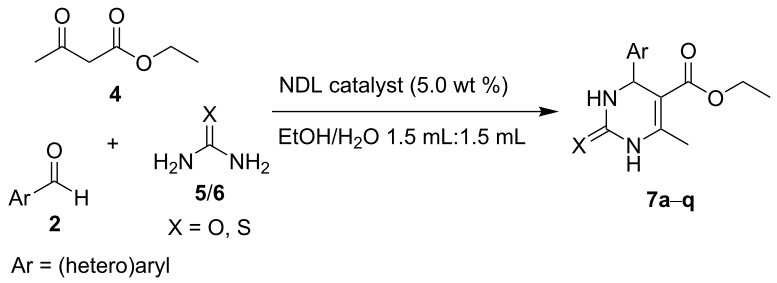

entry	reactants		product	AE (%)	E-factor[a]	PMI[b]	Curzon's RME[c] (%)	gRME[d] (%)
	Ar	**5**/**6**						
1	phenyl: **2a**	**5**	**7a**	88	45.254	46.254	85	2.2
2	4-methylphenyl: **2b**	**5**	**7b**	88	43.373	44.373	84	2.3
3	4-methoxyphenyl: **2e**	**5**	**7c**	89	41.036	42.036	85	2.4
4	3,4-dimethoxyphenyl: **2f**	**5**	**7d**	90	37.924	38.924	85	2.6
5	3-hydroxyphenyl: **2r**	**5**	**7e**	89	43.550	44.550	85	2.2
6	2-hydroxyphenyl: **2h**	**5**	**7f**	89	44.953	45.953	82	2.2
7	4-nitrophenyl: **2l**	**5**	**7g**	89	39.770	40.770	84	2.5
8	4-fluorophenyl: **2m**	**5**	**7h**	89	43.220	44.220	85	2.3
9	4-chlorophenyl: **2n**	**5**	**7i**	89	40.311	41.311	85	2.4
10	3-bromophenyl: **2s**	**5**	**7j**	90	36.254	37.254	84	2.7
11	2-furanyl: **2p**	**5**	**7k**	87	50.760	51.760	78	1.9
12	2-thienyl: **2q**	**5**	**7l**	88	46.600	47.600	81	2.1
13	phenyl: **2a**	**6**	**7m**	89	43.045	44.045	85	2.3
14	4-methylphenyl: **2b**	**6**	**7n**	89	41.341	41.341	85	2.4
15	4-methoxyphenyl: **2e**	**6**	**7o**	90	39.213	40.213	86	2.5
16	4-nitrophenyl: **2l**	**6**	**7p**	90	37.978	38.978	85	2.6
17	4-chlorophenyl: **2n**	**6**	**7q**	90	38.685	39.685	86	2.5

[a]E-factor = ^{m}inputs[e] – mass of the target product (^{m}**7**) – mass of the recovered materials/^{m}**7**. [b]PMI = (^{m}inputs – mass of the recovered materials)/^{m}**7** or 1 + E-factor. [c]Curzon's RME = ^{m}**7**/^{m}**2** + ^{m} **4** + ^{m}**5**/**6** or yield × AE × 1/SF; SF = 1. [d]gRME = 100·(^{m}**7**/(^{m}inputs – mass of the recovered materials)) or 100·(1/(1 + E-factor)). [em]inputs = ^{m}**2** + ^{m}**4** + ^{m}**5**/**6** + ^{m}S + ^{m}C + ^{m}WPM + ^{m}purification materials (PM).

separated by vacuum filtration, washed with ethyl acetate (1.0 mL), dried under vacuum, and reused in the next cycles. The study revealed that the obtained yields of the product, **3k** were 98, 98, 97, 97, 96, 97, and 98% for the first, second, third, fourth, fifth, sixth, and seventh cycle, respectively. Catalyst reusability tests were then conducted for the synthesis of compound **7a** using benzaldehyde (**2a**), ethyl acetoacetate (**4**), and urea (**5**) under USI for 15 min and for **11e** using 4-nitrobenzaldehyde (**2l**), malononitrile (**8**), and 2-mercaptopyridine (**9**) under USI for 32 min by following the same procedure as adopted for **3k**. The yields obtained for the compounds were 97, 97, 97, 96, 97, 97, and 97% for **7a** as well as 96, 96, 96, 97, 97, 97, and 98% for **11e** for the first, second, third, fourth, fifth, sixth, and seventh cycle, respectively. From this study, it was noticed that the catalyst could successfully be reused (at least) 7 times in the synthesis of the compounds **3k**, **7a**, and **11e** without a significant loss of the catalytic activity.

Effect of ultrasonication on the structure of the catalyst

The recovered catalyst after the 7th cycle of each synthesis was characterized by XRD to study the structural changes due to ultrasonication. As can be seen in Figure 8, the diffraction peak positions of the catalyst recovered after the synthesis of the compounds **3k**, **7a**, and **11e** (Figure 8b–d), respectively, remained the same as compared to the fresh catalyst (Figure 8a). It was also noticed that the broadening in the XRD pattern of the recovered catalyst had increased with an increase

Table 10: Green chemistry metrics for the synthesis of 2-amino-4-(hetero)aryl-3,5-dicarbonitrile-6-sulfanylpyridines **11**.

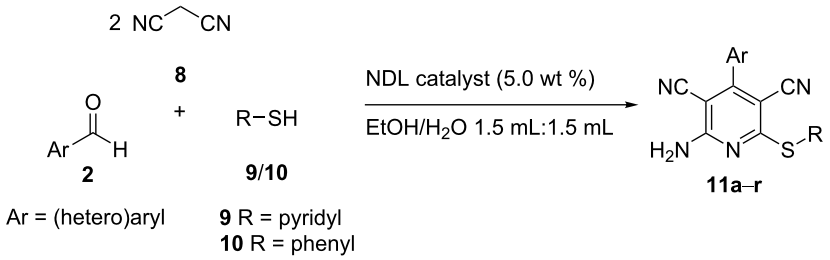

entry	reactants		product	AE (%)	E-factor[a]	PMI[b]	Curzon's RME[c] (%)	gRME[d] (%)
	Ar	R						
1	phenyl: **2a**	pyridyl: **9**	**11a**	94	36.054	37.054	90	2.7
2	4-methoxyphenyl: **2e**	pyridyl: **9**	**11b**	95	33.026.	34.026	91	2.9
3	3,4,5-trimethoxyphenyl: **2g**	pyridyl: **9**	**11c**	95	29.647	30.647	87	3.3
4	3-hydroxyphenyl: **2r**	pyridyl: **9**	**11d**	95	35.188	36.188	89	2.8
5	4-nitrophenyl: **2l**	pyridyl: **9**	**11e**	95	31.741	32.741	91	3.1
6	4-fluorophenyl: **2m**	pyridyl: **9**	**11f**	95	34.356	35.356	90	2.8
7	4-bromophenyl: **2o**	pyridyl: **9**	**11g**	95	29.698	30.698	89	3.3
8	3,4-difluorophenyl: **2t**	pyridyl: **9**	**11h**	95	34.699	35.699	86	2.8
9	pyridyl: **2u**	pyridyl: **9**	**11i**	94	37.143	38.143	87	2.6
10	Phenyl: **2a**	phenyl: **10**	**11j**	94	35.474	36.474	92	2.7
11	4-methylphenyl: **2b**	phenyl: **10**	**11k**	95	33.991	34.991	93	2.9
12	4-methoxyphenyl: **2e**	phenyl: **10**	**11l**	95	32.827	33.827	92	3.0
13	3,4,5-trimethoxyphenyl: **2g**	phenyl: **10**	**11m**	95	29.020	30.020	89	3.3
14	4-nitrophenyl: **2l**	phenyl: **10**	**11n**	95	32.021	33.021	90	3.0
15	4-fluorophenyl: **2m**	phenyl: **10**	**11o**	95	34.319	35.319	91	2.8
16	4-chlorophenyl: **2n**	phenyl: **10**	**11p**	95	32.744	33.744	91	3.0
17	3-bromophenyl: **2s**	phenyl: **10**	**11q**	95	29.775	30.775	89	3.2
18	pyridyl: **2u**	phenyl: **10**	**11r**	94	36.893	37.893	88	2.6

[a]E-factor = ^{m}inputs[f] – mass of the target product (^{m}**11**) – mass of the recovered materials/^{m}**11**. [b]PMI = (^{m}inputs – mass of the recovered materials)/^{m}**11** or 1 + E-factor. [c]Curzon's RME = ^{m}**11**/ ^{m}**2** + ^{m}**8** + ^{m}**9**/**10** or yield × AE × 1/SF; SF = 1. [d]gRME = 100·(^{m}**11**/(^{m}inputs – mass of the recovered materials)) or 100·(1/(1 + E-factor)). ^{em}inputs = ^{m}**2** + ^{m}**8** + ^{m}**9**/**10** + ^{m}S + ^{m}C + ^{m}WPM + ^{m}PM.

of the ultrasonication time. This clearly indicated that the amorphization of the recovered catalyst was enhanced by increasing the ultrasonication time.

Conclusion

An environmentally benign NDL catalyst was characterized and utilized as a heterogeneous catalyst for the synthesis of 2-aryl-1-arylmethyl-1*H*-benzo[*d*]imidazoles, dihydropyrimidinones/-thiones, and 2-amino-4-(hetero)aryl-3,5-dicarbonitrile-6-sulfanylpyridines in a mixture of ethanol and H_2O 1:1 under ultrasound irradiation. Notable advantages of this methodology include the clean reaction profile, broad substrate scope, simplicity of the process and handling, low catalyst loading, and the easy and quick isolation of the products in good to excellent yield. Besides, the products obtained were in an adequate purity without the need for chromatographic separation, and the catalyst was reused 7 times without a significant loss of the catalytic activity. Hence, the catalyst is a greener alternative for the synthesis of 1,2-disubstituted benzimidazoles, dihydropyrimidinones/-thiones, and highly substituted pyridines when compared to the existing reported catalysts. Further, the expansion of the catalyst scope and the generality for the synthesis of other privileged nitrogen- and sulfur-based heterocycles is under progress in our laboratory.

Experimental

See Supporting Information File 1 for full experimental data of compounds **3**, **7**, and **11**.

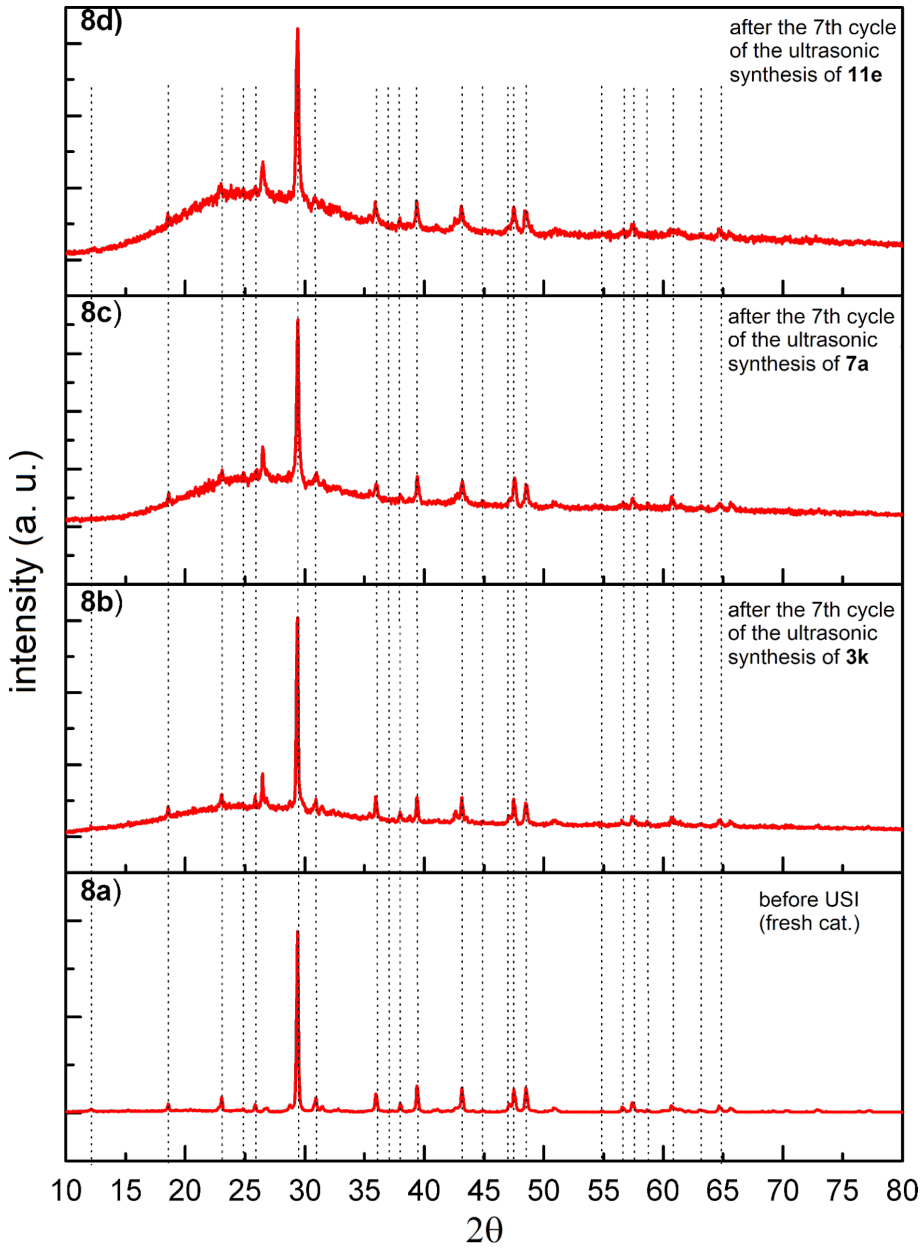

Figure 8: XRD pattern of a) the fresh NDL catalyst; b) the recovered NDL catalyst after the 7th cycle of the ultrasonic synthesis of **3k**; c) the recovered NDL catalyst after the 7th cycle of the ultrasonic synthesis of **7a**; and d) the recovered NDL catalyst after the 7th cycle of the ultrasonic synthesis of **11e**.

Supporting Information

Supporting Information File 1

Experimental procedures, characterization data, and copies of the ^{1}H and ^{13}C NMR, mass, and HRMS spectra of **3**, **7**, and **11**.
[https://www.beilstein-journals.org/bjoc/content/supplementary/1860-5397-16-156-S1.pdf]

Acknowledgements

The authors thank Dr. R. V. J. Kashyap, Dept. of English, Yogi Vemana University, for critical reading of the manuscript to ensure linguistic correctness.

Funding

The authors gratefully acknowledge the financial support for this work from the Department of Atomic Energy Board of Research in Nuclear Sciences (Bhabha Atomic Research Centre), Mumbai, Government of India, through a major

research project (No. 2011/37C/52/BRNS/2264) and the Council of Scientific and Industrial Research (CSIR), New Delhi, Government of India, under a major research project (No. 01 (2391)/10/EMR-II).

ORCID® iDs

Lakshmi Reddy Sanapareddy - https://orcid.org/0000-0001-9475-5516
Chinna Gangi Reddy Nallagondu - https://orcid.org/0000-0003-2088-802X

Preprint

A non-peer-reviewed version of this article has been previously published as a preprint doi:10.3762/bxiv.2020.39.v1

References

1. Joule, J. A.; Mills, K. *Heterocyclic Chemistry,* 4th ed.; Blackwell: Oxford, U.K., 2000.
2. Katritzky, A. R.; Ramsden, C. A.; Scriven, E. F. V.; Taylor, R. J. K., Eds. *Comprehensive Heterocyclic Chemistry III;* Elsevier: Oxford, U.K., 2008; Vol. 7.
3. Bull, J. A.; Mousseau, J. J.; Pelletier, G.; Charette, A. B. *Chem. Rev.* **2012,** *112,* 2642–2713. doi:10.1021/cr200251d
And references therein.
4. Nagarajaiah, H.; Mukhopadhyay, A.; Moorthy, J. N. *Tetrahedron Lett.* **2016,** *57,* 5135–5149. doi:10.1016/j.tetlet.2016.09.047
5. Suresh; Sandhu, J. S. *ARKIVOC* **2012,** No. i, 66–133. doi:10.3998/ark.5550190.0013.103
6. Perrier, V.; Wallace, A. C.; Kaneko, K.; Safar, J.; Prusiner, S. B.; Cohen, F. E. *Proc. Natl. Acad. Sci. U. S. A.* **2000,** *97,* 6073–6078. doi:10.1073/pnas.97.11.6073
7. Fredholm, B. B.; Ijzerman, A. P.; Jacobson, K. A.; Klotz, K.-N.; Linden, J. *Pharmacol. Rev.* **2001,** *53,* 527–552.
8. Nguyen, T. B.; Ermolenko, L.; Al-Mourabit, A. *J. Am. Chem. Soc.* **2013,** *135,* 118–121. doi:10.1021/ja311780a
9. Vitaku, E.; Smith, D. T.; Njardarson, J. T. *J. Med. Chem.* **2014,** *57,* 10257–10274. doi:10.1021/jm501100b
10. Preston, P. N. *Chem. Rev.* **1974,** *74,* 279–314. doi:10.1021/cr60289a001
11. Scott, L. J.; Dunn, C. J.; Mallarkey, G.; Sharpe, M. *Drugs* **2002,** *62,* 1503–1538. doi:10.2165/00003495-200262100-00006
12. Carcanague, D.; Shue, Y.-K.; Wuonola, M. A.; Uria-Nickelsen, M.; Joubran, C.; Abedi, J. K.; Jones, J.; Kühler, T. C. *J. Med. Chem.* **2002,** *45,* 4300–4309. doi:10.1021/jm020868v
13. Boiani, M.; Gonzalez, M. *Mini-Rev. Med. Chem.* **2005,** *5,* 409–424. doi:10.2174/1389557053544047
And references therein.
14. Shah, D. I.; Sharma, M.; Bansal, Y.; Bansal, G.; Singh, M. *Eur. J. Med. Chem.* **2008,** *43,* 1808–1812. doi:10.1016/j.ejmech.2007.11.008
15. Zhu, G.-D.; Gandhi, V. B.; Gong, J.; Thomas, S.; Luo, Y.; Liu, X.; Shi, Y.; Klinghofer, V.; Johnson, E. F.; Frost, D.; Donawho, C.; Jarvis, K.; Bouska, J.; Marsh, K. C.; Rosenberg, S. H.; Giranda, V. L.; Penning, T. D. *Bioorg. Med. Chem. Lett.* **2008,** *18,* 3955–3958. doi:10.1016/j.bmcl.2008.06.023
16. Ogino, Y.; Ohtake, N.; Nagae, Y.; Matsuda, K.; Moriya, M.; Suga, T.; Ishikawa, M.; Kanesaka, M.; Mitobe, Y.; Ito, J.; Kanno, T.; Ishihara, A.; Iwaasa, H.; Ohe, T.; Kanatani, A.; Fukami, T. *Bioorg. Med. Chem. Lett.* **2008,** *18,* 5010–5014. doi:10.1016/j.bmcl.2008.08.018
17. Molander, G. A.; Ajayi, K. *Org. Lett.* **2012,** *14,* 4242–4245. doi:10.1021/ol301956p
18. Asensio, J. A.; Gómez-Romero, P. *Fuel Cells* **2005,** *5,* 336–343. doi:10.1002/fuce.200400081
19. Schwartz, G.; Fehse, K.; Pfeiffer, M.; Walzer, K.; Leo, K. *Appl. Phys. Lett.* **2006,** *89,* 083509. doi:10.1063/1.2338588
20. Mariappan, G.; Hazarika, R.; Alam, F.; Karki, R.; Patangia, U.; Nath, S. *Arabian J. Chem.* **2015,** *8,* 715–719. doi:10.1016/j.arabjc.2011.11.008
And referenes therein.
21. Salahuddin; Shaharyar, M.; Mazumder, A.; Ahsan, M. J. *Arabian J. Chem.* **2014,** *7,* 418–424. doi:10.1016/j.arabjc.2013.02.001
And references therein.
22. Ravi, V.; Ramu, E.; Vijay, K.; Srinivas Rao, A. *Chem. Pharm. Bull.* **2007,** *55,* 1254–1257. doi:10.1248/cpb.55.1254
23. Wan, J.-P.; Gan, S.-F.; Wu, J.-M.; Pan, Y. *Green Chem.* **2009,** *11,* 1633–1637. doi:10.1039/b914286j
24. Sharma, S. D.; Konwar, D. *Synth. Commun.* **2009,** *39,* 980–991. doi:10.1080/00397910802448440
25. Reddy, L. S.; Reddy, N. C. G.; Reddy, T. R.; Lingappa, Y.; Mohan, R. B. *J. Korean Chem. Soc.* **2011,** *55,* 304–307. doi:10.5012/jkcs.2011.55.2.304
26. Chebolu, R.; Kommi, D. N.; Kumar, D.; Bollineni, N.; Chakraborti, A. K. *J. Org. Chem.* **2012,** *77,* 10158–10167. doi:10.1021/jo301793z
27. Zhang, L.-J.; Xia, J.; Zhou, Y.-Q.; Wang, H.; Wang, S.-W. *Synth. Commun.* **2012,** *42,* 328–336. doi:10.1080/00397911.2010.524337
And references therein.
28. Kumar, D.; Kommi, D. N.; Chebolu, R.; Garg, S. K.; Kumar, R.; Chakraborti, A. K. *RSC Adv.* **2013,** *3,* 91–98. doi:10.1039/c2ra21994h
29. Senthilkumar, S.; Kumarraja, M. *Tetrahedron Lett.* **2014,** *55,* 1971–1974. doi:10.1016/j.tetlet.2014.01.140
And references therein.
30. Herrera Cano, N.; Uranga, J. G.; Nardi, M.; Procopio, A.; Wunderlin, D. A.; Santiago, A. N. *Beilstein J. Org. Chem.* **2016,** *12,* 2410–2419. doi:10.3762/bjoc.12.235
And references therein.
31. Costanzo, P.; Nardi, M.; Oliverio, M. *Eur. J. Org. Chem.* **2020,** 3954–3964. doi:10.1002/ejoc.201901923
And references therein.
32. Berlinck, R. G. S.; Burtoloso, A. C. B.; Kossuga, M. H. *Nat. Prod. Rep.* **2008,** *25,* 919–954. doi:10.1039/b507874c
33. Hu, E. H.; Sidler, D. R.; Dolling, U.-H. *J. Org. Chem.* **1998,** *63,* 3454–3457. doi:10.1021/jo970846u
34. Sakata, K.-I.; Someya, M.; Matsumoto, Y.; Tauchi, H.; Kai, M.; Toyota, M.; Takagi, M.; Hareyama, M.; Fukushima, M. *Cancer Sci.* **2011,** *102,* 1712–1716. doi:10.1111/j.1349-7006.2011.02004.x
35. Ramesh, B.; Bhalgat, C. M. *Eur. J. Med. Chem.* **2011,** *46,* 1882–1891. doi:10.1016/j.ejmech.2011.02.052
36. Kaira, K.; Serizawa, M.; Koh, Y.; Miura, S.; Kaira, R.; Abe, M.; Nakagawa, K.; Ohde, Y.; Okumura, T.; Murakami, H.; Tsuya, A.; Nakamura, Y.; Naito, T.; Takahashi, T.; Kondo, H.; Nakajima, T.; Endo, M.; Yamamoto, N. *Lung Cancer* **2011,** *74,* 419–425. doi:10.1016/j.lungcan.2011.04.001
37. Schroeder, P. E.; Hasinoff, B. B. *Drug Metab. Dispos.* **2005,** *33,* 1367–1372. doi:10.1124/dmd.105.005546
38. Ma, Y.; Qian, C.; Wang, L.; Yang, M. *J. Org. Chem.* **2000,** *65,* 3864–3868. doi:10.1021/jo9919052
39. Fu, N.-Y.; Yuan, Y.-F.; Cao, Z.; Wang, S.-W.; Wang, J.-T.; Peppe, C. *Tetrahedron* **2002,** *58,* 4801–4807. doi:10.1016/s0040-4020(02)00455-6

40. Rodríguez-Domínguez, J. C.; Bernardi, D.; Kirsch, G. *Tetrahedron Lett.* **2007,** *48,* 5777–5780. doi:10.1016/j.tetlet.2007.06.104
41. Ahmed, N.; van Lier, J. E. *Tetrahedron Lett.* **2007,** *48,* 5407–5409. doi:10.1016/j.tetlet.2007.06.005
42. Chen, X.-H.; Xu, X.-Y.; Liu, H.; Cun, L.-F.; Gong, L.-Z. *J. Am. Chem. Soc.* **2006,** *128,* 14802–14803. doi:10.1021/ja065267y
43. Ryabukhin, S. V.; Plaskon, A. S.; Ostapchuk, E. N.; Volochnyuk, D. M.; Shishkin, O. V.; Shivanyuk, A. N.; Tolmachev, A. A. *Org. Lett.* **2007,** *9,* 4215–4218. doi:10.1021/ol701782v
44. Li, N.; Chen, X.-H.; Song, J.; Luo, S.-W.; Fan, W.; Gong, L.-Z. *J. Am. Chem. Soc.* **2009,** *131,* 15301–15310. doi:10.1021/ja905320q
45. Guggilapu, S. D.; Prajapati, S. K.; Nagarsenkar, A.; Lalita, G.; Vegi, G. M. N.; Babu, B. N. *New J. Chem.* **2016,** *40,* 838–843. doi:10.1039/c5nj02444g
And references therein.
46. Barbero, M.; Cadamuro, S.; Dughera, S. *Green Chem.* **2017,** *19,* 1529–1535. doi:10.1039/c6gc03274e
And references therein.
47. Oliverio, M.; Costanzo, P.; Nardi, M.; Rivalta, I.; Procopio, A. *ACS Sustainable Chem. Eng.* **2014,** *2,* 1228–1233. doi:10.1021/sc5000682
48. Ranu, B. C.; Hajra, A.; Jana, U. *J. Org. Chem.* **2000,** *65,* 6270–6272. doi:10.1021/jo000711f
49. Lu, J.; Bai, Y. *Synthesis* **2002,** 466–470. doi:10.1055/s-2002-20956
50. Gangadasu, B.; Palaniappan, S.; Rao, V. J. *Synlett* **2004,** 1285–1287. doi:10.1055/s-2004-822925
51. Russowsky, D.; Lopes, F. A.; da Silva, V. S. S.; Canto, K. F. S.; Montes D'Oca, M. G.; Godoi, M. N. *J. Braz. Chem. Soc.* **2004,** *15,* 165–169. doi:10.1590/s0103-50532004000200002
52. Tu, S.; Fang, F.; Zhu, S.; Li, T.; Zhang, X.; Zhuang, Q. *Synlett* **2004,** 537–539. doi:10.1055/s-2004-815419
53. Fazaeli, R.; Tangestaninejad, S.; Aliyan, H.; Moghadam, M. *Appl. Catal., A* **2006,** *309,* 44–51. doi:10.1016/j.apcata.2006.04.043
54. Ahmed, B.; Khan, R. A.; Habibullah; Keshari, M. *Tetrahedron Lett.* **2009,** *50,* 2889–2892. doi:10.1016/j.tetlet.2009.03.177
55. Phukan, M.; Kalita, M. K.; Borah, R. *Green Chem. Lett. Rev.* **2010,** *3,* 329–334. doi:10.1080/17518253.2010.487841
56. Zhang, X.; Gu, X.; Gao, Y.; Nie, S.; Lu, H. *Appl. Organomet. Chem.* **2017,** *31,* e3590. doi:10.1002/aoc.3590
And references therein.
57. Chitra, S.; Pandiarajan, K. *Tetrahedron Lett.* **2009,** *50,* 2222–2224. doi:10.1016/j.tetlet.2009.02.162
58. Han, B.; Han, R.-F.; Ren, Y.-W.; Duan, X.-Y.; Xu, Y.-C.; Zhang, W. *Tetrahedron* **2011,** *67,* 5615–5620. doi:10.1016/j.tet.2011.05.105
59. Shen, Z.-L.; Xu, X.-P.; Ji, S.-J. *J. Org. Chem.* **2010,** *75,* 1162–1167. doi:10.1021/jo902394y
60. Sheik Mansoor, S.; Syed Shafi, S.; Zaheer Ahmed, S. *Arabian J. Chem.* **2016,** *9,* S846–S851. doi:10.1016/j.arabjc.2011.09.018
61. Pandey, J.; Anand, N.; Tripathi, R. P. *Tetrahedron* **2009,** *65,* 9350–9356. doi:10.1016/j.tet.2009.09.002
62. Cocco, M. T.; Congiu, C.; Lilliu, V.; Onnis, V. *Eur. J. Med. Chem.* **2005,** *40,* 1365–1372. doi:10.1016/j.ejmech.2005.07.005
63. May, B. C. H.; Zorn, J. A.; Witkop, J.; Sherrill, J.; Wallace, A. C.; Legname, G.; Prusiner, S. B.; Cohen, F. E. *J. Med. Chem.* **2007,** *50,* 65–73. doi:10.1021/jm061045z
64. Reddy, T. R. K.; Mutter, R.; Heal, W.; Guo, K.; Gillet, V. J.; Pratt, S.; Chen, B. *J. Med. Chem.* **2006,** *49,* 607–615. doi:10.1021/jm050610f
65. Evdokimov, N. M.; Magedov, I. V.; Kireev, A. S.; Kornienko, A. *Org. Lett.* **2006,** *8,* 899–902. doi:10.1021/ol052994+
66. Evdokimov, N. M.; Kireev, A. S.; Yakovenko, A. A.; Antipin, M. Y.; Magedov, I. V.; Kornienko, A. *J. Org. Chem.* **2007,** *72,* 3443–3453. doi:10.1021/jo070114u
67. Ranu, B. C.; Jana, R.; Sowmiah, S. *J. Org. Chem.* **2007,** *72,* 3152–3154. doi:10.1021/jo070015g
68. Mamgain, R.; Singh, R.; Rawat, D. S. *J. Heterocycl. Chem.* **2009,** *46,* 69–73. doi:10.1002/jhet.32
69. Guo, K.; Thompson, M. J.; Chen, B. *J. Org. Chem.* **2009,** *74,* 6999–7006. doi:10.1021/jo901232b
70. Banerjee, S.; Sereda, G. *Tetrahedron Lett.* **2009,** *50,* 6959–6962. doi:10.1016/j.tetlet.2009.09.137
71. Shinde, P. V.; Sonar, S. S.; Shingate, B. B.; Shingare, M. S. *Tetrahedron Lett.* **2010,** *51,* 1309–1312. doi:10.1016/j.tetlet.2009.12.146
72. Srinivasula Reddy, L.; Ram Reddy, T.; Mohan, R. B.; Mahesh, A.; Lingappa, Y.; Gangi Reddy, N. C. *Chem. Pharm. Bull.* **2013,** *61,* 1114–1120. doi:10.1248/cpb.c13-00412
73. Tamaddon, F.; Tayefi, M.; Hosseini, E.; Zare, E. *J. Mol. Catal. A: Chem.* **2013,** *366,* 36–42. doi:10.1016/j.molcata.2012.08.027
74. Correia, L. M.; de Sousa Campelo, N.; Novaes, D. S.; Cavalcante, C. L., Jr.; Cecilia, J. A.; Rodríguez-Castellón, E.; Vieira, R. S. *Chem. Eng. J.* **2015,** *269,* 35–43. doi:10.1016/j.cej.2015.01.097
75. Vogel, A. I. *Quantitative inorganic analysis;* Longmans: London, U.K., 1951; p 582.
76. Gunasekaran, S.; Anbalagan, G.; Pandi, S. *J. Raman Spectrosc.* **2006,** *37,* 892–899. doi:10.1002/jrs.1518
77. Xu, B.; Poduska, K. M. *Phys. Chem. Chem. Phys.* **2014,** *16,* 17634–17639. doi:10.1039/c4cp01772b
78. Shawky, A.; El-Sheikh, S. M.; Rashed, M. N.; Abdo, S. M.; El-Dosoqy, T. I. *J. Environ. Chem. Eng.* **2019,** *7,* 103174. doi:10.1016/j.jece.2019.103174
79. Darezereshki, E.; Ranjbar, M.; Bakhtiari, F. *J. Alloys Compd.* **2010,** *502,* 257–260. doi:10.1016/j.jallcom.2010.04.163
80. Shao, M.; Ning, F.; Zhao, J.; Wei, M.; Evans, D. G.; Duan, X. *J. Am. Chem. Soc.* **2012,** *134,* 1071–1077. doi:10.1021/ja2086323
81. White, W. B.; Karr, C., Jr., Eds. *Infrared and Raman Spectroscopy of Lunar and Terrestrial Minerals;* Academic Press: New York, NY, USA, 1975.
82. Ramasesha, K.; De Marco, L.; Mandal, A.; Tokmakoff, A. *Nat. Chem.* **2013,** *5,* 935–940. doi:10.1038/nchem.1757
83. Shalaby, N. H.; Elsalamony, R. A.; El Naggar, A. M. A. *New J. Chem.* **2018,** *42,* 9177–9186. doi:10.1039/c8nj01479e
84. Lin, Y.-F.; Chen, H.-W.; Chang, C.-C.; Hung, W.-C.; Chiou, C.-S. *J. Chem. Technol. Biotechnol.* **2011,** *86,* 1449–1456. doi:10.1002/jctb.2665
85. Yadav, A. K.; Singh, P. *RSC Adv.* **2015,** *5,* 67583–67609. doi:10.1039/c5ra13043c
And references therein.
86. Debure, M.; Andreazza, P.; Canizarès, A.; Grangeon, S.; Lerouge, C.; Mack, P.; Madé, B.; Simon, P.; Veron, E.; Warmont, F.; Vayer, M. *ACS Earth Space Chem.* **2017,** *1,* 442–454. doi:10.1021/acsearthspacechem.7b00073
87. Makal, A.; Schilf, W.; Kamieński, B.; Szady-Chelmieniecka, A.; Grech, E.; Woźniak, K. *Dalton Trans.* **2011,** *40,* 421–430. doi:10.1039/c0dt00298d
88. Andraos, J.; Hent, A. *J. Chem. Educ.* **2015,** *92,* 1820–1830. doi:10.1021/acs.jchemed.5b00058

89. Dicks, A. P.; Hent, A. *Green Chemistry Metrics;* Springer International Publishing: Cham, Switzerland, 2015. doi:10.1007/978-3-319-10500-0

License and Terms

BEILSTEIN JOURNAL OF ORGANIC CHEMISTRY

Regiodivergent synthesis of functionalized pyrimidines and imidazoles through phenacyl azides in deep eutectic solvents

Paola Vitale*[1], Luciana Cicco[1], Ilaria Cellamare[1], Filippo M. Perna[1], Antonio Salomone[2,3] and Vito Capriati*[1]

Full Research Paper

Open Access

Address:
[1]Dipartimento di Farmacia-Scienze del Farmaco, Università di Bari "Aldo Moro", Consorzio C.I.N.M.P.I.S., Via E. Orabona 4, I-70125 Bari, Italy, [2]Dipartimento di Scienze e Tecnologie Biologiche ed Ambientali, Università del Salento, Prov.le Lecce-Monteroni, 73100 Lecce, Italy and [3]Dipartimento di Chimica, Università di Bari "Aldo Moro", Via E. Orabona 4, I-70125 Bari, Italy

Email:
Paola Vitale* - paola.vitale@uniba.it; Vito Capriati* - vito.capriati@uniba.it

* Corresponding author

Keywords:
deep eutectic solvents; imidazoles; phenacyl azides; phenacyl halides; pyrimidines

Beilstein J. Org. Chem. **2020,** *16,* 1915–1923.
doi:10.3762/bjoc.16.158

Received: 30 May 2020
Accepted: 20 July 2020
Published: 05 August 2020

This article is part of the thematic issue "Green chemistry II".

Guest Editor: L. Vaccaro

Abstract

We report that phenacyl azides are key compounds for a regiodivergent synthesis of valuable, functionalized imidazole (32–98% yield) and pyrimidine derivatives (45–88% yield), with a broad substrate scope, when using deep eutectic solvents [choline chloride (ChCl)/glycerol (1:2 mol/mol) and ChCl/urea (1:2 mol/mol)] as environmentally benign and non-innocent reaction media, by modulating the temperature (25 or 80 °C) in the presence or absence of bases (Et_3N).

Introduction

In a world with dwindling petroleum resources, the setting up of more and more sustainable routes for the preparation of heterocyclic compounds is an ongoing synthetic endeavor as these scaffolds are ubiquitous motifs in many biologically active compounds and pharmaceuticals. In this context, in the last decades, the so-called deep eutectic solvents (DESs) have received an increasing attention due to their biodegradability, high thermal stability, non-flammability, and low volatility. These are mixtures usually obtained from the combination of 2 or 3 safe, inexpensive and nature-inspired components able to engage in reciprocal hydrogen-bond interactions, and that form fluids at a specified mixing ratio at the desired temperature. Owing to the broad tunability of their physicochemical properties and the ability to act not only as solvents but also as catalysts and reagents, DESs have progressively replaced toxic and volatile organic solvents (VOCs) in countless heterocyclodehydration processes and multicomponent reactions (MCRs) [1-3].

As part of our ongoing research in DES chemistry, we reported recently on the preparation of valuable heterocycles by

(a) nucleophilic substitution (tetrahydrofuran derivatives) [4], (b) heterocyclodehydration reactions (2-aminoimidazoles, 2-pyrazinones, benzoxazines, thiophenes) [5-8], (c) carbon–sulfur bond-forming reactions [9], (d) directed *ortho*-metalation and nucleophilic acyl substitution strategies [10], (e) Pd-catalyzed aminocarbonylation of aryl iodides, Suzuki–Miyaura and Sonogashira cross-coupling reactions [11-13], (f) Cu-catalyzed C–N coupling reactions [14], and (g) heterogeneous "click" cycloaddition reactions [15] using DESs as environmentally responsible and non-innocent reaction media. Telescoped, one-pot transformations of phenacyl halides to symmetrical 2,5-disubstituted pyrazines (**A**), through phenacyl azides as intermediates, were also found to take place smoothly using such neoteric solvents (Scheme 1, path a) [16].

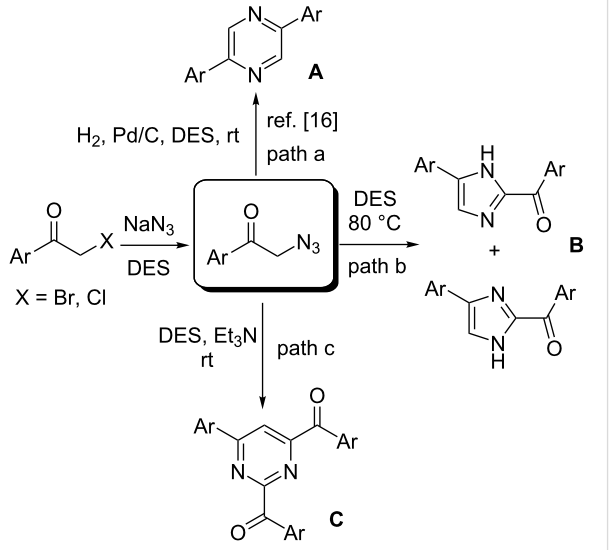

Scheme 1: One-pot synthesis of 2,5-diarylpyrazines (**A**) (path a) or 2-aroyl-(4 or 5)-aryl-(1*H*)-imidazoles (**B**) (path b), or 2,4-diaroyl-6-arylpyrimidines (**C**) (path c) in DES from phenacyl azides (rt = room temperature).

Among nitrogen-containing heterocyles, imidazoles and pyrimidines are important structural scaffolds commonly found in natural products [17,18], light-emitting devices [19,20], and pharmacologically active compounds as anticancer, anti-inflammatory, antitubercular, antihypertensive, antihistaminic, anti-obesity, antiviral, and other medicinal agents [21-27]. Herein, we wish to report that either 2-aroylimidazoles (**B**) (Scheme 1, path b) or 2,4-diaroylpyrimidines (**C**) (Scheme 1, path c) can regioselectively be prepared from the same phenacyl azide as starting material by properly selecting the nature of the eutectic mixture and the temperature, in the presence or absence of bases.

To the best of our knowledge, while there are a few reports for the synthesis of 2-aroylimidazoles (a) through the condensation of α-azido ketones in iPrOH in the presence of potassium ethylxanthate as a catalyst [28], (b) by exploiting the reaction of arylglyoxals with an excess amount of ammonium acetate in water [29], (c) by the cathodic reduction of 2-azido-1-phenylethanone in a DMF/$LiClO_4$ medium [30], (d) by radical chain reactions of α-azido ketones with tributyltin hydride [31], or (e) by a modified Radziszewski's synthesis when using phenylglyoxals, benzaldeydes, and ammonium acetate as ammonia source in acetic acid or methylene chloride or *N*,*N*-dimethylformamide as the solvent [32], there are no adequate studies covering the preparation of aroylpyrimidines. In 1995, Yamamoto et al. reported the direct introduction of acyl groups into pyrimidine rings by reacting trimethylstannyl derivatives with acylformyl chlorides in dry benzene under a N_2 stream [33].

Results and Discussion

During our studies on the synthesis of symmetrical pyrazines, we observed that phenacyl bromide (**1a**, 1.5 mmol) could be almost quantitatively converted into phenacyl azide (**2a**, 97% yield), within 4 h, when treated with NaN_3 (1.65 mmol) as the azide source in a choline chloride (ChCl)/glycerol (Gly) (1:2 mol/mol) eutectic mixture at room temperature (rt, 25 °C) (Scheme 2) [16]. By warming the mixture up to 50 °C, the yield of **2a** dropped to 89% after 1 h, and we noticed in the crude the appearance of an additional product, which was detected as a fluorescent spot on TLC, whose amount increased by increasing the temperature. After 4 h warming at 50 °C, we were able to isolate by column chromatography on silica gel a product which was characterized as 2-benzoyl-(4 or 5)-phenyl-(1*H*)-imidazole (**3a**/**3a'**, Scheme 2). This adduct was formed as a mixture of two tautomers (**3a** and **3a'**; **3a**/**3a'** ratio: 57:43, Supporting Information File 1) [28,29] in an overall 16% yield, the remaining being mainly **2a**, which was isolated in 75% yield (Scheme 2). We thus became interested in improving the yield of **3a**/**3a'**.

After careful evaluation of the reaction parameters (temperature and time) and the amount of NaN_3 used, we found that the treatment of phenacyl chloride (**1b**) with NaN_3 (1.5 equiv) in ChCl/Gly at 80 °C gave the best results, as it provided the adducts **3a**/**3a'** in an overall 88% yield after 12 h reaction time (Table 1, entries 1–4). Of note, imidazoles **3a**/**3a'** were found to precipitate directly from the aforementioned eutectic mixture during the reaction, and thus they could be isolated by simple decantation or centrifugation and washing with a few drops of EtOAc or Et_2O. This procedure left azide **2a** in solution. The latter could be quantified (10% yield) by simple dilution with an equal volume mixture of water and EtOAc, followed by the separation of the organic layer from water, and removal of the volatiles under reduced pressure.

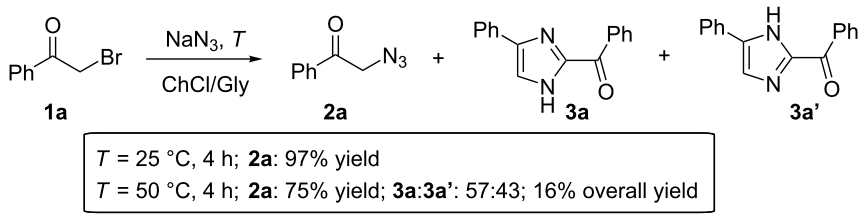

Scheme 2: Transformation of phenacyl bromide (**1a**) in ChCl/Gly into phenacyl azide (**2a**) and 2-benzoyl-(4 or 5)-phenyl-(1*H*)-imidazole (**3a** and **3a'**) depending on the temperature.

Table 1: Optimization of the reaction conditions for the synthesis of **3a**/**3a'**.[a]

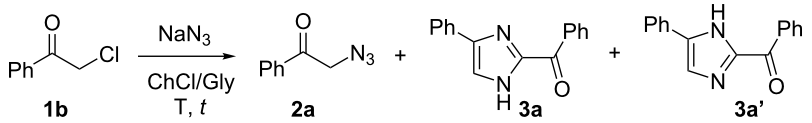

entry	*T* (°C)	*t* (h)	NaN_3 (equiv)	**2a** yield (%)[b]	**3a**/**3a'** yield (%)[b]
1	80	4	1.2	37	55
2	100	16	1.2	7	60[c]
3	80	16	0.9	68	32
4	80	12	1.5	10	88

[a]Reaction conditions: **1b** (0.5 mmol), ChCl/Gly (1.0 g); [b]yield refers to products isolated after column chromatography on silica gel; [c]15% of 2,4-dibenzoyl-6-phenylpyrimidine was also isolated (see main text and Table 2).

To examine the scope and limitation of this transformation, various functionalized phenacyl halides (**1c–i**) were tested as substrates. As can be seen from the results compiled in Scheme 3, the reaction is amenable to "neutral" (Me), electron-withdrawing (Cl, Br, CN) and electron-donating (MeO, OH) substituents as the desired imidazoles **3b**/**3b'–3h** were isolated in 78–98% yield. The presence of additional halogen groups such as chlorine and bromine in **3c**/**3c'** and **3d** allows further downstream diversification by cross-coupling reactions. A 4-fluoro-substituted phenacyl chloride as well as a bromomethyl 2-naphthyl ketone proved to be competent substrates as well, thus furnishing the corresponding imidazoles **3i**/**3i'** and **3j** in 67–87% yield. Conversely, a phenacyl halide decorated with an additional phenyl group at the *para*-position delivered the expected adduct **3k**/**3k'** in 32% yield even by prolonging the reaction time to 16 h, most probably because of the poor solubility in the eutectic mixture and/or the higher thermal stability towards the loss of N_2 (vide infra) of the corresponding phenacyl azide **2k** as it is formed. The latter was indeed isolated as the main product (68% yield, Scheme 3).

A plausible mechanism for the formation of the 2-aroylimidazoles **3**/**3'** is depicted in Scheme 4. A key intermediate may be the in situ generated α-imino ketone **5**. The latter is known to undergo dimerization to give **6** followed by dehydration. The two tautomers **3**/**3'** would most probably originate by two competitive pathways (a and b; Scheme 4) via a [1,5]-hydrogen shift [28,29]. Hydrogen-bond catalysis promoted by DES components may be playing an important role in favoring the loss of nitrogen under mild conditions from a putative azide tautomer **4**, the latter deriving from the corresponding α-phenacyl azide precursor **2** via an acid-catalyzed enolization process [34]. The pyrolysis of α-azido ketones in conventional VOCs (trichlorobenzene) is known to take place under harsh conditions, which are based on heating the mixture between 180 °C and 240 °C [35].

The investigation of the thermal stability of phenacyl azides **2** led to the fortuitous discovery of the competitive formation of a different heterocycle. Indeed, while phenacyl azide (**2a**) was stable per se in a ChCl/Gly mixture after stirring at rt for 12 h, a new fluorescent spot was detected on TLC plate in the presence of an excess of Et_3N (3 equiv). After column chromatography on silica gel, we were able to isolate a new product that was characterized as 2,4-dibenzoyl-6-phenylpyrimidine (**7a**, 55% yield) in addition to **3a**/**3a'** (26% yield), the remaining being starting material only (conversion: 81%, Table 2, entry 1). The employment of ChCl/urea (1:2 mol/mol) as the eutectic mix-

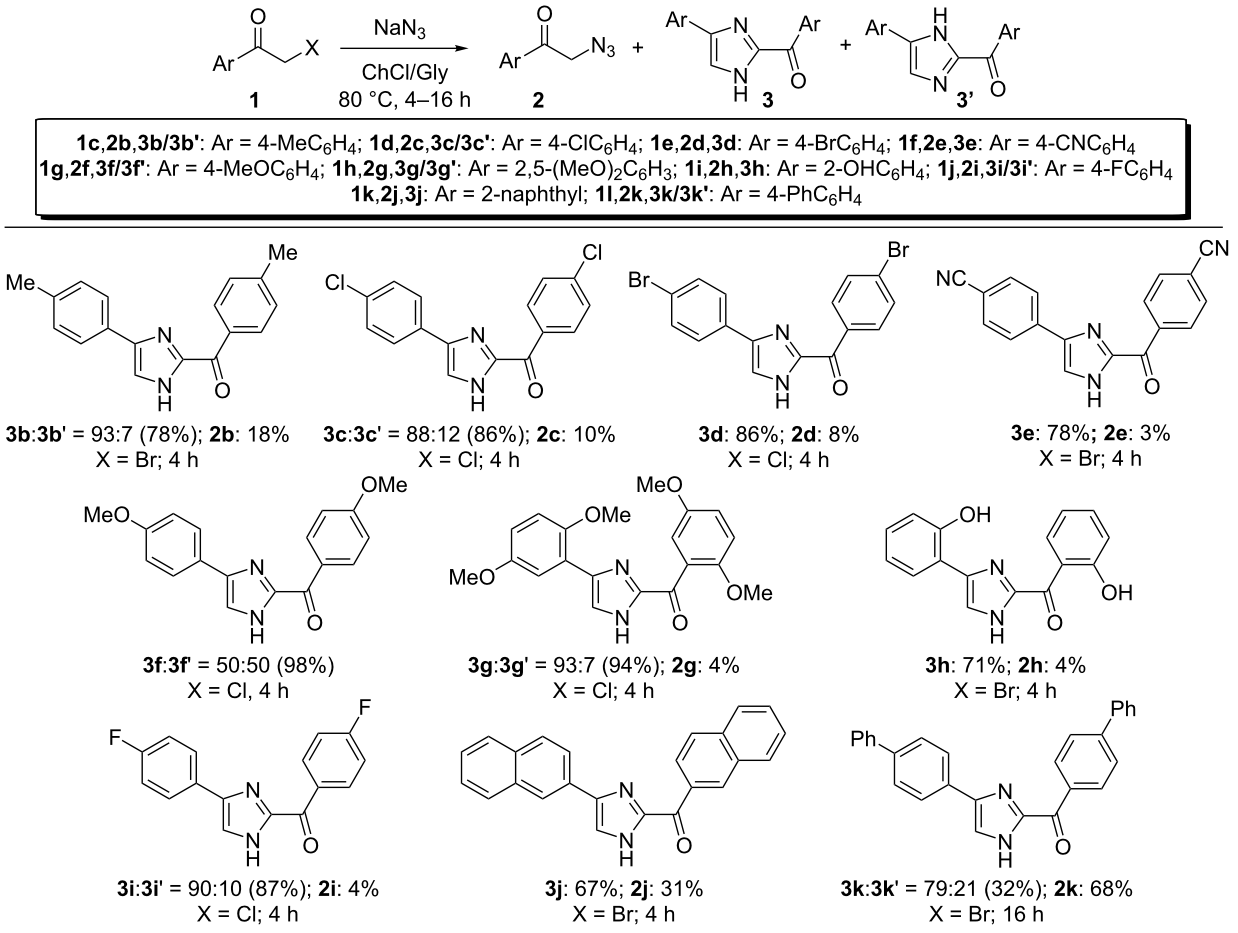

Scheme 3: Synthesis of 2-aroyl-(4 or 5)-aryl-(1*H*)-imidazoles **3**. Scope of the reaction. Typical conditions: **1** (0.5 mmol), NaN_3 (0.75 mmol), ChCl/Gly (1.0 g), 80 °C, 4–16 h; yield refers to products isolated after column chromatography on silica gel; only one tautomer has been depicted for simplicity; imidazoles **3c**/**3c'**, **3i**/**3i'**, **3j**, **3k**/**3k'** were found to precipitate as they formed, and were isolated by filtration/centrifugation and washing with a few drops of AcOEt or Et_2O; synthesis of imidazoles **3k**/**3k'**: 10% (w/w) EtOH was added to the eutectic mixture to improve the solubility of **2k**.

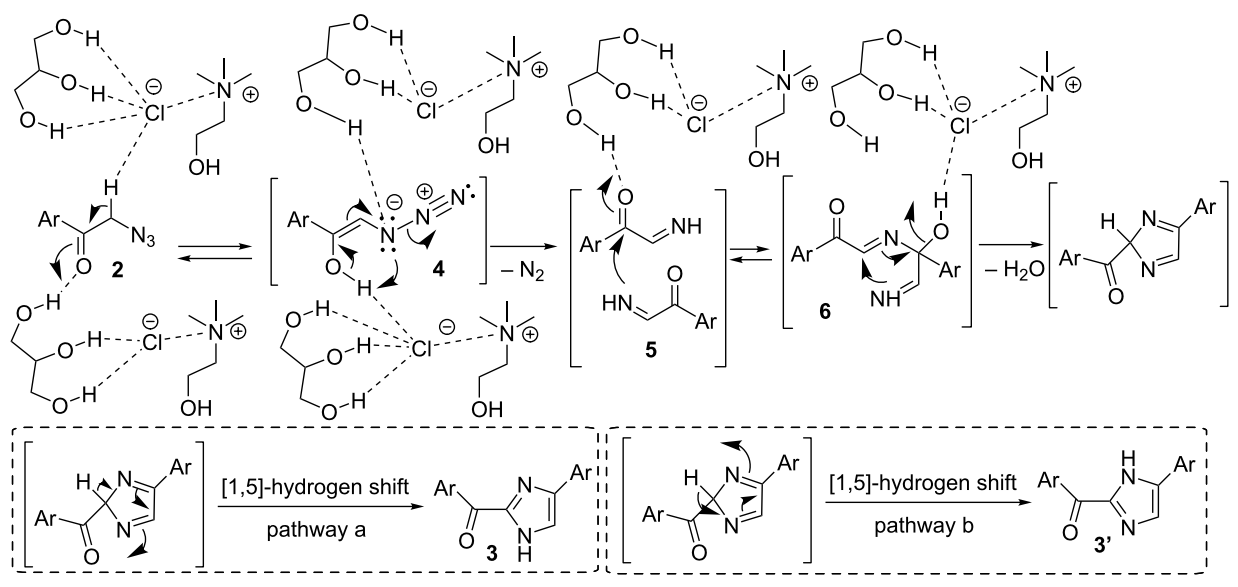

Scheme 4: Proposed mechanism for the formation of 2-aroyl-(4 or 5)-aryl-(1*H*)-imidazoles **3**/**3'** from α-phenacyl azides **2** in ChCl/Gly.

Table 2: Investigation of the reaction conditions in the synthesis of **7a**.[a]

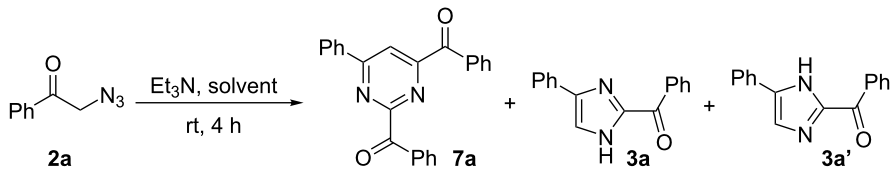

entry	solvent	**7a** yield (%)[b]	**3a**/**3a'** yield (%)[b]	conversion yield (%)
1	ChCl/Gly[c]	55	26	81
2	ChCl/urea[c]	57	43	full
3	ChCl/urea[d]	41	33	74
4	ChCl/urea[e]	37	25	62
5	ChCl/urea[f]	33	31	66
6	Gly[c]	52	37	89
7	Et_3N[c]	27	–	27

[a]Reaction conditions: **2a** (0.3 mmol), solvent (0.5 g); [b]yield refers to products isolated after column chromatography on silica gel; [c]Et_3N: 3 equiv; [d]Et_3N: 2 equiv; [e]Et_3N: 1 equiv; [f]K_2CO_3: 3 equiv.

ture provided **7a** in 57% yield and **3a**/**3a'** in 43% yield, but with full conversion (Table 2, entry 2). By lowering the equivalents of Et_3N up to 1, or alternatively using K_2CO_3 (3 equiv) as a base, in ChCl/urea, the yield of **7a** dropped down up to 33% and that of **3a**/**3a'** up to 25% (Table 2, entries 3–5). By changing the solvent to pure Gly, **7a** and **3a**/**3a'** now formed in 52 and 37% yield, respectively (Table 2, entry 6). When Et_3N (3 equiv) was alternatively used as the sole solvent, the formation of **7a** was suppressed dramatically (27% yield, Table 2, entry 7) [36]. This last result is consistent with a synergistic cooperation of the basic ChCl/urea eutectic mixture [37] with Et_3N in promoting the transformation at rt. α-Azido ketones are, indeed, known to be highly base sensitive and to undergo a base-promoted loss of nitrogen to form α-imino ketones upon protonation [38].

A plausible mechanism for the formation of pyrimidine derivative **7a** from **2a**, in competition with imidazoles **3a**/**3a'**, is depicted in Scheme 5.

The key intermediate **5a**, formed by elimination of nitrogen from the enol-azide **4a**, would undergo either dimerization to give **6a**, and then imidazoles **3a**/**3a'** after cyclization and dehydration (see Scheme 5), or trimerization to afford adduct **8a** further to an additional attack of **5a** to the internal imino group

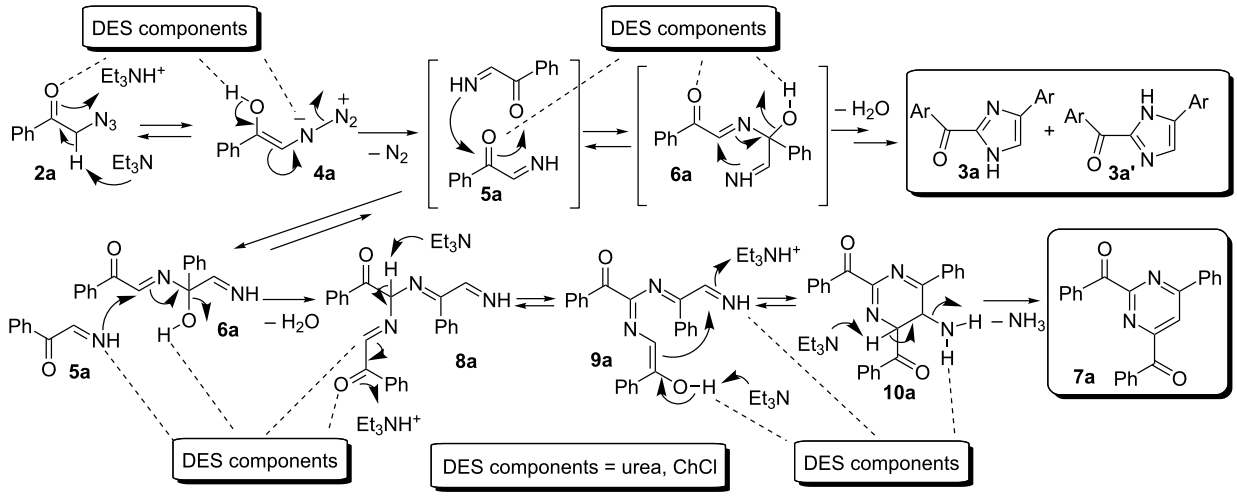

Scheme 5: Proposed mechanism for the formation of 2-benzoyl-(4 or 5)-phenyl-(1*H*)-imidazoles **3a**/**3a'** and 2,4-dibenzoyl-6-phenylpyrimidine (**7a**) from α-phenacyl azide (**2a**) in ChCl/urea in the presence of Et_3N.

of **6a** and dehydration. Consecutive tautomerization, followed by an intramolecular nucleophilic attack to the terminal imino group of **9a**, provides cyclized adduct **10a**, and finally pyrimidine derivative **7a** by aromatization/elimination of NH_3. To the best of our knowledge, this is the first one-pot synthesis of functionalized pyrimidines using phenacyl azides as the sole starting material [39]. Variation of the phenacyl azides was next investigated in the preparation of various pyrimidines **7** (Scheme 6).

The results shown in Scheme 6 demonstrate that this protocol allows the use of phenacyl azides as starting material also for the preparation of a variety of 2,4,6-trisubstituted pyrimidines. The cyclotrimerization of phenacyl azides containing an alkyl group (4-Me, **2b**), halides (4-Cl, 4-Br and 4-F, **2c**, **d**, and **2i**) or strong electron-withdrawing groups (2-CF_3, 4-CF_3, **2l**, **m**) occurs smoothly at rt generally within 4 h in a ChCl/urea eutectic mixture, thereby providing the desired pyrimidines **7b**–**h** in 45–88% yield. Variable amounts of difunctionalized imidazoles **3**/**3'** (20–40%), deriving from a dimerization process, also formed competitively in some cases under the aforementioned conditions. The latter, however, could be easily isolated by column chromatography. The presence of strong electron-donating groups like MeO was not tolerated. Indeed, phenacyl azides **2f**, and **2g** remained unreacted when stirred in ChCl/urea at rt even for 12 h.

Conclusion

In summary, we have shown that phenacyl halides can be straightforwardly converted, via phenacyl azides, into valuable 2-aroyl-(4 or 5)-aryl-(1*H*)-imidazoles when a solution in ChCl/Gly (1:2) is heated to 80 °C for 4–16 h in the presence of NaN_3 (1.5 equiv). In most cases, their isolation can be performed by a very gentle procedure: decantation/centrifugation as soon as they form from the above eutectic mixture. The reaction proceeds in very good yields (67–98%) when phenacyl azides are soluble in the eutectic mixture and is applicable to a range of substrates. Phenacyl azides, in turn, can also be competitively converted into 2,4-diaroyl-6-arylpyrimidines (45–88% yield) via an unprecedented cyclotrimerization reaction the key intermediate α-imino ketone undergoes when a solution in

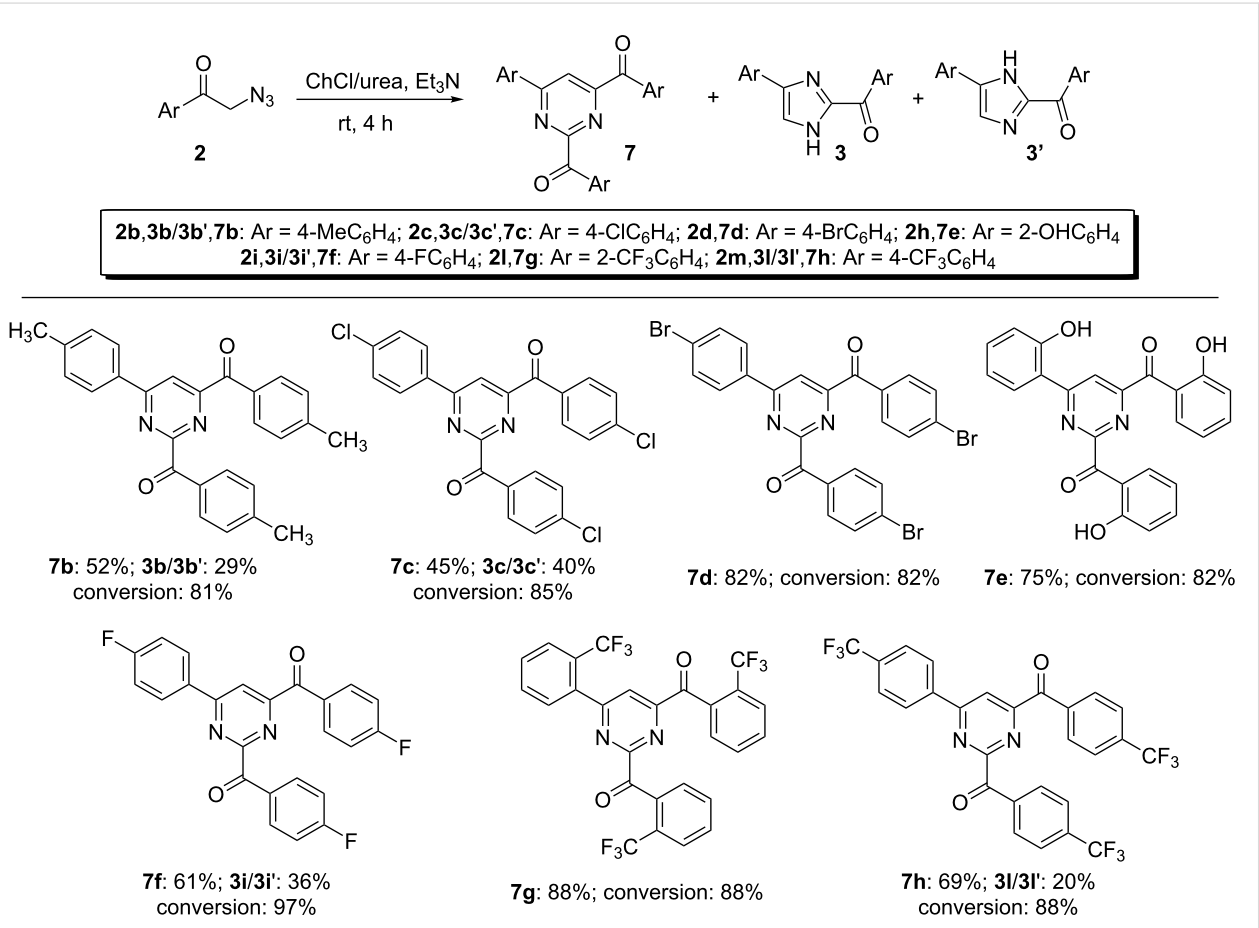

Scheme 6: Scope of the synthesis of 2,4-diaroyl-6-arylpyrimidines **7**. Typical conditions: **2** (0.3 mmol), Et_3N (0.9 mmol), ChCl/urea (0.5 g), rt, 4 h; yield refers to products isolated after column chromatography on silica gel; synthesis of pyrimidine derivatives **7b** and **7d**, reaction time: 12 h.

ChCl/urea is stirred at rt for 4 h in the presence of Et_3N (3 equiv) as a base. These cyclizations proved to be relatively sensitive to the electronic properties of the starting phenacyl azides as they did not take place in the presence of strong electron-donating groups like MeO. Studies to expand even more the scope and the selectivity of such DES-promoted heterocyclization reactions and to elucidate their mechanism are in progress.

Experimental

General methods

Deep eutectic solvents [choline chloride (ChCl)/glycerol (Gly) (1:2 mol/mol); choline chloride (ChCl)/urea (1:2 mol/mol)] were prepared by heating under stirring up to 80 °C for 10–15 min the corresponding individual components until a clear solution was obtained. ^{1}H NMR and ^{13}C NMR spectra were recorded on a Varian Mercury 300 or on a Bruker 400 or 600 MHz spectrometer and chemical shifts are reported in parts per million (δ); $CDCl_3$, $(CD_3)_2CO$ and $(CD_3)_2SO$ were used as solvents. GC–MS analyses were performed on a HP 6890 gas chromatograph, Series II by using a HP1 column (methyl siloxane; 30 m × 0.32 mm × 0.25 μm film thickness) equipped with a mass-selective detector operating at 70 eV. Analytical thin-layer chromatography (TLC) was carried out on pre-coated 0.25 mm thick plates of Kieselgel 60 F_{254}; visualization was accomplished by UV light (254 nm) or by spraying with a solution of 5% (w/v) ammonium molybdate and 0.2% (w/v) cerium(III) sulfate in 100 mL 17.6% (w/v) aq. sulfuric acid and heating to 473 K until blue spots appeared. Column chromatography was conducted by using silica gel 60 with a particle size distribution of 40–63 μm and 230–400 ASTM, using hexane/EtOAc mixtures as the eluent. High-resolution mass spectrometry (HRMS) analyses were performed using a Bruker microTOF QII mass spectrometer equipped with an electrospray ion source (ESI). NaN_3, 2-haloketones, and all other reagents, unless otherwise specified, were purchased from Sigma-Aldrich (Sigma-Aldrich, St. Louis, MO, USA), and used without any further purification.

Experimental procedures

General procedure for the synthesis of 2-azido ketones **2d**, **2e**, **2f**, **2k**, **2l** and **2m**

α-Haloketone **1** (1.5 mmol) and NaN_3 (107 mg, 1.65 mmol) were sequentially added to the ChCl/Gly (1:2 mol/mol, 2.0 g) eutectic mixture. The reaction mixture was stirred at 25 °C under air for 3–12 h until complete consumption of the starting material (monitored by thin-layer chromatography). Then, water was added, and the mixture was extracted with EtOAc (3 × 10 mL). The collected organic layers were dried using anhydrous Na_2SO_4, filtered, and the volatile evaporated under reduced pressure to afford the crude product, which was purified by column chromatography on silica gel (hexane/EtOAc 5:1–4:1) to afford the desired α-azido ketone **2**. Characterization data of the isolated 2-azido ketones are provided in Supporting Information File 1.

Synthesis of 2-benzoyl-4-phenyl-1*H*-imidazole (**3a**) and 2-benzoyl-5-phenyl-1*H*-imidazole (**3a'**). Typical procedure

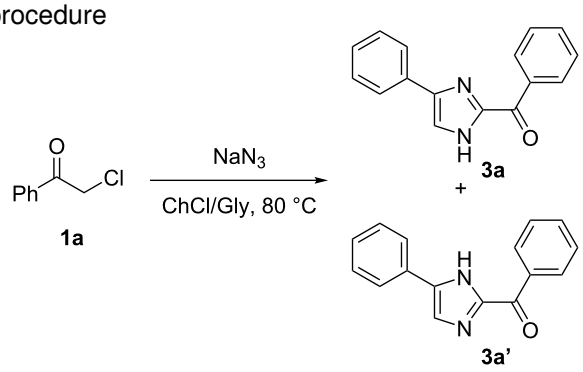

Sodium azide (0.75 mmol) was added to a solution of 2-chloroacetophenone (**1a**, 0.5 mmol) in ChCl/Gly (1:2 mol/mol, 1.0 g) under air and with vigorous stirring. The mixture was then warmed to 80 °C. After 12 h, 10 mL of water were added and the solid **3a** was recovered by decantation (or filtration) from the reaction mixture and washed with a few drops of EtOAc or Et_2O. The solution was extracted with EtOAc (3 × 10 mL). The combined organic phases were dried over anhydrous Na_2SO_4 and the solvent was concentrated in vacuo. The addition of Et_2O to the crude mixture allowed the further precipitation of **3a**, which was finally recovered in 88% yield. Characterization data of the isolated imidazoles are provided in Supporting Information File 1.

Synthesis of 2,4-dibenzoyl-6-phenylpyrimidine (**7a**). Typical procedure

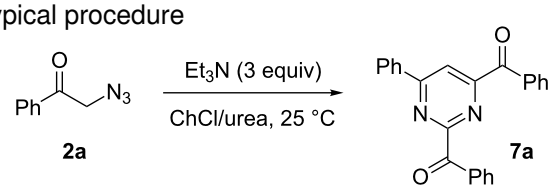

Et_3N (0.930 mmol, 0.130 mL) was added to a solution of 2-azidoacetophenone (**2a**, 0.31 mmol, 0.05 g) in ChCl/ urea (1:2 mol/mol, 0.5 g) eutectic mixture at 25 °C, under air and with vigorous stirring. The reaction was monitored by TLC (hexane/EtOAc 7:3). After 4 h, 5 mL of water were added and the reaction mixture was extracted with EtOAc (3 × 5 mL). The combined organic phases were dried over anhydrous Na_2SO_4 and the solvent was concentrated under reduced pressure. Purification by column chromatography on silica gel (hexane/EtOAc 9:1) provided pyrimidine **7a** in 57% yield. A mixture of

imidazoles **3a**/**3a'** (43% yield) was also isolated. Characterization data of the isolated pyrimidines are provided in Supporting Information File 1.

Supporting Information

Supporting Information File 1

Compound characterization data and NMR spectra.
[https://www.beilstein-journals.org/bjoc/content/supplementary/1860-5397-16-158-S1.pdf]

Acknowledgements

The authors are also indebted to Dr. Francesco Lavolpe, Dr. Walter Barella, Dr. Giuseppe Dilauro, and Dr. Francesco Messa for their contribution to the experimental work.

Funding

This work was carried out under the framework of the national PRIN project “Unlocking Sustainable Technologies Through Nature-inspired Solvents (NATUREChem) (grant number: 2017A5HXFC_002) financially supported by the University of Bari “A. Moro” (codes: SFARMA.RicercaLocale.Vitale Fondi Ateneo 17-18, PernaF.18 FondiAteneo15-16, VitaleP.18 FondiAteneo15-16), the University of Salento, the Interuniversity Consortium C.I.N.M.P.I.S., and the Ministero dell’Università e della Ricerca (MIUR-PRIN).

ORCID® iDs

Paola Vitale - https://orcid.org/0000-0001-8132-2893
Luciana Cicco - https://orcid.org/0000-0003-4126-3993
Filippo M. Perna - https://orcid.org/0000-0002-8735-8165
Antonio Salomone - https://orcid.org/0000-0002-3161-385X
Vito Capriati - https://orcid.org/0000-0003-4883-7128

References

1. Alonso, D. A.; Baeza, A.; Chinchilla, R.; Guillena, G.; Pastor, I. M.; Ramón, D. J. *Eur. J. Org. Chem.* **2016,** 612–632. doi:10.1002/ejoc.201501197
2. Ramón, D. J.; Guillena, G., Eds. *Deep Eutectic Solvents: Synthesis, Properties, and Applications;* Wiley-VCH: Weinheim, Germany, 2019. doi:10.1002/9783527818488
3. Perna, F. M.; Vitale, P.; Capriati, V. *Curr. Opin. Green Sustainable Chem.* **2020,** *21,* 27–33. doi:10.1016/j.cogsc.2019.09.004
4. Cicco, L.; Sblendorio, S.; Mansueto, R.; Perna, F. M.; Salomone, A.; Florio, S.; Capriati, V. *Chem. Sci.* **2016,** *7,* 1192–1199. doi:10.1039/c5sc03436a
5. Capua, M.; Perrone, S.; Perna, F. M.; Vitale, P.; Troisi, L.; Salomone, A.; Capriati, V. *Molecules* **2016,** *21,* 924. doi:10.3390/molecules21070924
6. Mancuso, R.; Maner, A.; Cicco, L.; Perna, F. M.; Capriati, V.; Gabriele, B. *Tetrahedron* **2016,** *72,* 4239–4244. doi:10.1016/j.tet.2016.05.062
7. Perrone, S.; Capua, M.; Messa, F.; Salomone, A.; Troisi, L. *Tetrahedron* **2017,** *73,* 6193–6198. doi:10.1016/j.tet.2017.09.013
8. Behalo, M. S.; Bloise, E.; Mele, G.; Salomone, A.; Messa, F.; Carbone, L.; Mazzetto, S. E.; Lomonaco, D. *J. Heterocycl. Chem.* **2020,** *57,* 768–773. doi:10.1002/jhet.3818
9. Dilauro, G.; Cicco, L.; Perna, F. M.; Vitale, P.; Capriati, V. *C. R. Chim.* **2017,** *20,* 617–623. doi:10.1016/j.crci.2017.01.008
10. Ghinato, S.; Dilauro, G.; Perna, F. M.; Capriati, V.; Blangetti, M.; Prandi, C. *Chem. Commun.* **2019,** *55,* 7741–7744. doi:10.1039/c9cc03927a
11. Messa, F.; Perrone, S.; Capua, M.; Tolomeo, F.; Troisi, L.; Capriati, V.; Salomone, A. *Chem. Commun.* **2018,** *54,* 8100–8103. doi:10.1039/c8cc03858a
12. Dilauro, G.; García, S. M.; Tagarelli, D.; Vitale, P.; Perna, F. M.; Capriati, V. *ChemSusChem* **2018,** *11,* 3495–3501. doi:10.1002/cssc.201801382
13. Messa, F.; Dilauro, G.; Perna, F. M.; Vitale, P.; Capriati, V.; Salomone, A. *ChemCatChem* **2020,** *12,* 1979–1984. doi:10.1002/cctc.201902380
14. Quivelli, A. F.; Vitale, P.; Perna, F. M.; Capriati, V. *Front. Chem. (Lausanne, Switz.)* **2019,** *7,* 723. doi:10.3389/fchem.2019.00723
15. Vitale, P.; Lavolpe, F.; Valerio, F.; Di Biase, M.; Perna, F. M.; Messina, E.; Agrimi, G.; Pisano, I.; Capriati, V. *React. Chem. Eng.* **2020,** *5,* 859–864. doi:10.1039/d0re00067a
16. Vitale, P.; Cicco, L.; Messa, F.; Perna, F. M.; Salomone, A.; Capriati, V. *Eur. J. Org. Chem.* **2019,** 5557–5562. doi:10.1002/ejoc.201900722
17. De Luca, L. *Curr. Med. Chem.* **2006,** *13,* 1–23.
18. Lagoja, I. M. *Chem. Biodiversity* **2005,** *2,* 1–50. doi:10.1002/cbdv.200490173
19. Han, H.-B.; Tu, Z.-L.; Wu, Z.-G.; Zheng, Y.-X. *Dyes Pigm.* **2019,** *160,* 863–871. doi:10.1016/j.dyepig.2018.09.017
20. Chen, W.-C.; Zhu, Z.-L.; Lee, C.-S. *Adv. Opt. Mater.* **2018,** *6,* 1800258. doi:10.1002/adom.201800258
21. Zhang, L.; Peng, X.-M.; Damu, G. L. V.; Geng, R.-X.; Zhou, C.-H. *Med. Res. Rev.* **2014,** *34,* 340–437. doi:10.1002/med.21290
22. Sharma, A.; Kumar, V.; Kharb, R.; Kumar, S.; Chander Sharma, P.; Pal Pathak, D. *Curr. Pharm. Des.* **2016,** *22,* 3265–3301. doi:10.2174/1381612822666160226144333
23. Kuzu, B.; Tan, M.; Taslimi, P.; Gülçin, İ.; Taşpınar, M.; Menges, N. *Bioorg. Chem.* **2019,** *86,* 187–196. doi:10.1016/j.bioorg.2019.01.044
24. Agarwal, A.; Srivastava, K.; Puri, S. K.; Chauhan, P. M. S. *Bioorg. Med. Chem.* **2005,** *13,* 4645–4650. doi:10.1016/j.bmc.2005.04.061
25. Shipe, W. D.; Sharik, S. S.; Barrow, J. C.; McGaughey, G. B.; Theberge, C. R.; Uslaner, J. M.; Yan, Y.; Renger, J. J.; Smith, S. M.; Coleman, P. J.; Cox, C. D. *J. Med. Chem.* **2015,** *58,* 7888–7894. doi:10.1021/acs.jmedchem.5b00983
26. Kaur, R.; Kaur, P.; Sharma, S.; Singh, G.; Mehndiratta, S.; Bedi, P. M. S.; Nepali, K. *Recent Pat. Anti-Cancer Drug Discovery* **2015,** *10,* 23–71. doi:10.2174/1574892809666140917104502
27. Farag, A. K.; Elkamhawy, A.; Londhe, A. M.; Lee, K.-T.; Pae, A. N.; Roh, E. J. *Eur. J. Med. Chem.* **2017,** *141,* 657–675. doi:10.1016/j.ejmech.2017.10.003
28. Chen, J.; Chen, W.; Yu, Y.; Zhang, G. *Tetrahedron Lett.* **2013,** *54,* 1572–1575. doi:10.1016/j.tetlet.2013.01.042

29. Khalili, B.; Tondro, T.; Hashemi, M. M. *Tetrahedron* **2009,** *65,* 6882–6887. doi:10.1016/j.tet.2009.06.082
30. Batanero, B.; Escudero, J.; Barba, F. *Org. Lett.* **1999,** *1,* 1521–1522. doi:10.1021/ol990200j
31. Benati, L.; Leardini, R.; Minozzi, M.; Nanni, D.; Spagnolo, P.; Strazzari, S.; Zanardi, G.; Calestani, G. *Tetrahedron* **2002,** *58,* 3485–3492. doi:10.1016/s0040-4020(02)00302-2
32. Zuliani, V.; Cocconcelli, G.; Fantini, M.; Ghiron, C.; Rivara, M. *J. Org. Chem.* **2007,** *72,* 4551–4553. doi:10.1021/jo070187d
33. Yamamoto, Y.; Ouchi, H.; Tanaka, T.; Morita, Y. *Heterocycles* **1995,** *41,* 1275–1290. doi:10.3987/com-95-7055
34. Skulcova, A.; Russ, A.; Jablonsky, M.; Sima, J. *BioResources* **2018,** *13,* 5042–5051.
35. Boyer, J. H.; Straw, D. *J. Am. Chem. Soc.* **1952,** *74,* 4506–4508. doi:10.1021/ja01138a011
36. Patonay, T.; Juhász-Tóth, É.; Bényei, A. *Eur. J. Org. Chem.* **2002,** 285–295. doi:10.1002/1099-0690(20021)2002:2<285::aid-ejoc285>3.0.co;2-j
37. Mjalli, F. S.; Ahmed, O. U. *Korean J. Chem. Eng.* **2016,** *33,* 337–343. doi:10.1007/s11814-015-0134-7
38. Reddy, C. N.; Sathish, M.; Adhikary, S.; Nanubolu, J. B.; Alarifi, A.; Maurya, R. A.; Kamal, A. *Org. Biomol. Chem.* **2017,** *15,* 2730–2733. doi:10.1039/c7ob00299h
39. Hu, M.; Wu, J.; Zhang, Y.; Qiu, F.; Yu, Y. *Tetrahedron* **2011,** *67,* 2676–2680. doi:10.1016/j.tet.2011.01.062

License and Terms

BEILSTEIN JOURNAL OF ORGANIC CHEMISTRY

Synergy between supported ionic liquid-like phases and immobilized palladium N-heterocyclic carbene–phosphine complexes for the Negishi reaction under flow conditions

Edgar Peris[1], Raúl Porcar[1], María Macia[1], Jesús Alcázar[2], Eduardo García-Verdugo[*1] and Santiago V. Luis[*1]

Full Research Paper

Open Access

Address:
[1]Dpt. of Inorganic and Organic Chemistry, Supramolecular and Sustainable Chemistry Group, University Jaume I, Avda Sos Baynat s/n, E-12071-Castellon, Spain and [2]Discovery Chemistry, Janssen Research and Development, Janssen-Cilag, S.A., C/ Jarama 75A, Toledo, Spain

Email:
Eduardo García-Verdugo[*] - cepeda@uji.es; Santiago V. Luis[*] - luiss@uji.es

* Corresponding author

Keywords:
immobilized catalyst; Negishi cross-coupling; NHC complex; palladium; supported ionic liquid

Beilstein J. Org. Chem. **2020,** *16,* 1924–1935.
doi:10.3762/bjoc.16.159

Received: 17 April 2020
Accepted: 20 July 2020
Published: 06 August 2020

This article is part of the thematic issue "Green chemistry II".

Guest Editor: L. Vaccaro

Abstract

The combination of supported ionic liquids and immobilized NHC–Pd–RuPhos led to active and more stable systems for the Negishi reaction under continuous flow conditions than those solely based on NHC–Pd–RuPhos. The fine tuning of the NHC–Pd catalyst and the SILLPs is a key factor for the optimization of the release and catch mechanism leading to a catalytic system easily recoverable and reusable for a large number of catalytic cycles enhancing the long-term catalytic performance.

Introduction

N-heterocyclic carbenes (NHCs) are known as efficient coordination ligands for different types of metals. The main feature of NHC complexes is their structural tunability [1]. Thus, their catalytic efficiency can be easily modulated through systematic variations of the steric and electronic design vectors of the NHC ligand [2]. These complexes have been used as highly efficient catalysts for a wide variety of C–C and C–X cross-coupling reactions [3]. Among others, different NHC–Pd complexes have been designed as efficient homogeneous catalysts for Negishi reactions [4]. Although these systems are highly efficient, their homogeneous nature hamper the separation of the products and recovery of the excess of the palladium from the reaction solution. A possible solution to this issue is the preparation of the related immobilized complexes enabling a simpler recovery and

reuse of the catalysts by filtration [5]. Furthermore, the immobilized NHC-complexes can be easily adapted to flow processes using a fix-bed reactor set-up increasing simultaneously the sustainability and the efficiency of the C–C coupling reactions [6,7]. In the pursuit of NHC immobilized metal complexes many different materials of organic and inorganic nature have been used as supports [5]. Several reports describe the synthesis of supported palladium–NHC complexes (Pd–NHC) and their application in cross-coupling reactions [8-10]. The main flaw of this type of systems is related with the mechanistic aspect of most C–C formation reactions catalyzed by palladium [11]. Careful studies of the reaction mechanism have revealed that, under certain conditions, palladium-supported species can act as mere pre-catalysts [12,13]. As suggested by Ananikov and co-worker, these in situ-generated catalytic species can give rise to cocktail-type systems with different active metal species present in solution [14]. In the case of immobilized catalysts, these palladium species can be released from the support reacting in the homogeneous medium transformed from Pd^0 to Pd^{II}. In this way, a "cocktail" of catalytic species, including molecular complexes, clusters and nanoparticles may be responsible for the catalytic activity [15]. In a continuous system, this can be accompanied by a significant leaching of the catalytic metal. In order to avoid a loss of activity by this leaching process, the role of the ligand and the support on the evolution of the catalytic systems should be carefully considered. It has been shown that the immobilization of Pd-catalysts or precatalysts onto supported ionic liquid-like materials can facilitate the recapture by the support of the released active species at the end of the reaction, in what has been called a "boomerang" mechanism [16,17]. Here, we report our efforts aiming a rational development for Negishi catalysts based on NHC–Pd complexes in conjunction with supported ionic liquid-like phases to enhance their catalytic stability under continuous flow conditions.

Results and Discussion

Scheme 1 summarizes the synthetic approach used for the preparation of the functionalized polymers considered in this work. A commercially available PS-DVB bead-type macroporous chloromethylated polymer **1** (Merrifield resin with 20% DVB and 1.2 mmol Cl/g,) was used as the starting material for the immobilization of *N*-arylimidazoles **2a** and **2b**, following the traditional alkylation protocol [18,19]. The preparation of these modified polymers was monitored by FT–ATR–IR, FT-Raman using a micro-spectroscopy accessory and the NBP test [20,21]. The corresponding Pd–NHC complexes **4a** and **4b** (Scheme 1) were obtained by treatment of the supported imidazolium species with $Pd(OAc)_2$ in the presence of a base. The amount of immobilized NHC ligand was determined by elemental analysis, while the palladium loaded on the polymer was determined by ICP analyses (see Table 1). The slightly lower value of the Pd loading is likely to be related to the partial formation of 2:1 NHC/Pd complexes. The experimental details for the synthesis of **2a**,**b**, **3a**,**b** and **4a**,**b** are given in Supporting Information File 1.

Table 1: Pd Loading for the different NHC-Pd synthesized.

Entry	Polymer	NHC loading[a]	Pd loading[b]
1	**4a**	0.75	0.43
2	**4b**	0.64	0.46

[a]As determined by elemental analysis (mmol functional group/g resin); [b]as determined by ICP analysis (mmol Pd/g resin).

The Negishi reaction of benzylzinc bromide (**5**) and methyl 4-bromobenzoate (**6**) to form methyl 4-benzylbenzoate (**7**) was used to evaluate the activity of the palladium catalysts on polymer support (Scheme 2). The Negishi reaction is a potent cross-coupling reaction in organic chemistry. Notably, it has

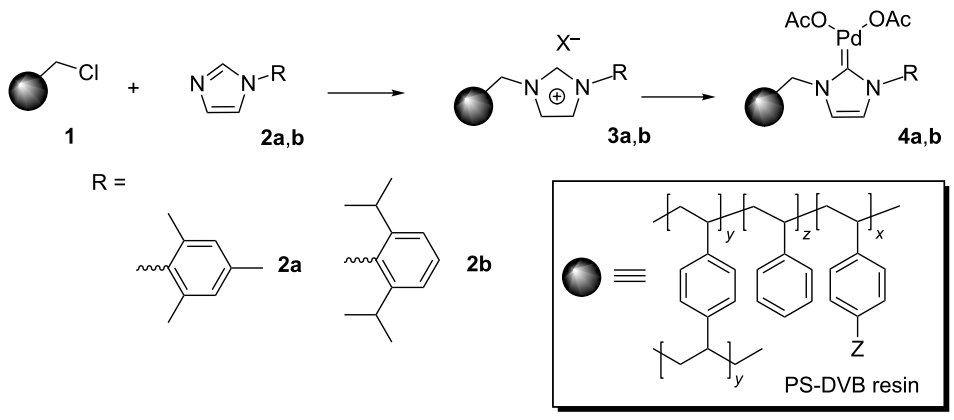

Scheme 1: Synthesis of NHC-supported catalysts.

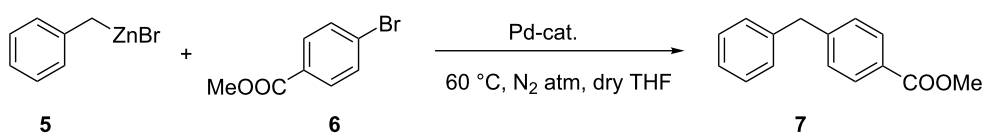

Scheme 2: Negishi benchmark reaction.

much value for the synthesis of fine chemicals and medicinal drugs [22]. The conditions selected for the benchmark reaction were the use of THF as the solvent, 60 °C and a catalyst loading based on the introduction of 5 mol % of Pd. The reaction was monitored by GC and the resulting conversions and yields were confirmed by ^{1}H NMR (see Supporting Information File 1).

The kinetic plots for this model reaction are represented in Figure 1. The NHC–Pd catalyst **4a** showed a rather reduced activity (less than 10% after two hours), while the catalyst bearing isopropyl moieties at the aromatic ring (**4b**) displayed a significant increase in the catalytic activity, reaching 67% yield after 120 min (Figure 1).

In order to improve the catalytic performance of these systems, the cooperative effect of an additional ligand was evaluated. Organ and co-workers have demonstrated that the introduction of pyridine ligands can be used to enhance the activity of such NHC complexes (pyridine enhanced precatalyst preparation, stabilization and initiation, PEPPSI) [23,24]. In addition to pyridine ligands, other compounds with coordinating atoms such as C, N or P have been reported to tune the catalytic activity of the NHC–Pd complexes [25-28]. Thus, a ligand containing P as the coordinating atom was selected for the activation of the NHC complexes. In this regard, RuPhos (2-dicyclohexylphosphino-2′,6′-diisopropoxybiphenyl) has been used as a palladium ligand for the Negishi reaction [29]. The preparation of the NHC–Pd–RuPhos complexes **8a**,**b** was carried out by mixing a suspension of **4a**,**b** with a solution of RuPhos for 2 hours (Scheme 3). The corresponding modified immobilized NHC–Pd–RuPhos complexes were isolated by filtration and thoroughly washed to remove any remaining non-coordinated RuPhos (0.37 and 0.57 mequiv of Pd/g for **8a** and **8b**, respectively).

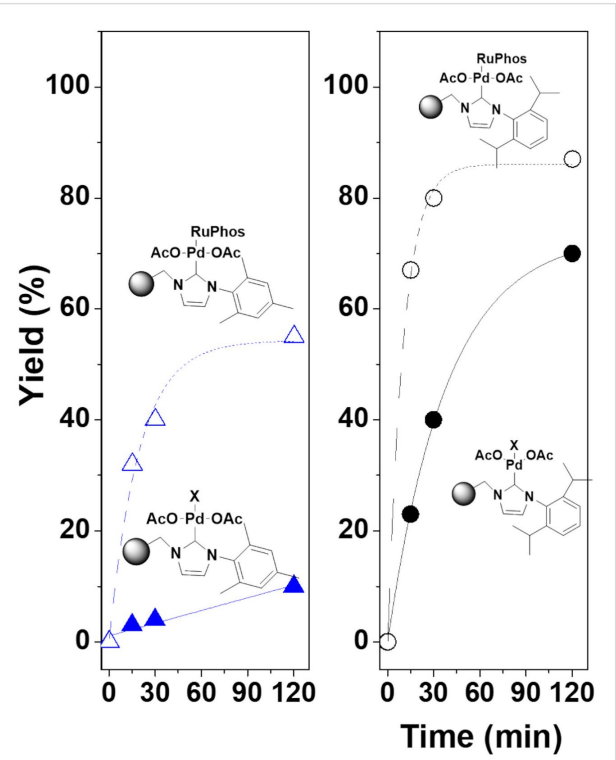

Figure 1: Negishi reaction catalyzed by immobilized NHC–Pd complexes. Conditions: methyl 4-bromobenzoate (0.25 mmol, 1 equiv), benzylzinc bromide (0.5 mmol, 2 equiv, 1 mL of a 0.5 M solution in THF), 5 mol % of Pd catalyst (0.0125 mmol) in dry THF (1 mL). N_2 atmosphere, 60 °C. Yields calculated by GC and confirmed by ^{1}H NMR.

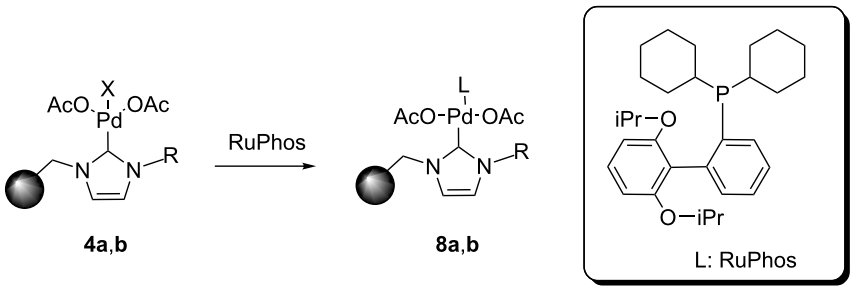

Scheme 3: Synthesis of immobilized NHC–Pd–RuPhos.

The introduction of the additional phosphine ligand produced a clear positive effect on the activity, enhancing the catalytic performance of the immobilized NHC–Pd complexes assayed as clearly shown in the kinetics profiles depicted in Figure 1. Both NHC–Pd–RuPhos catalysts showed an activity increase: ca. 10-fold for **8a** and ca. 2.9-fold for **8b**, according to the TOF values calculated at 15 minutes.

In the light of this initial screening under batch conditions with both kinds of catalytic complexes, NHC–Pd (**4a**,**b**) and NHC–Pd–RuPhos (**8a**,**b**), their activity and stability was evaluated under flow conditions. For this, the corresponding fixed-bed reactors were prepared, and the general flow reaction setup depicted in Supporting Information File 1. It should be mentioned that the catalyst **4a** showed, as in the batch process, low activity (<5% yield) under flow conditions. However, the catalyst **4b** yielded **7** under the selected flow conditions (flow rate of 0.214 mL/min, Figure 2). At initial times, yields for **7** were higher than those obtained in the batch process, which is remarkable considering the short residence time used (2.5 min). However, a strong deactivation was observed under prolonged use (Figure 2). The catalytic activity decay calculated in terms of productivity (g of **7** × g Pd^{-1} × h^{-1}) was of ca. 50% after only 2 h of continuous use. This decay in activity can be associated with the leaching of palladium from the heterogeneous phase [30]. The initial samples collected showed an elevated concentration of leached soluble palladium species as calculated by ICP–MS of the respective solutions (>15 ppm of Pd). The elemental analysis of the catalyst after its use was also consistent with this Pd loss from the NHC complex.

Additionally, the catalyst **8a** was also tested under continuous flow conditions. Although, this time a fivefold larger fixed bed reactor (2.9 mL vs 0.5 mL) was used, leading to a larger residence time (29 min vs 2.5 min). An increase in the residence time may favor the re-adsorption of the active species into the support limiting, at some extent, the Pd leaching. The results obtained under these conditions are depicted in Figure 3. As expected, the use of a larger residence time led to a high yield. Quantitative yields were initially obtained under these conditions, with a productivity of 1.73 g **7**/g Pd·h. This level of activity was kept constant during at least 5.5 h of continuous use. However, after this time a strong deactivation of the catalyst took place. An activity loss of ca. 50% of the initial value was observed. After this decay, between 8 and 15 h of continuous use, the productivity achieved was maintained around 0.8 g of **7** × g Pd^{-1} × h^{-1}.

These results agree with the ones observed by Organ and co-workers, who have developed silica-immobilized Pd–PEPPSI–*IPr*–SiO_2 [31] and Pd–PEPPSI–*IPent*–SiO_2 [32] catalysts. They observed a gradual catalyst deactivation due to the slow release of palladium over time. However, the high level of catalyst activity, especially for Pd–PEPPSI–*IPent*–SiO_2, made, in that case, the loss of Pd less relevant. With a reduction of palladium loading to half of its

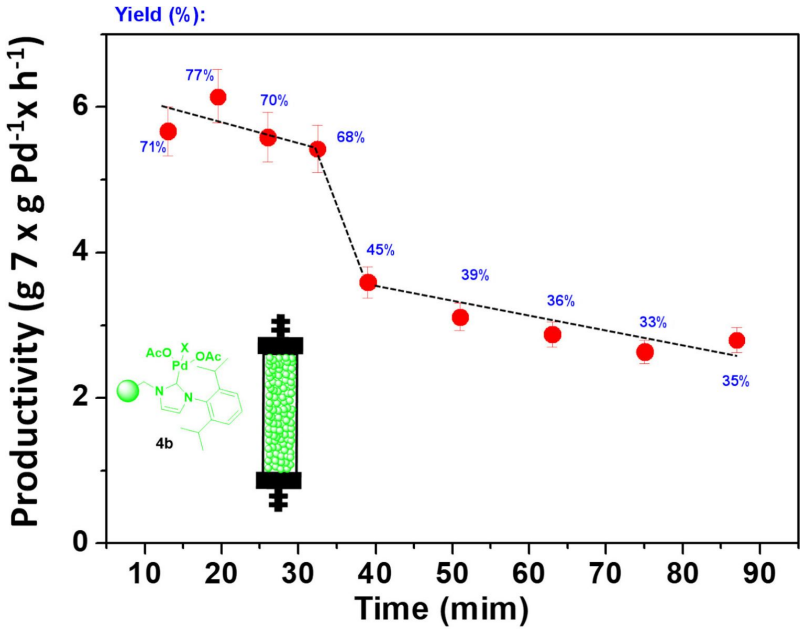

Figure 2: Negishi model reaction between **5** and **6** under flow conditions catalyzed by **4b**. *V* = 0.535 mL, 363 mg of **4b**, residence time = 2.5 min, total flow rate 0.214 mL/min. Productivity max: 7.97 g of **7** × g Pd^{-1} × h^{-1}. Yields calculated by GC and confirmed by ^{1}H NMR.

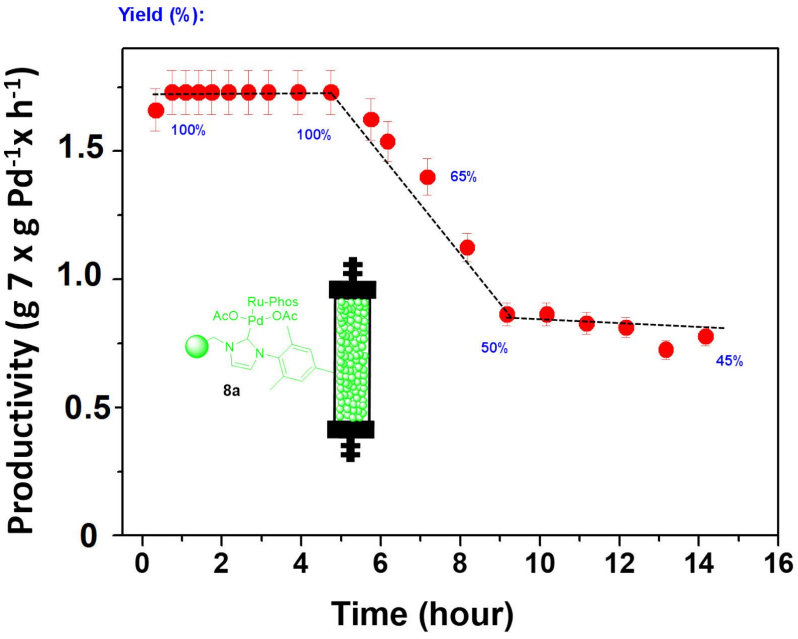

Figure 3: Negishi model reaction under flow conditions catalyzed by **8a**. *V* = 2.9 mL, 1.25 g of catalyst, residence time = 29 min, total flow rate: 1 mL/min, productivity max: 1.73 g of **7** × g Pd^{-1} × h^{-1}. Yields calculated by GC and confirmed by ^{1}H NMR.

initial value, still relatively efficient long-term flow runs could be carried out.

Different strategies have been evaluated to develop precatalysts/catalysts immobilized onto supported ionic liquid-like phases (SILLPs) [33-38]. In these systems, the microenvironment provided by the ionic liquid-like units can have a remarkable influence on the overall process, particularly on the catalytic activity and recyclability of the supported species. Indeed, the appropriate design of the SILLPs is a key factor for the optimization of release and catch systems leading to easily recoverable and reusable catalysts working for a large number of catalytic cycles without any loss in performance [33,34]. In this regard, the effect of the presence of different SILLPs in the catalytic behavior of the former catalytic complexes was evaluated. Thus, the benchmark Negishi reaction between **5** and **6** was performed using a polymeric mixture of two components: the immobilized NHC–Pd–RuPhos catalyst and a series of polymeric SILLPs in a 1:3 weight ratio. The first component can efficiently act as a catalyst but also will generate and release a series of Pd species accounting for the leaching. The second component, the SILLP, can act as scavenger of those species leached to the solution not only eliminating them from the solution but also contributing to their stabilization avoiding the formation of inactive species and keeping their activity for further catalytic cycles. Three different SILLPs were evaluated displaying different imidazolium substitution patterns and a loading of IL-like fragments of 13–24% by weight. Figure 4 summarizes the results obtained for this study. The presence of SILLPs affected both activity and Pd leaching. Regarding the activity, the presence of methyl imidazolium groups in SILLP **9a** slightly reduced the catalytic activity, while the presence of butyl- and methyldecylimidazolium units (SILLPs **9b** and **9c**, respectively) led to more active systems. This can be clearly appreciated when the TOF values at 15 minutes are compared (Figure 4b). The presence of the SILLPs **9c** and **9b** clearly led to a catalytic system more active than **8a**, while the presence of **9a** reduced the activity. The presence of the SILLPs also had a strong influence on the Pd leaching. In the absence of the SILLPs (**8a** as catalyst) the observed Pd leaching was 22.4 ppm, corresponding to ca. 7% of the initial Pd. In the presence of the SILLPs this leaching was reduced to 2.7, 14.4 and 17.1 ppm (ca. 0.8%, 4.5% and 5% of the initial Pd) for the polymeric mixtures **8a** + **9a**, **8a** + **9b** and **8a** + **9c**, respectively. This confirmed that the SILLPs act as scavengers for the leached Pd species. Noteworthy, the larger palladium leaching did not lead to higher activities, suggesting that in absence of the SILLP some deactivation for the leached species was taking place.

The TEM analysis of the polymers after the reactions showed the presence of palladium nanoparticles (Figure 5) confirming that during the reaction a part of the leached palladium was converted into PdNPs. The higher reactivity of the cocktails based on **9b** and **9c** can be associated with the presence of PdNPs with smaller size distributions. Our previous results obtained for AuNPs-SILLPs indicated that for the macroporous resins the

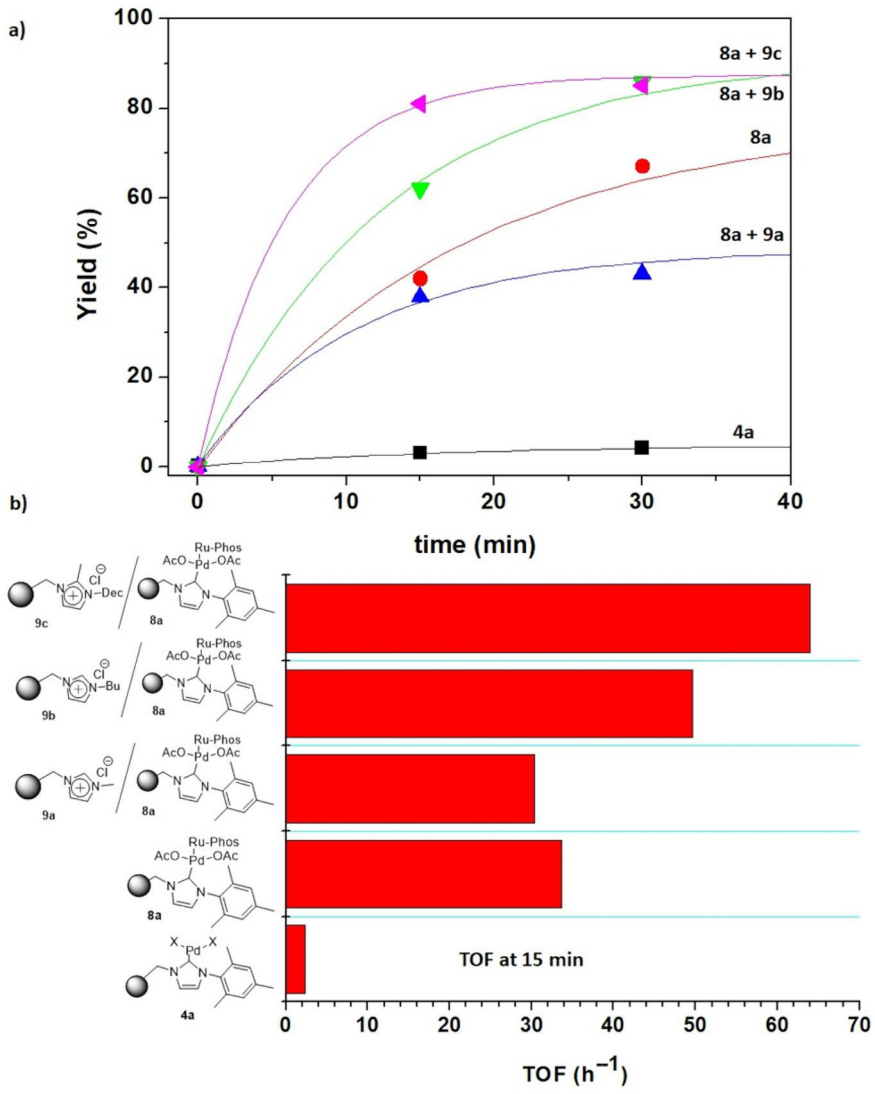

Figure 4: Negishi reaction between **5** and **6** catalyzed by **8a** in the presence of SILLPs**.** a) Yield (%) vs time for different catalytic mixtures. b) TOF values obtained at 15 minutes. Conditions: 1 equiv methyl 4-bromobenzoate (0.25 mmol), 2 equiv benzylzinc bromide (0.5 mmol, 1 mL of a 0.5 M solution in THF), 5 mol % Pd catalyst (0.0125 mmol) in dry THF (1 mL). N_2 atmosphere. Yields calculated by GC and confirmed by ^{1}H NMR.

NP size decreased when the size of the aliphatic residue of the imidazolium units increased with decyl N-substitution leading to smaller particle sizes [39]. The analysis of the polymeric samples revealed similar trends for the case of PdNPs. SILLPs with decyl and butyl N-substitution (**9c** and **9b**) presented the smallest size distributions, being also the most reactive ones.

In the light of these experiments, it can be concluded that the supported NHC–Pd–RuPhos **8a** acts as both catalyst and as a system releasing soluble Pd species, which can be partially catched by the SILLP acting as scavenger. The key is to find out if these recaptured species onto SILLP are still active for the Negishi reaction. The leaching of Pd from NHC–Pd–RuPhos is in agreement with previous studies for C–C palladium catalyzed reactions [33-35]. Recently, Ananikov and co-workers reported that for Pd–NHC systems the reactivity of the systems is mainly determined by the cleavage of the metal−NHC bond, while the catalyst performance is strongly affected by the stabilization of in situ-formed metal clusters [15,30,40]. In the mechanism suggested by these authors, Pd–NHC complexes can evolve through two different pathways towards the formation of a catalytically active cocktail of Pd species. In the first one, a reductive elimination takes place from the Pd(II) intermediate with the concomitant release of NHC-containing byproducts. In the second pathway, the dissociation of the M–NHC produces Pd intermediates from which metal clusters and MNPs can be readily formed while the carbene can react through C−NHC or H−NHC coupling. The presence of onium salts significantly

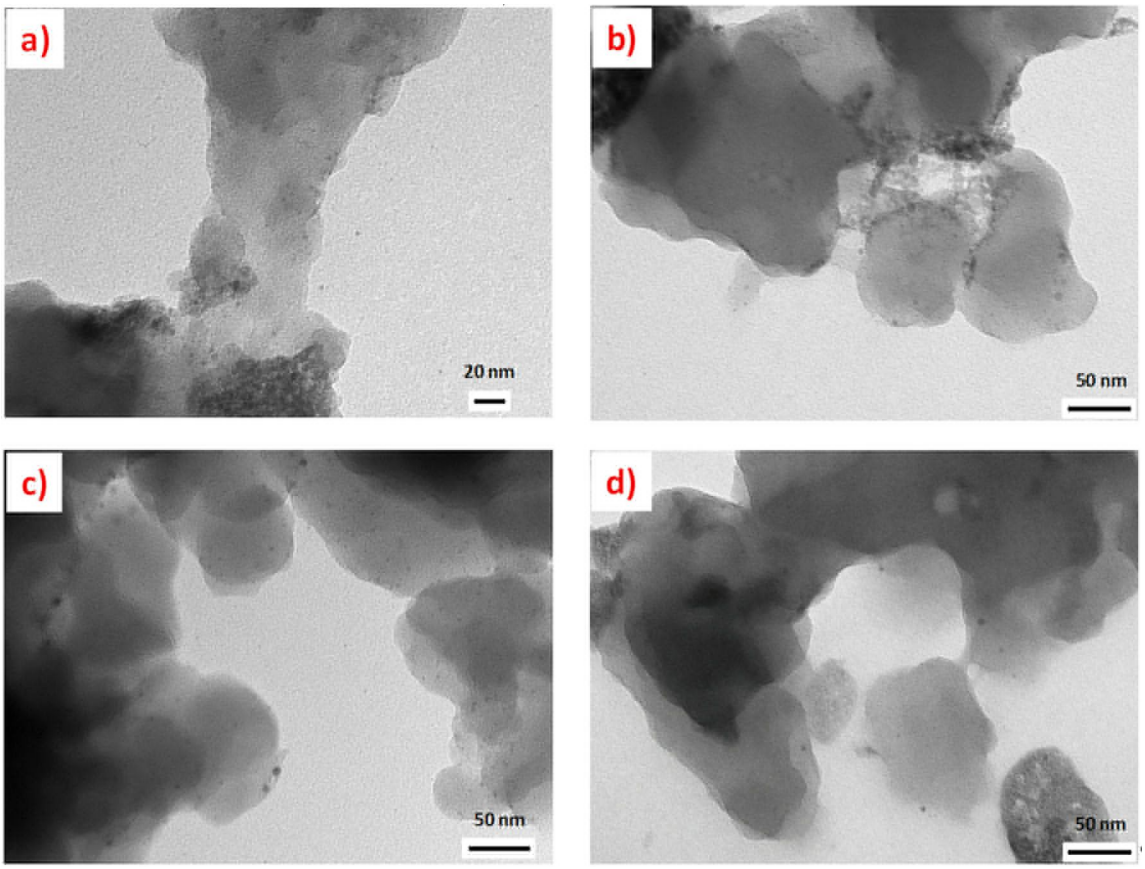

Figure 5: TEM images of the polymers after the Negishi reaction between **5** and **6**. a) **8a**, bar scale 20 nm, PdNP size distribution 4.91 ± 1.26 nm. b) **8a** + **9a**, bar scale 50 nm, PdNP size distribution 4.23 ± 1.65 nm. c) **8a** + **9b**, bar scale 50 nm, PdNP size distribution 3.61 ± 1.36 nm. d) **8a** + **9c**, bar scale 50 nm, PdNP size distribution 3.23 ± 0.81 nm.

contributes to the stabilization of both Pd clusters and PdNPs [40]. Thus, a combination of a classical molecular mode of operation and a cocktail-type mode of operation can also be involved in the Negishi reaction. Two different palladium species released from the NHC complex can act as catalyst for the Negishi reaction: i) soluble Pd(II) species or ii) palladium nanoparticles (PdNPs). Imidazolium moieties in SILLPs can scavenge and stabilize both types of palladium species. The possible catalytic effect of these Pd species immobilized onto SILLPs for the Negishi reaction was, thus, evaluated. Firstly, a solution of Pd(II) was adsorbed in the SILLP **10** similar to **9a** but with a high loading of methylimidazolium units leading to a Pd(II)-SILLP system **11** with 0.56 mequiv of Pd/g of SILLP and 3.79 mequiv of IL-like units/g of SILLP (Scheme 4). This

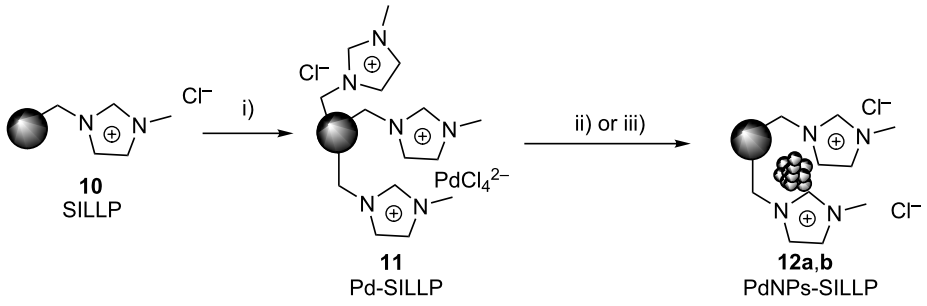

Scheme 4: Pd species immobilized onto SILLPs. i) 1 g SILLP **10,** 100 mg $PdCl_2$ in milli-Q® water (100 mL 1% HCl, 1000 ppm $PdCl_2$), orbitalic stirring, rt, 5 h. ii) 250 mg Pd-SILLP **11**, 0.2 g $NaBH_4$ in 12 mL EtOH/H_2O 1:4, rt, 3 h. iii) 250 mg Pd-SILLP **11**, 4 mL EtOH, MW (2 h, 200 °C, 300 psi, 120 W).

system was treated with either $NaBH_4$ or EtOH under microwave irradiation to produce the corresponding PdNPs immobilized onto SILLPs (**12a**,**b**).

The Pd-containing polymers **11** and **12a**,**b** were tested as potential catalysts for the benchmark Negishi reaction. Pd(II) adsorbed by ionic exchange (**11**) yielded 73% of **7** after 120 minutes of reaction under standard conditions, confirming that soluble Pd(II) species released from the immobilized systems and scavenged by SILLPs can act as catalysts for the Negishi reaction. The reaction was also evaluated in the presence of 0.05 equivalents of RuPhos, as some of this ligand should be released from the NHC–Pd–RuPhos complex along with Pd (Figure 6a). Under such conditions, the reaction took place with yields for **7** of ca. 90% for the first cycle. Noteworthy the levels of leaching were lower than the ones observed for **8a** (0.49 ppm vs 22.4 ppm for **8a**). The reaction was also assayed in the presence of one equivalent of RuPhos and SILLP **9a** as scavenger, by using a mixture of **11** and **9a** in a 1:3 weight ratio (Figure 6b). Under these conditions, the catalytic system was less active, but the leaching was reduced even further reaching a value of 0.04 ppm. The recyclability of the systems was also tested. In general, the catalysts assayed maintained the catalytic activity as far as an additional amount of RuPhos (0.05 equiv) was added for the new cycle. Under these conditions, the activity of **11** was kept constant for at least four catalytic cycles remaining the Pd leaching for each cycle rather small (ca. 0.04 ppm in the solution). The mixture of **11** and the scavenger **9a** was also active in successive cycles, under similar conditions, although the activity suffered from more fluctuations, probably due to the heterogeneity of the mixture. In any case, the systems were still active after six consecutive cycles being the Pd leaching per cycle in the 0.04–0.12 ppm range. It can be seen that in the absence of an additional amount of RuPhos after the first cycle the catalytic activity was lost but was recovered for the third cycle when RuPhos was added.

Regarding the activity of the PdNP-SILLPs **12a**,**b**, they showed no activity, with yields lower than 1%, in the absence of RuPhos, while providing good catalytic performance in the presence of one equivalent of the phosphine. The catalysts prepared by $NaBH_4$ reduction were slightly less reactive than those obtained with EtOH as reducing agent. Noteworthy, the supported catalysts were active in further catalytic cycles after separation of the product by filtration and polymer washing [41]. Catalytic systems **12a**,**b** were also recycled being **12a** even more active in a second than in the first cycle while **12b** reduced its activity (see Table 2). To understand these differences, it must be noted that the nature of the MNPs obtained in SILLPs is very sensitive to the procedure used for their preparation and this significantly affects its activity but also their recyclability [35,39]. The capacity to generate active catalytic species from the MNPs is essential in the first run, but the capacity of the system, including imidazolium fragments and remaining MNPs, to efficiently recapture the soluble species in an active form is key for the second and successive runs.

All these results suggest that the SILLPs can be used as efficient scavengers for the palladium-leached species released from NHC–Pd–RuPhos complexes, limiting the leaching and possibly improving the long-term system stability. In order to screen the effect of the SILLPs under continuous flow conditions, small flow fixed-bed reactors were prepared and evaluated. The first system was prepared by packing two layers, one

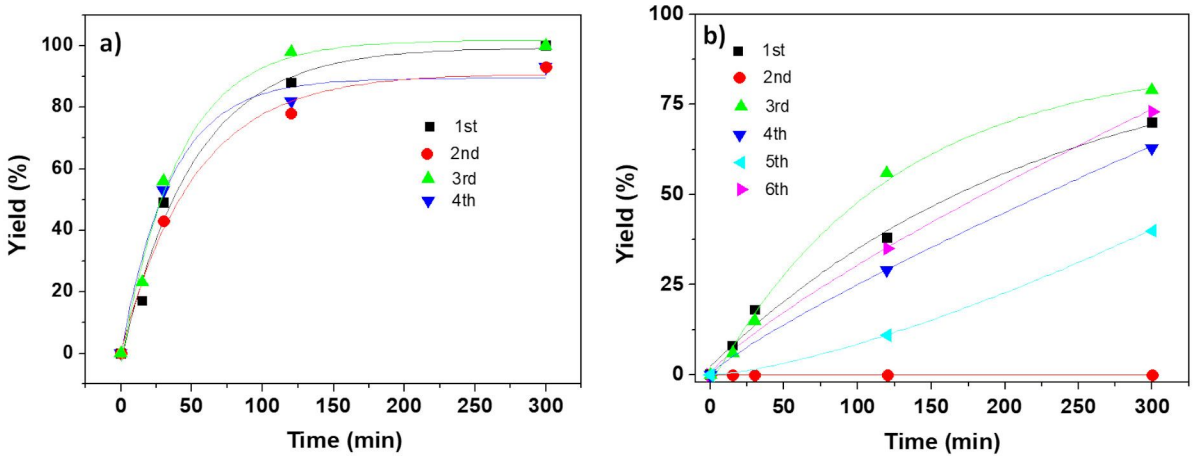

Figure 6: Negishi reaction between **5** and **6** catalyzed by **11**. 1 equiv methyl 4-bromobenzoate (**6**, 0.25 mmol), 2 equiv benzylzinc bromide (**5**, 0.5 mmol, 1 mL of a 0.5 M solution in THF), 5 mol % Pd catalyst in dry THF (1 mL). a) **11** in presence of RuPhos, Pd/RuPhos 1:0.05 molar ratio. RuPhos added for each cycle. b) **11** + **9a**, 1:3 weight ratio, in the presence of RuPhos, Pd/RuPhos 1:1 molar ratio, RuPhos added each cycle except for the 2nd cycle. N_2 atmosphere. Yields calculated by GC and confirmed by ^1H NMR.

Table 2: Negishi reaction between **5** and **6** catalyzed by **12a**,**b**.[a]

Entry	Catalyst	Pd/RuPhos	Cycle	Yield (time, min)[b]		
				15	30	120
1	**12a**	1:0	1	n.f.	n.f.	n.f.
2	**12b**	1:0	1	n.f.	n.f.	n.f.
3	**12a**	1:1	1	12	31	73
4	**12b**	1:1	1	42	50	73
5	**12a**	1:1	2	84	83	85
6	**12b**	1:1	2	11	21	66

[a]1 equiv methyl 4-bromobenzoate (**6**, 0.25 mmol), 2 equiv benzylzinc bromide (**5**, 0.5 mmol, 1 mL of a 0.5 M solution in THF), 5 mol % Pd catalyst in dry THF (1 mL). [b]Yield calculated by GC and confirmed by ^{1}H NMR; n.f.: product not found.

on the top of the other. The bottom layer was prepared with 200 mg of the scavenger SILLP **9a** (to recapture released Pd species) and the top layer with 200 mg of the catalyst **8a** (Figure 7a). However, this configuration did not contribute to improve the stability of the system, with a strong catalyst deactivation observed, reaching ca. 47% of the initial activity after 40 h on flow.

In an attempt to achieve a better performance a homogeneous distribution of the catalyst and the scavenger within the fixed bed reactor seems to be preferable as it has been observed in multicatalytic systems [42]. In this case, two different fixed bed reactors were prepared with a well-disperse mixture formed by 50 mg of the catalyst **8a** and 150 mg of a SILLP. Two different SILLPs were used, one with low loading of IL-like units (**9a**,1.09 mequiv/g, 13 wt %) and one with a high loading (**10**, 3.79 mequiv/g, 37 wt %). In the case of the continuous reactor containing the high loading SILLP the activity decay was lower than the previously observed (up to ca. 35% of the initial value). However, the system based on the use of the SILLP **9a** with a low loading kept a constant level of activity, with a productivity of ca. 15 g of **7** × g Pd^{-1} × h^{-1}.

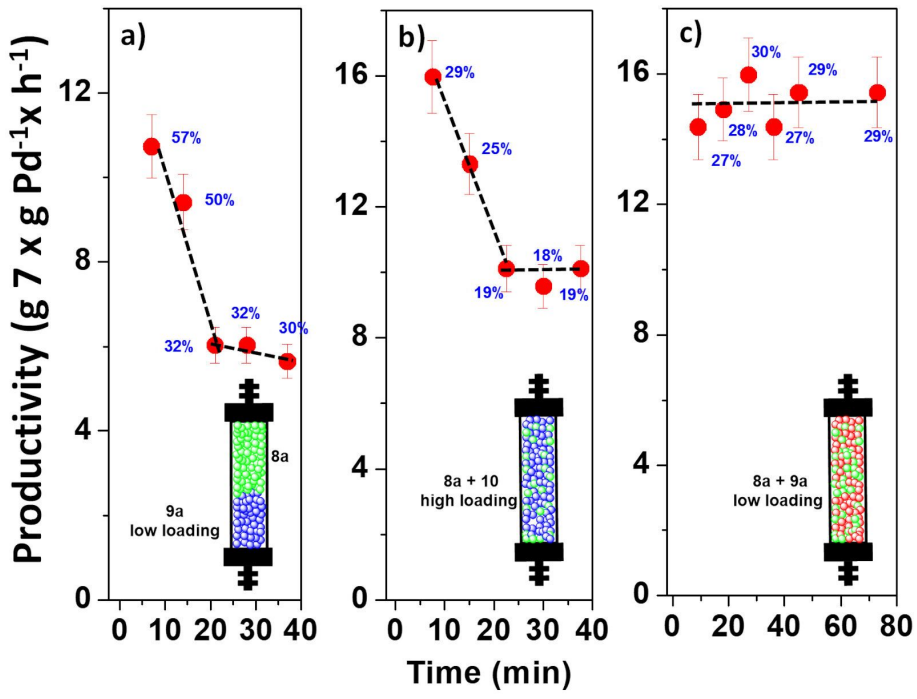

Figure 7: Negishi reaction between **5** and **6** under flow conditions catalyzed by **8a** in the presence of a scavenger SILLP (**9a** and **10**). a) 200 mg of **8a** (top) and 200 mg of **9a** (bottom). *V* = 0.535 mL, residence time = 2.5 min, productivity max: 18.84 g **7** × g Pd^{-1} × h^{-1}. b) 50 mg of **8a** and 150 mg of **10** (mixed), *V* = 0.38 mL, residence time = 2.5 min, Productivity max: 53.24 g **7** × g Pd^{-1} × h^{-1}. c) 50 mg of **8a** and 150 mg of **9a** (mixed), *V* = 0.35 mL, residence time = 2.5 min, productivity max: 53.24 g **7** × g Pd^{-1} × h^{-1}. Yield calculated by GC and confirmed by ^{1}H NMR.

Based on these results, two larger fixed bed reactors were prepared, and their performance evaluated for the benchmark Negishi reaction. A first one was filled with 250 mg of **8a** and 750 mg of the SILLP **9a**, while the second one contained the same amount of catalyst but using the SILLP **9c** instead of **9a**. The results are summarized in Figure 8. In agreement with results observed in the batch experiments, the mixture of the polymers **8a** + **9c** led to more active systems reaching >99% yield of **7**. However, the activity strongly decayed after 60 minutes of continuous use. This can be related with the leaching observed during this period with samples containing up to 10 ppm of leached palladium. The system based on **8a** and **9a** provided a more stable performance. Although the activity displayed was slightly lower, as observed in the batch experiments, it remained constant after an initial conditioning time. Thus, the initial samples showed up to ca. 85% yield of **7**, which after 80 minutes slightly decayed to ca. 70% yield, corresponding to a productivity of 4.87 g of **7** × g Pd^{-1} × h^{-1}. This level of productivity was maintained during at least five hours of continuous use.

The TEM images of the polymeric systems after their use under continuous flow conditions revealed again the presence of PdNPs (Figure 9). However, the images show that for the system **8a** + **9c** the number of particles and their size distribution are larger than for **8a** + **9a**. This trend is different to the one observed in batch experiments.

Conclusion

The results here presented confirm the viability of using polymeric cocktails formed by mixtures of supported NHC–Pd–RuPhos and SILLPs as efficient catalysts for the Neghishi reaction. In such cocktails, SILLPs act as scavengers of the palladium species released from the immobilized NHC–Pd–RuPhos, leading to complex mixtures of immobilized species still active for the considered reaction, while the leaching is minimized and the long-term catalyst life improved. This provides an opportunity for the development of active and stable Pd systems to be used under flow conditions, overcoming the limitations associated to the intrinsic mechanistic pathways of the Negishi reaction. A catch and release mecha-

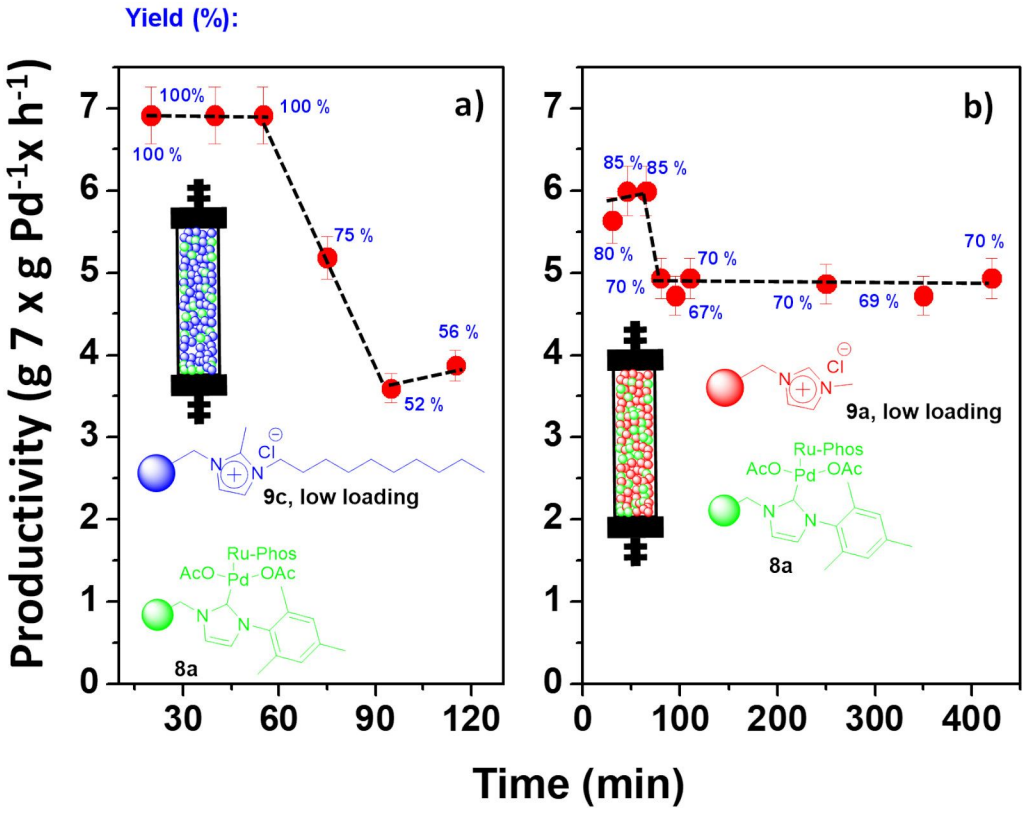

Figure 8: Effect of the structure of the SILLP scavenger for the Negishi reaction between **5** and **6** under flow conditions catalyzed by **8a** in the presence of SILLPs **9a** or **9c**. 60 °C. Total flow rate: 0.1 mL/min. 0.05 mL of a 0.2 M solution of **5** in THF and 0.05 mL/min of a 0.1 M solution of **6** in THF. *V* = 1.7 mL, residence time = 17 min. Productivity max: 7.08 g **7** × g Pd^{-1} × h^{-1}. a) 250 mg of **8a** and 750 mg of **9c** SILLP low loading, b) 250 mg of **8a** and 750 mg of **9a** SILLP low loading. Yield calculated by GC and confirmed by ^{1}H NMR.

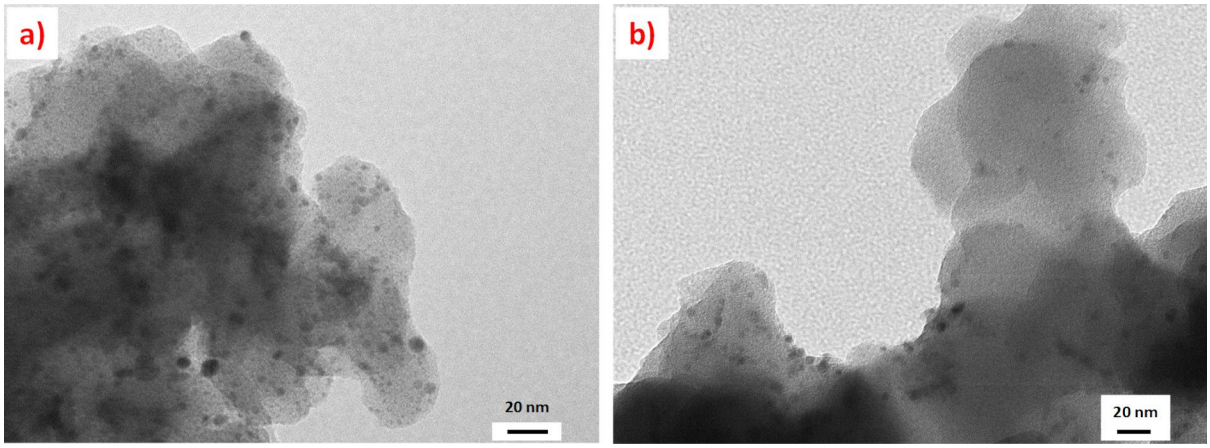

Figure 9: TEM images of the polymer after the Negishi reaction between **5** and **6** under flow conditions. a) **8a** + **9c**, bar scale 20 nm, PdNPs particle size distribution 4.72 ± 1.44 nm. b) **8a** + **9a** bar scale 20 nm, PdNPs particle size distribution 3.12 ± 0.97 nm.

nism can be established favored by the presence of the supported ionic liquid-like phases. SILLPs with a relatively low loading of methylimidazolium units provided the most efficient systems to be used in conjunction with the immobilized NHC–Pd–RuPhos.

Supporting Information

Supporting Information File 1

Experimental procedures and spectra. General flow reactions set-up.
[https://www.beilstein-journals.org/bjoc/content/supplementary/1860-5397-16-159-S1.pdf]

Acknowledgements

Technical support from the SCIC of the University Jaume I is acknowledged. The Ph.D. thesis of E.P. is the main source of the results here presented.

Funding

This work has been partially supported by projects UJI-B2019-40 (Pla de Promoció de la Investigació de la Universitat Jaume I) and RTI2018-098233-B-C22 (MINISTERIO DE CIENCIA, INNOVACIÓN Y UNIVERSIDADES). E. Peris thanks MICINN for financial support (FPU13/00685).

ORCID® iDs

Raúl Porcar - https://orcid.org/0000-0002-3345-0804
María Macia - https://orcid.org/0000-0002-0589-1696
Eduardo García-Verdugo - https://orcid.org/0000-0001-6867-6240
Santiago V. Luis - https://orcid.org/0000-0002-8159-3447

References

1. Peris, E. *Chem. Rev.* **2018,** *118,* 9988–10031. doi:10.1021/acs.chemrev.6b00695
2. Huynh, H. V. *Chem. Rev.* **2018,** *118,* 9457–9492. doi:10.1021/acs.chemrev.8b00067
3. Froese, R. D. J.; Lombardi, C.; Pompeo, M.; Rucker, R. P.; Organ, M. G. *Acc. Chem. Res.* **2017,** *50,* 2244–2253. doi:10.1021/acs.accounts.7b00249
4. Valente, C.; Çalimsiz, S.; Hoi, K. H.; Mallik, D.; Sayah, M.; Organ, M. G. *Angew. Chem., Int. Ed.* **2012,** *51,* 3314–3332. doi:10.1002/anie.201106131
5. Wang, W.; Cui, L.; Sun, P.; Shi, L.; Yue, C.; Li, F. *Chem. Rev.* **2018,** *118,* 9843–9929. doi:10.1021/acs.chemrev.8b00057
6. Len, C. Palladium-Catalyzed Cross-Coupling in Continuous Flow at Room and Mild Temperature. In *Sustainable Catalysis;* Luque, R.; Lam, F. L.-Y., Eds.; Wiley-VCH: Weinheim, Germany, 2018; pp 183–206. doi:10.1002/9783527693030.ch7
7. Busch, M.; Wodrich, M. D.; Corminboeuf, C. *ACS Catal.* **2017,** *7,* 5643–5653. doi:10.1021/acscatal.7b01415
8. Sommer, W. J.; Weck, M. *Coord. Chem. Rev.* **2007,** *251,* 860–873. doi:10.1016/j.ccr.2006.07.004
9. Zhong, R.; Lindhorst, A. C.; Groche, F. J.; Kühn, F. E. *Chem. Rev.* **2017,** *117,* 1970–2058. doi:10.1021/acs.chemrev.6b00631
10. Majeed, M. H.; Shayesteh, P.; Wallenberg, L. R.; Persson, A. R.; Johansson, N.; Ye, L.; Schnadt, J.; Wendt, O. F. *Chem. – Eur. J.* **2017,** *23,* 8457–8465. doi:10.1002/chem.201700777
11. Cantillo, D.; Kappe, C. O. *ChemCatChem* **2014,** *6,* 3286–3305. doi:10.1002/cctc.201402483
12. de Vries, J. G. *Dalton Trans.* **2006,** 421–429. doi:10.1039/b506276b
13. Astruc, D. *Inorg. Chem.* **2007,** *46,* 1884–1894. doi:10.1021/ic062183h
14. Kashin, A. S.; Ananikov, V. P. *J. Org. Chem.* **2013,** *78,* 11117–11125. doi:10.1021/jo402038p
15. Eremin, D. B.; Ananikov, V. P. *Coord. Chem. Rev.* **2017,** *346,* 2–19. doi:10.1016/j.ccr.2016.12.021
16. Bates, J. M.; Lummiss, J. A. M.; Bailey, G. A.; Fogg, D. E. *ACS Catal.* **2014,** *4,* 2387–2394. doi:10.1021/cs500539m
17. Genelot, M.; Dufaud, V.; Djakovitch, L. *Adv. Synth. Catal.* **2013,** *355,* 2604–2616. doi:10.1002/adsc.201300357

18. Sans, V.; Gelat, F.; Burguete, M. I.; Garcia-Verdugo, E.; Luis, S. V. *Catal. Today* **2012,** *196,* 137–147. doi:10.1016/j.cattod.2012.03.036
19. Burguete, M. I.; Erythropel, H.; García-Verdugo, E.; Luis, S. V.; Sans, V. *Green Chem.* **2008,** *10,* 401–407. doi:10.1039/b714977h
20. Altava, B.; Burguete, M. I.; Garcıa-Verdugo, E.; Luis, S. V.; Vicent, M. J. *Tetrahedron* **2001,** *57,* 8675–8683. doi:10.1016/s0040-4020(01)00831-6
21. Galindo, F.; Altava, B.; Burguete, M. I.; Gavara, R.; Luis, S. V. *J. Comb. Chem.* **2004,** *6,* 859–861. doi:10.1021/cc049871l
22. Haas, D.; Hammann, J. M.; Greiner, R.; Knochel, P. *ACS Catal.* **2016,** *6,* 1540–1552. doi:10.1021/acscatal.5b02718
23. Calimsiz, S.; Organ, M. G. *Chem. Commun.* **2011,** *47,* 5181–5183. doi:10.1039/c0cc04835f
24. Atwater, B.; Chandrasoma, N.; Mitchell, D.; Rodriguez, M. J.; Organ, M. G. *Chem. – Eur. J.* **2016,** *22,* 14531–14534. doi:10.1002/chem.201603603
25. Kim, M.; Shin, T.; Lee, A.; Kim, H. *Organometallics* **2018,** *37,* 3253–3258. doi:10.1021/acs.organomet.8b00413
26. Balcells, D.; Nova, A. *ACS Catal.* **2018,** *8,* 3499–3515. doi:10.1021/acscatal.8b00230
27. Yin, S.-C.; Zhou, Q.; Zhao, X.-Y.; Shao, L.-X. *J. Org. Chem.* **2015,** *80,* 8916–8921. doi:10.1021/acs.joc.5b01544
28. Arnold, P. L.; Sanford, M. S.; Pearson, S. M. *J. Am. Chem. Soc.* **2009,** *131,* 13912–13913. doi:10.1021/ja905713t
29. Ross, A. J.; Lang, H. L.; Jackson, R. F. W. *J. Org. Chem.* **2010,** *75,* 245–248. doi:10.1021/jo902238n
30. Khazipov, O. V.; Shevchenko, M. A.; Chernenko, A. Y.; Astakhov, A. V.; Pasyukov, D. V.; Eremin, D. B.; Zubavichus, Y. V.; Khrustalev, V. N.; Chernyshev, V. M.; Ananikov, V. P. *Organometallics* **2018,** *37,* 1483–1492. doi:10.1021/acs.organomet.8b00124
31. Price, G. A.; Bogdan, A. R.; Aguirre, A. L.; Iwai, T.; Djuric, S. W.; Organ, M. G. *Catal. Sci. Technol.* **2016,** *6,* 4733–4742. doi:10.1039/c6cy00331a
32. Price, G. A.; Hassan, A.; Chandrasoma, N.; Bogdan, A. R.; Djuric, S. W.; Organ, M. G. *Angew. Chem., Int. Ed.* **2017,** *56,* 13347–13350. doi:10.1002/anie.201708598
33. Burguete, M. I.; García-Verdugo, E.; Garcia-Villar, I.; Gelat, F.; Licence, P.; Luis, S. V.; Sans, V. *J. Catal.* **2010,** *269,* 150–160. doi:10.1016/j.jcat.2009.11.002
34. Sans, V.; Gelat, F.; Karbass, N.; Burguete, M. I.; García-Verdugo, E.; Luis, S. V. *Adv. Synth. Catal.* **2010,** *352,* 3013–3021. doi:10.1002/adsc.201000528
35. Karbass, N.; Sans, V.; Garcia-Verdugo, E.; Burguete, M. I.; Luis, S. V. *Chem. Commun.* **2006,** 3095–3097. doi:10.1039/b603224a
36. Gil, W.; Boczoń, K.; Trzeciak, A. M.; Ziółkowski, J. J.; Garcia-Verdugo, E.; Luis, S. V.; Sans, V. *J. Mol. Catal. A: Chem.* **2009,** *309,* 131–136. doi:10.1016/j.molcata.2009.05.007
37. Valentini, F.; Mahmoudi, H.; Bivona, L. A.; Piermatti, O.; Bagherzadeh, M.; Fusaro, L.; Aprile, C.; Marrocchi, A.; Vaccaro, L. *ACS Sustainable Chem. Eng.* **2019,** *7,* 6939–6946. doi:10.1021/acssuschemeng.8b06502
38. Mahmoudi, H.; Valentini, F.; Ferlin, F.; Bivona, L. A.; Anastasiou, I.; Fusaro, L.; Aprile, C.; Marrocchi, A.; Vaccaro, L. *Green Chem.* **2019,** *21,* 355–360. doi:10.1039/c8gc03228a
39. Burguete, M. I.; García-Verdugo, E.; Luis, S. V.; Restrepo, J. A. *Phys. Chem. Chem. Phys.* **2011,** *13,* 14831–14838. doi:10.1039/c1cp20970a
40. Astakhov, A. V.; Khazipov, O. V.; Chernenko, A. Y.; Pasyukov, D. V.; Kashin, A. S.; Gordeev, E. G.; Khrustalev, V. N.; Chernyshev, V. M.; Ananikov, V. P. *Organometallics* **2017,** *36,* 1981–1992. doi:10.1021/acs.organomet.7b00184
41. Biffis, A.; Centomo, P.; Del Zotto, A.; Zecca, M. *Chem. Rev.* **2018,** *118,* 2249–2295. doi:10.1021/acs.chemrev.7b00443
42. Lozano, P.; García-Verdugo, E.; Karbass, N.; Montague, K.; De Diego, T.; Burguete, M. I.; Luis, S. V. *Green Chem.* **2010,** *12,* 1803–1810. doi:10.1039/c0gc00076k

License and Terms

BEILSTEIN JOURNAL OF ORGANIC CHEMISTRY

A proposed sustainability index for synthesis plans based on input provenance and output fate: application to academic and industrial synthesis plans for vanillin as a case study

John Andraos

Full Research Paper

Open Access

Address:
CareerChem, 504-1129 Don Mills Road, Toronto, ON, M3B 2W4, Canada

Email:
John Andraos - c1000@careerchem.com

Keywords:
Borda count; green chemistry; input enthalpic energy; process mass intensity; poset dominance analysis; Rowan solvent greenness index; sacrificial reagent; sustainability; sustainable chemistry

Beilstein J. Org. Chem. **2020,** *16,* 2346–2362.
https://doi.org/10.3762/bjoc.16.196

Received: 04 October 2019
Accepted: 02 September 2020
Published: 25 September 2020

This article is part of the thematic issue "Green chemistry II".

Associate Editor: L. Vaccaro

Abstract

This paper describes a sustainability index (SI) as a quantitative measure of "sustainability" applicable to synthesis plans based on the provenance of input materials and energy sources and the fate of output waste products. The index is computed as the root-mean-square average of the following four parameters: mass fraction of valorized inputs (F_{VI}), mass fraction of valorized outputs (F_{VO}), mass fraction of valorized target product (F_{VP}), and input enthalpic energy fraction arising from renewable energy sources (F_{RE}). Valorized input materials originate from renewable, recycled, or reclaimed sources. Valorized output materials are destined for recycling or reclaiming so that they may be used in the same or other chemical processes. Valorized target product refers to that portion of the target product that is actually used for its intended purpose. Renewable energy sources are defined as originating from hydroelectric, wind, solar, geothermal, and biomass sources. The computation of SI is illustrated for 22 synthesis plans of the high commodity flavour ingredient vanillin from biofermentation, chemical synthesis, and solvent extraction processes. In addition, these plans are compared and ranked according to Borda count and poset (partially ordered set) pairwise dominance analyses using the following attributes: process mass intensity (PMI), sacrificial reagent (SR) consumption, input enthalpic energy (IEE) consumption, Rowan solvent greenness index (RSGI), and sustainability index (SI).

Introduction

The words "sustainable" and "sustainability" are nowadays routinely used throughout common speech and the popular press, including published modern chemistry literature, when discussing topics related to pressing issues such as preservation of the environment, climate change, and resource management. However, in all of this enormous volume of information avail-

able in the popular press, corporate mission statements, and scientific literature there does not exist an agreed consensus-based and widely used *quantitative* definition of what these words actually mean. A recent article published in Chemical and Engineering News in 2019 [1] nicely highlighted the problem in the context of distinguishing the terms *green chemistry* from *sustainable chemistry*. It was noted that "the term *sustainable chemistry* has been introduced more recently and possesses countless definitions put forth by individuals, companies, trade associations, non-profit organizations, and governmental entities". Also noted was the "key need [to come up with] a standardized approach for assessing the sustainability of chemical processes or products", and the need for "better information on product content throughout the supply chain and more complete data on the health and environmental impacts of chemicals throughout their life-cycle" in order for "stakeholders [to] make informed decisions that compare the sustainability of various products". A literature search on the subject of *sustainability metrics* in chemistry journals revealed a few publications that addressed the problem of quantifying and measuring what sustainability is [2-10]. Most of the discussions revolved around extended thermodynamics analysis, energy consumption, and energy resource considerations from fossil-fuel derived and renewable sources. Dutch and Belgian chemical engineers proposed an extended thermodynamic analysis considering exergy and lost work to address the sustainability potential of the chemical process industry [2-4]. Horvath and co-workers put forth the following sustainability metrics defined for biomass-based carbon chemicals using ethanol equivalent as a common basis: sustainability value of resource replacement, sustainability value of the fate of waste, and sustainability indicator [5-7]. Sikdar defined sustainability as the interplay of three domains: economic aspects, environmental aspects, and social aspects [8]. Sheldon and Sanders defined sustainability metrics for the production of chemicals from renewable biomass in terms of four criteria: material and energy efficiency, land use, and process economics [9]. Very recently, Egyptian and Lebanese scientists put forward an industrial environmental index obtained from process, environmental health and safety, and life cycle assessment metrics to assess the sustainability of industrial solvent-based processes [10].

Continuing our goal over the last decade of developing practical and easy-to-understand metrics that can be used by any chemist or chemical engineer, in this work we introduce a quantitative description of sustainability that is directly applicable to assess synthesis plans. Synthesis plans represent the heart and soul of what chemists create in the laboratory and chemical engineers scale up and optimize in the chemical plant. Hence, any chance of developing a quantitative definition of sustainability that addresses the needs and concerns already pointed out must focus on assessing the performance of synthesis plans according to some set of measurable parameters. This is a very important aspect in the evolution of scientific ideas that begin with qualitative statements often worded in fuzzy general language, but then develops into concrete statements written in the language of mathematics that make explicit what parameters need to be measured, how they are related to one another, and what outcome scenarios are predicted from them. The net result is that vagaries are removed from the discussion and hence the subject is presented in a rigorous and understandable format that is ultimately taken seriously. Since it is evident that synthesis plans begin with input resources and ultimately produce output products, it then becomes necessary to analyze both the origins of all inputs and the fate of all outputs in order to determine the sustainability potential of a given synthesis plan. In order to achieve our objective, we decided to begin from two already established main ideas. The first is the comparison of the rate of depletion of each resource (material or energy) used in a synthesis plan versus the rate of that resource's renewal as pointed out by Horvath and co-workers [5-7]. Clearly, sustainability is possible if the rate of renewal exceeds the rate of depletion. The second is the concept of "provenance" borrowed from the authentication of objects of art as genuine by art dealers and museum curators during the selling and purchasing of them at auctions. The provenance of an object of art potentially links it to its true creator. Obtaining provenance constitutes amassing traceable hard evidence that links the original artist and his or her work via the chain of its ownership through time from its creation to the present day. Provenances are necessary to establish the authenticity of a piece of art and thus distinguish it from a forgery. The concept of provenance or tracing has also been applied in other fields including computer science, data integrity management, petrology, archaeology, seed preservation, food authenticity, and palaeontology [11]. In the context of synthesis plans, it is possible to apply the concept of provenance to the origins of all material and energy resources used in a given plan in order to distinguish whether that resource originated from a renewable or non-renewable source. By the same reasoning, it is also possible to trace the fate of all waste outputs of a given plan in order to distinguish whether they will end up as useable or non-usable waste. From this discussion it becomes obvious that the success of tracing both provenance of inputs and fate of outputs involved in a synthesis plan in order to estimate the degree of its sustainability is based entirely on the full disclosure of supply chains and end-of-life chains throughout the chemistry enterprise. Such open access and transparent information, however, necessarily exposes vulnerabilities in those chains such as privacy with respect to business-to-business dealings and general proprietary protection that may not be comfortable to accept or possible to reveal

to producers, suppliers, vendors, and end users. These concerns are at the root cause of much of the vagueness and trepidation associated with the practical application of sustainability as already pointed out earlier [1]. Nevertheless, in this work we provide a framework that can be implemented to estimate the degree of sustainability of synthesis plans following these ideas once such information is made available whether internally for a privileged few or externally for all to see. With this view in mind, in the next sections we show a step-by-step development of our methodology and then apply it to the assessment of 22 synthesis plans of the high commodity flavour ingredient vanillin.

Methodology

We begin the development of a quantitative description of sustainability applied to synthesis plans by starting with the mathematical statement of the law of mass balance given by Equation 1.

$$M_{total\ inputs} = M_{total\ outputs} \tag{1}$$

where the M quantities refer to masses in grams. The left-hand side of Equation 1 will be governed by the provenance of input materials and the right-hand side will be governed by the fate of output materials. Hence, the mass of total inputs can be subdivided into two parts: mass of valorized inputs (M_{VI}) and mass of non-valorized inputs (M_{NVI}) according to Equation 2.

$$M_{total\ inputs} = M_{VI} + M_{NVI} \tag{2}$$

In this formulation, valorized inputs are defined as those that are derived from sources such that their rate of renewal is greater than or equal to their rate of depletion, and non-valorized inputs are defined as those that are derived from sources where the converse rate condition is true. Specifically, inputs derived from renewable or recycled sources such as biomass, scrap metals, or retrieved byproducts from other processes are considered valorized, and inputs derived from non-renewable sources such as fossil fuels and virgin mineral ores are considered non-valorized. The definition of F_{VI} used here extends that of renewables intensity [12]. Similarly, the mass of total outputs may be subdivided into three parts: waste mass of valorized outputs (W_{VO}), waste mass of non-valorized outputs (W_{NVO}), and mass of target product ($M_{product}$) as shown in Equation 3.

$$M_{total\,outputs} = W_{total} + W_{product} = W_{VO} + W_{NVO} + M_{product} \tag{3}$$

Valorized waste outputs are those that may be recycled or reclaimed for use in the same synthesis plan or other unrelated synthesis plans if they are sold to other chemical enterprises in the chemical commodity supply chain. These may include reaction and work-up solvents or reaction byproducts than can be chemically converted to starting materials, or byproducts that can be reclaimed for use in other chemical processes. Non-valorized waste outputs are those that will end up as "dead waste" whether or not they undergo treatment before release into the four main environmental compartments of air, water, soil, and sediment. Based on the definition of variables in Equations 1, 2, and 3 we can then define the following key parameters. The process mass intensity (PMI) [13] is defined according to Equation 4.

$$PMI = \frac{M_{VI} + M_{NVI}}{M_{product}} = \frac{M_{total\,inputs}}{M_{product}} \tag{4}$$

The mass fractions of valorized inputs (F_{VI}) and valorized waste outputs (F_{VO}) are defined according to Equation 5 and Equation 6.

$$F_{VI} = \frac{M_{VI}}{M_{total\,inputs}} = \frac{M_{VI}}{M_{VI} + M_{NVI}} \tag{5}$$

$$F_{VO} = \frac{W_{VO}}{W_{VO} + W_{NVO}} \tag{6}$$

We can also define a mass fraction of valorized target product (F_{VP}) according to Equation 7 that describes the proportion of target product of a synthesis plan that is actually used for its intended purpose. This takes into account the end-of-life stage of the life cycle of the target product where part of it will end up as "dead waste".

$$F_{VP} = \frac{M_{product} - M^*_{product}}{M_{product}} \tag{7}$$

where $M^*_{product}$ is the mass of target product that is destined to be wasted. For example, if the target product of a synthesis plan is a pharmaceutical compound a certain fraction of its manufacture will be used as intended by patients; however, there will be a remaining fraction that will be destined as non-usable waste via natural excretion by the human body and more importantly via disposal by pharmacies when the medicine passes its recommended safe expiry date. The estimation of F_{VP} will always rely on significant assumptions and guesswork since there are no proper centralized data kept for tracking end-of-life waste of any product manufactured in the chemical industry. Hence, for the purposes of calculating SI, estimating $M^*_{product}$ is the weakest link.

Having described the three mass fractions related to the provenance of input materials and fate of output materials, we may now examine the energy source provenance for conducting all heating and cooling operations involved in all reaction steps in a synthesis plan. We define a total input enthalpy energy, $(IEE)_{total}$, as shown in Equation 8 where it is divided into renewable and non-renewable energy sources.

$$(IEE)_{total} = (IEE)_{renewable} + (IEE)_{non-renewable} \quad (8)$$

The explicit formulation of $(IEE)_{total}$ is shown in Equation 9 where it is obtained as a sum of all energy consumptions as a result of heating and cooling over all input materials used in a synthesis plan above or below a reference state representing the ambient temperature and pressure conditions of 298 K and 1 atm, respectively. Temperature deviations are governed by temperature dependent heat capacity relationships for each substance, and pressure deviations are governed by volume-temperature relationships according to some specified equation of state. In practice, the contribution to IEE from temperature deviations far exceeds that from pressure deviations for reaction pressures below 100 atm. In cases where the reaction pressure exceeds 100 atm, the Redlich–Kwong equation of state formalism [14] was used in this work for computing IEE values.

$$(IEE)_{total} = \sum_{j=1}^{total\,inputs} (IEE)_j = \sum_{j=1}^{total\,inputs} \left[moles_j \left(\begin{array}{l} \int_{298}^{T_{rxn}} C_{p,j}(T)dt + \int_{1}^{0} \left[V - T\left(\frac{\partial V}{\partial T}\right)_p \right]_{T=298} dp \\ + \int_{0}^{p_{rxn}} \left[V - T\left(\frac{\partial V}{\partial T}\right)_p \right]_{T=T_{rxn}} dp \end{array} \right) \right] \quad (9)$$

Similar to the mass fractions defined in Equations 5–7, we can define an analogous input enthalpic energy fraction arising from renewable energy sources (F_{RE}) as shown in Equation 10. This definition is similar to renewability index proposed earlier [15].

$$F_{RE} = \frac{(IEE)_{renewable}}{(IEE)_{total}} \quad (10)$$

In the present formalism we define the following energy sources as renewable: hydroelectric, solar, wind, geothermal, and biofuels; and the following energy sources as non-renewable: coal, other fossil-fuels such as petroleum and natural gas, and nuclear. Furthermore, following recently published energy mix data [16,17] we set F_{RE} = 0.35 for all synthesis plans that were published on or after the year 2000 and F_{RE} = 0 for all synthesis plans that were published before 2000. We chose the year 2000 as an arbitrary boundary time frame since it marked the beginning of the 21st century when ideas of sustainability began to take root in the general societal consciousness.

Taking into account the four fractional values F_{VI}, F_{VO}, F_{VP}, and F_{RE} we can define an overall sustainability index (SI) which is the root-mean-square average of these four fractional quantities as shown in Equation 11.

$$SI = \frac{\sqrt{(F_{VI})^2 + (F_{VO})^2 + (F_{VP})^2 + (F_{RE})^2}}{\sqrt{4}} = \frac{1}{2}\sqrt{(F_{VI})^2 + (F_{VO})^2 + (F_{VP})^2 + (F_{RE})^2} \quad (11)$$

Since each of these fractions has values ranging between 0 and 1, then the magnitude of SI will also have a value ranging between 0 and 1. This mathematical formalism conveniently allows the writing down of a quantitative definition of sustainability applicable to synthesis plans. A given synthesis plan can therefore be said to be completely "sustainable" if the following conditions are satisfied: F_{VI} = 1, F_{VO} = 1, F_{VP} = 1, F_{RE} = 1, and SI = 1. Conversely, a given synthesis plan can be said to be completely "unsustainable", if the following conditions are satisfied: F_{VI} = 0, F_{VO} = 0, F_{VP} = 0, F_{RE} = 0, and SI = 0.

Having this new sustainability metric in hand, we can then use it along with process mass intensity (PMI), sacrificial reagent (SR) consumption, input enthalpic energy (IEE), and Rowan solvent greenness index (RSGI) as key attributes to rank any kind of synthesis plan or chemical process. PMI and IEE have already been defined in Equations 4 and 9. SR consumption defined in Equation 12 quantifies the mass fraction of reagents whose atoms do not contribute to the chemical structure of the final target product of the synthesis plan. Following the concept of atom economy [18], this attribute is important in designing syntheses that maximize the use of all atoms in input reagents towards the final product structure while minimizing waste byproducts as a consequence of producing the intended intermediates over the course of the synthesis sequence. The RSGI [19] given in Equation 13 is a convenient metric that is used to quantify the relative environmental, toxicological, and safety-hazard impacts of solvents used in reaction, work-up, and purification procedures. It is defined using an overall solvent index (OSI) that scales between 0 and 12 spanning the benign solvent water to the non-benign solvent benzene. Equation 14 and Equation 15 show the explicit dependence of OSI on 15 physical, toxicological, and hazard parameters.

$$SR = \frac{\sum mass\ sacrificial\ reagents}{\sum total\ mass\ reagents} \quad (12)$$

$$RSGI = \sum_i m_i (OSI_{12})_i \tag{13}$$

where m_i is the mass of solvent i and OSI_{12} is defined as a normalized quantity over a set of solvents as shown in Equation 14.

$$(OSI_{12})_i = 12\left(\frac{OSI_i - OSI_{\min}}{OSI_{\max} - OSI_{\min}}\right) \tag{14}$$

where OSI_{min} and OSI_{max} are the minimum and maximum values of OSI for a set of solvents and OSI_i for a given solvent i is given by Equation 15.

$$\begin{aligned} OSI_i = {} & 2\left(M_{OEL,i} + M_{LD50,i} + M_{LC50,i}\right) + M_{GWP,i} \\ & + M_{SEP,i} + M_{ODP,i} + M_{ABP,i} + M_{BCP,i} + M_{PER,i} \\ & + M_{soil,i} + M_{half\ life,i} + M_{aqua,i} + M_{Q-phrase,i} \\ & + M_{SD,i} + M_{FP,i} \end{aligned} \tag{15}$$

where the metric parameters (M) cover occupational exposure limit (OEL, ppm), LD_{50} (ingestion toxicity, mg/kg), LC_{50} (inhalation toxicity, g m^{-3} for 4 h), global warming potential (GWP, unitless), smog formation potential (SFP, unitless), ozone depletion potential (ODP, unitless), acidity-basicity potential (ABP, unitless), bioconcentration potential (BCP, unitless), persistence potential (PER, unitless), soil sorption coefficient (soil, K_{oc}), half-life of solvent in environment (half-life, h), aquatic toxicity to fish (aqua, mg/L for 96 h), Q-phrase potential (Q-phrase, unitless), skin dose (SD, mg), and flash point (FP, degrees K). Table 1 shows a revised and expanded formatted listing of normalized OSI values for various solvents used in the chemical industry.

In our past work [20] describing a presentation of a "standardized process green synthesis report" for chemical syntheses of pharmaceutical compounds we were able to demonstrate the Borda count [21-24] and poset (partially ordered set) pairwise dominance [25] ranking algorithms based on the four attributes PMI, SR, IEE, and RSGI. In the present work, we can now add SI as a fifth key attribute as part of those ranking algorithm analyses which takes into account sustainability potential as well as material and energy consumption and environmental and safety-hazard impacts. In order to demonstrate these ideas, we chose to examine 22 academic and industrial synthesis plans for the manufacture of 1 kg of vanillin since this high commodity flavour chemical is ideally suited to the present investigation owing to its varied methods of synthesis spanning classical chemical synthesis, biofermentation, and solvent ex-

Table 1: Revised summary of overall solvent index (OSI) for various organic solvents used in the pharmaceutical industry.

OSI_{12}[a]	solvent
12.000	benzene
10.597	chlorobenzene
10.350	aniline
10.150	toluene
10.130	nitrobenzene
10.077	pyridine
9.885	triethylamine
9.774	*o*-xylene
9.773	*p*-xylene
9.703	*m*-xylene
9.677	1,2-dichlorobenzene
9.653	1,2-dichloroethane
9.324	formaldehyde
9.048	*n*-hexane
8.879	methylcyclohexane
8.777	cyclohexane
8.534	2-methyltetrahydrofuran
8.451	carbon tetrachloride
8.421	diethyl ether
8.365	dimethylacetamide
8.309	acetic anhydride
8.090	chloroform
8.016	carbon disulfide
7.985	tetrahydrofuran
7.927	acetic acid
7.875	*tert*-butanol
7.852	cyclopentyl methyl ether
7.734	petroleum ether
7.727	1,4-dioxane
7.647	isopropyl acetate
7.603	acetonitrile
7.597	ethyl acetate
7.592	*p*-*N*,*N*-dimethyltoluidine
7.429	*n*-heptane
7.425	trifluorotoluene
7.402	dimethylformamide
7.365	methyl *tert*-butyl ether
7.323	hexamethylphosphoric triamide
7.278	methyl ethyl ketone
7.129	dichloromethane
7.074	acetone
6.966	1-heptanol
6.952	1-propanol
6.732	methyl propionate
6.719	isopropanol
6.706	trichloroethylene
6.644	*n*-butanol
6.547	nitromethane
6.505	*n*-pentane

Table 1: Revised summary of overall solvent index (OSI) for various organic solvents used in the pharmaceutical industry. (continued)

6.108	methyl formate
5.905	methyl acetate
5.859	ethylene glycol monomethyl ether
5.772	isoamyl alcohol
5.672	amyl acetate
5.620	isoamyl acetate
5.593	sec-butanol
5.495	*N*-methylpyrrolidinone
5.426	methanol
5.360	isobutyl acetate
5.352	anisole
5.298	*tert*-amylalcohol
5.268	cyclopentanone
5.210	trifluoroacetic acid
5.110	isopropyl ether
5.106	1-octanol
4.773	ethanol
4.751	ethylene glycol
4.538	thionyl chloride[b]
4.535	dimethoxymethane
4.474	isooctane
4.224	dimethyl carbonate
4.182	glycol diacetate
3.908	diglyme
3.795	sulfolane
3.679	sCO_2
3.266	ethylene glycol dimethyl ether
3.250	triethylene glycol monomethyl ether
3.027	propylene carbonate
2.803	dimethyl sulfoxide
2.485	propylene glycol
2.233	dimethylisosorbide
0.000	water

[a]Underlined entries indicate benign performance ($OSI_{12} \leq 5$); italicized entries indicate intermediate performance ($5 < OSI_{12} < 8$); and bold-formatted entries indicate worst performance ($OSI_{12} \geq 8$). [b]Missing LC_{50} (oral), LD_{50} (inhalation), and aquatic toxicity data; used as a dual reagent and solvent in industrial syntheses of acid chlorides from carboxylic acids.

traction procedures from the natural source vanilla beans. We chose these particular examples from the literature since they had the most detailed experimental procedures from which the set of discussed metrics could be reliably determined and then ranked. Figure S1 found in Part 1 of Supporting Information File 1 shows all of the schemes pertaining to the 22 synthesis plans listed in alphabetical order along with temperature and pressure conditions for each reaction step. Table 2 summarizes the same alphabetized list showing the plan codes, starting materials used, and type of chemical process employed. Four plans involved biofermentation from D-glucose, ferulic acid, or isoeugenol [26-30]; five plans involved chemical synthesis from wood-derived starting materials (lignosulfonic acid liquor or sawdust) [31-37]; seven plans involved chemical synthesis from either fossil-fuel or natural product-derived starting materials (guaiacol, eugenol, isoeugenol, and 4-hydroxybenzaldehyde) [38-43]; and five plans involved solvent extraction procedures either by percolation, Soxhlet, or supercritical fluid methods using cured vanilla beans that were either whole or were cut up as starting material [44-46].

Results and Discussion

Sustainability of vanillin plans

The exercise of partitioning input materials according to their provenance and output materials according to their fate is extremely challenging because it requires a completely transparent knowledge and access to the entire network supply and end-of-life chains that constitute the chemical industry enterprise. In practice, when reading experimental sections in journal publications and patents, one has limited or no access to such background knowledge even though authors may disclose the names of chemical suppliers of the starting materials they used in their own work. It is a fair comment to say that authors themselves may not know or care to know the chain of supply of those starting materials so long as they have them in hand in a sufficiently pure condition to carry out their own research agenda. In any event, the task of estimating a quantitative measure of sustainability of any given synthesis plan according to the formalism of Equation 11 will require significant assumptions to be made. For the purpose of our work, which is meant to be illustrative only in the numerical methods employed, we implemented the following assumptions in the calculation of SI for all 22 plans of vanillin:

(1) If ethanol is used as an input material then 10% of it was assumed to originate from renewable sources (i.e., biomass), if the publication is dated after 1990 since that is the approximate time frame when biofuels were made widely available in the market.

(2) Water was considered a renewable input material due to the circulating global hydrological cycle.

(3) Mineral salts, metal-derived catalysts, and all non-aqueous and non-biologically derived materials from fossil fuels or ores were considered non-renewable inputs since their rate of renewal occur on geological time scales that are several orders of magnitude longer than organism time scales.

(4) Lignosulfonic acid liquor and sawdust were considered renewable inputs since they ultimately originate from trees. Ferulic acid and D-glucose were considered renewable inputs

Table 2: Summary of plan codes, starting materials, and process types for 22 synthesis plans of vanillin.

Alphabetized list of vanillin synthesis plans	plan code	starting material	process
Borregaard synthesis	p1	lignosulfonic acid liquor	chemical synthesis
Collins chemical	p2	isoeugenol	chemical synthesis
Eilks Pt 1	p3	isoeugenol	chemical synthesis
Eilks Pt 2	p4	isoeugenol	chemical synthesis
Faith	p5	lignosulfonic acid liquor	chemical synthesis
Frost	p6	D-glucose	biofermentation
Givaudan–Roure	p7	ferulic acid	biofermentation
Haarmann and Reimer	p8	isoeugenol	biofermentation
Hibbert	p9	lignosulfonic acid liquor	chemical synthesis
Ji	p10	guaiacol	chemical synthesis
Lampman	p11	sawdust	chemical synthesis
Lesage–Meesen	p12	ferulic acid	biofermentation
Mayer	p13	eugenol	chemical synthesis
Mexican group SFE	p14	cured vanilla pods	solvent extraction
Mottern	p15	guaiacol	chemical synthesis
Ontario Paper Co.	p16	lignosulfonic acid liquor	chemical synthesis
percolation extraction cut	p17	cured vanilla pods	solvent extraction
percolation extraction whole	p18	cured vanilla pods	solvent extraction
Sorensen–Mehlum	p19	sawdust	chemical synthesis
Soxhlet extraction cut	p20	cured vanilla pods	solvent extraction
Soxhlet extraction ground	p21	cured vanilla pods	solvent extraction
Taber	p22	4-hydroxybenzaldehyde	chemical synthesis

since they originate from sugar beet biomass [47] and other cellulosic biomass feedstocks, respectively. Isoeugenol and eugenol were chosen to originate from the natural product clover oil since 80% by weight of this essential oil is eugenol [48], and isoeugenol is directly obtained from eugenol by base-catalyzed isomerization.

(5) Oxygen from air was considered a renewable input for the oxidation of lignosulfonic acid liquors since it is produced as a natural waste byproduct of photosynthesis.

(6) Spent vanilla beans were considered reusable waste since they can be composted into biomass.

(7) Supercritical carbon dioxide was considered reusable waste since it can be recycled in the same solvent extraction process via continuous pressurization and depressurization cycles.

(8) A renewable energy source contribution of 35% (F_{RE} = 0.35) was assigned, if the publication is dated on or after the year 2000 for reasons discussed earlier.

(9) Since vanillin is mainly used as a food flavouring agent, 70% of it was assumed to be actually used in the food industry (F_{VP} = 0.7) and 30% of it will end up as part of the food waste stream which mirrors recent statistics [49-53] that assert that about a third of all foodstuffs produced will end up wasted along supply chains and by end-of-use consumers.

In order to facilitate computation of SI an Excel-based calculator was developed that can be used for any synthesis plan once all inputs and outputs are identified (see Supporting Information File 2). Firstly, for a given synthesis plan, all scaled masses of input and output materials are entered for the production of 1 kg of vanillin. Scaled mass data for each plan are found in Part 2 of Supporting Information File 1. Secondly, valorized input and output materials are selected according to the assumptions listed above. Finally, F_{RE} is set to 0.35 or 0 for plans published after or before the year 2000, respectively and F_{VP} is set at 0.7. Figure 1 shows radial diamond diagrams depicting the four fractions for the leading eight most sustainable plans representing biofermentation and solvent extraction methods. The main reason for their high SI scores is the combined high values of F_{VI} and F_{VO} close to unity in each case. For the solvent extraction procedures low values of F_{VI} are found if the mass ratio of solvent to vanilla bean is very high as is the case for the percolation extraction cut, Soxhlet extraction cut, and Mexican group SFE plans. For the case of

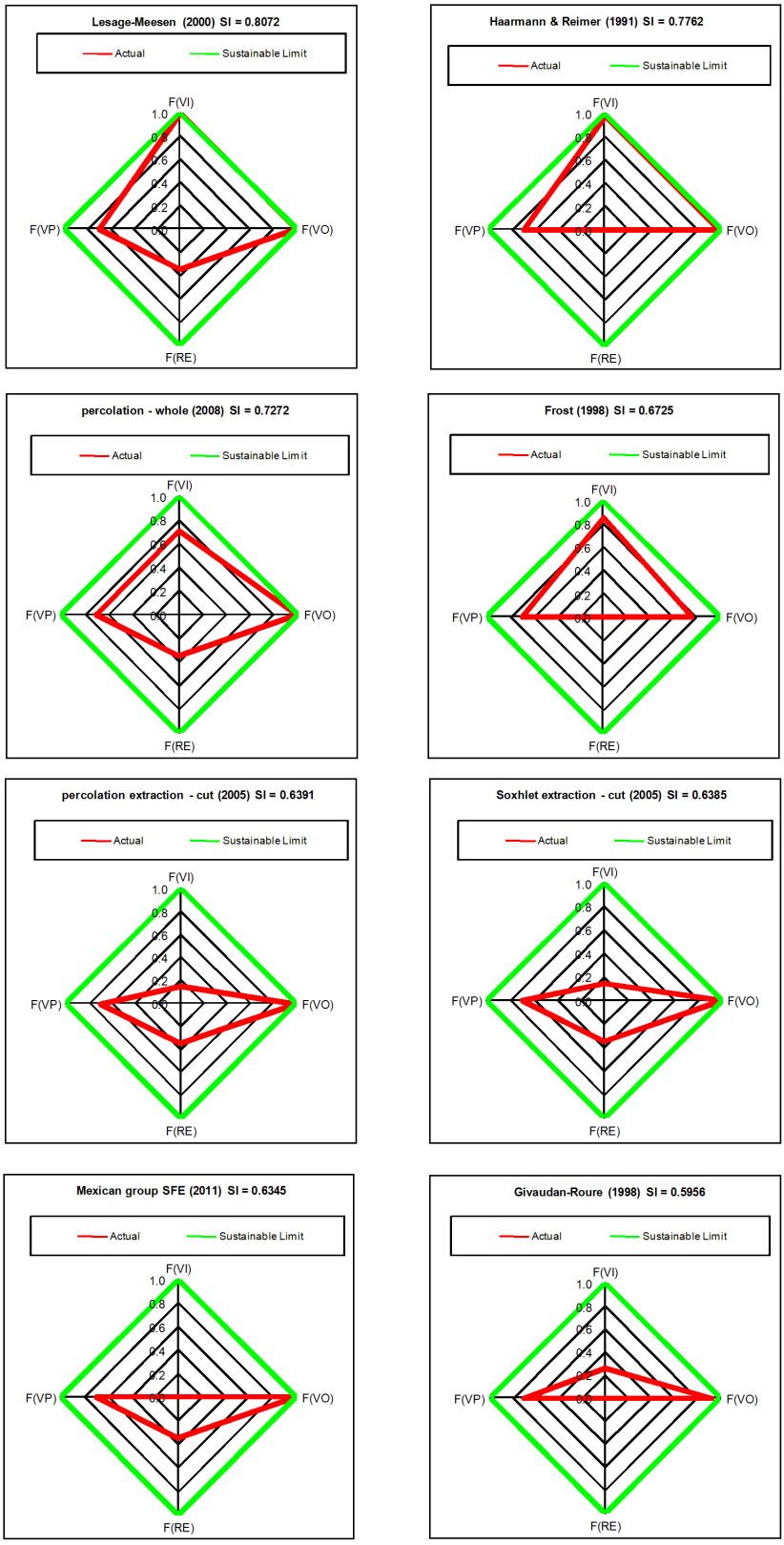

Figure 1: Radial diamond diagrams illustrating the sustainability index (SI) computed based on F_{VI}, F_{VO}, F_{VP}, and F_{RE} for the top eight scoring vanillin synthesis plans.

supercritical carbon dioxide used as an extraction solvent, the main drawback is that industrial carbon dioxide is classified as originating from a non-renewable mineral resource (mainly calcium carbonate) and that the mass ratio of sCO_2 solvent to vanilla beans is 435:1. Synthesis plans based on chemical syntheses from lignosulfonic acid liquor, guaiacol, eugenol and isoeugenol have F_{VO} values of 0 since none of their solvent and waste byproducts are reuseable. However, F_{VI} values for these syntheses range between 0 (Eilks – Pt 2) and 0.898 (Borregaard) with an average value of 0.414 over 14 plans. With respect to renewable energy sources, only nine out of the 22 plans were assigned a value of 0.35 for F_{RE} since their publications appeared on or after the year 2000.

Table 3 summarizes numerical results of the 5 attributes PMI, SR, IEE, RSGI, and SI for all 22 synthesis plans of vanillin. From this list we observe that chemical syntheses tend to have lower PMI values and biofermentation and solvent extraction methods tend to have higher PMI values due to higher solvent consumption in the latter group. Ten out of the 22 plans had SR values of 0 and the rest of the plans had higher values in the range 1.2 to 92, except for the Eilks – Pt 1 and Lampman plans that used isoeugenol and sawdust, respectively, as starting materials. With respect to energy consumption, the two percolation extraction procedures using cut or whole cured vanilla beans with no heating of solvents had the lowest IEE value of 0. The other plans had significant energy demands for various reasons. The methods starting from lignosulfonic acid liquors were conducted under elevated temperature and pressure conditions of 200 °C and 100 atm. The SFE method using a high amount of sCO_2 required pressurization conditions of about 200 atm. The biofermentation methods, though they were conducted under biologically ambient conditions of 37 °C and 1 atm, had high IEE values as a result of the high mass of aqueous nutrient broths required for their operation relative to the small mass of starting materials. For example, the most sustainable Lesage–Meesen plan with the highest SI value of 0.8072 had an IEE value of 939,475 kJ/kg owing to the 1254:1 combined aqueous nutrient medium-to-substrate ratio. With respect to solvent impacts, the Givaudan–Roure, Lesage-Meesen, and Haarmann and Reimer biofermentation procedures had RSGI values of 0. The only other plan with a zero solvent impact was the improved lignosulfonate method of Borregaard carried out in aqueous solution. The traditional chemical synthesis methods had more of a solvent impact due to the use of the following solvents listed in descending order of impact according to OSI values given in Table 1: benzene (12.000), aniline (10.350), toluene (10.150), nitrobenzene (10.130), cyclohexane (8.777), diethyl ether

Table 3: Summary of computed values for five attributes for 22 synthesis plans of vanillin.

Alphabetized list of vanillin synthesis plans	PMI (kg/kg)	SR (kg/kg)	IEE (kJ/kg)	RSGI (kg/kg)	SI
Borregaard synthesis	84	8.6	169046	0	0.5756
Collins chemical	38	1.2	50440	38	0.4603
Eilks Pt 1	1712	341	17309	4492	0.4866
Eilks Pt 2	147	0	2881	673	0.3907
Faith	50	0	29286	6	0.4519
Frost	15973	92	578763	16369	0.6725
Givaudan–Roure	21	0	795	0	0.5956
Haarmann and Reimer	1159	0	9388	0	0.7762
Hibbert	803	71	1005329	3768	0.4207
Ji	3843	45	325200	24670	0.3914
Lampman	32540	9845	2398980	112106	0.3676
Lesage–Meesen	19434	30	939475	0	0.8072
Mayer	26	10	20989	163	0.3704
Mexican group SFE	7513	0	1678005	27578	0.6345
Mottern	125	0	2181	277	0.4551
Ontario Paper Co.	730	32.5	688521	2101	0.4689
percolation extraction cut	831	0	0	3727	0.6391
percolation extraction whole	1028	0	0	1579	0.7272
Sorensen–Mehlum	563	29.5	653838	1952	0.4171
Soxhlet extraction cut	582	0	50219	2644	0.6385
Soxhlet extraction ground	5332	0	676694	16828	0.4246
Taber	1943	1.4	28138	12327	0.3946

(8.421), acetic anhydride (8.309), petroleum ether (7.734), ethyl acetate (7.597), *N,N*-dimethyltoluidine (7.592), methyl *tert*-butyl ether (7.365), dichloromethane (7.129), methanol (5.426), and ethanol (4.773). The Lampman plan had the highest overall RSGI value of 112,106 kg/kg vanillin due to the high masses of impactful solvents employed to obtain 1 kg of vanillin product, namely, nitrobenzene, diethyl ether, and cyclohexane.

Ranking of vanillin plans

Once numerical values of PMI, SR, IEE, RSGI, and SI are available for a given set of synthesis plans to a common target product, it is possible to use some kind of ranking algorithm to identify which ones have the highest overall performances based on these five attributes. From our previous work [20] we compared and contrasted the Borda positional counting method [21-24], established in 1781 by Jean-Charles de Borda (1733–1799), and the poset pairwise dominance analysis method [25] on 6 synthesis plans for the pharmaceutical apixaban. In implementing the Borda count method we first list the plans in ascending order of PMI, SR, IEE, and RSGI so that plans having the lowest values for these attributes are ranked highest; and we list the plans in descending order of SI so that plans having the highest values of SI are ranked highest. Since in this analysis there are 22 vanillin plans to consider the top ranking plan in any given list is assigned a point value of 22 and the lowest ranking plan is assigned a point value of 1 with all other plans having intermediate points accordingly. The maximum Borda count score corresponds to the number of plans considered in the set. In cases of plans having the same numerical values for a given attribute, they are assigned the same Borda count score. For example, for the SR attribute there are 10 plans that have an SR value of 0. Hence, each of them is assigned a Borda count score of 22 and the following lower ranking plans are successively given lower values in descending order. In this case the lowest ranking SR plan is given a Borda count score of 10. Once all Borda count scores are determined for all plans for each attribute, the scores for each plan are added up and these summed scores are ranked from highest to lowest. Table 4 shows the net results of the Borda count method implemented on all 22 synthesis plans for vanillin considered. Part 3 of Supporting Information File 1 contains all of the Borda count data. We observe that the Givaudan–Roure (102) and Haarmann and Reimer (92) biofermentation routes have the highest overall ranking across the 5 attributes according to the Borda count method followed closely by the percolation extraction of whole vanilla beans (90), Faith synthesis from lignosul-

Table 4: Summary of Borda count results for 22 synthesis plans of vanillin.[a]

Alphabetized list of vanillin synthesis plans	PMI points	SR points	IEE points	RSGI points	SI points	overall Borda count
Borregaard synthesis	18	19	11	**22**	14	84
Collins chemical	19	21	12	20	11	83
Eilks Pt 1	8	11	17	10	13	59
Eilks Pt 2	16	**22**	19	17	3	77
Faith	20	**22**	15	21	9	87
Frost	3	12	9	8	19	51
Givaudan–Roure	**22**	**22**	21	**22**	15	**102**
Haarmann and Reimer	9	**22**	18	**22**	21	**92**
Hibbert	12	13	4	11	7	47
Ji	6	14	10	6	4	40
Lampman	1	10	2	4	1	18
Lesage–Meesen	2	16	5	**22**	**22**	67
Mayer	21	18	16	19	2	76
Mexican group SFE	4	**22**	3	5	16	50
Mottern	17	**22**	20	18	10	87
Ontario Paper Co.	13	15	7	14	12	61
percolation extraction cut	11	**22**	**22**	12	18	85
percolation extraction whole	10	**22**	**22**	16	20	90
Sorensen–Mehlum	15	17	8	15	6	61
Soxhlet extraction cut	14	**22**	13	13	17	79
Soxhlet extraction ground	5	**22**	6	7	8	48
Taber	7	20	14	9	5	55

[a]Entries highlighted in bold represent the highest scores in each of the 5 attribute categories.

fonic acid liquor (87), and Mottern four-step chemical synthesis from guaiacol (87). The lowest ranking plan was found to be the Lampman synthesis from sawdust, which had the highest overall process mass intensity (PMI = 32,540 kg/kg), second highest energy consumption requirements (IEE = 2,398,980 kJ/kg), fourth-highest solvent impact ranking (RSGI = 112,106 kg/kg), and lowest sustainability index value (SI = 0.3676).

In implementing the poset pairwise dominance algorithm we determine the number of pairwise attributes and the number of pairwise plan comparisons for each pairwise attribute in order to determine the overall size of the ranking exercise. Since there are 5 attributes the number of pairwise attribute comparisons is C(5,2) = 5!/((5 – 2)! 2!) = 10. The explicit list is as follows: PMI versus SR, PMI versus IEE, PMI versus RSGI, PMI versus SI, SR versus IEE, SR versus RSGI, SR versus SI, IEE versus RSGI, IEE versus SI, and RSGI versus SI. Since there are 22 synthesis plans for vanillin the number of pairwise plan comparisons is C(22,2) = 22!/((22 – 2)! 2!) = 231. Hence, there are overall 10 × 231 = 2310 pairwise comparisons that need to be made in the entire poset analysis. In general, a complete poset analysis on K synthesis plans to a common target product based on m attributes will require C(K, 2)*C(m, 2) = (K!/(K – 2)! 2!)·(m!/(m – 2)! 2!) pairwise comparisons. For a given pairwise plan comparison for a pair of attributes there are two possible outcomes: (a) a comparable pair in which plan A dominates plan B for *both* attributes X and Y; and (b) an incomparable pair in which plan A dominates plan B for attribute X and plan B dominates plan A for attribute Y. For facile visual display of the results upper triangular 22 × 22 matrices are constructed showing green-coloured entries for comparable pairs and red-coloured entries for incomparable pairs. When a comparable pair for a given pairwise attribute comparison is found the dominant plan is identified. This sequence of steps is repeated for each pairwise attribute comparison and then the number of dominant occurrences for each plan are tallied up. Part 4 of Supporting Information File 1 summarizes the ten 22 × 22 matrices and the number of dominances for each plan for each pairwise attribute comparison. Supporting Information File 3 contains an Excel template file that facilitates carrying out the tedious task of pairwise comparisons involved in the poset analysis, particularly when the number of synthesis plans under consideration is large. Table 5 summarizes the main results of the poset dominance analysis for all vanillin plans considered. We observe that plans p7 (Givaudan–Roure), p8 (Haarmann and Reimer), and p18 (percolation extraction whole vanilla beans) have the highest number of pairwise dominances of 145, 105, and 101, respectively. Plans p11 (Lampman synthesis from sawdust), p10 (Ji synthesis from guaiacol), p14 (Mexican group SFE), p9 (Hibbert synthesis from lignosulfonic acid liquor), p21 (Soxhlet extraction from ground vanilla beans), and p6 (Frost biofermentation from D-glucose) have the fewest number of dominances of 0, 18, 23, 27, 28, and 29, respectively. Table 6 and Table 7 summarize the results of the two ranking algorithms. Both methods identify the same set of overall best plans and overall worst plans with 11 out of the 22 plans having exactly the same ranking. With respect to plans having different ranking orders we find that 5 out of 22 plans have +/− 1 rank positional change, 5 out of 22 plans have +/− 2 rank positional change, and 1 plan out of 22 having a +/− 3 rank positional change. Overall, the faster Borda count method is able to quickly identify the top and bottom performing plans with certainty. The more tedious poset pairwise dominance analysis

Table 5: Summary of pairwise poset dominance analysis for 22 synthesis plans of vanillin based on 5 attribute categories.[a]

pairwise attribute comparison	number of dominances																					
	p1	p2	p3	p4	p5	p6	p7	p8	p9	p10	p11	p12	p13	p14	p15	p16	p17	p18	p19	p20	p21	p22
PMI vs SR	8	10	1	9	10	1	**12**	6	3	2	0	1	8	3	9	5	6	6	7	8	3	4
PMI vs IEE	9	10	7	13	11	8	**19**	2	3	5	0	1	14	1	9	4	9	9	6	8	3	6
PMI vs RSGI	17	16	5	12	15	1	**21**	8	7	2	0	1	15	1	14	9	7	7	11	9	2	5
PMI vs SI	10	9	4	1	7	1	**14**	7	3	1	0	1	1	1	7	5	6	6	3	7	1	2
SR vs IEE	7	8	1	12	9	1	12	12	1	3	0	2	7	3	12	2	**13**	**13**	4	9	4	8
SR vs RSGI	8	9	1	9	9	1	**11**	**11**	3	1	0	6	7	1	8	5	6	8	6	6	2	3
SR vs SI	7	5	1	2	7	2	10	**11**	1	1	0	5	1	10	6	4	9	**11**	2	10	6	3
IEE vs RSGI	9	8	6	11	10	3	**18**	15	2	1	0	3	10	1	11	3	8	11	5	6	3	5
IEE vs SI	7	5	10	2	5	7	14	15	1	1	0	3	1	1	9	3	17	**18**	1	9	2	2
RSGI vs SI	13	8	3	1	8	4	14	**18**	3	1	0	**18**	1	1	8	5	7	12	3	7	2	2
TOTALS	95	88	39	72	91	29	**145**	105	27	18	0	41	65	23	93	45	88	101	48	79	28	40

[a]Entries highlighted in bold represent the highest dominances in each of the 10 pairwise attribute comparisons.

Table 6: Summary of Borda count and poset dominance analysis of 22 synthesis plans for vanillin listed alphabetically.

Alphabetized list of vanillin synthesis plans	plan code	Borda count	poset dominances
Borregaard synthesis	p1	84	95
Collins chemical	p2	83	88
Eilks Pt 1	p3	59	39
Eilks Pt 2	p4	77	72
Faith	p5	87	91
Frost	p6	51	29
Givaudan–Roure	p7	102	145
Haarmann and Reimer	p8	92	105
Hibbert	p9	47	27
Ji	p10	40	18
Lampman	p11	18	0
Lesage–Meesen	p12	67	41
Mayer	p13	76	65
Mexican group SFE	p14	50	23
Mottern	p15	87	93
Ontario Paper Co.	p16	61	45
percolation extraction cut	p17	85	88
percolation extraction whole	p18	90	101
Sorensen–Mehlum	p19	61	48
Soxhlet extraction cut	p20	79	79
Soxhlet extraction ground	p21	48	28
Taber	p22	55	40

Table 7: Summary of Borda count and poset dominance rankings of 22 synthesis plans for vanillin.[a,b]

Borda count ranking	plan	Poset dominance ranking	plan
102	*p7*	*145*	*p7*
92	*p8*	*105*	*p8*
90	*p18*	*101*	*p18*
87	**p5**	95	**p1**
87	*p15*	*93*	*p15*
85	**p17**	91	**p5**
84	**p1**	88	**p2**
83	**p2**	88	**p17**
79	*p20*	*79*	*p20*
77	*p4*	*72*	*p4*
76	*p13*	*65*	*p13*
67	**p12**	48	**p19**
61	*p16*	*45*	*p16*
61	**p19**	41	**p12**
59	**p3**	40	**p22**
55	**p22**	39	**p3**
51	*p6*	*29*	*p6*

Table 7: Summary of Borda count and poset dominance rankings of 22 synthesis plans for vanillin.[a,b] (continued)

50	**p14**	28	**p21**
48	**p21**	27	**p9**
47	**p9**	23	**p14**
40	*p10*	*18*	*p10*
18	*p11*	*0*	*p11*

[a]Line separated, italicized entries represent plans having exactly the same ranking order. [b]Bold entries represent plans having different ranking orders.

is more reliable in ranking the intermediate performing plans due to its thoroughness in considering all possible pairwise plan comparisons across all attributes considered.

Conclusion

We have introduced and demonstrated how a sustainability index (SI) can be computed specifically for synthesis plans based on the provenance of input materials and energy sources, and the fate of output waste materials. Reasonable and reliable estimates of SI based on provenance and fate of input and output materials respectively can only be made if full disclosure of both supply and disposal chains in the chemical enterprise exists. We note that this is a formidable challenge for the chemical community to accept and adopt in routine practice. We also note that the computation of SI will necessarily involve significant assumptions to be made in determining key parameters such as F_{RE} and F_{VP} and that these assumptions, in turn, will necessarily affect the ranking of synthesis plans. The nine assumptions listed for the analysis of vanillin are an illustrative example of what is entailed for the computation of SI. Other target products will require their own set of assumptions. Nevertheless, we believe that the protocols disclosed in this work are easily implementable once the necessary data are made available.

In our determination of the four fractions contributing to SI we implemented a binary approach based on whether or not a material or energy input arises from renewable or non-renewable sources; and on whether or not an output material could be recycled or reused. Specific rates of depletion versus renewal of a resource applied to inputs and specific rates of reusability versus accumulation of outputs require a complete macroscopic knowledge and connectivity of all elements pertaining to the network of all chemical processes involved in a given synthesis plan. At this time reliable estimates of these rates are not readily available to the average practicing chemist or chemical engineer in established open-access data collection databases for all commodity material resources, and so this significant limitation prevents estimation of time analyses pertaining to how long a given resource may exist under a so-called “sustainability condition”. For first generation chemical feedstocks arising from fossil fuels, the rate of finding new reserves of fossil fuel may be used as a rate of “renewal” rather than the geological rate of renewal which is several orders of magnitude lower. In any case, rates of finding new reserves of fossil fuels or mineral deposits depend on knowledge of counting existing reserves, which necessarily requires reliable databases that constantly track data annually. Such tracking is not always in industry’s best interest to disclose such information publicly for economic and political reasons. For example, providing inaccurate or incomplete information to governments and investors can leverage control of prices of crude oil, natural gas, and metals; whereas, disclosing accurate and up-to-date information can expose vulnerabilities among governments and investors that can be taken advantage of.

Furthermore, deciding where to terminate a chain of resources, i.e., which material to designate as the “starting material” for a given synthesis plan, remains a non-resolvable dilemma. What is known with certainty is that extending a starting material chain will necessarily amplify material consumption (PMI), enthalpic energy inputs (IEE), and associated environmental and safety-hazard impacts (RSGI). Hence, if the starting points of the vanillin plans in this work are changed, particularly for the chemical syntheses, then this will change the values of all of these parameters and ultimately the ranking order of the plans based on those parameters. There is also the problem of including the syntheses of all reagents and catalysts used in each reaction step involved in a given synthesis plan. Again, significant amplification of material consumption (PMI), enthalpic energy inputs (IEE), and associated environmental and safety-hazard impacts (RSGI) will result. For the case of F_{VI} which is the ratio of mass of valorized input to mass of total input, if we were to include the synthesis route of a catalyst used in the main synthesis chain we can envisage two case scenarios for how this will impact the computation of F_{VI} where the mass of total inputs (denominator) will obviously increase. In one case, if the mass of inputs to make the catalyst is considered valorized, then the numerator magnitude will also increase. Hence, the overall value of F_{VI} is expected to increase which will in turn increase

the value of SI. On the other hand, if the mass of inputs to make the catalyst is considered non-valorized, then the numerator magnitude does not change. Hence, the overall value of F_{VI} is expected to decrease which will in turn decrease the value of SI. Similar trends apply for F_{VO} and F_{RE}. Such a scenario will have a negative impact on chemical syntheses that primarily use non-renewable materials, reagents, and catalysts. The net effect is to drive down the ranking of chemical syntheses. Chemical syntheses have a lower likelihood of achieving moderate levels of sustainability compared to ones based on biofeedstocks and biofermentation processes mainly because they utilize fossil fuel-derived materials. In any event, the task of tracing starting materials, catalysts, and reaction solvent syntheses is very tedious, especially for time-pressed chemists who wish to practice green chemistry. However, such a task can be significantly alleviated if synthesis databases of first, second, and third generation feedstocks existed where all key metrics have been worked out in advance such as PMI, SR, IEE, and RSGI. It is then possible to tap into these databases in a cassette-like manner and insert these synthesis chain extensions to the main synthesis chain of interest as needed. The creation of such databases requires significant investment in time and energy but once done it is expected that they will have far-reaching utility in the long run. An important point to keep in mind in extending synthesis chains to first generation feedstocks of simple chemical complexity is that environmental and safety-hazard impacts of reactants and reagents become important since reaction solvent usage dramatically decreases. Reactions involving first generation feedstocks are typically gas-phase reactions run without any reaction solvent. However, as the synthesis chain extends to more complex intermediates and other materials, reaction solvent usage increases dramatically and becomes the bulk input mass of materials used. Hence, environmental and safety-hazard impacts of reaction solvents become important in the pharmaceutical industry, for example.

Deciding on where to terminate a chain is a contentious issue; however, general guidelines can be created to help direct and facilitate decision-making in the form of a decision tree. A first key question to ask is: "Does a plan trace to a renewable or reclaimed starting material?". If the answer is "yes", then all metrics analyses up to that renewable material need to be done. On the other hand, if the answer is "no", then there are three possible options in decreasing order of thoroughness. The first option is to trace to a non-renewable starting material that is common to all synthesis plans compared as far as possible. The second option, if no common starting material can be found, is to trace to a non-renewable starting material (i) that is a first generation feedstock such as coal, crude oil, or ores from the earth's crust; or (ii) whose molecular weight is less than 80 g/mol corresponding to benzene or pyridine starting materials. The third option is to trace to a "readily available" or commercially available starting material. An agreed consensus between academic, industry, and government stakeholders is needed to decide which option is most appropriate and feasible, or to decide other options. The main criterion for tracing each reaction step in a backwards fashion is to always choose literature examples with the least PMI, highest yields and atom economies, and least environmental-safety hazard impacts. As one goes towards virgin materials energy demands and hazard impacts generally increase. All synthesis plans should be compared in the same way to avoid biased ranking. For example, if reagents and catalysts are not traced further back, then this is done for all plans considered to a given target product. On the other hand, if they are traced back to earlier materials then this should be done for all plans. A key problem is that ranking positions can be arbitrarily selected for a given set of synthesis plans to a common target product simply by selecting the cut-off chain of starting materials. Hence, the computation of SI and subsequent ranking are most vulnerable to the apparent arbitrary choice of starting material cut-offs in the analyses. Transportation costs for getting starting materials to the manufacturing site also contribute to input energy; however, for the case of simplicity we have not considered these in the present analysis.

Based on the above challenges and limitations discussed above, we believe that our choice of starting materials used to carry out our metric analyses for all synthesis plans of vanillin considered as shown in Figure S1 (Supporting Information File 1) are reasonable and lead to fair ranking comparisons. We have also shown how synthesis plans may be compared and ranked using Borda count and poset pairwise dominance algorithms according to the following attributes: process mass intensity (PMI), sacrificial reagent consumption (SR), input enthalpy energy consumption (IEE), Rowan solvent greenness index (RSGI), and sustainability index (SI). The Borda count method is found to be adequate for rapid identification of best and worst plans in a given set of synthesis plans, whereas, the more detailed poset pairwise dominance analysis is appropriate for obtaining a precise ranking of intermediate performing plans. Application of these ranking methods to 22 synthesis plans for vanillin indicated that biofermentation processes from ferulic acid and isoeugenol starting materials were best performers overall followed closely by percolation solvent extraction processes from whole or cut cured vanilla beans. Chemical syntheses of vanillin from lignosulfonic acid liquors or guaiacol were surprisingly competitive when analyzed according to all of the 5 comparative attributes; however, they ranked low with respect to the sustainability index alone. The most sustainable processes were biofermentations and percolation solvent extractions.

Table 8: Abbreviations

Abbreviation	Explanation
ABP	acidification-basification potential
aqua	aquatic toxicity, mg/L for 96 h
BCP	bioconcentration potential, unitless
F_{VI}	mass fraction of valorized inputs
F_{NVI}	mass fraction of non-valorized inputs
F_{VO}	mass fraction of valorized outputs
F_{NVO}	mass fraction of non-valorized outputs
F_{RE}	input enthalpic energy fraction arising from renewable energy sources
F_{VP}	mass fraction of valorized target product
FP	flash point, degrees K
GWP	global warming potential, unitless
IEE	input enthalpic energy, kJ per kg product
K	number of synthesis plans to a common target product
LC_{50}	lethal concentration required to kill 50% of population, g/m^3 for 4 h
LD_{50}	lethal dose required to kill 50% of population, mg/kg body weight
m	number of attributes used in a ranking algorithm
M	metric
M_{VI}	mass of valorized or renewably sourced inputs
M_{NVI}	mass of non-valorized or non-renewably sourced inputs
$M_{product}$	mass of target product produced in a synthesis plan
$M^*_{product}$	mass of target product that is destined to be waste after its intended use
ODP	ozone depletion potential, unitless
OEL	occupational exposure limit, ppm
OSI	overall solvent index
PER	persistence potential, unitless
PMI	process mass intensity, kg total inputs per kg product
Q	quotient referring to risk phrases, unitless
r	rank number for a plan
RE	renewable energy
RSGI	Rowan solvent greenness index, kg per kg product
SD	skin dose, mg
SFE	supercritical fluid extraction
SFP	smog forming potential, unitless
SI	sustainability index, dimensionless
SR	sacrificial reagents
W_{VO}	mass of waste of valorized or reusable outputs
W_{NVO}	mass of waste of non-valorized outputs
W_{total}	total mass of waste produced in a synthesis plan

Supporting Information

Supporting Information File 1

Figure S1 comprising 22 vanillin synthesis plans, data for vanillin synthesis plans on production of 1 kg vanillin, Borda count results, and Poset analysis.
[https://www.beilstein-journals.org/bjoc/content/supplementary/1860-5397-16-196-S1.pdf]

Supporting Information File 2

Excel file of sustainability index (SI) calculator.
[https://www.beilstein-journals.org/bjoc/content/supplementary/1860-5397-16-196-S2.xls]

Supporting Information File 3

Excel template file for carrying out poset pairwise dominance analysis.
[https://www.beilstein-journals.org/bjoc/content/supplementary/1860-5397-16-196-S3.xls]

Acknowledgements

This paper is dedicated to the memory of Christopher R. Schmid, founding editor of *Organic Process Research and Development* and process chemist at Eli Lilly, who understood the true meaning and scope of both green chemistry and sustainability chemistry, and who foresaw their practical applications widely in the chemical industry. Facundo Jesus Salamanca from Don Mills Collegiate Institute Mathematics Club is thanked for checking the mathematical treatment.

ORCID® iDs

John Andraos - https://orcid.org/0000-0002-2982-2708

References

1. Hogue, C. *Chem. Eng. News* **2019,** *97,* 19.
2. Hinderink, A. P.; van der Kooi, H. J.; de Swaan Arons, J. *Green Chem.* **1999,** *1,* G176–G180. doi:10.1039/a909915h
3. Dewulf, J.; Van Langenhove, H.; Mulder, J.; van den Berg, M. M. D.; van der Kooi, H. J.; de Swaan Arons, J. *Green Chem.* **2000,** *2,* 108–114. doi:10.1039/b000015i
4. Lems, S.; van der Kooi, H. J.; de Swaan Arons, J. *Green Chem.* **2002,** *4,* 308–313. doi:10.1039/b203490p
5. Cséfalvay, E.; Akien, G. R.; Qi, L.; Horváth, I. T. *Catal. Today* **2015,** *239,* 50–55. doi:10.1016/j.cattod.2014.02.006
6. Horváth, I. T.; Cséfalvay, E.; Mika, L. T.; Debreczeni, M. *ACS Sustainable Chem. Eng.* **2017,** *5,* 2734–2740. doi:10.1021/acssuschemeng.6b03074
7. Cséfalvay, E.; Horváth, I. T. *ACS Sustainable Chem. Eng.* **2018,** *6,* 8868–8874. doi:10.1021/acssuschemeng.8b01213
8. Sikdar, S. K. *AIChE J.* **2003,** *49,* 1928–1932. doi:10.1002/aic.690490802

9. Sheldon, R. A.; Sanders, J. P. M. *Catal. Today* **2015,** *239,* 3–6. doi:10.1016/j.cattod.2014.03.032
10. Fadel, C.; Tarabieh, K. *Resources* **2019,** *8,* 115. doi:10.3390/resources8020115
11. Provenance. https://en.wikipedia.org/w/index.php?title=Provenance&oldid=918360247 (accessed Sept 30, 2019).
12. McElroy, C. R.; Constantinou, A.; Jones, L. C.; Summerton, L.; Clark, J. H. *Green Chem.* **2015,** *17,* 3111–3121. doi:10.1039/c5gc00340g
13. Jimenez-Gonzalez, C.; Ponder, C. S.; Broxterman, Q. B.; Manley, J. B. *Org. Process Res. Dev.* **2011,** *15,* 912–917. doi:10.1021/op200097d
14. Redlich, O.; Kwong, J. N. S. *Chem. Rev.* **1949,** *44,* 233–244. doi:10.1021/cr60137a013
15. Ruiz-Mercado, G. J.; Smith, R. L.; Gonzalez, M. A. *Ind. Eng. Chem. Res.* **2012,** *51,* 2309–2328. doi:10.1021/ie102116e
16. Ontario's System-Wide Electricity Supply Mix: 2017 Data. https://www.oeb.ca/sites/default/files/2017-supply-mix-data.pdf (accessed Sept 30, 2019).
17. Archived - 2017 Long-Term Energy Plan: Discussion Guide. https://www.ontario.ca/document/2017-long-term-energy-plan-discussion-guide/ontarios-energy-mix-end-2015 (accessed Sept 30, 2019).
18. Trost, B. M. *Science* **1991,** *254,* 1471–1477. doi:10.1126/science.1962206
19. Slater, C. S.; Savelski, M. *J. Environ. Sci. Health, Part A: Toxic/Hazard. Subst. Environ. Eng.* **2007,** *42,* 1595–1605. doi:10.1080/10934520701517747
20. Andraos, J. *Green Process. Synth.* **2019,** *8,* 787–801. doi:10.1515/gps-2019-0048
21. de Borda, J. C. *Mémoire de l'Académie Royale. Histoire de l'Académie des Sciences*, **1781**, 657–665. http://gerardgreco.free.fr/IMG/pdf/MA_c_moire-Borda-1781.pdf (accessed Sept 30, 2019).
22. Emerson, P. *Soc. Choice Welfare* **2013,** *40,* 353–358. doi:10.1007/s00355-011-0603-9
23. Levin, J.; Nalebuff, B. *J. Econ. Perspect.* **1995,** *9,* 3–26. doi:10.1257/jep.9.1.3
24. Saari, D. G. *The Optimal Ranking Method Is the Borda Count;* International Institute for Applied Systems Analysis: Laxenburg, Austria, 1985.
25. Restrepo, G.; Stadler, P. F. *ACS Sustainable Chem. Eng.* **2016,** *4,* 2191–2199. doi:10.1021/acssuschemeng.5b01649
26. Li, K.; Frost, J. W. *J. Am. Chem. Soc.* **1998,** *120,* 10545–10546. doi:10.1021/ja9817747
27. Muheim, A.; Müller, B.; Münch, T.; Wetli, M. Process for the production of vanillin. Eur. Pat. Appl. EP885968 A1, Dec 23, 1998.
28. Lesage-Meessen, L.; Delattre, M.; Haon, M.; Thibault, J.-F.; Ceccaldi, B. C.; Brunerie, P.; Asther, M. *J. Biotechnol.* **1996,** *50,* 107–113. doi:10.1016/0168-1656(96)01552-0
29. Lesage-Meesen, L.; Delattrea, M.; Haona, M.; Asther, M. Aspergillus niger which produces vanillic acid from ferulic acid. U.S. Patent US6162637, Dec 19, 2000.
30. Rabenhorst, J.; Hopp, R. Process for the preparation of vanillin. U.S. Patent US5017388, May 21, 1991.
31. Faith, W. L.; Keyes, D. B.; Clark, R. L. *Industrial Chemicals,* 3rd ed.; Wiley: New York, NY, USA, 1966; p 796.
32. Bjørsvik, H.-R.; Minisci, F. *Org. Process Res. Dev.* **1999,** *3,* 330–340. doi:10.1021/op9900028
33. Tomlinson, G. H., 2nd.; Hibbert, H. *J. Am. Chem. Soc.* **1936,** *58,* 345–348. doi:10.1021/ja01293a046
34. Hibbert, H.; Tomlinson, G. H. Manufacture of vanillin from waste sulphite pulp liquor. U.S. Patent US2069185, Jan 26, 1937.
35. Craig, D.; Logan, C. D. Method of producing vanillin and other useful products from lignosulfonic acid compounds. U.S. Patent US3054659, Sept 18, 1962.
36. Lampman, G. M.; Andrews, J.; Bratz, W.; Hanssen, O.; Kelley, K.; Perry, D.; Ridgeway, A. *J. Chem. Educ.* **1977,** *54,* 776–778. doi:10.1021/ed054p776
37. Sorensen, N. A.; Mehlum, J. Method of manufacturing vanillin. U.S. Patent US2752394, June 26, 1956.
38. Mayer, E. *Oesterr. Chem.-Ztg.* **1949,** *50,* 40–41.
39. Mottern, H. O. *J. Am. Chem. Soc.* **1934,** *56,* 2107–2108. doi:10.1021/ja01325a033
40. Fiecchi, A.; Mario, G.; Cabella, P.; Cicognani, G. Method of preparing vanillin from eugenol. U.S. Patent US3544621, Dec 1, 1970.
41. Garner, N.; Siole, A.; Eilks, I. J. *Sci. Educ.* **2016,** *17,* 25–28.
42. Huang, W.-B.; Du, C.-Y.; Jiang, J.-A.; Ji, Y.-F. *Res. Chem. Intermed.* **2013,** *39,* 2849–2856. doi:10.1007/s11164-012-0804-6
43. Taber, D. F.; Patel, S.; Hambleton, T. M.; Winkel, E. E. *J. Chem. Educ.* **2007,** *84,* 1158. doi:10.1021/ed084p1158
44. Sujalmi, S.; Suharso, S.; Supriyanto, R.; Buchari, B. *Indones. J. Chem.* **2010,** *5,* 7–10. doi:10.22146/ijc.21831
45. Sinha, A. K.; Sharma, U. K.; Sharma, N. *Int. J. Food Sci. Nutr.* **2008,** *59,* 299–326. doi:10.1080/09687630701539350
46. Castillo-Ruz, M. C.; Guillermo-Alcocer, C. G.; Bojorquez-Gamboa, R. R.; Rocha-Uribe, J. A. *Tecnol., Cienc., Educ.* **2011,** *26,* 80–84.
47. Couteau, D.; Mathaly, P. *Ind. Crops Prod.* **1997,** *6,* 237–252. doi:10.1016/s0926-6690(97)00014-9
48. Kaufman, T. S. *J. Braz. Chem. Soc.* **2015,** *26,* 1055–1086. doi:10.5935/0103-5053.20150086
49. Parfitt, J.; Barthel, M.; Macnaughton, S. *Philos. Trans. R. Soc., B* **2010,** *365,* 3065–3081. doi:10.1098/rstb.2010.0126
50. One Third of All Food Wasted! United Nations Regional Information Centre for Western Europe. https://www.unric.org/en/food-waste/27133-one-third-of-all-food-wasted (accessed Sept 30, 2019).
51. Gustavsson, J.; Cederberg, C.; Sonesson, U.; van Otterdijk, R.; Meybeck, A. *Global Food Losses and Food Waste – Extent, Causes, and Prevention.* Food and Agriculture Organization of the United Nations, Rome, 2011. http://www.fao.org/3/a-i2697e.pdf (accessed Sept 30, 2019).
52. Lipinski, B.; Hanson, C.; Lomax, J.; Kitinoja, L.; Waite, R.; Searchinger, T. Reducing Food Loss and Waste. Working Paper, Installment 2 of *Creating a Sustainable Food Future.* Washington, DC: World Resources Institute, 2013.. https://pdf.wri.org/reducing_food_loss_and_waste.pdf (accessed Sept 30, 2019).
53. S Department of Agriculture. Food Waste FAQs. https://www.usda.gov/foodwaste/faqs (accessed Sept 30, 2019).

BEILSTEIN JOURNAL OF ORGANIC CHEMISTRY

Palladium nanoparticles supported on chitin-based nanomaterials as heterogeneous catalysts for the Heck coupling reaction

Tony Jin[1], Malickah Hicks[1], Davis Kurdyla[2], Sabahudin Hrapovic[2], Edmond Lam[*2] and Audrey Moores[*1,3]

Letter

Open Access

Address:
[1]Department of Chemistry, McGill University, Montreal, Quebec H3A 0B8, Canada, [2]Aquatic and Crop Resource Development Research Centre, National Research Council of Canada, Montreal, Quebec H4P 2R2, Canada and [3]Department of Mining and Materials Engineering, McGill University, Montreal, Quebec H3A 0E9, Canada

Email:
Edmond Lam[*] - edmond.lam@cnrc-nrc.gc.ca; Audrey Moores[*] - audrey.moores@mcgill.ca

* Corresponding author

Keywords:
chitin; chitosan; Heck coupling; heterogeneous catalysis; nanomaterial

Beilstein J. Org. Chem. **2020,** *16,* 2477–2483.
https://doi.org/10.3762/bjoc.16.201

Received: 12 August 2020
Accepted: 22 September 2020
Published: 07 October 2020

This article is part of the thematic issue "Green chemistry II".

Associate Editor: L. Vaccaro

Abstract

In this report, chitin and chitosan nanocrystals were used as biomass-based supports for Pd nanoparticles (NPs) used as a heterogeneous catalyst for the Heck coupling reaction. By using a one-pot fabrication method, a Pd salt precursor was directly reduced and deposited onto these nanocrystal catalysts. Characterization of these nanocomposites showed disperse Pd NPs on the surfaces of the chitinous nanocrystals. Heck coupling model reactions revealed full product yield in relatively benign conditions, outcompeting the use of other catalysts supported on biomass-based nanomaterials, including cellulose nanocrystals. These initial results show the potential for using chitinous nanomaterials as effective catalyst supports in cross-coupling reactions.

Introduction

Over the past decades, biomass-based nanomaterials have become a highly prevalent topic of research owing to their sustainability, bioavailability, unique structural and morphological characteristics [1]. Particularly dominant in this field are cellulose nanocrystals (CNCs), which are rod-like nanocrystallites liberated from lignocellulosic biomass under acid hydrolysis conditions [2]. A spectrum of applications have been investigated over the years for this sustainable bio-nanomaterial including drug delivery [3], food packaging [4], environmental remediation [5], and catalysis [6]. With their high solubility and presence of functionalities such as hydroxy groups, sulfate half-esters, and carboxylates, CNCs are able to stabilize highly disperse metal nanoparticles (NPs), which can act as heterogeneous catalysts for a wide array of organic transformations [7-9]. Furthermore, the chiral nature of polysaccharides has also been used as a tool for enantioselective catalysis such as carbonyl

hydrogenations and amino acid hydrolysis, proving the unique ability of these biomass-based supports [10,11].

Chitin is another type of biomass feedstock that has attracted similar attention to cellulose. Found primarily in squid, insects, fungi, and the shells of crustaceans (shrimp, crab, and lobster), chitin is the second-most abundant biopolymer after cellulose, with an annual availability of over 6 million tons from crustacean shell waste alone [12]. With shell waste being often discarded back into the sea or in landfills, it is imperative that downstream applications be developed such that environmental concerns and disposal costs for this neglected resource are reduced through the creation of bio-based sustainable technologies [13]. In this manner, strategies for fabricating CNCs have been adapted for chitin nanocrystals (ChNCs). From the seminal discovery of ChNCs by Marchessault in 1959 [14], much work has been done to improve the monodispersity, morphology, and structure of this unique nanomaterial [15]. Very recently, we have reported the use of ammonium persulfate as a mild oxidizing agent to liberate the nanocrystallites existing within bulk chitin to yield ChNC with carboxylate functionalities [16]. Moreover, deacetylation of ChNCs in alkaline conditions, in the presence of $NaBH_4$, led to chitosan nanocrystals (ChsNCs) with abundant amine groups.

While groups are starting to investigate the usage of chitin and chitosan-based supports for heterogeneous catalysis, there are still scarce investigations on using these biomaterials on the nanoscale, which can allow for higher accessibility of their functionalities towards better stabilizing dispersed metal nanoparticle catalysts, along with increased solubility in aqueous media. Very recently, we have shown that these bio-based nanomaterials could stabilize highly disperse Au species on the surface of these nanocrystals to create a highly active catalyst for aromatic nitro reduction and aldehyde–amine–alkyne (A^3) coupling reactions [16]. Off this discovery, in this letter, we further expand the scope of using both ChNCs and ChsNCs as a catalyst support for Pd NPs to allow access towards other highly relevant C–C bond-forming reactions. A one-pot fabrication method is used to deposit Pd NPs directly onto both ChNCs and ChsNCs, and the as-made heterogeneous catalysts were tested with the Heck coupling reaction as a model for catalytic activity.

Findings

The fabrication of ChNC and ChsNCs was conducted using a procedure previously reported by our group (Lam) (see Supporting Information File 1) [16]. ChNCs were treated with ammonium persulfate (APS) for 16 h to form disperse ChNCs after washing. ChsNCs were made by deacetylating ChNCs in the presence of concentrated NaOH as well as a small amount of $NaBH_4$ (Scheme 1).

As seen through transmission electron microscopy (TEM) in Figure 1, a relatively uniform distribution for both ChNCs and ChsNCs with individual rod-like nanocrystals was observed,

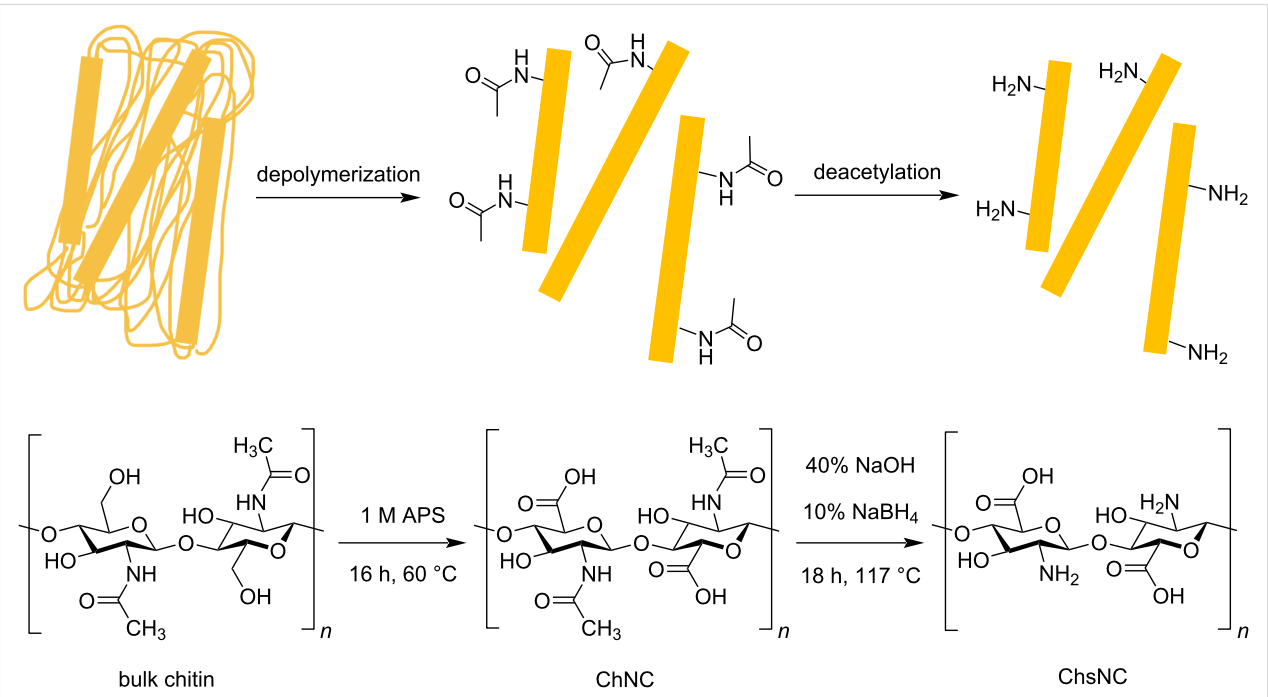

Scheme 1: Pathway for the formation of ChNC and subsequently ChsNCs from bulk chitin.

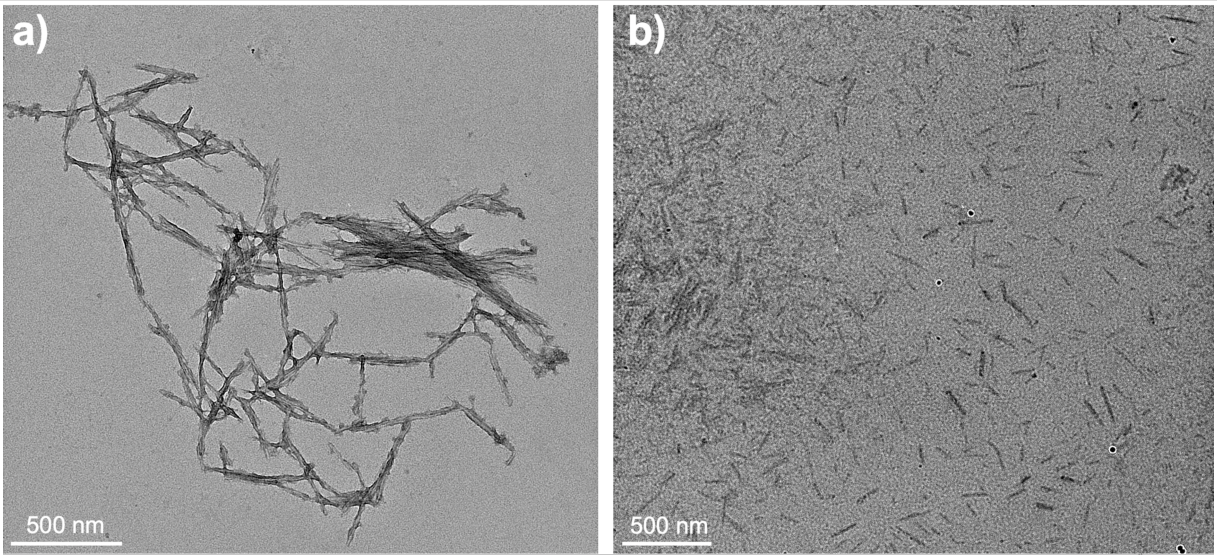

Figure 1: TEM micrographs of (a) ChNCs and (b) ChsNCs. Both samples were stained and prepared on glow-discharged C-coated Cu TEM grids.

with an average length of 231 ± 38 nm for the ChNC and 159 ± 34 nm for the ChsNC (Supporting Information File 1, Figure S1). These measures were made from parts in the grid where the nanocrystals were well separated. Larger aggregates of the individual nanocrystals were also observed in all samples. Glow-discharged carbon-coated TEM grids were used, along with uranyl acetate as a negative stain in order to provide higher contrast to the individual rods.

Further characterization of the ChNCs and ChsNCs confirmed the structural and chemical functional properties of these nanomaterials. We turned to Fourier transform infrared (FTIR) spectroscopy to access the degree of deacetylation (DDA) of the prepared materials (Supporting Information File 1, Figure S2). The ratio of primary amine over the sum of nitrogen-containing functionalities can be derived through the measurement of the N–H bend and C–O stretch peaks absorbance, found at 1560 cm^{-1} and 1030 cm^{-1}, respectively [17]. In general, bulk chitin has a DDA of 0–20%, while chitosan has a DDA of >80% [18]. The fabricated ChNCs had DDA values of 5–10%, while the ChsNCs had DDA values between 80–95%. A full spectral assignment for all of the FTIR peaks can be found in our recent report [16].

This transformation of the acetamide functionality into an amine one had drastic effects on the physicochemical properties of the nanomaterials. Specifically, the deacetylation of ChNC into ChsNC led to a decrease in crystallinity in the nanomaterial. Indeed, this can be seen in the FTIR with the broadening of the N–H and O–H stretches from 3000–3500 cm^{-1}. This was more notable in the powder X-ray diffraction (PXRD) spectra of ChNCs and ChsNCs (Supporting Information File 1, Figure S3) where broadening of the peaks was observed for ChsNC as amorphization of the internal ChNC structure occurred during the deacetylation process. ChsNCs were readily suspendable in aqueous media and formed a transparent solution, owing to their positively charged amino functionality, while ChNCs were less easily suspended. Zeta potential measurements of −24.6 mV for ChNCs and +36.8 mV for ChsNCs provided a rationale for these observations. With these differences between the two nanomaterials, we then explored how they behaved as catalyst supports for Pd NPs.

A one-pot synthesis method was used to both deposit Pd salts and reduce them into NPs onto the support material. First, $PdCl_2$ was mixed for 15 min with either ChNC or ChsNC in an acidic aqueous medium to form a dark yellow mixture. This step facilitated coordination of Pd salts onto the support, as evidenced when using CNC as support [7]. From their synthesis involving oxidative conditions, both ChNC and ChsNC featured carboxylate functionalities on their surface which we expected to be good chelating functionalities for Pd(II) (Scheme 1) [16]. For ChsNC, amines were unlikely to play any coordinating role, since they should be fully protonated under acidic conditions. Then, the mixtures were subjugated to 4 bar H_2 for 2 h at room temperature to reduce Pd(II) into metallic Pd NPs (Scheme 2), and the reaction mixture turned black. We also conducted a control study in the exact experimental parameters were performed on $PdCl_2$ and either ChNC or ChsNC, but with no H_2 reductant. In this case, the solution color remained yellow, indicating that using either ChNC or ChsNC alone cannot fully reduce $PdCl_2$. The resulting hybrid materials are noted PdNP@ChNC and PdNP@ChsNC, respectively.

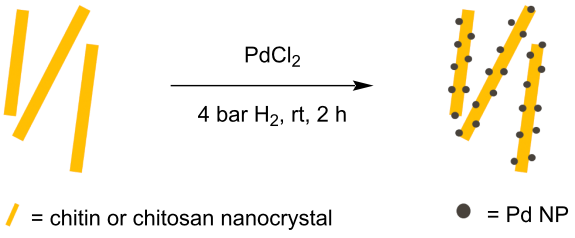

Scheme 2: Catalyst fabrication method for the deposition of Pd NPs onto chitin (PdNP@ChNC) and chitosan (PdNP@ChsNC).

Dihydrogen was selected here because it is one of cleanest reductants in this context as it will limit the production of by-products to chloride salts, by opposition to more classic reducing agents such as $NaBH_4$. Prior to characterization, the non-dried samples were purified by dialysis. The zeta potential measurements for PdNP@ChNC and PdNP@ChsNCs were −13.9 and +57.9 mV, respectively. PdNP@ChsNCs were, again, far more suspendable in aqueous solution as compared to PdNP@ChNCs. TEM micrographs of PdNP@ChNC (Figure 2a) and PdNP@ChsNC (Figure 2b) confirmed complete immobilization of Pd NPs onto both the ChNC and ChsNC, with energy dispersive X-ray (EDX) spectroscopy confirming the presence of Pd (Supporting Information File 1, Figure S4). PdNP@ChNCs self-aggregated while drying during the TEM sample preparation procedure, despite the use of glow discharged TEM grids. Conversely, the PdNP@ChsNCs were dispersed owing to the higher solubility of ChsNC. Both PdNP@ChNCs and PdNP@ChsNCs were imaged unstained to avoid any artefact in Pd imaging [19]. Dispersed "packets" of Pd NPs were observed for both samples, with far more packets observed for PdNP@ChNC (packet diameter of 42 ± 10 nm) samples compared to PdNP@ChsNC (packet diameter of 24 ± 7 nm) samples for the same wt/wt loading of the $PdCl_2$ salt to ChNC/ChsNC (initially set to 1.6 wt %). It is also noted that the packets found in PdNP@ChsNC were almost half as small relative to PdNP@ChNC. At higher magnification, these packets are seen to be extremely small Pd NPs agglomerated together (Supporting Information File 1, Figure S5). A similar packet formation was observed when the wt/wt loading of $PdCl_2$ was reduced by to 0.8 wt % to fabricate PdNP@ChNC (Supporting Information File 1, Figure S6).

X-ray photoelectron spectroscopy (XPS) was used to confirm the oxidation state of Pd on both the support materials (Figure 3). The experimental XPS spectra were deconvoluted and their match with thus obtained fitted data confirmed. Firstly, Pd on PdNP@ChNC was mainly Pd(0), with the Pd $3d_{5/2}$ peak residing at 335.1 eV, along with a small shoulder at higher binding energy indicating the presence of Pd(II) (Figure 3a). In contrast, Pd primarily exists as Pd(II) on PdNP@ChsNC (Figure 3b), which could be attributed to three possible reasons: 1) the presence of $PdCl_2$, 2) the oxidation of Pd NPs into PdO, and 3) the complexation of Pd(II) by ChsNCs. To address the first point, a survey XPS scan showed no Cl contribution to the overall atom distribution suggesting that no $PdCl_2$ species were present in the nanocomposites. For the second point, high-resolution XPS spectra on the O 1s scan of both the PdNP@ChNC and PdNP@ChsNC samples show

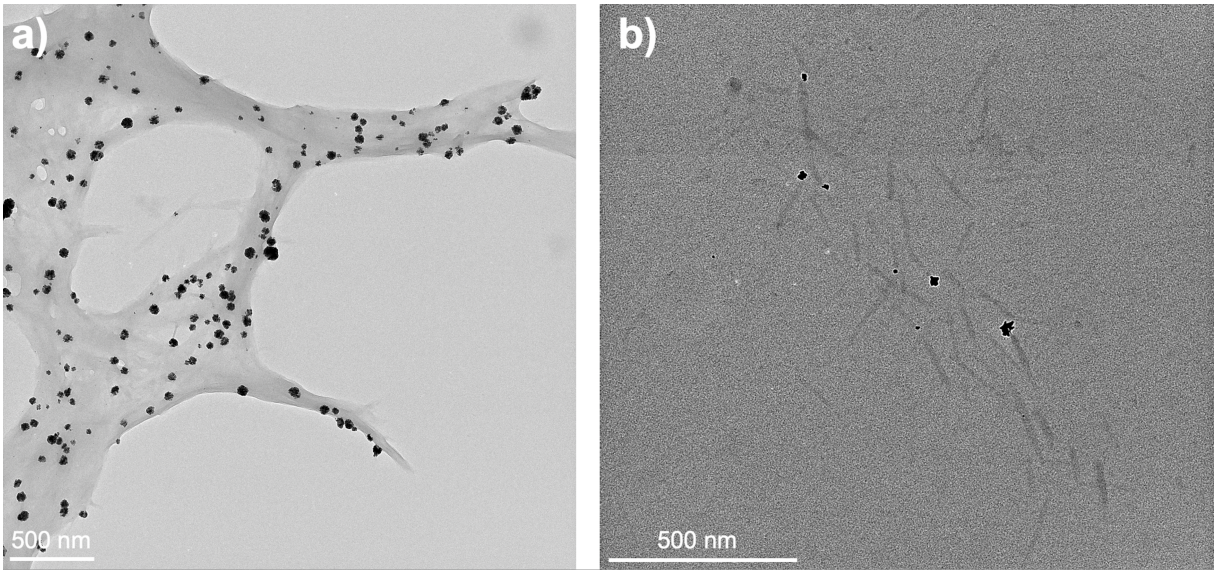

Figure 2: TEM micrographs of (a) PdNP@ChNCs and (b) PdNP@ChsNCs. The samples were placed on glow discharged TEM grids, but unstained. The images were taken purposefully with high contrast and large objective aperture to capture the nanocrystals.

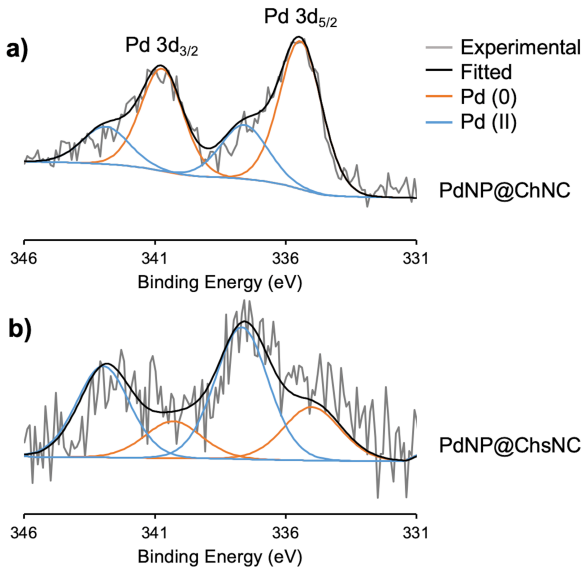

Figure 3: High-resolution X-ray photoelectron spectroscopy of the Pd 3d region of (a) PdNP@ChNC and (b) PdNP@ChsNC. Deconvolution of the experimental peaks (grey line) of each spectrum with a fitted (black line) leads to the Pd(0) (orange line) and Pd(II) (blue line) doublets.

the exact same symmetric peak, similar to that of bare ChNC and ChsNC, indicating that no formation of a Pd–O bond is present (Supporting Information File 1, Figure S7). A more accurate explanation is through the third point where Pd(II) is present on ChsNC over ChNC, an observation further validated by TEM micrographs that showed consistently fewer metallic Pd NPs on ChsNC than ChNCs. This point is corroborated by the very significant increase in zeta potential from +36.8 mV to +57.9 mV from ChsNCs to PdNPs@ChsNCs, which can only be explained by the integration at the nanocrystals surface of positively charged species, namely Pd(II). This resistance to reduction was surprising and in contradiction to what we observed with deposition onto CNC of Pd in the presence of H_2 [7], or Ag alone [20]. The striking difference between CNC on one hand and ChNC/ChsNC on the other is the presence of carboxylates on the latter. Carboxylates are expected to afford much stronger coordination to Pd(II) than OH typically present in CNC, and potentially prevent its full reduction.

Through FTIR (Supporting Information File 1, Figure S2) and XRD (Supporting Information File 1, Figure S3) analysis, there is little to no structural changes occurring in either the ChNC or the ChsNC during catalyst fabrication. The lack of metallic Pd peaks present in XRD is indicative of extreme broadening of the reflections of very small Pd NPs within the packets found.

Heck coupling is a prominent reaction for arene alkenylation, as the production of stilbene derivatives is highly relevant in areas of research such as pharmaceuticals and materials technology [21]. Furthermore, works in heterogeneous catalysis have shown that the catalyst support plays a major role in the activity of transition-metal NPs such as Pd [7]. A model reaction was performed under the conditions listed in Table 1, at 90 °C for 24 h using only PdNP@ChNC at 1 mol % Pd relative to iodobenzene. Full product yield was achieved, and another replicate

Table 1: Heck coupling reaction optimization.[a]

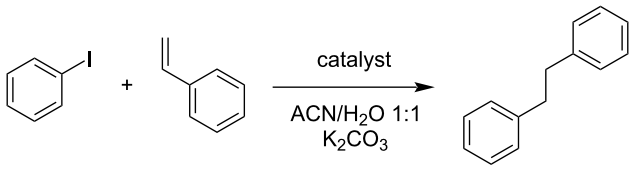

entry	catalyst	time (h)	temperature (°C)	yield[b]
1	PdNP@ChNC	24	90	100
2	PdNP@ChNC	24	70	<1
3	PdNP@ChNC	6	90	35
4	PdNP@ChNC[c]	24	90	38
5	PdNP@ChNC (0.8 wt % Pd)[d]	24	90	52
6	PdNP@ChsNC	24	90	3
7	ChNC[e]	24	90	0
8	$PdCl_2$ and ChNC	24	90	43

[a]All reactions listed used 0.2 mmol of iodobenzene and 0.24 mmol of styrene, and a Pd loading relative to iodobenzene of 1 mol %, unless otherwise specified. The solvent was 1:1 acetonitrile/water. [b]Yield was determined through GC–MS with hexamethylbenzene as an internal standard (Supporting Information File 1, Figure S8). [c]Reaction done with 0.5 mol % Pd loading relative to iodobenzene. [d]Reaction done with PdNP@ChNC using 0.8 wt % Pd relative to ChNC, as opposed to 1.6 wt % like the standard PdNP@ChNC. [e]Pd loading is 0 mol %.

was done for accuracy (Table 1, entry 1). However, a decrease in the reaction temperature to 70 °C yielded virtually no product (Table 1, entry 2). By keeping the system at 90 °C and shortening the time to 6 h, 35% product yield was already obtained, indicating a promising reaction rate (Table 1, entry 3). If the Pd loading was lowered to 0.5 mol %, a stark drop in the yield was observed (Table 1, entry 4). In entry 5 (Table 1), PdNP@ChNC with a lower Pd wt % relative to ChNC was used which yielded a lower product yield of 52% despite retention of 1 mol % loading relative to iodobenzene. The ChNC is potentially hindering the ability for substrates to interact with the Pd sites at such low wt % of Pd on the surface of the ChNC support.

In contrast to PdNP@ChNC, PdNP@ChsNC showed little product yield in the model reaction (Table 1, entry 6), which was surprising as our previous works showed that ChsNC was the superior catalyst support for Au-catalyzed A^3 coupling reactions [16]. The XPS analysis of PdNP@ChsNC suggests that Pd is complexed to ChsNC in the +2 oxidation state (Figure 3). These results align with our previous work where ChsNCs tend to stabilize Au in the +1 oxidation state as opposed to metallic Au. Since the Heck coupling primarily follows a classic oxidative addition/reductive elimination pathway with Pd(0) being the active catalytic site in most cases [22], Pd(II) would be inactive towards oxidative addition of the electrophilic iodobenzene, leading to no product formation. Importantly, even if mild reducers were present to initiate the cycle and afford Pd(0), as is often the case in Pd cross coupling chemistry, the fact that 4 bar H_2 pressure was not able to reduce these species is a strong indication of their stability against reduction. We also tested the controls to show that the ChNC support alone was catalytically inactive (Table 1, entry 7). We also demonstrated that direct mixing of $PdCl_2$ with ChNC had minor catalytic effect (Table 1, entry 8), likely because the partial reduction taking place under these conditions was ineffective in affording the well-defined nanoparticles we synthesized as PdNPs@ChNC.

Comparisons within the literature were made with similar Pd NP-based systems (Table S1 in Supporting Information File 1). Firstly, it can be seen that the PdNP@ChNC system outcompetes a similar system with Pd NP on CNCs, which led to 75% yield in 24 h and 100 °C, albeit with lower Pd loading [7]. Further comparisons with Pd NPs on other supports such as SiO_2 as reported by Jadhav et al. also suggest our system has higher catalytic activity in more benign conditions, with the Pd NP on SiO_2 system yielding 92% stilbene product at 110 °C and using dimethylformamide as the solvent [23]. Other examples using carbon-based supports such as carbon spheres [24] and graphene oxide [25] also have formidable yields, yet with either very high temperatures greater than 100 °C or using organic solvents such as toluene. The comparison with recent work in using chitin microspheres shows that chitin-based supports are potentially valuable support materials, with full product conversion in only 10 h, yet with mostly organic solvents (4:1 DMF/H_2O) [26].

Conclusion

ChNCs and ChsNCs were explored as sustainable supports for immobilizing Pd NPs to fabricate heterogeneous catalysts for the Heck coupling reaction. Through TEM and XPS analysis, metallic Pd NPs were formed and dispersed on the surface of the supports, while FTIR and PXRD showed little to no structural change to the biomaterials after metal deposition. Heck coupling results demonstrate the importance of using ChNCs as opposed to ChsNCs in order to control the redox chemistry of Pd, with full product yield in relatively mild conditions using PdNP@ChNC.

Supporting Information

Supporting Information features experimental procedures depicting the materials used, the syntheses of ChNC and ChsNC, fabrication methods for PdNP@ChNC and PdNP@ChsNC, the standard reaction protocol for Heck coupling, characterization information as well as additional characterization such as FTIR, PXRD, and supplemental TEM images.

Supporting Information File 1

Experimental part.
[https://www.beilstein-journals.org/bjoc/content/supplementary/1860-5397-16-201-S1.pdf]

Acknowledgements

We thank the Facility for Electron Microscopy Research of McGill University for help in data collection. We thank the MC^2 facility at McGill University for help in acquiring the FTIR spectra. Specifically, we thank Dr. Hatem Titi from the MC^2 facility for help in acquiring PXRD spectra along with fruitful scientific discussion.

Funding

We thank the Natural Science and Engineering Research Council of Canada (NSERC) Discovery Grant and Discovery Accelerator Supplement, the Canada Foundation for Innovation (CFI), the National Research Council (NRC) New Beginnings Initiative Ideation fund, the Fonds de Research du Quebec Nature et Technologie (FRQNT) - Centre du Chimie Verte et Catalyse (CCVC), the National Research Council Canada (NRC), and McGill University for their financial support.

ORCID® iDs

Tony Jin - https://orcid.org/0000-0003-2339-7218
Edmond Lam - https://orcid.org/0000-0003-4343-4469
Audrey Moores - https://orcid.org/0000-0003-1259-913X

References

1. Thomas, B.; Raj, M. C.; B, A. K.; H, R. M.; Joy, J.; Moores, A.; Drisko, G. L.; Sanchez, C. *Chem. Rev.* **2018,** *118,* 11575–11625. doi:10.1021/acs.chemrev.7b00627
2. Dufresne, A. *Mater. Today* **2013,** *16,* 220–227. doi:10.1016/j.mattod.2013.06.004
3. Seabra, A. B.; Bernardes, J. S.; Fávaro, W. J.; Paula, A. J.; Durán, N. *Carbohydr. Polym.* **2018,** *181,* 514–527. doi:10.1016/j.carbpol.2017.12.014
4. Chowdhury, R. A.; Nuruddin, M.; Clarkson, C.; Montes, F.; Howarter, J.; Youngblood, J. P. *ACS Appl. Mater. Interfaces* **2019,** *11,* 1376–1383. doi:10.1021/acsami.8b16897
5. Wang, N.; Ouyang, X.-K.; Yang, L.-Y.; Omer, A. M. *ACS Sustainable Chem. Eng.* **2017,** *5,* 10447–10458. doi:10.1021/acssuschemeng.7b02472
6. Kaushik, M.; Moores, A. *Green Chem.* **2016,** *18,* 622–637. doi:10.1039/c5gc02500a
7. Cirtiu, C. M.; Dunlop-Brière, A. F.; Moores, A. *Green Chem.* **2011,** *13,* 288–291. doi:10.1039/c0gc00326c
8. Lam, E.; Hrapovic, S.; Majid, E.; Chong, J. H.; Luong, J. H. T. *Nanoscale* **2012,** *4,* 997–1002. doi:10.1039/c2nr11558a
9. Seyednejhad, S.; Khalilzadeh, M. A.; Zareyee, D.; Sadeghifar, H.; Venditti, R. *Cellulose* **2019,** *26,* 5015–5031. doi:10.1007/s10570-019-02436-7
10. Kaushik, M.; Basu, K.; Benoit, C.; Cirtiu, C. M.; Vali, H.; Moores, A. *J. Am. Chem. Soc.* **2015,** *137,* 6124–6127. doi:10.1021/jacs.5b02034
11. Serizawa, T.; Sawada, T.; Wada, M. *Chem. Commun.* **2013,** *49,* 8827–8829. doi:10.1039/c3cc44416c
12. Chen, X.; Yang, H.; Yan, N. *Chem. – Eur. J.* **2016,** *22,* 13402–13421. doi:10.1002/chem.201602389
13. MacLeod, J. A.; Kuo, S.; Gallant, T. L.; Grimmett, M. *Can. J. Soil Sci.* **2006,** *86,* 631–640. doi:10.4141/s05-119
14. Marchessault, R. H.; Morehead, F. F.; Walter, N. M. *Nature* **1959,** *184,* 632–633. doi:10.1038/184632a0
15. Zeng, J.-B.; He, Y.-S.; Li, S.-L.; Wang, Y.-Z. *Biomacromolecules* **2012,** *13,* 1–11. doi:10.1021/bm201564a
16. Jin, T.; Kurdyla, D.; Hrapovic, S.; Leung, A. C. W.; Régnier, S.; Liu, Y.; Moores, A.; Lam, E. *Biomacromolecules* **2020,** *21,* 2236–2245. doi:10.1021/acs.biomac.0c00201
17. Shigemasa, Y.; Matsuura, H.; Sashiwa, H.; Saimoto, H. *Int. J. Biol. Macromol.* **1996,** *18,* 237–242. doi:10.1016/0141-8130(95)01079-3
18. Khor, E.; Lim, L. Y. *Biomaterials* **2003,** *24,* 2339–2349. doi:10.1016/s0142-9612(03)00026-7
19. Kaushik, M.; Chen, W. C.; van de Ven, T. G. M.; Moores, A. *Nord. Pulp Pap. Res. J.* **2014,** *29,* 77–84. doi:10.3183/npprj-2014-29-01-p077-084
20. Kaushik, M.; Li, A. Y.; Hudson, R.; Masnadi, M.; Li, C.-J.; Moores, A. *Green Chem.* **2016,** *18,* 129–133. doi:10.1039/c5gc01281c
21. Likhtenshtein, G. *Stilbenes: applications in chemistry, life sciences and materials science;* Wiley-VCH: Weinheim, Germany, 2009. doi:10.1002/9783527628087
22. Henriksen, S. T.; Norrby, P.-O.; Kaukoranta, P.; Andersson, P. G. *J. Am. Chem. Soc.* **2008,** *130,* 10414–10421. doi:10.1021/ja802991y
23. Jadhav, S.; Kumbhar, A.; Salunkhe, R. *Appl. Organomet. Chem.* **2015,** *29,* 339–345. doi:10.1002/aoc.3290
24. Kamal, A.; Srinivasulu, V.; Seshadri, B. N.; Markandeya, N.; Alarifi, A.; Shankaraiah, N. *Green Chem.* **2012,** *14,* 2513–2522. doi:10.1039/c2gc16430b
25. Premi, C.; Jain, N. *RSC Adv.* **2016,** *6,* 74961–74967. doi:10.1039/c6ra09996c
26. Pei, X.; Li, Y.; Deng, Y.; Lu, L.; Li, W.; Shi, R.; Lei, A.; Zhang, L. *Carbohydr. Polym.* **2021,** *251,* 117020. doi:10.1016/j.carbpol.2020.117020

License and Terms

BEILSTEIN JOURNAL OF ORGANIC CHEMISTRY

One-pot multicomponent green Hantzsch synthesis of 1,2-dihydropyridine derivatives with antiproliferative activity

Giovanna Bosica*[1], Kaylie Demanuele[1], José M. Padrón[2] and Adrián Puerta[2]

Full Research Paper

Open Access

Address:
[1]Department of Chemistry, University of Malta, Msida, MSD 2080 Malta and [2]BioLab, Instituto Universitario de Bio-Orgánica "Antonio González" (IUBO-AG), Universidad de La Laguna, c/Astrofísico Francisco Sánchez 2, 38206 La Laguna, Spain

Email:
Giovanna Bosica* - giovanna.bosica@um.edu.mt

* Corresponding author

Keywords:
antiproliferative activity; 1,2-dihydropyridines; green Hantzsch synthesis; heterogeneous catalysis; one-pot multicomponent reaction

Beilstein J. Org. Chem. **2020,** *16,* 2862–2869.
https://doi.org/10.3762/bjoc.16.235

Received: 29 August 2020
Accepted: 06 November 2020
Published: 24 November 2020

This article is part of the thematic issue "Green chemistry II". The article is dedicated to the memory of Prof. Bosica`s mother, Mrs. Maria Nespoli.

Associate Editor: L. Vaccaro

Abstract

A rapid route for obtaining unsymmetrical 1,2-dihydropyridines (1,2-DHPs) as opposed to 1,4-dihydropyridines (1,4-DHPs) has been achieved via a one-pot multicomponent Hantzsch reaction. A benign protocol has been developed for the preparation of various 1,2-dihydropyridine derivatives using heterogenized phosphotungstic acid on alumina support (40 wt %). High yields of over 75% have been accomplished in just 2–3.5 h after screening several heterogeneous catalysts and investigating the optimal reaction conditions. The catalyst chosen has passed the heterogeneity test and was shown to have the potential of being reused for up to 8 consecutive cycles before having a significant loss in activity. In addition, aromatic aldehydes gave the aforementioned regioisomer while the classical 1,4-DHPs were obtained when carrying out the reaction using aliphatic aldehydes. The preliminary study of the antiproliferative activity against human solid tumor cells demonstrated that 1,2-DHPs could inhibit cancer cell growth in the low micromolar range.

Introduction

A multicomponent approach towards the synthesis of the desired product offers a number of advantages over a stepwise method. Such advantages include the development of a design that is: cheaper, simpler, economical, and environmentally friendly [1,2]. Multicomponent reactions are not new to research. The pioneer multicomponent reactions are the Hantzsch (1882), Biginelli (1891), Mannich (1912), Passerini (1921), and Ugi (1959) reactions [3]. The significance of such a phenomenal approach for the synthesis of novel compounds first began as a way of increasing the chemical libraries and then shifted to obtaining products that are in high demand on an industrial scale at a cheaper and more benign way [4]. Recently, negative human impacts have been greatly witnessed as a result of population growth, so environmentally friendly design has

become one of the most important contributions. As a result, such research has grown exponentially in the past decade [5,6].

The work conducted by the German chemist Arthur Hantzsch exploded in the synthetic interest in dihydropyridines and pyridines when the pharmacological usefulness of these compounds in medicine was discovered [7]. The structural resemblance of these compounds to the coenzyme reduced nicotinamide adenine dinucleotide (NADH) sparked the potential pharmaceutical properties, and till today, the Hantzsch synthesis is the main route for obtaining such products, which are eventually used as active pharmaceutical ingredients in the pharmaceutical industry [3,8]. An analysis of the market shows that there are over 7000 drugs derived from dihydropyridines, some of which are blockbuster drugs, such as Tamiflu®, dioscorine, ibogaine, and isoquinuclidines [9,10].

Classically the Hantzsch synthesis involved the condensation of 2 equivalents of the β-ketoester ethyl acetoacetate (**2**) with benzaldehyde (**1a**) and ammonia (Scheme 1) [11]. This procedure was later optimized over the years using different substrates by varying the β-ketoesters and aldehydes in order to prepare a larger array of 1,4-dihydropyridines (1,4-DHPs) [12]. In addition, further developments were made to the methodology in order to enhance the reaction yield and also to reduce the reaction time. Other recent developments involve reducing the energy and waste that is produced in the reaction for a more environmentally friendly synthesis [13-16]. The source of nitrogen has also been varied from the classical use of ammonia. The most common nitrogen source reported in literature is ammonium acetate (**3**). Others include the use of oxahydrazines, primary amines, and urea. The oxidation of dihydropyridines to pyridines has been achieved using mild oxidizing agents [7,17,18].

One of the greatest limitations of this synthesis is however the fact that the dihydropyridines that are obtained are usually the 1,4-symmetrical ones. This multicomponent reaction has been thought to have one of the most complex mechanisms since various routes might take place, and the mechanism depends much on the identity of the substrates and the reaction conditions used [18]. Cao and collaborators have managed to synthesize the 1,2-dihydropyridine (1,2-DHP) regioisomer as the main product through the Hantzsch synthesis at room temperature and solvent-free conditions, irrespective of the electronic effect of the substituted benzaldehydes studied [19]. This was a further improvement of the reaction since the usual regioisomer has always been reported to be the 1,4-DHP. Cao et al. have suggested an alternative mechanism for this route. When the same reaction was conducted under argon, they obtained a mixture of the two regioisomers (1,4-DHP/1,2-DHP 32:68), proving further the complexity of this reaction [19].

Therefore, continuing our studies for the development and application of environmentally friendly methodologies for multicomponent reactions [20], we attempted to find a green catalyst that could provide a wide substrate scope for the Hantzsch synthesis of 1,2-dihydropyridines in a short reaction time.

In order to achieve a green method, apart from utilizing a multicomponent reaction as a route providing a high atom economy, heterogeneous catalysis should be used since it offers a greener

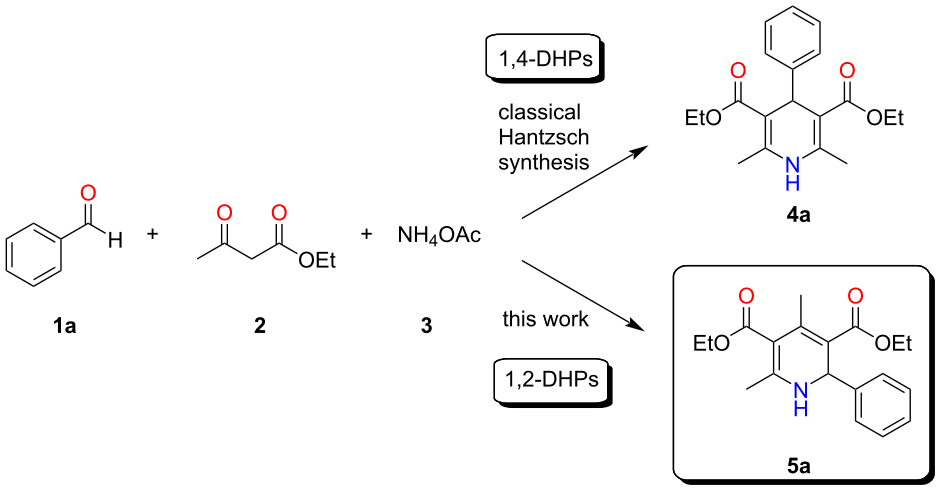

Scheme 1: The classical Hantzsch synthesis between benzaldehyde (**1a**), ethyl acetoacetate (**2**), and ammonium acetate (**3**) as well as the synthesis highlighted in this work.

alternative to homogeneous catalysis and ideally a solvent-free design to reduce the amount of solvent waste [21,22]. These two factors will reduce the amount of hazardous chemicals by reducing the amount of solvent in the reactor and during the workup of the product. A solid insoluble catalyst can easily be removed from the reaction mixture via filtration, unlike a soluble one [23-25].

Results and Discussion

According to literature, the reaction has shown to work best and most efficiently under acidic conditions since such conditions enhance the selectivity. When the model reaction between benzaldehyde (**1a**), ethyl acetoacetate (**2**), and ammonium acetate (**3**, Scheme 1) was carried out in the absence of any catalyst, it turned out to be very slow and, according to GC chromatograms, stopped in the early stages since the peaks of the corresponding starting materials of the model reaction appeared. A number of acidic catalysts was then analyzed before choosing the optimal catalyst (Table 1). The most significant result selected was based on the yield and reaction time.

The Nafion® catalysts showed the most promising results when carrying out the screenings. These catalysts were not further studied since they are no longer commercially available, and the preparation requires rather extreme conditions. The four catalysts chosen for further investigation according to the preliminary screenings shown in Table 1 were the activated resin Amberlyst® 15 (Table 1, entry 6), 40 wt % PW on silica (Table 1, entry 9), a 30 wt % PW loading on montmorillonite K30 clay (Table 1, entry 11), and a 40 wt % PW loading on alumina (Table 1, entry 12).

The study on the optimal reaction conditions shed a light on the acidity and the physical characteristics required for the reaction to be successful; the reaction requires strong acids. In addition, a peculiar result was obtained when analyzing the structure of the product obtained since the less frequently reported regioisomer, the unsymmetrical 1,2-DHP, was being obtained in a high yield and with a high selectivity. At this stage, further optimization and reaction trials were required in order to better understand the reaction conditions needed for the best results in terms of yield and selectivity of this transformation. The following investigation on each selected catalyst included changes in the molar ratio of the reagents, in the amount of catalyst, and in the temperature as well as the effect of the chosen green solvents (Figure 1).

Increasing the temperature did not significantly change the reaction yield or reduce the reaction time, while the presence of a green solvent, such as water or ethanol, negatively impacted the course of the reaction. Increasing the amount of catalyst did have a positive effect on the reaction, however, this was observed only up to a certain weight. The molar ratio of the reagents was altered by increasing the amount of ammonium acetate (**3**) in the model reaction. This again had no particularly positive effect. Since the presence of water was shown to be

Table 1: Screening of acidic heterogeneous catalysts.

entry[a]	catalyst	yield (%)[b]	reaction time (h)
1	Nafion® NR-50	88	5
2	Nafion® SAC-13	96	5
3	montmorillonite K30	72	4.5
4	Dowex® 50W	48	5.5
5	Amberlyst® 15	68	5.5
6[c]	activated Amberlyst® 15	82	5
7	40 wt % silicotungtstic acid on cellulose	49	6
8	40 wt % silicotungstic acid/Al_2O_3	37	6
9	40 wt % phosphotungstic acid (PW)/SiO_2	61	6
10	20 wt % silicotungstic acid/montmorillonite K10	40	6
11[d]	30 wt % PW/montmorillonite K30	83	2.5
12	40 wt % PW/Al_2O_3	94	3.5
13	40 wt % PW/acidic Al_2O_3	85	4
14	30 wt % PW/Amberlyst® 15	80	4.5
15	50 wt % H_3PO_4/Al_2O_3	74	5
16	30 wt % phosphomolybdic acid/Amberlyst® 15	43	6

[a]Reaction carried out under neat conditions using 0.04 g/mmol of the catalyst and a **1a**/**2**/**3** 1:2:1 ratio. [b]Yield of the pure isolated product. [c]Activation by heating overnight at 100 °C. [d]**1a**/**2**/**3** 1:2:2 ratio.

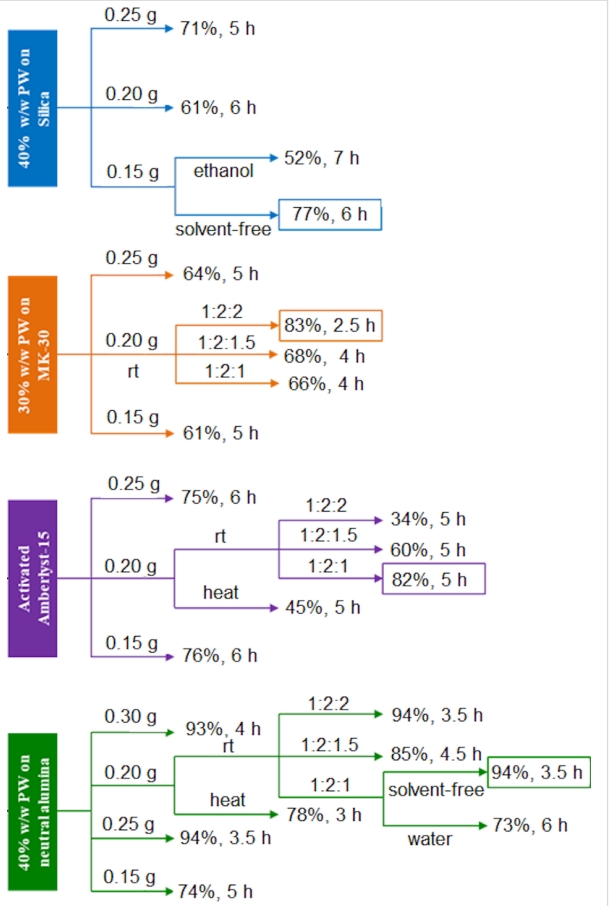

Figure 1: Optimization trials with the selected solid catalysts.

detrimental, the ammonium acetate (**3**) used was left to dry in a desiccator before use.

Reaction monitoring was mostly done using thin-layer chromatography (TLC) and at times also GC. These techniques showed the occurrence of at least three intermediates before reaching the ultimate product. No side products were observed at the end of all reactions, which shed a light on the selectivity obtained using the developed protocol. The results from the optimization trials are highlighted in Figure 1.

The optimal reaction conditions chosen included room temperature, a stoichiometric molar ratio of the reactants, using 40 wt % PW loaded on alumina under solvent-free conditions. These conditions satisfied the green protocol we were aiming for. Therefore, from this stage we moved onto the next one by changing the substrates to explore the versatility of the developed method.

The selectivity was promising even for the other substrates used (Table 2). Various substituted benzaldehydes were used, and all gave similar results. Deviations from the model reaction occurred in terms of the expected reaction time and yield, but generally, the deviations from the model reaction were minimal.

Unexpectedly, when carrying out the reaction using aliphatic aldehydes under the same conditions, a different regioisomer, the commonly reported 1,4-DHP instead of the 1,2-DHP, was

Table 2: Screening of different substrates.

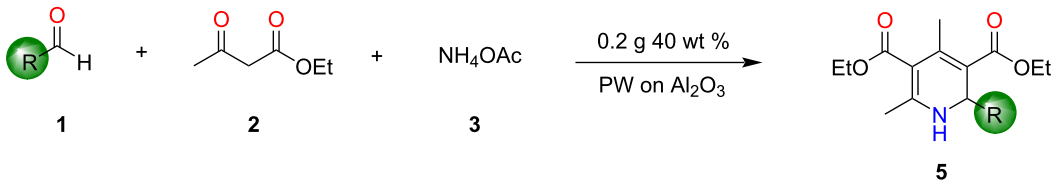

1 **2** **3** **5**

product[a]	R	yield of **5** (%)[b]	time (h)
5a	C_6H_5 (**1a**)	94	4.5
5b	2-OH-C_6H_4 (**1b**)	73	3.5
5c	2,4-$(OH)_2$-C_6H_3 (**1c**)	96	4
5d	2,4-Cl_2-C_6H_3 (**1d**)	65	6
5e	3-CH_3O-C_6H_4 (**1e**)	62	5
5f	2-CH_3O-C_6H_4 (**1f**)	62	5.5
5g	4-CH_3-C_6H_4 (**1g**)	64	4.5
5h	4-$N(CH_3)_2$-C_6H_4 (**1h**)	92	4
5i	naphthyl (**1i**)	90	4
5j	2,3-(methylenedioxy)-C_6H_3 (**1j**)	81	4.5

[a]The reactions were performed on a 5 mmol scale under neat conditions at room temperature and in the presence of 0.04 g/mmol 40 wt % PW on alumina at a molar ratio of 1:2:1. [b]Pure isolated product.

produced in the form of **4** with a high selectivity (Table 3), which was also reported by Cao and collaborators [19].

Catalyst characterization and recyclability

The catalyst was analyzed by X-ray fluorescence (XRF) spectroscopy in order to ascertain the PW/Al_2O_3-support ratio. The mass percentage ratio of tungsten, which is the main component of the catalyst, and aluminium, the major element of the support, was used to determine the percentage of PW in the ensemble. According to the data obtained by XRF spectroscopy, the PW loading of 38.4 wt % was concordant to the theoretical value of 40 wt %.

When the reusability test was carried out with the model reaction using the optimal catalyst, 40 wt % PW on alumina, a substantial yield loss of 13% was observed after the 8th cycle while the required reaction time increased by 30 minutes after the 7th cycle (Figure 2). This result confirmed the green character of the protocol, which is what we were aiming for.

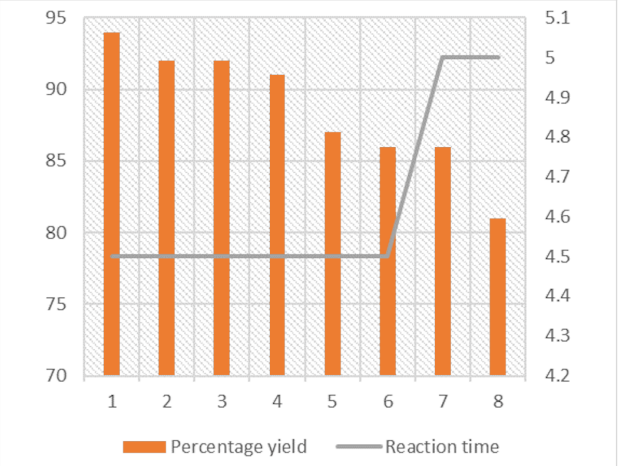

Figure 2: Graphical representation of the results obtained in the reusability test.

Green metrics

The green character of a reaction can be approximately quantified by calculating both the E-factor and the atom economy (AE), amongst other factors. The AE of the Hantzsch synthesis for the model reaction involving benzaldehyde (**1a**, 1 mol), ethyl acetoacetate (**2**, 2 mol) and ammonium acetate (**3**, 1 mol) is equal to 74%:

$$\mathrm{AE} = \frac{m\ (\text{product})}{m\ (\text{starting materials})} = \frac{329.39\ \text{g}}{2\cdot 130.14\ \text{g} + 106.12\ \text{g} + 77.08\ \text{g}} \cdot 100\% = 74.3\% \quad (1)$$

In order to take the amount of waste generated by the materials that are not directly involved in the reaction into consideration, the E-factor was also calculated:

$$\mathrm{E} = \frac{m\ (\text{product}) + m\ (\text{catalyst})}{m\ (\text{catalyst}) + m\ (\text{starting materials})} = \frac{1.548\ \text{g} + 0.2\ \text{g}}{0.2\ \text{g} + 0.385\ \text{g} + 0.531\ \text{g} + 1.301\ \text{g}} = 0.72 \quad (2)$$

The mass used for the calculation is that of the starting materials of the model reaction and that of the catalyst used in the general procedure.

Biological screening

The 1,4-DHP scaffold displays an extensive range of biological activities, including reversing multidrug resistance (through the inhibition of the P-glycoprotein) [26] and antiproliferative effects on human cancer cell lines [27]. We wondered whether the studied 1,2-DHPs could interfere with tumor cell growth. Thus, we selected a small subset of 1,2-DHPs and screened them against a panel of six human solid tumor cell lines. The

Table 3: Results obtained when using the aliphatic aldehydes **1** in the Hantzsch synthesis.

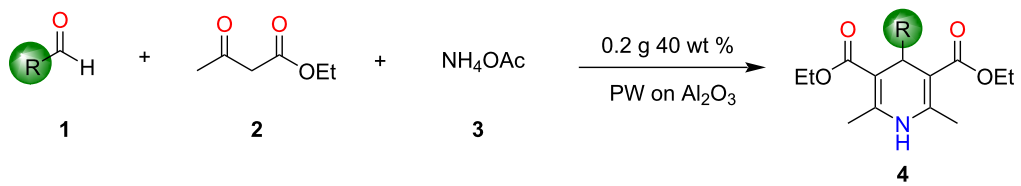

1 **2** **3** **4**

product[a]	aldehyde	yield of **4** (%)[b]	time (h)
4b	cyclohexanal (**1k**)	82	4
4c	penten-2-al (**1l**)	79	4

[a]The reactions were performed on a 5 mmol scale under neat conditions at room temperature and in the presence of 0.04 g/mmol 40 wt % PW on alumina at a molar ratio of 1:2:1. [b]Pure isolated product.

results are shown in Table 4. Interestingly, the majority of the 1,2-DHPs displayed antiproliferative activity against all cell lines, in the low micromolar range. The most active compound was **5e**, which exhibited GI_{50} values in the range of 2.7–5.6 μM. The results obtained are comparable to those of the standard anticancer drug cisplatin (CDDP), which was used as reference drug.

Conclusion

The one-pot multicomponent Hantzsch reaction for the synthesis of substituted dihydropyridines was performed under green heterogeneous and neat conditions in the presence of 0.04 g/mmol of a 40 wt % phosphotungstic acid on alumina catalyst, which is simple, safe and environmentally benign to prepare, fully recoverable, and reusable for up to 8 runs. A high AE of 74% and a low E-factor of 0.72 highlight the green character of the procedure. More importantly, PW/alumina was able to catalyze a wide range of reactions involving different aromatic aldehydes to give products in good to excellent yields and interestingly all with the same general structure, corresponding to the 1,2-DHP regioisomer, unless when using aliphatic aldehydes.

Experimental

General

All the chemicals used were purchased form Sigma-Aldrich. IR spectroscopy studies were conducted on a Shimadzu IRAffinity-1 FTIR spectrometer calibrated against 1602 cm^{-1} polystyrene absorbance spectra. The ^{1}H NMR and ^{13}C NMR spectra were measured on a Bruker Avance III HD® NMR spectrometer equipped with an Ascend 500 11.75 Tesla superconducting magnet, operating at 500.13 MHz for ^{1}H and 125.76 MHz for ^{13}C, and a multinuclear 5 mm PABBO probe. Melting points were recorded on a Stuart® SMP11 melting point apparatus. Reactions were monitored by TLC and GC. Mass spectra were measured via a Thermo Scientific GC/MS DSQ II device, which contained a column: EC-5 30 m × 0.25 mm i.d. × 0.25 μm or using the direct-infusion method using a Waters® ACQUITY® TQD system with a tandem quadrupole mass spectrometer. The software used was ThermoXcalibur 2.2 SP1.48. The XRF spectroscopy analysis of the catalyst was performed using a Bruker S2 Ranger®.

Catalyst preparation

The method previously reported by Zhu et al. was used to prepare several supported heteropoly acids (silicotungstic and PW) on various supports at different loadings [28]. For 1 g of a catalyst batch with a loading of 20 wt %, 0.8 g of the support and 0.2 g of a heteropoly acid were stirred in a minimum amount of distilled water to form a slurry for 8 hours at room temperature in a 10 mL round-bottomed flask. Then, the catalyst was dried overnight at 110 °C and ultimately calcined at 250 °C in a furnace under air for 4 h to obtain a white powder (1 g), which was stored in a calcium chloride/silica-filled desiccator.

General method

The general method involved the addition of 1 equiv of the aldehyde (5 mmol), 2 equiv ethyl acetoacetate (**2**, 10 mmol), and 1 equiv ammonium acetate (**3**, 5 mmol) in one vessel. The reactants were left to stir together with 0.2 g of the catalyst (40 wt % PW on alumina). At intervals of 30 minutes, the reaction mixture was analyzed using TLC, GC, or both. With time, the reaction mixture was observed to change from colorless to yellow, which darkened or brightened to orange or yellow and thickened with the occurrence of crystals on the sides of the flask. Once the spot or the peak corresponding to the benzaldehyde disappeared on the TLC plate or in the gas chromatogram,

Table 4: Antiproliferative activity (GI_{50} values) of selected 1,2-DHPs against human solid tumor cells.[a]

compound	cell line					
	A549	HBL-100	HeLa	SW1573	T-47D	WiDr
5a	29 ± 4.6	23 ± 1.8	21 ± 2.0	31 ± 0.7	21 ± 2.5	22 ± 2.4
5b	>100	>100	28 ± 7.5	>100	>100	>100
5d	14 ± 3.1	19 ± 3.0	12 ± 4.5	22 ± 1.2	17 ± 3.6	17 ± 1.2
5e	**5.1 ± 0.3**	**4.8 ± 0.4**	**2.7 ± 0.5**	**5.6 ± 1.0**	**4.0 ± 0.3**	**3.3 ± 0.5**
5f	43 ± 14	42 ± 6.2	26 ± 4.0	49 ± 12	33 ± 5.1	41 ± 9.6
5g	18 ± 4.9	20 ± 0.9	22 ± 6.6	18 ± 6.8	22 ± 2.1	18 ± 1.6
5h	34 ± 4.7	38 ± 4.0	28 ± 4.6	33 ± 6.1	31 ± 0.9	39 ± 8.9
5i	23 ± 6.8	26 ± 2.0	18 ± 5.0	30 ± 0.3	20 ± 2.0	33 ± 4.8
5j	16 ± 6.7	16 ± 3.5	**4.9 ± 1.0**	11 ± 1.7	15 ± 1.9	19 ± 3.3
CDDP	**4.9 ± 0.2**	**1.9 ± 0.2**	**1.8 ± 0.5**	**2.7 ± 0.4**	17 ± 3.3	23 ± 4.3

[a]GI_{50} values are given in μM. The standard deviation was calculated from at least two independent experiments. CDDP (cisplatin) was used as a reference compound. Values in bold face represent the best antiproliferative data against tumor cell lines (GI_{50} < 10 μM).

the time was taken as the reaction was finished. The reaction mixture, obtained as a viscous oil, was filtered through a sinter funnel to remove any catalyst and washed using acetone, which was then evaporated in a rotary evaporator. The resultant crystals were then recrystallized using hot ethanol. The products were then characterized via IR, NMR, and MS analysis.

Hot filtration test

The optimized model reaction was monitored by GC, and the catalyst was left in the reaction mixture for 30 minutes in order to confirm heterogeneity. During these 30 minutes, the reaction started. However, upon removal of the catalyst by filtration, the reaction was left to carry on but stopped, and therefore catalyst leaching was not evident.

Antiproliferative tests

We selected the cancer cell lines A549 and SW1573 (nonsmall-cell lung), HBL-100, as well as T-47D (breast), HeLa (cervix), and WiDr (colon) to evaluate the antiproliferative activity. The tests were performed in 96-well plates using the SRB assay [29] with the following specifications: the cell seeding density was 2500 cells/well for A549, HBL-100, HeLa, and SW1573, and 5000 cells/well for T-47D and WiDr. The drug incubation time was 48 h. The optical density of each well was measured at 530 (primary) and 620 nm (secondary). The antiproliferative activity, expressed as GI_{50} values, was calculated according to the NCI formulas [30].

Supporting Information

Supporting Information File 1

Analytical data of the products.
[https://www.beilstein-journals.org/bjoc/content/supplementary/1860-5397-16-235-S1.pdf]

Acknowledgements

The authors would like to thank Prof. Robert M. Borg for assistance with the acquisition of the NMR spectra and Mr. Godwin Sammut for MS analyses.

Funding

The authors thank the University of Malta and the ENDEAVOUR Scholarship Scheme (Malta), part-financed by the European Union–European Social Fund (ESF) under the Operational Programme II–Cohesion Policy 2014-2020, "Investing in human capital to create more opportunities and promote the well-being of society" for financial and technical support. A. P. and J. M. P. thank the Spanish Government for financial support through project PGC2018-094503-B-C22 (MCIU/AEI/FEDER, UE). A. P. thanks the EU Social Fund (FSE) and the Canary Islands ACIISI for a predoctoral grant TESIS2020010055.

ORCID® iDs

Giovanna Bosica - https://orcid.org/0000-0002-5674-870X
José M. Padrón - https://orcid.org/0000-0001-6268-6552
Adrián Puerta - https://orcid.org/0000-0002-7975-1960

References

1. Dömling, A.; AlQahtani, A. D. General Introduction to MCRs: Past, Present, and Future. In *Multicomponent Reactions in Organic Synthesis;* Zhu, J.; Wang, Q.; Wang, M.-X., Eds.; Wiley-VCH: Weinheim, Germany, 2014; pp 1–12. doi:10.1002/9783527678174.ch01
2. Ganem, B. *Acc. Chem. Res.* **2009,** *42,* 463–472. doi:10.1021/ar800214s
3. Alvim, H. G. O.; da Silva Júnior, E. N.; Neto, B. A. D. *RSC Adv.* **2014,** *4,* 54282–54299. doi:10.1039/c4ra10651b
4. Touré, B. B.; Hall, D. G. *Chem. Rev.* **2009,** *109,* 4439–4486. doi:10.1021/cr800296p
5. Sheldon, R. A. *Green Chem.* **2017,** *19,* 18–43. doi:10.1039/c6gc02157c
6. Ciriminna, R.; Pagliaro, M. *Org. Process Res. Dev.* **2013,** *17,* 1479–1484. doi:10.1021/op400258a
7. Abdel-Mohsen, H. T.; Conrad, J.; Beifuss, U. *Green Chem.* **2012,** *14,* 2686–2690. doi:10.1039/c2gc35950b
8. Ghorbani-Choghamarani, A.; Zolfigol, M. A.; Salehi, P.; Ghaemi, E.; Madrakian, E.; Nasr-Isfahani, H.; Shahamirian, M. *Acta Chim. Slov.* **2008,** *55,* 644–647.
9. Sharma, V. K.; Singh, S. K. *RSC Adv.* **2017,** *7,* 2682–2732. doi:10.1039/c6ra24823c
10. Javanbakht, S.; Shaabani, A. *ACS Appl. Bio Mater.* **2020,** *3,* 156–174. doi:10.1021/acsabm.9b00799
11. Lavilla, R. *J. Chem. Soc., Perkin Trans. 1* **2002,** 1141–1156. doi:10.1039/b101371h
12. Silva, E. M. P.; Varandas, P. A. M. M.; Silva, A. M. S. *Synthesis* **2013,** *45,* 3053–3089. doi:10.1055/s-0033-1338537
13. Nasr-Esfahani, M.; Montazerozohori, M.; Raeatikia, R. *Maejo Int. J. Sci. Technol.* **2014,** *8,* 32–40.
14. Pal, S.; Choudhury, L. H.; Parvin, T. *Synth. Commun.* **2013,** *43,* 986–992. doi:10.1080/00397911.2011.618283
15. Pacheco, S. R.; Braga, T. C.; da Silva, D. L.; Horta, L. P.; Reis, F. S.; Ruiz, A. L. T. G.; de Carvalho, J. E.; Modolo, L. V.; de Fatima, A. *Med. Chem.* **2013,** *9,* 889–896. doi:10.2174/1573406411309060014
16. Pramanik, A.; Saha, M.; Bhar, S. *ISRN Org. Chem.* **2012,** 1–7. doi:10.5402/2012/342738
17. Vanden Eynde, J.; Mayence, A. *Molecules* **2003,** *8,* 381–391. doi:10.3390/80400381
18. D'Alessandro, O.; Sathicq, Á. G.; Sambeth, J. E.; Thomas, H. J.; Romanelli, G. P. *Catal. Commun.* **2015,** *60,* 65–69. doi:10.1016/j.catcom.2014.11.022
19. Shen, L.; Cao, S.; Wu, J.; Zhang, J.; Li, H.; Liu, N.; Qian, X. *Green Chem.* **2009,** *11,* 1414–1420. doi:10.1039/b906358g
20. Bosica, G.; Abdilla, R. *Green Chem.* **2017,** *19,* 5683–5690. doi:10.1039/c7gc02038d
21. Sheldon, R. A. *Chem. Commun.* **2008,** 3352–3365. doi:10.1039/b803584a

22. Cave, G. W. V.; Raston, C. L.; Scott, J. L. *Chem. Commun.* **2001,** 2159–2169. doi:10.1039/b106677n
23. Heravi, M. M.; Bakhtiari, K.; Javadi, N. M.; Bamoharram, F. F.; Saeedi, M.; Oskooie, H. A. *J. Mol. Catal. A: Chem.* **2007,** *264,* 50–52. doi:10.1016/j.molcata.2006.09.004
24. Bitaraf, M.; Amoozadeh, A.; Otokesh, S. *J. Chin. Chem. Soc.* **2016,** *63,* 336–344. doi:10.1002/jccs.201500453
25. Liu, Y.; Zhao, G.; Wang, D.; Li, Y. *Natl. Sci. Rev.* **2015,** *2,* 150–166. doi:10.1093/nsr/nwv014
26. Firuzi, O.; Javidnia, K.; Mansourabadi, E.; Saso, L.; Mehdipour, A. R.; Miri, R. *Arch. Pharmacal Res.* **2013,** *36,* 1392–1402. doi:10.1007/s12272-013-0149-8
27. Sharma, M. G.; Vala, R. M.; Patel, D. M.; Lagunes, I.; Fernandes, M. X.; Padrón, J. M.; Ramkumar, V.; Gardas, R. L.; Patel, H. M. *ChemistrySelect* **2018,** *3,* 12163–12168. doi:10.1002/slct.201802537
28. Zhu, S.; Zhu, Y.; Gao, X.; Mo, T.; Zhu, Y.; Li, Y. *Bioresour. Technol.* **2013,** *130,* 45–51. doi:10.1016/j.biortech.2012.12.011
29. Orellana, E. A.; Kasinski, A. L. *Bio-Protoc.* **2016,** *6,* e1984. doi:10.21769/bioprotoc.1984
30. Monks, A.; Scudiero, D.; Skehan, P.; Shoemaker, R.; Paull, K.; Vistica, D.; Hose, C.; Langley, J.; Cronise, P.; Vaigro-Wolff, A.; Gray-Goodrich, M.; Campbell, H.; Mayo, J.; Boyd, M. *J. Natl. Cancer Inst.* **1991,** *83,* 757–766. doi:10.1093/jnci/83.11.757

License and Terms

BEILSTEIN JOURNAL OF ORGANIC CHEMISTRY

A novel and robust heterogeneous Cu catalyst using modified lignosulfonate as support for the synthesis of nitrogen-containing heterocycles

Bingbing Lai[1], Meng Ye[1], Ping Liu[2], Minghao Li[1], Rongxian Bai[*1] and Yanlong Gu[*1,3]

Full Research Paper

Open Access

Address:
[1]Key Laboratory of Material Chemistry for Energy Conversion and Storage, Ministry of Education. Hubei Key Laboratory of Material Chemistry and Service Failure, School of Chemistry and Chemical Engineering, Huazhong University of Science and Technology, 1037 Luoyu Road, Hongshan District, Wuhan 430074, P. R. China, [2]School of Chemistry and Chemical Engineering, the Key Laboratory for Green Processing of Chemical Engineering of Xinjiang Bingtuan, Shihezi University, Shihezi City, 832004, China and [3]State Key Laboratory for Oxo Synthesis and Selective Oxidation, Lanzhou Institute of Chemical Physics, Chinese Academy of Sciences, Lanzhou 730000, P. R. China

Email:
Rongxian Bai[*] - bairx@126.com; Yanlong Gu[*] - klgyl@hust.edu.cn

* Corresponding author

Keywords:
biomass; heterogeneous catalyst; immobilized copper catalyst; lignosulfonate; nitrogen-containing heterocycles; solid acid

Beilstein J. Org. Chem. **2020,** *16,* 2888–2902.
https://doi.org/10.3762/bjoc.16.238

Received: 28 August 2020
Accepted: 06 November 2020
Published: 26 November 2020

This article is part of the thematic issue "Green chemistry II".

Associate Editor: L. Vaccaro

Abstract

A waste biomass, sodium lignosulfonate, was treated with sodium 2-formylbenzenesulfonate, and the phenylaldehyde condensation product was then used as a robust supporting material to immobilize a copper species. The so-obtained catalyst was characterized by many physicochemical methods including FTIR, EA, FSEM, FTEM, XPS, and TG. This catalyst exhibited excellent catalytic activity in the synthesis of nitrogen-containing heterocycles such as tricyclic indoles bearing 3,4-fused seven-membered rings, 2-arylpyridines, aminonaphthalenes and 3-phenylisoquinolines. In addition, this catalyst showed to be recyclable and could be reused several times without significant loss in activity during the course of the reaction process.

Introduction

Heterogeneous metal catalysts have been continuously receiving considerable attention in the field of organic synthesis owing to the advantages of easy separation and recycling [1-4]. However, most of them often encounter the issues of poor stability and metal leaching [5], especially when the substrates and/or products have a powerful coordinating ability with the

immobilized metal [6,7]. For instance, nitrogen-containing substrates or target products sometimes may lead to the fast deactivation of catalysts, which consequently impair the recyclability of the catalysts [8-11]. Therefore, special efforts should be paid to enhancing the robustness of heterogeneous metal catalysts.

Sodium lignosulphonate (LS) is a waste from the paper-making industry, containing aryl- and sodium sulfonate groups [12]. As a category of polyanionic material, LS can easily load metal ions via an ion exchange process [13]. Given the desirable property, an array of heterogeneous metal catalysts using LS as support were successfully designed and utilized to catalyze some typical organic reactions in our previous work. In 2014 [14], LS were used by our group, for the first time, as a solid support of cationic catalysts. The obtained catalysts were then successfully applied to many organic transformations, in which the catalysts showed not only high activity but also good recyclability. However, the stability and durability of LS was very limited especially in polar solvents such as H_2O, EtOH and at harsh conditions. In a further study of our previous work [15], a LS/dicationic ionic liquid composite was prepared via an ion exchange process, and then used as catalyst support for preparing a heterogeneous Cu-based catalyst, the thereby obtained catalyst displayed remarkable performance in the Glaser heterocoupling reaction. Combining two successful attempts, a further study concerning improvement of the robustness of catalysts and active sites when using LS as support is urgently needed.

In this work, we present a novel heterogeneous Cu catalyst using modified LS as support by a consecutive process involving the phenol–aldehyde condensation of LS with 2-formylbenzenesulfonic acid sodium (FAS), ion exchange and acidification. Special interest is given in the application of the prepared catalyst for synthesizing nitrogen-containing heterocycles. The results showed that the grafting of FAS on LS provided the support with more ion exchange sites, significantly increasing the loading capability of the Cu species. The acidification process could transform the $–SO_3Na$ group left in the catalyst after ion exchange into $–SO_3H$, enabling the catalyst to catalyze the model reactions without the addition of protonic acid. The catalyst demonstrated impressive catalytic performance in the synthesis of nitrogen-containing heterocycles, and there was no deactivation even after 6 times of recycling, exhibiting enhanced stability compared to that without grafting of FAS. It is expected that this research would shed light on the design of heterogeneous metal catalysts with high activity and stability.

Results and Discussion

The whole preparation process of the catalyst is depicted in Figure 1. Firstly, the support was prepared through phenol–formaldehyde condensation reaction of LS and FAS. The FAS was chosen to embellish LS in consideration of the following reason: FAS skeleton consists of both aldehyde and sulfonic groups, so the grafting of FAS and LS can be easily realized via phenol–formaldehyde condensation reaction, and therefore equips the generated polymeric support with more sulfonic groups. The heterogeneous Cu catalyst (LS-FAS-Cu) was finally obtained through refluxing of LS-FAS with $Cu(OTf)_2$ in ethanol, and the loading capacity of Cu was confirmed to be 0.92 mmol/g by means of ICP. For comparison, two controlled heterogeneous catalysts, namely Resin-Cu and LS-FM-Cu were prepared using commercially available Amberlyst-15 and the material [13] was synthesized by condensation of formaldehyde and LS as supports, respectively (see Supporting Information File 1, Figure S1 and Figure S2), and the loading capacity of Cu was 0.45 mmol/g and 0.56 mmol/g, respectively.

Characterization of the prepared materials

The primary purpose of using FAS to modify LS was to increase the amount of $–SO_3Na$ groups in the supporting material. For the verification of this assumption, elemental analysis was firstly conducted and the results are listed in Table S1 (see Supporting Information File 1). From the results, it was found

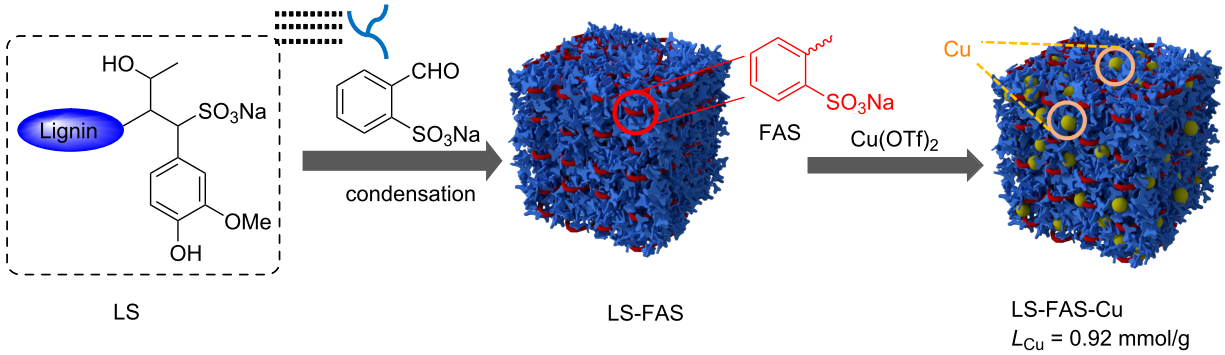

Figure 1: Schematic illustration for the preparation of the catalyst in this work.

that with introduction of the FAS moiety, LS-FAS showed a higher content of C, H and S elements compared to pristine LS, indicating the successful grafting of FAS on LS. According to the increment of the S element, the increment of $-SO_3Na$ groups was 1.26 mmol/g. The chemical compositions on the surfaces of LS, LS-FAS, LS-FAS-Cu were further characterized by FTIR. As shown in Figure 2, the broad and strong absorption peak at around 3000 cm^{-1} was associated with the stretching vibration of the –OH group in the skeleton of LS [16]. The tiny peak at approximately 2900 cm^{-1} was assigned to the stretching vibration of the $-CH_2-$ moiety. The characteristic peak of the aromatic benzene ring appeared at about 1500 cm^{-1} [17]. The vibration bands at 1000–1200 cm^{-1} were attributed to the $-SO_3$ and O–S–O stretching of the $-SO_3Na$ (or $-SO_3H$) group [18,19]. Grafting of the FAS moiety changed the peak pattern of $-SO_3Na$ in LS-FAS material, and the immobilization of the Cu complex shifted the corresponding peaks to a higher wavenumber position, implying the successful coordination of LS-FAS to the Cu complex.

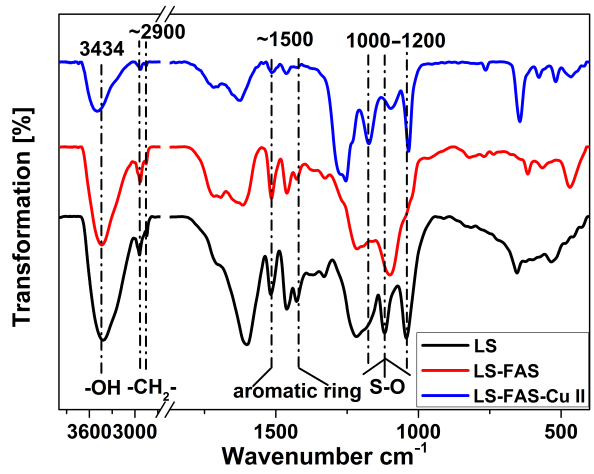

Figure 2: FTIR spectra of LS, LS-FAS, and LS-FAS-Cu.

The thermal behavior of LS-FAS and LS-FAS-Cu was investigated by TG in a temperature range of 40–800 °C (Figure 3). When the temperature was lower than 200 °C, both of them exhibited good stability with a slight drop of the curves, possibly due to the loss of a trace amount of absorbed water [20,21]. Two sharp weight losses were identified on the TG curves as temperature rose. The first loss within 224–327 °C may be caused by decomposition and elimination of the $-SO_3Na$ groups and the introduced small organic species in the materials [22], while the second loss at higher temperature of 327–448 °C may be attributed to decomposition of the support skeleton [23]. The thermal stability of referential Resin-Cu catalyst was also investigated by TG analysis (Supporting Information File 1, Figure S3), showing a high thermal stability as well [24-26]. The above results indicated that all prepared materials could remain stable in the system when used to catalyze organic reactions.

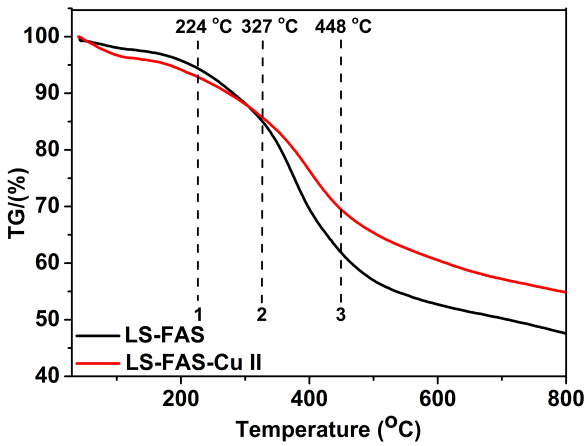

Figure 3: Thermogravimetric weight loss of the obtained materials LS-FAS and LS-FAS-Cu.

FSEM (field emission scanning electron microscopy) and FTEM (field emission transmission electron microscopy) were used to observe the surface morphologies of different catalysts, and the results are presented in Figure 4. The LS-FAS-Cu catalyst featured irregular and blocky morphology with uneven size from 100 nm to 400 nm (Figure 4a–d). In addition, the elemental mapping images clearly revealed the presence and uniform distribution of C, Cu, O, and S in LAS-FAS-Cu.

XPS was further utilized to analyze the chemical states of the elements on the surface of the catalyst (Figure 5). The wide survey spectrum of LS-FAS-Cu showed that all of the essential elements could be detected. In the high-resolution spectrum of C 1s, the peak at 284.9 eV was ascribed to C–C, and the peak at 286.3 eV corresponded to C–O/C–S [27,28]. The O 1s spectrum clearly evidenced the presence of oxygen atoms with three kinds of chemical environments: the peaks at 532.9 eV and 532.2 eV were attributed to –OH and –C–O– groups, respectively, while the peak at 533.7 eV was attributed to $-SO_3$ [12]. In the spectrum of Cu $2p_{3/2}$, the peak at ≈936 eV was assigned to Cu^{2+} in the spinel, accompanied by the characteristic Cu^{2+} shakeup satellite peaks at 938–948 eV, while the peak at ≈933 eV suggested the presence of Cu^+ and/or Cu^0 species. Because Cu $2p_{3/2}$ XPS cannot differentiate between Cu^+ and Cu^0, Auger Cu LMM spectra were further recorded, and the results confirmed the presence of Cu^+ at ≈570 eV, while Cu^0 at 565.6 eV [29-31], meaning that Cu^{2+} species were partially reduced during the course of immobilization.

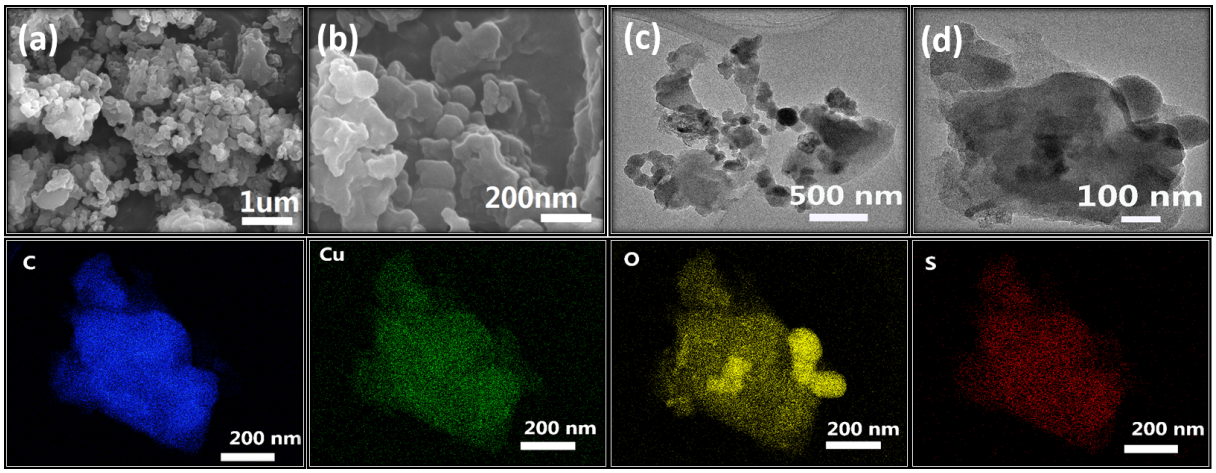

Figure 4: FSEM imagine of LS-FAS-Cu in different scale label a) 1 μm, b) 200 nm; FTEM images of LS-FAS-Cu in 500 nm (c) and 100 nm (d); and the elemental mapping of LS-FAS-Cu for C, Cu, O and S elements.

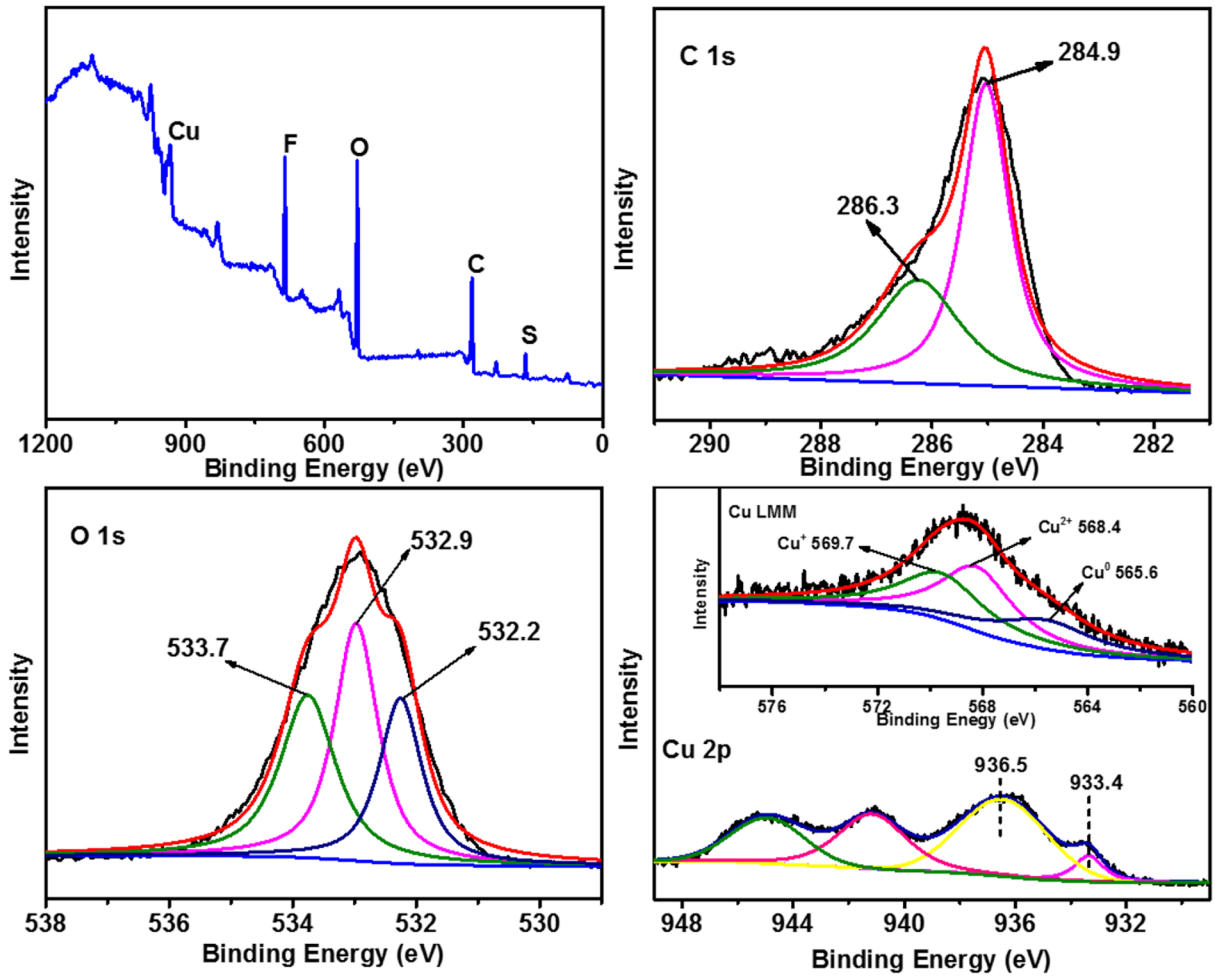

Figure 5: XPS spectra of LS-FAS-Cu in the regions of C 1s, O 1s, Cu $2p_{3/2}$ and Cu LMM (inset).

Catalytic activity of the catalysts

With the catalysts in hand, we investigated their catalytic activity in organic reactions. Tricyclic indole alkaloids bearing 3,4-fused seven-membered rings have attracted much attention because of their interesting molecular architectures and important biological activities [32,33]. Here the three-component reaction of 4-aminoindole (**1a**), 4-methylbenzaldehyde (**2a**) and diethyl acetylenedicarboxylate (**3a**) was performed to construct the seven-membered indole ring system with the aid of the LS-FAS-Cu catalyst, and the results are summarized in Table 1. At the beginning, the three-component reaction was conducted without the presence of any catalyst, but no products were formed (Table 1, entry 1). After screening different kind of solvents (Table 1, entries 2–8) at 60 °C, EtOH was found to be the best one, and the target product **4a** was obtained in 86% yield (Table 1, entry 8). The referential catalysts LS-FM-Cu and Resin-Cu showed inferior catalytic activity for this reaction, probably attributed to the low content of Cu species in the materials (Table 1, entries 9 and 10). Further investigation revealed that the reaction was also affected by the dosage of catalyst and the temperature. The yield was decreased significantly with the catalyst dosage decreasing (Table 1, entry 8 and 13). Decreasing the temperature will result in a significant loss of yields (Table 1, entry 11), prolong the time could increase the yield but still lower than that at 60 °C (Table 1, entry 12). Thus the optimal conditions were confirmed to be 20 mol % of LS-FAS-Cu (the Cu loading with reference to the substrates **1a**), 60 °C and 7 h. To our delight, the reaction could be easily scaled up to 10 mmol without significant loss of the efficiency and selectivity (Table 1, entry 14).

Under the optimal conditions, the substrate scope of the model reaction was extended and the results were shown in Scheme 1. Aldehydes **2** with different functional groups on the benzene ring could react smoothly with compounds **1a** and **3a**, producing the corresponding 3,4-fused tricyclic indoles **4b–d** with yields ranging from 46% to 64%. *o*-Anisaldehyde, with steric-hindrance effect, also reacted efficiently in this reaction and gave product **4e** in 55% yield. 2-Naphthaldehyde also proceeded well with **1a** and **3a** and the product **4f** was isolated in 60% yield. Aldehydes with multi-substituted functional groups also worked well in this reaction and the corresponding products were obtained in moderate yields (**4g** and **4h**). It should be noted that heterocyclic aldehydes such as

Table 1: Three-component reaction of **1a**, **2a**, and **3a** to synthesis of **4a**[a].

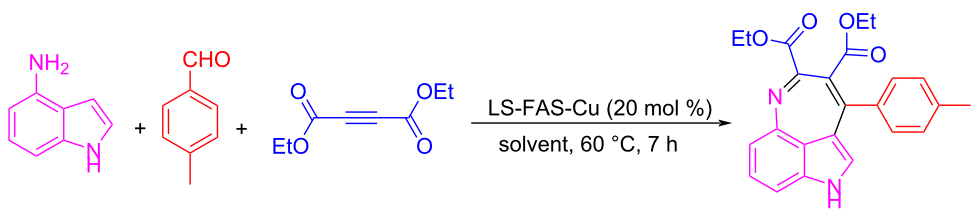

1a **2a** **3a** **4a**

Entry	Solvent	Yield [%][b]
1[c]	EtOH	0
2	AcOH	0
3	MeOH	59
4	THF	21
5	DMSO	trace
6	H_2O	0
7	CH_3NO_2	35
8	EtOH	86
9[d]	EtOH	62
10[e]	EtOH	57
11[f]	EtOH	49
12[g]	EtOH	71
13[h]	EtOH	37
14[i]	EtOH	84

[a]Reaction conditions: **1a**/**2a**/**3a** = 1.5:1:1.5; 1.0 mL. [b]Isolated yields. [c]Without the catalyst. [d]LS-FM-Cu was used. [e]Resin-Cu was used. [f]40 °C. [g]40 °C, 24 h. [h]10 mol % LS-FAS-Cu was used. [i]10 mmol scale reaction.

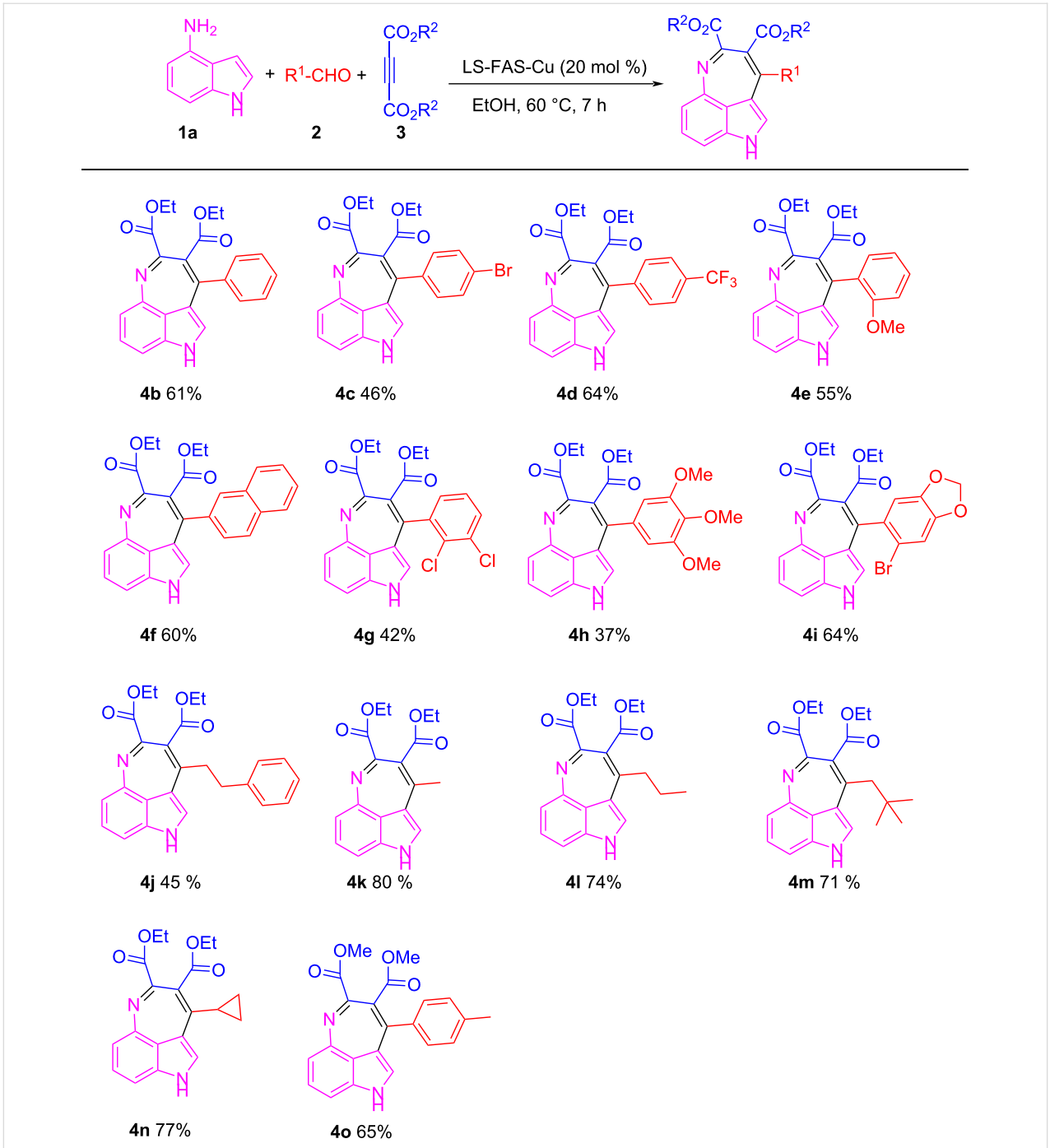

Scheme 1: Substrate scope of LS-FAS-Cu catalyzed three-component reactions of 4-aminoindoles, alkynes and aldehydes.

2-bromo-4,5-methylenedioxybenzaldehyde (**2i**) could also successfully engage in this reaction and the yield of product **4i** was up to 64%. In the following investigation, the aliphatic aldehydes **2j–m** were also successfully reacted, and the products **4j–m** were obtained in good to excellent yields. The acid-labile cyclopropanecarboxaldehyde (**2n**) could also participate well, and the product **4n** was obtained in 77% yield without damage of the cyclopropane structure. Dimethyl acetylenedicarboxylate (**3b**), **1a** and **2a** could tolerate the LS-FAS-Cu-promoted conditions as well, and gave the product **4o** in 65% yield. The successful attempts in the three-component reaction of 4-aminoindoles (**1a**), alkynes and aldehydes indicate that the heterogeneous catalyst LS-FAS-Cu is competent for catalyzing nitrogen-containing heterocyclic compounds without significant damage of the Cu species.

The pyridine-containing moiety, such as arylpyridines, widely exist in natural products, pharmaceutical agents and functional materials [34-37]. Traditional methods for synthesizing pyridine-containing derivatives include condensation reactions, cross-coupling, ring-closing, metathesis, cycloadditions, radical reactions and microwave-assisted reactions [38-40]. In this work, we attempt to develop a greener, simpler, more efficient and recyclable system to synthesize arylpyridine derivatives. Initially, the reaction of acetophenone (**5a**) and 1,3-diaminopropane (**6a**) was conducted with the aid of LS-FAS-Cu and $TsOH·H_2O$ in a variety of solvents at 100 °C for 24 h under an oxygen atmosphere (Table 2, entries 1–6). After comparing the yield, EtOH was found to be the optimal solvent, generating the target product 2-arylpyridine **7a** in 75% yield. Other kinds of solvents were ineffective (Table 2, entries 1–5 vs entry 6). Only the addition of $TsOH·H_2O$ showed a reluctant activity in this organic transformation (Table 2, entry 7). When homogeneous $Cu(OTf)_2$ was used, only 20% of **7a** was isolated (Table 2, entry 8). The two referential catalysts LS-FM-Cu and Resin-Cu exhibited low catalytic efficiencies in the model reaction, only 60% and 48% of **7a** were obtained, respectively (Table 2, entries 9 and 10). The results indicated that the yields were also greatly affected by the catalyst loading and proper acid additives. In the same solvent, the yield decreased with the decreasing of the catalyst loading (Table 2, entry 6 vs entries 9 and 10).

In order to utilize the residual $–SO_3Na$ groups in LS-FAS-Cu after immobilization of the Cu species, LS-FAS-Cu were further acidized by sulfuric acid solution (2 M) and denoted as LSA-FAS-Cu. The amount of $–SO_3H$ was determined through acid-base titration and elemental analysis, respectively (Table 3). The results showed that the density of $–SO_3H$ determined by acid-base titration was much lower than that confirmed by elemental analysis, indicating that a portion of sulfur existed in the form of Cu complex and $–SO_3Na$. Afterwards, the catalytic activity of LSA-FAS-Cu in the model reaction was investigated under the optimal conditions except for the absence of $TsOH·H_2O$. Considering that the density of $–SO_3H$ in LSA-FAS-Cu was a half of $TsOH·H_2O$, so the amount of LSA-FAS-Cu should be doubled. To our delight, although the reaction time was prolonged a little, LSA-FAS-Cu (Cu 40 mol %, $–SO_3H$ 0.5 equiv) could also promote the reaction smoothly and generated **7a** in 74% yield (Table 2, entry 11), suggesting that the acidification process enabled the catalyst to catalyze the model reaction without addition of $TsOH·H_2O$.

Using LSA-FAS-Cu as catalyst, the substrate scope of the reaction was subsequently investigated, and it was found that the reaction could tolerate a wide range of functionalities, including fluoro, chloro, iodo, cyclohexane and benzyloxy moieties. Acetophenones with an electron-donating group in the *para*-position of the aromatic ring afforded the target products in better

Table 2: Optimizing the reaction condition of acetophenones and 1,3-diaminopropane to synthesis 2-arylpyridine derivatives.[a]

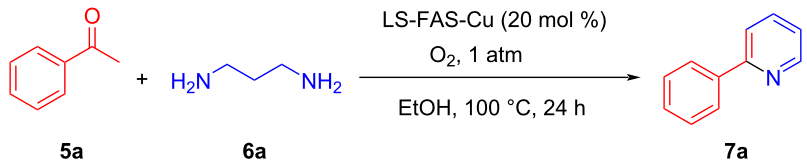

5a **6a** **7a**

Entry	Solvent	Yield [%][b]
1	CH_3CN	30
2	toluene	5
3	CH_2Cl_2	NR
4	H_2O	trace
5[c]	THF	trace
6	EtOH	75
7[d]	EtOH	NR
8[e]	EtOH	20
9[f]	EtOH	60
10[g]	EtOH	48
11[h]	EtOH	74

[a]Reaction conditions: **5a** (0.2 mmol), **6a** (0.6 mmol), solvent (1.0 mL), 0.6 equiv $TsOH·H_2O$, O_2 (1 atm), 24 h. [b]Isolated yield. [c]60 °C. [d]Only 0.5 equiv $TsOH·H_2O$ was used. [e]$Cu(OTf)_2$ (20 mol %) was used. [f]Referential catalyst LS-FM-Cu (20 mol %) was used. [g]Referential catalyst Resin-Cu (20 mol %) was used. [h]Catalyst: LSA-FAS-Cu [Cu (40 mol %), $–SO_3H$ (0.5 equiv)], 26 h.

Table 3: Acid density of catalyst.

Sample	Totally S content[a] (mmol/g)	SO_3H density[b] (mmol/g)
LSA-FAS-Cu	2.08	1.16

[a]Determined by EA. [b]Determined by acid–base titration.

yields than the electron-withdrawing groups (Table 4, **7b**–**j** and **7k**–**m**). 3'-Methylacetophenone (**5n**) and 2-acetonaphthone (**5o**) could also react with **6a**, and give the desired product **7n** and **7o** in 65% and 58% yield, respectively. Some disubstituted and trisubstituted acetophenones were also examined, and most of them could generate the desired products in moderate yields (**7p**–**t**). It was noted that heterocycles-substituted ketones also showed high reactivity in this reaction, and the corresponding products were obtained in good yields (**7u**–**w**).

In the following investigation, the LS-FAS-Cu was also found to be an efficient catalyst for the synthesis of aminonaphthalene derivatives (Table 5). The substituent effect of aniline was examined systematically, and the results showed that anilines bearing electron-donating groups such as Me, OMe and *t*-Bu at the *para*-position could convert smoothly and give the corresponding products in excellent yields (**10a**–**c**). The anilines with electron-withdrawing substituents such as 4-bromoaniline (**9d**) worked sluggishly and only a moderate yield of **10d** was obtained. Disubstituted anilines also tolerated the catalytic system, generating the product **10e** in 66% yield. Naphthylamine (**9f**)

Table 4: Substrate scope of the ketones catalyzed by LSA-FAS-Cu.

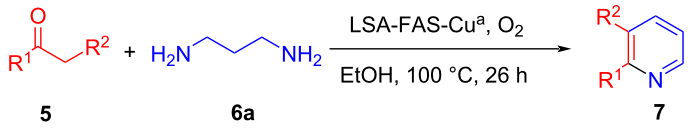

5 **6a** **7**

Entry	Product	Yield[b] (%)	Entry	Product	Yield[b] (%)
1	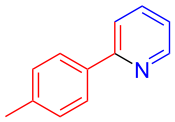 **7b**	71	12	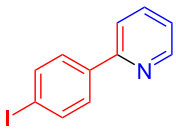 **7m**	39
2	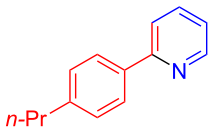 **7c**	70	13	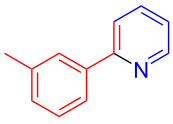 **7n**	65
3	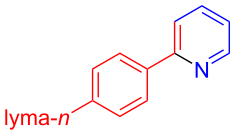 **7d**	68	14	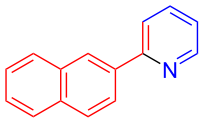 **7o**	58
4	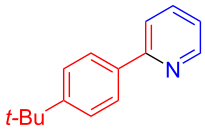 **7e**	63	15	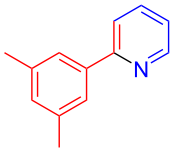 **7p**	68
5	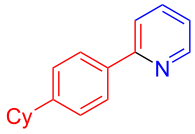 **7f**	60	16	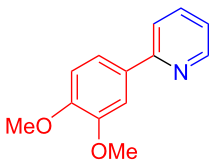 **7q**	56

Table 4: Substrate scope of the ketones catalyzed by LSA-FAS-Cu. (continued)

6	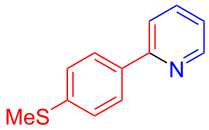 **7g**	82	17	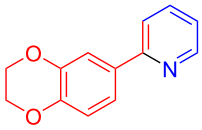 **7r**	64
7	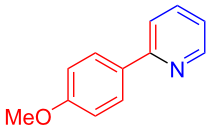 **7h**	65	18	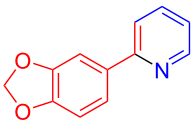 **7s**	71
8	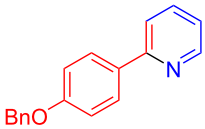 **7i**	67	19	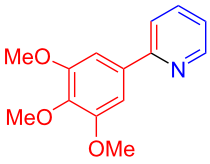 **7t**	73
9	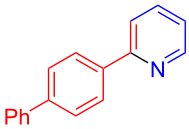 **7j**	63	20	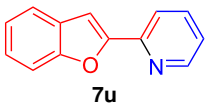 **7u**	76
10	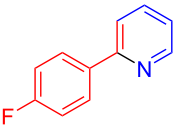 **7k**	45	21	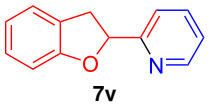 **7v**	75
11	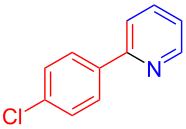 **7l**	40	22	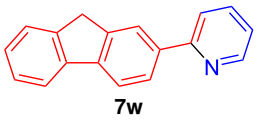 **7w**	69

[a]LSA-FAS-Cu [Cu (40 mol %), $-SO_3H$ (0.5 equiv). [b]Isolated yields.

also reacted positively with 2-(phenylethynyl)acetophenone (**8a**) and 70% of **10f** was obtained. The attempts of aliphatic amines were also successful, obtaining the corresponding products **10g–i** in good to excellent yields. It should be noted that secondary amines such as morpholine (**9j**) also showed high reactivity in this reaction and **10j** was obtained in 81% yield. The substituent effect of 2-(phenylethynyl)acetophenone was studied subsequently, and the results showed that fluoro, chloro, aliphatic chain and cycloolefin-substituted 2-(phenylethynyl)acetophenone could react smoothly, generating the target products **10k–o** in excellent yields. Unfortunately, aniline substituted with a strong electron-withdrawing group at the *para*-position and 2-(phenylethynyl)acetophenone substituted with an electron-donating group were reluctant to react under this catalytic system, and no desired products were determined (**10p** and **10q**).

Substituted isoquinoline derivatives are considered as an important class of N-heterocyclic compounds, showing attractive physiological, biological and pharmacological activities [41-45]. Therefore, the feasibility of synthesizing isoquinoline derivatives using LSA-FAS-Cu as catalyst was investigated. As shown in Table 6, LS-FAS-Cu could promote 2-(phenylethynyl)benzaldehyde (**11a**) and urea (**12a**) to generate 3-phenylisoquinoline (**13a**) in excellent yield, while the referential catalysts showed inferior catalytic activity, which may be ascribed to the low loading capacity of Cu species (Table 6, entry 1 vs entries 2 and 3). In addition, by increasing the amount of catalyst, the yields could reach the ideal level (Table 6, entries 4 and 5).

The recyclability of LS-FAS-Cu was investigated based on the three-component reaction of 4-aminoindole (**1a**), 4-methylben-

zaldehyde (**2a**) and diethyl acetylenedicarboxylate (**3a**). In order to confirm the heterogeneity of this reaction, we investigated the Cu leaching during the reaction process. The reaction mixture (including the catalyst) was allowed to stir for a period of time firstly, and then the catalyst was isolated by hot filtration. The remaining liquid mixture was divided into two portions,

Table 5: LS-FAS-Cu catalyzed synthesis of aminonaphthalene derivatives.[a]

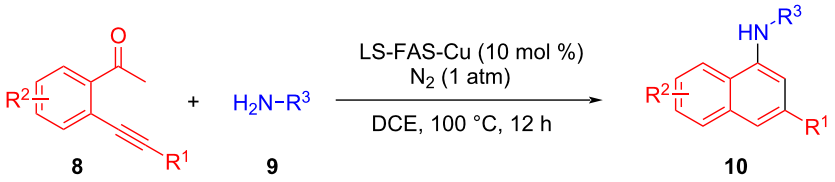

8 **9** **10**

Entry	R^1	R^2	R^3	Product	Yield[b] (%)
1	Ph	H	4-MeC_6H_4	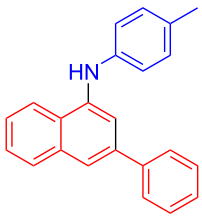 **10a**	81, (65)[c], (58)[d]
2	Ph	H	4-$OMeC_6H_4$	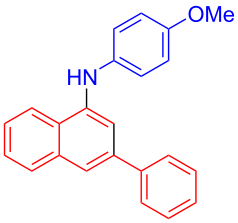 **10b**	85
3	Ph	H	4-*t*-BuC_6H_4	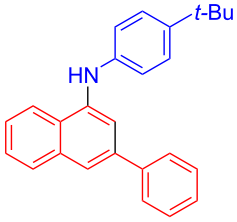 **10c**	79
4	Ph	H	4-BrC_6H_4	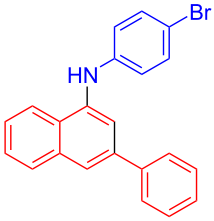 **10d**	55
5	Ph	H	3,4-$OMeC_6H_3$	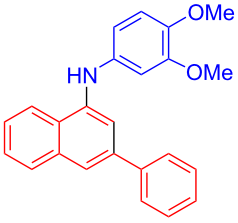 **10e**	66

Table 5: LS-FAS-Cu catalyzed synthesis of aminonaphthalene derivatives.[a] (continued)

6	Ph	H	1-naphthalene	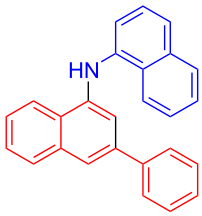 **10f**	70
7	Ph	H	Bn	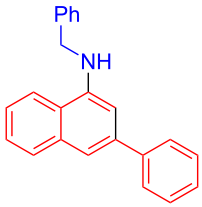 **10g**	61
8	Ph	H	*n*-Bu	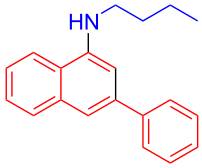 **10h**	83
9	Ph	H	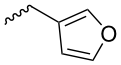	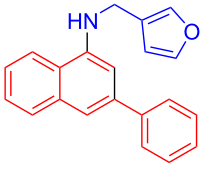 **10i**	88
10	Ph	H	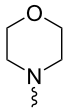	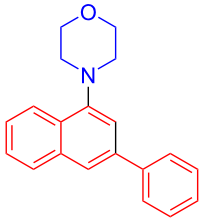 **10j**	81
11	Ph	Cl	4-MeC$_6$H$_4$	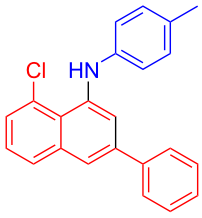 **10k**	78
12	Ph	F	4-MeC$_6$H$_4$	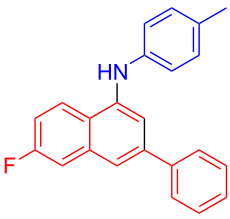 **10l**	63

Table 5: LS-FAS-Cu catalyzed synthesis of aminonaphthalene derivatives.[a] (continued)

13	4-FC_6H_4	H	4-MeC_6H_4	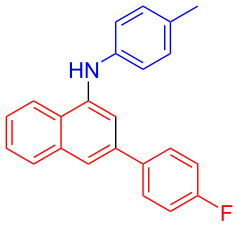 **10m**	71
14	*n*-hexyl	H	4-MeC_6H_4	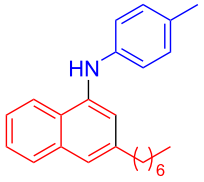 **10n**	54
15	cyclohexenyl	H	4-MeC_6H_4	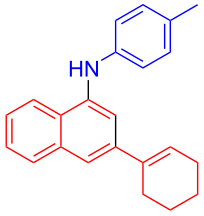 **10o**	42
16	Ph	H	4-$NO_2C_6H_4$	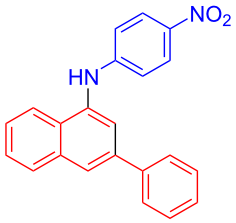 **10p**	n.d.
17	4-$OMeC_6H_4$	H	4-MeC_6H_4	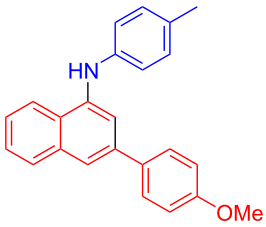 **10q**	n.d.

[a]Reaction conditions: **8** (0.2 mmol), **9** (0.24 mmol), DCE (1.0 mL), N_2, 12 h. [b]Isolated yields. [c]LS-FM-Cu (10 mol % was used) [d]Resin-Cu (10 mol %) was used.

one was isolated and used to calculate the target product yield, another one stirred for a period of time once again, and the latter did not show an increase in the yield. The Cu content in the reaction mixture after catalyst separation was confirmed to be 2.78 ppm by ICP. Besides, also with the aid of ICP-MS analysis, we found that there was no obvious change in the Cu content of the catalyst before and after the reaction (0.920 mmol/g vs 0.918 mmol/g). The above results not only verified the heterogeneous property of LS-FAS-Cu catalyst, but also implied that the loaded Cu species did not leach into the reaction system during the reaction process. The results associated with the recyclability of LS-FAS-Cu and two referential catalysts were summarized in Figure 6. After six runs of recycling (Figure 6a), LS-FAS-Cu was still capable of catalyzing the model reaction in 70% yield, indicating that the catalyst was robust and stable under the reaction conditions and could be recycled without obvious loss of catalytic activity. The slight decreasing of yield maybe caused by the mass loss of the catalyst during the recovery process (mass recovery 97.5%). In stark contrast, the two referential catalysts showed inferior re-

Table 6: Synthesis of the 3-phenylisoquinoline from **11a** and urea (**12a**).[a]

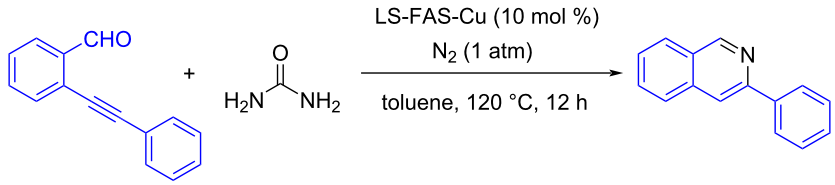

11a **12a** **13a**

Entry	Catalyst	Yield [%][b]
1	LS-FAS-Cu	85%, (84%)[3rd cycle]
2	LS-FM-Cu	74%
3	Resin-Cu	65%
4[c]	LS-FM-Cu	81%
5[c]	Resin-Cu	79%

[a]**11a**:**12a** = 1:1.2. [b]Isolated yield. [c]20 mol % of catalyst was used.

cyclability (Figure 6b and 6c) not only because the mass loss but also the low stability and capacity of the metals.

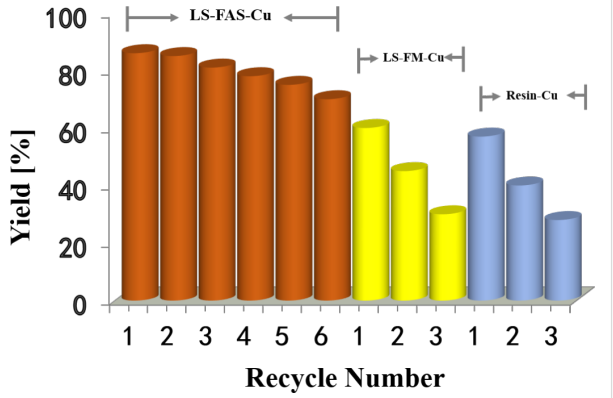

Figure 6: Recyclability of LS-FAS-Cu, LS-FM-Cu and Resin-Cu in the reaction between compounds **1a**, **2a** and **3a**.

Conclusion

A robust heterogeneous Cu catalyst was successfully prepared through immobilizing Cu on a novel and ecofriendly supporting material synthesized by the phenyl–aldehyde condensation reaction of FAS and LS. This catalyst could be used for the synthesis of several nitrogen-containing heterocycles and exhibited excellent catalytic activity. ICP-MS data showed that grafting of FAS on LS greatly increased the loading capability of the Cu species, which was considered to be responsible for the enhanced catalytic performance of the catalyst. This catalyst demonstrated a satisfying recyclability and could be reused several times without significant loss in activity. It is anticipated that this catalyst would have a broad application prospect considering the low cost and availability of the raw materials, as well as the facile preparation, multi-functionalities and recyclability of the catalyst.

Experimental

Experimental instrumentation

The chemical composition of the samples war characterized by Fourier transform infrared spectroscopy (FTIR, EQUINOX 55, Bruker) in the wavenumber range of 4000–400 cm^{-1} and X-ray photoelectron spectroscopy (XPS, AXIS-ULTRA DLD-600W, SHIMADZU) at a base pressure of 2×10^{-9} Pa. Elemental analyses (EA) were conducted using a Vario Micro cube Elemental Analyzer (Elementar, Germany). Thermogravimetric analyses (TGA) were performed under N_2 atmosphere by heating the materials from room temperature to 800 °C at a rate of 10 °C·min^{-1}. Before testing, all samples were degassed at 110 °C for 8 h under vacuum (10^{-5} bar) conditions. ICP-MS data were recorded on ELAN DRC-e device. The morphologies of samples were observed by scanning electron microscopy (SEM, Sirion 200, Holland) equipped with an energy dispersive X-ray (EDX) spectroscopy and transmission electron microscopy (TEM, Talos F200X), respectively. ^{1}H and ^{13}C NMR spectra were recorded on Bruker AV-400 spectrometer.

Catalyst preparation procedure

Typically, 3.0 g of LS were dissolved in 5.0 mL of deionized water, followed by adding 0.9 g of FAS. After the addition of 3.0 mL of concentrated HCl (37 wt %), the solution was continuously stirred at 90 °C for 8 h. Subsequently, the so-obtained support (denoted as LS-FAS) was filtered off, washed to be neutral and dried at 110 °C for 10 h.

Supporting Information

Supporting Information File 1

Characterization data, copies of NMR spectra and the preparation of the referential catalysts.
[https://www.beilstein-journals.org/bjoc/content/supplementary/1860-5397-16-238-S1.pdf]

Acknowledgements

The Cooperative Innovation Center of Hubei province and the testing center of HUST are acknowledged.

Funding

The authors thank the National Natural Science Foundation of China (21761132014, 21872060), the Fundamental Research Funds for the Central Universities of China (2016YXZD033), opening fund of Hubei Key Laboratory of Material Chemistry and Service Failure (No. 2017MCF01K) and Natural Science Foundation of Hubei province (No. 2019CFB219) for the financial support.

ORCID® iDs

Bingbing Lai - https://orcid.org/0000-0002-5450-0882
Ping Liu - https://orcid.org/0000-0002-3689-8364

References

1. Xie, F.; Lu, G.-P.; Xie, R.; Chen, Q.-H.; Jiang, H.-F.; Zhang, M. *ACS Catal.* **2019,** *9,* 2718–2724. doi:10.1021/acscatal.9b00037
2. Ma, Z.; Song, T.; Yuan, Y.; Yang, Y. *Chem. Sci.* **2019,** *10,* 10283–10289. doi:10.1039/c9sc04060a
3. Xie, C.; Niu, Z.; Kim, D.; Li, M.; Yang, P. *Chem. Rev.* **2020,** *120,* 1184–1249. doi:10.1021/acs.chemrev.9b00220
4. Dai, X.; Wang, B.; Wang, A.; Shi, F. *Chin. J. Catal.* **2019,** *40,* 1141–1146. doi:10.1016/s1872-2067(19)63397-8
5. Hübner, S.; de Vries, J. G.; Farina, V. *Adv. Synth. Catal.* **2016,** *358,* 3–25. doi:10.1002/adsc.201500846
6. Wei, Z.; Shao, F.; Wang, J. *Chin. J. Catal.* **2019,** *40,* 980–1002. doi:10.1016/s1872-2067(19)63336-x
7. Jin, T.; Hicks, M.; Kurdyla, D.; Hrapovic, S.; Lam, E.; Moores, A. *Beilstein J. Org. Chem.* **2020,** *16,* 2477–2483. doi:10.3762/bjoc.16.201
8. Han, Y.; Wang, Z.; Xu, R.; Zhang, W.; Chen, W.; Zheng, L.; Zhang, J.; Luo, J.; Wu, K.; Zhu, Y.; Chen, C.; Peng, Q.; Liu, Q.; Hu, P.; Wang, D.; Li, Y. *Angew. Chem., Int. Ed.* **2018,** *57,* 11262–11266. doi:10.1002/anie.201805467
9. Sardarian, A. R.; Eslahi, H.; Esmaeilpour, M. *ChemistrySelect* **2018,** *3,* 1499–1511. doi:10.1002/slct.201702452
10. Deraedt, C.; Ye, R.; Ralston, W. T.; Toste, F. D.; Somorjai, G. A. *J. Am. Chem. Soc.* **2017,** *139,* 18084–18092. doi:10.1021/jacs.7b10768
11. Liu, C.; Zhou, L.; Jiang, D.; Gu, Y. *Asian J. Org. Chem.* **2016,** *5,* 367–372. doi:10.1002/ajoc.201500497
12. Zhu, Y.; Li, Z.; Chen, J. *Green Energy Environ.* **2019,** *4,* 210–244. doi:10.1016/j.gee.2019.01.003
13. Zhang, X.; Zhang, Z.; Wang, F.; Wang, Y.; Song, Q.; Xu, J. *J. Mol. Catal. A: Chem.* **2013,** *377,* 102–107. doi:10.1016/j.molcata.2013.05.001
14. Sun, S.; Bai, R.; Gu, Y. *Chem. – Eur. J.* **2014,** *20,* 549–558. doi:10.1002/chem.201303364
15. Lai, B.; Bai, R.; Gu, Y. *ACS Sustainable Chem. Eng.* **2018,** *6,* 17076–17086. doi:10.1021/acssuschemeng.8b04451
16. Lee, C. M.; Kubicki, J. D.; Fan, B.; Zhong, L.; Jarvis, M. C.; Kim, S. H. *J. Phys. Chem. B* **2015,** *119,* 15138–15149. doi:10.1021/acs.jpcb.5b08015
17. Wang, K.; Jia, Z.; Yang, X.; Wang, L.; Gu, Y.; Tan, B. *J. Catal.* **2017,** *348,* 168–176. doi:10.1016/j.jcat.2017.02.024
18. Maggi, R.; Shiju, N. R.; Santacroce, V.; Maestri, G.; Bigi, F.; Rothenberg, G. *Beilstein J. Org. Chem.* **2016,** *12,* 2173–2180. doi:10.3762/bjoc.12.207
19. Gao, S.; Luo, T.; Zhou, Q.; Luo, W.; Li, H.; Jing, L. *J. Colloid Interface Sci.* **2018,** *517,* 9–17. doi:10.1016/j.jcis.2017.12.008
20. Parhizkar, J.; Habibi, M. H.; Mosavian, S. Y. *Silicon* **2019,** *11,* 1119–1129. doi:10.1007/s12633-018-9922-0
21. Jakab, E.; Faix, O.; Till, F.; Székely, T. *J. Anal. Appl. Pyrolysis* **1993,** *25,* 185–194. doi:10.1016/0165-2370(93)80039-3
22. Fiorani, G.; Perosa, A.; Selva, M. *Green Chem.* **2018,** *20,* 288–322. doi:10.1039/c7gc02118f
23. Li, S.; Liu, S.; Fu, Z.; Li, Q.; Wu, C.; Guo, W. *Surf. Interface Anal.* **2017,** *49,* 197–204. doi:10.1002/sia.6115
24. Xu, S.; Yin, C.; Pan, D.; Hu, F.; Wu, Y.; Miao, Y.; Gao, L.; Xiao, G. *Sustainable Energy Fuels* **2019,** *3,* 390–395. doi:10.1039/c8se00499d
25. Gunduz, H.; Kumbaraci, V.; Özkılıç, Y.; Tüzün, N. Ş.; Talinli, N. *ChemistrySelect* **2019,** *4,* 7278–7283. doi:10.1002/slct.201901403
26. Sakurai, H.; Koga, K.; Kiuchi, M. *Catal. Today* **2015,** *251,* 96–102. doi:10.1016/j.cattod.2014.11.004
27. Lai, B.; Huang, Z.; Jia, Z.; Bai, R.; Gu, Y. *Catal. Sci. Technol.* **2016,** *6,* 1810–1820. doi:10.1039/c5cy01012h
28. Lan, D.-H.; Chen, L.; Au, C.-T.; Yin, S.-F. *Carbon* **2015,** *93,* 22–31. doi:10.1016/j.carbon.2015.05.023
29. Li, H.; Cheng, R.; Liu, Z.; Du, C. *Sci. Total Environ.* **2019,** *683,* 638–647. doi:10.1016/j.scitotenv.2019.05.242
30. Dong, X.; Ren, B.; Sun, Z.; Li, C.; Zhang, X.; Kong, M.; Zheng, S.; Dionysiou, D. D. *Appl. Catal., B* **2019,** *253,* 206–217. doi:10.1016/j.apcatb.2019.04.052
31. Ghodsinia, S. S. E.; Akhlaghinia, B. *Green Chem.* **2019,** *21,* 3029–3049. doi:10.1039/c8gc03931c
32. Nemoto, T.; Harada, S.; Nakajima, M. *Asian J. Org. Chem.* **2018,** *7,* 1730–1742. doi:10.1002/ajoc.201800336
33. Chen, S.; Ravichandiran, P.; El-Harairy, A.; Queneau, Y.; Li, M.; Gu, Y. *Org. Biomol. Chem.* **2019,** *17,* 5982–5989. doi:10.1039/c9ob01045a
34. Zheng, S.; Zhong, Q.; Mottamal, M.; Zhang, Q.; Zhang, C.; LeMelle, E.; McFerrin, H.; Wang, G. *J. Med. Chem.* **2014,** *57,* 3369–3381. doi:10.1021/jm500002k
35. Hackenberger, D.; Weber, P.; Blakemore, D. C.; Goossen, L. J. *J. Org. Chem.* **2017,** *82,* 3917–3925. doi:10.1021/acs.joc.7b00046
36. Das, P.; Saha, D.; Saha, D.; Guin, J. *ACS Catal.* **2016,** *6,* 6050–6054. doi:10.1021/acscatal.6b01539
37. Shintani, R.; Misawa, N.; Takano, R.; Nozaki, K. *Chem. – Eur. J.* **2017,** *23,* 2660–2665. doi:10.1002/chem.201605000
38. Kuzmina, O. M.; Steib, A. K.; Markiewicz, J. T.; Flubacher, D.; Knochel, P. *Angew. Chem., Int. Ed.* **2013,** *52,* 4945–4949. doi:10.1002/anie.201210235

39. Donohoe, T. J.; Bower, J. F.; Basutto, J. A.; Fishlock, L. P.; Procopiou, P. A.; Callens, C. K. A. *Tetrahedron* **2009,** *65,* 8969–8980. doi:10.1016/j.tet.2009.07.076
40. Colby, D. A.; Bergman, R. G.; Ellman, J. A. *J. Am. Chem. Soc.* **2008,** *130,* 3645–3651. doi:10.1021/ja7104784
41. Sheng, J.; Fan, C.; Ding, Y.; Fan, X.; Wu, J. *Chem. Commun.* **2014,** *50,* 4188–4191. doi:10.1039/c4cc00691g
42. Jin, Y.; Makida, Y.; Uchida, T.; Kuwano, R. *J. Org. Chem.* **2018,** *83,* 3829–3839. doi:10.1021/acs.joc.8b00190
43. Wilson, T. A.; Koneru, P. C.; Rebensburg, S. V.; Lindenberger, J. J.; Kobe, M. J.; Cockroft, N. T.; Adu-Ampratwum, D.; Larue, R. C.; Kvaratskhelia, M.; Fuchs, J. R. *ACS Med. Chem. Lett.* **2019,** *10,* 215–220. doi:10.1021/acsmedchemlett.8b00633
44. Asako, T.; Suzuki, S.; Itami, K.; Muto, K.; Yamaguchi, J. *Chem. Lett.* **2018,** *47,* 968–970. doi:10.1246/cl.180429
45. Bertuzzi, G.; Pecorari, D.; Bernardi, L.; Fochi, M. *Chem. Commun.* **2018,** *54,* 3977–3980. doi:10.1039/c8cc01735b

License and Terms

BEILSTEIN JOURNAL OF ORGANIC CHEMISTRY

Three-component reactions of aromatic amines, 1,3-dicarbonyl compounds, and α-bromoacetaldehyde acetal to access *N*-(hetero)aryl-4,5-unsubstituted pyrroles

Wenbo Huang[1], Kaimei Wang[1], Ping Liu[2], Minghao Li[3], Shaoyong Ke[*1] and Yanlong Gu[*2,3]

Letter

Open Access

Address:
[1]National Biopesticide Engineering Research Centre, Hubei Biopesticide Engineering Research Centre, Hubei Academy of Agricultural Sciences, 8 Nanhu Avenue, Hongshan District, Wuhan 430064, China, [2]School of Chemistry and Chemical Engineering, The Key Laboratory for Green Processing of Chemical Engineering of Xinjiang Bingtuan, Shihezi University, Shihezi City 832004, China and [3]Key laboratory of Material Chemistry for Energy Conversion and Storage, Ministry of Education, Hubei Key Laboratory of Material Chemistry and Service Failure, School of Chemistry and Chemical Engineering, Huazhong University of Science and Technology, 1037 Luoyu road, Hongshan District, Wuhan 430074, China

Email:
Shaoyong Ke[*] - shaoyong.ke@nberc.com; Yanlong Gu[*] - klgyl@hust.edu.cn

* Corresponding author

Keywords:
acid catalyst; [1 + 2 + 2] annulation; KI; pyrazolo[3,4-*b*]pyridine; pyrroles

Beilstein J. Org. Chem. **2020,** *16,* 2920–2928.
https://doi.org/10.3762/bjoc.16.241

Received: 24 August 2020
Accepted: 17 November 2020
Published: 30 November 2020

This article is part of the thematic issue "Green chemistry II".

Associate Editor: L. Vaccaro

Abstract

N-(Hetero)aryl-4,5-unsubstituted pyrroles were synthesized from (hetero)arylamines, 1,3-dicarbonyl compounds, and α-bromoacetaldehyde acetal by using aluminum(III) chloride as a Lewis acid catalyst through [1 + 2 + 2] annulation. This new versatile methodology provides a wide scope for the synthesis of different functional *N*-(hetero)aryl-4,5-unsubstituted pyrrole scaffolds, which can be further derived to access multisubstituted pyrrole-3-carboxamides. In the presence of 1.2 equiv of KI, a polysubstituted pyrazolo[3,4-*b*]pyridine derivative was also successfully synthesized.

Introduction

Among nitrogen-containing heterocycles, pyrroles have garnered significant attention in the literature because of their presence in various natural products [1-4] and pharmaceutically relevant drugs [5,6]. Accordingly, numerous synthetic methods to construct pyrrole skeletons were reported, including the classical Hantzsch [7,8] and the Paal–Knorr pyrrole syntheses

[9-11], which have been developed to harvest the pyrrole frameworks. In the past few years, the interest in developing new methods to synthesize this heterocyclic motif has rapidly grown; transition metal-catalyzed cyclization [12-14] and multicomponent reactions [15-18] are some of the commonly used approaches for the construction of pyrrole scaffolds. Additionally, the biocatalytic synthesis of substituted pyrroles was also developed [19]. Though sustained efforts have been achieved to develop efficient synthetic methods for the preparation of this structural motif [20-23], the development of cost-effective methods to access functionalized pyrrole skeletons has remained an ongoing challenge.

N-(Hetero)aryl-4,5-unsubstituted pyrroles are one of the most important types of pyrroles, which are frequently used as a core scaffold in pharmaceuticals (Figure 1) [24,25]. Therefore, many efforts have been paid to the synthesis of these privileged pyrroles. (Hetero)arylamines are readily available chemicals. The direct conversion of (hetero)arylamines into *N*-(hetero)aryl-4,5-unsubstituted pyrroles has a high intrinsic synthetic potential. At present, the transformations can generally be realized through the following three approaches (Scheme 1): (i) [1 + 1 + 3] annulation, in which (hetero)arylamines are reacted with a C_3 donor and a C_1 donor to construct pyrrole scaffolds. Kumar et al. [26] developed a proline-catalyzed Mannich reaction–cyclization sequence of succinaldehyde and an in situ-generated arylimine, in which the succinaldehyde contributes three carbon atoms to the pyrrole ring. α,β-Unsaturated aldehydes have also been used as the C_3 donor to construct pyrrole scaffolds [27,28]; (ii) [1 + 4] annulation, in which (hetero)arylamines are reacted with a C_4 donor to form the pyrrole ring; many functional molecules, such as bioderived furans [29], (*Z*)-enynols [30], 1-vinylpropargyl alcohols [31], doubly activated cyclopropanes [32], and enynals [33], can be used as C_4 counter reagents. The carbon-based 1,4-biselectrophiles, such as the 1,4-dicarbonyl compounds [34,35], γ-carbonyl *tert*-butyl peroxides [36], and dihydrofurans [37] have also been reported to construct the pyrrole skeletons through this type of annulation; and (iii) [1 + 2 + 2] annulation, in which (hetero)arylamines are reacted with two different molecules, and each of them contributes two carbon atoms to construct a pyrrole ring [38-42]. Among these three approaches, the third is considered the most attractive route for *N*-(hetero)aryl-4,5-unsubstituted pyrrole synthesis. The reason is twofold: (i) the strategy uses easily available substrates and (ii) permits to synthesize pyrroles with a high potential of molecular diversity and complexity. However, to date, the productivity for creating molecular diversity and complexity has yet to be fully displayed. In addition, some of the reported approaches were established on the basis of using expensive and nonrecyclable homogeneous metal catalysts. To alleviate all these problems, herein, we used easily available α-bromoacetaldehyde acetal (**2a**) and a simple 1,3-dicarbonyl compound as a reagent couple to react with (hetero)arylamines. The established [1 + 2 + 2] annulation reaction provided a straightforward approach for accessing various *N*-(hetero)aryl-4,5-unsubstituted pyrroles, and some of the pyrrole products are not accessible with the methods reported hitherto.

Results and Discussion

Initially, a mixture of aniline (**1a**), α-bromoacetaldehyde acetal (**2a**), and ethyl acetoacetate (**3a**) was treated under the conditions; the obtained results are listed in Table 1. The mixture was heated in 1,4-dioxane at 80 °C. No reaction occurred in the absence of the catalyst (Table 1, entry 1); however, in the presence of the strong Lewis acid $Bi(OTf)_3$, the expected product **4a** was obtained in 36% yield after 6 h of reaction (Table 1, entry 2). To our surprise, the *N*-aryl-4,5-unsubstituted pyrrole derivative **4a** was isolated in 80% yield when 10 mol % of $AlCl_3$ was used as the catalyst (Table 1, entry 3). $FeCl_3$ and $NiCl_2$ were also proven to catalyze this reaction, but the yield of **4a** was inferior to those obtained with $AlCl_3$ (Table 1, entries 4 and 5).

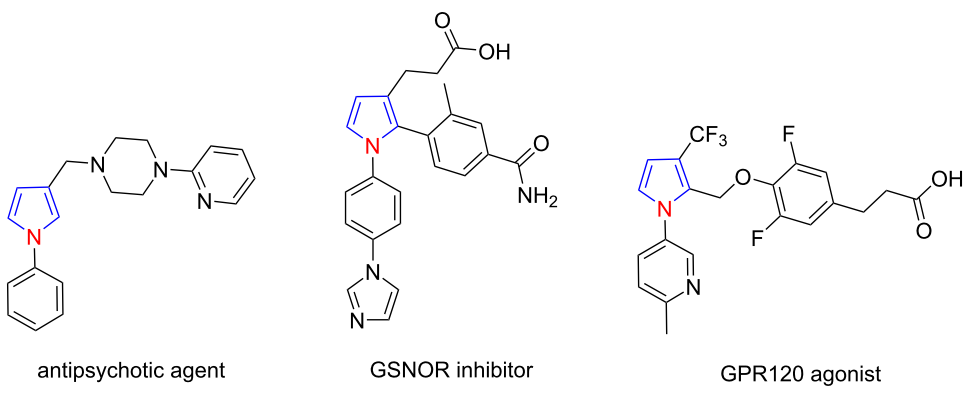

Figure 1: Representative biologically active *N*-(hetero)aryl-4,5-unsubstituted pyrrole scaffolds.

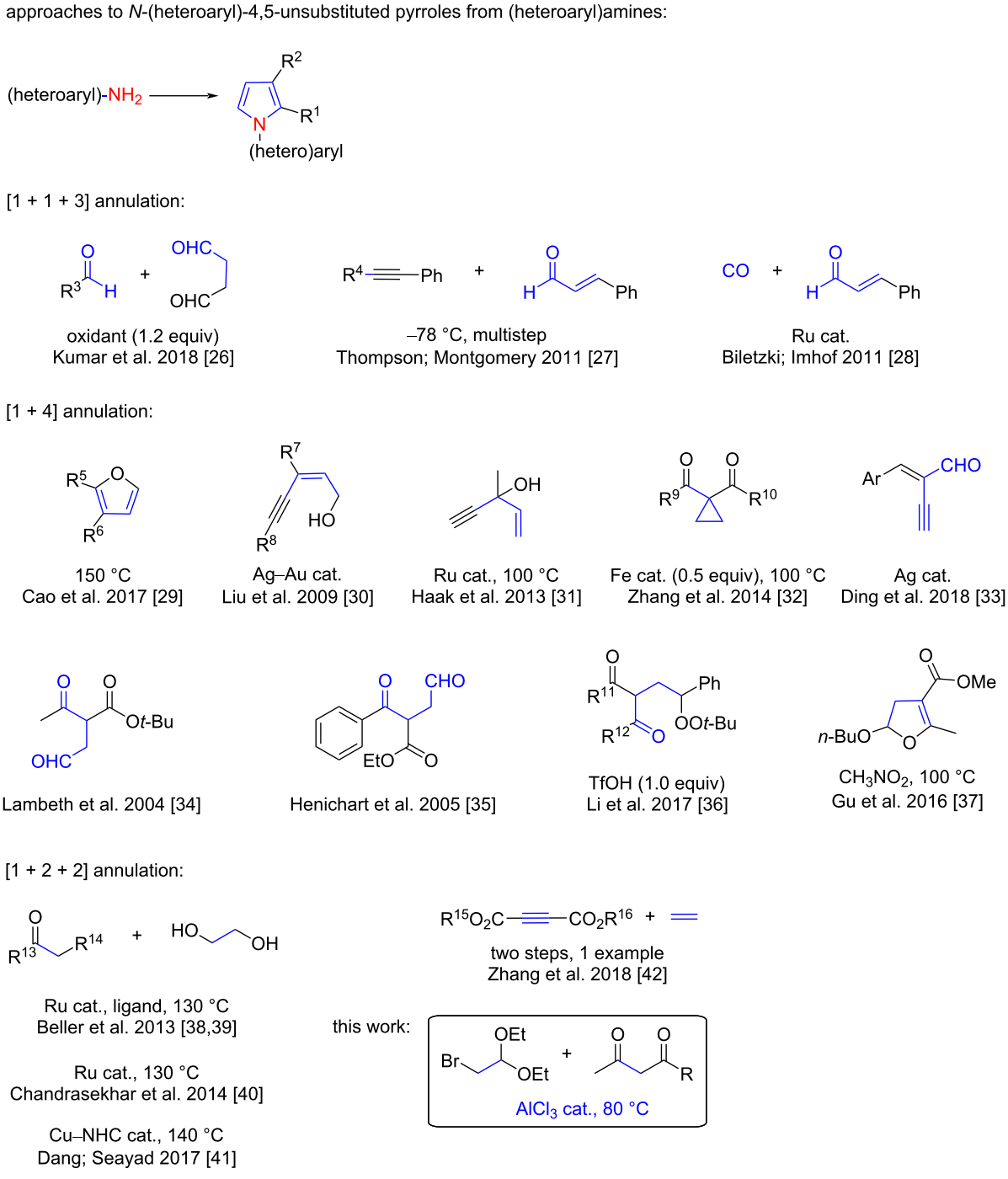

Scheme 1: Typical routes to *N*-(heteroaryl)-4,5-unsubstituted pyrroles.

p-Toluenesulfonic acid (PTSA), a strong Brønsted acid, also exhibited a promising catalytic ability, and the yield of **4a** reached 73% (Table 1, entry 6). When HOAc was used, only unreacted starting materials were recovered (Table, entry 7). The effect of the solvent on the model reaction was also examined. Anhydrous ethanol, acetonitrile, toluene, and DMSO did not bring any improvement with respect to the yield of **4a** (Table 1, entries 8–11). The decrease of the catalyst loading from 10 to 5 mol % resulted in a slight decrease of the reaction yield (Table 1, entry 12). Further investigations revealed that the reaction was also affected by the temperature and time; a yield of only 51% was obtained at 50 °C (Table 1, entries 13 and 14). Therefore, the optimized reaction conditions were confirmed as the following: 10 mol % of $AlCl_3$ as a catalyst, 1,4-

Table 1: Optimization of the conditions for the reaction between **1a**, **2a**, and **3a**.[a]

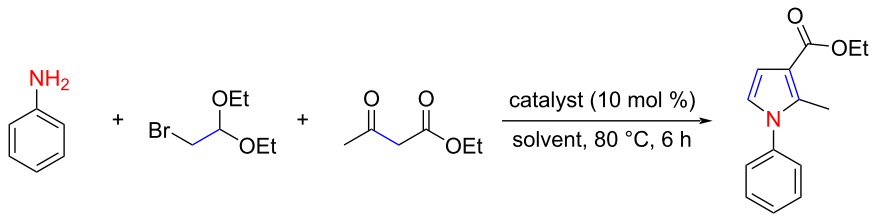

1a **2a** **3a** **4a**

entry	catalyst	solvent	yield (%)[b]
1	—	1,4-dioxane	0
2	$Bi(OTf)_3$	1,4-dioxane	36
3	$AlCl_3$	1,4-dioxane	80
4	$FeCl_3$	1,4-dioxane	44
5	$NiCl_2$	1,4-dioxane	21
6	PTSA	1,4-dioxane	73
7	HOAc	1,4-dioxane	trace
8	$AlCl_3$	EtOH	31
9	$AlCl_3$	MeCN	50
10	$AlCl_3$	PhMe	27
11	$AlCl_3$	DMSO	62
12[c]	$AlCl_3$	1,4-dioxane	55
13[d]	$AlCl_3$	1,4-dioxane	51
14[e]	$AlCl_3$	1,4-dioxane	40
15[f]	$AlCl_3$	1,4-dioxane	72

[a]**1a**: 0.5 mmol, **2a**: 0.6 mmol, **3a**: 0.6 mmol, catalyst: 0.05 mmol, solvent: 1 mL, 80 °C, 6 h. [b]Isolated yield, calculated with respect to **1a**. [c]$AlCl_3$: 0.025 mmol. [d]50 °C. [e]2 h. [f]10 mmol-scale reaction.

dioxane as a solvent, 6 h, and 80 °C. It is worth noting that the reaction can be effectively scaled up with similar efficiency. In a gram-scale synthesis of **4a**, the corresponding pyrrole product was obtained in 72% yield (Table 1, entry 15).

The scope of this synthetic protocol for pyrroles was then investigated under the optimized reaction conditions. The substrate scope of the 1,3-dicarbonyl component was first examined (Scheme 2). Acetylacetone reacted smoothly with **1a** and **2a** to form **4b** in 52% yield. 1,3-Dicarbonyl compounds bearing an ester group readily participated in this reaction, affording the desired pyrroles **4c**–**e** in moderate to good yield. Notably, methyl 2-methyl-1-phenyl-1*H*-pyrrole-3-carboxylate (**4c**) is a key intermediate in the synthesis of a TRPM8 antagonist [43]. The substrate scope of the aromatic amine component was then examined, and the remarkable efficiency of our pyrrole synthesis was reflected by the tolerance of a broad range of functional groups attached to the aromatic amine. For example, anilines bearing methyl (in **4f**), phenyl (in **4g**), and halo functionalities (in **4h**–**m**) were readily compatible with the $AlCl_3$ and 1,4-dioxane system. In these cases, the pyrrole products were isolated in moderate to good yield. The presence of an electron-donating group in the phenyl ring facilitated the progress of the reaction to some extent, resulting in **4n**. Anilines with electron-withdrawing groups, such as an acetyl or carboxy group, can also be used in the reaction, but the yields obtained for **4o** and **4p** were slightly inferior. Gratifyingly, a 3,5-dichloro-4-(1,1,2,2-tetrafluoroethoxy)aniline also participated smoothly in this reaction, and the expected product **4q** can be obtained in 75% yield. This fluorinated substituent on the aniline ring has been identified as the key precursor to access the insect-growth regulators [44]. It is noteworthy that the sulfonamide group persisted during this transformation, and the desired pyrrole product **4r** could be obtained in 69% yield. A high yield was also obtained when the phenyl group was replaced with a naphthyl group in **4s**. Subsequently, aliphatic primary amines and ammonia, such as benzylamine and *N*-butylamine, were also examined as nitrogen donors; however, no desired product was detected.

Then, we attempted to synthesize pharmaceutically active N-heterocyclic pyrrole derivatives with the aid of this three-

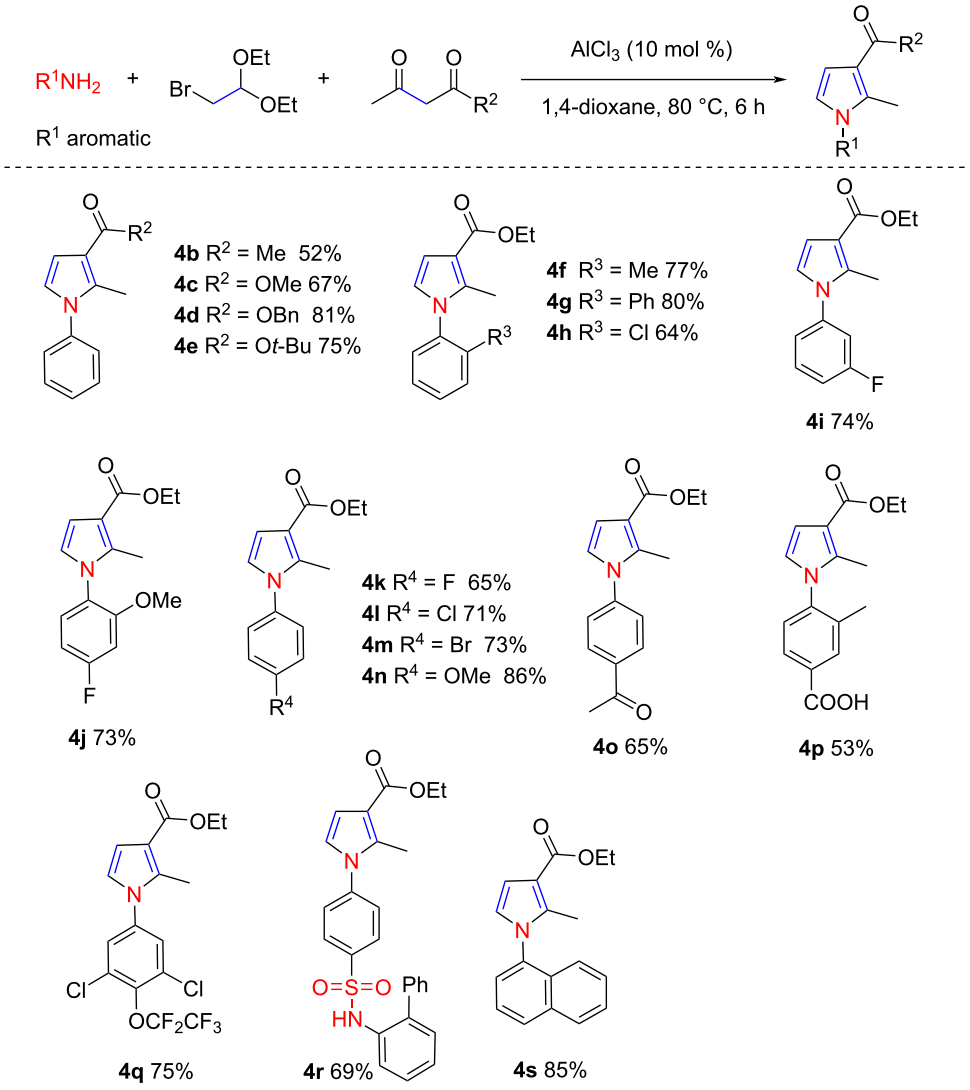

Scheme 2: Substrate scope of the pyrrole synthesis.

component reaction. To our great delight, the N-heterocyclic pyrrole skeletons **4t–v** were successfully synthesized in 51–85% yield by using our protocol (Scheme 3). It should be mentioned that the obtained *N*-pyridylpyrroles **4t** and **4u** are a class of very important intermediates for synthesizing the soluble guanylyl cyclase (sGC) activator. A reported method for accessing these similar scaffolds suffers from a low product yield and harsh reaction conditions (32%, 130 °C) [45,46].

One of the obtained *N*-aryl-4,5-unsubstituted pyrroles, **4l**, could undergo hydrolysis to form the (pyrrol-3-yl)carboxylic acid **4w**. The latter can react readily with aniline (**1a**) or amantadine in the presence of HATU or EDCI to form the multisubstituted pyrrole-3-carboxamide derivatives **4x** and **4y** (Scheme 4). These skeletons have been proven to be promising inhibitors for the production of cytokines [47].

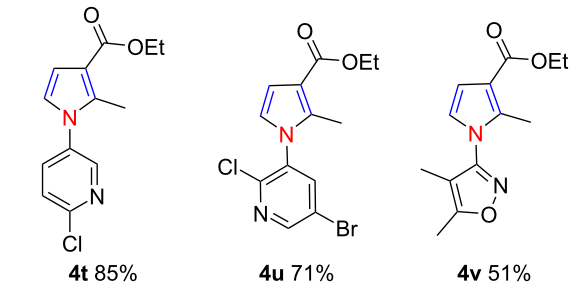

Scheme 3: Synthesis of N-heterocyclic pyrroles.

A plausible mechanism for the model reaction was proposed and is depicted in Scheme 5. Initially, a reaction of **1a** and **3a** occurred, providing an imine intermediate **I**, which tautomerized to the corresponding enamine form. Meanwhile, the activa-

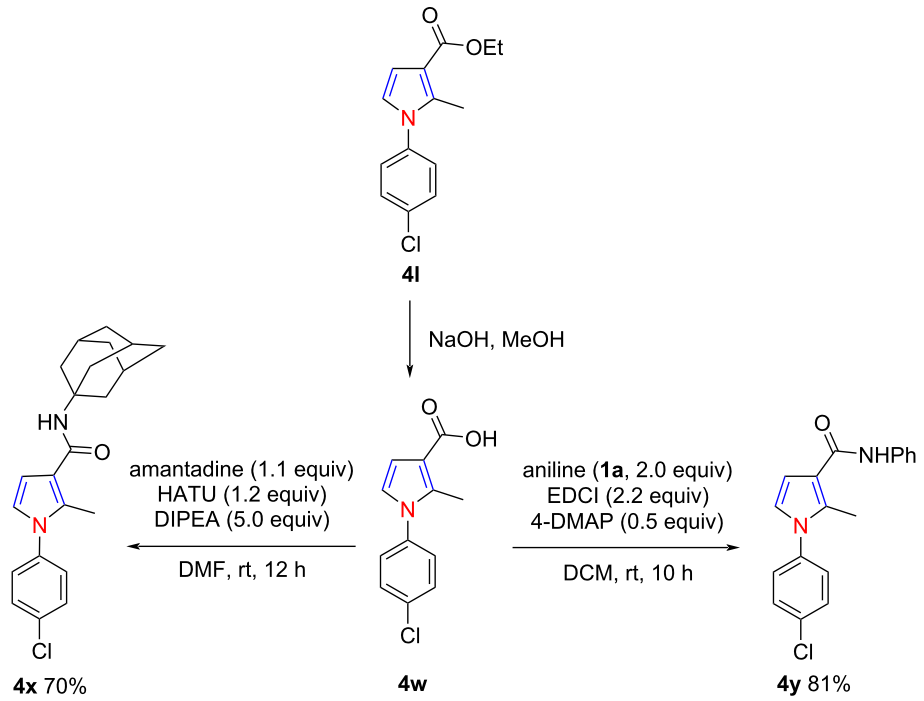

Scheme 4: Direct synthesis of pyrrole-3-carboxamide derivatives.

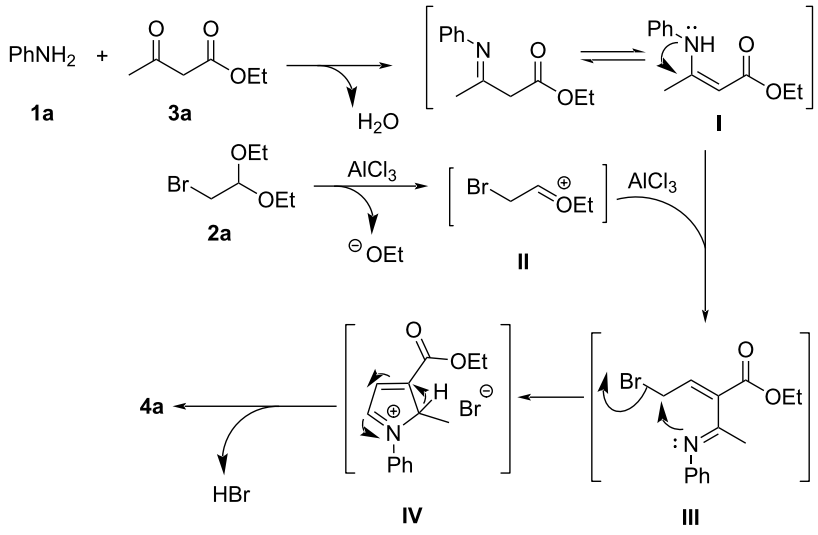

Scheme 5: Plausible mechanism of the three-component reaction.

tion of **2a** with $AlCl_3$ allowed the formation of a carbocation intermediate **II**, which was then trapped by the enamine intermediate **I** to generate another intermediate **III**. Subsequently, **III** underwent an intramolecular electrophilic substitution to form the intermediate **IV**. Finally, **IV** underwent an elimination of HBr and a spontaneous aromatization to afford the pyrrole product **4a** [48,49].

Apart from the pyrrole synthesis, we also observed an unexpected reaction in which the pyrazolo[3,4-*b*]pyridine scaffold was constructed under analogous conditions. As shown in Scheme 6, In the presence of a catalytic amount of $AlCl_3$ and 1.2 equiv of KI, 3-methyl-1-phenyl-1*H*-pyrazol-5-amine (**1b**) reacted smoothly with **2a** and **3a**, affording the polysubstituted pyrazolo[3,4-*b*]pyridine **5a** in 53% yield. The formation of an

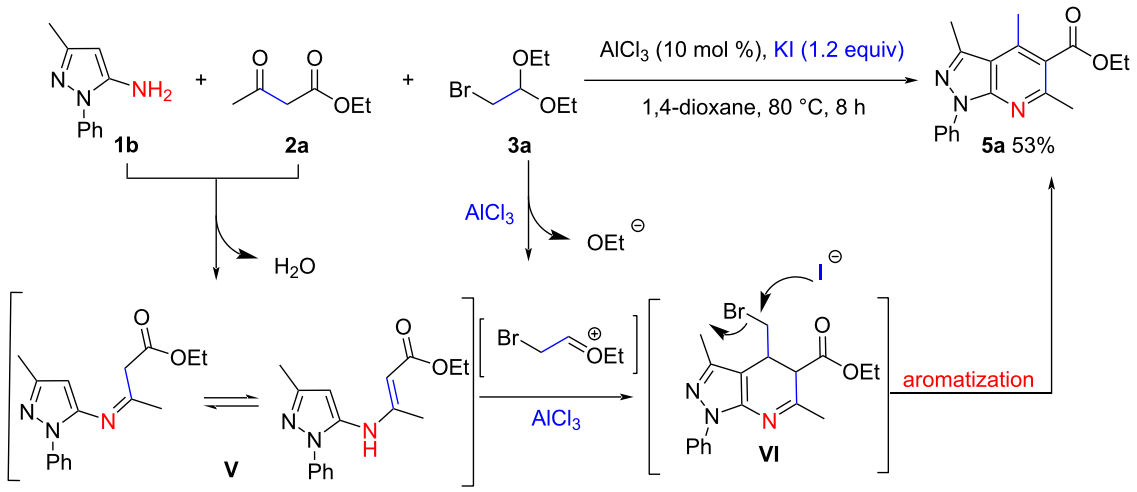

Scheme 6: Synthesis of polysubstituted pyrazolo[3,4-b]pyridine derivatives.

imine intermediate **V** may be involved in the reaction mechanism, and the enamine form of **V** contained two nucleophilic sites to react with a molecule of **3a**, which generated the intermediate **VI**. Finally, **VI** underwent an aromatization to produce **5a**. KI may play a key role in the last step, and we suspected that it can promote the removal of bromide. Although **5a** can theoretically be synthesized through a three-component reaction of **1b**, **2a**, and an appropriate aldehyde, for example, acetaldehyde [50,51] owing to the insufficient reactivity of aliphatic aldehydes, the reaction in Scheme 6 should be a wise choice for the synthesis of products similar in type to **5a**. This point deserves further investigation.

Conclusion

In summary, an efficient and practical one-pot multicomponent reaction of (hetero)arylamines with α-bromoacetaldehyde acetal (**2a**) and 1,3-dicarbonyl compounds was developed by using $AlCl_3$ as a catalyst. The developed chemistry is also successful for the synthesis of functionalized pyrazolo[3,4-*b*]pyridine derivatives. This study offered a complementary method to construct pyrrole scaffolds through [1 + 2 + 2] annulation, and thus enriching the product diversity of the pyrrole derivatives.

Supporting Information

Supporting Information File 1

Experimental procedures and copies of NMR spectra.
[https://www.beilstein-journals.org/bjoc/content/supplementary/1860-5397-16-241-S1.pdf]

Funding

The authors thank the Program for Leading Talents of Hubei Academy of Agricultural Sciences (L2018031) and the Natural Science Foundation of Hubei Province (2020CFB717), and the authors also thank the partial support from the Projects in the Youth Science Foundation of Hubei Academy of Agricultural Sciences (2021NKYJJ17) and Hubei Key Laboratory of Crop Diseases, Insect Pests and Weeds Control (2020ZTSJJ5), the Natural Science Foundation of Hubei Province (2019CFB219), and the National Natural Science Foundation of China (2171101076 and 21872060).

ORCID® iDs

Wenbo Huang - https://orcid.org/0000-0003-1507-6123

Preprint

A non-peer-reviewed version of this article has been previously published as a preprint: https://doi.org/10.3762/bxiv.2020.94.v1

References

1. O'Hagan, D. *Nat. Prod. Rep.* **2000,** *17,* 435–446. doi:10.1039/a707613d
2. Walsh, C. T.; Garneau-Tsodikova, S.; Howard-Jones, A. R. *Nat. Prod. Rep.* **2006,** *23,* 517–531. doi:10.1039/b605245m
3. Trost, B. M.; Dong, G. *Org. Lett.* **2007,** *9,* 2357–2359. doi:10.1021/ol070742y
4. Lindel, T.; Hochgürtel, M.; Assmann, M.; Köck, M. *J. Nat. Prod.* **2000,** *63,* 1566–1569. doi:10.1021/np000160o
5. Khajuria, R.; Dham, S.; Kapoor, K. K. *RSC Adv.* **2016,** *6,* 37039–37066. doi:10.1039/c6ra03411j
6. Osman, N. A.; Ligresti, A.; Klein, C. D.; Allarà, M.; Rabbito, A.; Di Marzo, V.; Abouzid, K. A.; Abadi, A. H. *Eur. J. Med. Chem.* **2016,** *122,* 619–634. doi:10.1016/j.ejmech.2016.07.012

7. Hantzsch, A. *Ber. Dtsch. Chem. Ges.* **1890,** *23,* 1474–1476. doi:10.1002/cber.189002301243
8. Leonardi, M.; Estévez, V.; Villacampa, M.; Menéndez, J. C. *Synthesis* **2019,** *51,* 816–828. doi:10.1055/s-0037-1610320
9. Knorr, L. *Ber. Dtsch. Chem. Ges.* **1884,** *17,* 1635–1642. doi:10.1002/cber.18840170220
10. Paal, C. *Ber. Dtsch. Chem. Ges.* **1885,** *18,* 367–371. doi:10.1002/cber.18850180175
11. Balakrishna, A.; Aguiar, A.; Sobral, P. J. M.; Wani, M. Y.; Almeida e Silva, J.; Sobral, A. J. F. N. *Catal. Rev.: Sci. Eng.* **2019,** *61,* 84–110. doi:10.1080/01614940.2018.1529932
12. Bunrit, A.; Sawadjoon, S.; Tšupova, S.; Sjöberg, P. J. R.; Samec, J. S. M. *J. Org. Chem.* **2016,** *81,* 1450–1460. doi:10.1021/acs.joc.5b02581
13. Billedeau, R. J.; Klein, K. R.; Kaplan, D.; Lou, Y. *Org. Lett.* **2013,** *15,* 1421–1423. doi:10.1021/ol400062w
14. Andreou, D.; Kallitsakis, M. G.; Loukopoulos, E.; Gabriel, C.; Kostakis, G. E.; Lykakis, I. N. *J. Org. Chem.* **2018,** *83,* 2104–2113. doi:10.1021/acs.joc.7b03051
15. Firoozi, N.; Torres, G. M.; Arndtsen, B. A. *J. Org. Chem.* **2016,** *81,* 11145–11152. doi:10.1021/acs.joc.6b02102
16. Zheng, Y.; Wang, Y.; Zhou, Z. *Chem. Commun.* **2015,** *51,* 16652–16655. doi:10.1039/c5cc05624a
17. Singh, K.; Kabadwal, L. M.; Bera, S.; Alanthadka, A.; Banerjee, D. *J. Org. Chem.* **2018,** *83,* 15406–15414. doi:10.1021/acs.joc.8b02666
18. Herath, A.; Cosford, N. D. P. *Org. Lett.* **2010,** *12,* 5182–5185. doi:10.1021/ol102216x
19. Xu, J.; Green, A. P.; Turner, N. J. *Angew. Chem., Int. Ed.* **2018,** *57,* 16760–16763. doi:10.1002/anie.201810555
20. Chelucci, G. *Coord. Chem. Rev.* **2017,** *331,* 37–53. doi:10.1016/j.ccr.2016.09.014
21. Estévez, V.; Villacampa, M.; Menéndez, J. C. *Chem. Soc. Rev.* **2014,** *43,* 4633–4657. doi:10.1039/c3cs60015g
22. Gulevich, A. V.; Dudnik, A. S.; Chernyak, N.; Gevorgyan, V. *Chem. Rev.* **2013,** *113,* 3084–3213. doi:10.1021/cr300333u
23. Estévez, V.; Villacampa, M.; Menéndez, J. C. *Chem. Soc. Rev.* **2010,** *39,* 4402–4421. doi:10.1039/b917644f
24. Ahmad, S.; Alam, O.; Naim, M. J.; Shaquiquzzaman, M.; Alam, M. M.; Iqbal, M. *Eur. J. Med. Chem.* **2018,** *157,* 527–561. doi:10.1016/j.ejmech.2018.08.002
25. Winters, M. P.; Sui, Z.; Wall, M.; Wang, Y.; Gunnet, J.; Leonard, J.; Hua, H.; Yan, W.; Suckow, A.; Bell, A.; Clapper, W.; Jenkinson, C.; Haug, P.; Koudriakova, T.; Huebert, N.; Murray, W. V. *Bioorg. Med. Chem. Lett.* **2018,** *28,* 841–846. doi:10.1016/j.bmcl.2018.02.013
26. Singh, A.; Mir, N. A.; Choudhary, S.; Singh, D.; Sharma, P.; Kant, R.; Kumar, I. *RSC Adv.* **2018,** *8,* 15448–15458. doi:10.1039/c8ra01637b
27. Thompson, B. B.; Montgomery, J. *Org. Lett.* **2011,** *13,* 3289–3291. doi:10.1021/ol201133n
28. Biletzki, T.; Imhof, W. *Synthesis* **2011,** 3979–3990. doi:10.1055/s-0031-1289584
29. Tao, L.; Wang, Z.-J.; Yan, T.-H.; Liu, Y.-M.; He, H.-Y.; Cao, Y. *ACS Catal.* **2017,** *7,* 959–964. doi:10.1021/acscatal.6b02953
30. Lu, Y.; Fu, X.; Chen, H.; Du, X.; Jia, X.; Liu, Y. *Adv. Synth. Catal.* **2009,** *351,* 129–134. doi:10.1002/adsc.200800490
31. Thies, N.; Gerlach, M.; Haak, E. *Eur. J. Org. Chem.* **2013,** 7354–7365. doi:10.1002/ejoc.201300803
32. Zhang, Z.; Zhang, W.; Li, J.; Liu, Q.; Liu, T.; Zhang, G. *J. Org. Chem.* **2014,** *79,* 11226–11233. doi:10.1021/jo5018487
33. Kong, H.-H.; Pan, H.-L.; Ding, M.-W. *J. Org. Chem.* **2018,** *83,* 12921–12930. doi:10.1021/acs.joc.8b01984
34. Tracey, M. R.; Hsung, R. P.; Lambeth, R. H. *Synthesis* **2004,** 918–922. doi:10.1055/s-2004-815976
35. Delayen, A.; Goossens, L.; Goossens, R.; Henichart, J.-P. *Heterocycles* **2005,** *65,* 1673–1678. doi:10.3987/com-05-10386
36. Lu, S.; Qi, L.; Li, Z. *Asian J. Org. Chem.* **2017,** *6,* 313–321. doi:10.1002/ajoc.201600608
37. Wang, M.; Liu, C.; Gu, Y. *Tetrahedron* **2016,** *72,* 6854–6865. doi:10.1016/j.tet.2016.09.014
38. Zhang, M.; Neumann, H.; Beller, M. *Angew. Chem., Int. Ed.* **2013,** *52,* 597–601. doi:10.1002/anie.201206082
39. Zhang, M.; Fang, X.; Neumann, H.; Beller, M. *J. Am. Chem. Soc.* **2013,** *135,* 11384–11388. doi:10.1021/ja406666r
40. Chandrasekhar, S.; Patro, V.; Chavan, L. N.; Chegondi, R.; Grée, R. *Tetrahedron Lett.* **2014,** *55,* 5932–5935. doi:10.1016/j.tetlet.2014.08.105
41. Dang, T. T.; Seayad, A. M. *Chem. – Asian J.* **2017,** *12,* 2383–2387. doi:10.1002/asia.201701045
42. Zeng, J.-C.; Xu, H.; Huang, R.-L.; Yu, F.; Zhang, Z. *Tetrahedron Lett.* **2018,** *59,* 1576–1580. doi:10.1016/j.tetlet.2018.03.025
43. Shishido, Y.; Ohmi, M.; Ando, K. Azaspiro derivatives as trpm8 antagonists. WO Patent WO2015136947A1, Sept 17, 2015.
44. Sun, R.; Liu, Y.; Zhang, Y.; Xiong, L.; Wang, Q. *J. Agric. Food Chem.* **2011,** *59,* 2471–2477. doi:10.1021/jf104578j
45. Hirth-Dietrich, C.; Sandner, P.; Stasch, J.-P.; Hahn, M.; Follmann, M. The use of sGC stimulators, sGC activators, alone and combinations with PDE5 inhibitors for the treatment of systemic sclerosis (SSc). Eur. Patent EP2594270A2, May 22, 2013.
46. Boyer, T.; Dodic, N.; Evans, B.; Kirk, B. E. 2,6-disubstituted pyridines and 2,4-disubstituted pyrimidines as soluble guanylate cyclase activators. WO Patent WO2009068652A1, June 4, 2009.
47. Ushio, H.; Hamada, M.; Watanabe, M.; Numata, A.; Fujie, N.; Takashima, T.; Furukawa, H.; Ando, J. Amide derivative and use thereof. WO Patent WO2012050159A1, April 19, 2012.
48. Huang, W.; Liu, C.; Gu, Y. *Adv. Synth. Catal.* **2017,** *359,* 1811–1818. doi:10.1002/adsc.201700074
49. Huang, W.; Chen, S.; Chen, Z.; Yue, M.; Li, M.; Gu, Y. *J. Org. Chem.* **2019,** *84,* 5655–5666. doi:10.1021/acs.joc.9b00596
50. Tu, S.; Wang, Q.; Zhang, Y.; Xu, J.; Zhang, J.; Zhu, X.; Shi, F. *J. Heterocycl. Chem.* **2007,** *44,* 811–814. doi:10.1002/jhet.5570440409
51. Gunasekaran, P.; Indumathi, S.; Perumal, S. *RSC Adv.* **2013,** *3,* 8318–8325. doi:10.1039/c3ra00136a

BEILSTEIN JOURNAL OF ORGANIC CHEMISTRY

Ultrasound-assisted Strecker synthesis of novel 2-(hetero)aryl-2-(arylamino)acetonitrile derivatives

Emese Gal[1], Luiza Gaina[1], Hermina Petkes[1], Alexandra Pop[2], Castelia Cristea[*1], Gabriel Barta[3], Dan Cristian Vodnar[3] and Luminița Silaghi-Dumitrescu[1]

Full Research Paper

Open Access

Address:
[1]Faculty of Chemistry and Chemical Engineering, Research Center on Fundamental and Applied Heterochemistry, Babes-Bolyai University, 11 Arany Janos street, RO-400028, Cluj-Napoca, Romania, [2]Department of Chemistry, Babes-Bolyai University, 11 Arany Janos street, RO-400028, Cluj-Napoca, Romania and [3]Department of Food Science and Technology, University of Agricultural Sciences and Veterinary Medicine 3-5 Mănăștur Street, RO-400372 Cluj-Napoca, Romania

Email:
Castelia Cristea[*] - castelia@chem.ubbcluj.ro

* Corresponding author

Keywords:
Ames test; α-aminoacetonitriles; ferrocene; phenothiazine; SEM; single crystal XRD; sonochemistry

Beilstein J. Org. Chem. **2020,** *16,* 2929–2936.
https://doi.org/10.3762/bjoc.16.242

Received: 04 August 2020
Accepted: 20 November 2020
Published: 30 November 2020

This article is part of the thematic issue "Green chemistry II".

Associate Editor: L. Vaccaro

Abstract

This work describes an efficient, simple, and ecofriendly sonochemical procedure for the preparation of new α-(arylamino)acetonitrile derivatives C-substituted with phenothiazine or ferrocene units. The synthetic protocol is based on the Strecker reaction of a (hetero)aryl aldimine substrate with trimethylsilyl cyanide (TMSCN) in poly(ethylene glycol) (PEG) solution. The advantages of the sonochemical versus the conventional α-(arylamino)acetonitrile synthesis are the significantly shorter reaction time (30 min instead of 72 hours), the higher purity and the easier separation of the product that precipitated from the reaction mixture in crystalline form as depicted by scanning electron microscopy (SEM) analysis. The single crystal X-ray diffraction analysis disclosed the arrangement of the α-(arylamino)acetonitrile molecules in the aggregated crystalline state as a racemic mixture. The mutagenic/antimutagenic potential for three representative derivatives containing phenothiazinyl, ferrocenyl, and phenyl units, respectively, was evaluated by the Ames Salmonella/microsome test using *S. typhimurium* TA98 and TA100 strains with and without metabolic activation. The preliminary screening results pointed out that the C-(hetero)aryl-α-(arylamino)acetonitrile derivatives can be considered genotoxically safe and possibly antimutagenic.

Introduction

Sonochemistry can be considered as a major contributor to green chemistry mainly due to the ability of minimizing the energy consumption required by chemical transformations and allowing the development of environmentally friendly chemical procedures which may be eventually scaled up for industrial applications [1]. For the synthesis of organic heterocyclic compounds, the use of ultrasound irradiation became a powerful tool by proving to be superior in terms of reaction rates, yields,

and the purity of the products as compared to traditional convective heating methods [2]. Sonochemical syntheses can be successfully performed in homogeneous media using "green" solvents, for example, low vapor pressure solvents such as ionic liquids [3], low volatile solvents such as glycerol, ethylene glycol and its oligomers, or nontoxic water solvent, as well as in heterogeneous media under solvent-free conditions [4]. Other advantages induced by sonication are related to the possibility of controlling the crystal structure properties of the final product in nanomaterials syntheses [5]. For this reason, theoretical scientific research is currently directed towards the understanding of the physical phenomena involved in sonocrystallization mechanisms [6]. A major benefit of sonocrystallization appeared to be the induction of nucleation and therefore, crystallization improvements were operated for several organic compounds of low to medium molecular weight with the possibility of scaling up of this technology for industrial use [7]. Low ultrasonic frequencies between 20 and 100 kHz were reported in the literature as optimal to enhance the nucleation and fragmentation rates, but the exact optimal frequency is probably reactor and system specific [8].

The exciting properties of the heterocyclic phenothiazine core displaying tunable chemical, redox, optical, and biological properties upon a careful selection of the substitution pattern [9], continually encouraged the scientific community to search for new powerful representatives and to elaborate advantageous synthetic protocols. Under chemical, biochemical, or electrochemical conditions the ferrocene unit displays a remarkably reversible one-electron oxidation behavior offering interesting fields of applications for its derivatives as redox mediators in sensor applications [10]. Medicinal applications of ferrocene derivatives grafted on different pharmacophoric units greatly benefit from the lipophilic character of the metallocene [11]. However, only a limited number of reports described the application of ultrasonic irradiation for the synthesis of phenothiazine derivatives, and included the N-alkylation of 10*H*-phenothiazine [12], condensation of phenothiazine carbaldehyde with hydrazino-benzoxazole [13] or different other acetohydrazines [14], complexation of phenothiazinyl-chalcone using diiron nonacarbonyl [15], and regioselective oxidation [16].

α-Aminonitriles are versatile synthetic intermediates that are readily obtainable by a Strecker reaction involving the addition of a cyanide nucleophile to an imine C–N bond. Among the various cyanide transferring agents, which were largely documented in the search for advantageous synthetic procedures of these synthetic intermediates [17], trimethylsilyl cyanide (TMSCN) gave the possibility of accomplishing Strecker reactions using a wide variety of aldimine and ketoimine substrates under mild conditions [18]. Early studies reported a positive effect of sonication on the classical aminocyanation procedures. The reaction rate of the classical Strecker reaction using cyanide salts, amines and aromatic carbonyl derivatives [19] or piperidone [20] appeared improved under ultrasound-assisted conditions, which also enhanced the yields of the final α-aminonitrile derivatives. The Strecker reaction of cyclopropanone acetal substrates with sodium cyanide and several amines was also facilitated by sonication conditions which afforded cleaner N-alkylated α-(amino)cyanocyclopropane derivatives not contaminated by intermediates or ring-opening byproducts [21], whereas the asymmetric Strecker synthesis induced by chiral amines was successfully conducted by sonication in the presence of silica gel [22].

Pursuing our interest in developing environmentally friendly procedures for the synthesis of new phenothiazine and ferrocene derivatives [23-27] and perceiving the importance of α-aminoacetonitrile derivatives as pharmaceutical and agrochemical intermediates with a great number of α-aminonitrile derivatives which were proved to have remarkable biological properties exhibiting enzymatic activity as potent and selective protease inhibitors, fungicidal and herbicidal activity [17], we designed an efficient, simple, and ecofriendly synthetic procedure for the preparation of new synthetic compounds containing joint phenothiazine/ferrocene and α-amino-nitrile pharmacophoric units. In this work we report the experimental procedure for the ultrasound-assisted addition of the TMSCN nucleophile to heterocyclic aldimines. The substrates tested were mostly represented by a series of phenothiazinyl aldimines, but the scope of the new synthetic procedure was broadened by the preparation of new α-(arylamino)acetonitrile derivatives containing ferrocenyl and phenyl units. In order to evaluate the carcinogenic potential hazard of the newly prepared α-(arylamino)acetonitrile derivatives, the mutagenic potential of C-substituted derivatives containing phenothiazine, ferrocene or benzene units was screened by the *Salmonella* mutagenicity assay (Ames test) [28] using *S. typhimurium* TA98 and TA100 strains.

Results and Discussions

Ultrasound-assisted synthesis

The Strecker reaction between (hetero)aromatic aldimines and TMSCN in poly(ethylene glycol) (PEG)–water medium [18] was customized for phenothiazinyl aldimine substrates (Scheme 1), but an extremely long reaction time was required (72 hours) for the reaction to complete. In order to enhance the reaction rate, alternative energy sources were taken into consideration and ultrasonic irradiation was selected as a green chemistry protocol capable of inducing a more efficient energy input. Indeed, the reaction rate was significantly increased by applying the new protocol modified by means of an indirect ultrasound

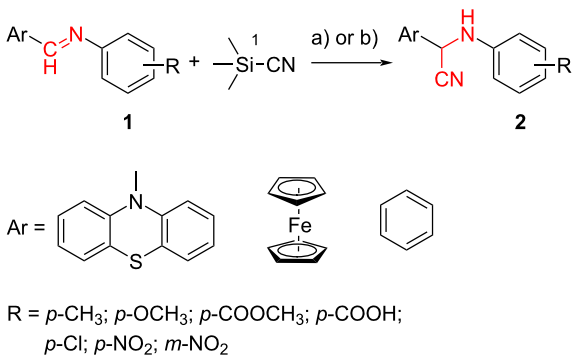

Scheme 1: Synthesis of α-amino-acetonitrile derivatives. Reaction conditions: Aldimine (1 equiv), TMSCN (1 equiv), reaction medium PEG–H_2O a) ultrasound-assisted reaction conditions: ultrasound frequency 37 kHz, power 95 W, temperature 25 °C, sonication time 30 min, b) classical reaction conditions: rt, 72 hours.

irradiation technique and high yields of the α-(arylamino)acetonitrile products were obtained after 30 minutes of sonication in a commercially available ultrasonic bath. The ferrocene and phenothiazine derivatives behaved in a similar manner and excellent yields of the corresponding α-(arylamino)acetonitrile derivatives were obtained in each case (Table 1), indicative of a good tolerance for the presence of (hetero)aromatic units and either electron-donating (methyl, methoxy) or electron-withdrawing groups (carboxy, nitro, etc.) pending on the imine substrate.

The molecular structures of all synthesized α-(arylamino)acetonitriles **2a–j** were fully characterized by spectroscopic methods. The MS spectra confirmed the molecular weight of the new compounds, while high-resolution ^{1}H and ^{13}C NMR spectroscopy afforded the complete characterization of the molecular

Table 1: Synthesis and characterization of 2-arylamino-2-(hetero)arylacetonitrile derivatives.

entry	α-(arylamino)acetonitrile	yield (%)		mp (°C)	FTIR $\nu_{C\equiv N}$ (cm^{-1})
		classical	ultrasound		
	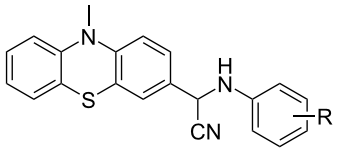				
2a	R = *p*-CH_3	95	98	90	2245
2b	R = *p*-O-CH_3	95	97	145	2247
2c	R = *p*-$COOCH_3$	91	95	85	2230
2d	R = *p*-COOH	97	97	206	2260
2e	R = *p*-Cl	93	93	86	2260
2f	R = *p*-NO_2	96	96	101	2234
2g	R = *m*-NO_2	98	98	128	2231
	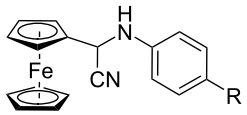				
2h	R = -O-CH_3	90	92	85	2247
2i	R = -$COOCH_3$	94	94	78	2250
2j	R = *p*-Cl	92	92	108	2239
2k	R = *p*-COOH	94	94	178	2239
	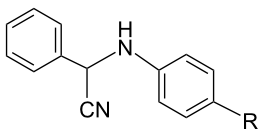				
2l	R = -$COOCH_3$	94	95	129	2251

skeleton. In the ^{1}H NMR spectra of compounds **2c**, **2e–l** a vicinal coupling constant between the protons in the >CH–NH– unit ($^3J \approx 7.5–8.7$ Hz) was recorded suggesting the reduced mobility for the proton in the amino group. The presence of the cyano functional group was confirmed by the FTIR spectra displaying an absorption band typical for the stretching vibration of the C≡N bond situated in the 2230–2260 cm^{-1} region, its position appearing slightly influenced by the electronic effects induced by the substituents of the aniline unit (Table 1). Detailed information about characterization data for compounds **2a–l** is given in Supporting Information File 1.

X-ray crystallographic data

In order to bring evidence of the geometry and arrangement of the molecules of the synthesized α-(arylamino)acetonitrile derivatives in the aggregated crystalline state, single crystals suitable for X-ray analysis were obtained by crystallization from isopropanol. The crystallographic data for the structure **2a** reported in this paper have been deposited at the Cambridge Crystallographic Data Centre as supplementary publication (CCDC 2018198) (deposit@ccdc.cam.ac.uk). The molecular structure for the representative compound **2a** is depicted in Figure 1.

As revealed from the crystal packing structure shown in Figure 1, compound **2a** forms a single crystalline phase containing both enantiomers of the chiral molecular structure in an ordered 1:1 ratio in the elementary cell. The phenothiazine unit shows a quasi-equatorial orientation of the methyl group attached to the heterocyclic nitrogen atom and a folding angle of 143.3°, a value close to the typical folding angle for unsubstituted 10-methylphenothiazine which was reported to be 143.7° [29], thus revealing a negligible electron-withdrawing effect of the substituent. The aromatic plane situated on the edge of the phenothiazine and the plane of the aromatic unit attached to the amino substituent appear twisted with a dihedral angle of 64.5°. The intermolecular distances are situated in the range 2.3–2.6 Å disclosing the lack of intermolecular interactions in the crystal structure.

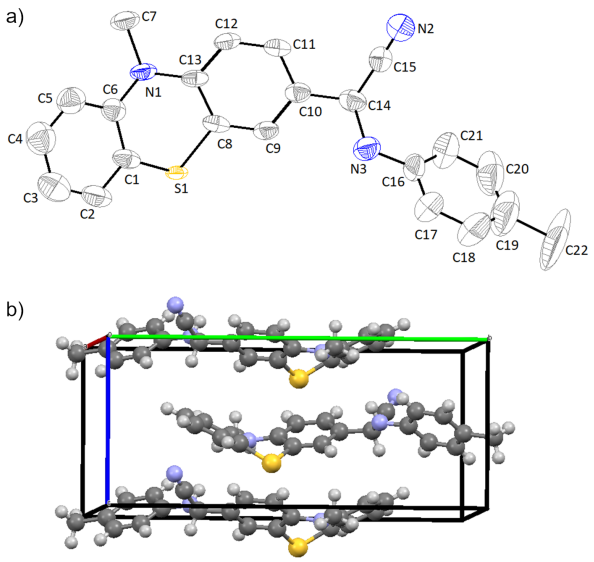

Figure 1: Crystal structure of 2-phenothiazinyl-2-(*p*-tolylamino)acetonitrile **2a**. a) ORTEP plot and b) crystallographic cell unit.

Scanning electron microscopy (SEM) analysis

Besides process intensification leading to a shorter reaction time, another advantage of the ultrasound-assisted reaction conditions was the formation of the product in crystalline form which was further investigated by SEM analysis. For comparison, the SEM micrographs recorded for the α-(arylamino)acetonitriles **2b** (Figure 2) and **2c** (Figure 3) obtained by ultrasound-

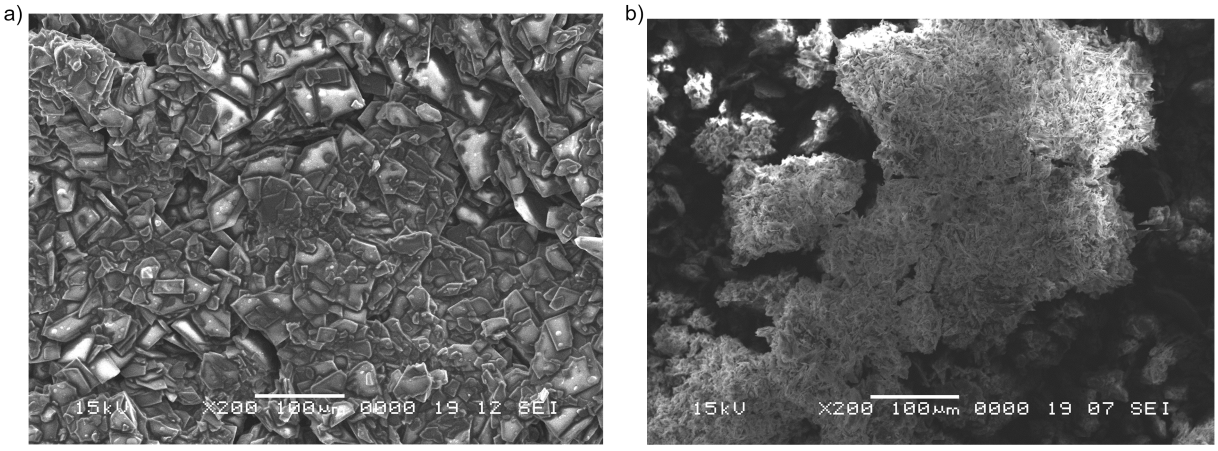

Figure 2: SEM images recorded at 200× for the raw reaction product **2b** obtained through a) ultrasound-assisted reaction conditions and b) classical reaction conditions.

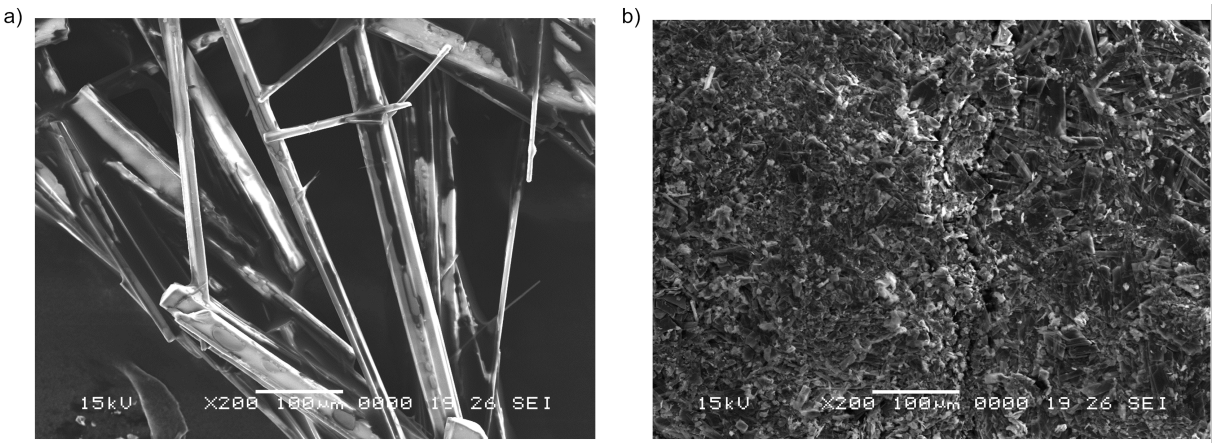

Figure 3: SEM image recorded at 200× for the raw reaction product **2c** obtained through a) ultrasound-assisted reaction conditions and b) classical reaction conditions.

assisted versus classical conditions are presented. In Figure 2a the magnification at 200× clearly shows higher crystallite sizes of the reaction product **2b** isolated by direct filtration of the reaction mixture obtained after the ultrasound-assisted protocol as compared to the same product obtained under classical conditions (Figure 2b).

In Figure 3a, the magnification at 200× indicates sharp rod-like natured crystals of the amino-acetonitrile **2c** obtained by the ultrasound-assisted reaction conditions in comparison with the crystallite aggregates obtained by the classical procedure (Figure 3b).

Biological assay

We chose the well-recognized Ames test to screen the mutagenic potential for three selected C-substituted α-amino-acetonitriles comprising different hetero(aromatic) units: phenothiazinyl (**2c**), ferrocenyl (**2i**), and phenyl (**2l**), respectively. The similarity of the tested aminoacetonitrile series was set aside by the N-functionalization of the methyl 4-((cyano-methyl)amino)benzoate skeleton, while dissimilarity was introduced by the C-functionalization with distinctive phenothiazinyl (**2c**), ferrocenyl (**2i**), and phenyl (**2l**) units, respectively, each of the constituent structural units being susceptible of imparting biological activity. The viability of *Salmonella typhimurium* TA98 and TA 100, respectively, was assessed by exposing the histidine dependent bacteria to compound **2c**, **2i**, and **2l**, respectively, directly on minimal glucose agar plates in the presence or absence of the metabolic activation system S9. The number of histidine independent revertant colonies was scored on the test plates after 72 hours of incubation at 37 °C. The mutagenicity test results confirmed spontaneous colony numbers within the regular range (comparable to the number scored on the (negative) solvent control plates), thus indicating that no toxicity effects are predictable for the new compounds **2c**, **2i**, and **2l** at concentrations ranging at their solubility maxima.

The possible antimutagenic effect of the selected C-substituted α-aminoacetonitriles **2c**, **2i**, and **2l**, respectively, in the presence of 2-aminoantracene, daunomycin (mutagens for TA 98), or sodium azide (known mutagen for TA 100), was also examined using the plate incorporation procedure and the results are summarized in Table 2 and Table 3. This assay proved a strong antimutagenic activity of all tested α-(arylamino)acetonitrile derivatives, with a better inhibition exhibited in the case of the TA98 strain (44–95%), but nevertheless considerable for TA100 strain (46–79%).

The results of the antimutagenicity assay indicate a lower inhibition exhibited in the presence of liver homogenate (S9), pointing out that metabolizing enzymes could interfere with the activation of the synthetic compounds.

Conclusion

An efficient reaction protocol for the ultrasound-assisted synthesis of new 2-(arylamino)-2-(hetero)arylacetonitrile derivatives containing phenothiazine units was developed. It was proved that the protocol can be more generally applied, affording excellent yields of the substituted α-(arylamino)acetonitrile derivatives with a high tolerance to the variation of (hetero)aromatic units and electron-donating/withdrawing substituents present in the structure of the aldimine substrate. The comparison between the classical and the ultrasound-assisted reaction protocols recommends the ultrasound irradiation technique as a greener chemical protocol affording significantly enhanced reaction rates and higher crystallite size of the

Table 2: The antimutagenicity assay results of the newly synthesized C-substituted α-aminoacetonitriles for *S. typhimurium* TA98 and TA100 strain with the metabolic activation system S9.

test item	TA98		TA100	
	number of revertants	inhibition (%)	number of revertants	inhibition (%)
negative control	25		170	
2c	14	44	42	75.3
2i	10	60	35	79.4
2l	16	36	43	74.7
2-aminoanthracene[a]	28	–	114	–

[a]2-Aminoanthracene was used as the positive control for the *S. typhimurium* TA98 and TA100 strains.

Table 3: The antimutagenicity assay results of the newly synthesized C-substituted α-aminoacetonitriles for *S. typhimurium* TA98 and TA100 strain without the metabolic activation system S9.

test item	TA98		TA100	
	number of revertants	inhibition (%)	number of revertants	inhibition (%)
negative control	58		184	
2c	3	94.8	98	46.7
2i	14	75.8	38	79.3
2l	12	79.3	85	53.8
NaN_3[a]	–	–	147	–
daunomycin[a]	95	–	–	–

[a]NaN_3 and daunomycin were used as the positive controls for the *S. typhimurium* TA98 and TA100 strains.

products, thus increasing the energy efficiency of the Strecker synthesis.

An initial screening of the mutagenic potential of the newly synthetized α-amino-C-substituted-acetonitriles pointed out that the compounds **2c**, **2i**, and **2l** can be considered as genotoxically safe at concentrations in the range of their solubility limit in DMSO/water media. The tested compounds also exhibited antimutagenic activity by interfering with the effect of known mutagenic compounds such as 2-aminoantracene and sodium azide.

Experimental

General procedures for the preparation of 2-(arylamino)-2-(hetero)arylacetonitrile derivatives

Ultrasound-assisted reaction conditions (a)

Ultrasound-assisted reactions were carried out by indirect sonication using a commercially available ultrasonic bath (Elmasonic S 15 (H), Germany) of rectangular geometry (tank internal dimensions 151 × 137 × 100 mm) with sandwich transducer systems, an ultrasonic frequency of 37 kHz, power 95 W, and temperature-controlled ultrasonic operation. For the reactions, a stopper-sealed pear-shaped glass flask (25 mL) containing the reaction mixture was placed in the central position of the ultrasonic bath tank filled with a 5% Na_2CO_3 aqueous solution and subjected to sonication by setting the bath operation period to 30 min and the temperature to 25 °C. The reaction mixture was prepared by adding TMSCN (1 equiv) to a solution containing the aldimine (1 equiv) dissolved in PEG (5 mL) and water (1 mL). After completion of the reaction, the product was collected by filtration directly from the reaction mixture, or after being poured into water. The crystalline product was dried and if necessary, further purified by recrystallization from a suitable solvent.

Classical conditions (b)

The reaction mixture, prepared as described to general procedure (a), was stirred at room temperature for 3 days. After completion of the reaction, the mixture was poured into water and the product was extracted in diethyl ether. After evaporation of the organic solvent the solid product was collected and purified by recrystallization from a suitable solvent.

Supporting Information

Supporting Information File 1

Experimental procedures, characterization data, biological assay, and copies of the ^{1}H and ^{13}C NMR spectra.
[https://www.beilstein-journals.org/bjoc/content/supplementary/1860-5397-16-242-S1.pdf]

Acknowledgements

The authors greatly acknowledge Dr. Florin Popa from Technical University of Cluj-Napoca, Materials Science and Engineering Department, for recording the SEM images.

Funding

This work was partially supported by a Joint Research Project Romanian Academy - National Academy of Sciences of Belarus, Belarusian Republican Foundation for Fundamental Research, code: AR-FRBCF-2020-2021

ORCID® iDs

Alexandra Pop - https://orcid.org/0000-0002-2355-3682
Castelia Cristea - https://orcid.org/0000-0003-1138-2596
Gabriel Barta - https://orcid.org/0000-0001-5501-2744
Luminița Silaghi-Dumitrescu - https://orcid.org/0000-0001-8800-4839

References

1. Leonelli, C.; Mason, T. J. *Chem. Eng. Process.* **2010,** *49,* 885–900. doi:10.1016/j.cep.2010.05.006
2. Patil, R.; Bhoir, P.; Deshpande, P.; Wattamwar, T.; Shirude, M.; Chaskar, P. *Ultrason. Sonochem.* **2013,** *20,* 1327–1336. doi:10.1016/j.ultsonch.2013.04.002
3. Kaur, G.; Sharma, A.; Banerjee, B. *ChemistrySelect* **2018,** *3,* 5283–5295. doi:10.1002/slct.201800326
4. Lupacchini, M.; Mascitti, A.; Giachi, G.; Tonucci, L.; d'Alessandro, N.; Martinez, J.; Colacino, E. *Tetrahedron* **2017,** *73,* 609–653. doi:10.1016/j.tet.2016.12.014
5. Pokhrel, N.; Vabbina, P. K.; Pala, N. *Ultrason. Sonochem.* **2016,** *29,* 104–128. doi:10.1016/j.ultsonch.2015.07.023
6. Nalesso, S.; Bussemaker, M. J.; Sear, R. P.; Hodnett, M.; Lee, J. *Ultrason. Sonochem.* **2019,** *57,* 125–138. doi:10.1016/j.ultsonch.2019.04.020
7. Ruecroft, G.; Hipkiss, D.; Ly, T.; Maxted, N.; Cains, P. W. *Org. Process Res. Dev.* **2005,** *9,* 923–932. doi:10.1021/op050109x
8. Jordens, J.; Gielen, B.; Xiouras, C.; Hussain, M. N.; Stefanidis, G. D.; Thomassen, L. C. J.; Braeken, L.; Van Gerven, T. *Chem. Eng. Process.* **2019,** *139,* 130–154. doi:10.1016/j.cep.2019.03.017
9. Pluta, K.; Morak-Młodawska, B.; Jeleń, M. *Eur. J. Med. Chem.* **2011,** *46,* 3179–3189. doi:10.1016/j.ejmech.2011.05.013
10. Saleem, M.; Yu, H.; Wang, L.; Zain-ul-Abdin; Khalid, H.; Akram, M.; Abbasi, N. M.; Huang, J. *Anal. Chim. Acta* **2015,** *876,* 9–25. doi:10.1016/j.aca.2015.01.012
11. Ludwig, B. S.; Correia, J. D. G.; Kühn, F. E. *Coord. Chem. Rev.* **2019,** *396,* 22–48. doi:10.1016/j.ccr.2019.06.004
12. Zhao, S.; Kang, J.; Du, Y.; Kang, J.; Zhao, X.; Xu, Y.; Chen, R.; Wang, Q.; Shi, X. *J. Heterocycl. Chem.* **2014,** *51,* 683–689. doi:10.1002/jhet.1652
13. Parsaee, Z.; Joukar Bahaderani, E.; Afandak, A. *Ultrason. Sonochem.* **2018,** *40,* 629–643. doi:10.1016/j.ultsonch.2017.08.010
14. Venkatesan, K.; Satyanarayana, V. S. V.; Mohanapriya, K.; Khora, S. S.; Sivakumar, A. *Res. Chem. Intermed.* **2015,** *41,* 595–607. doi:10.1007/s11164-013-1213-1
15. Găină, L.; Iftimia, A.; Surducan, M.; Cristea, C.; Silaghi-Dumitrescu, L. *Stud. Univ. Babes-Bolyai, Chem.* **2008,** *53* (4), 35–41.
16. Găină, L.; Csámpai, A.; Túrós, G.; Lovász, T.; Zsoldos-Mády, V.; Silberg, I. A.; Sohár, P. *Org. Biomol. Chem.* **2006,** *4,* 4375–4386. doi:10.1039/b608455a
17. Kouznetsov, V. V.; Puerto Galvis, C. E. *Tetrahedron* **2018,** *74,* 773–810. doi:10.1016/j.tet.2018.01.005
18. Kumar, M. A.; Babu, M. F. S.; Srinivasulu, K.; Kiran, Y. B.; Reddy, C. S. *J. Mol. Catal. A: Chem.* **2007,** *265,* 268–271. doi:10.1016/j.molcata.2006.10.030
19. Hanafusa, T.; Ichihara, J.; Ashida, T. *Chem. Lett.* **1987,** *16,* 687–690. doi:10.1246/cl.1987.687
20. Menéndez, J. C.; Trigo, G. G.; Söllhuber, M. M. *Tetrahedron Lett.* **1986,** *27,* 3285–3288. doi:10.1016/s0040-4039(00)84777-2
21. Fadel, A. *Tetrahedron* **1991,** *47,* 6265–6274. doi:10.1016/s0040-4020(01)86558-3
22. Fadel, A. *Synlett* **1993,** 503–505. doi:10.1055/s-1993-22507
23. Găină, L. I.; Mătărângă-Popa, L. N.; Gal, E.; Boar, P.; Lönnecke, P.; Hey-Hawkins, E.; Bischin, C.; Silaghi-Dumitrescu, R.; Lupan, I.; Cristea, C.; Silaghi-Dumitrescu, L. *Eur. J. Org. Chem.* **2013,** 5500–5508. doi:10.1002/ejoc.201300480
24. Găină, L.; Torje, I.; Gal, E.; Lupan, A.; Bischin, C.; Silaghi-Dumitrescu, R.; Damian, G.; Lönnecke, P.; Cristea, C.; Silaghi-Dumitrescu, L. *Dyes Pigm.* **2014,** *102,* 315–325. doi:10.1016/j.dyepig.2013.10.044
25. Găină, L.; Gal, E.; Mătărângă-Popa, L.; Porumb, D.; Nicolescu, A.; Cristea, C.; Silaghi-Dumitrescu, L. *Tetrahedron* **2012,** *68,* 2465–2470. doi:10.1016/j.tet.2012.01.068
26. Ignat, A.; Lovasz, T.; Vasilescu, M.; Fischer-Fodor, E.; Tatomir, C. B.; Cristea, C.; Silaghi-Dumitrescu, L.; Zaharia, V. *Arch. Pharm. (Weinheim, Ger.)* **2012,** *345,* 574–583. doi:10.1002/ardp.201100355
27. Gál, E.; Cristea, C.; Silaghi-Dumitrescu, L.; Lovász, T.; Csámpai, A. *Tetrahedron* **2010,** *66,* 9938–9944. doi:10.1016/j.tet.2010.10.046
28. Maron, D. M.; Ames, B. N. *Mutat. Res.* **1983,** *113,* 173–215. doi:10.1016/0165-1161(83)90010-9
29. Chu, S. S. C.; Van der Helm, D. *Acta Crystallogr., Sect. B: Struct. Crystallogr. Cryst. Chem.* **1974,** *30,* 2489–2490. doi:10.1107/s0567740874007394

License and Terms

BEILSTEIN JOURNAL OF ORGANIC CHEMISTRY

Metal-free synthesis of biarenes via photoextrusion in di(tri)aryl phosphates

Hisham Qrareya[1,2], Lorenzo Meazza[1], Stefano Protti[1] and Maurizio Fagnoni[*1]

Full Research Paper

Open Access

Address:
[1]PhotoGreen Lab, Department of Chemistry, viale Taramelli 12, 27100 Pavia, Italy and [2]Industrial Chemistry Department, Arab American University, 240 Jenin 13, Zababdeh, Palestine

Email:
Maurizio Fagnoni[*] - fagnoni@unipv.it

* Corresponding author

Keywords:
aryl phosphates; biarenes; metal-free synthesis; photochemistry; photoextrusion

Beilstein J. Org. Chem. **2020,** *16,* 3008–3014.
https://doi.org/10.3762/bjoc.16.250

Received: 25 September 2020
Accepted: 23 November 2020
Published: 08 December 2020

This article is part of the thematic issue "Green chemistry II".

Associate Editor: L. Vaccaro

Abstract

A metal-free route for the synthesis of biarenes has been developed. The approach is based on the photoextrusion of a phosphate moiety occurring upon irradiation of biaryl- and triaryl phosphates. The reaction involves an exciplex as the intermediate and it is especially suitable for the preparation of electron-rich biarenes.

Introduction

It is difficult to overestimate the importance of aromatics in drug development. Indeed, introducing an aromatic or a heteroaromatic ring, most often a (substituted) phenyl ring, into a biologically active compound is a common practice in medicinal chemistry [1-3]. In particular, the biaryl moiety is a privileged scaffold largely present in the skeleton of natural substances [4-7] and in useful chiral ligands [8-10]. The synthesis of biaryl derivatives remains, however, a considerable challenge [11-13]. Common methods, such as the Ullmann and Gomberg synthesis [14-16] have been nowadays supplanted by the much more versatile metal-catalyzed cross-coupling reactions [17-23]. This excellent approach still encounters some limitation in the scope and in the practical application, due to the use of labile and expensive reagents. Moreover, the elimination of metal trace residues and wastes is of some concern particularly for products destined to pharmaceutical applications as it is imperative operating under 'green' conditions. As for the last issue, there is nowadays a growing interest in the forging of Ar–Ar bonds under transition-metal-free conditions [24,25]. Apart the most common pathways, e.g., the Friedel–Crafts functionalization [26] or nucleophilic aromatic substitution [27], alternative approaches have emerged that make use of photogenerated intermediates (triplet aryl cations [28,29] or aryl radicals [30,31]). As for the former case, the intermolecular formation of a biaryl arose from the photoheterolysis of an Ar–N bond (in arene diazonium salts or their derivatives [32,33]), of an Ar–Cl bond [34,35], of an Ar–O bond (in aryl phosphates [36], aryl sulfonates [36], and in aryl trifluoroethyl sulfate [37],

Scheme 1a) followed by the reaction of the thus formed aryl cation with an aromatic substrate. In an alternative approach, aryl radicals may be generated under photoredox catalysis conditions (mostly from arene diazonium salts or aryl iodides) [30,31] or by the direct photolysis of arylazo sulfones [38-40] and employed for the desired arylations. These reactions have the advantage of being applied to non-functionalized arenes but have the drawback to require a large excess of the nucleophilic reagent (the arene Ar–H) in up to 10–20-fold amount. Furthermore, the aryl radical/cation addition onto the aromatic reactant may lead to a mixture of regioisomers when using non-symmetrical Ar–H. A possible solution is having recourse to an intramolecular free radical ipso substitution reaction where an XSO_2 tether is placed between two aromatic rings to direct the selective Ar–Ar bond formation (Scheme 1b) [41-43]). In this case, *N*-methyl sulfonamides were the elective substrates albeit a part of the tether is maintained in the final structure. This is common even for other related metal-free biaryl syntheses exploiting the Truce–Smiles rearrangement in aryl sulfonamides and aryl phenylsulfonates [44-46] or the [3,3]-sigmatropic rearrangement of sulfonium salts arising from the reaction of aryl sulfoxides and phenols [47]. To overcome this problem, the use of a metal catalyst (mainly Ni) was mandatory as reported for the real extrusion of CO in diaryl ketones [48,49] or of SO_2 in diaryl sulfones (Scheme 1c) [50]. Nevertheless, a recent publication demonstrated that a metal-free photoextrusion was feasible when starting from benzene sulfonamides **I** (Scheme 1d, path a) [51]. Following the same approach, sparse reports described that in some cases biaryls may be obtained in variable yields starting from biaryl phosphates [52], biaryl phosphonates **II** [53-56], and triaryl phosphates [57-61] (Scheme 1d, path b). In search for alternative ways for the preparation of biaryls under photoinduced metal-free ecosustainable conditions we reinvestigated the photochemistry of di- and triaryl phosphates **III** and **IV** (Scheme 1e), compounds that can be easily achieved from the corresponding phenols [62,63].

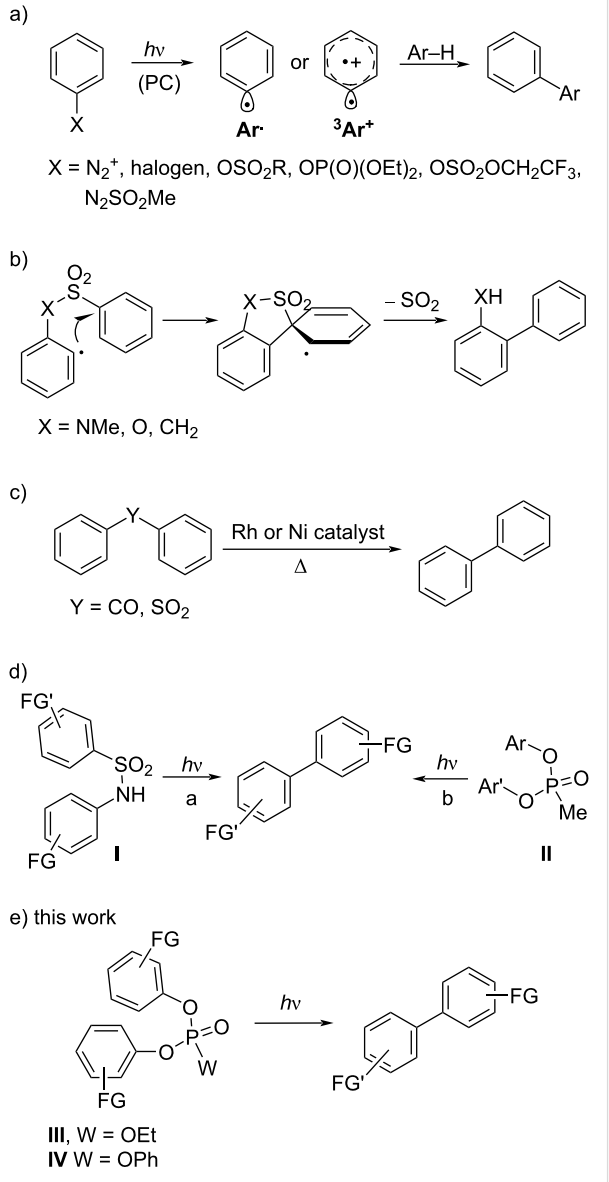

Scheme 1: Synthesis of biarenes via a) photogenerated triplet aryl cations and aryl radicals (PC = photocatalyst), b) intramolecular free radical ipso substitution, c) thermally catalyzed extrusion of CO and SO_2, d) photoinduced photoextrusion from benzene sulfonamides **I** and phosphonates **II**, and e) photoextrusion from diaryl- (**III**) and triaryl (**IV**) phosphates.

Results and Discussion

At the onset of our investigation, we tested a triaryl phosphate such as 4-chlorophenyl diphenyl phosphate (**1a**), as the model compound in different solvents by irradiation in a multilamp reactor (wavelength centered at 310 nm, see Supporting Information File 1 for details). The obtained results are depicted in Table 1. Compound **1a** (0.02 M) was quite photostable in dichloromethane, acetonitrile, and acetone (Table 1, entries 1–3), whereas 4-chlorobiphenyl (**2a**) was observed in traces as the only product in neat methanol (30% of **1a** consumption, Table 1, entry 4). Interestingly, the addition of water (a methanol/water 2:1 mixture) increased the overall yield of the product **2a** (up to 16%) along with negligible amounts of biphenyl (**2b**). Decreasing the concentration of **1a** (to 10^{-2} M) in the examined conditions was found noxious for the reaction course (Table 1, entry 6), but shifting the wavelength to 254 nm led to significant amounts of the desired biaryl (Table 1, entry 7). The yields started to be satisfactory, however, when performing the reaction at 310 nm using 2,2,2-trifluoroethanol (TFE) as the solvent (45% yield, entry 8 in Table 1). We thus decided to replace part of the rather expensive and toxic solvent TFE with acetone (Table 1, entries 9–12) and the best results were obtained when using a TFE/acetone 4:1 mixture (Table 1, entry 10) with an

Table 1: Optimization of the reaction conditions.

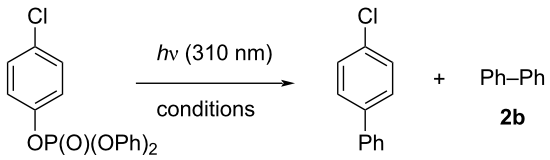

1a **2a**

entry	reaction conditions	λ_{irr} (nm)	products, yield (%)
1	**1a** (0.02 M), CH_2Cl_2	310	–[a]
2	**1a** (0.02 M), CH_3CN	310	–[a]
3	**1a** (0.02 M), acetone	310	–[a]
4	**1a** (0.02 M), CH_3OH	310	**2a**, 3[b]
5	**1a** (0.02 M), CH_3OH/H_2O 2:1	310	**2a**, 16; **2b**, 1
6	**1a** (0.01 M), CH_3OH/H_2O 2:1	310	**2a**, 6
7	**1a** (0.01 M), CH_3OH/H_2O 2:1	254	**2a**, 44
8	**1a** (0.02 M), CF_3CH_2OH	310	**2a**, 45; **2b**, 2
9	**1a** (0.02 M), CF_3CH_2OH/acetone 9:1	310	**2a**, 38; **2b**, 2
10	**1a (0.02 M), CF_3CH_2OH/acetone 4:1**	**310**	**2a, 67; 2b, 4**
11	**1a** (0.02 M), CF_3CH_2OH/acetone 7:3	310	**2a**, 48; **2b**, 3
12	**1a** (0.02 M), CF_3CH_2OH/acetone 1:1	310	**2a**, 14; **2b**, 2
13	**1a** (0.04 M), CF_3CH_2OH/acetone 4:1	310	**2a**, 57; **2b**, 2
14	**1a** (0.06 M), CF_3CH_2OH/acetone 4:1	310	**2a**, 67; **2b**, 12
15	**1a** (0.02 M), CF_3CH_2OH/acetone 4:1[c]		–[a]

[a]No consumption of **1a** observed; [b]30% consumption of **1a** measured; [c]the reaction mixture was stored in the dark for 24 h.

isolated yield of **2a** of 67% along with **2b** (4% yield) as the by-product. A further increase in the concentration of the substrate (Table 1, entries 13 and 14) resulted in a lowering of the selectivity (the undesired product **2b** was detected in up to 12% yield). Finally, no reaction took place when the solution was covered by an aluminum foil and stored in the photochemical apparatus for 24 h (Table 1, entry 15).

Encouraged by the results collected in Table 1, in particular with the fact that the byproduct **2b** was formed in such small amounts, we used the conditions described in entry 10 (Table 1) to explore the scope of the process by investigating other *n*-substituted phenyl diphenyl phosphates (**1a–l**, see Scheme 2). Thus, the irradiation of triphenyl phosphate (**1b**) gave the corresponding biphenyl (**2b**) in 67% yield. Similar results were obtained with 4-alkylphenyl diphenyl phosphates, that afforded the 4-substituted biaryls **2c–e** in up to 83% yield. However, when examining substrates bearing a strong electron-donating substituent (G = 4-OMe, 4-OPh, 3-OMe), the efficiency of the process decreased (see the yields of **2f, g**, and **2i** in Scheme 2). On the other hand, the presence of an electron-withdrawing group (e.g., 4-CN, compound **1h**) completely inhibited the reaction and **1h** was recovered unaltered after the irradiation. Better results have been, however, obtained with polysubstituted derivatives **1j–l**. In these cases, the expected phenylated arenes **2j–l** were isolated in the 50–64% range.

We were then intrigued to extend the scope of the reaction by focusing on a few ethyl diaryl phosphates **3a–e**. Gratifyingly, the formation of the symmetric biaryls **4** took place efficiently with the substrates bearing strong electron-donating substituents, especially when present in the *para*-position (see the case of **4a–c**). Unfortunately, the unsymmetric biaryl **4e** was detected in a very poor amount.

To investigate the reaction mechanism, some photophysical parameters of compounds **1** and **3** were determined. All the phosphates examined were barely fluorescent in methanol, with an emission quantum yield (Φ_{em}) in the 0.005–0.06 range (see Table 2 and Supporting Information File 1 for further details).

We thus focused on compounds **1e**, **1h**, **3a** and **3c** as the model substrates. In the case of compounds **1e** and **1h**, we observed that the fluorescence is significantly red shifted (about 30 nm) with respect to that of the corresponding diethyl aryl phosphates (see Figure 1 and Figure 2). On the other hand, when focusing on compound **3a**, we noticed the presence of two emission bands located at 307 and 360 nm, respectively (see

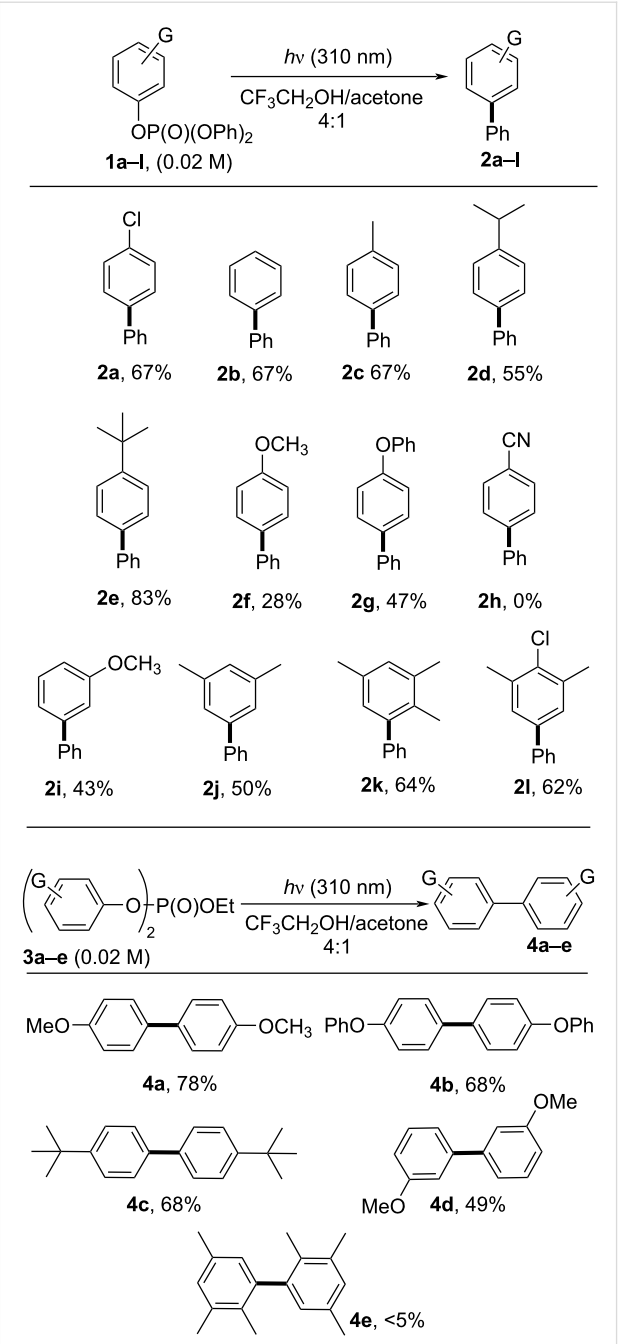

Scheme 2: Metal-free photochemical synthesis of biaryls **2** and **4**.

Figure 3) and their relative intensity was solvent dependent. Indeed, the band at 360 nm is favored and slightly blue shifted when increasing the proticity of the medium (see the comparison of the fluorescence spectra obtained in methanol and in a methanol/TFE 4:1 mixture, Figure 3). A similar behavior was observed with compound **3c**, where a single emission band located at ca. 290 nm is observable in neat methanol, whereas the presence of TFE causes a lowering of that emission, in favor of a second band in the 330–350 nm region (Figure 4). These two

Table 2: Emission data of selected diaryl- and triaryl phosphates **1** and **3**.

compound	λ_{em} (nm)	Φ_{em}[a]
1a	300	0.005
1b	315	0.017
1e	319	0.025
1f	312	0.059
1h	335	0.023
3a	307, 360	0.030
3c	294	0.062

[a]Measured by comparison with 4-chloroanisole (Φ_F = 0.019 in MeOH) [64].

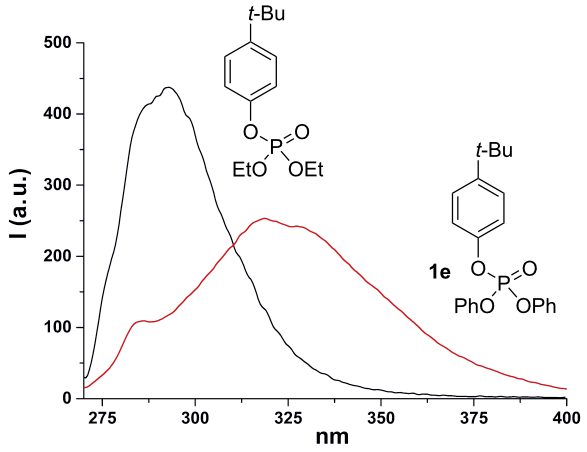

Figure 1: Emission spectrum of compound **1e** (red) and of diethyl *p-tert*-butylphenyl phosphate (black) in methanol.

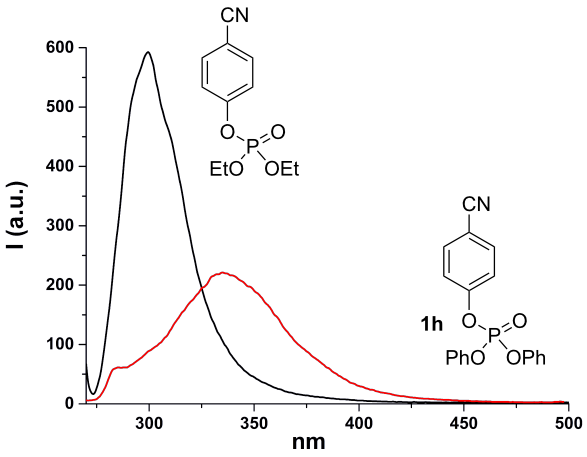

Figure 2: Emission spectrum of compound **1h** (red) and of diethyl *p*-cyanophenyl phosphate (black) in methanol.

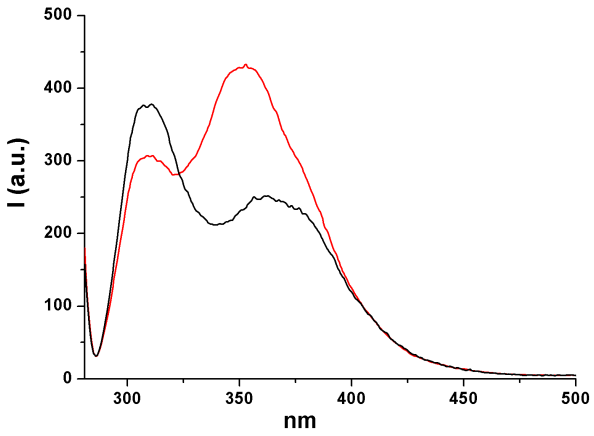

Figure 3: Emission spectrum of compound **3a** in methanol (black) and in a methanol/TFE 4:1 mixture (red).

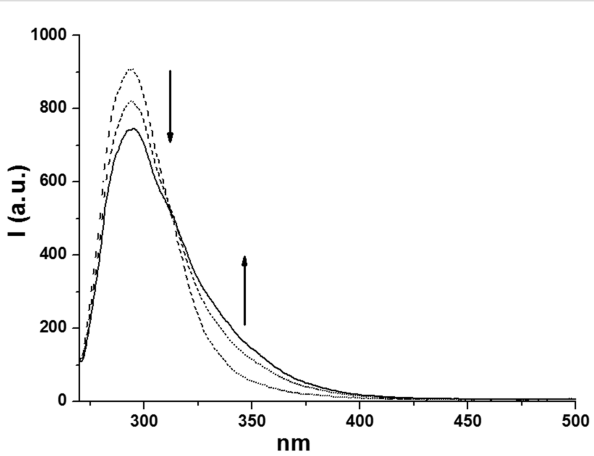

Figure 4: Emission spectrum of **3c** in MeOH (dotted line) and in the presence of increasing amounts of TFE (up to 20% v/v, continuous line).

emissions have been assigned, on the basis of our results and of the reported literature [58,61], to the singlet monomeric excited state and to the exciplex, respectively.

While aryl phosphates have been only sparsely used as substrates in thermal cross-coupling reactions [65-67], their photochemical behavior has been the subject of various investigations in the last decades [28,29,64,68]. Simple (electron-rich) monoaryl phosphates are known to undergo the photoheterolysis of the Ar–O bond to form aryl cations [28,36]. The presence of an electron-withdrawing group (e.g., NO_2) may, however, divert the reactivity since a photoinduced solvolysis occurred as demonstrated by Havinga more than 70 years ago [69]. In alternative, the irradiation of monoaryl phosphates in the presence of a strong nucleophile (e.g., a tin anion) led to an ipso substitution reaction via an $ArS_{RN}1$ process [70].

The situation dramatically changes when a further aryl group is present in the phosphates since none of the above-mentioned processes took place. In fact, our investigations, in according with early works [52,71], suggested that both diaryl and triaryl phosphates are prone to generate an intramolecular exciplex **5*** under irradiation (Scheme 3, path (a)), on the route to the extrusion of the phosphate moiety. This is demonstrated by the formation of a new emission band when more than one aryl group is present in the aryl phosphate (see Figure 1). In our investigation, we likewise stated that the formation of **5*** (from **1** and **3**) is highly favored in highly protic solvents such as TFE, as well evidenced, among the others, in the cases of **1e** and **4c**, and as already reported in the formation of other intramolecular aromatic exciplexes [72].

The so generated exciplex apparently plays a key role in the formation of the biaryls **2** and **4** probably via the formation of the biradical intermediate **6** [55] preceding the loss of $ROP(O)(OH)_2$ (paths (b), (c), Scheme 3). The long irradiation time required to achieve a complete consumption of the substrates **1** and **3** is in accordance with the low quantum yield values reported for this process [58,61]. Furthermore, a dependence on the nature of the aromatic substituents G was apparent, since arylation took place (in variable yields) with electron-rich aromatic substituents, while it was completely in-

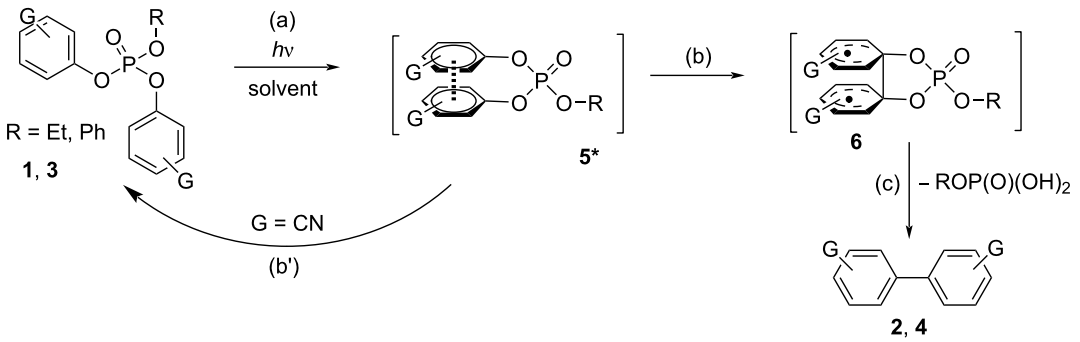

Scheme 3: Photoreactivity of aryl phosphates **1** and **3** in protic media.

hibited in the presence of electron-withdrawing groups (path (b'), in Scheme 3). In the case of the triaryl phosphates, biphenyl (**1b**) is formed as the byproduct in <5% yield.

Conclusion

We demonstrated that biaryls can be smoothly prepared via the photoextrusion of diaryl- and triaryl phosphates in protic media, with the concomitant release of a molecule of phosphoric acid monoester. The reaction takes place in moderate yields but under very mild conditions with no need of any (photo)catalyst or additive, despite the scope of the process is in part limited since the presence of at least one electron-withdrawing group on an aromatic ring completely suppressed the reaction.

Supporting Information

Supporting Information File 1

Experimental section, fluorescence, and ^{1}H and ^{13}C NMR spectra.
[https://www.beilstein-journals.org/bjoc/content/supplementary/1860-5397-16-250-S1.pdf]

Funding

H. Q. thanks the Arab American University-Palestine (AAUP) for financial support, and the University of Pavia (Italy) for hosting.

ORCID® iDs

Hisham Qrareya - https://orcid.org/0000-0003-0909-3760
Stefano Protti - https://orcid.org/0000-0002-5313-5692
Maurizio Fagnoni - https://orcid.org/0000-0003-0247-7585

Preprint

A non-peer-reviewed version of this article has been previously published as a preprint: https://doi.org/10.3762/bxiv.2020.110.v1

References

1. Hajduk, P. J.; Bures, M.; Praestgaard, J.; Fesik, S. W. *J. Med. Chem.* **2000,** *43,* 3443–3447. doi:10.1021/jm000164q
2. Horton, D. A.; Bourne, G. T.; Smythe, M. L. *Chem. Rev.* **2003,** *103,* 893–930. doi:10.1021/cr020033s
3. Klekota, J.; Roth, F. P. *Bioinformatics* **2008,** *24,* 2518–2525. doi:10.1093/bioinformatics/btn479
4. Goa, K. L.; Wagstaff, A. J. *Drugs* **1996,** *51,* 820–845. doi:10.2165/00003495-199651050-00008
5. McElroy, W. T.; DeShong, P. *Tetrahedron* **2006,** *62,* 6945–6954. doi:10.1016/j.tet.2006.04.074
6. Torres, J. C.; Pinto, A. C.; Garden, S. J. *Tetrahedron* **2004,** *60,* 9889–9900. doi:10.1016/j.tet.2004.08.030
7. Bringmann, G.; Price Mortimer, A. J.; Keller, P. A.; Gresser, M. J.; Garner, J.; Breuning, M. *Angew. Chem., Int. Ed.* **2005,** *44,* 5384–5427. doi:10.1002/anie.200462661
8. Noyori, R.; Takaya, H. *Acc. Chem. Res.* **1990,** *23,* 345–350. doi:10.1021/ar00178a005
9. Wallace, T. W. *Org. Biomol. Chem.* **2006,** *4,* 3197–3210. doi:10.1039/b608470m
10. Berthod, M.; Mignani, G.; Woodward, G.; Lemaire, M. *Chem. Rev.* **2005,** *105,* 1801–1836. doi:10.1021/cr040652w
11. Vasconcelos, S. N. S.; Reis, J. S.; de Oliveira, I. M.; Balfour, M. N.; Stefani, H. A. *Tetrahedron* **2019,** *75,* 1865–1959. doi:10.1016/j.tet.2019.02.001
12. Nguyen, T. T. *Org. Biomol. Chem.* **2019,** *17,* 6952–6963. doi:10.1039/c9ob01304k
13. Felpin, F.-X.; Sengupta, S. *Chem. Soc. Rev.* **2019,** *48,* 1150–1193. doi:10.1039/c8cs00453f
14. Fanta, P. E. *Chem. Rev.* **1946,** *38,* 139–196. doi:10.1021/cr60119a004
15. Sambiagio, C.; Marsden, S. P.; Blacker, A. J.; McGowan, P. C. *Chem. Soc. Rev.* **2014,** *43,* 3525–3550. doi:10.1039/c3cs60289c
16. Amaya, T.; Jin, Y.; Tobisu, M. *Tetrahedron Lett.* **2019,** *60,* 151062. doi:10.1016/j.tetlet.2019.151062
17. de Meijere, A.; Diederich, F., Eds. *Metal-Catalyzed Cross-Coupling Reactions,* 2nd ed.; Wiley-VCH: Weinheim, Germany, 2004. doi:10.1002/9783527619535
18. Cepanec, I. *Synthesis of biaryls;* Elsevier: Oxford, U.K., 2004. doi:10.1016/b978-0-08-044412-3.x5000-3
19. Hussain, I.; Singh, T. *Adv. Synth. Catal.* **2014,** *356,* 1661–1696. doi:10.1002/adsc.201400178
20. García-López, J.-A.; Greaney, M. F. *Chem. Soc. Rev.* **2016,** *45,* 6766–6798. doi:10.1039/c6cs00220j
21. Hassan, J.; Sévignon, M.; Gozzi, C.; Schulz, E.; Lemaire, M. *Chem. Rev.* **2002,** *102,* 1359–1470. doi:10.1021/cr000664r
22. Nicolaou, K. C.; Bulger, P. G.; Sarlah, D. *Angew. Chem., Int. Ed.* **2005,** *44,* 4442–4489. doi:10.1002/anie.200500368
23. Hussain, I.; Capricho, J.; Yawer, M. A. *Adv. Synth. Catal.* **2016,** *358,* 3320–3349. doi:10.1002/adsc.201600354
24. Sun, C.-L.; Shi, Z.-J. *Chem. Rev.* **2014,** *114,* 9219–9280. doi:10.1021/cr400274j
25. Sun, C.-L.; Li, H.; Yu, D.-G.; Yu, M.; Zhou, X.; Lu, X.-Y.; Huang, K.; Zheng, S.-F.; Li, B.-J.; Shi, Z.-J. *Nat. Chem.* **2010,** *2,* 1044–1049. doi:10.1038/nchem.862
26. Sawama, Y.; Asai, S.; Kawajiri, T.; Monguchi, Y.; Sajiki, H. *Chem. – Eur. J.* **2015,** *21,* 2222–2229. doi:10.1002/chem.201405558
27. Guo, L.; Liu, F.; Wang, L.; Yuan, H.; Feng, L.; Kürti, L.; Gao, H. *Org. Lett.* **2019,** *21,* 2894–2898. doi:10.1021/acs.orglett.9b00927
28. Dichiarante, V.; Protti, S.; Fagnoni, M. *J. Photochem. Photobiol., A* **2017,** *339,* 103–113. doi:10.1016/j.jphotochem.2017.02.007
29. Lazzaroni, S.; Ravelli, D.; Protti, S.; Fagnoni, M.; Albini, A. *C. R. Chim.* **2017,** *20,* 261–271. doi:10.1016/j.crci.2015.11.024
30. Hofmann, J.; Heinrich, M. R. *Tetrahedron Lett.* **2016,** *57,* 4334–4340. doi:10.1016/j.tetlet.2016.08.034
31. Ghosh, I.; Marzo, L.; Das, A.; Shaikh, R.; König, B. *Acc. Chem. Res.* **2016,** *49,* 1566–1577. doi:10.1021/acs.accounts.6b00229
32. Milanesi, S.; Fagnoni, M.; Albini, A. *Chem. Commun.* **2003,** 216–217. doi:10.1039/b210243a
33. Barragan, E.; Poyil, A. N.; Yang, C.-H.; Wang, H.; Bugarin, A. *Org. Chem. Front.* **2019,** *6,* 152–161. doi:10.1039/c8qo00938d
34. Fagnoni, M.; Mella, M.; Albini, A. *Org. Lett.* **1999,** *1,* 1299–1301. doi:10.1021/ol990982g

35. Dichiarante, V.; Fagnoni, M.; Albini, A. *Angew. Chem., Int. Ed.* **2007,** *46,* 6495–6498. doi:10.1002/anie.200701462
36. De Carolis, M.; Protti, S.; Fagnoni, M.; Albini, A. *Angew. Chem., Int. Ed.* **2005,** *44,* 1232–1236. doi:10.1002/anie.200461444
37. Qrareya, H.; Protti, S.; Fagnoni, M. *J. Org. Chem.* **2014,** *79,* 11527–11533. doi:10.1021/jo502172c
38. Crespi, S.; Protti, S.; Fagnoni, M. *J. Org. Chem.* **2016,** *81,* 9612–9619. doi:10.1021/acs.joc.6b01619
39. da Silva Júnior, P. E.; Amin, H. I. M.; Nauth, A. M.; da Silva Emery, F.; Protti, S.; Opatz, T. *ChemPhotoChem* **2018,** *2,* 878–883. doi:10.1002/cptc.201800125
40. Qiu, D.; Lian, C.; Mao, J.; Fagnoni, M.; Protti, S. *J. Org. Chem.* **2020,** *85,* 12813–12822. doi:10.1021/acs.joc.0c01895
41. Motherwell, W. B.; Pennell, A. M. K. *J. Chem. Soc., Chem. Commun.* **1991,** 877–879. doi:10.1039/c39910000877
42. da Mata, M. L. E. N.; Motherwell, W. B.; Ujjainwalla, F. *Tetrahedron Lett.* **1997,** *38,* 137–140. doi:10.1016/s0040-4039(96)02236-8
43. da Mata, M. L. E. N.; Motherwell, W. B.; Ujjainwalla, F. *Tetrahedron Lett.* **1997,** *38,* 141–144. doi:10.1016/s0040-4039(96)02237-x
44. Holden, C. M.; Sohel, S. M. A.; Greaney, M. F. *Angew. Chem., Int. Ed.* **2016,** *55,* 2450–2453. doi:10.1002/anie.201510236
45. Rasheed, O. K.; Hardcastle, I. R.; Raftery, J.; Quayle, P. *Org. Biomol. Chem.* **2015,** *13,* 8048–8052. doi:10.1039/c5ob01239b
46. Yanagi, T.; Nogi, K.; Yorimitsu, H. *Chem. – Eur. J.* **2020,** *26,* 783–787. doi:10.1002/chem.201903570
47. Yanagi, T.; Otsuka, S.; Kasuga, Y.; Fujimoto, K.; Murakami, K.; Nogi, K.; Yorimitsu, H.; Osuka, A. *J. Am. Chem. Soc.* **2016,** *138,* 14582–14585. doi:10.1021/jacs.6b10278
48. Morioka, T.; Nishizawa, A.; Furukawa, T.; Tobisu, M.; Chatani, N. *J. Am. Chem. Soc.* **2017,** *139,* 1416–1419. doi:10.1021/jacs.6b12293
49. Somerville, R. J.; Martin, R. *Angew. Chem., Int. Ed.* **2017,** *56,* 6708–6710. doi:10.1002/anie.201702188
50. Takahashi, F.; Nogi, K.; Yorimitsu, H. *Org. Lett.* **2018,** *20,* 6601–6605. doi:10.1021/acs.orglett.8b02972
51. Kloss, F.; Neuwirth, T.; Haensch, V. G.; Hertweck, C. *Angew. Chem., Int. Ed.* **2018,** *57,* 14476–14481. doi:10.1002/anie.201805961
52. Okamoto, Y.; Nakamura, M.; And, M. S.; Takamuku, S. *Photochem. Photobiol.* **1992,** *56,* 403–407. doi:10.1111/j.1751-1097.1992.tb02178.x
53. Shi, M.; Okamoto, Y.; Takamuku, S. *Tetrahedron Lett.* **1991,** *32,* 6899–6902. doi:10.1016/0040-4039(91)80438-c
54. Nakamura, M.; Sawasaki, K.; Okamoto, Y.; Takamuku, S. *J. Chem. Soc., Perkin Trans. 1* **1994,** 141–146. doi:10.1039/p19940000141
55. Nakamura, M.; Shi, M.; Okamoto, Y.; Takamuku, S. *J. Photochem. Photobiol., A* **1995,** *85,* 111–118. doi:10.1016/1010-6030(94)03894-z
56. Okamoto, Y.; Tatsuno, T.; Takamuku, S. *Phosphorus, Sulfur Silicon Relat. Elem.* **1996,** *117,* 129–138. doi:10.1080/10426509608038780
57. Finnegan, R. A.; Matson, J. A. *J. Am. Chem. Soc.* **1972,** *94,* 4780–4782. doi:10.1021/ja00768a084
58. Shi, M.; Yamamoto, K.; Okamoto, Y.; Takamuku, S. *Phosphorus, Sulfur Silicon Relat. Elem.* **1991,** *60,* 1–14. doi:10.1080/10426509108233919
59. Nakamura, M.; Sawasaki, K.; Okamoto, Y.; Takamuku, S. *Bull. Chem. Soc. Jpn.* **1995,** *68,* 3189–3197. doi:10.1246/bcsj.68.3189
60. Nakamura, M.; Okamoto, Y.; Takamuku, S. *Phosphorus, Sulfur Silicon Relat. Elem.* **1995,** *106,* 137–144. doi:10.1080/10426509508027899
61. Okamoto, Y.; Tatsuno, T.; Takamuku, S. *Heteroat. Chem.* **1996,** *7,* 257–261. doi:10.1002/(sici)1098-1071(199608)7:4<257::aid-hc7>3.0.co;2-2
62. Genkina, G. K.; Shipov, A. E.; Mastryukova, T. A.; Kabachnik, M. I. *Russ. J. Gen. Chem.* **1996,** *66,* 1742–1744.
63. Bruice, T. C.; Blaskó, A.; Petyak, M. E. *J. Am. Chem. Soc.* **1995,** *117,* 12064–12069. doi:10.1021/ja00154a005
64. Dichiarante, V.; Dondi, D.; Protti, S.; Fagnoni, M.; Albini, A. *J. Am. Chem. Soc.* **2007,** *129,* 5605–5611. doi:10.1021/ja068647s
65. Protti, S.; Fagnoni, M. *Chem. Commun.* **2008,** 3611–3621. doi:10.1039/b801888j
66. Chen, X.; Chen, Z.; So, C. M. *J. Org. Chem.* **2019,** *84,* 6337–6346. doi:10.1021/acs.joc.9b00669
67. Chen, Z.; Chen, X.; So, C. M. *J. Org. Chem.* **2019,** *84,* 6366–6376. doi:10.1021/acs.joc.9b00703
68. Ravelli, D.; Fagnoni, M. Photochemistry of Phosphate and Sulfonate Esters. In *CRC Handbook of Organic Photochemistry and Photobiology,* 3rd ed.; Griesbeck, A.; Oelgemoeller, M.; Ghetti, F., Eds.; CRC Press: Boca Raton, FL, USA, 2012; pp 393–417.
69. Cornelisse, J.; Havinga, E. *Chem. Rev.* **1975,** *75,* 353–388. doi:10.1021/cr60296a001
70. Chopa, A. B.; Silbestri, G. F.; Lockhart, M. T. *J. Organomet. Chem.* **2005,** *690,* 3865–3877. doi:10.1016/j.jorganchem.2005.05.023
71. Naito, I.; Kinoshita, A.; Okamoto, Y.; Takamuku, S. *ACS Symp. Ser.* **1995,** *579,* 139–150. doi:10.1021/bk-1994-0579.ch011
72. Siqintuya; Sueishi, Y.; Yamamoto, S. *J. Photochem. Photobiol., A* **2007,** *186,* 41–46. doi:10.1016/j.jphotochem.2006.07.010

License and Terms

BEILSTEIN JOURNAL OF ORGANIC CHEMISTRY

An atom-economical addition of methyl azaarenes with aromatic aldehydes via benzylic C(sp^3)–H bond functionalization under solvent- and catalyst-free conditions

Divya Rohini Yennamaneni[1,2], Vasu Amrutham[1,2], Krishna Sai Gajula[1,2], Rammurthy Banothu[1,2], Murali Boosa[1,2] and Narender Nama[*1,2,§]

Letter

Open Access

Address:
[1]Catalysis and Fine Chemicals Division, CSIR-Indian Institute of Chemical Technology, Hyderabad, Telangana, 500 007, India and [2]Academy of Scientific and Innovative Research, CSIR-HRDC Campus, Sector 19, Kamala Nehru Nagar, Ghaziabad, UP-201002, India

Email:
Narender Nama[*] - nama.iict@gov.in

* Corresponding author
§ Tel.: +91-40-27191703; Fax: +91-40-27160387/27160757

Keywords:
aldehydes; azaarenes; benzylic addition; green chemistry; solvent-free conditions

Beilstein J. Org. Chem. **2020,** *16,* 3093–3103.
https://doi.org/10.3762/bjoc.16.259

Received: 05 October 2020
Accepted: 01 December 2020
Published: 23 December 2020

This article is part of the thematic issue "Green chemistry II".

Associate Editor: L. Vaccaro

Abstract

A convenient practical approach for the synthesis of 2-(pyridin-2-yl)ethanols by direct benzylic addition of azaarenes and aldehydes under catalyst- and solvent-free conditions is reported. This reaction is metal-free, green, and was carried out in a facile operative environment without using any hazardous transition metal catalysts or any other coupling reagents. Different aromatic aldehydes and azaarenes were monitored, and the yields of the resulting products were moderate to excellent. We accomplished several azaarene derivatives under neat conditions through a highly atom-economical pathway. To evaluate the preparative potential of this process, gram-scale reactions were performed up to a 10 g scale.

Introduction

Azaarenes are a distinct class of heterocyclic compounds possessing wide compatibility in the field of synthetic organic chemistry. The recent advancements in nitrogen-containing carbon compounds have marked them as an unusual moiety due to their attractive applications in biology and as materials [1-4]. Among various nitrogen-containing heterocyclic compounds, pyridine and quinolines are readily found in bioactive compounds [5]. The functionalization of alkylpyridines and quinolines is significant and plays a remarkable role in the efficient drug design [6-8]. Due to their conformational diversity, these

compounds constitute a motif in various natural alkaloid products, such as chimanine and those derived from lobelia, sedum, etc. These compounds act as anti-HIV and anti-asthma drugs [9-11]. Mainly, 2-substituted quinolines and their analogues exhibits magnificent bioactivity [12,13]. The synthesis of higher cores of nitrogen-containing heterocyclic compounds through C(sp^3)–H functionalization of simple compounds like methyl azaarenes allows direct transformation without any critical reaction conditions. Thus, in this regard the further development of this approach is still in need to be developed [14].

The formation of new C–C bonds through direct C–H bond functionalization in organic chemistry is attractive [15]. Such methodologies are omnipresent and facilitate sustainable organic transformations for the synthesis of complex natural products and pharmaceuticals. In the past years, C−H bond functionalization catalyzed by transition metals received a strong emphasis, and other different catalytic systems have also been encouraged [16-20]. Huang and co-workers first realized the addition of alkylazaarenes directly to unsaturated bonds via C(sp^3)–H functionalization [21,22]. The synthesis of pyridine and related azaarene derivatives involve the C(sp^3)–H activation of 2-methylpyridines using different transition-metal compounds, Lewis acids, and Brønsted acids [23-28]. Recently, C(sp^3)–H functionalizations of methylazaarenes with isatins and malononitrile under catalyst-free conditions have been reported [29]. Wang et al. reported the functionalization of benzylic C–H bonds of 2-methylazaarenes by nucleophilic addition to aromatic aldehydes catalyzed by acetic acid using harmful chlorinated solvent, and this reaction suffers from longer reaction times [30]. Rao et al. performed similar reactions without catalyst under microwave irradiation in the presence of water as a solvent [31], but when considering an industrial scale, there are numerous factors that serves as obstacles for the usage of microwave reactors, such as escalated heat loss, variations in the absorption, an inadequate penetrating ability of the radiation into the reaction medium, and further reflection of the microwaves. Nevertheless, the solvent was water, which required long extraction processes compared to solvent-free conditions. Castro and co-workers have also reported the synthesis of 1-phenyl-2-(2-pyridyl)ethanol and 1-phenyl-2-(2-pyridyl)ethene under catalyst- and solvent-free conditions. Despite the low yield of the product of around 4%, this work described crystallographic data and the influence of reaction conditions such as the temperature and the reaction time on the stability of 1-phenyl-2-(2-pyridyl)ethanol [32]. Different catalysts such as ionic liquids [33], $CuFe_2O_4$ [34], and $Ca(OTf)_2$ [35] were also utilized. Due to the abundant importance of these products, several different approaches were reported (Scheme 1 and Scheme 2). These higher azaarene products were also achieved from other starting materials, such as 2-methyl-6-(phenylethynyl)pyridine [36], 2,6-dimethylpyridine (**1a**) and (*E*)-*N*-benzylidene-4-methylbenzenesulfonamide [22], 2-bromo-6-methylpyridine and (*E*)-styrylboronic acid [37], as well as 2-methylpyridine and phenylmethanamine [38]. Most recently, Yaragorla et al. published a review on C(sp^3)–H bond functionalization of 2-methylazaarenes [39]. These strategies are proficient, but due to the involvement of drastic reaction conditions, the use of expensive reagents, toxic metals, harmful solvents, and tedious workup procedures, they need to be reevaluated. Therefore, alternatives with environmentally benign reagents are much in focus.

Correspondingly, considering the exemplar shift from conventional synthetic methodologies towards green chemistry, there have been some alternatives or replacements of toxic catalysts and hazardous solvents in chemical reactions [40]. These conversions play a vital role for the syntheses of active pharma-

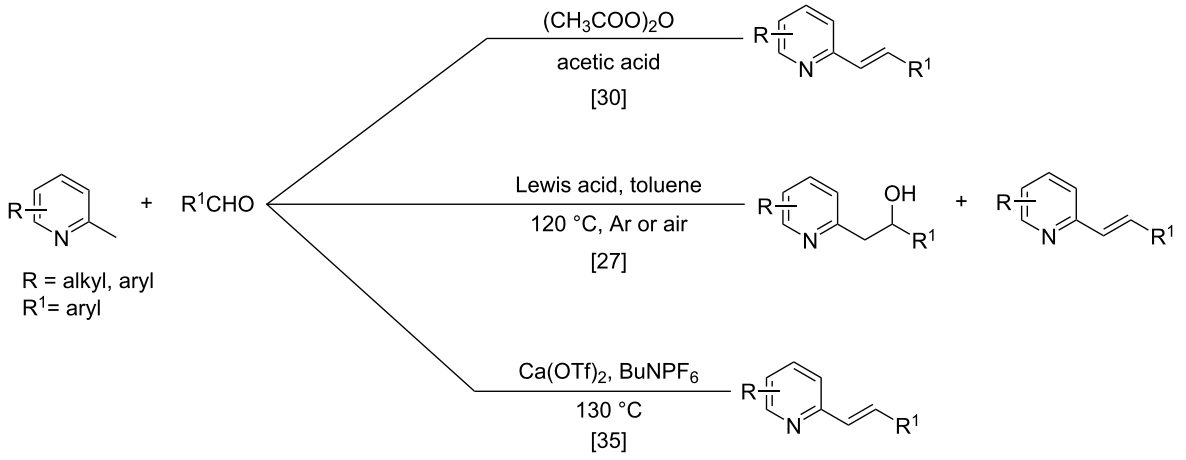

Scheme 1: Benzylic addition of aldehydes to azaarenes using different catalysts.

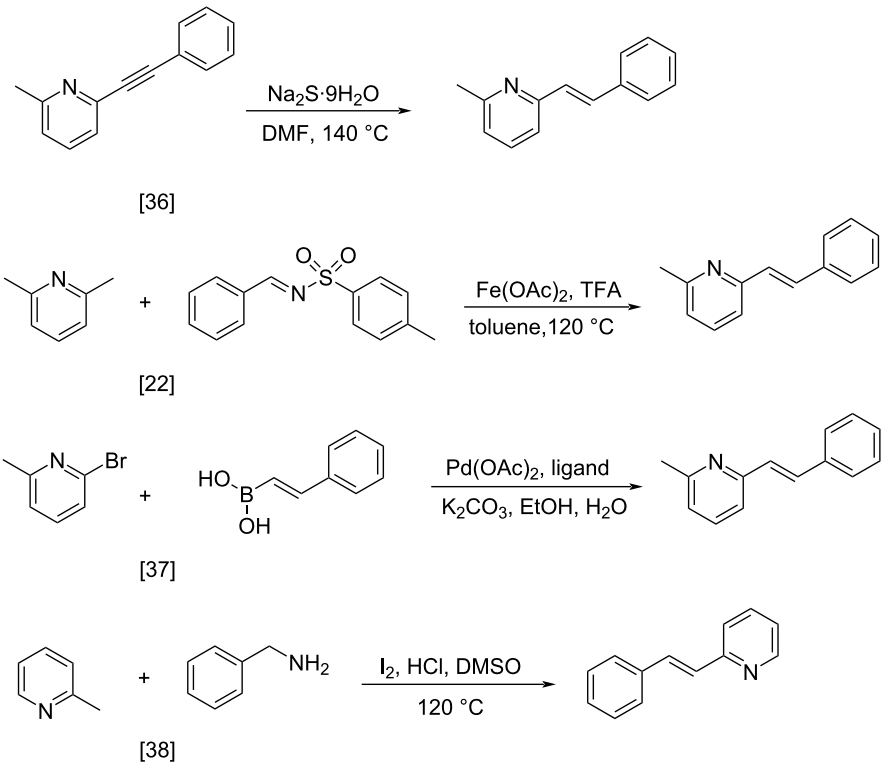

Scheme 2: Synthesis of azaarene derivatives from different precursors.

ceutical ingredients as these approaches reduce the contamination in an industrial setting. In addition, the replacement of toxic reagents by environmentally benign reagents can decrease pollution to some extent [41,42].

However, to develop advantageous eco-friendly, atom-economical, simple, and efficient synthetic-organic processes under solvent- and catalyst-free conditions in order to synthesize highly demanding pharmaceuticals or natural products can be quite backbreaking [43-45]. From this perspective, we herein disclose environmentally benign, atom-economical, catalyst-free nucleophilic additions of benzylic-like azaarene C–H groups to various benzaldehydes under neat conditions (Scheme 3).

Results and Discussion

With the purpose to develop an environmentally benign process, we first examined *p*-nitrobenzaldehyde (**2a**) and 2,6-dimethylpyridine (**1a**) as model substrates. Our investigation started with the reaction of *p*-nitrobenzaldehyde (**2a**) and 2,6-dimethylpyridine (**1a**) in the presence of Hβ zeolite as a catalyst at 120 °C in toluene for 24 h in a sealed vial (Table 1, entry 1). However, the desired compound **3a** was observed in traces. We thought that the catalyst pore size may be an obstruction to a higher yield and used a mesoporous material, MCM-41, as a catalyst, which slightly improved the yield (Table 1, entry 2). At the same time, increasing the temperature to 130 °C enhanced the yield of the product **3a** (Table 1, entry 3). In order to address the economic cost and ecological impact, we tried this reaction without using a solvent (Table 1, entry 4). Further, this reaction was screened using various zeolites, such as Hβ, H-mordenite, H-ZSM, HY, NaY, and MCM-41 under solvent-free conditions (Table 1, entries 5–9). In addition, to justify the role of the catalyst, this reaction was carried out in the absence of a catalyst. Thankfully, the yield of the product enhanced to

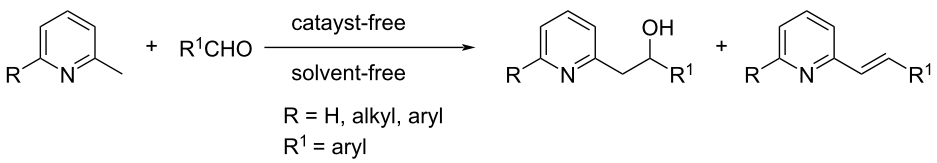

Scheme 3: Our work: catalyst- and solvent-free benzylic addition of aldehydes to azaarenes.

Table 1: Optimization of the reaction conditions.[a]

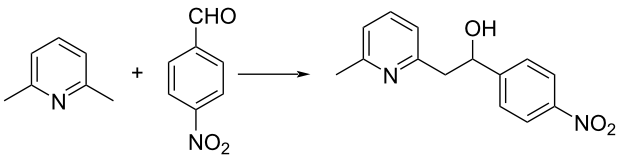

1a **2a** **3a**

entry	catalyst	solvent	temperature (°C)	yield (%)[b]
1	Hβ	toluene	120	4
2	MCM-41	toluene	120	10
3	MCM-41	toluene	130	23
4	MCM-41	—	130	62
5	Hβ	—	130	76
6	H-mordenite	—	130	38
7	H-ZSM	—	130	72
8	HY	—	130	30
9	NaY	—	130	6
10	—	—	130	79
11	—	—	135	84
12	—	—	140	82
13	—	—	120	36
14	—	—	135	36[c]
15	—	—	135	80[d]
16	—	—	135	58[e]
17	—	—	135	63[f]
18	—	—	135	85[g]
19	—	—	135	85[h]
20	—	—	135	92[i]

[a]1 mmol **1a**, 1 mmol **2a**, 24 h. [b]Based on **2a**. [c]18 h. [d]30 h. [e]Open atmosphere. [f]0.8 mmol **1a**. [g]1.5 mmol **1a**. [h]1.75 mmol **1a**. [i]2 mmol **1a**.

79% (Table 1, entry 10). We managed to increase the yield of the desired product **3a** by further screening of the reaction conditions under catalyst- as well as solvent-free conditions. As we increased the temperature to 135 °C, the yield of the product increased to 84% (Table 1, entry 11). An additional increase of the temperature to 140 °C did not exhibit any promising change, but decreasing the temperature to 120 °C reduced the yield of the product **3a** (Table 1, entries 12 and 13). Hence, we carried out further reactions at 135 °C. Generally, the temperature of the reaction plays a crucial role, in formation of a uniform reaction mixture of the reactants under solvent-free conditions. Increasing the reaction time did not produce a remarkable change, but when decreasing the reaction time, a drastic effect on the yield of the product **3a** was observed (Table 1, entries 14 and 15). Surprisingly, when the reaction was carried out in an open atmosphere, the yield of the required product **3a** was drastically reduced (Table 1, entry 16). Different reactant stoichiometries were analyzed to maximize the yield of the desired product **3a** (Table 1, entries 17–20). After these tests, we concluded the best yield of **3a** to be 92% (Table 1, entry 20), which was achieved from a reaction mixture of 2 mmol 2,6-dimethylpyridine (**1a**) and 1 mmol *p*-nitrobenzaldehyde (**2a**) at 135 °C for 24 h in a sealed vial without any catalysts or additive under solvent-free conditions.

Thereupon, these optimized conditions were utilized to validate the substrate scope of this direct C–C coupling reaction. A variety of aldehydes, **2a**–**r**, was reacted with 2,6-dimethylpyridine (**1a**) to obtain the corresponding products **3a**–**r** with a moderate to excellent yield (Table 2). The substrates **2a**–**d** with nitro substituents were well reacted to achieve the desired products **3a**–**d** in 68–95% yield (Table 2, entries 1–4). Distinctly, 2-nitrobenzaldehyde (**2c**) gave the expected product **3c** along with the dehydrated product **4c** (Table 2, entry 3). Substrates

Table 2: Variation of the aldehyde component **2**.[a]

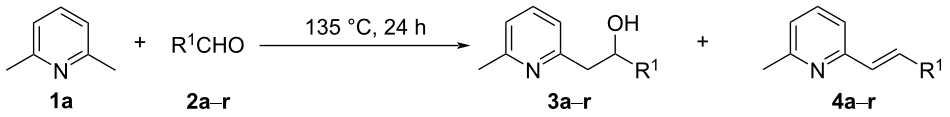

1a **2a–r** **3a–r** **4a–r**

entry	substrate **2**	product **3**	product **4**	yield (%)[b]	
				3	**4**
1	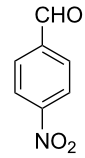 **2a**	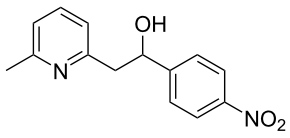 **3a**	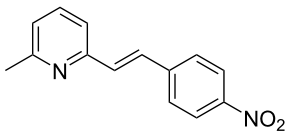 **4a**	92	0
2	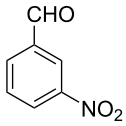 **2b**	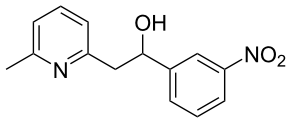 **3b**	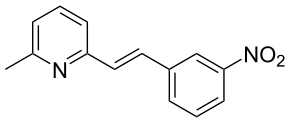 **4b**	68	0
3	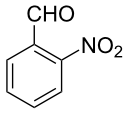 **2c**	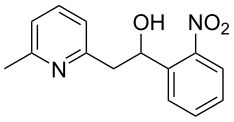 **3c**	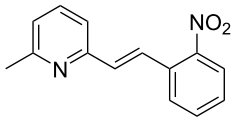 **4c**	74	17
4	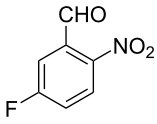 **2d**	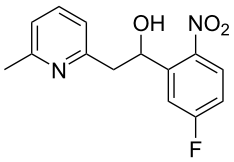 **3d**	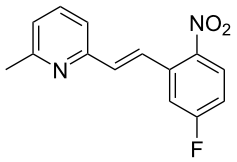 **4d**	95	0
5	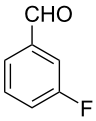 **2e**	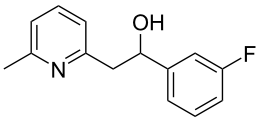 **3e**	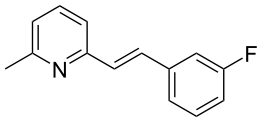 **4e**	55	19
6	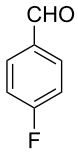 **2f**	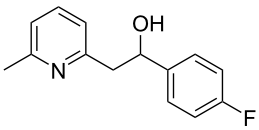 **3f**	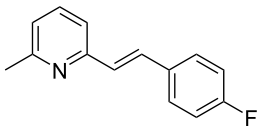 **4f**	52	0
7	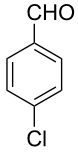 **2g**	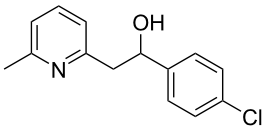 **3g**	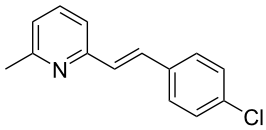 **4g**	48	0
8	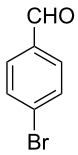 **2h**	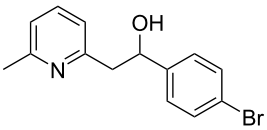 **3h**	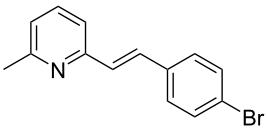 **4h**	42	0

Table 2: Variation of the aldehyde component **2**.[a] (continued)

9	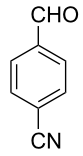 **2i**	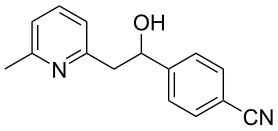 **3i**	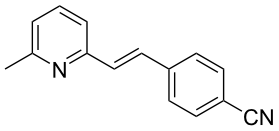 **4i**	0	77
10	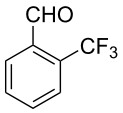 **2j**	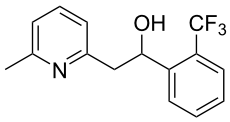 **3j**	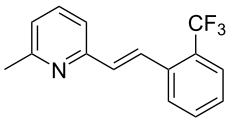 **4j**	0	71
11	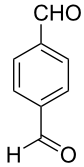 **2k**	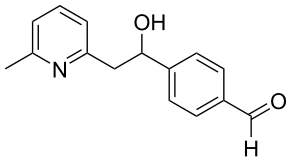 **3k**	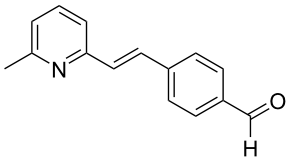 **4k**	0	92
12	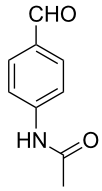 **2l**	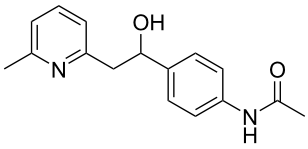 **3l**	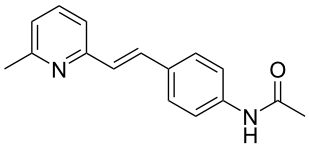 **4l**	22	0
13	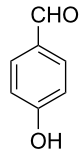 **2m**	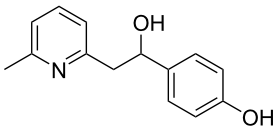 **3m**	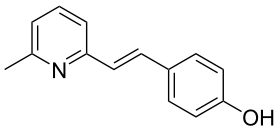 **4m**	0	58
14	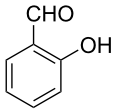 **2n**	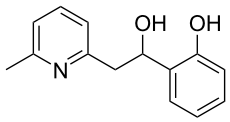 **3n**	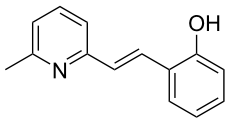 **4n**	0	34
15	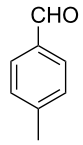 **2o**	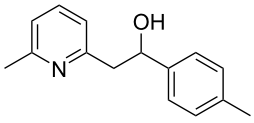 **3o**	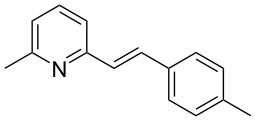 **4o**	0	46[c]
16	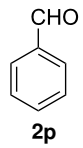 **2p**	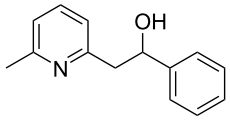 **3p**	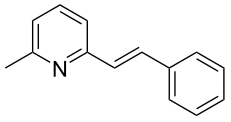 **4p**	45	0
17	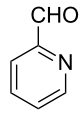 **2q**	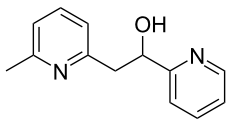 **3q**	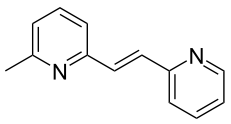 **4q**	0	96

Table 2: Variation of the aldehyde component **2**.[a] (continued)

18	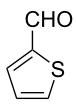 **2r**	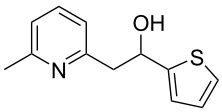 **3r**	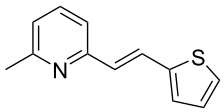 **4r**	29[c]	0

[a]2 mmol **1a**, 1 mmol **2**, 24 h. [b]Based on **2**. [c]48 h.

containing a halogen, such as fluorine, chlorine, and bromine, were efficiently reacted to afford the products **3e–h** in successively moderate yields (Table 2, entries 5–8). Notably, 3-fluorobenzaldehyde (**2e**) also reacted well and provided the alcohol **3e** in 55% yield along with the alkene product **4e** in 19% yield (Table 2, entry 5). Exceptionally, substrates with groups such as cyano, trifluoromethyl, and formyl were reacted and provided the respective dehydrated alkenylpyridine compounds **4i–k** in 77%, 71%, and 92% yield, respectively (Table 2, entries 9–11). 4-Acetamidobenzaldehyde (**2l**) also reacted but provided a low product yield of 22% **3l** (Table 2, entry 12). Starting materials with a *para*- and *ortho*-hydroxy group provided the corresponding alkenylpyridine products **4m** and **4n** in 58% and 34% yield, respectively (Table 2, entries 13 and 14). 4-Methylbenzaldehyde (**2o**) gave the respective dehydrated product **4o** in 46% yield upon reaction for 48 h (Table 2, entry 15). Simple benzaldehyde (**2p**) was also tolerated well and furnished the corresponding product **3p** in 45% yield (Table 2, entry 16). The heteroaromatic aldehyde 2-pyridinecarbaldehyde (**2q**) gave the respective dehydrated product **4q** in 96% yield, whereas 2-thiophene (**2r**) resulted in the desired product **3r** but in a low yield (Table 2, entries 17 and 18).

Subsequently, several azaarenes in combination with 4-nitrobenzaldehyde (**2a**) were also evaluated under optimized conditions to extend the substrate scope. Firstly 2,4,6-collidine (**1b**) was successfully reacted for 48 h to obtain the successive product **5b** in 87% yield (Table 3, entry 1). Next, 2-ethylpyridine (**1c**) was made to react under standard reaction conditions. To our surprise, 1-(4-nitrophenyl)-2-(pyridin-2-yl)propan-1-ol (**5c**) was formed in 53% yield, and the formation of this product displays the reactivity of the benzylic C–H group attached in the *ortho* position of the pyridine ring (Table 3, entry 2). The reaction of 2-methylpyridine (**1d**) with **2a** for 48 h gave the desired alcohol **5d** in 42% yield along with the corresponding dehydrated alkenylpyridine compound **6d** in 16% yield (Table 3, entry 3). Different from the 2,6-substitution pattern, 3,5-dimethylpyridine (**1e**) was also tested under standard reaction conditions upon increasing the reaction time to 48 h, which did not furnish the corresponding products (Table 3, entry 4). Later, to screen the compatibility of the azaarenes, various quinolines were screened (Table 3, entries 5–8). Among these, only 2-methylquinoline (**1f**) and 6-fluoro-2-methylquinoline (**1g**) gave the dehydrated alkenylazaarenes **6f** and **6g** as the products in 48% and 45% yield, respectively (Table 3,

Table 3: Variation of the azaarene component **1**.[a]

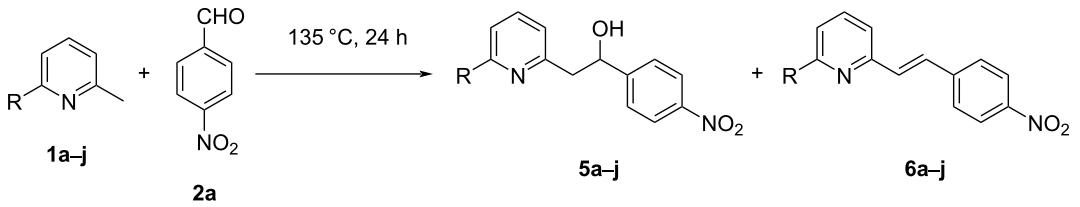

1a–j **2a** **5a–j** **6a–j**

entry	substrate	product **5**	product **6**	yield (%)[b]	
				5	**6**
1	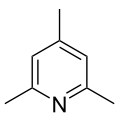 **1b**	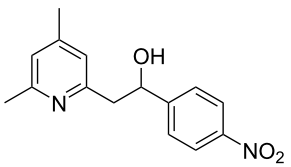 **5b**	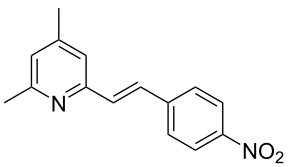 **6b**	87[c]	0

Table 3: Variation of the azaarene component **1**.[a] (continued)

2	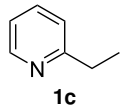 **1c**	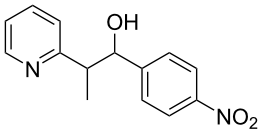 **5c**	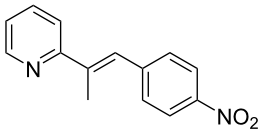 **6c**	53[c]	0
3	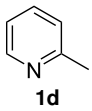 **1d**	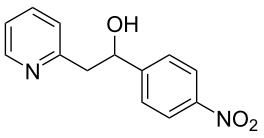 **5d**	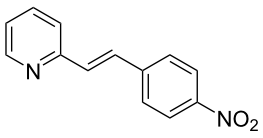 **6d**	42[c]	16[c]
4	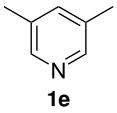 **1e**	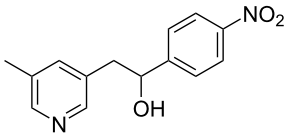 **5e**	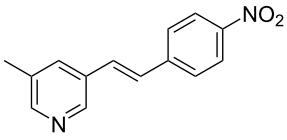 **6e**	0	0
5	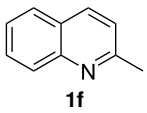 **1f**	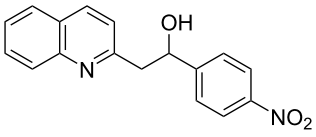 **5f**	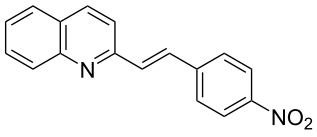 **6f**	0	48
6	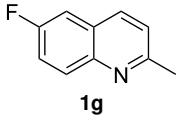 **1g**	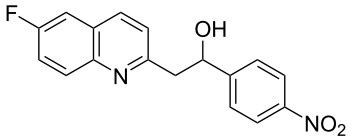 **5g**	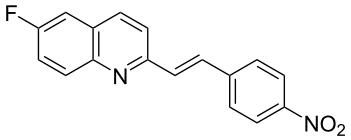 **6g**	0	45
7	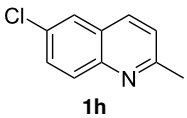 **1h**	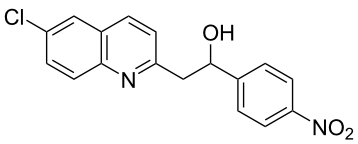 **5h**	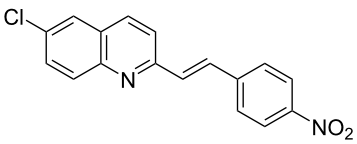 **6h**	0	0
8	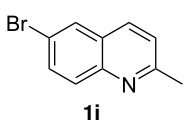 **1i**	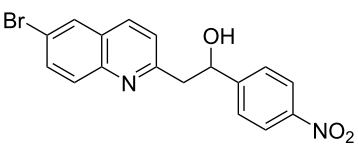 **5i**	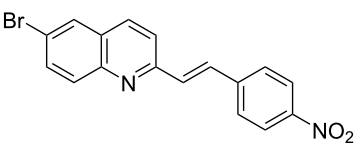 **6i**	0	0

[a]2 mmol **1**, 1 mmol **2a**, 24 h. [b]Based on **2a**. [c]48 h.

entries 5 and 6). We also tried this reaction with 6-chloro-2-methylquinoline (**1h**) and 6-bromo-2-methylquinoline (**1g**), but unfortunately the reactions did not proceed well, and the desired products **6h** and **6i** were not formed (Table 3, entries 7 and 8).

However, some dehydrated alkenyl products were obtained, which may possess wide biological activities of great demand. This reaction was also carried out on a gram scale, and the results display the potential for large-scale applications as the yields were not drastically changed when shifting from a mmol scale to a gram scale (1 g, 5 g, and 10 g). These results are shown in Scheme 4.

Based on the experimental investigations and literature reports [46], conclusions were drawn, and a plausible mechanism was suggested. Under standard reaction conditions, 2 mmol of 2,6-dimethylpyridine participates in inter reaction (1 mmol of **1a** will inter react to another 1 mmol of **1a**) and this inter reaction influences the nitrogen atom present in the compound to act as a Brønsted base. This resulting Brønsted base accepts benzylic C–H protons to furnish the respective enamine **A**, which facili-

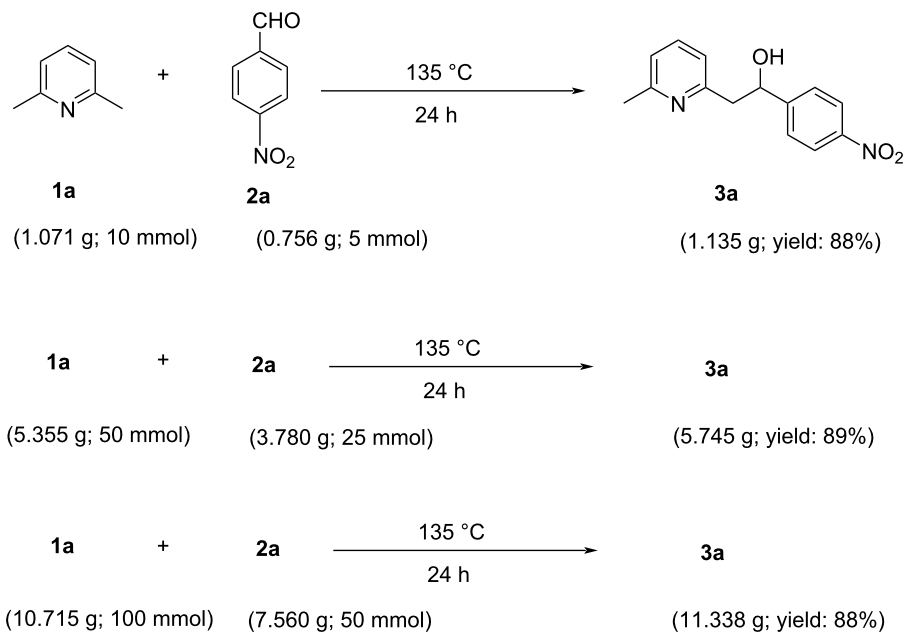

Scheme 4: Large-scale experiments for the synthesis of 2-(6-methylpyridin-2-yl)-1-(4-nitrophenyl)ethan-1-ol (**3a**) from 2,6-dimethylpyridine (**1a**) and 4-nitrobenzaldehyde (**2a**).

tates the further nucleophilic addition to 4-nitrobenzaldehyde (**2a**). The product of this is the intermediate **B**, which favors the formation of the corresponding desired product **3a**, as shown in Scheme 5.

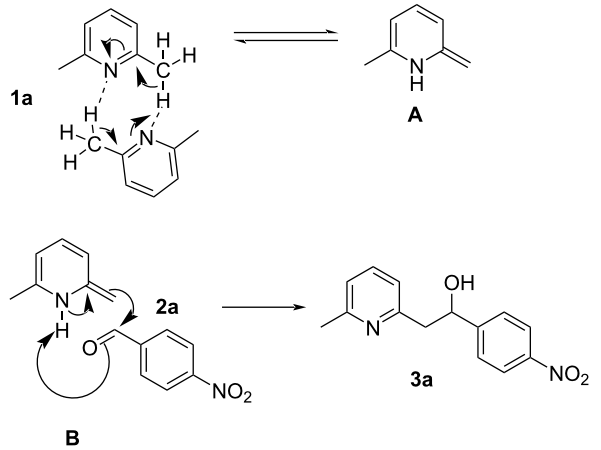

Scheme 5: Plausible mechanism for the formation of 2-(6-methylpyridin-2-yl)-1-(4-nitrophenyl)ethan-1-ol (**3a**) under standard reaction conditions from 2,6-dimethylpyridine (**1a**) and 4-nitrobenzaldehyde (**2a**).

Conclusion

In summary, this work provides a green and simple synthetic methodology for the synthesis of higher azaarenes from pyridines and quinolines with aromatic aldehydes, avoiding the use of solvents and a catalyst. Despite of previous reports under catalyst- and solvent-free conditions, this approach features specific traits, such as good yields and simple reaction conditions. This method requires no reagent purification and is a new and clean process. A variety of aromatic aldehydes, including electron-donating, electron-withdrawing, as well as halogen groups was screened, affording the products in moderate to excellent yields. Azaarenes such as pyridines with various substitution patterns and a few quinolines were also reacted with moderate to excellent yields. This draws the conclusion that the benzylic C–H unit of 2-alkylpyridine/quinolines actively participates in this addition reaction. However, in some cases, 2-alkenyl compounds were formed. Nevertheless, these are of equivalent significance. Moreover, this method has a high atom economy and reduces large amounts of waste generated by the unnecessary utilization of catalysts and solvents. Notably, this reaction is compatible with a gram scale, and further research is yet to be developed towards more sustainability.

Supporting Information

Supporting Information File 1

Experimental procedures, compound characterization data, and NMR spectra.
[https://www.beilstein-journals.org/bjoc/content/supplementary/1860-5397-16-259-S1.pdf]

Acknowledgements

We thank the Director, CSIR-IICT (IICT/Pubs./2020/288) for providing all the required facilities to carry out the work.

Funding

We thank the DST, New Delhi for financial support under the Indo-Russia (DST-RSF, No. INT/RUS/RSF/P-7) program. Y. D., A. V., G. K., and B. M. acknowledge the CSIR, B. R. acknowledges the UGC, India for financial support in the form of a fellowship.

References

1. Chelucci, G.; Orrù, G.; Pinna, G. A. *Tetrahedron* **2003,** *59,* 9471–9515. doi:10.1016/j.tet.2003.09.066
2. Prehn, K.; Warburg, A.; Schilling, T.; Bron, M.; Schulte, K. *Compos. Sci. Technol.* **2009,** *69,* 1570–1579. doi:10.1016/j.compscitech.2008.09.006
3. Kem, W. R.; Soti, F.; Rittschof, D. *Biomol. Eng.* **2003,** *20,* 355–361. doi:10.1016/s1389-0344(03)00049-2
4. Friesen, R. W.; Brideau, C.; Chan, C. C.; Charleson, S.; Deschênes, D.; Dubé, D.; Ethier, D.; Fortin, R.; Gauthier, J. Y.; Girard, Y.; Gordon, R.; Greig, G. M.; Riendeau, D.; Savoie, C.; Wang, Z.; Wong, E.; Visco, D.; Xu, L. J.; Young, R. N. *Bioorg. Med. Chem. Lett.* **1998,** *8,* 2777–2782. doi:10.1016/s0960-894x(98)00499-5
5. Capdeville, R.; Buchdunger, E.; Zimmermann, J.; Matter, A. *Nat. Rev. Drug Discovery* **2002,** *1,* 493–502. doi:10.1038/nrd839
6. Solomon, V. R.; Lee, H. *Curr. Med. Chem.* **2011,** *18,* 1488–1508. doi:10.2174/092986711795328382
7. Wilson, K. J.; van Niel, M. B.; Cooper, L.; Bloomfield, D.; O'Connor, D.; Fish, L. R.; MacLeod, A. M. *Bioorg. Med. Chem. Lett.* **2007,** *17,* 2643–2648. doi:10.1016/j.bmcl.2007.01.098
8. Michael, J. P. *Nat. Prod. Rep.* **2005,** *22,* 627–646. doi:10.1039/b413750g
9. Strunz, G. M.; Findlay, J. A. Pyridine and Piperidine Alkaloids. In *The Alkaloids;* Brossi, A., Ed.; Academic Press: New York, NY, USA, 1985; pp 89–183. doi:10.1016/s0099-9598(08)60194-7
10. Meth-Cohn, O.; Yau, C. C.; Yu, C.-Y. *J. Heterocycl. Chem.* **1999,** *36,* 1549–1553. doi:10.1002/jhet.5570360615
11. Houghton, P. J.; Woldemariam, T. Z.; Watanabe, Y.; Yates, M. *Planta Med.* **1999,** *65,* 250–254. doi:10.1055/s-1999-13988
12. Kumar, S.; Bawa, S.; Gupta, H. *Mini-Rev. Med. Chem.* **2009,** *9,* 1648–1654. doi:10.2174/138955709791012247
13. Fournet, A.; Barrios, A. A.; Muñoz, V.; Hocquemiller, R.; Roblot, F.; Cavé, A.; Richomme, P.; Bruneton, J. *Phytother. Res.* **1994,** *8,* 174–178. doi:10.1002/ptr.2650080312
14. Nakamura, I.; Yamamoto, Y. *Chem. Rev.* **2004,** *104,* 2127–2198. doi:10.1021/cr020095i
15. Campeau, L.-C.; Rousseaux, S.; Fagnou, K. *J. Am. Chem. Soc.* **2005,** *127,* 18020–18021. doi:10.1021/ja056800x
16. Kanyiva, K. S.; Nakao, Y.; Hiyama, T. *Angew. Chem., Int. Ed.* **2007,** *46,* 8872–8874. doi:10.1002/anie.200703758
17. Wu, J.; Cui, X.; Chen, L.; Jiang, G.; Wu, Y. *J. Am. Chem. Soc.* **2009,** *131,* 13888–13889. doi:10.1021/ja902762a
18. Mousseau, J. J.; Bull, J. A.; Charette, A. B. *Angew. Chem., Int. Ed.* **2010,** *49,* 1115–1118. doi:10.1002/anie.200906020
19. Deng, G.; Ueda, K.; Yanagisawa, S.; Itami, K.; Li, C.-J. *Chem. – Eur. J.* **2009,** *15,* 333–337. doi:10.1002/chem.200801893
20. Tobisu, M.; Hyodo, I.; Chatani, N. *J. Am. Chem. Soc.* **2009,** *131,* 12070–12071. doi:10.1021/ja9053509
21. Qian, B.; Guo, S.; Shao, J.; Zhu, Q.; Yang, L.; Xia, C.; Huang, H. *J. Am. Chem. Soc.* **2010,** *132,* 3650–3651. doi:10.1021/ja910104n
22. Qian, B.; Xie, P.; Xie, Y.; Huang, H. *Org. Lett.* **2011,** *13,* 2580–2583. doi:10.1021/ol200684b
23. Jazzar, R.; Hitce, J.; Renaudat, A.; Sofack-Kreutzer, J.; Baudoin, O. *Chem. – Eur. J.* **2010,** *16,* 2654–2672. doi:10.1002/chem.200902374
24. Lyons, T. W.; Sanford, M. S. *Chem. Rev.* **2010,** *110,* 1147–1169. doi:10.1021/cr900184e
25. Kalyani, D.; Deprez, N. R.; Desai, L. V.; Sanford, M. S. *J. Am. Chem. Soc.* **2005,** *127,* 7330–7331. doi:10.1021/ja051402f
26. Shabashov, D.; Daugulis, O. *Org. Lett.* **2005,** *7,* 3657–3659. doi:10.1021/ol051255q
27. Mao, D.; Hong, G.; Wu, S.; Liu, X.; Yu, J.; Wang, L. *Eur. J. Org. Chem.* **2014,** 3009–3019. doi:10.1002/ejoc.201400073
28. Yaragorla, S.; Dada, R.; Singh, G. *Synlett* **2016,** *27,* 912–918. doi:10.1055/s-0035-1560385
29. Yaragorla, S.; Singh, G.; Dada, R. *Tetrahedron Lett.* **2016,** *57,* 591–594. doi:10.1016/j.tetlet.2015.12.096
30. Wang, F.-F.; Luo, C.-P.; Wang, Y.; Deng, G.; Yang, L. *Org. Biomol. Chem.* **2012,** *10,* 8605–8608. doi:10.1039/c2ob26604k
31. Nageswara Rao, N.; Meshram, H. M. *Tetrahedron Lett.* **2013,** *54,* 5087–5090. doi:10.1016/j.tetlet.2013.07.053
32. Percino, M. J.; Chapela, V. M.; Cerón, M.; Soriano-Moro, G.; Castro, M. E. *Res. Chem. Intermed.* **2015,** *41,* 3563–3572. doi:10.1007/s11164-013-1471-y
33. Zhang, X.-Y.; Dong, D.-Q.; Yue, T.; Hao, S.-H.; Wang, Z.-L. *Tetrahedron Lett.* **2014,** *55,* 5462–5464. doi:10.1016/j.tetlet.2014.08.034
34. Wang, Z.-L. *RSC Adv.* **2015,** *5,* 5563–5566. doi:10.1039/c4ra14486d
35. Yaragorla, S.; Singh, G.; Dada, R. *Tetrahedron Lett.* **2015,** *56,* 5924–5929. doi:10.1016/j.tetlet.2015.09.035
36. Chen, Z.; Luo, M.; Wen, Y.; Luo, G.; Liu, L. *Org. Lett.* **2014,** *16,* 3020–3023. doi:10.1021/ol501137x
37. Nallasivam, J. L.; Fernandes, R. A. *Eur. J. Org. Chem.* **2015,** 3558–3567. doi:10.1002/ejoc.201500353
38. Sharma, R.; Abdullaha, M.; Bharate, S. B. *J. Org. Chem.* **2017,** *82,* 9786–9793. doi:10.1021/acs.joc.7b00856
39. Latha, D. S.; Yaragorla, S. *Eur. J. Org. Chem.* **2020,** 2155–2179. doi:10.1002/ejoc.201901899
40. Anastas, P. T.; Heine, L. G.; Williamson, T. C. *Green Chemical Syntheses and Processes;* Oxford University Press: Oxford, U.K., 2000.
41. Anastas, P. T.; Warner, J. C. *Green chemistry: theory and practice;* Oxford University Press: Oxford, U.K., 1998.
42. Varma, R. S. In *Green chemistry: challenging perspectives;* Tundo, P.; Anastas, P. T., Eds.; Oxford University Press: Oxford, U.K., 2000; pp 221–244.
43. Xu, L.; Shao, Z.; Wang, L.; Zhao, H.; Xiao, J. *Tetrahedron Lett.* **2014,** *55,* 6856–6860. doi:10.1016/j.tetlet.2014.10.079
44. Malviya, B. K.; Singh, K.; Jaiswal, P. K.; Shukla, M.; Verma, V. P.; Vanangamudi, M.; Jassal, A. K.; Punjabi, P. B.; Sharma, S. *ACS Omega* **2019,** *4,* 12146–12155. doi:10.1021/acsomega.9b01514
45. Goutam, B. *Catalyst-free Organic Synthesis;* Royal Society of Chemistry: Cambridge. U.K., 2017. doi:10.1039/9781788012782

46. Rao, Y. S.; Latha, D. S.; Devunuri, N.; Almansour, A. I.; Arumugam, N.; Yaragorla, S. *Eur. J. Org. Chem.* **2020,** 4134–4145. doi:10.1002/ejoc.202000511

BEILSTEIN JOURNAL OF ORGANIC CHEMISTRY

A sustainable strategy for the straightforward preparation of 2*H*-azirines and highly functionalized *NH*-aziridines from vinyl azides using a single solvent flow-batch approach

Michael Andresini, Leonardo Degannaro* and Renzo Luisi*

Letter

Open Access

Address:
Flow Chemistry and Microreactor Technology FLAME-Lab, Department of Pharmacy – Drug Sciences, University of Bari "A. Moro", Via E. Orabona 4, Bari, 70125, Italy

Email:
Leonardo Degannaro* - leonardo.degennaro@uniba.it; Renzo Luisi* - renzo.luisi@uniba.it

* Corresponding author

Keywords:
aziridines; 2*H*-azirines; flow chemistry; green chemistry; organolithium compounds

Beilstein J. Org. Chem. **2021,** *17,* 203–209.
https://doi.org/10.3762/bjoc.17.20

Received: 16 November 2020
Accepted: 29 December 2020
Published: 20 January 2021

This article is part of the thematic issue "Green chemistry II".

Associate Editor: L. Vaccaro

Abstract

The reported flow-batch approach enables the easy preparation of 2*H*-azirines and their stereoselective transformation into highly functionalized *NH*-aziridines, starting from vinyl azides and organolithium compounds. The protocol has been developed using cyclopentyl methyl ether (CPME) as an environmentally benign solvent, resulting into a sustainable, safe and potentially automatable method for the synthesis of interesting strained compounds.

Introduction

Since their conception in the early 1990s, Green Chemistry Principles (GCP) have been applied with increasing effort towards the design of efficient production processes [1-3]. As a result, a number of sustainable synthetic strategies has been recently developed, lowering the environmental impact and reducing the chemical hazards associated with the preparation of highly valuable compounds [4]. Among the elements that affect the sustainability of a synthetic method, the choice of the solvent is crucial [5]. In fact, chemical solvents represent most of the total amount of chemical species used in manufacturing processes, and therefore, strongly affect waste disposal requirements and process related risks [6]. Recently, a variety of sustainable solvents has been therefore identified, and their use have been combined with those of enabling technologies. In this scenario, the development of continuous flow synthetic methodologies has found its fortune in the past two decades [7-9]. Several chemical hazards can be effectively controlled through the use of microfluidic systems, because of the utilization of a reduced confined space and the exquisite control over heating and mass transfer [10]. In fact, the utilization of the microfluidic technology results in smaller temperature gradients due to the large surface–volume ratio of microreactors, and may prevent the formation of undesirable byproducts that are not avoidable under the traditional batch conditions. As a consequence, efforts have been devoted to the development of syn-

thetic processes combining GCP and enabling technologies [11].

Within the synthetic chemistry context, the preparation of aziridines still generates interest, mostly because of their importance as source for drug prototypes and drug discovery leads [12]. Interestingly, important advances have been recently addressed in the synthesis of *NH*-aziridines directly from olefins [13,14]. Aziridines are otherwise accessible from a variety of acyclic precursors [15-17], even stereoselectively [18-20], and through derivatization of 2*H*-azirines. The reactions using 2*H*-azirines as electrophiles proceed with several nitrogen, oxygen and sulfur nucleophiles, enabling to access aziridines with great structural variability [21]. The reaction of azirines with Grignard and organolithium reagents has been poorly investigated, and only without using green and renewable solvents [22,23]. In turn, 2*H*-azirines can be smoothly obtained through intramolecular cyclization of vinyl azides, or by other strategies involving oximes, imines and oxazoles [24].

One appealing strategy for the preparation of 2*H*-azirines involves the use of readily available vinyl azides [25-30]. However, the batch cyclization of vinyl azides into the corresponding 2*H*-azirines could generate some risks, due to the explosive nature of organic azides, and possible overpressure issues caused by nitrogen generation at high temperatures. Consequently, scalability and control of this processes represents a real challenge. The exploitation of microfluidic technologies has therefore resulted in safer procedures for the preparation of 2*H*-azirines, offering valuable alternatives for production purposes. In 2013, Kirschning harnessed the photoinduced electrocyclization of vinyl azides in a microfluidic photoreactor yielding 2*H*-azirines as precursors of 1,3-dipolarophiles (Scheme 1a) [27]. Similarly, Maurya developed a microfluidic

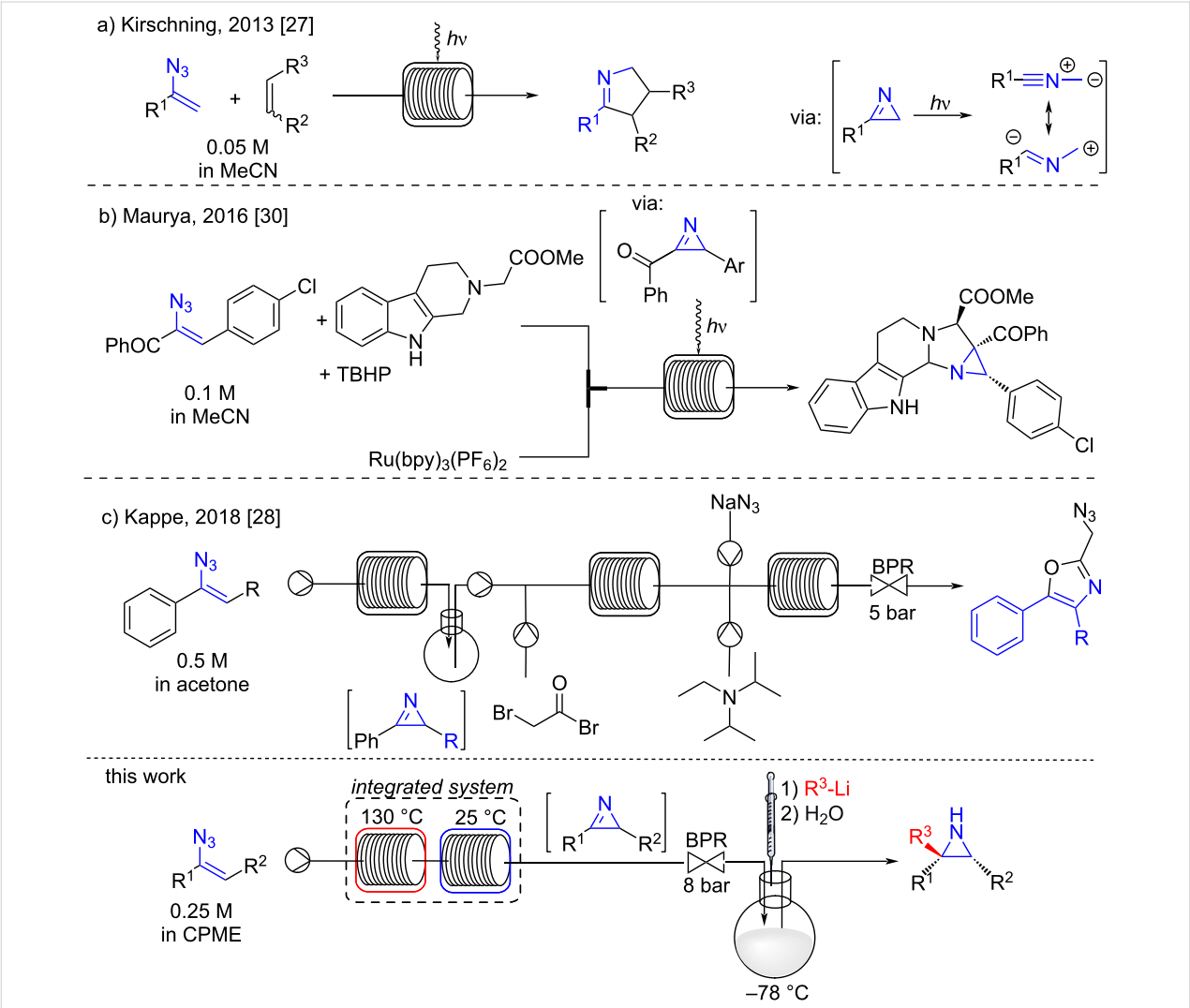

Scheme 1: Flow generation and transformation of 2*H*-azirines.

photoreactor for the synthesis of a fused β-carboline from an α-ketovinyl azide and a 1,2,3,4-tetrahydro-β-carboline (Scheme 1b) [30]. More recently, Kappe reported the generation of 2*H*-azirines under continuous flow conditions, and their transformation into functionalized oxazoles using acetone as the solvent (Scheme 1c) [28]. Inspired by these recent reports, we became interested in the development of an eco-friendly strategy for the safe preparation of highly functionalized *NH*-aziridines from acyclic precursors. Herein, we report a sustainable mixed flow-batch approach that enables the direct preparation of functionalized *NH*-aziridines from vinyl azides.

Results and Discussion

At the earliest stage of our research, we focused on the choice of the most suitable solvent for azide cyclization and organolithium addition reactions. Most of the previously reported flow procedures involved acetonitrile, dichloromethane and acetone as solvents, however, incompatible with the utilization of reactive alkali organometals. An exception is made for toluene, used by Kirschning for the photoinduced azirine formation [27]. Therefore, we investigated the thermally induced cyclisation of 1-(1-azidovinyl)-4-methylbenzene (**1a**) in refluxing 2-MeTHF and cyclopentyl methyl ether (CPME) as green solvent candidates, and compared the results with the reaction conducted in toluene (Table 1).

The reaction proceeded rapidly in CPME, while the use of 2-MeTHF resulted in longer reaction times if compared with toluene. We therefore selected CPME as the most suitable solvent for our purposes. Interestingly, besides being characterized by low toxicity, CPME has a very low affinity to water, making it suitable for moisture sensitive reactions, without previous distillation [31-33]. Subsequently, the process was examined under continuous flow conditions employing a special integrated coil reactor with two different operating temperatures (see Supporting Information File 1). A solution of 1-(1-azidovinyl)-4-methylbenzene (**1a**, 0.25 M in CPME) was introduced, via a high pressure syringe pump, into the coil reactor maintained at the temperature of 130 °C, and the residence time varied by adjusting the flow rate (Table 2). The reaction yield was calculated by ^{1}H NMR analysis of the crude. In details, conversion of **1a** in **2a** increased from 33% to >99% by adjusting the residence time from 4 min to 16 min, respectively. The complete transformation of vinyl azide **1a** was therefore achieved above the boiling point of CPME (106 °C), as enabled by the utilization of a microfluidic reactor. From a technical point of view, the pressure generated during the course of the

Table 1: Thermally induced cyclization of 1-(1-azidovinyl)-4-methylbenzene (**1a**) under batch conditions.

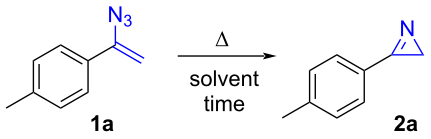

Solvent	Temperature	Time[a]
toluene	110 °C	1.5 h
2-MeTHF	80 °C	4.0 h
CPME	106 °C	45 min

[a]Time needed for complete consumption of **1a**.

Table 2: Flow cyclization of 1-(1-azidovinyl)-4-methylbenzene (**1a**).

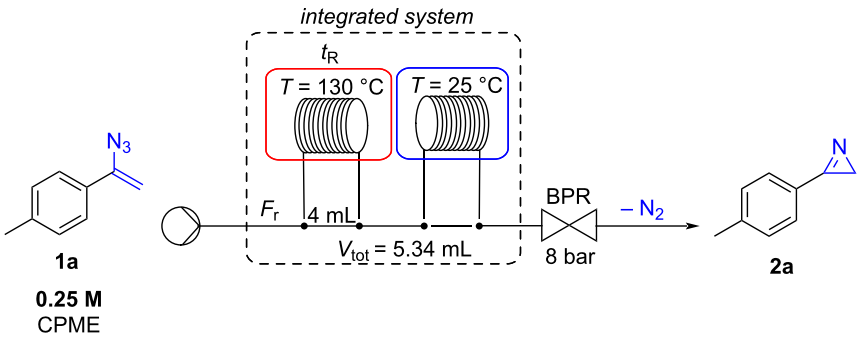

Entry	Flow rate (F_r)	Residence time (t_R)	Yield of **2a**
1	1.00 mL/min	4 min	33%
2	0.50 mL/min	8 min	65%
3	0.25 mL/min	16 min	>99%

reaction, due to nitrogen evolution, could be managed by using a high pressure pump, a stainless-steel reactor and a back-pressure regulator at 8 bar.

Under the optimized conditions, the scope of the reaction was explored on vinyl azides **1a**–**l** that were transformed into the corresponding 2*H*-azirines **2a**–**l** (Scheme 2). The methodology was found to be efficient with vinyl azides carrying aryls substituted with chlorine (**2b**), fluorine (**2c**), and bromide (**2e**–**g**). In details, *ortho*-, *meta*-, and *para*-bromophenyl derivatives were quantitatively transformed into the corresponding 2*H*-azirines **2e–g** without substantial differences. Similarly, 3-(*o*-tolyl)-2*H*-azirine (**2d**) and 2,3-diphenyl-2*H*-azirine (**2l**) were also obtained in excellent yields. When 1-(1-azidovinyl)-2,3,4,5,6-pentafluorobenzene (**1k**) was reacted under optimal flow conditions, a mixture of **1k** and 2*H*-azirine **2k** (20:80 ratio) was recovered. Unfortunately, it was not possible to isolate 3-(perfluorophenyl)-2*H*-azirine (**2k**) due to its rapid polymerization in the crude mixture.

Interestingly, aliphatic vinyl azides **1h–j** were found less reactive, and the corresponding azirines **2h–j** were obtained in just 74–77% yield, in mixtures with unreacted starting materials. However, when the reaction crudes were re-introduced into the flow reactor under the same conditions, azirines **2h–j** were obtained quantitatively (**2h**, 98%; **2i**, 97%; **2j**, 97%).

Pursuing in our aim to develop a green approach to prepare substituted *NH*-aziridines from vinyl azides in a single procedure, the solution of **2a** from the microfluidic system was collected in a round bottom flask cooled at −78 °C, and reacted with 1.2 equivalents of phenyllithium (PhLi) [34,35]. The mixture was stirred at the same temperature for 5 minutes, before quenching with water. To our delight, product **3a** was isolated

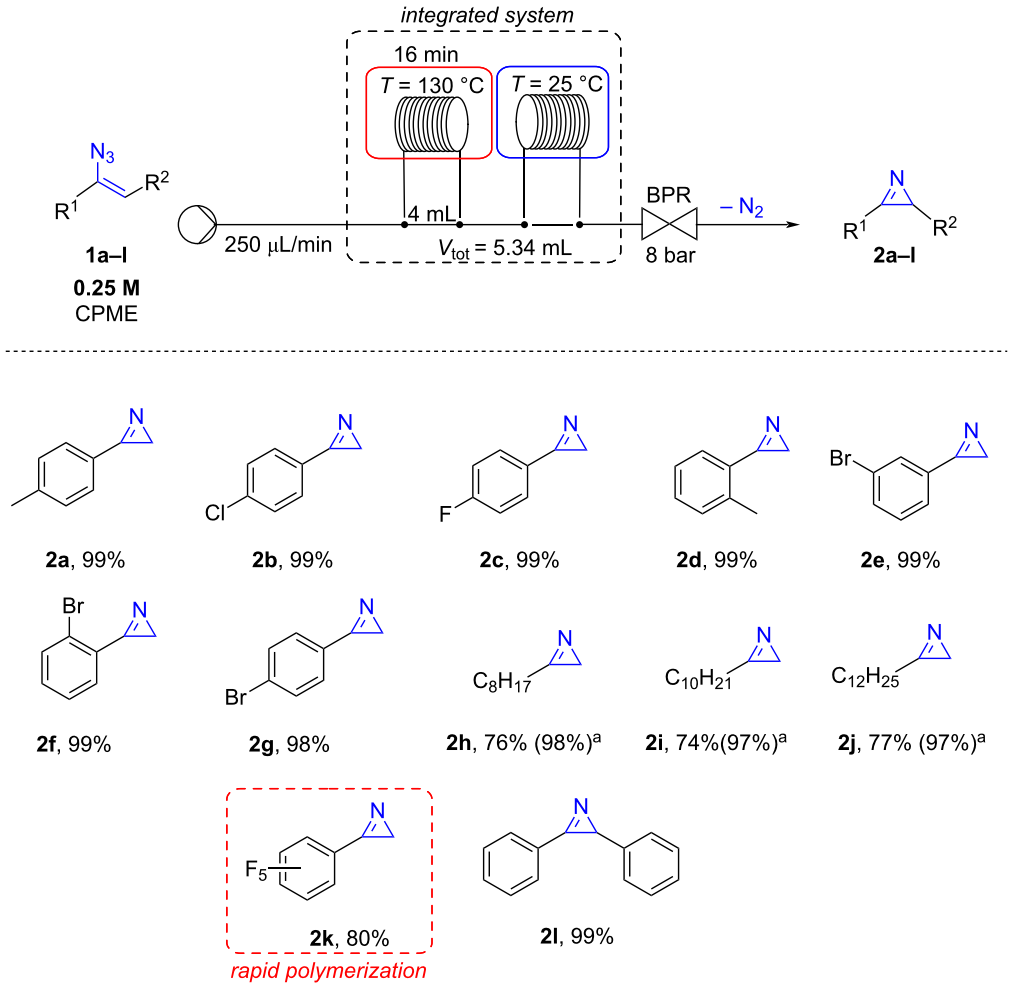

Scheme 2: Flow synthesis of 2*H*-azirines from vinyl azides. [a]The solution of vinyl azide was re-introduced twice into the flow system to achieve full conversion.

in 49% yield. Next, the reactions of several commercially available organolithium compounds were examined. As shown in Scheme 3, the reaction of **2a**, generated in flow from **1a**, proceeded smoothly also with hexyllithium (HexLi), *n*-butyllithium (*n*-BuLi) and isobutyllithium (iBuLi) affording the corresponding *NH*-aziridines **3b–d** in good yields. Subsequently, other vinyl azides were tested for this flow-batch two-step procedure (Scheme 3).

Starting from vinyl azide **1d**, the corresponding 3-(*o*-tolyl)-2*H*-azirine (**2d**) was generated under flow conditions, and reacted with PhLi, HexLi and BuLi, furnishing *NH*-azirdines **3e**–**g**. Aliphatic vinyl azides **1i** and **1j** were also subjected to this mixed flow-batch protocol, generating *NH*-aziridines **3h**,**i** in good yields (Scheme 3). The reaction was found to be efficient when PhLi was added to the collected solution of 2,3-diphenyl-2*H*-azirine (**2m**), affording 2,2,3-triphenylaziridine (**3j**) in 62% yield. Moreover, the reaction was found fully diastereoselective when HexLi or iBuLi were added to **2m**. In fact, only products deriving from the attack of the organolithium on the less hindered face (i.e., *anti* with respect to the phenyl substituent at C3), leading to **3k** (52%), and **3l** (45%), were observed. The relative stereochemistry was assigned by NOESY experiments (see Supporting Information File 1). Unfortunately, when the protocol was applied to 1-(1-azidovinyl)-2,3,4,5,6-pentafluorobenzene (**1k**), only a complex mixture was recovered likely

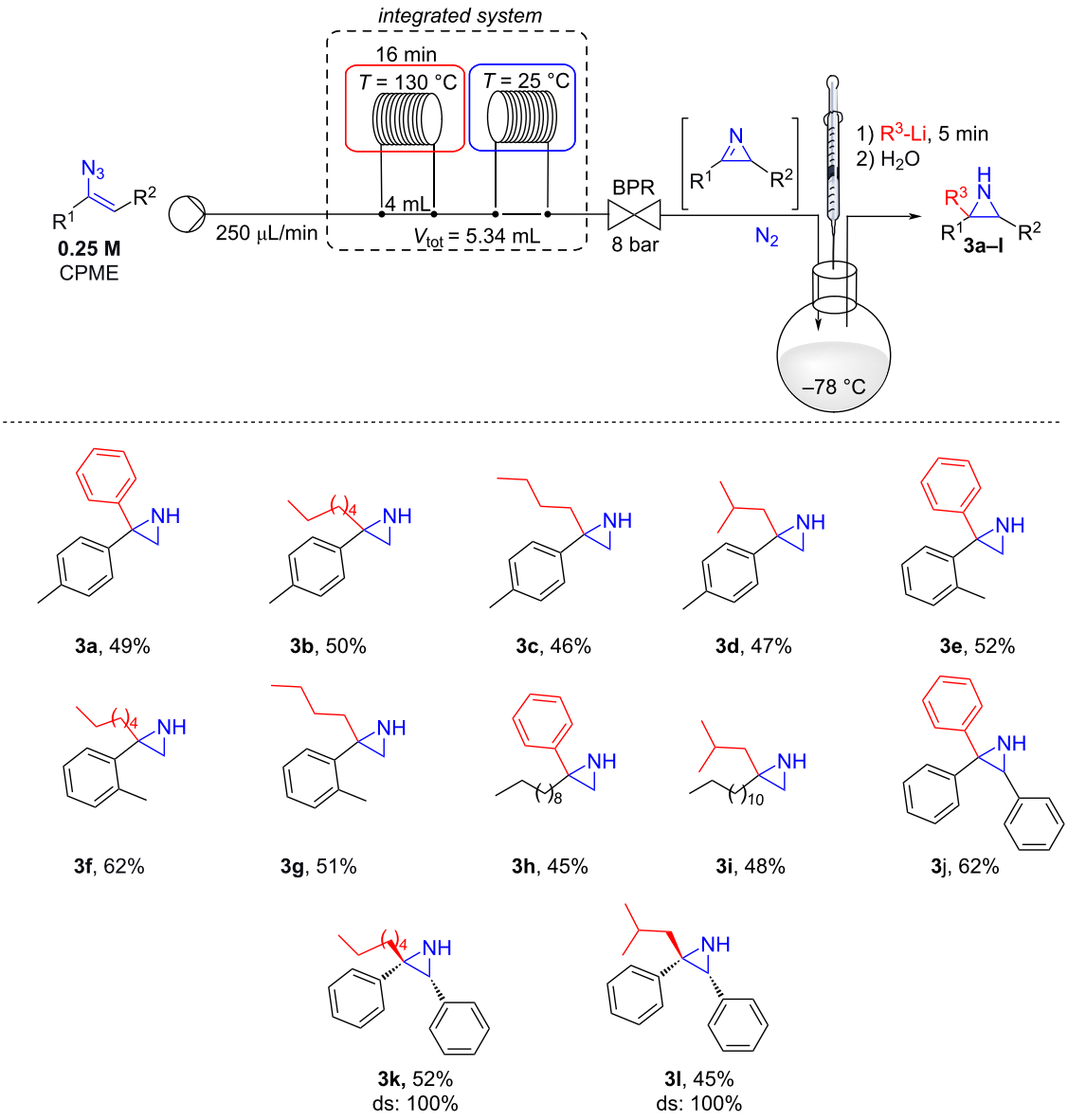

Scheme 3: Mixed flow-batch approach for the preparation of functionalized *NH*-aziridines from vinyl azides.

because of the instability of the corresponding 2*H*-azirine **2k** (vide infra).

Conclusion

In summary, we have developed a sustainable mixed flow-batch approach for the synthesis of functionalized *NH*-aziridines starting from vinyl azides using a single green solvent for two reaction steps. Several vinyl azides have been quantitatively transformed into the corresponding 2*H*-azirines in a microfluidic reactor, overcoming the hazards associated with this transformation under batch conditions. A small library of functionalized aryl and alkyl-substituted *NH*-aziridines has been created under operationally simple conditions. Notably, the addition reaction was found to proceed stereoselectively when organolithium compounds were added to 2,3-diphenyl-2*H*-azirine. This is a fast, safe, green and convenient method to access this interesting structural motif without requiring protection/deprotection steps or long synthetic pathways.

Supporting Information

Supporting Information File 1

Description of general methods, general procedures, characterization data for all compounds and copies of ^{1}H,^{13}C,^{19}F, NOESY spectra.
[https://www.beilstein-journals.org/bjoc/content/supplementary/1860-5397-17-20-S1.pdf]

Acknowledgements

We thank the CNR ICCOM section of Bari.

Funding

This research was supported by the project MISE, Horizon 2020 (PON 2014/2020 FARMIDIAB “code 338”) and the University of Bari (Fin. Ateneo Degennaro2019).

ORCID® iDs

Michael Andresini - https://orcid.org/0000-0003-4523-8488
Renzo Luisi - https://orcid.org/0000-0002-9882-7908

Preprint

A non-peer-reviewed version of this article has been previously published as a preprint: https://doi.org/10.3762/bxiv.2020.130.v1

References

1. Chen, T.-L.; Kim, H.; Pan, S.-Y.; Tseng, P.-C.; Lin, Y.-P.; Chiang, P.-C. *Sci. Total Environ.* **2020,** *716,* 136998. doi:10.1016/j.scitotenv.2020.136998
2. Ratti, R. *SN Appl. Sci.* **2020,** *2,* No. 263. doi:10.1007/s42452-020-2019-6
3. Loste, N.; Roldán, E.; Giner, B. *Environ. Sci. Pollut. Res.* **2020,** *27,* 6215–6227. doi:10.1007/s11356-019-07177-5
4. Sharma, S.; Das, J.; Braje, W. M.; Dash, A. K.; Handa, S. *ChemSusChem* **2020,** *13,* 2859–2875. doi:10.1002/cssc.202000317
5. Osei Akoto, C. *Industrial Applications of Green Solvents in Organic and Drug Synthesis for Sustainable Development of Chemical Process and Technologies*. In *Applications of Nanotechnology for Green Synthesis;* Inamuddin, A. A., Ed.; Nanotechnology in the Life Sciences; Springer: Cham, Switzerland, 2020; pp 19–40. doi:10.1007/978-3-030-44176-0_2
6. Häckl, K.; Kunz, W. *C. R. Chim.* **2018,** *21,* 572–580. doi:10.1016/j.crci.2018.03.010
7. Fanelli, F.; Parisi, G.; Degennaro, L.; Luisi, R. *Beilstein J. Org. Chem.* **2017,** *13,* 520–542. doi:10.3762/bjoc.13.51
8. Porta, R.; Benaglia, M.; Puglisi, A. *Org. Process Res. Dev.* **2016,** *20,* 2–25. doi:10.1021/acs.oprd.5b00325
9. Degennaro, L.; Carlucci, C.; De Angelis, S.; Luisi, R. *J. Flow Chem.* **2016,** *6,* 136–166. doi:10.1556/1846.2016.00014
10. Plutschack, M. B.; Pieber, B.; Gilmore, K.; Seeberger, P. H. *Chem. Rev.* **2017,** *117,* 11796–11893. doi:10.1021/acs.chemrev.7b00183
11. Bogdan, A. R.; Dombrowski, A. W. *J. Med. Chem.* **2019,** *62,* 6422–6468. doi:10.1021/acs.jmedchem.8b01760
12. Dembitsky, V. M.; Terent’ev, A. O.; Levitsky, D. O. *Aziridine Alkaloids: Origin, Chemistry and Activity*. *Natural Products;* Springer: Berlin, Heidelberg, Germany, 2013; pp 977–1006. doi:10.1007/978-3-642-22144-6_93
13. Jat, J. L.; Paudyal, M. P.; Gao, H.; Xu, Q.-L.; Yousufuddin, M.; Devarajan, D.; Ess, D. H.; Kürti, L.; Falck, J. R. *Science* **2014,** *343,* 61–65. doi:10.1126/science.1245727
14. Oseka, M.; Laudadio, G.; van Leest, N. P.; Dyga, M.; de Andrade Bartolomeu, A.; Goossen, L.; de Bruin, B.; Thiago de Oliveira, K.; Noel, T. *ChemRxiv* **2020**. doi:10.26434/chemrxiv.12824135.v1
15. Ielo, L.; Touqeer, S.; Roller, A.; Langer, T.; Holzer, W.; Pace, V. *Angew. Chem., Int. Ed.* **2019,** *58,* 2479–2484. doi:10.1002/anie.201812525
16. Ielo, L.; Pace, V.; Pillari, V.; Miele, M.; Castiglione, D. *Synlett* **2021**. doi:10.1055/s-0040-1706404
17. Monticelli, S.; Colella, M.; Pillari, V.; Tota, A.; Langer, T.; Holzer, W.; Degennaro, L.; Luisi, R.; Pace, V. *Org. Lett.* **2019,** *21,* 584–588. doi:10.1021/acs.orglett.8b04001
18. Degennaro, L.; Trinchera, P.; Luisi, R. *Chem. Rev.* **2014,** *114,* 7881–7929. doi:10.1021/cr400553c
19. de Ceglie, M. C.; Musio, B.; Affortunato, F.; Moliterni, A.; Altomare, A.; Florio, S.; Luisi, R. *Chem. – Eur. J.* **2011,** *17,* 286–296. doi:10.1002/chem.201002172
20. Dammacco, M.; Degennaro, L.; Florio, S.; Luisi, R.; Musio, B.; Altomare, A. *J. Org. Chem.* **2009,** *74,* 6319–6322. doi:10.1021/jo9011943
21. Alves, M. J.; Teixeira Costa, F. 2*H*-Azirines as electrophiles. In *Heterocyclic Targets in Advanced Organic Synthesis,* 1st ed.; do Carmo Carreiras, M.; Marco-Contelles, J., Eds.; Research Signpost: Kerala, India, 2010; pp 145–172.
22. Davis, F. A.; Liang, C.-H.; Liu, H. *J. Org. Chem.* **1997,** *62,* 3796–3797. doi:10.1021/jo9702610
23. Carlson, R. M.; Lee, S. Y. *Tetrahedron Lett.* **1969,** *10,* 4001–4004. doi:10.1016/s0040-4039(01)88598-1

24. Ramkumar, N.; Voskressensky, L. G.; Sharma, U. K.; Van der Eycken, E. V. *Chem. Heterocycl. Compd.* **2019,** *55,* 795–801. doi:10.1007/s10593-019-02539-w
25. Tiwari, D. K.; Maurya, R. A.; Nanubolu, J. B. *Chem. – Eur. J.* **2016,** *22,* 526–530. doi:10.1002/chem.201504292
26. O'Brien, A. G.; Lévesque, F.; Seeberger, P. H. *Chem. Commun.* **2011,** *47,* 2688–2690. doi:10.1039/c0cc04481d
27. Cludius-Brandt, S.; Kupracz, L.; Kirschning, A. *Beilstein J. Org. Chem.* **2013,** *9,* 1745–1750. doi:10.3762/bjoc.9.201
28. Rossa, T. A.; Suveges, N. S.; Sá, M. M.; Cantillo, D.; Kappe, C. O. *Beilstein J. Org. Chem.* **2018,** *14,* 506–514. doi:10.3762/bjoc.14.36
29. Koo, H.; Kim, H. Y.; Oh, K. *Org. Lett.* **2019,** *21,* 10063–10068. doi:10.1021/acs.orglett.9b04010
30. Chandrasekhar, D.; Borra, S.; Nanubolu, J. B.; Maurya, R. A. *Org. Lett.* **2016,** *18,* 2974–2977. doi:10.1021/acs.orglett.6b01321
31. Azzena, U.; Carraro, M.; Pisano, L.; Monticelli, S.; Bartolotta, R.; Pace, V. *ChemSusChem* **2019,** *12,* 40–70. doi:10.1002/cssc.201801768
32. Perna, F. M.; Vitale, P.; Capriati, V. *Curr. Opin. Green Sustainable Chem.* **2020,** *21,* 27–33. doi:10.1016/j.cogsc.2019.09.004
33. Watanabe, K.; Yamagiwa, N.; Torisawa, Y. *Org. Process Res. Dev.* **2007,** *11,* 251–258. doi:10.1021/op0680136
34. Zenzola, M.; Degennaro, L.; Trinchera, P.; Carroccia, L.; Giovine, A.; Romanazzi, G.; Mastrorilli, P.; Rizzi, R.; Pisano, L.; Luisi, R. *Chem. – Eur. J.* **2014,** *20,* 12190–12200. doi:10.1002/chem.201403141
35. Parisi, G.; Capitanelli, E.; Pierro, A.; Romanazzi, G.; Clarkson, G. J.; Degennaro, L.; Luisi, R. *Chem. Commun.* **2015,** *51,* 15588–15591. doi:10.1039/c5cc06323j

License and Terms

BEILSTEIN JOURNAL OF ORGANIC CHEMISTRY

Deoxygenative C2-heteroarylation of quinoline *N*-oxides: facile access to α-triazolylquinolines

Geetanjali S. Sontakke, Rahul K. Shukla and Chandra M. R. Volla*

Letter

Open Access

Address:
Department of Chemistry, Indian Institute of Technology Bombay, Powai-400076, Mumbai, India

Email:
Chandra M. R. Volla* - chandra.volla@chem.iitb.ac.in

* Corresponding author

Keywords:
amination; heteroarylation; quinoline *N*-oxides; regioselective; triazoles

Beilstein J. Org. Chem. **2021,** *17,* 485–493.
https://doi.org/10.3762/bjoc.17.42

Received: 13 July 2020
Accepted: 30 January 2021
Published: 17 February 2021

This article is part of the thematic issue "Green chemistry II".

Associate Editor: L. Vaccaro

Abstract

A metal- and additive-free, highly efficient, step-economical deoxygenative C2-heteroarylation of quinolines and isoquinolines was achieved from readily available *N*-oxides and *N*-sulfonyl-1,2,3-triazoles. A variety of α-triazolylquinoline derivatives were synthesized with good regioselectivity and in excellent yields under mild reaction conditions. Further, a gram-scale and one-pot synthesis illustrated the efficacy and simplicity of the developed protocol. The current transformation was also found to be compatible for the late-stage modification of natural products.

Introduction

Quinoline is a key heterocyclic moiety found in many natural products [1-4], agrochemicals and pharmaceuticals having potent biological activities, such as antimalarial, antibacterial and anticancer activities [5-11]. Due to their wide range of applications, selective functionalization of quinolines at various positions has gained significant interest in the last few years [12,13]. In particular, the C2-functionalization of quinolines has been well studied, and various methodologies were established for C–C [14-23], C–O [24,25] and C–S [26,27] bond formation. Recently C2-selective C–N bond formation has also attracted considerable attention due to the importance of the 2-aminoquinoline motif in medicinal chemistry and pharmaceuticals [28-45]. Some of the representative examples of biologically relevant derivatives containing a 2-aminoquinoline motif are shown in Figure 1 [46,47].

As a result, a variety of transition metal-catalyzed C2-selective aminations of azine *N*-oxides were explored extensively [28-34]. Additionally, various transition metal-free C2-aminations of these scaffolds were also investigated [35-45]. For example, Yin and co-workers developed a protocol for the deoxygenative C2-amination of pyridine/quinoline *N*-oxides using *t*-$BuNH_2$ and Ts_2O/TFA in 2007 (Scheme 1a) [48].

Later, Londregan and co-workers were successful in achieving C2-amination employing secondary amines as the nucleophiles

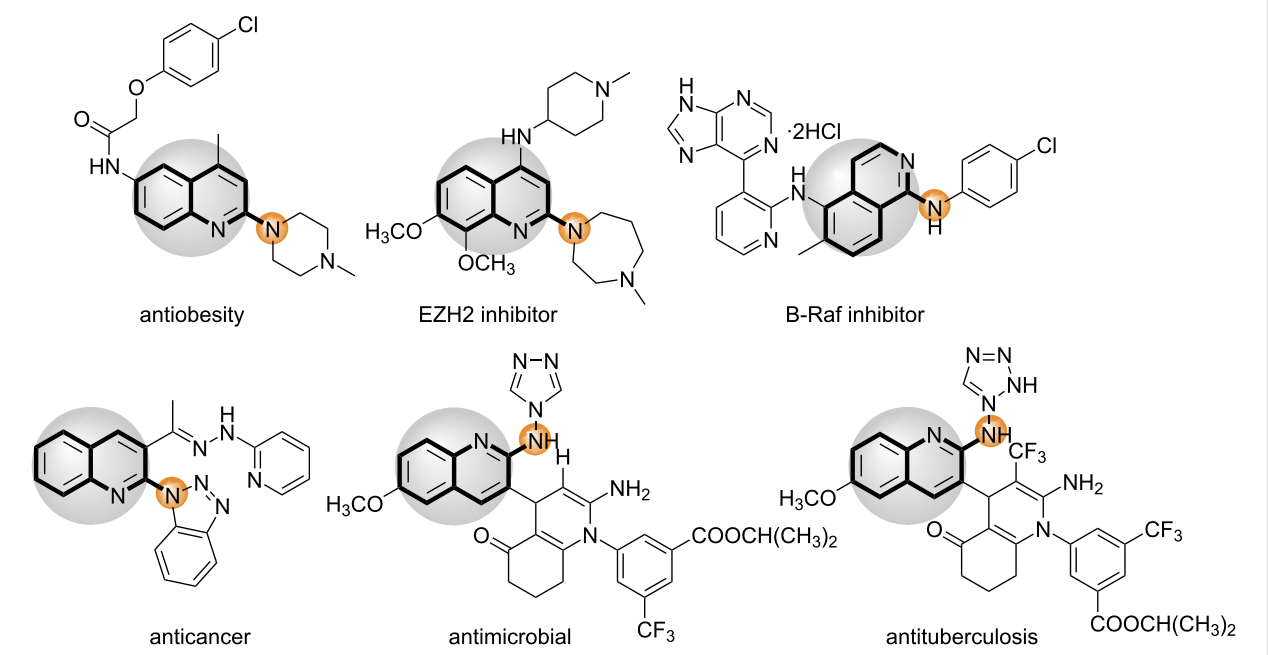

Figure 1: Bioactive molecules containing the 2-aminoquinoline motif.

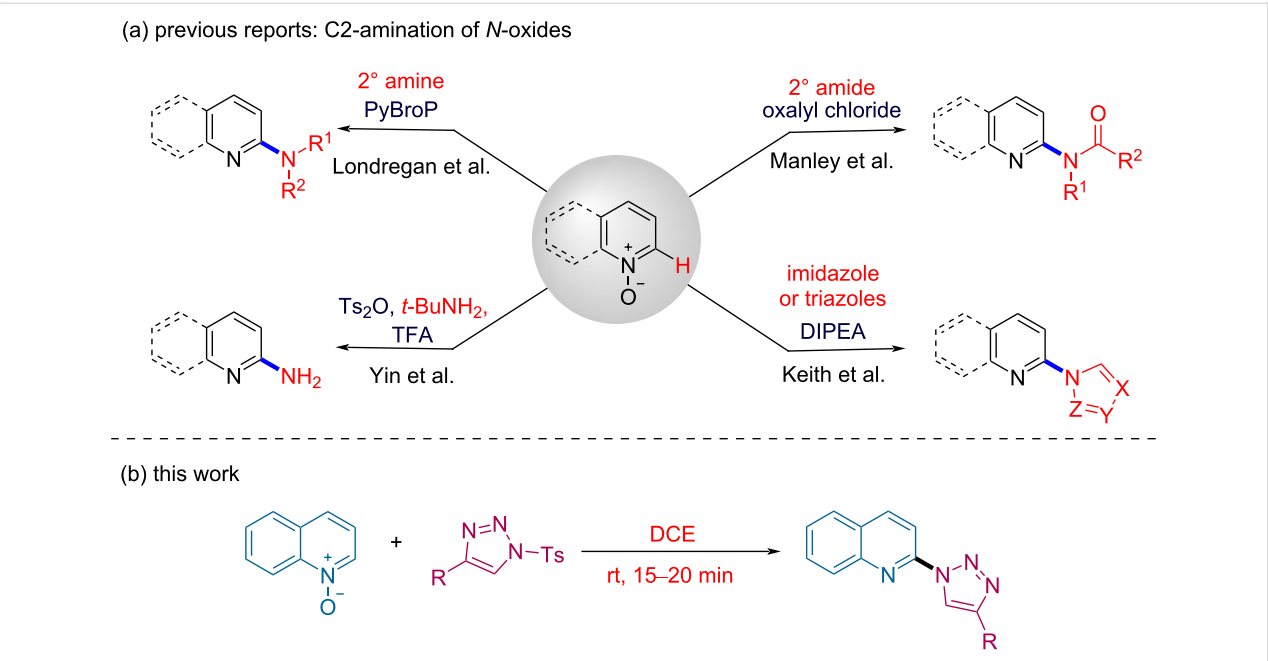

Scheme 1: C2-selective C–N bond formation of *N*-oxides.

[49]. In their protocol, the regioselectivity is controlled by PyBroP catalyst, which acts as the *N*-oxide activator. Manley and Bilodeau reported the amidation of heterocyclic *N*-oxides at the C2-position using oxalyl chloride for activating the *N*-oxides [50]. In addition to amination and amidation, there are few reports on metal-free C2-heteroarylation of pyridine *N*-oxides. In 1984, Rogers demonstrated the synthesis of 2-triazolylpyridines from 2-azidopyridines and phenylacetylene [51]. Along the same lines, Keith reported methodologies for the C2-imidazolylation and triazolylation of various heterocyclic *N*-oxides using sulfuryldiimidazole and 1,2,4-triazole, respectively. However, their protocol affords a mixture of C2- and C4-heteroarylated products [52,53]. More recently, Muthusubramanian and co-workers further expanded the scope of Keith's

protocol to a variety of pyridine *N*-oxides [54]. Despite the versatility of these methods, the above reports involve the use of external additives for activating the *N*-oxides and suffer from other disadvantages, including prolonged reaction time, high temperature and limited substrate scope. At the same time, with the advent of Cu-catalyzed "Click" chemistry, *N*-sulfonyl-1,2,3-triazoles have become useful precursors for accessing a variety of heterocyclic moieties [55,56].

In spite of the above methods for the C2-amination, the establishment of a simple, efficient and atom-economical method for the synthesis of 2-triazolylquinoline derivatives is highly desired. The continuous interest and efforts of our group for the derivatization of quinoline moieties [57] and use of *N*-sulfonyl-1,2,3-triazoles as heterocyclic precursors encouraged us to develop a new strategy for the regioselective C2-triazolylation of quinoline *N*-oxide under mild reaction conditions (Scheme 1b) [58-62].

Results and Discussion

We initiated our trials employing easily accessible quinoline *N*-oxide (**1a**) and 1-tosyl-4-phenyl-1,2,3-triazole (**2a**) as model substrates. Subjecting the reaction mixture to 100 °C in the presence of DIPEA in 1,2-dichloroetane (DCE), we were pleased to observe the formation of C2-triazolylquinoline **3a** selectively in 15% NMR yield (Table 1, entry 1). Replacing DIPEA with DABCO or K_2CO_3 did not further increase the yield of **3a** (Table 1, entries 2 and 3). Interestingly, while doing the control studies to understand the role of the base, we found that the reaction indeed proceeds in the absence of the base to afford **3a** in a better yield (40%, Table 1, entry 4). We further optimized the reaction conditions by lowering the temperature to 80 °C and then to 60 °C, which afforded **3a** with a moderate yield increment up to 52% (Table 1, entries 5 and 6). However, when the reaction was performed at room temperature, surprisingly, the yield of **3a** increased to 95% within 15 minutes (Table 1, entry 7). To examine the influence of solvent on the reaction, we screened other solvents, such as DCM, $CHCl_3$ and toluene, which provided **3a** only in inferior yields (Table 1, entries 8–10).

Table 1: Optimization of the reaction conditions.[a]

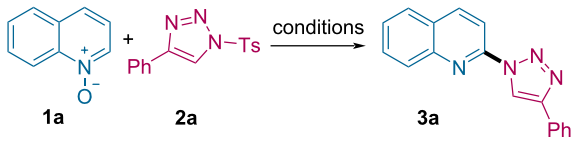

entry	solvent	base	*T* (°C)	yield (%)[b]
1	DCE	DIPEA	100	15
2	DCE	DABCO	100	8
3	DCE	K_2CO_3	100	<5
4	DCE	–	100	40
5	DCE	–	80	45
6	DCE	–	60	52
7	DCE	–	rt	95 (92)[c]
8	DCM	–	rt	78
9	chloroform	–	rt	65
10	toluene	–	rt	58

[a]Reaction conditions: 0.1 mmol of **1a** and 0.12 mmol of **2a** in 1 mL solvent. [b]NMR yield was taken by using 0.1 mmol of 1,3,5-trimethoxybenzene as an internal standard. [c]Yield of the isolated product in parentheses for 0.2 mmol **1a**.

Using the optimized reaction conditions, we explored the substrate scope of our developed strategy using quinoline *N*-oxide (**1a**) with triazoles **2** having variable functional groups (Scheme 2). We examined the impact of electronic and steric effects of the substituents and observed that triazoles bearing electron-donating groups on the aromatic ring, such as alkyl or methoxy moieties, were well tolerated, furnishing the corresponding products **3b–h** in 83–95% yield. For electron-poor substituents (CF_3 and F) on the aryl ring of the triazole, the corresponding products **3i** and **3j** were isolated in slightly lower yield (81% and 84%, respectively). Triazoles bearing halide substituents (Cl and Br) at the *meta*- or *para*-positions were also found to be viable substrates to afford the products **3k** and **3l** with 85–90% yield. Additionally, the reaction protocol is compatible with the heteroaromatic substrates and afforded **3m** in 82% yield.

Gratifyingly, alkenylated and aliphatic triazoles also showed similar reactivity and furnished desired products **3n–p** in moderate yield (73–77%). Motivated by the above results, we further extended the scope of triazoles by using different heteroatom-tethered triazoles. The -O-, -S- and -N-linked triazoles smoothly reacted under standard reaction conditions to provide the corresponding functionalized C2-triazolylquinolines **3q–x** in 67–83% yield. Cyclohexadienone-tethered triazole afforded the corresponding product **3y** in 66% yield. It is worth mentioning that when pyridine *N*-oxide was employed instead of **1a**, only traces of the corresponding product were observed even after prolonged reaction time.

Subsequently, the substrate scope was evaluated by analyzing electronic and steric effects of substituents present on the quinoline *N*-oxides **1** (Scheme 3). Electronically rich Me and OMe groups at the 4- or 6-positions of *N*-oxides were tolerated and delivered the corresponding C2-triazolylquinolines **3z**, **3aa** and **3ab** in 85–90% yield. Further, the structure was unambiguously confirmed by the single-crystal X-ray diffraction analysis of **3z** [63]. Halogenated substrates also furnished the 2-heteroary-

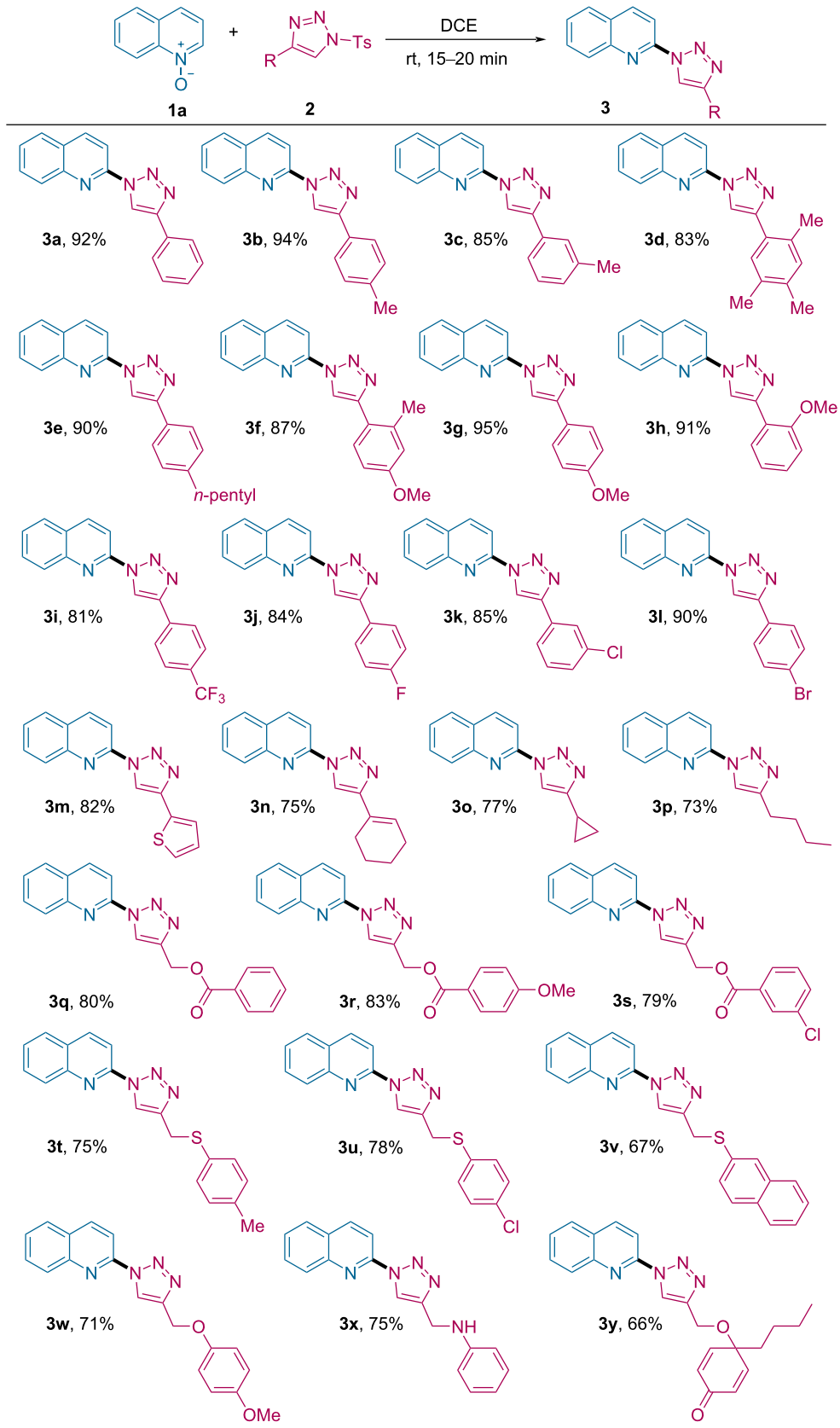

Scheme 2: Substrate scope of *N*-sulfonyl-1,2,3-triazoles. Reaction conditions: **1a** (0.2 mmol), **2** (0.24 mmol) and DCE (2 mL) at rt for 15–20 min.

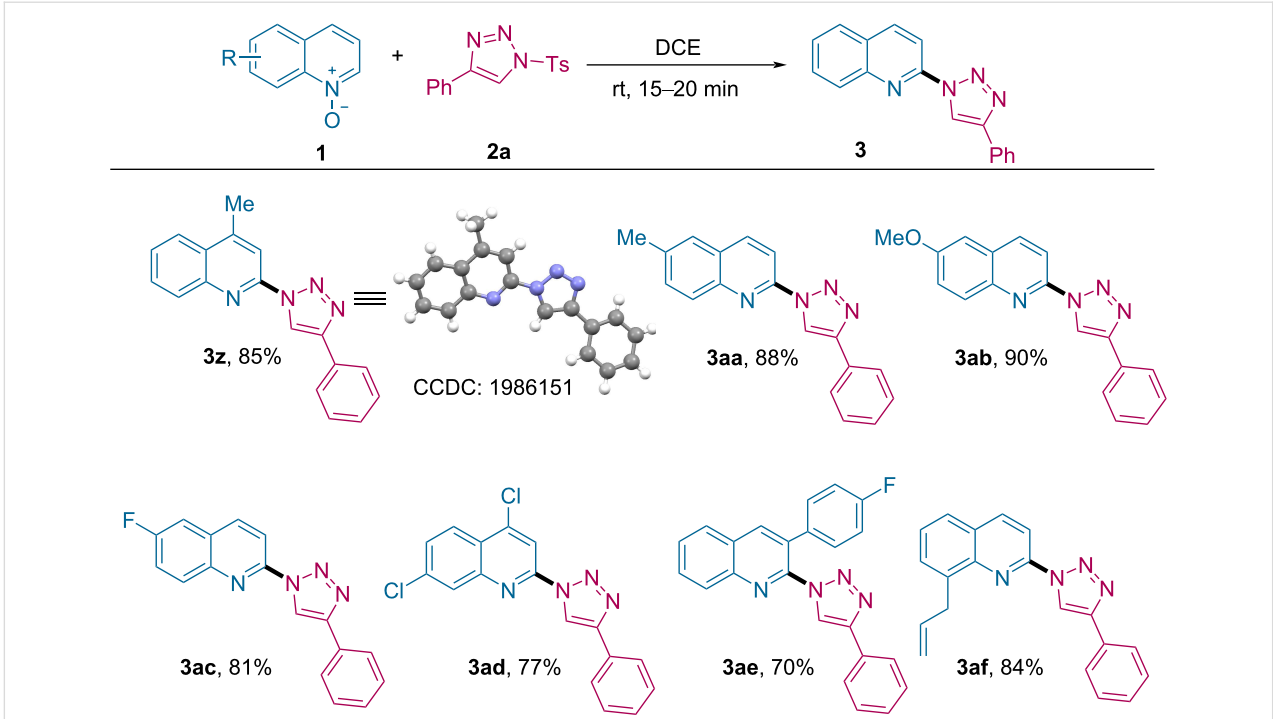

Scheme 3: Substrate scope of quinoline *N*-oxides. Reaction conditions: **1** (0.2 mmol), **2a** (0.24 mmol) and DCE (2 mL) at rt for 15–20 min.

lated products **3ac** and **3ad** in 81% and 77% yield, respectively. For 3-substituted quinoline *N*-oxides, a slight decrease in the yield to 70% was observed for **3ae**. The 8-allylated quinoline *N*-oxide cleanly provided **3af** in 84% yield.

In addition, the compatibility of this transformation for late-stage modification of complex natural products was explored, and as shown in Scheme 4, the protocol was tested with various natural-product-derived triazoles. Novel C2-tria-

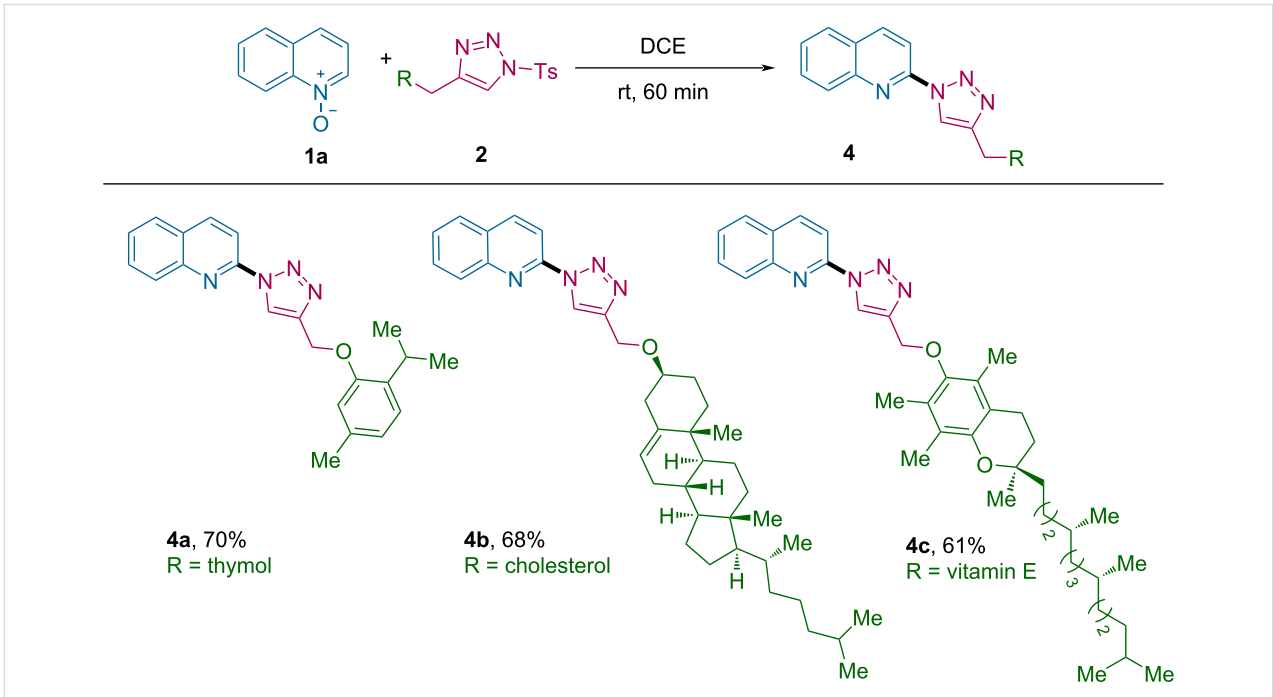

Scheme 4: Late-stage modification of natural products.

zolyl products **4a–c** were synthesized in good yield of 61–70% from triazoles derived from thymol, cholesterol and vitamin E, respectively.

To our delight, this protocol could also be extended for selective C1-functionalization of isoquinoline *N*-oxide (**5**, Scheme 5). Treating **5** with triazole **2a** under standard reaction conditions, the C1-heteroarylated isoquinoline product **6a** was obtained in 85% yield. Both the aromatic and aliphatic triazoles were suitable substrates for the reaction and afforded **6b–d** in good to excellent yield of 71–89%.

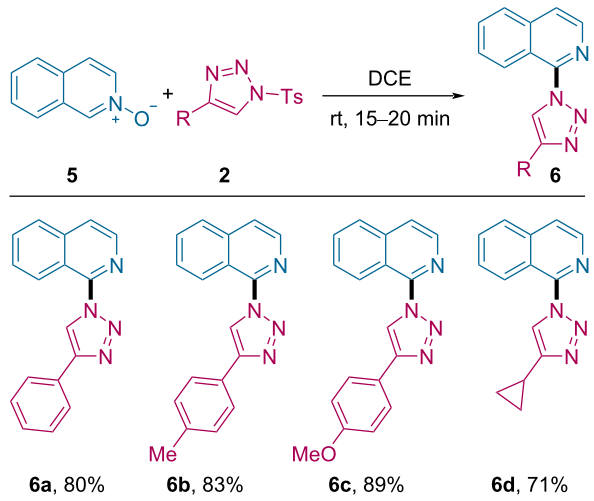

Scheme 5: Substrate scope for the reaction of substituted triazoles with isoquinoline *N*-oxide.

In order to investigate the synthetic utility of the current methodology, a gram-scale reaction was carried out (Scheme 6a). Upon treating quinoline *N*-oxide (**1a**, 6.9 mmol, 1.0 g) with 4-phenyl-1-tosyl-1*H*-1,2,3-triazole (**2a**, 8.3 mmol, 1.2 equiv) at room temperature for 1 h, the reaction worked equally well and produced the desired product **3a** in 87% yield (1.6 g). In addition, to enlarge the simplicity of the developed protocol for selective C2-triazolylation of quinoline derivatives, we performed a sequential one-pot synthesis by combining a Cu(I)-catalyzed "Click" reaction of phenylacetylene (**7**) with TsN_3 and a metal-free C2-heteroarylation of quinoline *N*-oxide (**1a**, Scheme 6b). Remarkably, the yield of the desired product **3a** in the one-pot synthesis (80%) was comparable to the stepwise pathway.

The plausible mechanism for the C2-triazolylation of quinoline *N*-oxides is presented in Scheme 7 [64]. The reaction initiates by the nucleophilic attack of quinoline *N*-oxide, e.g., **1a**, on the sulfonyl group of *N*-sulfonyl-1,2,3-triazole **2**, leading to the formation of intermediate **A**. This on elimination of a free triazolyl anion generates intermediate **B**. In next step, the triazolyl anion attacks the electrophilic C2-position of the quinoline *N*-oxide, providing the intermediate **C**, which, upon rearomatization, affords the desired 2-triazolylquinoline product **3**, along with the transfer of the oxygen atom from quinoline to the sulfonyl group of the triazole to form *p*-toluenesulfonic acid as the byproduct.

Conclusion

In summary, we have developed an operationally simple and metal-free protocol for the synthesis of α-triazolylquinolines utilizing *N*-sulfonyl-1,2,3-triazoles as the aminating source. The reaction proceeds at room temperature in a short reaction time with excellent regioselectivity. The methodology was also found to be compatible with isoquinoline *N*-oxides and diversely functionalized *N*-sulfonyl-1,2,3-triazoles to establish a broad substrate scope for a variety of scaffolds. The late-stage

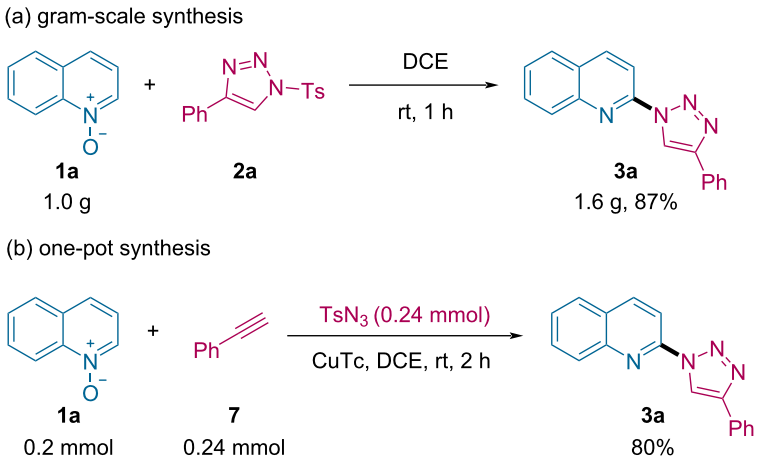

Scheme 6: Gram-scale and one-pot synthesis.

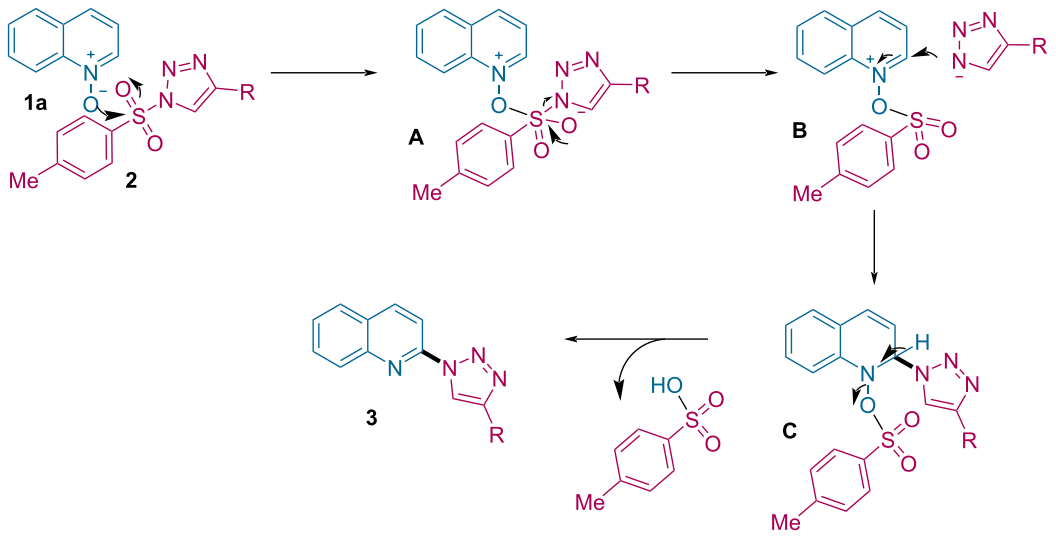

Scheme 7: Proposed mechanism.

modification of natural products is the salient feature of this current transformation.

Experimental

General procedure for the C2-selective synthesis of α-triazolylquinolines **3**

To an oven-dried reaction tube equipped with a magnetic stirring bar were added quinoline *N*-oxide (**1a**, 29 mg, 0.2 mmol, 1.0 equiv) and 4-phenyl-1-tosyl-1*H*-1,2,3-triazole (**2a**, 72 mg, 0.24 mmol, 1.2 equiv), followed by DCE (2 mL) via syringe. The reaction mixture was allowed to stir at rt for 15–20 min. After completion of the reaction, the solvent was evaporated under reduced pressure, and the residue was purified by column chromatography (ethyl acetate/petroleum ether 1:9) to get the desired product **3a** in 92% yield (50 mg, 0.18 mmol).

Supporting Information

Supporting Information File 1

Experimental details.
[https://www.beilstein-journals.org/bjoc/content/supplementary/1860-5397-17-42-S1.pdf]

Funding

The activity was generously supported by Science and Engineering Research Board (SERB), India: CRG/2019/005059. G.S.S and R.S. would like to thank CSIR and UGC, India for the fellowships, respectively.

ORCID® iDs

Geetanjali S. Sontakke - https://orcid.org/0000-0003-1253-3640
Rahul K. Shukla - https://orcid.org/0000-0002-4646-8341
Chandra M. R. Volla - https://orcid.org/0000-0002-8497-1538

References

1. Madapa, S.; Tusi, Z.; Batra, S. *Curr. Org. Chem.* **2008,** *12,* 1116–1183. doi:10.2174/138527208785740300
2. Michael, J. P. *Nat. Prod. Rep.* **2008,** *25,* 166–187. doi:10.1039/b612168n
3. Roughley, S. D.; Jordan, A. M. *J. Med. Chem.* **2011,** *54,* 3451–3479. doi:10.1021/jm200187y
4. Peng, H.-K.; Lin, C.-K.; Yang, S.-Y.; Tseng, C.-K.; Tzeng, C.-C.; Lee, J.-C.; Yang, S.-C. *Bioorg. Med. Chem. Lett.* **2012,** *22,* 1107–1110. doi:10.1016/j.bmcl.2011.11.121
5. Ridley, R. G. *Nature* **2002,** *415,* 686–693. doi:10.1038/415686a
6. Foley, M.; Tilley, L. *Pharmacol. Ther.* **1998,** *79,* 55–87. doi:10.1016/s0163-7258(98)00012-6
7. Solomon, V. R.; Lee, H. *Curr. Med. Chem.* **2011,** *18,* 1488–1508. doi:10.2174/092986711795328382
8. Garuti, L.; Roberti, M.; Pizzirani, D. *Mini-Rev. Med. Chem.* **2007,** *7,* 481–489. doi:10.2174/138955707780619626
9. Priya, N.; Gupta, A.; Chand, K.; Singh, P.; Kathuria, A.; Raj, H. G.; Parmar, V. S.; Sharma, S. K. *Bioorg. Med. Chem.* **2010,** *18,* 4085–4094. doi:10.1016/j.bmc.2010.04.011
10. Tseng, C.-H.; Chen, Y.-L.; Chung, K.-Y.; Wang, C.-H.; Peng, S.-I.; Cheng, C.-M.; Tzeng, C.-C. *Org. Biomol. Chem.* **2011,** *9,* 3205–3216. doi:10.1039/c0ob01225d
11. Gorka, A. P.; de Dios, A.; Roepe, P. D. *J. Med. Chem.* **2013,** *56,* 5231–5246. doi:10.1021/jm400282d
12. Iwai, T.; Sawamura, M. *ACS Catal.* **2015,** *5,* 5031–5040. doi:10.1021/acscatal.5b01143
13. Murakami, K.; Yamada, S.; Kaneda, T.; Itami, K. *Chem. Rev.* **2017,** *117,* 9302–9332. doi:10.1021/acs.chemrev.7b00021

14. Campeau, L.-C.; Stuart, D. R.; Leclerc, J.-P.; Bertrand-Laperle, M.; Villemure, E.; Sun, H.-Y.; Lasserre, S.; Guimond, N.; Lecavallier, M.; Fagnou, K. *J. Am. Chem. Soc.* **2009,** *131,* 3291–3306. doi:10.1021/ja808332k
15. Cho, S. H.; Hwang, S. J.; Chang, S. *J. Am. Chem. Soc.* **2008,** *130,* 9254–9256. doi:10.1021/ja8026295
16. Odani, R.; Hirano, K.; Satoh, T.; Miura, M. *J. Org. Chem.* **2015,** *80,* 2384–2391. doi:10.1021/acs.joc.5b00037
17. Xi, P.; Yang, F.; Qin, S.; Zhao, D.; Lan, J.; Gao, G.; Hu, C.; You, J. *J. Am. Chem. Soc.* **2010,** *132,* 1822–1824. doi:10.1021/ja909807f
18. Larionov, O. V.; Stephens, D.; Mfuh, A.; Chavez, G. *Org. Lett.* **2014,** *16,* 864–867. doi:10.1021/ol403631k
19. Ryu, J.; Cho, S. H.; Chang, S. *Angew. Chem., Int. Ed.* **2012,** *51,* 3677–3681. doi:10.1002/anie.201200120
20. Wu, J.; Cui, X.; Chen, L.; Jiang, G.; Wu, Y. *J. Am. Chem. Soc.* **2009,** *131,* 13888–13889. doi:10.1021/ja902762a
21. Cho, S. H.; Kim, J. Y.; Kwak, J.; Chang, S. *Chem. Soc. Rev.* **2011,** *40,* 5068–5083. doi:10.1039/c1cs15082k
22. Kumar, R.; Kumar, I.; Sharma, R.; Sharma, U. *Org. Biomol. Chem.* **2016,** *14,* 2613–2617. doi:10.1039/c5ob02600h
23. Kumar, R.; Kumar, R.; Dhiman, A. K.; Sharma, U. *Asian J. Org. Chem.* **2017,** *6,* 1043–1053. doi:10.1002/ajoc.201700267
24. Chen, X.; Zhu, C.; Cui, X.; Wu, Y. *Chem. Commun.* **2013,** *49,* 6900–6902. doi:10.1039/c3cc43947j
25. Lian, Y.; Coffey, S. B.; Li, Q.; Londregan, A. T. *Org. Lett.* **2016,** *18,* 1362–1365. doi:10.1021/acs.orglett.6b00295
26. Du, B.; Qian, P.; Wang, Y.; Mei, H.; Han, J.; Pan, Y. *Org. Lett.* **2016,** *18,* 4144–4147. doi:10.1021/acs.orglett.6b02289
27. Wu, Z.; Song, H.; Cui, X.; Pi, C.; Du, W.; Wu, Y. *Org. Lett.* **2013,** *15,* 1270–1273. doi:10.1021/ol400178k
28. Li, G.; Jia, C.; Sun, K. *Org. Lett.* **2013,** *15,* 5198–5201. doi:10.1021/ol402324v
29. Li, G.; Jia, C.; Sun, K.; Lv, Y.; Zhao, F.; Zhou, K.; Wu, H. *Org. Biomol. Chem.* **2015,** *13,* 3207–3210. doi:10.1039/c5ob00135h
30. Zhu, C.; Yi, M.; Wei, D.; Chen, X.; Wu, Y.; Cui, X. *Org. Lett.* **2014,** *16,* 1840–1843. doi:10.1021/ol500183w
31. Yu, H.; Dannenberg, C. A.; Li, Z.; Bolm, C. *Chem. – Asian J.* **2016,** *11,* 54–57. doi:10.1002/asia.201500875
32. Xie, L.-Y.; Peng, S.; Jiang, L.-L.; Peng, X.; Xia, W.; Yu, X.; Wang, X.-X.; Cao, Z.; He, W.-M. *Org. Chem. Front.* **2019,** *6,* 167–171. doi:10.1039/c8qo01128a
33. Sun, K.; Wang, X.; Liu, L.; Sun, J.; Liu, X.; Li, Z.; Zhang, Z.; Zhang, G. *ACS Catal.* **2015,** *5,* 7194–7198. doi:10.1021/acscatal.5b02411
34. Dhiman, A. K.; Chandra, D.; Kumar, R.; Sharma, U. *J. Org. Chem.* **2019,** *84,* 6962–6969. doi:10.1021/acs.joc.9b00739
35. Li, P.; Zhao, J.; Xia, C.; Li, F. *Org. Chem. Front.* **2015,** *2,* 1313–1317. doi:10.1039/c5qo00204d
36. Aithagani, S. K.; Kumar, M.; Yadav, M.; Vishwakarma, R. A.; Singh, P. P. *J. Org. Chem.* **2016,** *81,* 5886–5894. doi:10.1021/acs.joc.6b00593
37. Bering, L.; Antonchick, A. P. *Org. Lett.* **2015,** *17,* 3134–3137. doi:10.1021/acs.orglett.5b01456
38. Chen, X.; Cui, X.; Yang, F.; Wu, Y. *Org. Lett.* **2015,** *17,* 1445–1448. doi:10.1021/acs.orglett.5b00330
39. Xia, H.; Liu, Y.; Zhao, P.; Gou, S.; Wang, J. *Org. Lett.* **2016,** *18,* 1796–1799. doi:10.1021/acs.orglett.6b00522
40. Tang, R.-J.; Kang, L.; Yang, L. *Adv. Synth. Catal.* **2015,** *357,* 2055–2060. doi:10.1002/adsc.201500268
41. Couturier, M.; Caron, L.; Tumidajski, S.; Jones, K.; White, T. D. *Org. Lett.* **2006,** *8,* 1929–1932. doi:10.1021/ol060473w
42. Xie, L.-Y.; Peng, S.; Liu, F.; Yi, J.-Y.; Wang, M.; Tang, Z.; Xu, X.; He, W.-M. *Adv. Synth. Catal.* **2018,** *360,* 4259–4264. doi:10.1002/adsc.201800918
43. Xie, L.-Y.; Peng, S.; Lu, L.-H.; Hu, J.; Bao, W.-H.; Zeng, F.; Tang, Z.; Xu, X.; He, W.-M. *ACS Sustainable Chem. Eng.* **2018,** *6,* 7989–7994. doi:10.1021/acssuschemeng.8b01358
44. Chen, X.; Peng, M.; Huang, H.; Zheng, Y.; Tao, X.; He, C.; Xiao, Y. *Org. Biomol. Chem.* **2018,** *16,* 6202–6205. doi:10.1039/c8ob00862k
45. Londregan, A. T.; Jennings, S.; Wei, L. *Org. Lett.* **2011,** *13,* 1840–1843. doi:10.1021/ol200352g
46. Clark, D. E.; Higgs, C.; Wren, S. P.; Dyke, H. J.; Wong, M.; Norman, D.; Lockey, P. M.; Roach, A. G. *J. Med. Chem.* **2004,** *47,* 3962–3971. doi:10.1021/jm040762v
47. Smith, A. L.; DeMorin, F. F.; Paras, N. A.; Huang, Q.; Petkus, J. K.; Doherty, E. M.; Nixey, T.; Kim, J. L.; Whittington, D. A.; Epstein, L. F.; Lee, M. R.; Rose, M. J.; Babij, C.; Fernando, M.; Hess, K.; Le, Q.; Beltran, P.; Carnahan, J. *J. Med. Chem.* **2009,** *52,* 6189–6192. doi:10.1021/jm901081g
48. Yin, J.; Xiang, B.; Huffman, M. A.; Raab, C. E.; Davies, I. W. *J. Org. Chem.* **2007,** *72,* 4554–4557. doi:10.1021/jo070189y
49. Londregan, A. T.; Jennings, S.; Wei, L. *Org. Lett.* **2010,** *12,* 5254–5257. doi:10.1021/ol102301u
50. Manley, P. J.; Bilodeau, M. T. *Org. Lett.* **2002,** *4,* 3127–3129. doi:10.1021/ol0264556
51. Rogers, R. B.; Gerwick, B. C.; Egli, E. A. 1-(Pyridyl)-1*H*-1,2,3-triazole derivatives, and use as herbicidal agents. U.S. Patent US4474599A, Oct 2, 1984.
52. Keith, J. M. *J. Org. Chem.* **2008,** *73,* 327–330. doi:10.1021/jo702038g
53. Keith, J. M. *J. Org. Chem.* **2010,** *75,* 2722–2725. doi:10.1021/jo1001017
54. Harisha, M. B.; Nagaraj, M.; Muthusubramanian, S.; Bhuvanesh, N. *RSC Adv.* **2016,** *6,* 58118–58124. doi:10.1039/c6ra10452e
55. Chattopadhyay, B.; Gevorgyan, V. *Angew. Chem., Int. Ed.* **2012,** *51,* 862–872. doi:10.1002/anie.201104807
56. Davies, H. M. L.; Alford, J. S. *Chem. Soc. Rev.* **2014,** *43,* 5151–5162. doi:10.1039/c4cs00072b
57. Shukla, R. K.; Nair, A. M.; Khan, S.; Volla, C. M. R. *Angew. Chem., Int. Ed.* **2020,** *59,* 17042–17048. doi:10.1002/anie.202003216
58. Dey, A.; Thrimurtulu, N.; Volla, C. M. R. *Org. Lett.* **2019,** *21,* 3871–3875. doi:10.1021/acs.orglett.9b01392
59. Nallagonda, R.; Thrimurtulu, N.; Volla, C. M. R. *Adv. Synth. Catal.* **2018,** *360,* 255–260. doi:10.1002/adsc.201701162
60. Thrimurtulu, N.; Dey, A.; Maiti, D.; Volla, C. M. R. *Angew. Chem., Int. Ed.* **2016,** *55,* 12361–12365. doi:10.1002/anie.201604956
61. Sontakke, G. S.; Pal, K.; Volla, C. M. R. *J. Org. Chem.* **2019,** *84,* 12198–12208. doi:10.1021/acs.joc.9b01924
62. Pal, K.; Sontakke, G. S.; Volla, C. M. R. *Org. Lett.* **2019,** *21,* 3716–3720. doi:10.1021/acs.orglett.9b01174
63. Supplementary crystallographic data for this paper can be obtained free of charge from the Cambridge Crystallographic Data Centre using the associated CCDC numbers via http://www.ccdc.cam.ac.uk/data_request/cif. CCDC 1986151 (**3z**).
64. Dong, H.; Zhang, D.; Fang, R.; Du, Q.; Dong, Z.; Wei, H.; Shi, M.; Wang, F. *Synth. Commun.* **2018,** *48,* 1227–1234. doi:10.1080/00397911.2018.1440316

License and Terms

BEILSTEIN JOURNAL OF ORGANIC CHEMISTRY

Designed whole-cell-catalysis-assisted synthesis of 9,11-secosterols

Marek Kõllo[1], Marje Kasari[2], Villu Kasari[2], Tõnis Pehk[3], Ivar Järving[1], Margus Lopp[1], Arvi Jõers[2] and Tõnis Kanger*[1]

Full Research Paper

Open Access

Address:
[1]Department of Chemistry and Biotechnology, School of Science, Tallinn University of Technology, Akadeemia tee 15, 12618 Tallinn, Estonia, [2]Institute of Technology, University of Tartu, Nooruse 1, 50104 Tartu, Estonia and [3]National Institute of Chemical Physics and Biophysics, Akadeemia tee 23, 12618 Tallinn, Estonia

Email:
Tõnis Kanger* - tonis.kanger@taltech.ee

* Corresponding author

Keywords:
chemoenzymatic synthesis; cortisol; hydroxylation; secosterol; whole-cell catalysis

Beilstein J. Org. Chem. **2021,** *17,* 581–588.
https://doi.org/10.3762/bjoc.17.52

Received: 07 January 2021
Accepted: 17 February 2021
Published: 01 March 2021

This article is part of the thematic issue "Green chemistry II".

Associate Editor: L. Vaccaro

Abstract

A method for the synthesis of 9,11-secosteroids starting from the natural corticosteroid cortisol is described. There are two key steps in this approach, combining chemistry and synthetic biology. Stereo- and regioselective hydroxylation at C9 (steroid numbering) is carried out using whole-cell biocatalysis, followed by the chemical cleavage of the C–C bond of the vicinal diol. The two-step method features mild reaction conditions and completely excludes the use of toxic oxidants.

Introduction

Developments in the chemistry of steroids have stimulated extensive research interest in the exploration of new synthetic methods since the 1960s. Advances in synthetic biology and the increasing importance of methods of sustainable chemistry have brought chemoenzymatic approaches for obtaining natural products, or derivatives thereof, with complex structure into focus [1]. Various enzymatic or semisynthetic methods have also been exploited in the synthesis of steroids [2-4]. A more challenging synthesis of secosteroids with unique broken tetracyclic carbon skeletons and abeo-steroids with migrated bonds has received attention only recently [5,6]. As the bond cleavage may occur at the 5,6-, 9,11-, 9,10-, 8,9-, 8,14- or 13,17-positions (Figure 1A), the selection of synthetic methods for secosteroids is wide. However, usually these are multistep sequences exploiting toxic oxidants.

Marine invertebrates are a rich source of oxidated and highly functionalized steroidal metabolites, including secosteroids. Since the first isolation of 9,11-secosterol from *Pseudopterogorgia americana* in 1972 (Figure 1B) [7], several others from

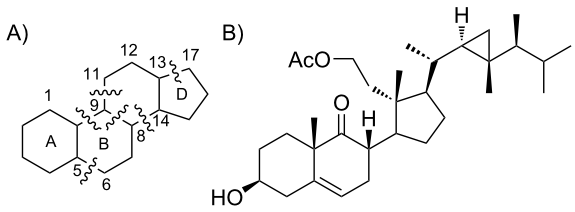

Figure 1: A) Tetracyclic core of steroids and possible sites of bond cleavages for secosteroids. B)The first 9,11-secosteroid isolated in 1972 [7].

the family have been reported [8-14]. The 9,11-secosterols exhibit diverse biological activities, including antihistaminic, antiproliferative, anti-inflammatory, cytotoxic and protein kinase C (PKC) inhibition activities [8-10,15]. Biochemical characterization of 9,11-secosterols has so far mainly relied on the identification and purification of natural products from marine invertebrates. The intriguing profile of biological properties has prompted synthetic studies of this class of secosterols. The majority of synthetic schemes starts with natural steroids, taking advantage of the appropriate stereochemistry of existing stereogenic centres [16-20]. However, the synthesis of target compounds is a multistep procedure, often including several protections and deprotections of functional groups.

Our approach to 9,11-secosterols is depicted in the retrosynthetic analysis in Scheme 1. There are two key steps in obtaining the skeleton of the secosterol. The first is (di)hydroxylation at C9 (C11), and the second is C9–C11-bond cleavage, which can be carried out by a well-developed chemical oxidation of 1,2-diols. Starting with a compound already possessing a hydroxy group at the position C11, only hydroxylation at C9 is needed. Commercially available corticosteroid cortisol already possesses a hydroxy group at the position C11, and therefore only hydroxylation at C9 is needed, making cortisol (**1**) an ideal starting compound for this synthesis.

Chemical oxidation methods for the synthesis of steroids often require stoichiometric amounts of toxic reagents, and the selectivity of the oxidation is still an unsolved problem [21].

Typically, toxic oxidants, such as OsO_4, SeO_2 and $Pb(OAc)_4$ are used in this total synthesis sequence. Inspired by several enzymatic oxidations [22-25], we envisioned to carry out oxidation at C9 in an environmentally benign way using an oxidation by a whole-cell biocatalysis method.

The first, and so far the only chemoenzymatic synthesis of 9,11-secosterols using cellular lysate of the marine gorgonian *Pseudopterogorgia americana* was published by Keliman et al. in 1996 [26]. They carried out quite effective transformations of a variety of sterols to 9,11-secosteroid derivatives in high yields. However, it is unclear which enzymes were responsible for each oxidation step through the whole secosteroid synthesis pathway. Also, the use of cellular lysate from a nonlaboratory organism prevents any widespread adoption of this method.

Herein, we present a new combined route towards 9,11-secosterols via stereo- and regiospecific enzymatic hydroxylation at C9, followed by the chemical oxidative cleavage of the 9,11-C–C bond. For the hydroxylation, we used a biocatalyst derived from an *Escherichia coli* laboratory strain BL21 (DE3) overexpressing the *kshA5* and *kshB* genes from *Rhodococcus. rhodochrous*. Cortisol (**1**) was chosen as a model steroidal structure.

Results and Discussion

Synthesis of starting compounds for enzymatic hydroxylation

In order to estimate the possible diversity of the substrates as starting materials for the biocatalytic transformation, cortisol (**1**) was converted to a hydroxylated steroid derivative **2** by reduction of the C20 carbonyl group with $NaBH_4$ and subsequent oxidative cleavage of the intermediate 17,20,21-trihydroxy side chain with $NaIO_4$ in 99% total yield (Scheme 2) [27].

The C11 hydroxy group was protected with acetic anhydride in the presence of a base, resulting in C11-protected product **3** in 93% yield. Performing the same reaction under microwave irradiation, a mixture of monoacylated and diacylated products **3** and **4** in 52% and 33% yield, respectively, was isolated [28].

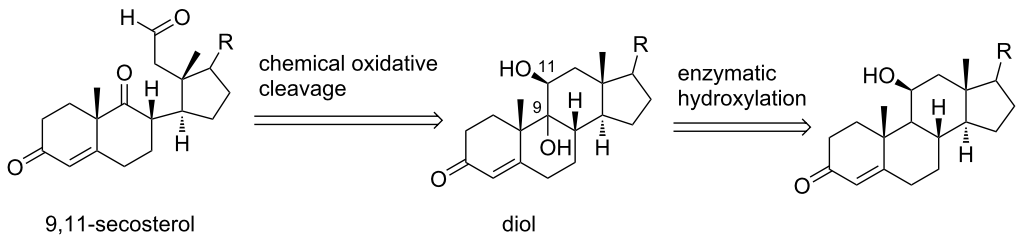

Scheme 1: Retrosynthetic analysis of 9,11-secosterols.

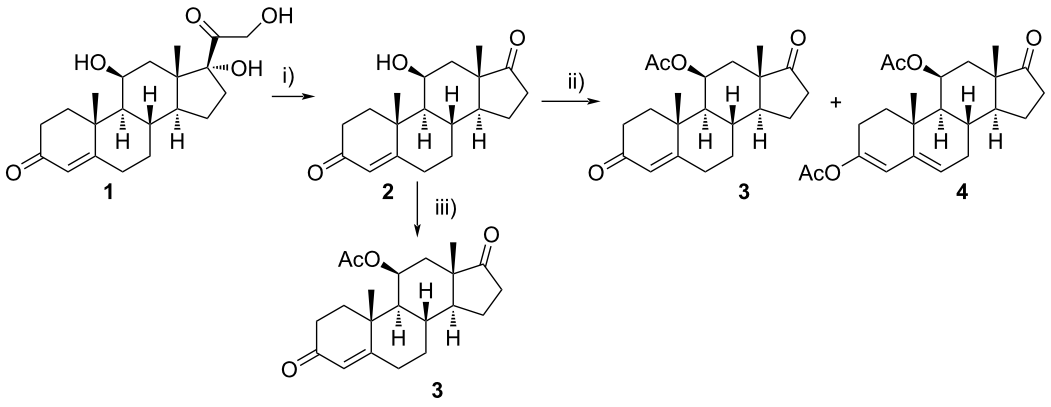

Scheme 2: Synthesis of starting materials. Reagents and conditions: i) $NaBH_4$, EtOH/CH_2Cl_2 1:1, 2 h, rt, then acetone, H_2O, $NaIO_4$, overnight, rt, 99%; ii) Ac_2O, *p*-TsOH (1 mol %), MW (800 W), 6 min, 52% for **3** and 33% for **4**; iii) Ac_2O, DMAP, Et_3N, CH_2Cl_2, overnight, rt, 93%.

Enzymatic hydroxylation

3-Ketosteroid 9α-hydroxylase (KSH) from *R. rhodochrous* has been shown to oxidize C9 in several steroids [29]. This enzyme consists of two polypeptides: KshA (terminal oxygenase) and KshB (ferredoxin reductase). When expressed together in *E. coli*, active KSH is formed, and several steroids can be oxidized in the C9 position [29,30]. Out of five KshA homologues found in *R. rhodochrous*, only KshA5 is able to utilize C11-hydroxylated cortisone, 11β-hydrocortisone, as a substrate [30].

For the construction of the biocatalyst, *kshA5* and *kshB* genes from *R. rhodochrous* were codon-optimized for enhanced expression in *E. coli* and cloned into a pET21a protein expression plasmid. To obtain an active biocatalyst, the plasmid was transformed into an *E. coli* BL21 (DE3) strain, and protein expression was induced by the addition of IPTG. Substrates of biocatalysis were added together with the IPTG inducer. The whole-cell biocatalysis was performed overnight at 30 °C in a rich medium with continuous shaking. Cell pellet and culture supernatant were collected the next morning for further analysis. A typical reaction contained approximately 40 mg of substrate in 200 mL culture medium, depending on the solubility and availability of substrates. This reaction can be scaled up by increasing the culture volume; the substrate concentration cannot be increased due to the low solubility of corticosteroids in aqueous solution. The expression of KshA5 and KshB was verified from the cell lysate by polyacrylamide gel electrophoresis and western blotting (see Supporting Information File 1, Figure S1). The product distribution between the cellular pellet and supernatant was approximately 1:10 (estimated by HRMS analysis). The steroid compounds were extracted from the supernatant and purified by column chromatography on silica gel as the stationary phase. The outcome of the enzymatic hydroxylation in position C9 using KSH-based biocatalysis is given in Table 1.

With substrates **1** and **2**, enzymatic hydroxylation proceeded efficiently and selectively at C9, affording *trans*-9,11-dihydroxysteroids **5** and **6** , respectively. For compound **5**, 67% of the starting compound was isolated. In Table 1, entry 2, several unidentified products were also formed. With 11-acetoxy steroid **3**, the C9-hydroxylated product **7** was isolated together with unreacted starting steroid **2**. Conjugated enol ester **4** did not react, and only the starting compound was detected in the reaction mixture. This indicates that the C3 carbonyl group in substrates is essential for enzymatic hydroxylation, as has been shown before [29]. A positive control experiment with the same batch of KSH-expressing *E. coli* cells using cortisol (**1**) as a substrate yielded C9-hydroxylated product **5**. From the results, we can also conclude that a protected C11 hydroxy group decreases the effectiveness of enzymatic transformation. Also, the substituent at C17 does not affect the KSH performance: steroids with C17 keto functionality (i.e., **2** and **3**) or cholesterol-like side chains at C20 (i.e., **1**) were all transformed efficiently to the corresponding 9,11-dihydroxylated products. ^1H and ^{13}C 1D and 2D (COSY, HSQ and HMBC) NMR spectra from samples **5** and **6** were analyzed, as were the spectra of the starting compounds **1** and **2**. The assignment of all ^1H and ^{13}C signals confirmed the preservation of the configuration of the ring system and substituents in these whole-cell transformations, as well as the OH group connections to C9.

Chemical oxidation of 9,11-dihydroxysteroids

In the final step, the obtained *trans*-diols **5** and **6** were subjected to the chemical oxidation of the 9,11 carbon bond. Lead tetraacetate is a classic oxidant for the cleavage of vicinal diols. However, there are serious drawbacks when using $Pb(OAc)_4$. In addition to its toxicity, the oxidation rate affording *trans*-diols was very slow in comparison to that for *cis*-diols. Using an even longer reaction time and stoichiometric amount of the reagent, diol **5** was not oxidized to the corresponding dicarbonyl com-

Table 1: Enzymatic hydroxylation.

entry	substrate	product	yield (%)[a]
1	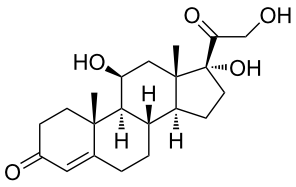 **1**	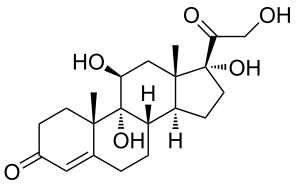 **5**	29
2	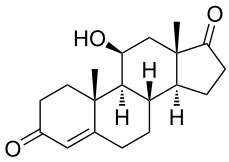 **2**	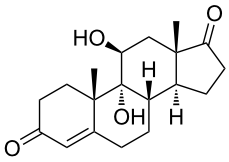 **6**	27
3[b]	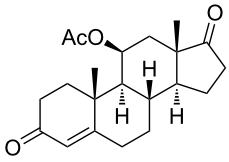 **3**	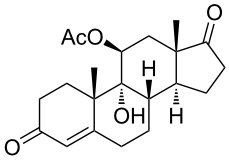 **7**	9
4[c]	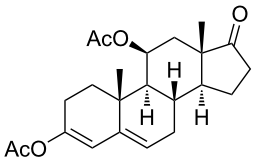 **4**	–	

[a]Isolated yield after column chromatography. [b]23% of starting material was recovered. [c]No products were formed, only starting substrate was detected.

pound **8**. However, using $NaOCl{\cdot}5H_2O$ as an oxidant [31], diols **5** and **6** were effectively converted to the corresponding 9,11-secosterols **8** and **9** within one hour at 0 °C (Scheme 3).

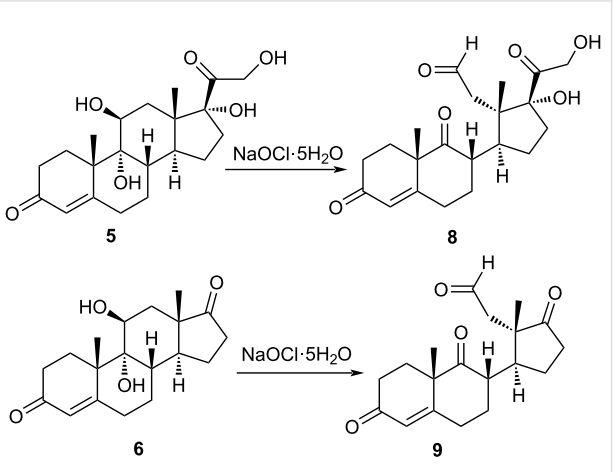

Scheme 3: Oxidation of diols **5** and **6** with $NaOCl{\cdot}5H_2O$.

Compound **8** was isolated as 2:1 mixture together with starting diol **5** and purified further by preparative TLC. Compound **9** was isolated as a single product in 87% yield.

Conclusion

We have presented the results of the synthesis of the 9,11-secosteroid carbon skeleton by using the designed whole-cell biotransformation of natural steroids with a genetically engineered biocatalyst. The enzymatic oxidation of cortisol derivatives is completely stereo- and regioselective, affording only 9α-hydroxylated diol. The following oxidative cleavage of the C–C bond with a mild oxidant leads to the steroid with an appropriately broken steroid skeleton. The method provides the target compound in only two steps, without any manipulations involving protecting groups. The present method features mild reaction conditions, and the protocol tolerates several functional groups. It is an environmentally benign approach, totally excluding the use of highly toxic oxidants. Our synthetic scheme provides a direct entry to structurally diverse 9,11-secosterols, enabling also studies of their biological properties.

Further research to broaden the scope of the presented synthetic scheme is ongoing.

Experimental

General data

Full assignment of ^{1}H and ^{13}C chemical shifts were based on the 1D and 2D FT NMR spectra, measured with a Bruker Avance III 400 MHz or a Bruker Avance III 800 MHz instrument. Residual solvent signals were used ($CDCl_3$: δ = 7.26 for ^{1}H NMR, δ = 77.2 for ^{13}C NMR or CD_3OD: δ = 3.31 for ^{1}H NMR, δ = 49.0 for ^{13}C NMR) as internal standards. Optical rotations were obtained by using an Anton Paar GWB Polarimeter MCP500. High-resolution mass spectra were recorded with an Agilent Technologies 6540 UHD Accurate-Mass QTOF LC/MS spectrometer by using AJ-ESI as an ionization method.

Construction of biocatalyst

Plasmid cloning and amplification were performed in *E. coli* DH5 strain. *E. coli* strain BL21 (DE3) was used for biocatalysis experiments. Lysogeny broth (LB) medium was used for all cell-growth incubations. For the selection of plasmids, 100 μg/mL ampicillin was used.

Plasmid pAJ30 for heterologous expression of *kshA5* and *kshB* was constructed using the CPEC method [32]. *kshA5* and *kshB* gene sequences from *R. rhodochrous* were codon-optimized for high-level expression in *E. coli* using the IDT codon optimization tool (to eliminate rare codons). Synthetic DNA was ordered from Twist Bioscience and inserted into pET21a backbone as one operon (see Supporting Information File 2) under the control of an IPTG-inducible tac promoter. The obtained plasmid was verified by DNA sequencing. To obtain the biocatalyst strain, the plasmid pAJ30 was transformed into chemically competent *E. coli* BL21 (DE3) cells.

Enzymatic hydroxylation

3 mL precultures of BL21(DE3) transformed with pAJ30 plasmid (biocatalyst) or without plasmid (negative control) were grown overnight at 37 °C. The next morning, 200 mL of LB medium in a 2 L baffled flask was inoculated with 1 mL of a preculture. The cultures were grown until OD_{600} = 0.1 at 37 °C with continuous shaking at 220 rpm, and then the expression was induced by adding 1 mM IPTG and a substrate (compound **1**–**4**, respectively) at a final concentration of 225 μg/mL, 175 μg/mL, 190 μg/mL or 122 μg/mL, respectively. The biocatalysis was carried out for 20 hours at 30 °C with continuous shaking at 220 rpm. The next morning, the cells were harvested by centrifugation at 4,000*g*, and cell pellet and culture supernatant were stored at a temperature of −20 °C until further analysis.

Synthesis of substrates

11β-Hydroxyandrost-4-ene-3,17-dione (**2**)

To a stirred solution of cortisol (**1**, 1.2 g, 3.36 mmol) in a 1:1 mixture of EtOH and CH_2Cl_2 (23 mL), $NaBH_4$ (51.2 mg, 1.35 mmol) was added in one portion at room temperature. After 2 h, acetone (5.8 mL) was added, followed by water (5.8 mL) and $NaIO_4$ (1.8 g, 8.41 mmol). The solution was stirred overnight at room temperature. Water (115 mL) was added, and the reaction mixture was extracted with $CHCl_3$ (3 × 50 mL). The combined organic layers were dried over sodium sulfate and filtered. After evaporation of the solvent, ketone **2** (1.01 g, 99%) was isolated as white amorphous solid. $[\alpha]_D^{20}$ +177.4 (*c* 0.46, $CHCl_3$); ^{1}H NMR ($CDCl_3$, 400 MHz) δ 5.69 (d, *J* = 1.3 Hz, 1H), 4.45 (q, *J* = 3.0 Hz, 1H), 2.58–1.97 (m, 10H), 1.95 (dd, *J* = 14.4, 2.7 Hz, 1H), 1.85 (td, *J* = 13.5, 4.6 Hz, 1H), 1.73–1.58 (m, 1H), 1.52–1.47 (m, 1H), 1.46 (s, 3H), 1.34–1.18 (m, 2H), 1.16 (s, 3H), 1.14–1.06 (m, 1H), 1.00 (dd, *J* = 11.1, 3.3 Hz, 1H); ^{13}C NMR ($CDCl_3$, 101 MHz) δ 219.19, 199.48, 171.63, 122.70, 68.07, 56.80, 52.49, 46.84, 41.13, 39.43, 35.41, 35.15, 33.93, 31.95, 31.62, 31.09, 21.80, 21.20, 15.99; HRMS (*m*/*z*): $[M + H]^+$ calcd, 303.1955; found, 303.1961.

11β-Acetoxyandrost-4-ene-3,17-dione (**3**)

Starting steroid **2** (202 mg, 0.67 mmol, 1 equiv) was dissolved in dry dichloromethane (9.8 mL), and after that 4-(dimethylamino)pyridine (8.2 mg, 0.067 mmol, 0.1 equiv), triethylamine (373 μL, 2.67 mmol, 4 equiv) and acetic anhydride (316 μL, 3.34 mmol, 5 equiv) were added. The mixture was stirred under argon atmosphere overnight at room temperature. Saturated aqueous NH_4Cl (4.11 mL) was added, and the reaction mixture was extracted with CH_2Cl_2 (4 × 6 mL). The combined organic layers were dried over sodium sulfate, filtered and then concentrated in vacuo. The residue was chromatographed on silica gel with gradient 10% to 40% acetone in petroleum ether to give acetate **3** (213.2 mg, 93%) as pale yellow oil. $[\alpha]_D^{20}$ +180.0 (*c* 0.58, $CHCl_3$); ^{1}H NMR ($CDCl_3$, 400 MHz) δ 5.68 (d, *J* = 1.4 Hz, 1H), 5.47 (q, *J* = 3.1 Hz, 1H), 2.57–2.21 (m, 6H), 2.20–2.05 (m, 4H), 2.04 (s, 3H), 1.99 (m, 1H), 1.85–1.74 (m, 1H), 1.69–1.60 (m, 1H), 1.42 (dd, *J* = 14.9, 3.3 Hz, 1H), 1.28 (s, 3H), 1.21–1.10 (m, 3H), 1.03 (s, 3H); ^{13}C NMR ($CDCl_3$, 101 MHz) δ 217.94, 198.85, 170.13, 169.58, 123.08, 69.41, 55.60, 52.11, 46.48, 38.76, 36.99, 35.48, 35.27, 33.71, 31.82, 31.65, 31.34, 21.90, 21.71, 20.87, 15.56; HRMS (*m*/*z*): $[M + H]^+$ calcd, 345.2060; found, 345.2078.

3,11β-Bis(acetyloxy)androsta-3,5-dien-17-one (**4**)

The general procedure of Marwah et al. [28] was followed with modifications. A mixture of steroid **2** (254 mg, 0.84 mmol, 1 equiv), acetic anhydride (475 μL, 5.03 mmol, 6 equiv) and

p-toluenesulfonic acid monohydrate (2.8 mg, 0,008 mmol, 0,01 equiv) in a beaker was subjected to continuous mode of microwave irradiation (800 W) at high power setting in a domestic microwave oven for 6 min. After this, the mixture was cooled to room temperature, and saturated aqueous $NaHCO_3$ (5 mL) was added, after which this was mixed and extracted with EtOAc (5 mL). The organic layer was dried over magnesium sulfate, filtered and concentrated in vacuo. The residue was chromatographed on silica gel with gradient 7% to 30% acetone in petroleum ether to give monoacetate **3** (151 mg, 52%) and diacetate **4** (107 mg, 33%). Diacetate **4**: ^{1}H NMR ($CDCl_3$, 400 MHz) δ 5.66 (d, *J* = 2.1 Hz, 1H), 5.50 (q, *J* = 3.2 Hz, 1H), 5.33 (t, *J* = 3.8 Hz, 1H), 2.67–2.36 (m, 4H), 2.29 (m, 1H), 2.12 (s, 3H), 2.11–2.04 (m, 4H), 2.03 (s, 3H), 2.01–1.96 (m, 1H), 1.95–1.84 (m, 1H), 1.75 (dd, *J* = 12.7, 4.2 Hz, 1H), 1.70–1.62 (m, 1H), 1.51–1.12 (m, 2H), 1.08 (s, 3H), 1.03 (s, 3H); ^{13}C NMR ($CDCl_3$, 101 MHz) δ 218.48, 169.85, 169.41, 147.42, 140.45, 122.24, 116.12, 69.66, 53.31, 50.99, 46.72, 37.01, 35.38, 34.90, 33.49, 30.73, 28.37, 24.60, 21.96, 21.79, 21.54, 21.21, 15.50; HRMS (*m*/*z*): $[M + H]^+$ calcd, 387.2166; found, 387.2167.

Isolation of 9-hydroxysteroids

A frozen culture supernatant was melted at room temperature or in a warm water bath, then poured into the separation funnel, saturated by the addition of solid sodium chloride and extracted with EtOAc. The extract was concentrated in vacuo to give a solid residue that was chromatographed on silica gel. Elution with acetone/petroleum ether solvent system (30% to 50% for **5** and **6**, 10% to 30% for **7**) afforded the product.

9-Hydroxysteroids

9α,11β,17α,21-Tetrahydroxypregn-4-ene-3,20-dione (**5**)

Compound **5** was further purified by column chromatography on silica gel with 10% MeOH/$CHCl_3$. $[\alpha]_D^{20}$ +119.2 (*c* 0.66, MeOH); ^{1}H NMR (MeOD, 400 MHz) δ 5.72 (s, 1H), 4.64 (d, *J* = 19.2 Hz, 1H), 4.26 (d, *J* = 19.1 Hz, 1H), 4.05 (t, 1H), 2.73 (ddd, *J* = 14.2, 11.2, 2.7 Hz, 1H), 2.67–2.54 (m, 1H), 2.53–2.46 (m, 2H), 2.43–2.22 (m, 8H), 2.02–1.94 (m, 1H), 1.70 (dt, *J* = 10.9, 5.6 Hz, 2H), 1.58 (s, 3H), 1.49 (ddd, *J* = 14.9, 9.2, 6.4 Hz, 1H), 1.42–1.36 (m, 2H), 0.87 (s, 3H); ^{13}C NMR (CD_3OD, 201 MHz) δ 213.08, 202.81, 176.40, 124.85, 90.50, 78.81, 73.87, 67.69, 48.27, 46.75, 46.25, 36.83, 35.36, 34.86, 34.75, 32.33, 29.11, 26.84, 24.54, 22.49, 17.60; HRMS (*m*/*z*): $[M + H]^+$ calcd, 303.1955; found, 303.1961.

9α,11β-Dihydroxyandrost-4-ene-3,17-dione (**6**)

^{1}H NMR (CD_3OD, 800 MHz) δ 5.74 (ddd, *J* = 2.1, 0.8, 0.5 Hz, 1H), 4.03 (dd, *J* = 3.3, 2.6 Hz, 1H), 2.64 (dddd, *J* = 15.4, 13.3, 6.9, 2.1 Hz, 1H), 2.53 (ddd, *J* = 12.5, 11.2, 4.7 Hz, 1H), 2.52 (ddd, *J* = 16.1, 14.4, 5.3 Hz, 1H), 2.48 (ddd, 19.2, 8.8, 0.9 Hz, 1H), 2.45 (dddd, *J* = 14.4, 13.0, 4.3, 0.5 Hz, 1H), 2.34 (dddd, *J* = 16.1, 4.3, 3.1, 0.8 Hz, 1H), 2.30 (dddd, *J* = 15.4, 5.6, 1.5, 0.5 Hz, 1H), 2.06 (dt, *J* = 19.2, 8.8, 8.8 Hz, 1H), 1.99 (ddd, *J* = 13.0, 5.3, 3.2 Hz, 1H), 1.91 (m, 1H), 1.89 (m, 1H), 1.82 (ddddd, *J* = 13.3, 6.9, 4.7, 1.5, 0.5 Hz, 1H), 1.73 (bdd, *J* = 14.0, 3.3 Hz, 1H), 1.72 (dd, *J* = 14.0, 2.6 Hz, 1H), 1.68 (m, 1H), 1.66 (dddd, *J* = 13.3, 13.3, 12.5, 5.6 Hz, 1H), 1.61 (d, *J* = 0.5 Hz, 3H), 1.16 (s, 3H); ^{13}C NMR (CD_3OD, 201 MHz) δ 222.73, 202.58, 175.91, 124.93, 79.13, 73.30, 48.17, 46.78, 46.50, 37.32, 36.34, 34.80, 34.76, 32.08, 29.01, 25.55, 22.46, 22.35, 15.89; HRMS (*m*/*z*): $[M + H]^+$ calcd, 319.1904; found, 319.1866.

9α-Hydroxy-11β-acetyloxyandrost-4-ene-3,17-dione (**7**)

$[\alpha]_D^{20}$ +157.3 (*c* 0.23, $CHCl_3$); ^{1}H NMR (MeOD, 400 MHz) δ 5.75 (d, *J* = 1.9 Hz, 1H), 5.10 (t, *J* = 3.0 Hz, 1H), 2.60–2.41 (m, 4H), 2.38–2.27 (m, 2H), 2.16 (d, *J* = 9.5 Hz, 4H), 2.07 (s, 3H), 2.05–1.91 (m, 1H), 1.85 (dddd, *J* = 13.4, 6.8, 4.8, 1.7 Hz, 1H), 1.78 (d, *J* = 3.0 Hz, 2H), 1.73–1.64 (m, 1H), 1.62–1.52 (m, 1H), 1.49 (s, 3H), 1.05 (s, 3H); ^{13}C NMR (MeOD, 101 MHz) δ 221.00, 201.81, 174.03, 170.77, 125.22, 56.05, 47.45, 46.22, 46.01, 36.17, 35.43, 34.63, 33.93, 32.02, 29.74, 29.53, 25.38, 22.82, 22.25, 21.63, 15.59; HRMS (*m*/*z*): $[M + Na]^+$ calcd, 383.1829; found, 383.1825.

Chemical oxidation of 9,11-dihydroxysteroids

The general procedure of Kirihara et al. [31] was followed. Sodium hypochlorite pentahydrate (3 equiv) was added to a stirred solution of diol (1 equiv) and tetrabutylammonium hydrogen sulfate (0.1 equiv) in dichloromethane (8 mL/mmol diol) and water (2.7 mL/mmol diol) at 0 °C. The resulting mixture was stirred for 1 h and monitored by TLC analysis (10% MeOH in $CHCl_3$). Water (2.7 mL/mmol diol) was added, and the reaction mixture was extracted with CH_2Cl_2 (2 × 32 mL/mmol diol). The combined organic layers were dried over anhydrous sodium sulfate, filtered and then concentrated in vacuo.

17α,21-Dihydroxy-3,9,20-trioxo-9,11-seco-pregn-4-en-11-al (**8**)

Compound **8** was obtained as a mixture with **5** in the ratio 2:1. Compound **8** was further purified by preparative TLC (10% MeOH in $CHCl_3$); ^{1}H NMR (MeOD, 400 MHz) δ 9.60 (s, 1H, H-11), 5.81 (d, *J* = 2.3 Hz, 1H, H-4), 1.50 (s, 3H, 19-Me), 0.83 (s, 3H, 18-Me); ^{13}C NMR ($CDCl_3$, 101 MHz) δ 221.31 (C9), 211.52 (C20), 200.50 (C11), 198.19 (C3), 165.72 (C5), 125.90 (C4); HRMS (*m*/*z*): $[M + H]^+$ calcd, 377.1959; found, 377.1944.

3,9-Dioxo-9,11-secoandrost-4-en-11-al (**9**)

Compound **9** was obtained as pure compound with a yield of 87%. $[\alpha]_D^{20}$ +57.1 (*c* 0.42, $CHCl_3$); ^1H NMR ($CDCl_3$, 400 MHz) δ 9.69 (d, *J* = 0.8 Hz, 1H), 5.83 (d, *J* = 2.0 Hz, 1H), 3.40–3.28 (m, 1H), 3.00–2.73 (m, 5H), 2.66–2.54 (m, 2H), 2.51–2.36 (m, 2H), 2.30–2.16 (m, 1H), 2.10–2.01 (m, 1H), 1.95 (ddd, *J* = 14.1, 4.8, 3.2 Hz, 1H), 1.74–1.53 (m, 1H), 1.51 (s, 3H), 1.49–1.37 (m, 2H), 0.84 (s, 3H); ^{13}C NMR ($CDCl_3$, 101 MHz) δ 221.30, 211.50, 200.48, 198.17, 165.72, 125.87, 51.55, 51.30, 48.56, 47.37, 39.82, 36.20, 33.60, 32.45, 29.62, 28.98, 23.72, 22.99, 18.49; HRMS (*m*/*z*): $[M + H]^+$ calcd, 317.1747; found, 317.1755.

Supporting Information

Supporting Information File 1

General material and methods for the construction of the biocatalyst as well as NMR spectra of synthesized compounds.
[https://www.beilstein-journals.org/bjoc/content/supplementary/1860-5397-17-52-S1.pdf]

Supporting Information File 2

DNA sequence.
[https://www.beilstein-journals.org/bjoc/content/supplementary/1860-5397-17-52-S2.gb]

Funding

The authors thank the Estonian Ministry of Education and Research (Grant Nos. PRG657 and PRG1031) and the Centre of Excellence in Molecular Cell Engineering (2014-2020.4.01.15-0013) for financial support.

ORCID® iDs

Marje Kasari - https://orcid.org/0000-0002-2177-3753
Villu Kasari - https://orcid.org/0000-0002-2970-2001
Ivar Järving - https://orcid.org/0000-0001-6047-4759
Arvi Jõers - https://orcid.org/0000-0003-2083-3977
Tõnis Kanger - https://orcid.org/0000-0001-5339-9682

References

1. Li, J.; Amatuni, A.; Renata, H. *Curr. Opin. Chem. Biol.* **2020,** *55,* 111–118. doi:10.1016/j.cbpa.2020.01.005
2. Fryszkowska, A.; Peterson, J.; Davies, N. L.; Dewar, C.; Evans, G.; Bycroft, M.; Triggs, N.; Fleming, T.; Gorantla, S. S. C.; Hoge, G.; Quirmbach, M.; Timmanna, U.; Poreddy, S. R.; Reddy, D. N. K.; Dahanukar, V.; Holt-Tiffin, K. E. *Org. Process Res. Dev.* **2016,** *20,* 1520–1528. doi:10.1021/acs.oprd.6b00215
3. Carvalho, J. F. S.; Silva, M. M. C.; Moreira, J. N.; Simões, S.; Melo, M. L. S. *J. Med. Chem.* **2009,** *52,* 4007–4019. doi:10.1021/jm9003973
4. Contente, M. L.; Molinari, F.; Serra, I.; Pinto, A.; Romano, D. *Eur. J. Org. Chem.* **2016,** 1260–1263. doi:10.1002/ejoc.201501557
5. Noack, F.; Heinze, R. C.; Heretsch, P. *Synthesis* **2019,** *51,* 2039–2057. doi:10.1055/s-0037-1611576
6. Duecker, F. L.; Reuß, F.; Heretsch, P. *Org. Biomol. Chem.* **2019,** *17,* 1624–1633. doi:10.1039/c8ob02325e
7. Enwall, E. L.; van der Helm, D.; Hsu, I. N.; Pattabhiraman, T.; Schmitz, F. J.; Spraggins, R. L.; Weinheimer, A. J. *J. Chem. Soc., Chem. Commun.* **1972,** 215–216. doi:10.1039/c39720000215
8. Koljak, R.; Pehk, T.; Järving, I.; Liiv, M.; Lopp, A.; Varvas, K.; Vahemets, A.; Lille, Ü.; Samel, N. *Tetrahedron Lett.* **1993,** *34,* 1985–1986. doi:10.1016/s0040-4039(00)91981-6
9. Lopp, A.; Pihlak, A.; Paves, H.; Samuel, K.; Koljak, R.; Samel, N. *Steroids* **1994,** *59,* 274–281. doi:10.1016/0039-128x(94)90113-9
10. Koljak, R.; Lopp, A.; Pehk, T.; Varvas, K.; Müürisepp, A.-M.; Järving, I.; Samel, N. *Tetrahedron* **1998,** *54,* 179–186. doi:10.1016/s0040-4020(97)10268-x
11. Huang, C.-Y.; Su, J.-H.; Duh, C.-Y.; Chen, B.-W.; Wen, Z.-H.; Kuo, Y.-H.; Sheu, J.-H. *Bioorg. Med. Chem. Lett.* **2012,** *22,* 4373–4376. doi:10.1016/j.bmcl.2012.05.002
12. Chang, Y.-C.; Hwang, T.-L.; Kuo, L.-M.; Sung, P.-J. *Mar. Drugs* **2017,** *15,* 11.
13. He, Y.-Q.; Lee Caplan, S.; Scesa, P.; West, L. M. *Steroids* **2017,** *125,* 47–53. doi:10.1016/j.steroids.2017.06.008
14. Chang, Y.-C.; Lai, K.-H.; Kumar, S.; Chen, P.-J.; Wu, Y.-H.; Lai, C.-L.; Hsieh, H.-L.; Sung, P.-J.; Hwang, T.-L. *Mar. Drugs* **2020,** *18,* 271.
15. Sica, D.; Musumeci, D. *Steroids* **2004,** *69,* 743–756. doi:10.1016/j.steroids.2004.09.001
16. Adinolfi, R.; Migliuolo, A.; Piccialli, V.; Sica, D. *J. Nat. Prod.* **1994,** *57,* 1220–1226. doi:10.1021/np50111a005
17. Jäälaid, R.; Järving, I.; Pehk, T.; Lille, Ü. *Proc. Est. Acad. Sci., Chem.* **1998,** *47,* 39–43.
18. Kuhl, A.; Kreiser, W. *Tetrahedron Lett.* **1998,** *39,* 1145–1148. doi:10.1016/s0040-4039(97)10875-9
19. Jäälaid, R.; Järving, I.; Pehk, T.; Parve, O.; Lille, Ü. *Nat. Prod. Lett.* **2001,** *15,* 221–228. doi:10.1080/10575630108041285
20. Kongkathip, B.; Hasakunpaisarn, A.; Boonananwong, S.; Kongkathip, N. *Steroids* **2010,** *75,* 834–847. doi:10.1016/j.steroids.2010.05.003
21. Salvador, J. A. R.; Silvestre, S. M.; Moreira, V. M. *Curr. Org. Chem.* **2012,** *16,* 1243–1276. doi:10.2174/138527212800564204
22. Warnke, M.; Jung, T.; Dermer, J.; Hipp, K.; Jehmlich, N.; von Bergen, M.; Ferlaino, S.; Fries, A.; Müller, M.; Boll, M. *Angew. Chem., Int. Ed.* **2016,** *55,* 1881–1884. doi:10.1002/anie.201510331
23. Ferrandi, E. E.; Bertuletti, S.; Monti, D.; Riva, S. *Eur. J. Org. Chem.* **2020,** 4463–4473. doi:10.1002/ejoc.202000192
24. Li, A.; Acevedo-Rocha, C. G.; D'Amore, L.; Chen, J.; Peng, Y.; Garcia-Borràs, M.; Gao, C.; Zhu, J.; Rickerby, H.; Osuna, S.; Zhou, J.; Reetz, M. T. *Angew. Chem., Int. Ed.* **2020,** *59,* 12499–12505. doi:10.1002/anie.202003139
25. Acevedo-Rocha, C. G.; Gamble, C. G.; Lonsdale, R.; Li, A.; Nett, N.; Hoebenreich, S.; Lingnau, J. B.; Wirtz, C.; Fares, C.; Hinrichs, H.; Deege, A.; Mulholland, A. J.; Nov, Y.; Leys, D.; McLean, K. J.; Munro, A. W.; Reetz, M. T. *ACS Catal.* **2018,** *8,* 3395–3410. doi:10.1021/acscatal.8b00389

26. Kerr, R. G.; Rodriguez, L. C.; Keliman, J. *Tetrahedron Lett.* **1996,** *37,* 8301–8304. doi:10.1016/0040-4039(96)01942-9
27. Wüst, F.; Carlson, K. E.; Katzenellenbogen, J. A. *Steroids* **2003,** *68,* 177–191. doi:10.1016/s0039-128x(02)00171-x
28. Marwah, P.; Marwah, A.; Lardy, H. A. *Tetrahedron* **2003,** *59,* 2273–2287. doi:10.1016/s0040-4020(03)00207-2
29. Petrusma, M.; Dijkhuizen, L.; van der Geize, R. *Appl. Environ. Microbiol.* **2009,** *75,* 5300–5307. doi:10.1128/aem.00066-09
30. Petrusma, M.; Hessels, G.; Dijkhuizen, L.; van der Geize, R. *J. Bacteriol.* **2011,** *193,* 3931–3940. doi:10.1128/jb.00274-11
31. Kirihara, M.; Osugi, R.; Saito, K.; Adachi, K.; Yamazaki, K.; Matsushima, R.; Kimura, Y. *J. Org. Chem.* **2019,** *84,* 8330–8336. doi:10.1021/acs.joc.9b01132
32. Quan, J.; Tian, J. *Nat. Protoc.* **2011,** *6,* 242–251. doi:10.1038/nprot.2010.181

License and Terms

BEILSTEIN JOURNAL OF ORGANIC CHEMISTRY

Valorisation of plastic waste via metal-catalysed depolymerisation

Francesca Liguori, Carmen Moreno-Marrodán and Pierluigi Barbaro*

Review

Open Access

Address:
Consiglio Nazionale delle Ricerche, Istituto di Chimica dei Composti Organo Metallici, Via Madonna del Piano 10, 50019 Sesto Fiorentino, Firenze, Italy

Email:
Pierluigi Barbaro* - pierluigi.barbaro@iccom.cnr.it

* Corresponding author

Keywords:
catalysis; depolymerisation; plastic; recycling; sustainable

Beilstein J. Org. Chem. **2021,** *17,* 589–621.
https://doi.org/10.3762/bjoc.17.53

Received: 23 November 2020
Accepted: 05 February 2021
Published: 02 March 2021

This article is part of the thematic issue "Green chemistry II".

Associate Editor: L. Vaccaro

Abstract

Metal-catalysed depolymerisation of plastics to reusable building blocks, including monomers, oligomers or added-value chemicals, is an attractive tool for the recycling and valorisation of these materials. The present manuscript shortly reviews the most significant contributions that appeared in the field within the period January 2010–January 2020 describing selective depolymerisation methods of plastics. Achievements are broken down according to the plastic material, namely polyolefins, polyesters, polycarbonates and polyamides. The focus is on recent advancements targeting sustainable and environmentally friendly processes. Biocatalytic or unselective processes, acid–base treatments as well as the production of fuels are not discussed, nor are the methods for the further upgrade of the depolymerisation products.

Review

1. Introduction

In a circular-economy perspective, wastes are deemed precious feedstock usable in the production of fertilisers, fuels, chemicals and a variety of materials for packaging, housing, transport and clothing [1,2]. A considerable fraction of the waste currently produced by our society is due to plastics, which is a major problem [3,4]. Plastics are usually synthetic polymers recalcitrant to decomposition, and hence liable to accumulate in landfills or the environment when discarded [5,6]. Not all plastics can be reused, and thus having limited economic value [7,8]. Plastics may release toxic compounds dangerous to human health and the habitat [9,10]. Plastic materials are ubiquitous in our everyday life, which accounts for a global production of plastics of around 360 million tons in 2018 [11], of which more than 60% are disposed [12,13]. As a consequence, pollution from plastics is impressive, resulting in the diffusion of microplastics into soil [14,15], oceans [16,17], crustaceans [18] and rain [19].

Valorisation of plastic waste, via chemical conversion into reusable building blocks, may contribute to solving these prob-

lems while representing a strategy to reduce the carbon footprint of the chemical industry [20,21]. The approach deepens the concept of plastic recycling [22,23], first of all requiring a careful design of efficient and controlled depolymerisation processes. Despite of this hurdle, the implementation of effective plastics value chains through recovery, reprocessing and upgrade would be a tangible mean to turn a challenge into an opportunity [24,25]. The waste-to-products strategy is already in place for both animal [26,27] and plant biomass polymeric waste [28,29], for which mature technologies are operative [30].

When referring to polymers in general, there is often a lack of univocal definitions, which may lead to confusion between terminologies used as synonyms, though they are not [31,32]. The IUPAC recommendations provide a useful reference to this aim [33]. Thus, “degradation” is a broad term describing the “progressive loss of the performance or of the characteristics of a substance" due to the action of chemical (acids, air, halogens, solvents) or physical agents (heat, light). For polymers, the properties involved are, for instance, tensile strength, colour or shape, the change of which is usually associated with a modification of the chemical composition (e.g., as a consequence of oxidation, cross-linkage, bond cleavage). The term “biodegradation” indicates a “degradation caused by enzymatic processes resulting from the action of cells”. Although commonly used, also for artificial polymers, the term “biodegradable” specifically refers to biorelated polymers (i.e., proteins, nucleic acids, polysaccharides), which are "susceptible to degradation by biological activity by lowering of the molar masses of macromolecules". Therefore, in this situation, “chain cleavage” and “degradation” are used interchangeably. To avoid confusion, instead of “(bio)degradation”, in the present review, we will use the term “depolymerisation” to identify the “process of converting a macromolecule into (recoverable) monomers or a mixture of monomers". Another relevant definition is that of “bioplastic”, meaning “biobased polymer derived from the biomass or issued from monomers derived from the biomass”, wherein “biobased” indicates “composed or derived in whole or in part of biological products issued from the biomass”. Also, there is no universally accepted definition for “compostable”, as it differs between diverse issuers [34]. The criteria indicated by the European Commission through the standard EN 13432 “Packaging–Requirements for packaging recoverable through composting and biodegradation” include disintegration (i.e., breakdown of material to particles of a defined size), biodegradability, absence of negative effects on the composting process and amount of heavy metals below given maximum values [35,36].

“Recycling” itself is a general term for which multiple definitions exist, depending on the year and the author [37]. Plastics manufacturers have also delivered their own guidelines under the name “Design for Recycling” [38,39]. A generally accepted definition for plastic recycling is “the process of recovering scrap or waste plastics and reprocessing the material into useful products, sometimes completely different in form from their original state” [40,41]. A possible classification of reported plastic recycling techniques is schematically shown in Figure 1 [42], wherein breakdown by the recycled polymer, the final product or the process involved further differentiates between methods, which may lead to occasional overlaps and inconsistencies [43,44].

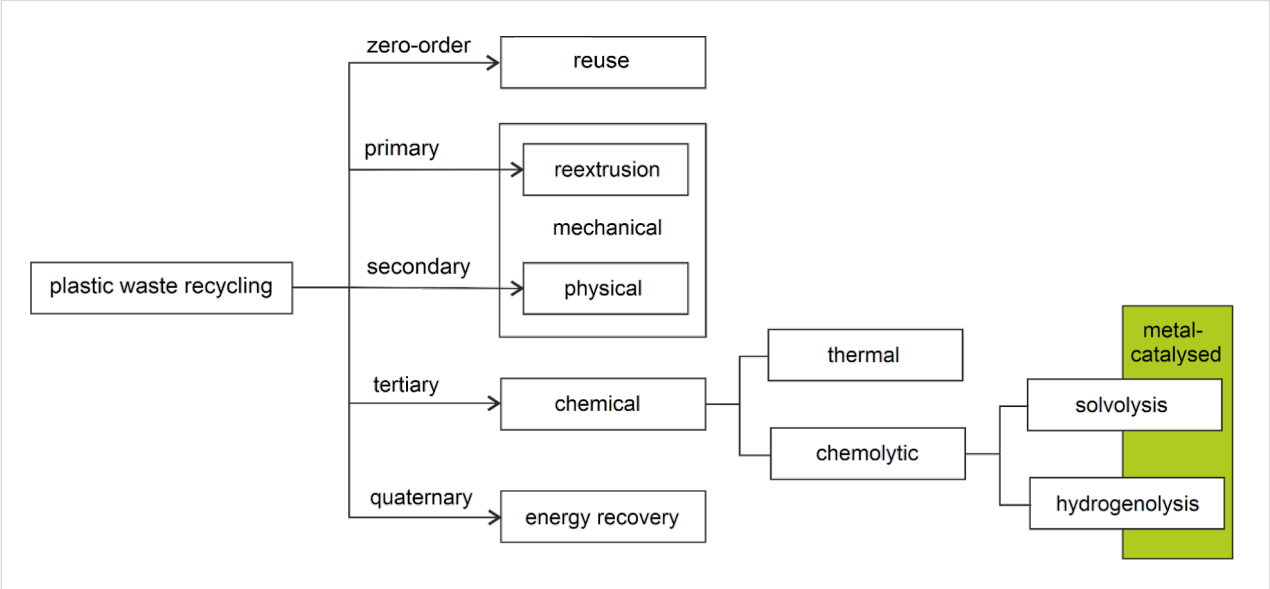

Figure 1: Potential classification of plastic recycling processes. The area covered by the present review is highlighted in green.

"Reuse" is considered a zero-order recycling option, meaning "any operation by which products or components that are not waste are used again for the same purpose for which they were conceived" [45]. A typical example are plastic containers that are washed and reused as they are [46]. True recycling includes "any recovery operation by which waste materials are reprocessed into products, materials or substances whether for the original or other purposes. It includes the reprocessing of organic material but does not include energy recovery and the reprocessing into materials that are to be used as fuels" [45]. Therein, three options can be distinguished. "Reextrusion" (also known as closed-loop recycling) refers to the recycling of clean, uncontaminated single-polymer materials to give products with analogous performance and applications [47]. For example, polyethylene bottles are recycled into new bottles. Similarly, in "physical recycling", the polymeric structure of the original material is maintained, although purification steps, the addition of additives or blending with fresh polymers may be included [48]. For this reason, both reextrusion and physical recycling are also referred to as "mechanical recycling", primary and secondary, respectively [49,50]. However, materials of lower quality and economic value can be obtained [51,52]. By contrast, the term "chemical recycling" (or feedstock recycling) refers to those processes involving an alteration of the polymeric chain due to breakage of chemical bonds [53,54]. This definition may be confusing since chain scission may actually occur using either physical (heat) or chemical agents. Indeed, chemical recycling processes can be divided into two main categories: thermochemical and chemolytic routes. All of these processes may result in a variety of valuable products and the mixture thereof, including C1 molecules (CO, CO_2, CH_4), H_2O and H_2 due to complete decomposition of the polymeric chain, monomers or oligomers, depending on the waste polymer and the process. The as-obtained compounds can be reused as raw materials for the process industry (hence the term feedstock) to produce chemicals, fuels or other polymers. Thermochemical processes include pyrolysis [55], catalytic cracking [56] and gasification [57]. These are usually unselective, high-temperature treatments (300–1000 °C) that may efficiently provide light hydrocarbons or small molecules [58,59]. Chemolytic processes, wherein a chemical reagent is used to achieve depolymerisation, mainly involve solvolysis (a solvent is the reagent and solvolyses include hydrolysis, glycolysis, alcoholysis and aminolysis) and hydrogenolysis reactions (H_2 as reagent). Hydrolysis (sometimes called hydrocracking) is in between thermochemical and chemolytic processing, basically consisting of depolymerisation by the combined action of heat and dihydrogen [60]. Chemolytic processes may or may not be catalytic. They will be discussed in detail in the following section. A fourth option is "energy recovery". Strictly speaking, this cannot be considered as recycling, consisting in the recovery of the energy contained in a material rather than the material itself, and it is usually achieved by combustion or incineration [61,62]. This method is generally used for plastics that cannot be economically recycled by other means [63,64]. However, it often entails the emission of toxic volatile compounds (furans, dioxins) [65]. The tar obtained may be used for road construction [66].

The present paper shortly reviews the most significant contributions that appeared in the literature, from January 2010 to January 2020, in the field of metal-catalysed selective depolymerisation of plastics to reusable monomers, oligomers or added-value chemicals (see Figure 1). Scientific achievements will be described according to the plastic substrate, irrespective of the metal catalyst. Uncatalysed depolymerisations, full chain-cracking or unselective processes, acid–base treatments, as well as the production of fuels from plastics, will not be covered. Conversion of plastic waste to fuels [67,68] and biocatalytic depolymerisation methods [69,70] have been extensively and recently reviewed elsewhere, hence they will not be considered herein.

2. Depolymerisation of plastics

As outlined above, depolymerisation of plastic waste to reusable building blocks is an attractive option for effective recycling and valorisation. This is most conveniently achieved through chemolytic processes because of the higher selectivity and lower energy inputs compared to thermochemical approaches [71]. This is a "hot" research topic, mainly due to the few industrial applications developed in the field so far, despite the urgent need for innovative technologies that overcome the high costs of recycling, the legal constraints for dumping, the accumulation of plastic scraps and the dependence on nonrenewable (fossil) sources [72,73]. A reason for this underdevelopment is that chemolysis of plastics is still challenging due to multiple critical factors: i) the achievement of selective depolymerisation is only possible by carefully controlled reaction conditions, ii) the related processes must be "green" and economically viable and, iii) tailored solutions are required to overcome the chemical inertness for, and the thermodynamic limitations of the reversal of each polymer. Indeed, the ease (and outcome) of chain scission does not depend on the origin of the polymer but on its chemical structure [74,75]. For instance, plastics derived from biomass are not necessarily biodegradable, particularly if similar to those obtained from petroleum sources [76,77]. For depolymerisation to be effective at reasonable operating temperature and selective, the plastic substrate should in principle originate from low-exergonic polymerisation reactions [78]. This justifies for the easier depolymerisation of polyesters and polycarbonates compared to polyolefins [79,80]. By contrast, poor selectivity and slow kinetics of depolymerisation can be circumvented using a catalyst.

2.1 Chemolysis

Several catalytic depolymerisation processes of plastics have been developed, using a solvent or molecular hydrogen as cleaving agents [81]. The main solvolytic process include:

- hydrolysis (water)
- alcoholysis (methanol, ethanol, 1-butanol, 2-ethyl-1-hexanol, phenol)
- glycolysis (ethylene glycol (EG), 1,2-propanediol (PD), 1,3- and 1,4-butanediol (BD)), diethylene glycol (DEG), dipropylene glycol (DPG))
- aminolysis (2-aminoethanol, 3-amino-1-propanol, ethylenediamine).

Advantages of catalytic processes are obvious and can be witnessed in the hydrolysis and the glycolysis reactions of poly(ethylene terephthalate) (PET) [82,83]. Representative data are reported in graphical format in Figure 2 for the glycolysis reaction of PET, using titanium(IV) *n*-butoxide as the catalyst. Compared to the uncatalysed process, benefits include milder reaction conditions, higher selectivity and productivity and reduced generation of waste; in short, improved sustainability [84,85]. However, solvolytic methods are usually not cost-competitive and energy-intensive [86], while they may involve the management of large amounts of noxious solvents and a variety of (decomposition) byproducts [87,88]. Depolymerisation products of course depend on the polymer, the solvent and the reaction conditions. For instance, for polyesters, alcoholysis may provide mixed monomers formally derived from transesterification reactions [89,90], while aminolysis provides amides and alcohols [91,92].

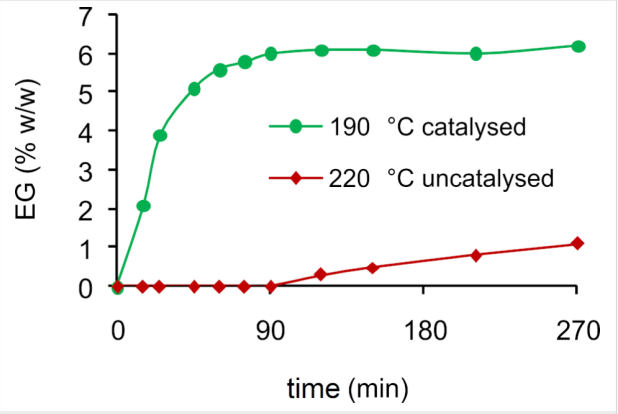

Figure 2: EG produced during glycolytic depolymerisation of PET using DEG + DPG as solvent and titanium(IV) *n*-butoxide as catalyst. Data from reference [92].

In the search of "greener" technologies for plastic recycling, catalytic hydrogenolysis processes have been developed that benefit from the use of H_2 as clean reagent and that usually result in a limited number of secondary products [93,94]. The excess of H_2 reagent can also be easily removed from the reaction mixture. The approach, referred to as hydrodeoxygenation [95,96], is already in use for the valorisation of naturally-occurring polymeric waste, i.e., lignocellulosic biomass [97,98], particularly lignin [99,100] and cellulose [101], to monomers or added-value platform molecules [102,103]. Here the main drawbacks concern safety hazards, supply, transport and storage costs of hydrogen. Catalytic transfer hydrogenation (CTH) methods from safer reagents have thus been developed and successfully applied to lignocellulose polymers [104,105].

2.2 Catalysts

Catalysts of various types, including homogeneous and heterogeneous, have been reported for the above-mentioned depolymerisation processes of plastics. Heterogeneous systems are preferred by industry due to the easier separation from the reaction mixture, reuse and integration into existing reactor equipment [106,107]. Metal-based catalysts have been used for both solvolytic and hydrogenolytic methods, wherein the latter are usually achieved by supported metal species (Ru, Ir), due to the ability to activate molecular hydrogen, functioning as redox centres. The mechanisms of the metal-catalysed solvolytic reactions of plastics are all very similar and typical of conventional organic processes: a metal ion acts as Lewis acid centre for the activation of the chain-linking group of the polymer (either an ester, carbonate, ketone or amide) toward the nucleophilic attack of the various solvents. Specific examples, broken down according to the nature of the polymer and the process, will be reported in the next sections, in which metal catalysts are described in detail. Solvolytic depolymerisations can also be promoted by metal-free soluble acid or base catalysts. However, concentrated solutions, quasistoichiometric amounts or strong mineral acids (HNO_3, H_2SO_4, H_3PO_4) or bases (NaOH, KOH, potassium butoxide) are often required, particularly for hydrolysis reactions [108,109], which may result in corrosion problems, troublesome neutralisation and purification procedures as well as a considerable generation of waste, which makes these process economically and environmentally unappealing [110,111]. These systems are not considered in the present review.

Biological catalysts for the deconstruction of plastics were extensively studied in the past years, and several hydrolytic-enzymes-containing microorganisms have been shown to be usable for this purpose [112,113]. However, enzymatic depolymerisation is hampered by high molecular weight and crystallinity, reduced chain mobility and hydrophobicity of polymers [114,115], which makes biodegradation often ineffective and time-consuming, particularly for polyolefins, such as polyethylene, polyvinyl chloride (PVC), polystyrene or PET

[116,117]. Thus, abiotic pretreatments may be required, including UV irradiation [118], oxidation [119] or acidic degradation [120].

It is worth mentioning that organocatalytic depolymerisation methods have also been reported [121,122]. Despite these systems represent promising "greener" options, they still are in an early development stage. Uses are mainly limited to nitrogen-based catalysts, ionic liquids [123,124] and alcoholysis of oxygen-containing polymers, such as polyesters, polycarbonates and polyamides, i.e., glycolysis of PET, wherein high temperatures and nearly stoichiometric amounts of catalysts are often required to achieve moderate yields of monomers [125,126].

3. Selective depolymerisation of plastics via metal catalysis

Research in depolymerisation of plastics by artificial metal catalysts is relatively recent as most of the earliest studies are related to biocatalytic systems. Metal salts are the conventional catalysts for these processes, wherein acetates, phosphates and chlorides of heavy metals (Ti, Zn, Mg, Co, Fe) or lead oxide are commonly used in the alcoholysis and glycolysis of polyesters [127,128]. Despite that these systems ensure high conversions and selectivity, shortcomings relate to the harsh reaction conditions, slow kinetics, cost of metals, toxicity, difficulty in catalyst reusing and need of downstream processing. Significant efforts have thus been made to develop greener and sustainable catalytic systems featuring high efficiency under mild conditions. The use of sodium carbonate or bicarbonate as ecofriendly catalyst replacements for zinc acetate in the glycolysis of PET are examples of this direction [129,130]. Recent studies focused on molecular complexes as homogeneous catalysts, whereas heterogeneous systems based on solid-supported metal nanoparticles (NPs) have been scarcely investigated.

3.1 Polyolefins

Due to the intrinsic chemical resistance of the hydrocarbon skeleton devoid of functional groups, polyolefins are neither prone to chemical recycling nor biodegradable [131,132]. Hence, they are more commonly repurposed via mechanical recycling, burned or just discarded [133,134]. Depolymerisation of polyolefins usually requires thermal treatments at high temperature [54,135].

3.1.1 Polyethylene (PE): PE is the most used thermoplastic material today, having a variety of uses in several fields. Applications of PE depend on the mechanical and physical properties (particularly the tensile strength, hardness and melting point T_m), which are, in turn, ruled by the molecular weight and degree of branching [136,137]. Various types of PE exist, which are classified according to the density, the most common being high-density polyethylene (HDPE) and low-density polyethylene (LDPE). HDPE (0.94–0.97 g·cm^{-3}, T_m 130 °C) is a highly crystalline material with a low degree of short chain branching. Owing to the high stiffness, tensile strength, resistance to moisture and gas permeability, it is mainly used in the manufacture of water pipes, toys, beverage bottles, outdoor furniture, housewares and electrical cables [138,139]. LDPE (0.91–0.94 g·cm^{-3}, T_m 120 °C) is a poorly crystalline material having a high degree of short chain and long chain branching. It is featured by a good flexibility, transparency and high impact strength, which make it suitable for short-term applications, such as films, food packaging, squeezable bottles, plastic bags and medical devices [140]. PEs (except cross-linked samples) are partially soluble in (hot) aromatic hydrocarbons or in chlorinated solvents [141].

Depolymerisation of PE by catalytic pyrolysis or cracking into liquid fuels was recently reviewed [67,142]. Most of these processes are promoted by heterogeneous acid catalysts (e.g., zeolites, alumina, silica) and are usually unselective, resulting in a broad distribution of gas (C_3 and C_4 hydrocarbons), liquids (cycloparaffins, oligomers, aromatics) and solid products (char, coke) as a consequence of the random scission of C–C bonds into radicals, which leads to a complex mixture of olefinic and cross-linked compounds [143].

In a few cases, good selectivity to a liquid fraction was achieved. For instance, nanostructured $BaTiO_3$ doped with Pb provided a mixture of liquid products, which includes alkanes (73.4%), olefins (22.5%) and naphthalene (4.1%) at total HDPE conversion at 350 °C [144]. In another example, hydrocracking of PE was performed over Pt NPs supported on $SrTiO_3$ perovskite nanocuboids [145]. Virgin PE (M_w = 18000–420000 g·mol^{-1}) or PE from single-use plastic bags (M_w = 115000 g·mol^{-1}) was converted in >97% yield into liquid hydrocarbon (alkane) products having a narrow distribution of the molecular weight (960–1130 g·mol^{-1}) under 11.7 bar H_2 at 300 °C and solvent-free conditions [146]. The pyrolysis oils produced may be used as lubricants, waxes or further processed into detergents and cosmetics [147]. The catalyst could be recycled, however, with reduced performance due to Pt nanoparticle oxidation.

3.1.2 Polybutadiene (PBD): Partial depolymerisation of 1,4-PBD (*cis*, *trans*, M_w 1800–500000 g·mol^{-1}) was achieved by an unconventional tandem ring-opening–ring-closing metathesis route mediated by commercially available Ru homogeneous catalysts [148]. The process afforded C_{16} to C_{44} mixtures of macrocyclic oligobutadienes with up to 98% selectivity at moderate conversions (59–88%) using first-generation Ru com-

plexes bearing a tricyclohexylphosphine (PCy_3) ligand, mild reaction temperature (35 °C) but toxic CH_2Cl_2 solvent (Scheme 1). The reaction using second-generation N-heterocyclic carbene ligands was faster and preferably yielded cyclododecatriene. Larger cyclic butadienes may be used in the production of flame retardants, lubricants and specialty polymers [149,150].

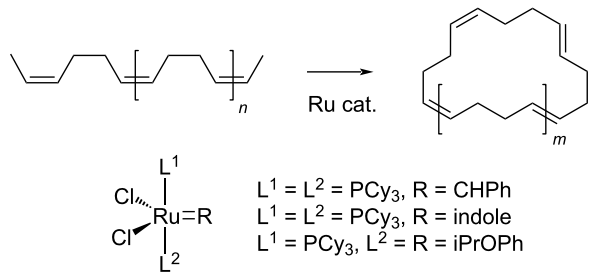

Scheme 1: Simplified representation of the conversion of 1,4-PBD to C_{16}–C_{44} macrocycles using Ru metathesis catalysts.

3.1.3 Polystyrene (PS): PS is a low-cost, hard and brittle plastic used both as a solid or foam in protective packaging, containers and trays [151]. It is a nonbiodegradable material accounting for about 10% of municipal solid waste [135]. It is soluble in benzene, carbon disulfide, chlorinated hydrocarbons, lower ethers and *N*-methyl-2-pyrrolidone (NMP) and has a melting point around 240 °C [152]. Most methods for PS recycling are not economically advantageous [153]. Mechanical recycling, based on pelletizing and moulding, produces low-grade plastics with poor mechanical strength and low market value. Solid PS products, such as coffee cups or take-away containers, can be recycled into videocassette cases or office equipment. Incineration at a temperature below 1000 °C and insufficient air is believed to produce a mixture of volatile compounds, including hazardous polycyclic aromatic hydrocarbons, alkylbenzenes and benzoperylene [154,155]. As for other polymers, pyrolytic methods end up to be poorly selective.

In some cases, metal-catalysed depolymerisation processes of PS were described, showing significant selectivity. In an earlier example, thermal treatment of PS waste over a Fe–K@Al_2O_3 catalyst at 400 °C provided a hydrocarbon oil in 92% yield, 71.4% of which were attributable to styrene monomer [156]. A decrease of 56 kJ mol^{-1} for the activation energy of PS depolymerisation was calculated in the presence of the catalysts. More recently, high-porosity montmorillonite (Mt) was used to prepare Mg-, Zn-, Al-, Cu- or Fe-decorated heterogeneous catalysts [157,158]. An oil yield around 89% was obtained at 450 °C over 20% Fe@Mt, composed by 51%, 10% and 6% (wt) styrene, toluene and ethylbenzene, respectively, and additional oligomers.

3.2 Polyesters

3.2.1 PET: PET is one of the most widely used thermoplastic polyesters, particularly in the textile and food packaging industry (e.g., soft-drink and water bottles, food container, films) due to the excellent thermal and mechanical properties, durability, inertness and transparency. The global production of PET exceeds 50 million tons pear year, while PET accounts for around 8% by weight and 12% by volume of the world's solid waste [159,160]. PET is a copolymer of terephthalic acid (TPA) and EG [161]. It is best soluble in chlorophenol, tetrachloroethane, *m*-cresol, NMP, nitrobenzene and 1,1,1,3,3,3-hexafluoro-2-propanol, insoluble in common alcohols and water and has a melting point of 250 °C and a glass transition temperature T_g of 76 °C [162,163]. It was suggested that under certain circumstances, PET may leach phthalates [164], which are known for potentially adverse health effects and subject to ECHA regulation restrictions [165,166]. Coupled with the fact that TPA is produced from petrochemical sources, bioderived 2,5-furandicarboxylic acid has been proposed as TPA replacement in the production of plastic bottles, representing one of the rare examples of industrial manufacture of biobased polymers [167,168].

From the chemical recycling point of view, PET is one of the most studied plastics, so as to represent a case study in the field [169,170]. A variety of added-value, reusable chemicals and monomers can be recovered from PET via chemolytic depolymerisation, including 1,4-benzenedimethanol (BDM), TPA, dimethylterephthalate (DMT), bis(2-hydroxyethyl)terephthalate (BHET), terephthalamides (TPM [171]) and EG (Figure 3). Cat-

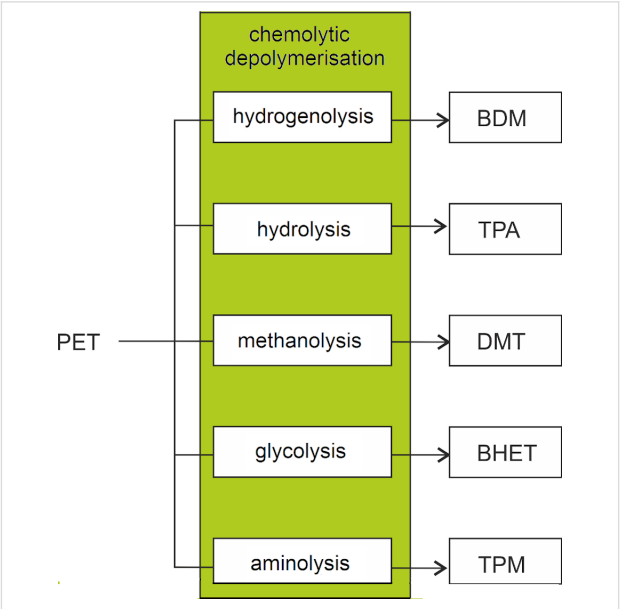

Figure 3: Main added-value monomers obtainable by catalytic depolymerisation of PET via chemolytic methods.

alytic hydrogenolysis, hydrolysis, methanolysis and glycolysis reactions of (postconsumer) PET have been reviewed, each showing their own advantages and disadvantages [172,173]. For instance, glycolysis usually requires more problematic purifications than methanolysis, which, on the other hand, is generally more energy-intensive. Some solvolytic processes of PET are already in operation at the industrial or pilot scale [174,175]. However, they often rely on the use of considerable amounts of strong alkali bases and chlorinated solvents [176,177], which makes them neither economically competitive nor environmentally friendly [178,179]. A survey of patents related to the chemical recycling of PET up to 2005 can be found in the literature [180].

Hydrogenolysis. In the recent years, hydrogenolysis reactions of PET were developed mostly using Ru metal-based catalysts, due to their higher affinity for C=O bond (ester) hydrogenation compared to other metals (Scheme 2) [181,182]. Thus, a 73% BDM yield was obtained using a soluble Ru(II)–PNN complex at 110 °C in THF/anisole solvent, 50 bar of hydrogen and a 20:1 excess of strong base potassium *tert*-butoxide as cocatalyst (Table 1, entry 1) [183]. Although the reaction mechanism was not investigated in detail, it was suggested that cleavage of the ester linkage may occur in a concerted manner through the reported heterolytic route [184,185]. The role of butoxide was postulated to be the activation of the heterogeneous splitting of dihydrogen. BDM is an important building block for the production of resins and polyesters other than PET [186,187]. Analogously, a similar Milstein-type ruthenium–PNN complex, generated in situ by treatment of the chloride catalyst precursor with potassium butoxide in a 2:1 molar ratio, resulted in a nearly quantitative yield of BDM and EG at a slightly higher reaction temperature (160 °C, 54 bar H_2, Table 1, entry 2). Interestingly, PET flakes from postconsumer bottles could be used, showing the catalytic system to be resistant to the presence of contaminants and impurities (e.g., additives, pigments) [188]. More recently, effective PET depolymerisation was accomplished by a ruthenium molecular catalysts bearing the well-known tripodal phosphorous ligand 1,1,1-tri(diphenylphosphinomethyl)ethane (triphos) [189,190]. Thus, use of Ru(triphos)tmm (tmm = trimethylenemethane) and acidic bis(trifluoromethane)sulfonimide ($HNTf_2$) cocatalyst (1:1) in noxious 1,4-dioxane solvent resulted in 41% PET conversion and 64% BDM selectivity at 140 °C and 100 bar H_2 due to the formation of ether byproducts (Table 1, entry 3) [191]. No hypotheses for the reaction mechanism were formulated. Higher conversion (64%) and selectivity (99%) were observed using the bulkier xylyl derivative Ru(triphos-xyl)tmm (Table 1, entry 4), which was attributed to reduced catalyst degradation [192]. The catalyst could be employed for the depolymerisation of PET flakes from various sources (water bottles, dyed soda bottles, pillow filling, yoghurt pots). However, the role of $HNTf_2$ was unclear.

In a different approach, hydrogenolysis-like depolymerisation was achieved through a hydrosilylation strategy, using the pincer Ir(III) complex $[Ir(POCOP)H(THF)][B(C_6F_5)_4]$ (POCOP = 1,3-(*t*-$Bu_2PO)_2C_6H_3$) as catalyst and an excess of Et_3SiH as reagent (chlorobenzene solvent, 70 °C) [193]. BDM could be obtained in an overall 58% yield from PET from fibres or bottles, after hydrolysis of the intermediate silyl ether using $Bu_4NF{\cdot}3H_2O$ in THF (Scheme 3).

Hydrolysis. Methods for the metal-catalysed hydrolysis of PET were developed, allowing for the recovery of costly TPA monomer (Scheme 4, top). TPA was obtained in 97.1% yield at full PET conversion, using 70 wt % aqueous $ZnCl_2$ as catalyst at 180 °C and no organic solvent [194]. However, a high $ZnCl_2$/PET weight ratio of 35 was required. The catalyst could be reused, showing significant activity decrease starting from the fourth cycle due to biochar formation. A mechanism was hypothesised in which Zn^{2+} ions act as a Lewis acid activator for the carbonyl ester bond. In a previous work, complete depolymerisation of PET was achieved using zinc acetate as catalyst in hot compressed water [195]. A TPA yield of 90.5% was obtained at 240 °C after 30 min reaction time, using a $ZnAc_2$/PET weight ratio as low as 0.015. For this, a mechanism was speculated in which proton ions act as activators.

Methanolysis. To the best of our knowledge, only one example of a depolymerisation reaction of PET through alcoholysis was recently reported, which is however devoid of any catalysts [196]. Therein, a 97.3% yield of DMT was obtained at full PET conversion, by treatment of PET with methanol at 200 °C for

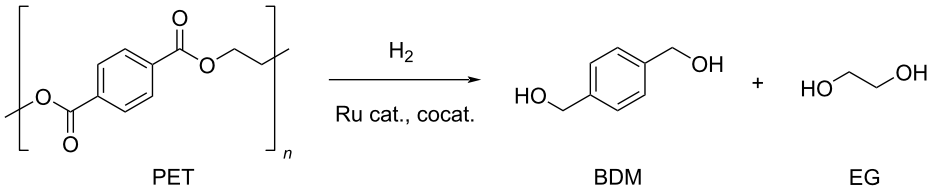

Scheme 2: Hydrogenolytic depolymerisation of PET by ruthenium complexes.

Table 1: Hydrogenolysis of PET by soluble Ru molecular catalysts.

entry	catalyst	cocatalyst[a]	reaction conditions[b]			conv.[c] (%)	BDM		ref.
			T (°C)	H_2 (bar)	solvent		sel.[d] (%)	TOF[e] ($mol_{BDM}·mol_{cat.}^{-1}·h^{-1}$)	
1	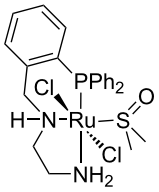	K*t*-BuO[f]	110	50	anisole/THF[g]	73	100	0.76	[183]
2	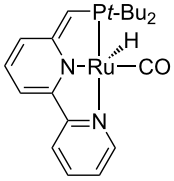	K*t*-BuO	160	54	anisole/THF[g]	99	100	1.03	[188]
3	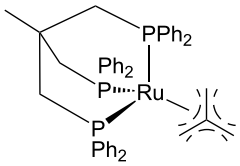	HNTf[h]	140	100	1,4-dioxane	42	64	1.68	[191]
4	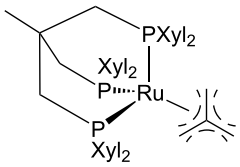	HNTf[h]	140	100	1,4-dioxane	64	99	3.96	[191]

[a]Catalyst loading 2 mol %, calculated based on repetition units in PET, cocatalyst molar ratio 2:1. [b]Reaction temperature, hydrogen pressure, reaction time 48 h. [c]PET conversion. [d]Selectivity to BDM. [e]Turnover frequency, calculated based on repetition units in PET and moles of Ru catalyst. [f]Cocatalyst molar ratio 20:1. [g]1:1 v/v. [h]Catalyst loading 1 mol %. Reaction time 16 h.

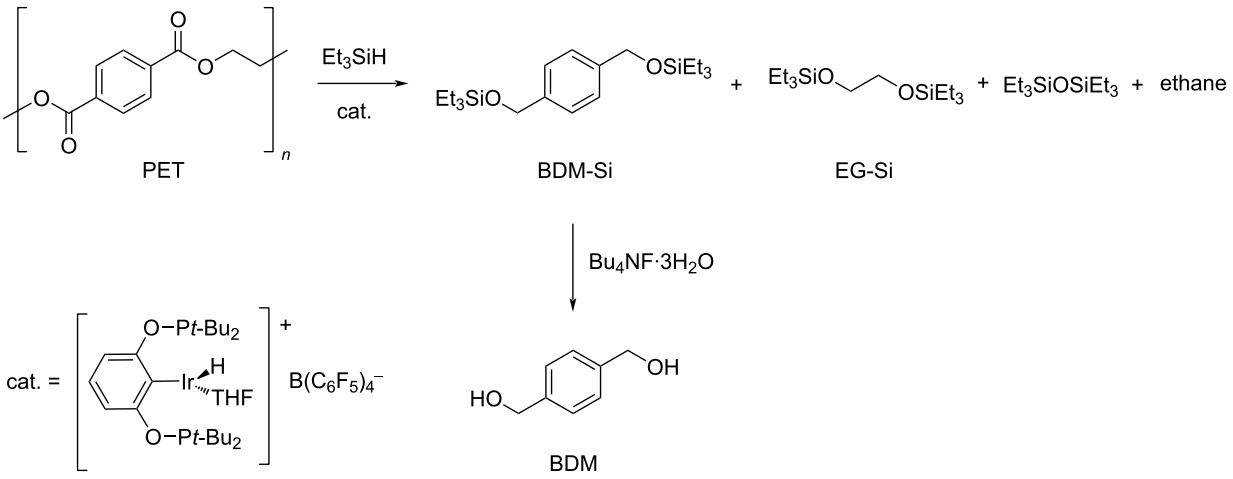

Scheme 3: Depolymerisation of PET via catalytic hydrosilylation by Ir(III) pincer complex.

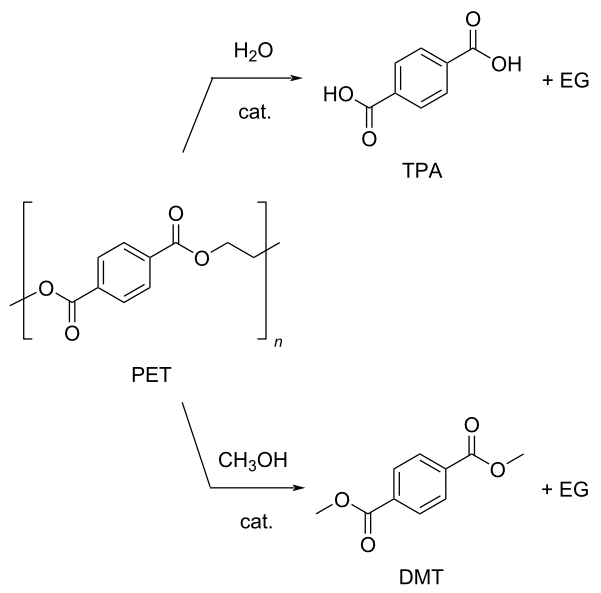

Scheme 4: Catalytic hydrolysis (top) and methanolysis (bottom) reactions of PET.

3.5 h (Scheme 4, bottom). No details of byproducts were provided. Ethanol and butanol were much less reactive under identical reaction conditions. The as-prepared DMT could be used for the production of hydrocarbon jet fuels by catalytic hydrogenation. Metal-catalysed methanolysis of PET was described in previous years [109,197].

Glycolysis. Glycolysis is a convenient process for PET chemical recycling, owing to the low cost, relatively mild reaction conditions and the potential for the production of useful monomers and oligomers. These compounds can be used in the synthesis of recycled polyesters, polyurethanes, polyisocyanurates and resins [43]. Among the various glycols, EG is the most popular, resulting in the formation of BHET, formally through a (reversible) transesterification reaction (Scheme 5) [198]. Drawbacks of this method are the difficulty of purification of BHET, the need of an excess of EG and the possible product contamination by homogeneous catalysts [199]. The conventional catalysts for this reaction are EG-soluble metal acetates, the activity of which showed a decrease in the order Zn^{2+} > Mn^{2+} > Co^{2+}, which was attributed to the diverse interaction between the metal cation promoter and the carbonyl group of polyester [200]. Indeed, several studies showed Zn-based catalysts to provide the best performances. A summary of recent findings and reaction conditions is reported in Table 2. In an earlier study, a 85.6% BHET yield was obtained at 196 °C, using an EG/PET ratio of 5:1 (w/w) and 1 wt % $Zn(OAc)_2$ loading (Table 2, entry 1) [201]. The system resulted in partial selectivity to BHET due to the formation of significant amounts of oligomers, mainly BHET dimers, which increased upon standing. The kinetic of the zinc acetate-promoted process was studied over a range of reaction conditions, showing the best combination to be 196 °C, an EG/PET ratio of 2.45:1 (w/w) and a catalyst loading of 0.3 wt % (Table 2, entry 2) [129]. Under these conditions, an equilibrium yield of BHET around 65% was achieved within short reaction times (1 h), much faster than in the absence of catalysts or using alkali salt promoters (Na_2CO_3, $NaHCO_3$, Na_2SO_4 or K_2SO_4, Figure 4). PET wastes, including highly coloured and multilayered PET, could be used as substrate. More recently, it was demonstrated that the addition of a cosolvent for PET, such as dimethyl sulfoxide (DMSO), NMP, nitrobenzene or aniline to the conventional PET-insoluble EG system, greatly enhanced the depolymerisation kinetics, resulting in improved conversions (the solubility of PET at T > 130 °C was aniline > NMP > nitrobenzene > DMSO) [202]. For instance, the use of a DMSO/EG 2:1, w/w solvent mixture resulted in an increase of PET conversion from 43.0% to 83.9% compared to pure EG (190 °C, 5 wt % catalyst loading, 5 min reaction time, Table 2, entry 4 vs entry 3). Using the same reaction conditions and solvent mixture, Mn, Co, Cu and Ni acetate catalysts were less active than Zn (Table 2, entries 5 and 6). In a further study, glycolysis of PET was performed under microwave heating in the presence of $Zn(OAc)_2$, yielding BHET with an 80% selectivity at 97% conversion due to formation of dimers (Table 2, entry 7) [203,204]. Soluble metal chlorides (zinc, magnesium, iron, zirconium, cobalt, nickel) were also explored as catalysts in the glycolytic depolymerisation of PET [128,205]. The highest BHET yield (74.7%) was achieved using zinc chloride (0.5% w/w), an EG/PET ratio of 14:1 and reflux conditions (Table 2, entry 8). The use of

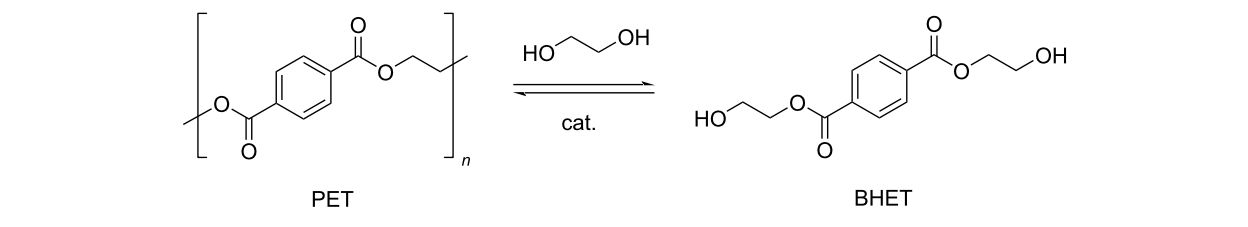

Scheme 5: Depolymerisation of PET by glycolysis with ethylene glycol.

Table 2: Catalytic EG glycolysis of PET by metal acetates or other soluble metal salts.

entry	material	catalyst	EG/PET[a] (w/w)	T[b] (°C)	conv.[c] (%)	BHET		reference
						sel.[d] (%)	TOF[e] ($mol_{BHET}·mol_{cat.}^{-1}·h^{-1}$)	
1	PET bottle chips	$Zn(OAc)_2$	5:1	196	n.a.[f]	85.6[g]	27.0	[201]
2	PET waste	$Zn(OAc)_2$	2.45:1	196	65	100	207.1	[129]
3	PET pellets	$Zn(OAc)_2$	6:1	190	43.0	100	118.4	[202]
4	PET pellets	$Zn(OAc)_2$	2:1[h]	190	83.9	100	230.9	[202]
5	PET pellets	$Mn(OAc)_2$	2:1[h]	190	80.8	100	222.0	[202]
6	PET pellets	$Co(OAc)_2$	2:1[h]	190	78.7	100	216.3	[202]
7	PET bottle flakes	$Zn(OAc)_2$	5:1	196[i]	97.1	80.3	73.7	[203]
8	PET	$ZnCl_2$	14:1	196	n.a.[f]	74.4[g]	n.a.[f]	[128]
9	PET pellets	Zn POM[j]	4:1	185	100	84.1	1292.3	[210]

[a]EG as solvent. [b]Reaction temperature. [c]PET conversion. [d]Selectivity to BHET. [e]Turnover frequency calculated based on PET repetition units and moles of metal catalyst. [f]Not available. [g]BHET yield (%). [h]Solvent DMSO/EG 2:1, w/w. [i]Microwave irradiation 500 W. [j]Zn polyoxometalate formula $K_6SiW_{11}ZnO_{39}(H_2O)$.

preformed soluble Co(II) complexes bearing bidentate phosphorus ligands (e.g., 1,2-bis(dicyclophosphino)ethane) showed minimal improvements compared to the chloride salt catalyst [205]. The use of transition metal-substituted polyoxometallates (POMs), of the general formula $K_6SiW_{11}MO_{39}(H_2O)$ (M = Zn^{2+}, Mn^{2+}, Co^{2+}, Cu^{2+}, Ni^{2+}) [206,207], was also investigated [208]. The catalytic activity was found to decrease in the order Zn > Mn > Co > Cu > Ni, consistent with previous reports [209]. The best catalyst afforded BHET in 84.1% yield (Table 2, entry 9), which was rather constant over eight catalyst reuses [210]. A stepwise depolymerisation mechanism was proposed, via intermediate oligomers, in which Zn ions act as Lewis acid activators for the C=O ester bonds toward nucleophilic attack by EG.

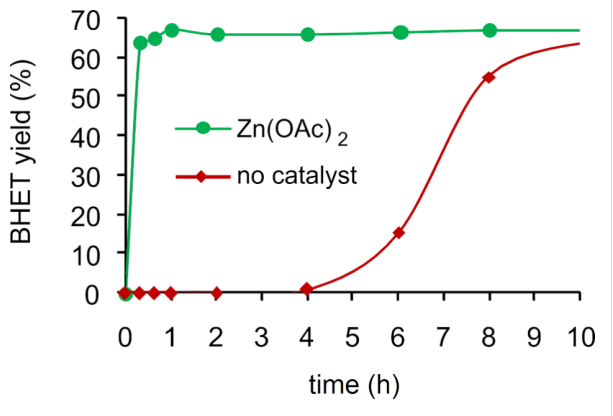

Figure 4: Glycolysis of PET: evolution of BHET yield over time, with and without zinc acetate catalyst (196 °C, EG/PET ratio 2.45 (w/w). Data from reference [129].

In addition to soluble catalysts, metal-containing insoluble materials, namely solid acid catalysts, were developed for the glycolytic depolymerisation of PET by EG. Representative data are summarised in Table 3, wherein the catalyst productivity is reported for comparison as $mol_{BHET}·g_{cat.}^{-1}·h^{-1}$. Despite that both catalyst and PET were insoluble in EG at the reaction temperature, most systems displayed substantial activity. Thus, sulfated titania, zinc oxide and mixed oxides (SO_4^{2-}/TiO_2, SO_4^{2-}/ZnO and $SO_4^{2-}/ZnO–TiO_2$) were prepared, showing the amount of Lewis acid sites and the high surface area of the solid material to be critical in affecting the catalytic efficiency [211]. Best results were obtained for the binary oxide $SO_4^{2-}/ZnO–TiO_2$ calcined at 200–300 °C (surface area 192 $m^2·g^{-1}$, density of acidic sites 4.34 $mmol·g^{-1}$), which provided BHET in 73% selectivity at full PET conversion at 180 °C reaction temperature and a moderate excess of EG (5.5:1, w/w, Table 3, entry 1). The formation of a significant amount of oligomers was detected. The catalyst could be recovered by centrifugation and reused over four cycles with no efficiency decay. Similar effects were reported for Zn-substituted titanate nanotube (TiNT) catalysts [212,213]. Therein, a positive role of Zn^{2+} Lewis acid sites was demonstrated by the higher efficiency compared to the Na^+ catalyst counterpart (Table 3, entry 2 vs entry 3), whilst a high surface area around 150 $m^2·g^{-1}$ was proposed to increase the number of exposed sites [214]. Zn@TiNT afforded BHET in 87% yield at 196 °C reaction temperature. TiNT have received significant general interest in heterogeneous catalysis because of the better active-site-accessibility compared to 2D materials, thanks to a typical 8–16 nm outer diameter tubular morphology [215,216] and the potential for facile metal doping via ion-exchange of the solid support

Table 3: Glycolysis of PET using EG and insoluble, solid-supported metal catalysts.

entry	material	catalyst	EG/PET (w/w)	T[a] (°C)	conv.[b] (%)	BHET		reference
						sel.[c] (%)	productivity[d] ($mol_{BHET} \cdot g_{cat.}^{-1} \cdot h^{-1}$)	
1	PET pellets	SO_4^{2-}/ZnO–TiO_2	5.5:1	180	100	73.0	0.42	[211]
2	PET bottle grains	Zn@TiNT	4:1	196	99	87.0	0.45	[214]
3	PET bottle grains	Na@TiNT	4:1	196	99	80.1	0.42	[214]
4	PET	γ-Fe_2O_3 NPs	3.7:1	300	100	90	0.09	[219]
5	PET granules	GO–Mn_3O_4	3.7:1	300	100	96.4	0.38	[220]
6	PET bottles	$ZnMn_2O_4$	5.5	260	100	92.2	0.48	[222]
7	PET pellets	(Mg–Zn)–Al LDH	10:1	196	100	75.0	0.13	[223]

[a]Reaction temperature. [b]PET conversion. [c]Selectivity to BHET. [d]Catalyst productivity calculated based on PET repetition units, moles of BHET and grams of solid catalyst.

[217,218]. Lewis acid-type catalytic activity was also postulated for γ-Fe_2O_3 NPs, which provided BHET in 90% yield at 300 °C (Table 3, entry 4) [219]. Therein, thanks to the superparamagnetic properties, easy recovery of the highly dispersed solid catalyst (11 nm size) was possible by application of a magnetic field. The catalyst could be reused over ten cycles without significant activity loss. Other solid-supported nanostructured metal oxides were tested as catalysts for PET glycolysis. Thus, a graphene oxide (GO)–Mn_3O_4 nanocomposite (Table 3, entry 5) [220] and silica NPs-supported Mn_3O_4 [221] resulted in a good yield of BHET (>90%), however, at a high reaction temperature. A zinc manganite spinel $ZnMn_2O_4$ gave BHET in 92% yield at 260 °C and 5 atm pressure (Table 3, entry 6) [222]. On the other hand, amphoteric solid catalysts have also shown usability in EG depolymerisation of PET. For instance, a BHET yield of 75% was achieved over (Mg–Zn)–Al-layered double hydroxides (LDH) catalysts at 196 °C (Table 2, entry 7) [223]. A cooperative mechanism was proposed in which Lewis acid sites (Mg^{2+}, Al^{3+}, Zn^{2+}) activate the C=O ester bond, while the basic sites (OH^-) deprotonate EG, enhancing the nucleophilic cleavage of the ester unit [224].

Notably, the depolymerisation of PET by EG was also reported using metal-containing catalysts in the form of ionic liquids (ILs) [209]. Advantages of metallated ILs include low flammability, high thermal stability and versatility. However, their "greenness" and toxicity are still debated [225,226]. Thus, amim[$ZnCl_3$] (amin = 1-allyl-3-methylimidazolium, Table 4, entry 1) [227] and amim[$ZnCl_3$] (bmim = 1-butyl-3-methylimidazolium, Table 4, entry 2) [228] were recently studied, showing higher catalytic activity compared to metal-free ionic liquids (i.e., bmim chloride), the conventional catalysts (i.e., $ZnCl_2$, $Zn(OAc)_2$) or the analogous Mn, Co and Cu ionic liquids. Typically, 80–85% BHET yields were observed for metallated ILs, while under the same experimental conditions, $ZnCl_2$ gave BHET in ≈70% yield (Table 4, entry 5). Similar results were reported for the bmim$_2$[MCl_4] (M = Cr, Fe, Co, Zn, Ni, Cu) catalysts, wherein the cobalt derivative resulted in the best performance (Table 4, entry 3) [229]. Based on infrared studies, the higher catalytic activities of the metallated ILs was attributed to their higher Lewis acidity compared to both the metal-free catalysts and the metal salts. A mechanism was therefore proposed in which a synergistic effect of the metallated ILs takes place, based on the activation of the C=O bond by the IL Lewis acid cation and of the hydroxy group in EG by the IL anion (Scheme 6). The IL catalysts could be easily separated by distillation and reused up to six times with no significant efficiency drop. Catalytic glycolysis by heterogenised, metallated ionic liquids was also investigated [230], however, showing a lower performance compared to the soluble systems. Thus, PET pellets were fully converted by a bmim[$Fe(OAc)_3$] catalyst immobilised onto bentonite, affording BHET in 44% yield (Table 4, entry 4) [231]. The solid catalyst could be recovered by filtration and reused.

As an alternative to ILs, metal-based deep eutectic solvent (DES) systems were also explored as catalysts for the glycolysis reaction of PET using EG. DES have similar properties to metallated ILs, but they are cheaper and less toxic [232,233]. Because of this, they have found application in many fields [234,235], though they cannot be considered inherently "green" [236]. In a recent work, the DES combination zinc acetate and 1,3-dimethylurea (1:4) showed the highest catalytic activity among a series of transition metal acetates (Zn, Mn, Co, Ni, Cu), affording BHET with 82% yield and noticeable productivity (TOF = 129 h^{-1}, based on the moles of Zn) at 190°C, EG/PET 4:1, w/w and 5 wt % catalyst [237]. A mechanism was proposed analogous to that depicted in Scheme 6, but in which Zn^{2+} acts as Lewis acid and dimethylurea acts as base promoter for EG hydroxy deprotonation [238]. The remarkable activity

Table 4: Catalytic EG glycolysis of PET using metallated ionic liquids.

entry	catalyst		EG/PET (w/w)	T[a] (°C)	conv.[b] (%)	BHET		reference
	formula	loading (wt %)				sel.[c] (%)	TOF[d] ($mol_{BHET}·mol_{cat.}^{-1}·h^{-1}$)	
1	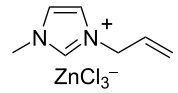 $ZnCl_3^-$	10	4:1	175	100	80.1	9.8	[227]
2	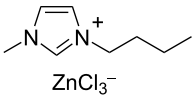 $ZnCl_3^-$	1.25	11:1	190	100	84.9	55.2	[228]
3	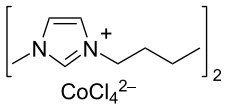 $CoCl_4^{2-}$	17	12:1	175	100	81.1	8.5	[229]
4	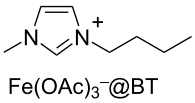 $Fe(OAc)_3^-$@BT	30[e]	7:1	190	100	44.0	2.9[f]	[231]
5	$ZnCl_2$[g]	1.25	4:1	175	94	76.2	4.0	[227]

[a]Reaction temperature. [b]PET conversion. [c]Selectivity to BHET. [d]Turnover frequency calculated based on PET repetition units and moles of metal catalyst. [e]Loading of bmim[$Fe(OAc)_3$] immobilised onto bentonite. [f]Calculated with respect to the moles of iron. [g]Metal salt.

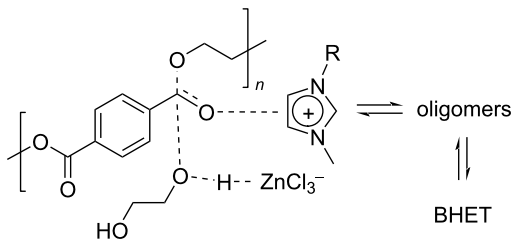

Scheme 6: Potential activated complex for the glycolysis reaction of PET catalysed by metallated ILs and evolution toward products.

was attributed to the dual effect of base and acid catalysis, in addition to the solubility of the catalyst in EG.

It is worth mentioning that, in addition to the recovery of chemicals via chemolytic processes, repurposing techniques of PET were developed based on one-pot, two-step glycolysis-reprocessing strategies, wherein the depolymerisation products are directly used in a polymerisation reaction, without intermediate purifications. In order to avoid the presence of free glycols in the polymerisation mixture, most of these processes were performed using (sub)stoichiometric amounts of diol cleaving agents, other than EG (for instance, PD [239], DEG [240,241]). As a consequence, the depolymerisation step usually results in complex mixtures of oligomers. Moreover, reacting diols may be unstable under the reaction conditions adopted. Hence, if used in excess, a significant formation of decomposition by-products may be observed (i.e., dioxane and acetaldehyde for DEG [242]). Because of that, these metal-catalysed depolymerisations cannot be strictly considered as selective, although the overall processes are interesting from a practical and sustainability point of view. Some recent examples are cited herein. Postconsumer PET was depolymerised in the melt (at 250 °C) using DEG and Ca/Zn stearate as catalyst, and the product mixture was used in situ in conjunction with bis(2-ethylhexyl)phthalate and the same metal promoter for the production of flexible poly(vinyl chloride) compounds [243]. One-pot depolymerisation–polycondensation reactions were developed to produce random copolyesters poly(ethylene terephthalate-*co*-adipate) from PET in the presence of EG and adipic acid [244]. The depolymerisation step was carried out using a zinc acetate catalyst (1 wt %), with no need of excess of chemicals. Polymerisation was then achieved by raising the reaction temperature, without purification of the intermediate oligomers being required. An interesting one-pot process was developed that combines the use of bioderived chemicals, isosorbide and succinic acid, with PET chemical recycling to produce novel polyesters [245]. In this process, isosorbide was used as depolymerising diol to give a mixture of differently composed oligomers, whereas succinic acid was added in the second step as polymerising comonomer (Scheme 7). Both steps were efficiently catalysed by monobutyltin oxide, using substoichiometric amounts of isosorbide and succinic acid and no solvent at

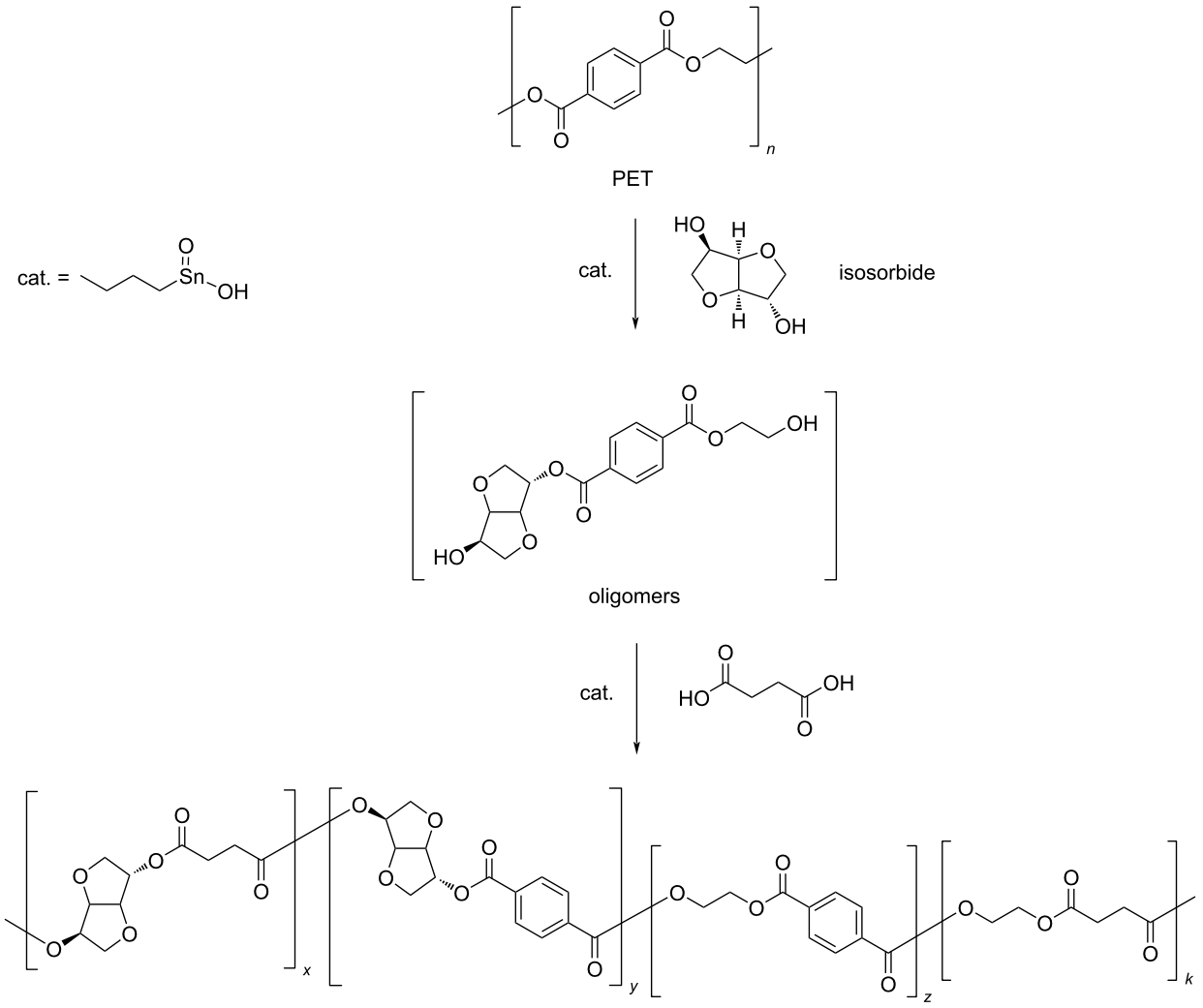

Scheme 7: One-pot, two-step process for PET repurposing via chemical recycling.

230 °C reaction temperature. Isosorbide is a safe chemical [246] that is obtainable on the large scale from renewable glucose [247,248]. Because of this and due to the inherent rigid structure, conferring the resulting polymers with excellent mechanical properties (e.g., stiffness, toughness, hardness), isosorbide is used as monomer in the production of a variety of plastics [249,250]. By contrast, the rigidity results in a poor reactivity as depolymerising agent [251].

3.2.2 Polylactic acid (PLA): PLA is a bioderived plastic [252] that is manufactured on a 190 kton scale directly from lactic acid by condensation or from lactide by ring-opening polymerisation (Scheme 8) [253,254]. The main renewable raw material for lactic acid is starch, e.g., from corn, cassava, sugarcane or beet pulp [255]. Owing to the chirality of lactic acid, three forms of PLA (L, PLLA; D, PDLA; DL, PDLLA) with slightly different properties (crystallinity, T_g 60–65 °C, T_m 130–180 °C)

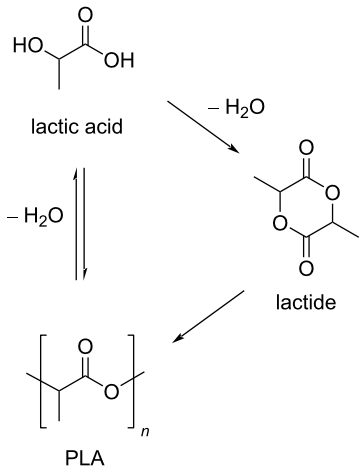

Scheme 8: Synthetic routes to PLA.

exist [256]. PLA is soluble in benzene, tetrahydrofuran, ethyl acetate, propylene carbonate and dioxane [257], and it is biodegradable [258,259]. Because of these features, PLA is largely employed in several applications: microelectronics, biomedicine and food packaging [260].

Although chemical recycling of PLA is possible by thermal methods over metal catalysts [261,262], these often result in a poor selectivity and in a variety of volatile compounds, with the notable exception of calcium oxide, which gave L,L-lactide from PLLA in ≈98% yield at 250 °C [263].

Alcoholysis. The solvolytic depolymerisation of PLA was mostly reported using zinc-based catalysts, ethanol or methanol agents, wherein a higher reactivity of the latter was ascribed to the better nucleophilicity. Indeed, a methyl lactate (Me-La) and ethyl lactate yield of 70% and 21% was obtained, respectively, using soluble zinc acetate at reflux temperature [264]. Interestingly, under the same reaction conditions, PET was unreactive, thus enabling the selectively recycle of mixed PET/PLA plastic waste. It was suggested that the different reactivity between PLA and PET is attributable to the amorphous, less rigid structure of PLA and to the potential of forming five-membered chetate ring intermediates between Zn(II) ions and lactate units, which favour the transesterification process. More recently, the use of soluble Zn(II) molecular catalysts was investigated. An in-depth study of the methanolysis reaction of PLA was carried out via design of experiments technique, using a series of imino monophenolate–Zn complexes and THF solvent. Different commercial samples of PLA were examined, showing the critical operational parameters to be temperature and catalyst concentration, whereas the process was not significantly affected by particle size or stirring speed. Thus, up to 100% Me-La yield was obtained using the six-coordinated Zn(ligand)$_2$ complex sketched in Scheme 9a, either at 90 °C and 16 wt % catalyst or 130 °C and 8 wt % catalyst [265]. Higher efficiency was provided by the tetrahedral complex ZnA_2 bearing a similar ligand, as shown in (Scheme 9b), which resulted in 81% Me-La selectivity at full PLA conversion at under 50 °C and 4 wt % catalyst loading [266]. However, in the absence of THF solvent, the latter catalysts gave a 98% Me-La yield at 130 °C. The comparable complexes ZnL^1_2, ZnL^2_2 and ZnL^3_2 shown in Scheme 9c resulted in a lower catalytic efficiency (Me-La yield 41–88%, 50 °C, 8 wt % catalyst loading, 18 h), and thus indicating a significant steric and electronic effect of the ligand [267]. A reaction mechanism for PLA depolymerisation was proposed, consisting of two consecutive first-order steps, in which Me-La production follows the formation of chain-end groups intermediates [265]. A zinc–N-heterocyclic carbene complex was used as catalysts for the methanolysis reaction of PLLA via a two-step, one-pot procedure using CH_2Cl_2 solvent and an excess of methanol at room temperature (Scheme 10) [268]. At full sub-

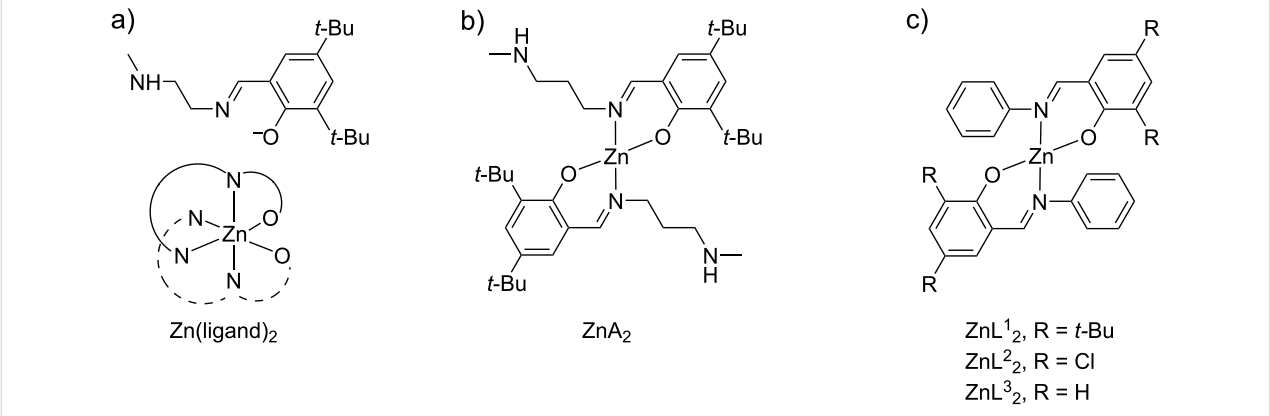

Scheme 9: Structures of the zinc molecular catalysts used for PLA-methanolysis in various works. a) See [265], b) see [266], c) see [267].

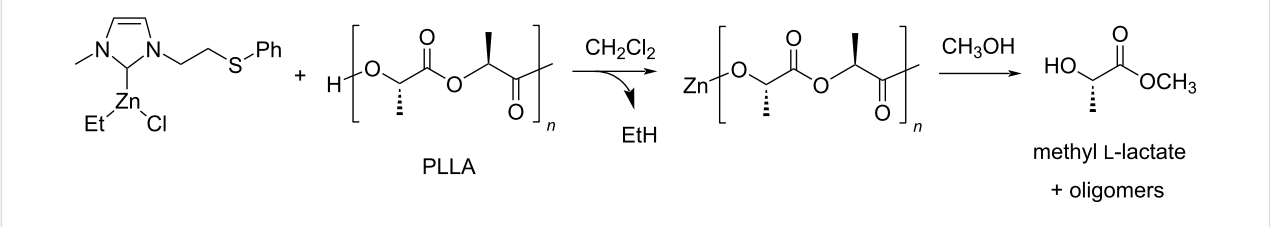

Scheme 10: Depolymerisation of PLLA by Zn–N-heterocyclic carbene complex.

strate conversion, a Me-La/oligomers ratio around 10:1 was detected by GPC analysis. Notably, mutatis mutandis, almost all of the above described zinc complexes could be used as catalysts, both in PLA alcoholysis and in PLA synthesis via lactide polymerisation.

Metal species other than zinc were reported as effective catalysts for PLA methanolysis. Group 4 metal complexes with salalen ligands of the formula M(ligand)$(OiPr)_2$ (M = Ti, Zr, Hf) were used in the methanolysis reaction of PLA at room temperature with an excess of methanol and CH_2Cl_2 cosolvent (Scheme 11) [269,270]. A 75% yield of Me-La and residual oligomers with M_n 500 g·mol^{-1} were obtained by conversion of M_n 200000 g·mol^{-1} PLA using the hafnium derivative. As an alternative to expensive metal (complex) catalysts, methanolysis of PLA was recently described using alkali metal halides [271]. In an optimised experiment, PLA from various goods (cups, fork, spoons, containers, M_w 120000–260000 g·mol^{-1}) was converted into Me-La in up to 97% yield using 2.5 mol % KF, 180 °C microwave heating and 23.1 equiv CH_3OH. The potassium fluoride catalyst could be reused in up to three runs with no change in performance, while a 50% drop of the yield was observed afterwards.

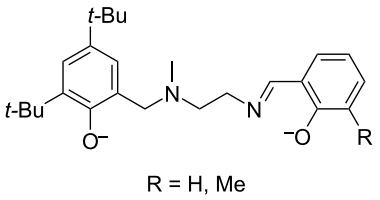

Scheme 11: Salalen ligands.

Me-La is a low-toxic chemical used as substitute for hydrocarbon solvents, with applications in the field of paints, lacquers and cleaning agents [272,273]. It should be finally mentioned that during the alcoholysis reaction of PLA using alkoxide catalysts, alkaline earth metal adducts (typically of Ca^{2+}) were isolated, and thus suggesting a potential involvement of the metal centre in the depolymerisation mechanism [274,275].

Hydrogenolysis. The Ru(triphos)tmm/$HNTf_2$ catalytic system described above for the hydrogenolysis reaction of PET was also successfully applied in PLA hydrogenative depolymerisation (Scheme 12) [191]. PLA was directly converted to 1,2-propanediol in 99% yield using 1 mol % catalyst (with respect to lactic acid units) and 1,4-dioxane solvent at 140 °C and 100 bar H_2. A TOF of 6.19 $mol_{PD}·mol_{Ru}^{-1}·h^{-1}$ can be calculated based on this. Scale-up using PLA granulates and beverage cups was also possible using a lower catalyst loading. In addition, the method allowed for the selective recycle of equimolar mixtures of PET and PLA using the [Ru(triphos-xyl)methylallyl]NTf_2 catalyst congener at 45 °C reaction temperature, wherein insoluble PET was filtered out, while PLA was fully converted to PD. Similarly to PET, the ruthenium(II)–PNN complex sketched in Table 1, entry 2 was also used in PLA hydrogenolysis to give PD in 99% yield at 160 °C, 54 bar H_2 and in anisole/THF solvent [182,188]. PD is a safe chemical that is mainly produced from propylene oxide or catalytically from lactic acid intermediate, and it serves in the polymer and food industry or as antifreezing agent [276,277].

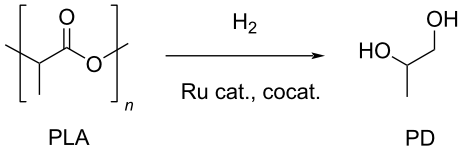

Scheme 12: Catalytic hydrogenolysis of PLA.

Under milder reaction conditions, PLA could be converted to the corresponding silyl ether in 92% yield, propane and silicon byproducts (8%) using the above mentioned Brookhart pincer complex [Ir(POCOP)H(THF)][$B(C_6F_5)_4$] shown in Scheme 3, an excess of Et_3SiH and chlorobenzene solvent at 90 °C (Scheme 13) [193]. The use of 6 equiv of 1,1,3,3-tetramethyldisiloxane (TMDS) led to the total conversion to propane and polydimethylsiloxane (PDMS), a silicon oil with several applications (lubricants, food-additives, breast implants).

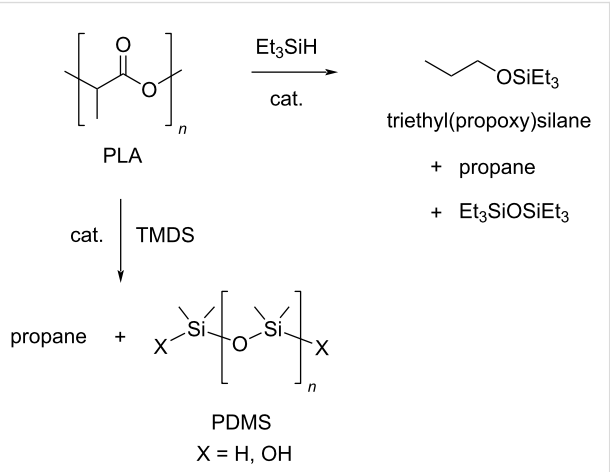

Scheme 13: Catalytic hydrosilylation of PLA.

3.2.3 Other polyesters: The hydrogenolysis reaction of esters other than PET and PLA was carried out using the above described soluble Ru(triphos)tmm/$HNTf_2$ catalytic system [191]. Thus, poly(butylene terephthalate) (PBT) and polycaprolactone

(PCL) were depolymerised into the corresponding (co)monomeric diols at 140 °C and 100 bar H_2 in 1,4-dioxane solvent (Scheme 14). A 99% selectivity to 1,6-hexanediol was observed at full PCL conversion, whereas the selectivity to diols was only 22% for PBT (due to the formation of ethers byproducts), which could be raised to 99% by using the bulkier Ru(triphos-xyl)tmm catalyst derivative.

PCL could be converted to 1,6-hexanediol in 68% yield also through a two-step procedure involving hydrosilylation by the above mentioned cationic Ir catalyst complex [Ir(POCOP)H(THF)][$B(C_6F_5)_4$] and TMDS reagent (chlorobenzene solvent, 90 °C), followed by alkaline hydrolysis (10% NaOH in CH_3OH/H_2O) [193]. PCL is a biodegradable polymer with a low melting point (≈60 °C) and glass transition temperature (−60 °C). It is commonly used in the manufacture of polyurethanes, to which it imparts improved solvent resistance, flexibility and toughness [278].

The glycolysis of poly(1,4-cyclohexylenedimethylene terephthalate) (PCT) was reported using DEG as reagent and zinc acetate as catalyst (0.12 mol %, Scheme 15) [279]. A 56% yield of bis(2-hydroxydiethylene terephthalate) (BHDET) was obtained at 196 °C and a DEG/PCT 15:1, w/w ratio, which was five times lower than that using PET under the same reaction conditions. This finding was attributed to the steric hindrance of the 1,4-cyclohexanedimethanol (CHDM)-based chain that hampers the transesterification process. A 90% BHDET yield was achieved using $Zn(OCH_3)_2$ catalysts under the same conditions.

Recently, a quantitatively and selectively depolymerisable novel polyester was developed based on a *trans*-fused six-membered γ-butyrolactone ring, 3,4-T6GBL (Scheme 16) [280]. This material joins the advantages of the ease of depolymerisation (97% monomer yield, 180 °C, toluene, 2 mol % $ZnCl_2$ catalyst), rigid structure of the monomer (which provides the polymer with

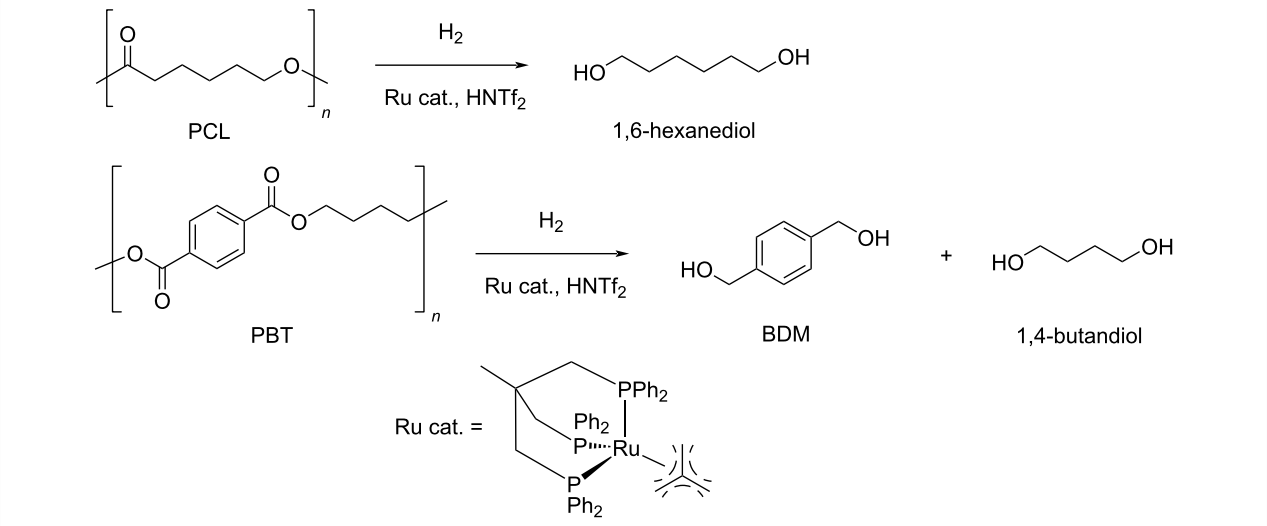

Scheme 14: Hydrogenative depolymerisation of PBT and PCL by molecular Ru catalysts.

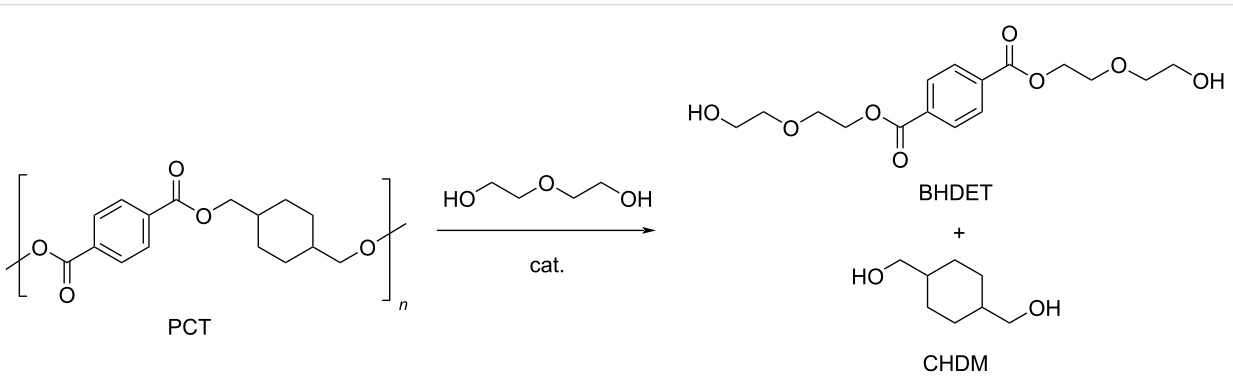

Scheme 15: Glycolysis reaction of PCT by diethylene glycol.

good thermal and mechanical properties) and facile synthesis (ring-opening polymerisation, solvent-free, room temperature, La, Y or Zn catalyst), significantly contributing to a closed-loop concept of plastics recycle. The approach enabled to perform the polymerisation–depolymerisation cycle over three times and on a multigram scale, using both linear and cyclic polymers. These advantages are not provided, for example, by more conventional poly(γ-butyrolactone) plastics, which require high depolymerisation temperatures (260–300 °C) and undesirable synthetic conditions (−40 °C) [281].

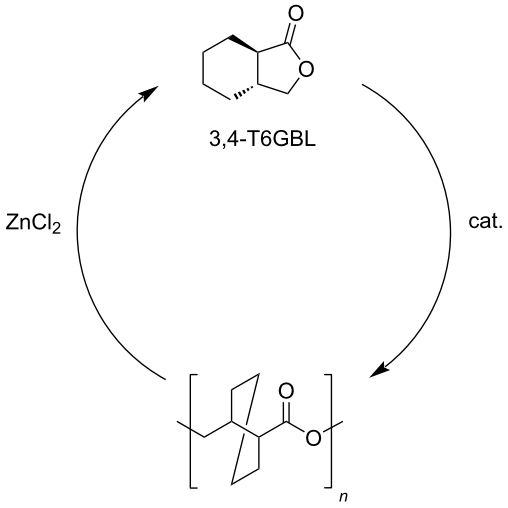

Scheme 16: Polymerisation–depolymerisation cycle of 3,4-T6GBL.

Following the same approach to purposely designed, chemically recyclable polymers, it was reported that poly(2-(2-hydroxyethoxybenzoate) (P2HEB) is reversibly depolymerised to 2,3-dihydro-5*H*-1,4-benzodioxepin-5-one (2,3-DHB) in 94% yield by an aluminium–salen catalyst at room temperature (Scheme 17) [282]. Thus, a polymerisation–depolymerisation cycle could be established using the same metal catalyst, simply by adjusting the initial monomer concentration in a one-pot process.

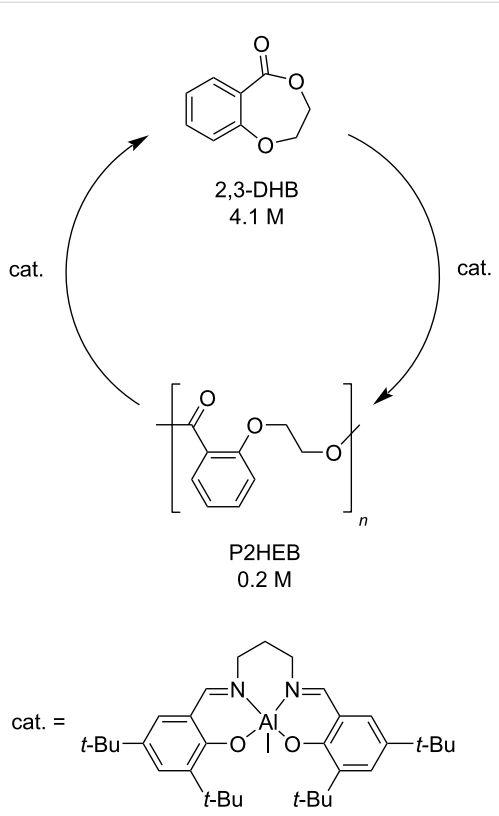

Scheme 17: Polymerisation–depolymerisation cycle of 2,3-HDB.

3.3 Polycarbonates

3.3.1 Poly(bisphenol A carbonate) (PBPAC): Bisphenol A (BPA) is a monomer for a variety of polymers widespread in our everyday life, namely polycarbonates, polyesters, polyethers, polysulphones and epoxy resins [249,283]. Particularly, PBPAC is used in the manufacture of plastics for food and beverage containers, safety helmets, optical lenses, electronic and medical equipment, phones, automotive components and toys [284,285]. This justifies for BPA to be one of the highest-volume chemicals produced worldwide, with a global market of around 6 million tons in 2017, 68% of which account for the manufacture of polycarbonates [286,287]. However, BPA is considered a hazardous substance [288,289] and an endocrine disrupting agent [290,291]. BPA can leach from the corresponding polymers, including water- and temperature-sensitive polycarbonates [292,293]. BPA is industrially obtained by the condensation reaction of phenol with acetone, using an excess of phenol [294]. All byproducts of the process, including unreacted phenol, are toxic [295,296], whereas a purity greater than 98% is required for most BPA applications [297,298]. PBPAC is then produced by the condensation of BPA and a carbonyl source, usually phosgene or diphenyl carbonate [299,300]. Commercial PBPAC is a tough material with an average M_w of 50000 g·mol^{-1} and T_g around 150 °C. It is soluble in THF, hazardous NMP and chlorinated solvents and insoluble in alcohols and water [301]. A number of chemolytic processes have been developed in the recent years for the selective depolymerisation of PBPAC, including hydrogenolysis, hydrolysis, alcoholysis and aminolysis, some of which are metal-catalysed [302,303].

Hydrogenolysis. The hydrogenative depolymerisation of PBPAC was accomplished through the Ru–triphos molecular catalyst described above for PET, PLA, PBT and PCL polyesters [191]. Thus, use of the soluble Ru(triphos)tmm complex,

in conjunction with acid $HNTf_2$ cocatalyst (1:1) in 1,4-dioxane, resulted in complete conversion and selectivity to BPA and methanol under the moderate conditions of using 100 bar H_2 at 140 °C (Scheme 18 and Table 5, entry 1). The protocol could be successfully extended to the depolymerisation of consumer goods, such as compact discs and beverage cups. Notably, pure BPA could be recovered in >70% yield after simple CH_2Cl_2 extraction. A similar approach was recently reported using commercially available Ru(II) catalysts, namely the Milstein [304] and the Ru–MACHO–BH [305] complexes bearing tridentate PN ligands, as shown in Table 5, entries 2 and 3, which are known as efficient hydrogenation catalysts of organic carbonates [306,307]. High BPA yields were obtained in those experiments as well, though with lower hydrogen pressure and catalyst productivity in terms of turnover frequency ($mol_{BPA}{\cdot}mol_{Ru\ cat.}{}^{-1}{\cdot}h^{-1}$). Potassium *tert*-butoxide was used as cocatalyst, the role of which was speculated to activate the carbonate group of the polymer [308]. The depolymerisation of a digital versatile disc (DVD) using the latter catalyst afforded BPA in an estimated 97% yield after THF pretreatment.

Hydrolysis. The hydrolytic depolymerisation of PBPAC in hot compressed water was achieved via manganese acetate catalyst (Scheme 19, top) [309]. Under optimal conditions (280 °C, catalyst loading 2 wt %), the reaction resulted in 55% selectivity to BPA and 19% to phenol at full polymer conversion. A higher selectivity to BPA was obtained by simple Lewis acid treatment using rare earth metal triflate catalysts [310]. The process occurred in the homogeneous phase using a THF/H_2O solvent mixture and a H_2O/PBPAC weight ratio of ≤1. The highest BPA yield (97% at 160 °C) was observed for $La(CF_3SO_3)_3$ due to the reduced decomposition of BPA to phenol, 4-isopropenylphenol and 4-isopropylphenol. A comparison with triflic acid catalyst ruled out the possibility of a proton-catalysed depolymerisation process.

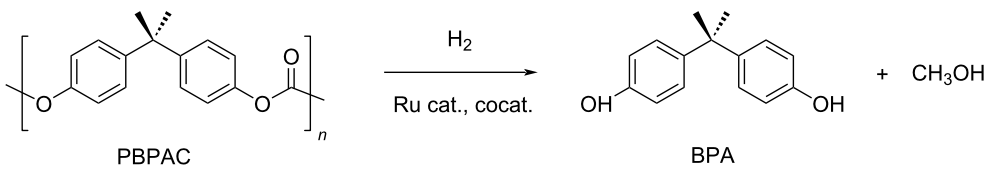

Scheme 18: Hydrogenative depolymerisation of PBPAC by molecular Ru catalysts.

Table 5: Hydrogenolysis of PBPAC by soluble Ru molecular catalysts.

entry	catalyst	cocatalyst[a]	reaction conditions[b]			conv.[c] (%)	BPA		reference
			T (°C)	H_2 (bar)	solvent		sel.[d] (%)	TOF[e] ($mol_{BPA}{\cdot}mol_{cat.}{}^{-1}{\cdot}h^{-1}$)	
1	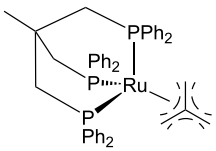	$HNTf_2$[f]	140	100	1,4-dioxane	99	99	6.12[g]	[191]
2	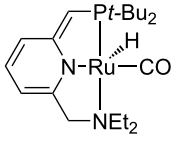	K*t*-BuO	140	45	THF	99	99	1.10	[304]
3	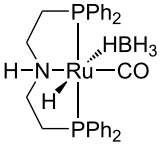	K*t*-BuO	140	45	THF	99	99	0.06	[305]

[a]Catalyst loading 5 mol %, calculated based on PBPAC repetition units, cocatalyst molar ratio = 1:1. [b]Reaction temperature, hydrogen pressure, 24 h reaction time. [c]PBPAC conversion. [d]Selectivity to BPA. [e]Turnover frequency, calculated based on PBPAC repetition units and moles of Ru catalyst. [f]Catalyst loading 1 mol %. [g]Reaction time 16 h.

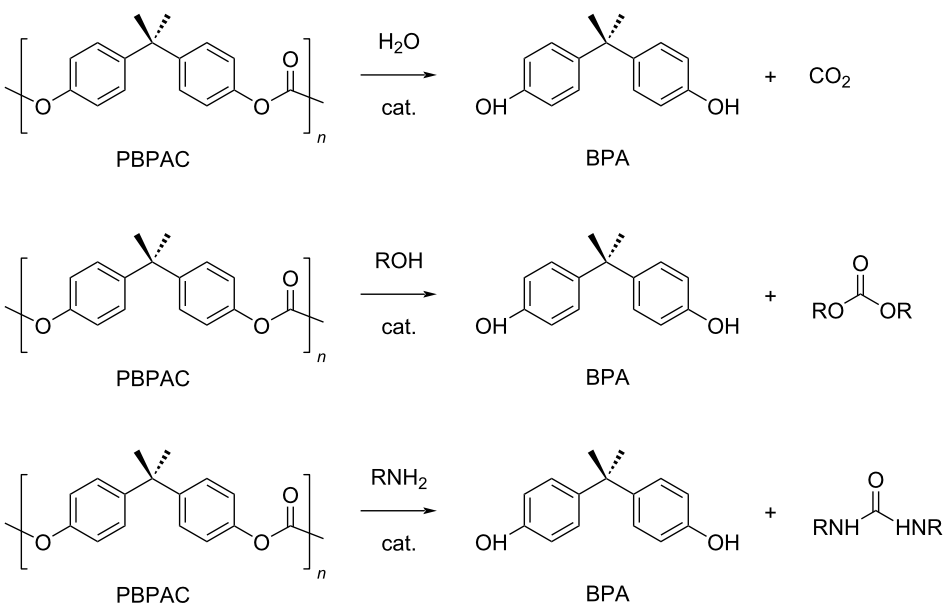

Scheme 19: Catalytic hydrolysis (top), alcoholysis (middle) and aminolysis (bottom) reactions of PBPAC.

Alcoholysis. A variety of metal-based catalytic systems was recently described for the alcoholysis reaction of PBPAC using diverse alcohols (Scheme 19, middle). Thus, a Lewis acid catalyst consisting of a soluble $FeCl_3$–ionic liquid adduct, namely BmimCl·2$FeCl_3$, was reported for the methanolysis of PBPAC, providing BPA in 97% yield at 120 °C [311]. Higher alcohols resulted in lower BPA yields. A mechanism was hypothesised in which the iron centre activates the carbonyl group of the polymer toward nucleophilic attack of methanol. The catalyst could be efficiently recovered and reused over six runs, after ethyl acetate/water extraction. On the other hand, CeO_2–CaO particles onto hollow ZrO_2 nanospheres were used as heterogeneous catalyst for the methanolysis of PBPAC, yielding around 95% BPA at 100 °C in a THF/methanol mixture [312]. The basic sites, due to lattice O^{2-} of CeO_2, were attributed to be responsible for the deprotonation of methanol, and thus initiating the solvolytic process in that reaction. Depolymerisation of PBPAC was reported using various alcohols (methanol, phenol, benzyl alcohol, 1-naphthol, PD, glycerol), a mechanical mixture of zinc oxide NPs and tetrabutylammonium chloride as catalyst as well as THF cosolvent to give BPA and the corresponding carbonates in >98% yield at 100 °C reaction temperature (Scheme 19) [313]. The insoluble Lewis acid ZnO catalyst could be removed from the reaction mixture by centrifugation and reused five times with a minor loss of activity. However, Bu_4NCl was only partially recovered and had to be integrated with fresh cocatalyst after each run. Remarkably, the reaction with glycerol enabled the recycling of two industrial wastes (PBPAC and glycerol) into the valuable chemicals BPA and glycerol carbonate in one process only, with the latter compound being industrially used as synthetic intermediate, solvent and in the formulation of cosmetics [314].

Aminolysis. The ZnO–Bu_4NCl Lewis acid catalytic mixture was also successfully used in the aminolytic depolymerisation of PBPAC by different amines (cyclohexylamine, aniline, imidazole, 1,2-diaminopropane, 1,3-diaminopropane) to give the corresponding substituted (cyclic) ureas in >97% yield (Scheme 19, bottom) [313]. The reaction with 2-amino-1-propanol gave 4-methyloxazolidin-2-one. Despite the complications due to separation from BPA, the process provides ureas of industrial relevance as anticancer or antiviral agents [315,316].

3.3.2 Poly(propylene carbonate) (PPC) and poly(ethylene carbonate) (PEC): PPC is a thermoplastic material obtained by the copolymerisation of CO_2 with propylene oxide or propylenediol, which is mainly used as a packing material and in binder applications [317]. It has a low thermal stability, with a decomposition temperature around 200 °C and a T_g around 40 °C, depending on the molecular weight. PPC may be readily dissolved in many solvents (e.g., chlorinated hydrocarbons, THF, benzene, ethyl acetate and lower ketones), but it is insoluble in longer-chain alkanes, alcohols and water [318].

Hydrogenative depolymerisation of PPC and PEC to methanol and the respective glycols (PD and EG, respectively) was achieved using the soluble Milstein ruthenium catalysts described above for the hydrogenolysis of PET (Scheme 20) [188]. Thus, more than 91% glycol yield was obtained using a

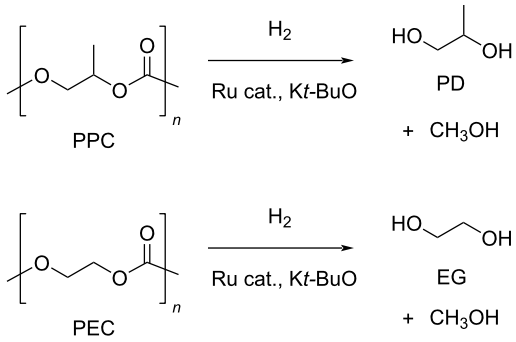

Scheme 20: Hydrogenative depolymerisation of PPC (top) and PEC (bottom) by molecular Ru catalysts.

1:2 Ru catalyst/butoxide molar ratio, 160 °C reaction temperature, 55 bar H_2 pressure and an anisole/THF 1:1 solvent mixture (Table 6, entries 1 and 2). The same approach was adopted using a Ru(II)–PNP pincer complex, showing higher catalytic activity (TOF 41.3 h^{-1}) under similar reaction conditions (Table 6, entry 3) [319]. The role of butoxide was proposed to be the conversion of the staring molecular complex in the catalytically active species by elimination of HCl. Similarly, a nonprecious PNN–manganese carbonyl complex was reported to afford PD from PPC in 91% yield (Table 6, entry 4) [320]. By contrast, use of a comparable Mn complex and KH as activator resulted in a much lower selectivity to PD (68%) at full PPC conversion (110 °C, 50 bar H_2, in toluene), resulting in the formation of a propylene carbonate byproduct [321].

Table 6: Hydrogenolysis of PPC by molecular metal catalysts.

entry	catalyst	cocatalyst[a]	reaction conditions[b]			conv.[c] (%)	PD		reference
			T (°C)	H_2 (bar)	solvent		sel.[d] (%)	TOF[e] ($mol_{PD}·mol_{cat.}^{-1}·h^{-1}$)	
1	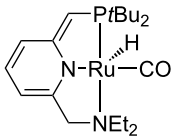	Kt-BuO	160	55	anisole/THF[f]	99	100	4.12	[188]
2	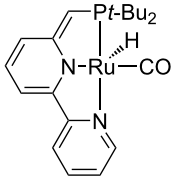	Kt-BuO	160	55	anisole/THF[f]	99	100	4.12	[188]
3	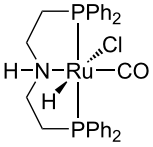	Kt-BuO[g]	140	50	THF	99	99	41.25	[319]
4	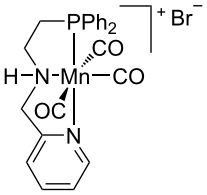	Kt-BuO[h]	140	50	1,4-dioxane	91	100	2.84[i]	[320]
5	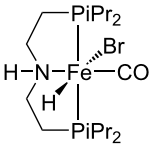	Kt-BuO[j]	140	—	iPrOH/THF[k]	65	100	0.43	[322]

[a]Catalyst loading 1 mol %, calculated based on PPC repetition units, cocatalyst molar ratio = 2:1. [b]Reaction temperature, hydrogen pressure, 24 h reaction time. [c]PPC conversion. [d]Selectivity to PD. [e]Turnover frequency, calculated based on PPC repetition units and moles of Ru catalyst. [f]1:1, v/v. [g]Catalyst loading 0.1 mol %, cocatalyst molar ratio = 1:1. [h]Catalyst loading 0.2 mol %, cocatalyst molar ratio = 2:1. [i]Reaction time 16 h. [j]Catalytic hydrogen transfer. Catalyst loading 5 mol %, cocatalyst molar ratio = 1:1, reaction time 30 h. [k]4:1, v/v.

In the search of safer and "greener" alternatives, a slightly different approach to controlled PPC depolymerisation was recently proposed, based on catalytic hydrogen transfer rather than hydrogenation reaction, and thus to avoid involvement of high H_2 pressures [322]. Thus, hydrogen transfer from isopropanol to PPC using a soluble iron pincer-type catalyst resulted in a 65% PD yield at 140 °C (Table 6, entry 5). However, a relatively high amount of catalyst was required. Potassium butoxide and THF were used as precatalyst activator and cosolvent, respectively.

3.3.3 Other carbonates: A polycarbonate suitable for smooth chemical recycle was engineered based on 1-benzyloxycarbonyl-3,4-epoxypyrrolidine (BEP) units [323]. In fact, a one-pot copolymerisation–depolymerisation cycle was enabled using a dinuclear salen–chromium complex in the presence of a bis(triphenylphosphine)iminium cocatalyst (Scheme 21). Therein, the BEP monomer was fully converted to the polycarbonate at 60 °C reaction temperature, while complete and selective depolymerisation back to BEP was achieved at 100 °C. The process could be repeated several times with no changes in either the monomer or the copolymer structure. After removing the catalyst, the polymer was stable at 200 °C for 10 h.

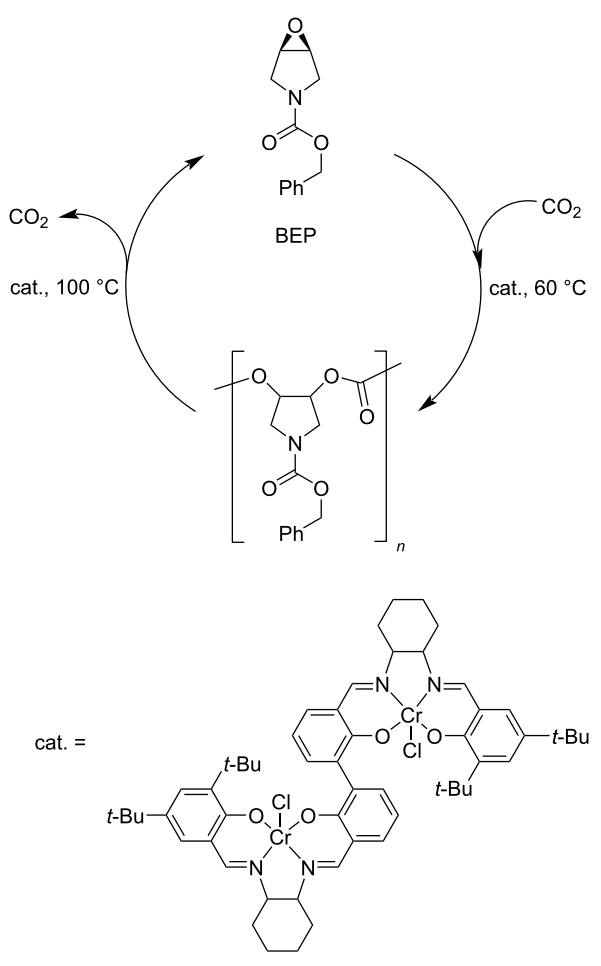

Scheme 21: Polymerisation-depolymerisation cycle of BEP.

3.4 Polyamides (PA)

Polyamides may be natural (e.g., silk, wool) or synthetic polymers (e.g., nylons, aramids, polyaspartates) that are largely used in the manufacture of fibres and automotive components as well as in biomedicine, due to their excellent mechanical and thermal properties [324,325]. The widespread use of polyamides and the high price of the starting monomers, such as ε-caprolactam, have led to the development of several methods for their chemical recycling. Most of these are based on mineral acid [326], organic base (e.g., 4-dimethylaminopyridine, triethylenetetramine) [327,328] or organic acid (e.g., glycolic, lactic, benzoic acid) [329] catalysis, using supercritical methanol or ionic liquids as solvent [330]. Few literature reports exist on the depolymerisation of polyamides using metal catalysts. In an earlier paper, the hydrolysis of nylon-6 was achieved by a combination of zinc chloride (40 wt %) and phosphoric acid (20 wt %) under microwave irradiation, however, resulting in a mixture of linear and cyclic oligomers at 89% polymer conversion [121,331]. While drafting the present review, the first example of catalytic hydrogenative depolymerisation of polyamides and polyurethanes was described, using soluble Milstein-type Ru–pincer complexes (2 mol %), DMSO solvent and K*t*-BuO cocatalyst at 150 °C and 70 bar H_2 [332]. Typically, a selectivity to the corresponding diols/diamines/amino alcohols in the range of 20–80% was observed at 60–99% conversion, depending on the polymeric substrate. For instance, 6-amino-hexan-1-ol and BDM were obtained in 24% and 80% yield, respectively, from nylon-6 and the polyamide shown in Scheme 22.

3.5 Other plastics

3.5.1 Epoxy resins (EP): EP are thermosetting polymers featuring high thermal and chemical resistance. They are widely used in the manufacture of paints, metal coatings, electronic components and adhesives [333]. EP are usually reinforced with fibres to give composite materials for the aeronautical, automotive and sport industries. Actually, recycling efforts of EP were mainly focused on the recovery of valuable (expensive) carbon fibres rather than the polymers themselves. Recently, a metal-catalysed route was reported for the degradation of the epoxy resin of bisphenol A diglycidyl ether (BADGE)–carbon fibres composites [334]. Therein, low-coordinated aquo ions of zinc enabled the selective cleavage of the R_2CH–N bond while keeping intact RCH_2–N, C–C and C–O bonds (Scheme 23). The method was previously adopted for the conversion of cellulose to hydroxymethylfurfural and required the use of highly soluble zinc chloride to obtain a concentrated aqueous solution of metal

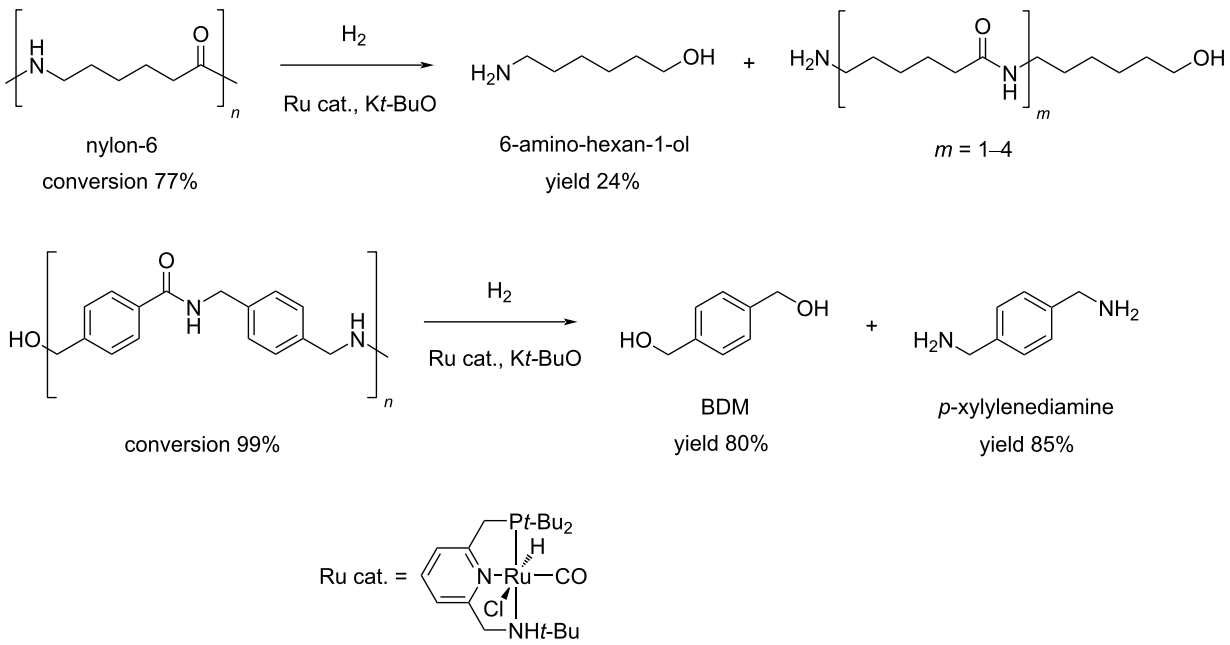

Scheme 22: Hydrogenolysis of polyamides using soluble Ru catalysts.

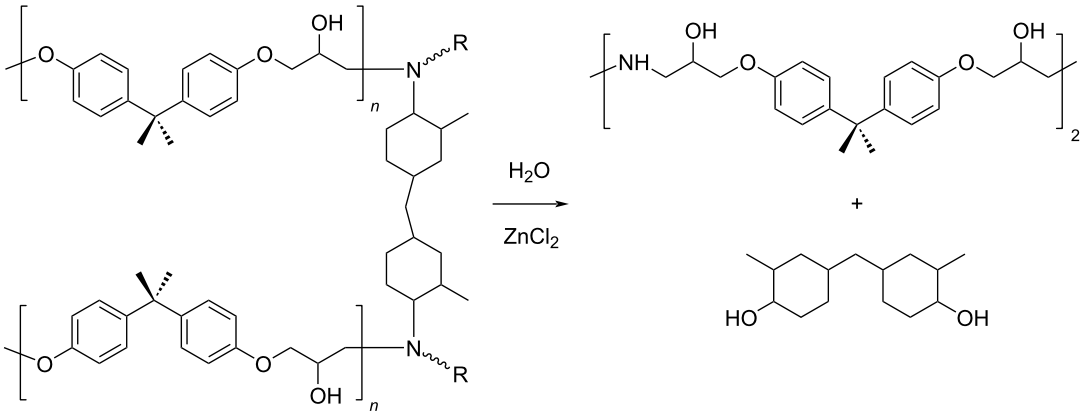

Scheme 23: Catalytic depolymerisation of epoxy resin/carbon fibres composite.

(60 wt % $ZnCl_2$) [335]. On this basis, the small, incompletely coordinated Zn^{2+} ions were proposed to activate the selective cleavage of C–N bonds, acting as Lewis acid centres. The process carried out at 220 °C led to carbon fibres, a dimer of DGEBA reused for the synthesis of new EP, and 4,4'-methylenebis(2-methylcyclohexanol). The concentrated $ZnCl_2$ solution showed good reusability, and thus adding some advantages to common highly energy-consuming methods.

3.5.2 Polyethers: Polyethers are polymers with a solubility that depends heavily on the solvent used, including water, and they find applications in the cosmetic, pharmacy or paint industries [336]. Thermal decomposition or disposal into landfills are consolidated management systems of "end-of-life" polyethers [337,338], whereas very few studies cope with the catalytic depolymerisation through selective C–O bond cleavage into specific low-molecular-weight chemicals.

The group of Enthaler reported a number of research with a common strategy for polyethers depolymerisation [339-341]: Basically, the solvent-free reaction of a polyether with an acyl chloride in the presence of a catalytic amount (5 mol %) of zinc or iron salts as Lewis acid catalysts results in monomeric chloroesters, which are valuable chemicals reprocessable into other polymers (Scheme 24). A deep study was carried out investigating the effect of key reaction parameters: metal salt,

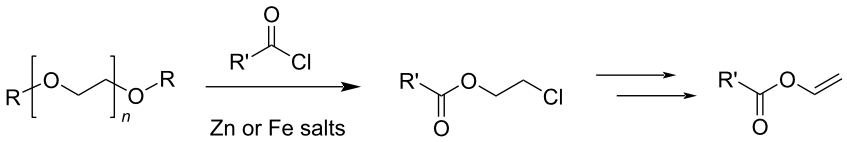

Scheme 24: Depolymerisation of polyethers with metal salt catalysts and acyl chlorides.

catalyst loading, temperature, depolymerisation agent and the applicability to a variety of polyethers. Successful examples include depolymerisation of polyethylene glycol (PEG) and polytetrahydrofuran (polyTHF) to chloroesters in 70–78% and 92% yield, respectively, using $ZnCl_2$ at 130 °C or $Zn(OTf)_2$ catalyst when acetic anhydride was used as depolymerising agent [339,340]. Chloroester yields in the range 89–95% were obtained for PEG depolymerisation at 100 °C using $FeCl_2$ as catalyst [341]. A mechanism was postulated in which the ether bond is cleaved via formation of an iron alkoxide intermediate (Scheme 25). Sustainability issues relate to the hazardous properties of low-molecular-weight acyl chlorides, which could be partially circumvented by the use of bioderived fatty acid chlorides [340].

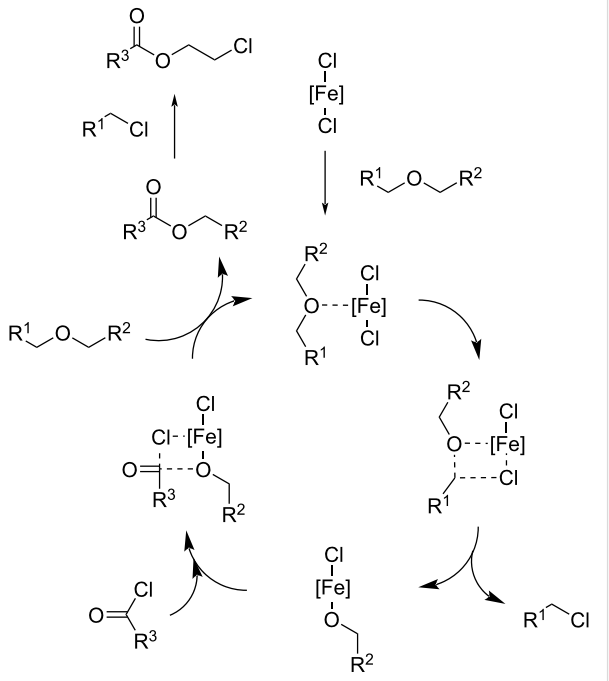

Scheme 25: Proposed mechanism for the iron-catalysed depolymerisation reaction of polyethers. Adapted with permission from [341], Copyright © 2012 WILEY-VCH Verlag GmbH & Co. KGaA, Weinheim. Used with permission from Stephan Enthaler and Maik Weidauer, "Low-Temperature Iron-Catalysed Depolymerization of Polyethers", ChemSusChem, John Wiley and Sons.

In a different approach, selective ring-closing depolymerisation of polyTHF to THF was achieved in 92% and 95% yield, respectively, using Lewis acid catalysis by $FeCl_3$ (5 mol %, 180 °C) [342] or phosphotungstic acid (10 wt %, 130 °C) [343].

Conclusion

The implementation of a value chain for plastics, in which design is coupled with production, use, depolymerisation and reprocessing, may substantially contribute to the development of a truly circular economy model for plastic materials, wherein scraps are converted into useful chemicals and reusable building blocks [344]. This model addresses three grand challenges of our century: pollution of the habitat, carbon dioxide emissions and dependence on fossil sources. However, performing plastics recycling via chemical processing is not enough. This must be achieved at competitive economic and environmental costs [345]. A perusal of the recent literature indicates that, despite their urgency and significance, strategies for sustainable chemical recycling are surprisingly still rather underdeveloped. Most methods for controlled and selective depolymerisation rely on harsh reaction conditions, use of an excess of reagents, toxic solvents and troublesome downstream treatments often generating a considerable amount of waste. Metal catalysis may represent a useful tool to overcome these issues, provided that significant improvements are achieved in relation to key challenges.

Catalysts

Most processes, particularly if based on solvolysis reactions, are carried out using traditional metal salt-based catalysts (e.g., zinc chloride, zinc acetate), the role of which is merely to act as Lewis acid centres, and they are often needed in a large amount with respect to the plastic to be depolymerised (i.e., >2 and up to 60 wt %). In some cases, toxic metals (e.g., Co, Ni) result in the highest catalytic efficiency. A significant improvement is represented by the use of molecular complex catalysts, particularly based on ruthenium for use in hydrogenolysis. These systems, typically used in up to 2 wt %, are quite efficient under relatively mild reaction conditions, although a strong acid or basic cocatalyst is usually required. On the other hand, soluble catalysts were mainly investigated so far, with clear limitations in terms of catalyst separation and reuse, purification, scale-up

and cost. The use of meal-based ionic liquids and deep eutectic solvents has also been explored; however, their viability for practical application at large is uncertain [346]. Thus, inventive catalysts shall be developed with particular attention to heterogeneous systems, for instance, solid-supported metal species based on low-cost metals and solid materials featured by enhanced mass transfer and thermal resistance properties. Bifunctional solid catalysts bearing arrays of metal and acid single-sites may be useful in the same instances and processes [347,348].

Polymers

Easily and selectively depolymerisable plastics are relatively uncommon, owing to the poor mechanical and physical properties and to the low temperature required to achieve their polymerisation [280]. Specifically designed, chemically recyclable polymers have been developed in some cases, which may offer an affordable solution to this regard (see, e.g., Section 3.2.3). These materials are indeed usable in closed polymerisation–depolymerisation loops, and hence appropriate to extend the life cycle of plastics. Excellent reviews describe the recent developments in the field [71].

Processes

Large-scale chemical recycling of plastics is thus far hampered by the higher costs compared to mechanical recycling. A reason for this lays in the scarce development of effective catalysts. On the other hand, most processes for chemical recycling are still based on conventional organic reactions, requiring an excess of (unstable) decomposing agents or high temperature (e.g., for transesterifications). Moreover, performing the reactions in the homogeneous phase improves their kinetics, which, however, is limited by the usual poor solubility of polymers, and thus often ending up in the use of toxic solvents (e.g., chlorinated ones). Hence, besides the need for more efficient catalysts, the use of renewable and safer reagents and solvents is certainly desirable [349,350]. More importantly, novel processes and depolymerisation strategies have to be designed. Whereas glycolysis and methanolysis methods have reached commercial maturity (e.g., for PET), at high energy costs, however, in other instances (e.g., for polyolefins), no efficient processes for selective depolymerisation are in place yet. Hydrogenative depolymerisation represents a promising contribution to this end, owing to the use of the clean reducing agent H_2, no need for organic reactants, reduced amount of metal catalyst, milder reaction conditions and limited formation of byproducts. Issues related to hydrogen supply may be circumvented, e.g., by in situ-generated hydrogen. Novel processes have thus to be developed, with special emphasis on those based on reaction sequences in one-pot or depolymerisation–polymerisation cycles as they clearly benefit from reduced energy inputs, reactor volumes and units, no need for intermediate purification/separation steps and better automation. Notably, methods for the direct reprocessing of plastics into valuable chemicals or polymers take advantage of metal catalysts (see Sections 3.2.3 and 3.3.3). Finally, coupling one-pot techniques with the use of lytic agents other than the conventional ones may remarkably enlarge the scenario of depolymerisation products beyond that of the simple plastic components. Table 7 summarises the most common monomers obtainable in the metal-catalysed depolymerisation of plastics described in the present review. It is predictable that a greater variety of added-value products, such as monomers, oligomers and the chemically derived, functionalised compounds thereof, may be obtained by developing alternative depolymerisation pathways and reprocessing strategies.

In conclusion, as it was previously outlined, circular chemistry is a precondition for a truly circular economy, particularly in the field of production of goods and materials [351]. Chemical recycling via metal catalysts may effectively contribute to a circular recycling vision for postconsumer plastics, provided that the strategy is further developed and improved, aiming to reduce costs and environmental impact of selective depolymerisation processes. The design of novel versatile catalysts and more sustainable processes are key in this direction.

Table 7: Common monomeric products of metal-catalysed chemolytic depolymerisation reactions of plastics.[a]

polymer type	chemolytic method				
	hydrogenolysis	hydrolysis	alcoholysis	glycolysis	aminolysis
polyolefins	hydrocarbons[b]	—	—	—	—
polyesters	diols	acids (+ diols)	esters (+ diols)	esters	amides + diols
polycarbonates	diols + CH_3OH	diols + CO_2	diols + carbonates[c]	diols + cyclic carbonates[c]	diols + ureas[d]
polyamides	amines, alcohols	amines, acids	—	—	—

[a]The monomeric products indicated (e.g., diols) are those corresponding to the repeating units in the polymer. [b]Usually liquid mixtures. [c]Organic carbonates. [d]N-substituted ureas.

ORCID® iDs

Francesca Liguori - https://orcid.org/0000-0002-5520-1550
Carmen Moreno-Marrodán - https://orcid.org/0000-0003-0805-0726
Pierluigi Barbaro - https://orcid.org/0000-0002-7298-5756

References

1. Circular Economy Action Plan, European Commission, Brussels, Belgium, 2020. https://ec.europa.eu/environment/circular-economy/pdf/new_circular_economy_action_plan.pdf (accessed Jan 27, 2021).
2. Towards a circular economy - Waste management in the EU, PE 581.913, European Parliamentary Research Service, Brussels, Belgium, 2017. https://www.europarl.europa.eu/RegData/etudes/STUD/2017/581913/EPRS_STU%282017%29581913_EN.pdf (accessed Jan 27, 2021).
3. Heidbreder, L. M.; Bablok, I.; Drews, S.; Menzel, C. *Sci. Total Environ.* **2019,** *668,* 1077–1093. doi:10.1016/j.scitotenv.2019.02.437
4. Narancic, T.; O'Connor, K. E. *Microbiology (London, U. K.)* **2019,** *165,* 129–137. doi:10.1099/mic.0.000749
5. Moharir, R. V.; Kumar, S. *J. Cleaner Prod.* **2019,** *208,* 65–76. doi:10.1016/j.jclepro.2018.10.059
6. Raddadi, N.; Fava, F. *Sci. Total Environ.* **2019,** *679,* 148–158. doi:10.1016/j.scitotenv.2019.04.419
7. Sardon, H.; Dove, A. P. *Science* **2018,** *360,* 380–381. doi:10.1126/science.aat4997
8. Thomas, P.; Rumjit, N. P.; Lai, C. W.; Johan, M. R. B.; Saravanakumar, M. P. Polymer-Recycling of Bulk Plastics. *Encyclopedia of Renewable and Sustainable Materials;* Elsevier: Amsterdam, Netherlands, 2020; Vol. 2, pp 432–454. doi:10.1016/b978-0-12-803581-8.10765-9
9. Wright, S. L.; Kelly, F. J. *Environ. Sci. Technol.* **2017,** *51,* 6634–6647. doi:10.1021/acs.est.7b00423
10. Lehner, R.; Weder, C.; Petri-Fink, A.; Rothen-Rutishauser, B. *Environ. Sci. Technol.* **2019,** *53,* 1748–1765. doi:10.1021/acs.est.8b05512
11. Plastics - the Facts 2019, Plastics Europe, Association of Plastics Manufacturers, Brussels, Belgium, 2019. https://www.plasticseurope.org/application/files/9715/7129/9584/FINAL_web_version_Plastics_the_facts2019_14102019.pdf (accessed Jan 27, 2021).
12. Geyer, R.; Jambeck, J. R.; Law, K. L. *Sci. Adv.* **2017,** *3,* e1700782. doi:10.1126/sciadv.1700782
13. The New Plastics Economy: Rethinking the future of plastics & catalysing action, Ellen MacArthur Foundation, 2017. https://www.ellenmacarthurfoundation.org/assets/downloads/publications/NPEC-Hybrid_English_22-11-17_Digital.pdf (accessed Jan 27, 2021).
14. Li, J.; Song, Y.; Cai, Y. *Environ. Pollut.* **2020,** *257,* 113570. doi:10.1016/j.envpol.2019.113570
15. Wang, J.; Liu, X.; Li, Y.; Powell, T.; Wang, X.; Wang, G.; Zhang, P. *Sci. Total Environ.* **2019,** *691,* 848–857. doi:10.1016/j.scitotenv.2019.07.209
16. Peng, L.; Fu, D.; Qi, H.; Lan, C. Q.; Yu, H.; Ge, C. *Sci. Total Environ.* **2020,** *698,* 134254. doi:10.1016/j.scitotenv.2019.134254
17. Jambeck, J. R.; Geyer, R.; Wilcox, C.; Siegler, T. R.; Perryman, M.; Andrady, A.; Narayan, R.; Law, K. L. *Science* **2015,** *347,* 768–771. doi:10.1126/science.1260352
18. Iannilli, V.; Pasquali, V.; Setini, A.; Corami, F. *Environ. Res.* **2019,** *179,* 108811. doi:10.1016/j.envres.2019.108811
19. Brahney, J.; Hallerud, M.; Heim, E.; Hahnenberger, M.; Sukumaran, S. *Science* **2020,** *368,* 1257–1260. doi:10.1126/science.aaz5819
20. Zheng, J.; Suh, S. *Nat. Clim. Change* **2019,** *9,* 374–378. doi:10.1038/s41558-019-0459-z
21. Dormer, A.; Finn, D. P.; Ward, P.; Cullen, J. *J. Cleaner Prod.* **2013,** *51,* 133–141. doi:10.1016/j.jclepro.2013.01.014
22. Hopewell, J.; Dvorak, R.; Kosior, E. *Philos. Trans. R. Soc., B* **2009,** *364,* 2115–2126. doi:10.1098/rstb.2008.0311
23. Kiser, B. *Nature* **2016,** *531,* 443–446. doi:10.1038/531443a
24. A European Strategy for Plastics in a Circular Economy, European Commission, Brussels, Belgium, 2018. https://ec.europa.eu/environment/circular-economy/pdf/plastics-strategy-brochure.pdf (accessed Jan 27, 2021).
25. Xu, C.; Nasrollahzadeh, M.; Selva, M.; Issaabadi, Z.; Luque, R. *Chem. Soc. Rev.* **2019,** *48,* 4791–4822. doi:10.1039/c8cs00543e
26. Maschmeyer, T.; Luque, R.; Selva, M. *Chem. Soc. Rev.* **2020,** *49,* 4527–4563. doi:10.1039/c9cs00653b
27. Kanani, F.; Heidari, M. D.; Gilroyed, B. H.; Pelletier, N. *J. Cleaner Prod.* **2020,** *262,* 121129. doi:10.1016/j.jclepro.2020.121129
28. Cavani, F.; Albonetti, S.; Basile, F.; Gandini, A., Eds. *Chemicals and Fuels from Bio-Based Building Blocks;* Wiley-VCH: Weinheim, Germany, 2016. doi:10.1002/9783527698202
29. Jérôme, F.; Chatel, G.; De Oliveira Vigier, K. *Green Chem.* **2016,** *18,* 3903–3913. doi:10.1039/c6gc00814c
30. Breakthrough Innovations Enabling Waste-to-Product, Report ID 4900532, Research and Markets, Dublin, Ireland, Dec 2019.
31. Müller, R. J. In *Biodegradability of Polymers: Regulations and Methods for Testing;* Steinbüchel, A., Ed.; Biopolymers Online; John Wiley & Sons: Hoboken, NJ, USA, 2005. doi:10.1002/3527600035.bpola012
32. Niaounakis, M. *Biopolymers: Applications and Trends;* Elsevier: Amsterdam, Netherlands, 2015. doi:10.1016/c2014-0-00936-7
33. Vert, M.; Doi, Y.; Hellwich, K.-H.; Hess, M.; Hodge, P.; Kubisa, P.; Rinaudo, M.; Schué, F. *Pure Appl. Chem.* **2012,** *84,* 377–410. doi:10.1351/pac-rec-10-12-04
34. Rudnik, E. Compostable Polymer Materials: Definitions, Structures, and Methods of Preparation. *Handbook of Biopolymers and Biodegradable Plastics;* Elsevier: Amsterdam, Netherlands, 2013; pp 189–211. doi:10.1016/b978-1-4557-2834-3.00010-0
35. Commission Decision of 28 June 2001 relating to the publication of references for standards EN 13428:2000, EN 13429:2000, EN 13430:2000, EN 13431:2000 and EN 13432:2000 in the Official Journal of the European Communities in connection with Directive 94/62/EC on packaging and packaging waste, L 190, 12/07/2001, 21-23, 2001/524/EC, European Commission, Brussels, Belgium, 2001. https://op.europa.eu/en/publication-detail/-/publication/17d5b3cd-42a7-45ef-a821-2f773d551f1f (accessed Jan 27, 2021).
36. EN 13432 Certified bioplastic performance in industrial composting, European Bioplastics e.V., Berlin, Germany, 2015. https://docs.european-bioplastics.org/publications/bp/EUBP_BP_En_13432.pdf (accessed Jan 27, 2021).
37. Datta, J.; Kopczyńska, P. *Crit. Rev. Environ. Sci. Technol.* **2016,** *46,* 905–946. doi:10.1080/10643389.2016.1180227
38. The APR Design® Guide for Plastics Recyclability, Association of Plastic Recyclers, Washington, DC, 2018. https://plasticsrecycling.org/apr-design-guide (accessed Jan 27, 2021).

39. Plastic Recyclers Europe, Brussels, Belgium. https://www.plasticsrecyclers.eu/design-recycling (accessed June 1, 2020).
40. Merrington, A. Recycling of Plastics. *Applied Plastics Engineering Handbook,* 2nd ed.; Elsevier: Amsterdam, Netherlands, 2017; pp 167–189. doi:10.1016/b978-0-323-39040-8.00009-2
41. *Guide for Waste Reduction, Resource Recovery, and Use of Recycled Polymeric Materials and Products, ASTM D7209-06;* ASTM International: West Conshohocken, PA, U.S.A.. doi:10.1520/d7209-06
42. Sahajwalla, V.; Gaikwad, V. *Curr. Opin. Green Sustainable Chem.* **2018,** *13,* 102–107. doi:10.1016/j.cogsc.2018.06.006
43. Nikles, D. E.; Farahat, M. S. *Macromol. Mater. Eng.* **2005,** *290,* 13–30. doi:10.1002/mame.200400186
44. Hamad, K.; Kaseem, M.; Deri, F. *Polym. Degrad. Stab.* **2013,** *98,* 2801–2812. doi:10.1016/j.polymdegradstab.2013.09.025
45. Directive 2008/98/EC of the European Parliament and of the Council of 19 November 2008 on waste and repealing certain Directives, European Commission, Brussels, Belgium, 2008. https://eur-lex.europa.eu/legal-content/EN/TXT/?uri=celex%3A32008L0098 (accessed Jan 27, 2021).
46. Reuse - Rethinking Packaging, Ellen MacArthur Foundation, 2019. https://www.ellenmacarthurfoundation.org/assets/downloads/Reuse.pdf (accessed Jan 27, 2021).
47. Al-Salem, S. M.; Lettieri, P.; Baeyens, J. *Waste Manage. (Oxford, U. K.)* **2009,** *29,* 2625–2643. doi:10.1016/j.wasman.2009.06.004
48. Chandrasekaran, S. R.; Sharma, B. K. From Waste to Resources: How to Integrate Recycling Into the Production Cycle of Plastics. *Plastics to Energy;* Elsevier: Amsterdam, Netherlands, 2019; pp 345–364. doi:10.1016/b978-0-12-813140-4.00013-3
49. Ignatyev, I. A.; Thielemans, W.; Vander Beke, B. *ChemSusChem* **2014,** *7,* 1579–1593. doi:10.1002/cssc.201300898
50. Vilaplana, F.; Karlsson, S. *Macromol. Mater. Eng.* **2008,** *293,* 274–297. doi:10.1002/mame.200700393
51. Kaminsky, W.; Hartmann, F. *Angew. Chem., Int. Ed.* **2000,** *39,* 331–333. doi:10.1002/(sici)1521-3773(20000117)39:2<331::aid-anie331>3.0.co;2-h
52. Welle, F. Food Law Compliance of Poly(ethylene Terephthalate) (PET) Food Packaging Materials. In *Food Additives and Packaging;* Komolprasert, V.; Turowski, P., Eds.; ACS Symposium Series, Vol. 1162; American Chemical Society: Washington, DC, USA, 2014; pp 167–195. doi:10.1021/bk-2014-1162.ch016
53. Sethi, B. Methods of Recycling. In *Recycling of Polymers - Methods, Characterization and Applications;* Francis, R., Ed.; Wiley-VCH: Weinheim, Germany, 2017; pp 55–114. doi:10.1002/9783527689002.ch3
54. Thiounn, T.; Smith, R. C. *J. Polym. Sci. (Hoboken, NJ, U. S.)* **2020,** *58,* 1347–1364. doi:10.1002/pol.20190261
55. Al-Salem, S. M.; Antelava, A.; Constantinou, A.; Manos, G.; Dutta, A. *J. Environ. Manage.* **2017,** *197,* 177–198. doi:10.1016/j.jenvman.2017.03.084
56. Serrano, D. P.; Aguado, J.; Escola, J. M. *ACS Catal.* **2012,** *2,* 1924–1941. doi:10.1021/cs3003403
57. Panda, A. K.; Singh, R. K. *J. Fuel Chem. Technol. (Beijing, China)* **2011,** *39,* 198–202. doi:10.1016/s1872-5813(11)60017-0
58. Butler, E.; Devlin, G.; McDonnell, K. *Waste Biomass Valorization* **2011,** *2,* 227–255. doi:10.1007/s12649-011-9067-5
59. Ciesielski, P. N.; Pecha, M. B.; Bharadwaj, V. S.; Mukarakate, C.; Leong, G. J.; Kappes, B.; Crowley, M. F.; Kim, S.; Foust, T. D.; Nimlos, M. R. *Wiley Interdiscip. Rev.: Energy Environ.* **2018,** *7,* e297. doi:10.1002/wene.297
60. Munir, D.; Irfan, M. F.; Usman, M. R. *Renewable Sustainable Energy Rev.* **2018,** *90,* 490–515. doi:10.1016/j.rser.2018.03.034
61. Al-Salem, S. M.; Lettieri, P.; Baeyens, J. *Prog. Energy Combust. Sci.* **2010,** *36,* 103–129. doi:10.1016/j.pecs.2009.09.001
62. Verma, R.; Vinoda, K. S.; Papireddy, M.; Gowda, A. N. S. *Procedia Environ. Sci.* **2016,** *35,* 701–708. doi:10.1016/j.proenv.2016.07.069
63. Gente, V.; La Marca, F. Study on the Feasibility of Hazardous Waste Recycling: The Case of Pharmaceutical Packaging. In *Material Recycling-Trends and Perspectives;* Achilias, D. S., Ed.; IntechOpen: Rijeka, Croatia, 2012; pp 237–264. doi:10.5772/34389
64. Keane, M. A. *ChemSusChem* **2009,** *2,* 207–214. doi:10.1002/cssc.200900001
65. Veethahavya, K. S.; Rajath, B. S.; Noobia, S.; Kumar, B. M. *Procedia Environ. Sci.* **2016,** *35,* 709–713. doi:10.1016/j.proenv.2016.07.072
66. Brems, A.; Baeyens, J.; Dewil, R. *Therm. Sci.* **2012,** *16,* 669–685. doi:10.2298/tsci120111121b
67. Burange, A. S.; Gawande, M. B.; Lam, F. L. Y.; Jayaram, R. V.; Luque, R. *Green Chem.* **2015,** *17,* 146–156. doi:10.1039/c4gc01760a
68. Ma, C.; Yu, J.; Wang, B.; Song, Z.; Xiang, J.; Hu, S.; Su, S.; Sun, L. *Renewable Sustainable Energy Rev.* **2016,** *61,* 433–450. doi:10.1016/j.rser.2016.04.020
69. Pathak, V. M.; Navneet. *Bioresour. Bioprocess.* **2017,** *4,* 15. doi:10.1186/s40643-017-0145-9
70. Urbanek, A. K.; Mirończuk, A. M.; García-Martín, A.; Saborido, A.; de la Mata, I.; Arroyo, M. *Biochim. Biophys. Acta, Proteins Proteomics* **2020,** *1868,* 140315. doi:10.1016/j.bbapap.2019.140315
71. Hong, M.; Chen, E. Y.-X. *Green Chem.* **2017,** *19,* 3692–3706. doi:10.1039/c7gc01496a
72. Circular economy in Europe - Developing the knowledge base, Report No. 2/2016, European Environment Agency, 2016. https://www.eea.europa.eu/publications/circular-economy-in-europe (accessed Jan 27, 2021).
73. Carey, J. *Proc. Natl. Acad. Sci. U. S. A.* **2017,** *114,* 612–616. doi:10.1073/pnas.1620655114
74. Haider, T. P.; Völker, C.; Kramm, J.; Landfester, K.; Wurm, F. R. *Angew. Chem., Int. Ed.* **2019,** *58,* 50–62. doi:10.1002/anie.201805766
75. Webb, H. K.; Arnott, J.; Crawford, R. J.; Ivanova, E. P. *Polymers (Basel, Switz.)* **2013,** *5,* 1–18. doi:10.3390/polym5010001
76. Schneiderman, D. K.; Hillmyer, M. A. *Macromolecules* **2017,** *50,* 3733–3749. doi:10.1021/acs.macromol.7b00293
77. Wei, R.; Zimmermann, W. *Microb. Biotechnol.* **2017,** *10,* 1308–1322. doi:10.1111/1751-7915.12710
78. Zhang, X.; Fevre, M.; Jones, G. O.; Waymouth, R. M. *Chem. Rev.* **2018,** *118,* 839–885. doi:10.1021/acs.chemrev.7b00329
79. Fiorentino, G.; Ripa, M.; Ulgiati, S. *Biofuels, Bioprod. Biorefin.* **2017,** *11,* 195–214. doi:10.1002/bbb.1729
80. Achilias, D. S.; Antonakou, E.; Roupakias, C.; Megalokonomos, P.; Lappas, A. *Global NEST J.* **2008,** *10,* 114–122. doi:10.30955/gnj.000468
81. Ragaert, K.; Delva, L.; Van Geem, K. *Waste Manage. (Oxford, U. K.)* **2017,** *69,* 24–58. doi:10.1016/j.wasman.2017.07.044
82. Pardal, F.; Tersac, G. *Polym. Degrad. Stab.* **2007,** *92,* 611–616. doi:10.1016/j.polymdegradstab.2007.01.008

83. Achilias, D. S.; Karayannidis, G. P. *Water, Air, Soil Pollut.: Focus* **2004,** *4,* 385–396. doi:10.1023/b:wafo.0000044812.47185.0f
84. El Dorado of Chemical Recycling -State of play and policy challenges, Zero Waste Europe, Aug 2019. https://zerowasteeurope.eu/library/el-dorado-of-chemical-recycling-state-of-play-and-policy-challenges/ (accessed Jan 27, 2021).
85. Sudarsanam, P.; Peeters, E.; Makshina, E. V.; Parvulescu, V. I.; Sels, B. F. *Chem. Soc. Rev.* **2019,** *48,* 2366–2421. doi:10.1039/c8cs00452h
86. George, N.; Kurian, T. *Ind. Eng. Chem. Res.* **2014,** *53,* 14185–14198. doi:10.1021/ie501995m
87. Sabu, T.; Ajay, V. R.; Krishnan, K.; Abitha, V. K.; Martin, G. T., Eds. *Recycling of Polyurethane Foams;* Elsevier: Amsterdam, Netherlands, 2018. doi:10.1016/c2016-0-01054-9
88. Carta, D.; Cao, G.; D'Angeli, C. *Environ. Sci. Pollut. Res.* **2003,** *10,* 390–394. doi:10.1065/espr2001.12.104.8
89. Di Serio, M.; Tesser, R.; Ferrara, A.; Santacesaria, E. *J. Mol. Catal. A: Chem.* **2004,** *212,* 251–257. doi:10.1016/j.molcata.2003.10.032
90. Awaja, F.; Pavel, D. *Eur. Polym. J.* **2005,** *41,* 1453–1477. doi:10.1016/j.eurpolymj.2005.02.005
91. Lorenzetti, C.; Manaresi, P.; Berti, C.; Barbiroli, G. *J. Polym. Environ.* **2006,** *14,* 89–101. doi:10.1007/s10924-005-8711-1
92. Pardal, F.; Tersac, G. *Polym. Degrad. Stab.* **2006,** *91,* 2567–2578. doi:10.1016/j.polymdegradstab.2006.05.016
93. Kandasamy, S.; Samudrala, S. P.; Bhattacharya, S. *Catal. Sci. Technol.* **2019,** *9,* 567–577. doi:10.1039/c8cy02035c
94. McElvery, R. *Chem. Eng. News* **2019,** *97,* No. 10.
95. Kim, S.; Kwon, E. E.; Kim, Y. T.; Jung, S.; Kim, H. J.; Huber, G. W.; Lee, J. *Green Chem.* **2019,** *21,* 3715–3743. doi:10.1039/c9gc01210a
96. De, S.; Saha, B.; Luque, R. *Bioresour. Technol.* **2015,** *178,* 108–118. doi:10.1016/j.biortech.2014.09.065
97. Espro, C.; Gumina, B.; Paone, E.; Mauriello, F. *Catalysts* **2017,** *7,* 78. doi:10.3390/catal7030078
98. Van den Bosch, S.; Koelewijn, S.-F.; Renders, T.; Van den Bossche, G.; Vangeel, T.; Schutyser, W.; Sels, B. F. *Top. Curr. Chem.* **2018,** *376,* 36. doi:10.1007/s41061-018-0214-3
99. Kärkäs, M. D. *ChemSusChem* **2017,** *10,* 2111–2115. doi:10.1002/cssc.201700436
100. Cheng, C.; Shen, D.; Gu, S.; Luo, K. H. *Catal. Sci. Technol.* **2018,** *8,* 6275–6296. doi:10.1039/c8cy00845k
101. Xin, H.; Hu, X.; Cai, C.; Wang, H.; Zhu, C.; Li, S.; Xiu, Z.; Zhang, X.; Liu, Q.; Ma, L. *Front. Chem. (Lausanne, Switz.)* **2020,** *8,* 333. doi:10.3389/fchem.2020.00333
102. Farmer, T. J.; Mascal, M. Platform Molecules. *Introduction to Chemicals from Biomass,* 2nd ed.; John Wiley & Sons: Hoboken, NJ, USA, 2015; pp 89–155. doi:10.1002/9781118714478.ch4
103. Fang, Z.; Smith, R. L., Jr.; Qi, X., Eds. *Production of Platform Chemicals from Sustainable Resources;* Springer Nature Singapore Pte, Ltd.: Singapore, 2017. doi:10.1007/978-981-10-4172-3
104. Tang, X.; Chen, H.; Hu, L.; Hao, W.; Sun, Y.; Zeng, X.; Lin, L.; Liu, S. *Appl. Catal., B* **2014,** *147,* 827–834. doi:10.1016/j.apcatb.2013.10.021
105. Margellou, A.; Triantafyllidis, K. S. *Catalysts* **2019,** *9,* 43. doi:10.3390/catal9010043
106. Cole-Hamilton, D. J.; Tooze, R. P., Eds. *Catalyst Separation, Recovery and Recycling - Chemistry and Process Design;* Catalysis by Metal Complexes, Vol. 30; Springer: Dordrecht, Netherlands, 2006. doi:10.1007/1-4020-4087-3
107. Sheldon, R. A.; van Bekkum, H., Eds. *Fine Chemicals Through Heterogeneous Catalysis;* Wiley-VCH: Weinheim, Germany, 2001. doi:10.1002/9783527612963
108. Yoshioka, T.; Sato, T.; Okuwaki, A. *J. Appl. Polym. Sci.* **1994,** *52,* 1353–1355. doi:10.1002/app.1994.070520919
109. Paszun, D.; Spychaj, T. *Ind. Eng. Chem. Res.* **1997,** *36,* 1373–1383. doi:10.1021/ie960563c
110. Aguado, J.; Serrano, D. P.; Escola, J. M. *Ind. Eng. Chem. Res.* **2008,** *47,* 7982–7992. doi:10.1021/ie800393w
111. Sinha, V.; Patel, M. R.; Patel, J. V. *J. Polym. Environ.* **2010,** *18,* 8–25. doi:10.1007/s10924-008-0106-7
112. Taniguchi, I.; Yoshida, S.; Hiraga, K.; Miyamoto, K.; Kimura, Y.; Oda, K. *ACS Catal.* **2019,** *9,* 4089–4105. doi:10.1021/acscatal.8b05171
113. Kawai, F.; Kawabata, T.; Oda, M. *Appl. Microbiol. Biotechnol.* **2019,** *103,* 4253–4268. doi:10.1007/s00253-019-09717-y
114. Witt, U.; Yamamoto, M.; Seeliger, U.; Müller, R.-J.; Warzelhan, V. *Angew. Chem., Int. Ed.* **1999,** *38,* 1438–1442. doi:10.1002/(sici)1521-3773(19990517)38:10<1438::aid-anie1438>3.0.co;2-u
115. Koshti, R.; Mehta, L.; Samarth, N. *J. Polym. Environ.* **2018,** *26,* 3520–3529. doi:10.1007/s10924-018-1214-7
116. Kumar Sen, S.; Raut, S. *J. Environ. Chem. Eng.* **2015,** *3,* 462–473. doi:10.1016/j.jece.2015.01.003
117. Bornscheuer, U. T. *Science* **2016,** *351,* 1154–1155. doi:10.1126/science.aaf2853
118. Verma, R.; Singh, S.; Dalai, M. K.; Saravanan, M.; Agrawal, V. V.; Srivastava, A. K. *Mater. Des.* **2017,** *133,* 10–18. doi:10.1016/j.matdes.2017.07.042
119. Devi, R. S. K.; Natarajan, K.; Nivas, D.; Kannan, K.; Chandra, S.; Antony, A. R. The Role of Microbes in Plastic Degradation. In *Environmental waste management;* Chandra, R., Ed.; CRC Press: Boca Raton, FL, USA, 2015; pp 341–370. doi:10.1201/b19243
120. Hadad, D.; Geresh, S.; Sivan, A. *J. Appl. Microbiol.* **2005,** *98,* 1093–1100. doi:10.1111/j.1365-2672.2005.02553.x
121. Jehanno, C.; Pérez-Madrigal, M. M.; Demarteau, J.; Sardon, H.; Dove, A. P. *Polym. Chem.* **2019,** *10,* 172–186. doi:10.1039/c8py01284a
122. Fukushima, K.; Coulembier, O.; Lecuyer, J. M.; Almegren, H. A.; Alabdulrahman, A. M.; Alsewailem, F. D.; Mcneil, M. A.; Dubois, P.; Waymouth, R. M.; Horn, H. W.; Rice, J. E.; Hedrick, J. L. *J. Polym. Sci., Part A: Polym. Chem.* **2011,** *49,* 1273–1281. doi:10.1002/pola.24551
123. Liu, M.; Guo, J.; Gu, Y.; Gao, J.; Liu, F.; Yu, S. *ACS Sustainable Chem. Eng.* **2018,** *6,* 13114–13121. doi:10.1021/acssuschemeng.8b02650
124. McKeown, P.; Kamran, M.; Davidson, M. G.; Jones, M. D.; Román-Ramírez, L. A.; Wood, J. *Green Chem.* **2020,** *22,* 3721–3726. doi:10.1039/d0gc01252a
125. Wang, Q.; Yao, X.; Tang, S.; Lu, X.; Zhang, X.; Zhang, S. *Green Chem.* **2012,** *14,* 2559–2566. doi:10.1039/c2gc35696a
126. Quaranta, E.; Minischetti, C. C.; Tartaro, G. *ACS Omega* **2018,** *3,* 7261–7268. doi:10.1021/acsomega.8b01123
127. Troev, K.; Grancharov, G.; Tsevi, R.; Gitsov, I. *J. Appl. Polym. Sci.* **2003,** *90,* 1148–1152. doi:10.1002/app.12711
128. Pingale, N. D.; Palekar, V. S.; Shukla, S. R. *J. Appl. Polym. Sci.* **2010,** *115,* 249–254. doi:10.1002/app.31092
129. López-Fonseca, R.; Duque-Ingunza, I.; de Rivas, B.; Arnaiz, S.; Gutiérrez-Ortiz, J. I. *Polym. Degrad. Stab.* **2010,** *95,* 1022–1028. doi:10.1016/j.polymdegradstab.2010.03.007

130. Pingale, N. D.; Shukla, S. R. *Eur. Polym. J.* **2008,** *44,* 4151–4156. doi:10.1016/j.eurpolymj.2008.09.019
131. Mukherjee, S.; RoyChaudhuri, U.; Kundu, P. P. *J. Chem. Technol. Biotechnol.* **2018,** *93,* 1300–1311. doi:10.1002/jctb.5489
132. Yang, J.; Yang, Y.; Wu, W.-M.; Zhao, J.; Jiang, L. *Environ. Sci. Technol.* **2014,** *48,* 13776–13784. doi:10.1021/es504038a
133. Yin, S.; Tuladhar, R.; Shi, F.; Shanks, R. A.; Combe, M.; Collister, T. *Polym. Eng. Sci.* **2015,** *55,* 2899–2909. doi:10.1002/pen.24182
134. Grigore, M. E. *Recycling* **2017,** *2,* 24. doi:10.3390/recycling2040024
135. Achilias, D. S.; Andriotis, L.; Koutsidis, I. A.; Louka, D. A.; Nianias, N. P.; Siafaka, P.; Tsagkalias, I.; Tsintzou, G. Recent Advances in the Chemical Recycling of Polymers (PP, PS, LDPE, HDPE, PVC, PC, Nylon, PMMA). *Material Recycling - Trends and Perspectives;* IntechOpen Ltd.: Rijeka, Croatia, 2012. doi:10.5772/33457
136. Peacock, A. *Handbook of Polyethylene: Structures: Properties, and Applications;* CRC Press: Boca Raton, FL, USA, 2000. doi:10.1201/9781482295467
137. Ugbolue, S. C. O., Ed. *Polyolefin Fibres: Structure, Properties and Industrial Applications,* 2nd ed.; Elsevier: Amsterdam, Netherlands, 2017.
138. Emblem, A. Plastics properties for packaging materials. *Packaging Technology Fundamentals, Materials and Processes;* Elsevier: Amsterdam, Netherlands, 2012; pp 287–309. doi:10.1533/9780857095701.2.287
139. Rahimi, A.; García, J. M. *Nat. Rev. Chem.* **2017,** *1,* 0046. doi:10.1038/s41570-017-0046
140. Jordan, J. L.; Casem, D. T.; Bradley, J. M.; Dwivedi, A. K.; Brown, E. N.; Jordan, C. W. *J. Dyn. Behav. Mater.* **2016,** *2,* 411–420. doi:10.1007/s40870-016-0076-0
141. Whiteley, K. S.; Heggs, T. G.; Koch, H.; Mawer, R. L.; Immel, W. Polyolefins. *Ullmann's Encyclopedia of Industrial Chemistry;* Wiley-VCH: Weinheim, Germany, 2000. doi:10.1002/14356007.a21_487
142. Kumar, S.; Panda, A. K.; Singh, R. K. *Resour., Conserv. Recycl.* **2011,** *55,* 893–910. doi:10.1016/j.resconrec.2011.05.005
143. Jin, H.; Gonzalez-Gutierrez, J.; Oblak, P.; Zupančič, B.; Emri, I. *Polym. Degrad. Stab.* **2012,** *97,* 2262–2272. doi:10.1016/j.polymdegradstab.2012.07.039
144. Ahmad, I.; Khan, M. I.; Ishaq, M.; Khan, H.; Gul, K.; Ahmad, W. *Polym. Degrad. Stab.* **2013,** *98,* 2512–2519. doi:10.1016/j.polymdegradstab.2013.09.009
145. Christensen, S. T.; Elam, J. W.; Rabuffetti, F. A.; Ma, Q.; Weigand, S. J.; Lee, B.; Seifert, S.; Stair, P. C.; Poeppelmeier, K. R.; Hersam, M. C.; Bedzyk, M. J. *Small* **2009,** *5,* 750–757. doi:10.1002/smll.200801920
146. Celik, G.; Kennedy, R. M.; Hackler, R. A.; Ferrandon, M.; Tennakoon, A.; Patnaik, S.; LaPointe, A. M.; Ammal, S. C.; Heyden, A.; Perras, F. A.; Pruski, M.; Scott, S. L.; Poeppelmeier, K. R.; Sadow, A. D.; Delferro, M. *ACS Cent. Sci.* **2019,** *5,* 1795–1803. doi:10.1021/acscentsci.9b00722
147. Liang, Z.; Chen, L.; Alam, M. S.; Zeraati Rezaei, S.; Stark, C.; Xu, H.; Harrison, R. M. *Fuel* **2018,** *220,* 792–799. doi:10.1016/j.fuel.2017.11.142
148. Dewaele, A.; Renders, T.; Yu, B.; Verpoort, F.; Sels, B. F. *Catal. Sci. Technol.* **2016,** *6,* 7708–7717. doi:10.1039/c6cy00933f
149. Bahr, S.; Doyle, N.; Wang, J.; Winckler, S.; Takekoshi, T.; Wang, Y. F. Macrocyclic polyster oligomers as carriers and/or flow modifier additives for thermoplastics. W.O. Pat. Appl. WO2007011684 A2, Jan 25, 2007.
150. Laurent, B. A.; Grayson, S. M. *J. Am. Chem. Soc.* **2011,** *133,* 13421–13429. doi:10.1021/ja2024355
151. Scheirs, J.; Priddy, D. B., Eds. *Modern Styrenic Polymers: Polystyrenes and Styrenic Copolymers;* John Wiley & Sons: Hoboken, NJ, USA, 2003. doi:10.1002/0470867213
152. Wypych, G. PS polystyrene. *Handbook of Polymers;* Elsevier: Amsterdam, Netherlands, 2012; pp 541–547. doi:10.1016/b978-1-895198-47-8.50162-4
153. Samper, M. D.; Garcia-Sanoguera, D.; Parres, F.; López, J. *Prog. Rubber, Plast. Recycl. Technol.* **2010,** *26,* 83–92. doi:10.1177/147776061002600202
154. Hawley-Fedder, R. A.; Parsons, M. L.; Karasek, F. W. *J. Chromatogr.* **1984,** *315,* 201–210. doi:10.1016/s0021-9673(01)90737-x
155. Ergut, A.; Levendis, Y. A.; Carlson, J. *Fuel* **2007,** *86,* 1789–1799. doi:10.1016/j.fuel.2007.01.009
156. Kim, J.-S.; Lee, W.-Y.; Lee, S.-B.; Kim, S.-B.; Choi, M.-J. *Catal. Today* **2003,** *87,* 59–68. doi:10.1016/j.cattod.2003.10.004
157. Adnan; Shah, J.; Jan, M. R. *J. Anal. Appl. Pyrolysis* **2014,** *109,* 196–204. doi:10.1016/j.jaap.2014.06.013
158. Shah, J.; Jan, M. R.; Adnan. *J. Taiwan Inst. Chem. Eng.* **2017,** *80,* 391–398. doi:10.1016/j.jtice.2017.07.026
159. Yoshida, S.; Hiraga, K.; Takehana, T.; Taniguchi, I.; Yamaji, H.; Maeda, Y.; Toyohara, K.; Miyamoto, K.; Kimura, Y.; Oda, K. *Science* **2016,** *351,* 1196–1199. doi:10.1126/science.aad6359
160. Atta, A. M.; El-Kafrawy, A. F.; Aly, M. H.; Abdel-Azim, A.-A. A. *Prog. Org. Coat.* **2007,** *58,* 13–22. doi:10.1016/j.porgcoat.2006.11.001
161. Köpnick, H.; Schmidt, M.; Brügging, W.; Rüter, J.; Kaminsky, W. Polyesters. *Ullmann's Encyclopedia of Industrial Chemistry;* Wiley-VCH: Weinheim, Germany, 2000; pp 623–649. doi:10.1002/14356007.a21_227
162. Mahalingam, S.; Raimi-Abraham, B. T.; Craig, D. Q. M.; Edirisinghe, M. *Chem. Eng. J.* **2015,** *280,* 344–353. doi:10.1016/j.cej.2015.05.114
163. Weisskopf, K. *J. Polym. Sci., Part A: Polym. Chem.* **1988,** *26,* 1919–1935. doi:10.1002/pola.1988.080260718
164. Sax, L. *Environ. Health Perspect.* **2010,** *118,* 445–448. doi:10.1289/ehp.0901253
165. Sathyanarayana, S. *Curr. Probl. Pediatr. Adolesc. Health Care* **2008,** *38,* 34–49. doi:10.1016/j.cppeds.2007.11.001
166. Commission Regulation (EU) 2018/2005 of 17 December 2018 amending Annex XVII to Regulation (EC) No 1907/2006 of the European Parliament and of the Council concerning the Registration, Evaluation, Authorisation and Restriction of Chemicals (REACH) as regards bis(2-ethylhexyl) phthalate (DEHP), dibutyl phthalate (DBP), benzyl butyl phthalate (BBP) and diisobutyl phthalate (DIBP). https://eur-lex.europa.eu/legal-content/EN/TXT/PDF/?uri=CELEX:32018R2005&from=EN (accessed Jan 27, 2021).
167. De Clercq, R.; Dusselier, M.; Sels, B. F. *Green Chem.* **2017,** *19,* 5012–5040. doi:10.1039/c7gc02040f
168. Liguori, F.; Barbaro, P.; Calisi, N. *ChemSusChem* **2019,** *12,* 2558–2563. doi:10.1002/cssc.201900833
169. Al-Sabagh, A. M.; Yehia, F. Z.; Eshaq, G.; Rabie, A. M.; ElMetwally, A. E. *Egypt. J. Pet.* **2016,** *25,* 53–64. doi:10.1016/j.ejpe.2015.03.001
170. Garcia, J. M.; Robertson, M. L. *Science* **2017,** *358,* 870–872. doi:10.1126/science.aaq0324

171. Hoang, C. N.; Dang, Y. H. *Polym. Degrad. Stab.* **2013,** *98,* 697–708. doi:10.1016/j.polymdegradstab.2012.12.026
172. Sabu, T.; Ajay, V. R.; Krishnan, K.; Abitha, V. K.; Martin, G. T., Eds. *Recycling of Polyethylene Terephthalate Bottles;* Elsevier: Amsterdam, Netherlands, 2018. doi:10.1016/c2016-0-01084-7
173. Raheem, A. B.; Noor, Z. Z.; Hassan, A.; Abd Hamid, M. K.; Samsudin, S. A.; Sabeen, A. H. *J. Cleaner Prod.* **2019,** *225,* 1052–1064. doi:10.1016/j.jclepro.2019.04.019
174. Vilaplana Artigas, M.; Mestrom, L.; De Groot, R.; Philipp, V.; Guerreo Sanchez, C.; Hooghoudt, T. Polymer Degradation. U.S. Pat. Appl. US2019185406A1, June 20, 2019.
175. Inada, S.; Sato, K. Methods for the preparation or purification of bis-beta-hydroxythethyl terephthalate. W.O. Pat. Appl. WO2001010812 A1, Feb 15, 2001.
176. Essaddam, H.; Hostetler, M. J. Polyethylene terephthalate depolymerisation. W.O. Pat. Appl. WO2017007965 A1, Jan 12, 2017.
177. Parravicini, M.; Crippa, M.; Bertelè, M. V. Method and apparatus for the recycling of polymeric materials via depolymerization process. W.O. Pat. Appl. WO2013014650 A1, Jan 31, 2013.
178. Barla, F. G.; Showalter, T.; Su, H. C.; Jones, J.; Bobe, I. Methods for recycling cotton and polyester fibers from waste textiles. W.O. Pat. Appl. WO2019140245 A1, July 18, 2019.
179. Cornell, D. D. Recycling Polyesters by Chemical Depolymerization. *Modern Polyesters: Chemistry and Technology of Polyesters and Copolyesters;* John Wiley & Sons: Hoboken, NJ, USA, 2003; pp 563–590. doi:10.1002/0470090685.ch16
180. Han, M. Depolymerization of PET Bottle via Methanolysis and Hydrolysis. In *Recycling of Polyethylene Terephthalate Bottles;* Sabu, T.; Ajay, V. R.; Krishnan, K.; Abitha, V. K.; Martin, G. T., Eds.; Elsevier: Amsterdam, Netherlands, 2019; pp 85–108. doi:10.1016/b978-0-12-811361-5.00005-5
181. Michel, C.; Gallezot, P. *ACS Catal.* **2015,** *5,* 4130–4132. doi:10.1021/acscatal.5b00707
182. Balaraman, E.; Fogler, E.; Milstein, D. *Chem. Commun.* **2012,** *48,* 1111–1113. doi:10.1039/c1cc15778g
183. Fuentes, J. A.; Smith, S. M.; Scharbert, M. T.; Carpenter, I.; Cordes, D. B.; Slawin, A. M. Z.; Clarke, M. L. *Chem. – Eur. J.* **2015,** *21,* 10851–10860. doi:10.1002/chem.201500907
184. Takebayashi, S.; Bergens, S. H. *Organometallics* **2009,** *28,* 2349–2351. doi:10.1021/om9002076
185. Hasanayn, F.; Baroudi, A. *Organometallics* **2013,** *32,* 2493–2496. doi:10.1021/om400122n
186. Martello, M. T.; Hillmyer, M. A. *Macromolecules* **2011,** *44,* 8537–8545. doi:10.1021/ma201063t
187. Luo, Y.; Zhang, S.; Ma, Y.; Wang, W.; Tan, B. *Polym. Chem.* **2013,** *4,* 1126–1131. doi:10.1039/c2py20914d
188. Krall, E. M.; Klein, T. W.; Andersen, R. J.; Nett, A. J.; Glasgow, R. W.; Reader, D. S.; Dauphinais, B. C.; Mc Ilrath, S. P.; Fischer, A. A.; Carney, M. J.; Hudson, D. J.; Robertson, N. J. *Chem. Commun.* **2014,** *50,* 4884–4887. doi:10.1039/c4cc00541d
189. Ghilardi, C. A.; Midollini, S.; Orlandini, A.; Sacconi, L. *Inorg. Chem.* **1980,** *19,* 301–306. doi:10.1021/ic50204a005
190. Phanopoulos, A.; Miller, P. W.; Long, N. J. *Coord. Chem. Rev.* **2015,** *299,* 39–60. doi:10.1016/j.ccr.2015.04.001
191. Westhues, S.; Idel, J.; Klankermayer, J. *Sci. Adv.* **2018,** *4,* eaat9669. doi:10.1126/sciadv.aat9669
192. vom Stein, T.; Meuresch, M.; Limper, D.; Schmitz, M.; Hölscher, M.; Coetzee, J.; Cole-Hamilton, D. J.; Klankermayer, J.; Leitner, W. *J. Am. Chem. Soc.* **2014,** *136,* 13217–13225. doi:10.1021/ja506023f
193. Monsigny, L.; Berthet, J.-C.; Cantat, T. *ACS Sustainable Chem. Eng.* **2018,** *6,* 10481–10488. doi:10.1021/acssuschemeng.8b01842
194. Wang, Y.; Zhang, Y.; Song, H.; Wang, Y.; Deng, T.; Hou, X. *J. Cleaner Prod.* **2019,** *208,* 1469–1475. doi:10.1016/j.jclepro.2018.10.117
195. Liu, Y.; Wang, M.; Pan, Z. *J. Supercrit. Fluids* **2012,** *62,* 226–231. doi:10.1016/j.supflu.2011.11.001
196. Tang, H.; Li, N.; Li, G.; Wang, A.; Cong, Y.; Xu, G.; Wang, X.; Zhang, T. *Green Chem.* **2019,** *21,* 2709–2719. doi:10.1039/c9gc00571d
197. Kurokawa, H.; Ohshima, M.-a.; Sugiyama, K.; Miura, H. *Polym. Degrad. Stab.* **2003,** *79,* 529–533. doi:10.1016/s0141-3910(02)00370-1
198. López-Fonseca, R.; Duque-Ingunza, I.; de Rivas, B.; Flores-Giraldo, L.; Gutiérrez-Ortiz, J. I. *Chem. Eng. J.* **2011,** *168,* 312–320. doi:10.1016/j.cej.2011.01.031
199. Commission regulation No 10/2011 of 14 January 2011 on plastic materials and articles intended to come into contact with food, European Commission, Brussels, Belgium, 2011. https://eur-lex.europa.eu/legal-content/EN/TXT/PDF/?uri=CELEX:32011R0010&from=EN (accessed Jan 27, 2021).
200. Ghaemy, M.; Mossaddegh, K. *Polym. Degrad. Stab.* **2005,** *90,* 570–576. doi:10.1016/j.polymdegradstab.2005.03.011
201. Xi, G.; Lu, M.; Sun, C. *Polym. Degrad. Stab.* **2005,** *87,* 117–120. doi:10.1016/j.polymdegradstab.2004.07.017
202. Liu, B.; Lu, X.; Ju, Z.; Sun, P.; Xin, J.; Yao, X.; Zhou, Q.; Zhang, S. *Ind. Eng. Chem. Res.* **2018,** *57,* 16239–16245. doi:10.1021/acs.iecr.8b03854
203. Chen, F.; Wang, G.; Shi, C.; Zhang, Y.; Zhang, L.; Li, W.; Yang, F. *J. Appl. Polym. Sci.* **2013,** *127,* 2809–2815. doi:10.1002/app.37608
204. Chaudhary, S.; Surekha, P.; Kumar, D.; Rajagopal, C.; Roy, P. K. *J. Appl. Polym. Sci.* **2013,** *129,* 2779–2788. doi:10.1002/app.38970
205. Esquer, R.; García, J. J. *J. Organomet. Chem.* **2019,** *902,* 120972. doi:10.1016/j.jorganchem.2019.120972
206. Ammam, M. *J. Mater. Chem. A* **2013,** *1,* 6291–6312. doi:10.1039/c3ta01663c
207. Kamata, K.; Sugahara, K. *Catalysts* **2017,** *7,* 345. doi:10.3390/catal7110345
208. Zhang, L.; Gao, J.; Zou, J.; Yi, F. *J. Appl. Polym. Sci.* **2013,** *130,* 2790–2795. doi:10.1002/app.39497
209. Zhou, X.; Lu, X.; Wang, Q.; Zhu, M.; Li, Z. *Pure Appl. Chem.* **2012,** *84,* 789–801. doi:10.1351/pac-con-11-06-10
210. Geng, Y.; Dong, T.; Fang, P.; Zhou, Q.; Lu, X.; Zhang, S. *Polym. Degrad. Stab.* **2015,** *117,* 30–36. doi:10.1016/j.polymdegradstab.2015.03.019
211. Zhu, M.; Li, S.; Li, Z.; Lu, X.; Zhang, S. *Chem. Eng. J.* **2012,** *185–186,* 168–177. doi:10.1016/j.cej.2012.01.068
212. Ritter Lima, G.; Monteiro, W. F.; Ligabue, R.; Campomanes Santana, R. M. *Mater. Res. (Sao Carlos, Braz.)* **2017,** *20* (Suppl. 2), 588–595. doi:10.1590/1980-5373-mr-2017-0645
213. Monteiro, W. F.; Vieira, M. O.; Aquino, A. S.; de Souza, M. O.; de Lima, J.; Einloft, S.; Ligabue, R. *Appl. Catal., A* **2017,** *544,* 46–54. doi:10.1016/j.apcata.2017.07.011
214. Lima, G. R.; Monteiro, W. F.; Toledo, B. O.; Ligabue, R. A.; Santana, R. M. C. *Macromol. Symp.* **2019,** *383,* 1800008. doi:10.1002/masy.201800008
215. Kitano, M.; Nakajima, K.; Kondo, J. N.; Hayashi, S.; Hara, M. *J. Am. Chem. Soc.* **2010,** *132,* 6622–6623. doi:10.1021/ja100435w
216. Yang, X.; Wu, L.; Ma, L.; Li, X.; Wang, T.; Liao, S. *Catal. Commun.* **2015,** *59,* 184–188. doi:10.1016/j.catcom.2014.10.031

217. Linares, N.; Moreno-Marrodan, C.; Barbaro, P. *ChemCatChem* **2016,** *8,* 1001–1011. doi:10.1002/cctc.201501126
218. Jiao, S.; Chen, Y.; Xu, M.; Zhang, Y.; Wang, D.; Pang, G.; Feng, S. *Mater. Lett.* **2010,** *64,* 1704–1706. doi:10.1016/j.matlet.2010.05.007
219. Bartolome, L.; Imran, M.; Lee, K. G.; Sangalang, A.; Ahn, J. K.; Kim, D. H. *Green Chem.* **2014,** *16,* 279–286. doi:10.1039/c3gc41834k
220. Park, G.; Bartolome, L.; Lee, K. G.; Lee, S. J.; Kim, D. H.; Park, T. J. *Nanoscale* **2012,** *4,* 3879–3885. doi:10.1039/c2nr30168g
221. Imran, M.; Lee, K. G.; Imtiaz, Q.; Kim, B.-K.; Han, M.; Cho, B. G.; Kim, D. H. *J. Nanosci. Nanotechnol.* **2011,** *11,* 824–828. doi:10.1166/jnn.2011.3201
222. Imran, M.; Kim, D. H.; Al-Masry, W. A.; Mahmood, A.; Hassan, A.; Haider, S.; Ramay, S. M. *Polym. Degrad. Stab.* **2013,** *98,* 904–915. doi:10.1016/j.polymdegradstab.2013.01.007
223. Eshaq, G.; ElMetwally, A. E. *J. Mol. Liq.* **2016,** *214,* 1–6. doi:10.1016/j.molliq.2015.11.049
224. Di Cosimo, J. I.; Dıez, V. K.; Xu, M.; Iglesia, E.; Apesteguıa, C. R. *J. Catal.* **1998,** *178,* 499–510. doi:10.1006/jcat.1998.2161
225. Deetlefs, M.; Seddon, K. R. *Green Chem.* **2010,** *12,* 17–30. doi:10.1039/b915049h
226. Thuy Pham, T. P.; Cho, C.-W.; Yun, Y.-S. *Water Res.* **2010,** *44,* 352–372. doi:10.1016/j.watres.2009.09.030
227. Wang, Q.; Lu, X.; Zhou, X.; Zhu, M.; He, H.; Zhang, X. *J. Appl. Polym. Sci.* **2013,** *129,* 3574–3581. doi:10.1002/app.38706
228. Yue, Q. F.; Xiao, L. F.; Zhang, M. L.; Feng Bai, X. F. *Polymers (Basel, Switz.)* **2013,** *5,* 1258–1271. doi:10.3390/polym5041258
229. Wang, Q.; Geng, Y.; Lu, X.; Zhang, S. *ACS Sustainable Chem. Eng.* **2015,** *3,* 340–348. doi:10.1021/sc5007522
230. Valkenberg, M. H.; deCastro, C.; Hölderich, W. F. *Green Chem.* **2002,** *4,* 88–93. doi:10.1039/b107946h
231. Al-Sabagh, A. M.; Yehia, F. Z.; Eshaq, G.; ElMetwally, A. E. *Ind. Eng. Chem. Res.* **2015,** *54,* 12474–12481. doi:10.1021/acs.iecr.5b03857
232. Abbott, A. P.; Ahmed, E. I.; Harris, R. C.; Ryder, K. S. *Green Chem.* **2014,** *16,* 4156–4161. doi:10.1039/c4gc00952e
233. Wagle, D. V.; Zhao, H.; Baker, G. A. *Acc. Chem. Res.* **2014,** *47,* 2299–2308. doi:10.1021/ar5000488
234. Paiva, A.; Craveiro, R.; Aroso, I.; Martins, M.; Reis, R. L.; Duarte, A. R. C. *ACS Sustainable Chem. Eng.* **2014,** *2,* 1063–1071. doi:10.1021/sc500096j
235. Pena-Pereira, F.; Namieśnik, J. *ChemSusChem* **2014,** *7,* 1784–1800. doi:10.1002/cssc.201301192
236. Smith, E. L.; Abbott, A. P.; Ryder, K. S. *Chem. Rev.* **2014,** *114,* 11060–11082. doi:10.1021/cr300162p
237. Liu, B.; Fu, W.; Lu, X.; Zhou, Q.; Zhang, S. *ACS Sustainable Chem. Eng.* **2019,** *7,* 3292–3300. doi:10.1021/acssuschemeng.8b05324
238. Wang, Q.; Yao, X.; Geng, Y.; Zhou, Q.; Lu, X.; Zhang, S. *Green Chem.* **2015,** *17,* 2473–2479. doi:10.1039/c4gc02401j
239. Cakić, S. M.; Ristić, I. S.; M-Cincović, M.; Nikolić, N. Č.; Ilić, O. Z.; Stojiljković, D. T.; B-Simendić, J. K. *Prog. Org. Coat.* **2012,** *74,* 115–124. doi:10.1016/j.porgcoat.2011.11.024
240. Essawy, H. A.; Tawfik, M. E.; Elsayed, N. H. *J. Appl. Polym. Sci.* **2012,** *123,* 2377–2383. doi:10.1002/app.34750
241. Chaudhary, S.; Surekha, P.; Kumar, D.; Rajagopal, C.; Roy, P. K. *J. Appl. Polym. Sci.* **2013,** *129,* 2779–2788. doi:10.1002/app.38970
242. Hoang, C. N.; Le, T. T. N.; Hoang, Q. D. *Polym. Bull.* **2019,** *76,* 23–34. doi:10.1007/s00289-018-2369-z
243. Amaro, L. P.; Coiai, S.; Ciardelli, F.; Passaglia, E. *Waste Manage. (Oxford, U. K.)* **2015,** *46,* 68–75. doi:10.1016/j.wasman.2015.09.005
244. Kárpáti, L.; Fogarassy, F.; Kovácsik, D.; Vargha, V. *J. Polym. Environ.* **2019,** *27,* 2167–2181. doi:10.1007/s10924-019-01490-3
245. Gioia, C.; Vannini, M.; Marchese, P.; Minesso, A.; Cavalieri, R.; Colonna, M.; Celli, A. *Green Chem.* **2014,** *16,* 1807–1815. doi:10.1039/c3gc42122h
246. Substance Infocard 1,4:3,6-dianhydro-D-glucitol, European Chemicals Agency. https://echa.europa.eu/it/substance-information/-/substanceinfo/100.010.449 (accessed Sept 1, 2020).
247. Dussenne, C.; Delaunay, T.; Wiatz, V.; Wyart, H.; Suisse, I.; Sauthier, M. *Green Chem.* **2017,** *19,* 5332–5344. doi:10.1039/c7gc01912b
248. Delbecq, F.; Khodadadi, M. R.; Rodriguez Padron, D.; Varma, R.; Len, C. *Mol. Catal.* **2020,** *482,* 110648. doi:10.1016/j.mcat.2019.110648
249. Liguori, F.; Moreno-Marrodan, C.; Barbaro, P. *Chem. Soc. Rev.* **2020,** *49,* 6329–6363. doi:10.1039/d0cs00179a
250. Saxon, D. J.; Luke, A. M.; Sajjad, H.; Tolman, W. B.; Reineke, T. M. *Prog. Polym. Sci.* **2020,** *101,* 101196. doi:10.1016/j.progpolymsci.2019.101196
251. Feng, X.; East, A. J.; Hammond, W. B.; Zhang, Y.; Jaffe, M. *Polym. Adv. Technol.* **2011,** *22,* 139–150. doi:10.1002/pat.1859
252. Jem, K. J.; Tan, B. *Adv. Ind. Eng. Polym. Res.* **2020,** *3,* 60–70. doi:10.1016/j.aiepr.2020.01.002
253. Auras, R.; Lim, L.-T.; Selke, S. E. M.; Tsuji, H., Eds. *Poly(Lactic Acid): Synthesis, Structures, Properties, Processing, and Applications;* John Wiley & Sons: Hoboken, NJ, USA, 2010. doi:10.1002/9780470649848
254. Lunt, J. *Polym. Degrad. Stab.* **1998,** *59,* 145–152. doi:10.1016/s0141-3910(97)00148-1
255. Datta, R.; Henry, M. *J. Chem. Technol. Biotechnol.* **2006,** *81,* 1119–1129. doi:10.1002/jctb.1486
256. Garlotta, D. *J. Polym. Environ.* **2001,** *9,* 63–84. doi:10.1023/a:1020200822435
257. Sato, S.; Gondo, D.; Wada, T.; Kanehashi, S.; Nagai, K. *J. Appl. Polym. Sci.* **2013,** *129,* 1607–1617. doi:10.1002/app.38833
258. Castro-Aguirre, E.; Iñiguez-Franco, F.; Samsudin, H.; Fang, X.; Auras, R. *Adv. Drug Delivery Rev.* **2016,** *107,* 333–366. doi:10.1016/j.addr.2016.03.010
259. Anderson, J. M.; Shive, M. S. *Adv. Drug Delivery Rev.* **2012,** *64,* 72–82. doi:10.1016/j.addr.2012.09.004
260. Niaounakis, M. *Biopolymers: Processing and Products;* Elsevier: Amsterdam, Netherlands, 2014. doi:10.1016/c2013-0-09982-3
261. Garg, M.; White, S. R.; Sottos, N. R. *ACS Appl. Mater. Interfaces* **2019,** *11,* 46226–46232. doi:10.1021/acsami.9b17599
262. Lizundia, E.; Ruiz-Rubio, L.; Vilas, J. L.; León, L. M. *RSC Adv.* **2016,** *6,* 15660–15669. doi:10.1039/c5ra24604k
263. Fan, Y.; Nishida, H.; Mori, T.; Shirai, Y.; Endo, T. *Polymer* **2004,** *45,* 1197–1205. doi:10.1016/j.polymer.2003.12.058
264. Carné Sánchez, A.; Collinson, S. R. *Eur. Polym. J.* **2011,** *47,* 1970–1976. doi:10.1016/j.eurpolymj.2011.07.013
265. Román-Ramírez, L. A.; Mckeown, P.; Jones, M. D.; Wood, J. *ACS Catal.* **2019,** *9,* 409–416. doi:10.1021/acscatal.8b04863
266. McKeown, P.; Román-Ramírez, L. A.; Bates, S.; Wood, J.; Jones, M. D. *ChemSusChem* **2019,** *12,* 5233–5238. doi:10.1002/cssc.201902755

267. Payne, J.; McKeown, P.; Mahon, M. F.; Emanuelsson, E. A. C.; Jones, M. D. *Polym. Chem.* **2020,** *11,* 2381–2389. doi:10.1039/d0py00192a
268. Fliedel, C.; Vila-Viçosa, D.; Calhorda, M. J.; Dagorne, S.; Avilés, T. *ChemCatChem* **2014,** *6,* 1357–1367. doi:10.1002/cctc.201301015
269. Whitelaw, E. L.; Davidson, M. G.; Jones, M. D. *Chem. Commun.* **2011,** *47,* 10004–10006. doi:10.1039/c1cc13910j
270. Chmura, A. J.; Cousins, D. M.; Davidson, M. G.; Jones, M. D.; Lunn, M. D.; Mahon, M. F. *Dalton Trans.* **2008,** 1437–1443. doi:10.1039/b716304e
271. Alberti, C.; Damps, N.; Meißner, R. R. R.; Hofmann, M.; Rijono, D.; Enthaler, S. *Adv. Sustainable Syst.* **2020,** *4,* 1900081. doi:10.1002/adsu.201900081
272. Bowmer, C. T.; Hooftman, R. N.; Hanstveit, A. O.; Venderbosch, P. W. M.; van der Hoeven, N. *Chemosphere* **1998,** *37,* 1317–1333. doi:10.1016/s0045-6535(98)00116-7
273. Calvo-Flores, F. G.; Monteagudo-Arrebola, M. J.; Dobado, J. A.; Isac-García, J. *Top. Curr. Chem.* **2018,** *376,* 18. doi:10.1007/s41061-018-0191-6
274. Petrus, R.; Bykowski, D.; Sobota, P. *ACS Catal.* **2016,** *6,* 5222–5235. doi:10.1021/acscatal.6b01009
275. Bykowski, D.; Grala, A.; Sobota, P. *Tetrahedron Lett.* **2014,** *55,* 5286–5289. doi:10.1016/j.tetlet.2014.07.103
276. Dusselier, M.; Van Wouwe, P.; Dewaele, A.; Makshina, E.; Sels, B. F. *Energy Environ. Sci.* **2013,** *6,* 1415–1442. doi:10.1039/c3ee00069a
277. Sullivan, C. J.; Kuenz, A.; Vorlop, K. D. Propanediols. *Ullmann's Encyclopedia of Industrial Chemistry;* Wiley-VCH: Weinheim, Germany, 2018. doi:10.1002/14356007.a22_163.pub2
278. Guarino, V.; Gentile, G.; Sorrentino, L.; Ambrosio, L. Polycaprolactone: Synthesis, Properties, and Applications. *Encyclopedia of Polymer Science and Technology,* 4th ed.; John Wiley & Sons: Hoboken, NJ, USA, 2017. doi:10.1002/0471440264.pst658
279. Nguyet Thi Ho, L.; Minh Ngo, D.; Cho, J.; Jung, H. M. *Polym. Degrad. Stab.* **2018,** *155,* 15–21. doi:10.1016/j.polymdegradstab.2018.07.003
280. Zhu, J.-B.; Watson, E. M.; Tang, J.; Chen, E. Y.-X. *Science* **2018,** *360,* 398–403. doi:10.1126/science.aar5498
281. Hong, M.; Chen, E. Y.-X. *Angew. Chem., Int. Ed.* **2016,** *55,* 4188–4193. doi:10.1002/anie.201601092
282. MacDonald, J. P.; Shaver, M. P. *Polym. Chem.* **2016,** *7,* 553–559. doi:10.1039/c5py01606a
283. Czub, P. Bisphenol-A. In *Handbook of Engineering and Specialty Thermoplastics, Polyethers and Polyesters;* Sabu, T.; Visakh, P. M., Eds.; John Wiley & Sons: Hoboken, NJ, USA, 2011; Vol. 3, pp 221–269. doi:10.1002/9781118104729.ch7
284. Fukuoka, S.; Fukawa, I.; Adachi, T.; Fujita, H.; Sugiyama, N.; Sawa, T. *Org. Process Res. Dev.* **2019,** *23,* 145–169. doi:10.1021/acs.oprd.8b00391
285. Morgan, S. E.; Li, J. Polycarbonate (PC). In *Encyclopedia of Chemical Processing;* Lee, S., Ed.; CRC Press: Boca Raton, FL, USA, 2005; Vol. 4, pp 2277–2290. doi:10.1201/noe0824755638
286. Bisphenol A (BPA) Market - Growth, Trends, and Forecast (2019 - 2024), Report ID 4520075, Research and Markets, Dublin, Ireland, Apr 2019.
287. http://bisphenol-a-europe.org/ (accessed July 18, 2020).
288. Bisphenol A (BPA) hazard assessment protocol, EFSA supporting publication 2017:EN-1354, European Food Safety Authority (EFSA), 2017. https://pdfs.semanticscholar.org/baa6/8fcf927e969202d76ce06d43d4e4a9576d33.pdf (accessed Jan 27, 2021).
289. Ma, Y.; Liu, H.; Wu, J.; Yuan, L.; Wang, Y.; Du, X.; Wang, R.; Marwa, P. W.; Petlulu, P.; Chen, X.; Zhang, H. *Environ. Res.* **2019,** *176,* 108575. doi:10.1016/j.envres.2019.108575
290. Giulivo, M.; Lopez de Alda, M.; Capri, E.; Barceló, D. *Environ. Res.* **2016,** *151,* 251–264. doi:10.1016/j.envres.2016.07.011
291. Alonso-Magdalena, P.; Ropero, A. B.; Soriano, S.; García-Arévalo, M.; Ripoll, C.; Fuentes, E.; Quesada, I.; Nadal, Á. *Mol. Cell. Endocrinol.* **2012,** *355,* 201–207. doi:10.1016/j.mce.2011.12.012
292. Mercea, P. *J. Appl. Polym. Sci.* **2009,** *112,* 579–593. doi:10.1002/app.29421
293. Kang, J.-H.; Kito, K.; Kondo, F. *J. Food Prot.* **2003,** *66,* 1444–1447. doi:10.4315/0362-028x-66.8.1444
294. de Angelis, A.; Ingallina, P.; Perego, C. *Ind. Eng. Chem. Res.* **2004,** *43,* 1169–1178. doi:10.1021/ie030429+
295. Eco-profiles and Environmental Product Declarations of the European Plastics Manufacturers - Bisphenol A (BPA), Plastics Europe, Brussels, Belgium, Jan 2019. https://www.plasticseurope.org/en/resources/eco-profiles (accessed Jan 27, 2021).
296. Toxicological profile for phenol, U.S. Department of Health and Human Services, Agency for Toxic Substances and Disease Registry, Atlanta, GA, Sept 2008. https://www.atsdr.cdc.gov/toxprofiles/tp115.pdf (accessed Jan 27, 2021).
297. Belfadhel, H. W.; de Brouwer, J.; Vieveen, M.; Wold, C.; Brander, E. Process for producing Bisphenol A with reduced sulfur content, polycarbonate made from the Bisphenol A, and containers formed from the polycarbonate. W.O. Pat. Appl. WO2013061274 A1, May 2, 2013.
298. Kissinger, G. M.; Wynn, N. P. Process and composition. U.S. Pat. Appl. US5362900A, Nov 8, 1994.
299. Brunelle, D. J. *ACS Symp. Ser.* **2005,** *898,* 1–5. doi:10.1021/bk-2005-0898.ch001
300. Serini, V. Polycarbonates. *Ullmann's Encyclopedia of Industrial Chemistry;* Wiley-VCH: Weinheim, Germany, 2000. doi:10.1002/14356007.a21_207
301. Samperi, F.; Montaudo, M. S.; Montaudo, G. Polycarbonates. In *Handbook of Engineering and Specialty Thermoplastics, Polyethers and Polyesters;* Sabu, T.; Visakh, P. M., Eds.; John Wiley & Sons: Hoboken, NJ, USA, 2011; Vol. 3, pp 493–528. doi:10.1002/9781118104729.ch12
302. Kim, J. G. *Polym. Chem.* **2020,** *11,* 4830–4849. doi:10.1039/c9py01927h
303. Antonakou, E. V.; Achilias, D. S. *Waste Biomass Valorization* **2013,** *4,* 9–21. doi:10.1007/s12649-012-9159-x
304. Alberti, C.; Eckelt, S.; Enthaler, S. *ChemistrySelect* **2019,** *4,* 12268–12271. doi:10.1002/slct.201903549
305. Kindler, T.-O.; Alberti, C.; Sundermeier, J.; Enthaler, S. *ChemistryOpen* **2019,** *8,* 1410–1412. doi:10.1002/open.201900319
306. Balaraman, E.; Gunanathan, C.; Zhang, J.; Shimon, L. J. W.; Milstein, D. *Nat. Chem.* **2011,** *3,* 609–614. doi:10.1038/nchem.1089
307. Dixneuf, P. H. *Nat. Chem.* **2011,** *3,* 578–579. doi:10.1038/nchem.1103
308. Alberti, C.; Scheliga, F.; Enthaler, S. *ChemistrySelect* **2019,** *4,* 2639–2643. doi:10.1002/slct.201900556

309. Pan, Z.; Hu, Z.; Shi, Y.; Shen, Y.; Wang, J.; Chou, I.-M. *RSC Adv.* **2014,** *4,* 19992–19998. doi:10.1039/c4ra00680a
310. Quaranta, E. *Appl. Catal., B* **2017,** *206,* 233–241. doi:10.1016/j.apcatb.2017.01.007
311. Guo, J.; Liu, M.; Gu, Y.; Wang, Y.; Gao, J.; Liu, F. *Ind. Eng. Chem. Res.* **2018,** *57,* 10915–10921. doi:10.1021/acs.iecr.8b02201
312. Liu, F.; Xiao, Y.; Sun, X.; Qin, G.; Song, X.; Liu, Y. *Chem. Eng. J.* **2019,** *369,* 205–214. doi:10.1016/j.cej.2019.03.048
313. Iannone, F.; Casiello, M.; Monopoli, A.; Cotugno, P.; Sportelli, M. C.; Picca, R. A.; Cioffi, N.; Dell'Anna, M. M.; Nacci, A. *J. Mol. Catal. A: Chem.* **2017,** *426,* 107–116. doi:10.1016/j.molcata.2016.11.006
314. de Caro, P.; Bandres, M.; Urrutigoïty, M.; Cecutti, C.; Thiebaud-Roux, S. *Front. Chem. (Lausanne, Switz.)* **2019,** *7,* 308. doi:10.3389/fchem.2019.00308
315. Adams, J. L.; Meek, T. D.; Mong, S. M.; Johnson, R. K.; Metcalf, B. W. *J. Med. Chem.* **1988,** *31,* 1355–1359. doi:10.1021/jm00402a018
316. Katritzky, A. R.; Oliferenko, A.; Lomaka, A.; Karelson, M. *Bioorg. Med. Chem. Lett.* **2002,** *12,* 3453–3457. doi:10.1016/s0960-894x(02)00741-2
317. Luinstra, G. A. *Polym. Rev. (Philadelphia, PA, U. S.)* **2008,** *48,* 192–219. doi:10.1080/15583720701834240
318. Luinstra, G. A.; Borchardt, E. Material Properties of Poly(Propylene Carbonates). In *Synthetic Biodegradable Polymers;* Rieger, B.; Künkel, A.; Coates, G.; Reichardt, R.; Dinjus, E.; Zevaco, T., Eds.; Advances in Polymer Science, Vol. 245; Springer: Berlin, Heidelberg, 2011; pp 29–48. doi:10.1007/12_2011_126
319. Han, Z.; Rong, L.; Wu, J.; Zhang, L.; Wang, Z.; Ding, K. *Angew. Chem., Int. Ed.* **2012,** *51,* 13041–13045. doi:10.1002/anie.201207781
320. Zubar, V.; Lebedev, Y.; Azofra, L. M.; Cavallo, L.; El-Sepelgy, O.; Rueping, M. *Angew. Chem., Int. Ed.* **2018,** *57,* 13439–13443. doi:10.1002/anie.201805630
321. Kumar, A.; Janes, T.; Espinosa-Jalapa, N. A.; Milstein, D. *Angew. Chem., Int. Ed.* **2018,** *57,* 12076–12080. doi:10.1002/anie.201806289
322. Liu, X.; de Vries, J. G.; Werner, T. *Green Chem.* **2019,** *21,* 5248–5255. doi:10.1039/c9gc02052g
323. Liu, Y.; Zhou, H.; Guo, J.-Z.; Ren, W.-M.; Lu, X.-B. *Angew. Chem., Int. Ed.* **2017,** *56,* 4862–4866. doi:10.1002/anie.201701438
324. Palmer, R. J. Polyamides, Plastics. *Encyclopedia of Polymer Science and Technology;* John Wiley & Sons: Hoboken, NJ, USA, 2001. doi:10.1002/0471440264.pst251
325. Zhang, C. *e-Polym.* **2018,** *18,* 373–408. doi:10.1515/epoly-2018-0094
326. Shukla, S. R.; Harad, A. M.; Mahato, D. *J. Appl. Polym. Sci.* **2006,** *100,* 186–190. doi:10.1002/app.22775
327. Alberti, C.; Figueira, R.; Hofmann, M.; Koschke, S.; Enthaler, S. *ChemistrySelect* **2019,** *4,* 12638–12642. doi:10.1002/slct.201903970
328. Datta, J.; Błażek, K.; Włoch, M.; Bukowski, R. *J. Polym. Environ.* **2018,** *26,* 4415–4429. doi:10.1007/s10924-018-1314-4
329. Matsumoto, H.; Akinari, Y.; Kaiso, K.; Kamimura, A. *J. Mater. Cycles Waste Manage.* **2017,** *19,* 326–331. doi:10.1007/s10163-015-0425-4
330. Kamimura, A.; Shiramatsu, Y.; Kawamoto, T. *Green Energy Environ.* **2019,** *4,* 166–170. doi:10.1016/j.gee.2019.01.002
331. Klun, U.; Kržan, A. *Polym. Adv. Technol.* **2002,** *13,* 817–822. doi:10.1002/pat.250
332. Kumar, A.; von Wolff, N.; Rauch, M.; Zou, Y.-Q.; Shmul, G.; Ben-David, Y.; Leitus, G.; Avram, L.; Milstein, D. *J. Am. Chem. Soc.* **2020,** *142,* 14267–14275. doi:10.1021/jacs.0c05675
333. May, C. A., Ed. *Epoxy Resins: Chemistry and Technology,* 2nd ed.; Taylor & Francis: Boca Raton, FL, USA, 1988. doi:10.1201/9780203756713
334. Deng, T.; Liu, Y.; Cui, X.; Yang, Y.; Jia, S.; Wang, Y.; Lu, C.; Li, D.; Cai, R.; Hou, X. *Green Chem.* **2015,** *17,* 2141–2145. doi:10.1039/c4gc02512a
335. Deng, T.; Cui, X.; Qi, Y.; Wang, Y.; Hou, X.; Zhu, Y. *Chem. Commun.* **2012,** *48,* 5494–5496. doi:10.1039/c2cc00122e
336. Ensing, B.; Tiwari, A.; Tros, M.; Hunger, J.; Domingos, S. R.; Pérez, C.; Smits, G.; Bonn, M.; Bonn, D.; Woutersen, S. *Nat. Commun.* **2019,** *10,* 2893. doi:10.1038/s41467-019-10783-z
337. Maeno, Z.; Torii, H.; Yamada, S.; Mitsudome, T.; Mizugaki, T.; Jitsukawa, K. *RSC Adv.* **2016,** *6,* 89231–89233. doi:10.1039/c6ra20864a
338. Maeno, Z.; Yamada, S.; Mitsudome, T.; Mizugaki, T.; Jitsukawa, K. *Green Chem.* **2017,** *19,* 2612–2619. doi:10.1039/c7gc00817a
339. Enthaler, S.; Weidauer, M. *Chem. – Eur. J.* **2012,** *18,* 1910–1913. doi:10.1002/chem.201103677
340. Enthaler, S. *Catal. Lett.* **2014,** *144,* 850–859. doi:10.1007/s10562-014-1214-8
341. Enthaler, S.; Weidauer, M. *ChemSusChem* **2012,** *5,* 1195–1198. doi:10.1002/cssc.201200125
342. Enthaler, S.; Trautner, A. *ChemSusChem* **2013,** *6,* 1334–1336. doi:10.1002/cssc.201300380
343. Wang, Y.; Hou, Y.; Song, H. *Polym. Degrad. Stab.* **2017,** *144,* 17–23. doi:10.1016/j.polymdegradstab.2017.08.001
344. Vollmer, I.; Jenks, M. J. F.; Roelands, M. C. P.; White, R. J.; van Harmelen, T.; de Wild, P.; van der Laan, G. P.; Meirer, F.; Keurentjes, J. T. F.; Weckhuysen, B. M. *Angew. Chem., Int. Ed.* **2020,** *59,* 15402–15423. doi:10.1002/anie.201915651
345. Sheldon, R. A.; Norton, M. *Green Chem.* **2020,** *22,* 6310–6322. doi:10.1039/d0gc02630a
346. Plechkova, N. V.; Seddon, K. R. *Chem. Soc. Rev.* **2008,** *37,* 123–150. doi:10.1039/b006677j
347. Climent, M. J.; Corma, A.; Iborra, S. *ChemSusChem* **2009,** *2,* 500–506. doi:10.1002/cssc.200800259
348. Felpin, F.-X.; Fouquet, E. *ChemSusChem* **2008,** *1,* 718–724. doi:10.1002/cssc.200800110
349. Moreno-Marrodan, C.; Liguori, F.; Barbaro, P. *Mol. Catal.* **2019,** *466,* 60–69. doi:10.1016/j.mcat.2019.01.014
350. Clarke, C. J.; Tu, W.-C.; Levers, O.; Bröhl, A.; Hallett, J. P. *Chem. Rev.* **2018,** *118,* 747–800. doi:10.1021/acs.chemrev.7b00571
351. Keijer, T.; Bakker, V.; Slootweg, J. C. *Nat. Chem.* **2019,** *11,* 190–195. doi:10.1038/s41557-019-0226-9

License and Terms

BEILSTEIN JOURNAL OF ORGANIC CHEMISTRY

Synthesis of β-triazolylenones via metal-free desulfonylative alkylation of *N*-tosyl-1,2,3-triazoles

Soumyaranjan Pati[1], Renata G. Almeida[2], Eufrânio N. da Silva Júnior[*2] and Irishi N. N. Namboothiri[*1]

Letter

Open Access

Address:
[1]Department of Chemistry, Indian Institute of Technology Bombay, Mumbai, 400 076, India and [2]Institute of Exact Sciences, Department of Chemistry, Federal University of Minas Gerais, CEP 31270-901, Belo Horizonte, MG, Brazil

Email:
Eufrânio N. da Silva Júnior[*] - eufranio@ufmg.br;
Irishi N. N. Namboothiri[*] - irishi@chem.iitb.ac.in

* Corresponding author

Keywords:
azoles; cycloaddition; enones; heterocycles; 1,2,3-triazoles

Beilstein J. Org. Chem. **2021,** *17,* 762–770.
https://doi.org/10.3762/bjoc.17.66

Received: 26 November 2020
Accepted: 19 March 2021
Published: 31 March 2021

This article is part of the thematic issue "Green chemistry II".

Associate Editor: L. Vaccaro

Abstract

Desulfonylative alkylation of *N*-tosyl-1,2,3-triazoles under metal-free conditions leading to β-triazolylenones is reported here. The present study encompasses the synthesis of triazoles with a new substitution pattern in a single step from cyclic 1,3-dicarbonyl compounds and *N*-tosyl triazole in moderate to high yields. Our synthesis takes place with complete regioselectivity as confirmed by crystallographic analysis which is rationalized by a suitable mechanistic proposal. This method provides an efficient, versatile and straightforward strategy towards the synthesis of new functionalized 1,2,3-triazoles.

Introduction

1,2,3-Triazoles are significant non-natural heterocyclic scaffolds with extensive applications in biochemistry, agrochemistry and materials chemistry [1-5]. This class of heterocycles presents important biological properties, such as antiviral, anti-inflammatory, antimicrobial etc. and are considered as key building blocks in pharmaceutical industry [6-9]. Thus, they marked their presence as prominent scaffolds in many drug molecules such as tazobactam, cefatrizine, rufinamide and JNJ-54175446 (Scheme 1a) [10].

In addition to their biological activities, triazolic compounds are widely employed in organic synthesis and have outstanding synthetic versatility. In this sense, extensive scientific research has been conducted using triazoles as synthetic precursors in denitrogenative transannulation reactions under metal-catalysed conditions to form other heterocycles such as functionalized pyrroles, imidazoles and pyridines (Scheme 1b) [11-13].

The traditional method for the synthesis of triazole unit is the Huisgen 1,3-dipolar cycloaddition between azides and alkynes [14,15]. However, the formation of the nitrogenated azoles by the classical Huisgen methodology is slow due to its high activation energies and also lack of regiochemical control, in general, leading to a mixture of 1,4- and 1,5-regioisomers of

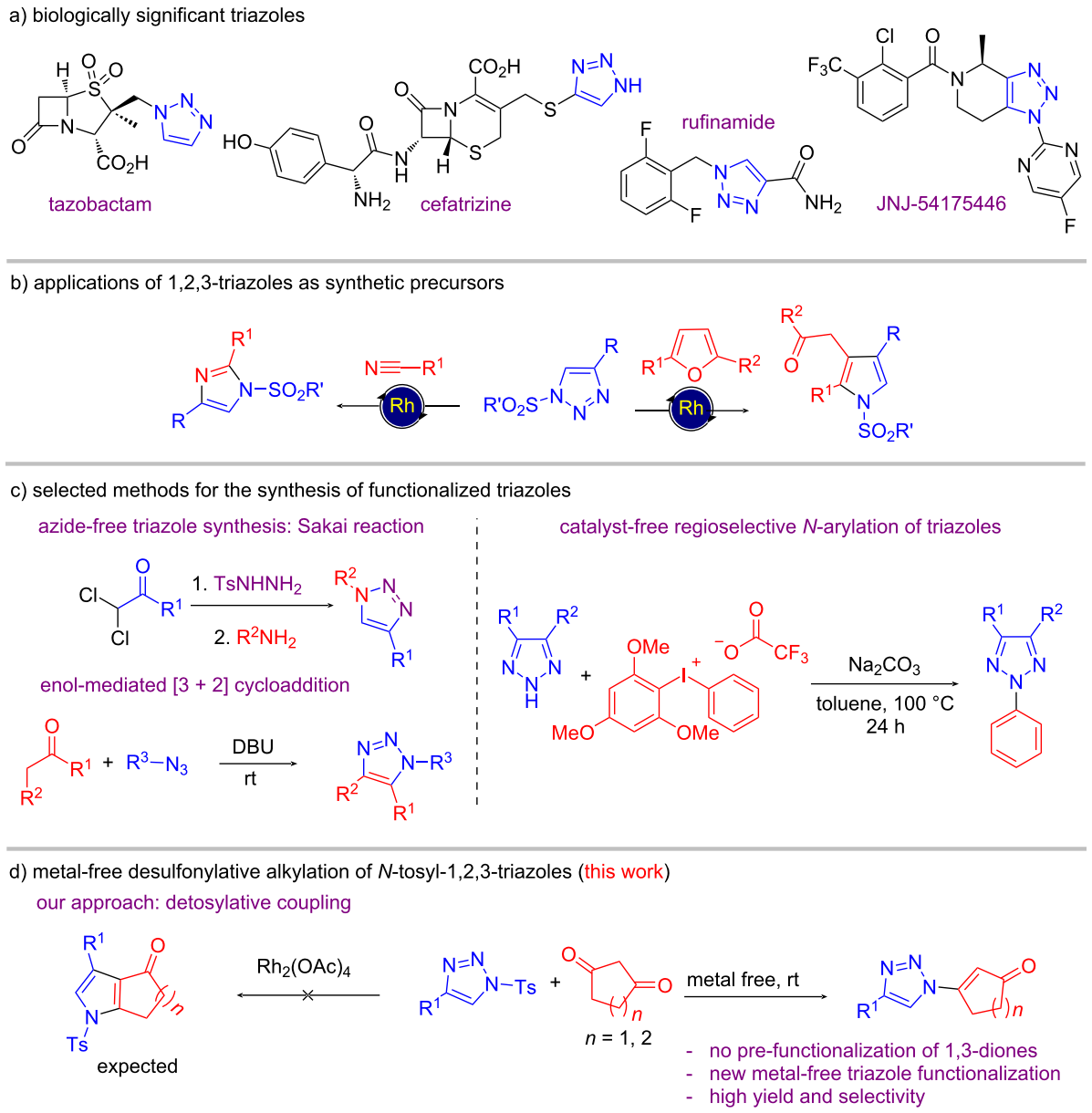

Scheme 1: Synthesis, functionalization and applications of triazoles.

1,2,3-triazoles. Later, Sharpless and Meldal have independently developed a copper-catalysed azide–alkyne cycloaddition that accelerated the rate of the reaction and allowed the selective preparation of 1,5-disubstituted 1,2,3-triazoles [16-19].

As noted above, a wide range of methods are available in the literature for the efficient synthesis of triazoles with different substitution pattern. One important methodology developed by the Sakai group involved the reaction of α,α-dichloroketone, tosyl hydrazide and primary amine [20]. However, in this case, the unstable α,α-dichlorohydrazone intermediate had to be isolated which paved the way for further modification of the protocol (Scheme 1c).

Direct functionalization of triazoles is an alternative strategy to access triazoles with the desired substitution pattern. However, such approaches are complicated by a low energy barrier between the N^1 and N^2 tautomers in solution leading to poor N^1/N^2 selectivity, for instance, in the direct *N*-alkylation of triazoles [21-23]. Despite these challenges, a number of N^1- and N^2-selective alkylation methods have been developed employing transition metal catalysts which include Au-catalysed desul-

fonylative coupling *N*-tosyl-1,2,3-triazoles with alkynes and Rh catalysed N^1 and N^2 selective alkylations [24,25].

As for metal-free approaches, besides synthesizing *N*-alkylated triazoles via 1,3-dipolar cycloaddition of alkyl azide with enols generated from carbonyl compounds under transition metal-free conditions [26], a direct functionalization of triazoles under metal-free conditions has been reported. These include the Broensted acid-catalysed N^2 alkylation [27], organocatalytic N^1 alkylation [28,29], N^2-arylation using hypervalent iodine (Scheme 1c) [30], N^2-alkylation involving radical intermediate [31], pyridine-*N*-oxide-mediated N^1-arylation [32], NIS-mediated N^2-arylation [33], etc. Although these are significant advances towards metal-free functionalization of triazoles, many of them suffer from poor regioselectivity. Therefore, a new method for N^1-selective alkylation of the triazole moiety under simple, mild and metal-free conditions is highly desirable.

From another perspective, compounds containing a 1,3-dicarbonyl moiety are essential building blocks in organic synthesis whose reactivity is well-established in the literature [34,35]. Besides, these are the precursors of β-enamines which are employed for the synthesis of many bioactive heterocycles [36]. These are also important precursors of diazo adducts which are used in insertion, cyclopropanation, and various rearrangements to construct various cyclic as well as acyclic moieties under metal-catalysed conditions [37,38]. On the contrary, under basic conditions, these diazo compounds undergo [3 + 2] cycloadditions with suitable substrates to render various nitrogen-rich heterocycles [39]. In addition to their synthetic importance, these are frequently encountered as ligands in many metal complexes [40-43]. Our group have also employed 1,3-dicarbonyl compounds as binucleophiles for the construction of various carbocycles, heterocycles as well as in asymmetric catalysis [44-50]. Our initial objective to trap the aza vinyl rhodium carbenoid using 1,3-dicarbonyl compounds to form pyrazolone was unsuccessful which instead led to the formation of an unexpected product, i.e., β-triazolylenone. Being inspired by the results, we intended to use 1,3-dicarbonyl compounds as detosylative alkylating agents that would lead to the formation of β-triazolylenones in a highly regioselective manner under mild conditions (Scheme 1d).

Results and Discussion

In order to execute our idea, triazole **1a** and 1,3-cyclohexanedione (**2a**) were selected as our model substrates and the reaction was performed using 4 mol % of $Rh_2(OAc)_4$ in chloroform under reflux conditions which afforded the β-1,2,3-triazolylcyclohexenone **3a** in 66% yield (Table 1, entry 1). The alternative approach for the synthesis of such triazole moiety **3a** is the [3 + 2] cycloaddition between alkynes and the corresponding azides. However, the major disadvantage of such a strategy is the use of 3-azidoenone which is difficult to handle owing to its

Table 1: Optimization studies.[a]

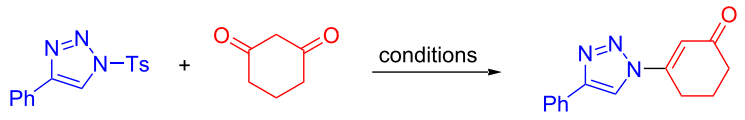

1a **2a** **3a**

Entry	Catalyst (mol %)	Solvent	Temp. (°C)	Time (h)	Yield (%)[b]
1	$Rh_2(OAc)_4$ (4)	$CHCl_3$	60	2.5	66
2	$Cu(OAc)_2$ (4)	$CHCl_3$	60	6	65
3	…	$CHCl_3$	60	5	49
4	**…**	**$CHCl_3$**	**rt**	**24**	**78**
5	…	THF	rt	48	NR
6	…	EtOAc	rt	48	trace
7	…	toluene	rt	72	trace
8	…	CH_2Cl_2	rt	96	56
9	…	1,2-DCE	rt	72	trace
10	…	2-MeTHF	rt	72	[c]
11	…	isopropanol	rt	72	[c]
12	…	acetone	rt	72	[c]

[a]Performed by using 0.1 mmol 4-phenyl-*N*-tosyl-1*H*-1,2,3- triazole (**1a**) and 0.1 mmol of cycloalkan-1,3-dione **2**. [b]After silica gel column chromatography. [c]**1a** decomposed.

explosive nature. Therefore, our method provides an easy pathway to synthesize such triazolylenones.

Inspired by this result, we proceeded to optimize the reaction conditions to further improve the yield. Replacement of rhodium by copper (II) acetate slowed down the reaction with a marginal change in the yield of the product **3a** (Table 1, entry 2). Surprisingly, when the reaction was conducted in the absence of any metal catalyst, the reaction proceeded sluggishly and the coupling product **3a** was isolated in 49% yield (Table 1, entry 3). This suggested that the reaction could also proceed even in the absence of metal catalyst. However, the lower yield of the product **3a** might be attributed to certain side products obtained at high temperature as evident from TLC analysis. To avoid such side reactions, the reaction was performed at room temperature and to our delight, the product **3a** was obtained in 78% yield (Table 1, entry 4). For further improvement in the yield, the reaction was carried out in different solvents such as THF, EtOAc, toluene, DCM, 1,2-DCE, 2-MeTHF, isopropanol and acetone. Unfortunately, these attempts led to inferior results (Table 1, entries 5–12). Since, there was no further improvement in the yield, the conditions described in Table 1, entry 4 were considered as the best to generalize the scope of the reaction.

At the outset, various triazoles **1** were screened under the optimized conditions (Scheme 2). As mentioned earlier, the model triazole **1a** afforded the product **3a** in 78% yield within 24 h.

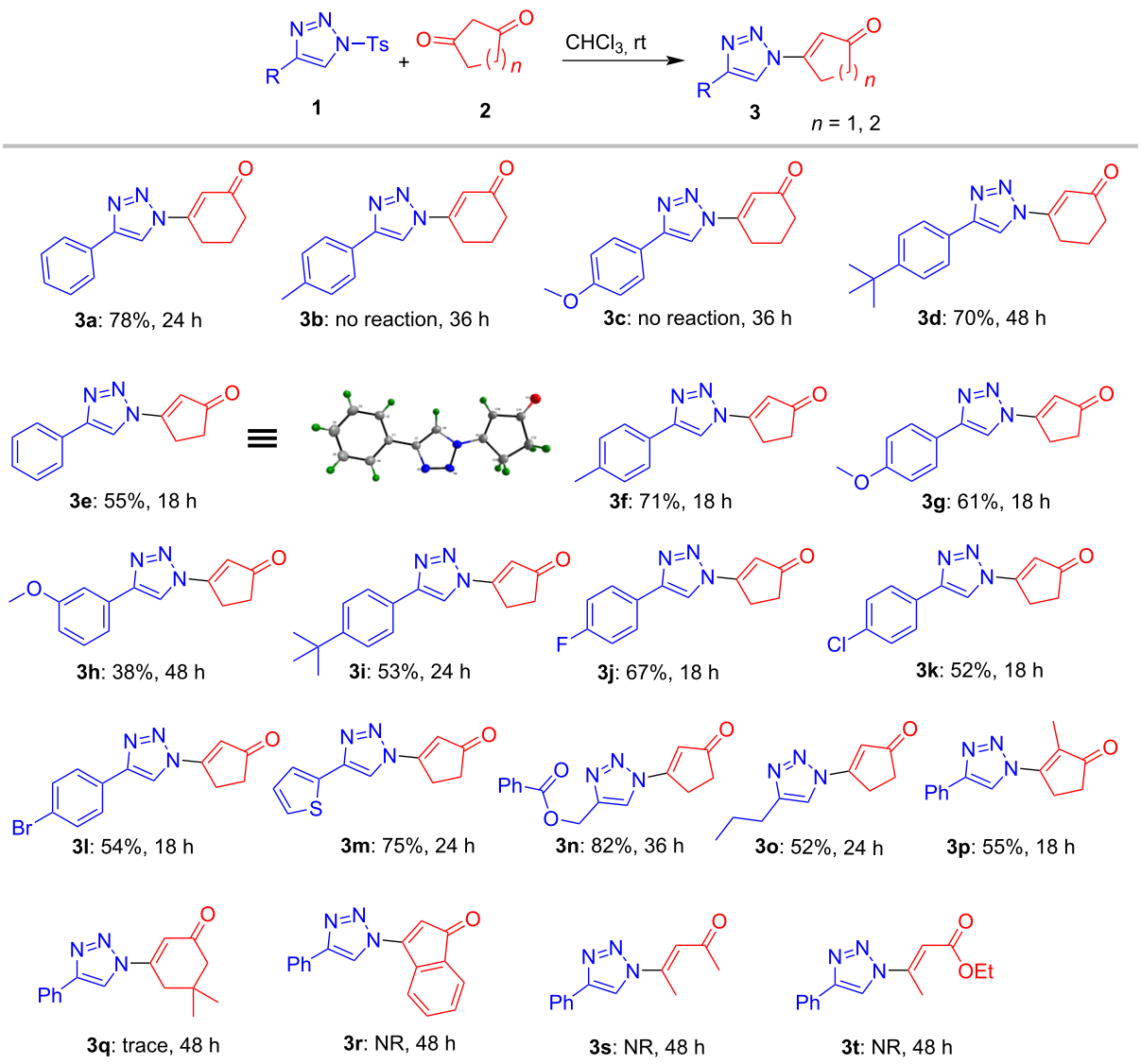

Scheme 2: The reaction was performed using 0.2 mmol *N*-tosyl-1,2,3-triazole **1** and 0.2 mmol of cyclohexyl-1,3-dione **2**. Yields are determined after silica gel column chromatography. NR = no reaction.

But to our surprise, triazoles **1b** and **1c** containing electron donating 4-tolyl and 4-methoxyphenyl groups did not deliver the products **3b** and **3c**, respectively, even after prolonged reaction time. This is attributable to the greater reactivity of their corresponding triazolyl anion which preferred protonation over Michael addition (see mechanism, Scheme 4, vide infra). On the other hand, 4-*tert*-butyl analog **1d** underwent the reaction smoothly to form the corresponding product **3d** in 70% yield. However, due to the inconsistent results with cyclohexanedione **2a**, further scope was investigated by employing cyclopentane-1,3-dione **2b**. The model triazole **1a** furnished the product **3e** in 55% yield within 18 h. To our delight, triazoles **1b** and **1c**, bearing 4-tolyl and 4-methoxyphenyl groups, which did not react with 1,3-cyclohexanedione **2a** reacted smoothly with cyclopentane-1,3-dione **2b** to deliver the products **3f** and **3g** in 71% and 61% yields, respectively. The reaction of mild electron withdrawing 3-methoxyphenyl-1,2,3-triazole **1e** led to product **3h** in low yield (38%) whereas the corresponding 4-*tert*-butylphenyl-1,2,3-triazole **1f** afforded the product **3i** in 53% yield. Later, the reaction was performed using various haloaryltriazoles, such as 4-fluorophenyl **1f**, 4-chlorophenyl **1g** and 4-bromophenyl **1h**, which also gave the corresponding products **3j**, **3k** and **3l** in 67%, 52% and 54%, respectively.

Further, the heteroaryl derivative thienyltriazole **1i** also reacted well to afford the product **3m** in 75% yield. While the benzoyloxymethyltriazole **1j** furnished the product **3n** in excellent (82%) yield, the performance of another alkyltriazole **1k** was less impressive giving the corresponding product **3o** only in moderate (52%) yield. The reaction of model triazole **1a** with 2-methyl-1,3-cyclopentanedione (**2c**) also led to the product **3p** in moderate (55%) yield. Unfortunately, the reaction was not successful with dimedone (**2d**), 1,3-indanedione (**2e**) and acyclic 1,3-dicarbonyl compounds such as acetylacetone (**2e**) and ethyl acetoacetate (**2f**).

The structure and regiochemistry of all the products were confirmed by detailed analysis of their spectral data (IR, ^{1}H, ^{13}C and Mass) which were further unambiguously established by single crystal X-ray analysis of a representative compound **3e** (Scheme 2 and Supporting Information File 3).

Although triazole **1a** reacted with cyclohexanedione **2a** (vide supra), its reaction with dimedone **2d** provided a complex mixture. Therefore, we employed triazole **1a'** bearing a mesyl group for the reaction with **2d** (Scheme 3a). Surprisingly, this reaction delivered the 5,5-dimethyl-3-oxocyclohex-1-en-1-yl

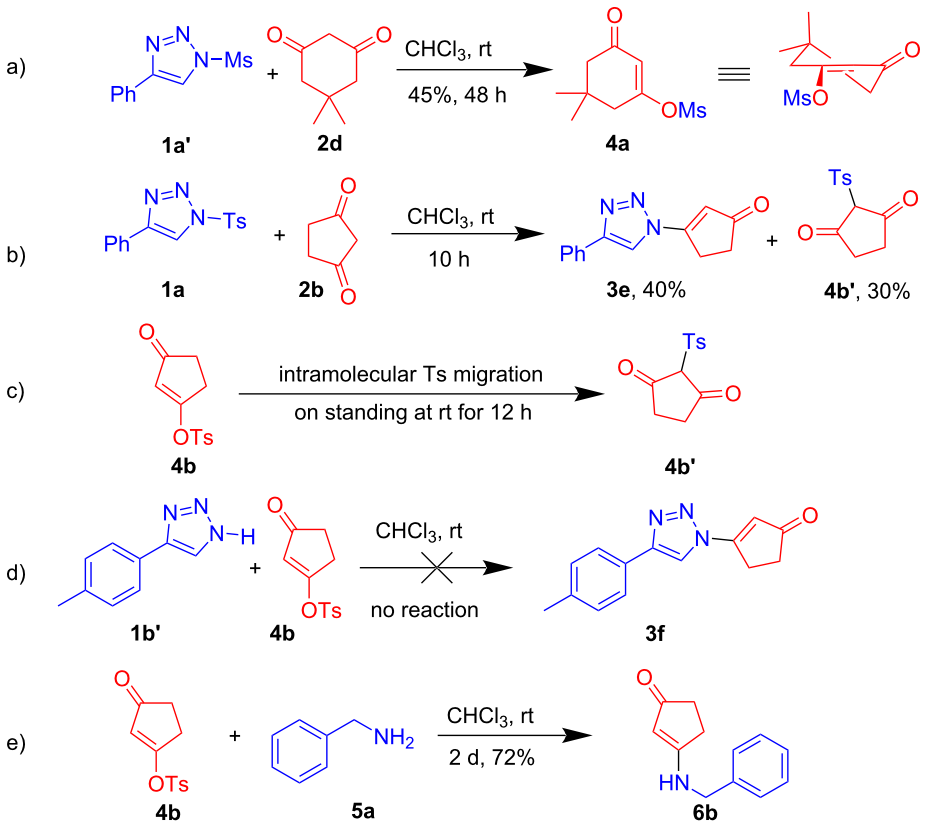

Scheme 3: Control experiments.

methanesulfonate (**4a**), instead of the expected β-triazolylenone **3q**, in 45% yield. In order to further ascertain the reaction mechanism, the crude reaction mixture of **1a** with **2b** after 10 h was analysed by NMR which suggested the formation of C-tosyl intermediate **4b'** besides the expected product **3e** (Scheme 3b). The two compounds were later purified and characterized. Subsequently, the cyclopentan-1,3-dione derived *O*-tosyl intermediate **4b** was prepared following a literature procedure [51]. Even though the *O*-tosyl intermediate **4b** was stable at low temperature (0 °C), surprisingly, it got converted to C-tosyl intermediate on standing overnight at room temperature (Scheme 3c). However, treatment of this *O*-tosyl intermediate **4b** with triazole **1b'** did not afford the expected product **3f** (Scheme 3d). This suggests that triazole **1b'** is not the active nucleophile in this transformation. However, when the *O*-tosyl intermediate **4b** was treated with a more nucleophilic amine, namely benzyl amine **5a**, it indeed afforded the Michael addition–elimination product **6b** in good yield. These results provided crucial evidence for the mechanism of the reaction which suggested that β-sulfonyloxyenone could be the key intermediate in the formation of β-triazolylenone **3**.

Based on the above control experiments, the following mechanism is proposed. Initially, the enol form of 1,3-dicarbonyl **2** attacks the sulfonyl group in **1** to form intermediate **I** which later undergoes proton transfer to form intermediate **II**. Cleavage of the N–S bond in intermediate **II** generates the β-*O*-tosylcycloalkenone **4** and triazolyl anion **III**. Subsequent counter-attack of the triazolyl anion **III** on the enone intermediate **4** (path A), followed by elimination of OTs affords the corresponding β-triazolylenone **3** (Scheme 4) [52]. The β-*O*-tosylcyclopentenone intermediate **4b** can also undergo intramolecular tosyl migration to form a stable C-tosylated product **4b'** (see also Scheme 3b and c). This might also be attributed to the lower yields obtained in certain cases.

It may be noted that the outcome of the reaction is highly dependent on the nature of the 1,3-dicarbonyl compound. In the case of cyclic-1,3-dicarbonyls, cyclopentane-1,3-dione **2b** reacts smoothly in almost all cases whereas the scope of cyclohexane-1,3-dione **2a** is limited. On the contrary, dimedone (**2d**) did not react with *N*-tosyl-1,2,3-triazole, but reacted with *N*-mesyl-1,2,3-triazole to form the 5,5-dimethyl-3-oxocyclohex-1-en-1-yl methanesulfonate intermediate **4a**. The highly substrate-dependent nature of the reaction can be explained by taking both hydrogen bonding and steric factors into consideration. In the solid as well as in the solution state, all the three above-mentioned 1,3-dicarbonyls exist in the enol form which are considerably stable and therefore undergo tosylation easily to form the corresponding *O*-tosylenone

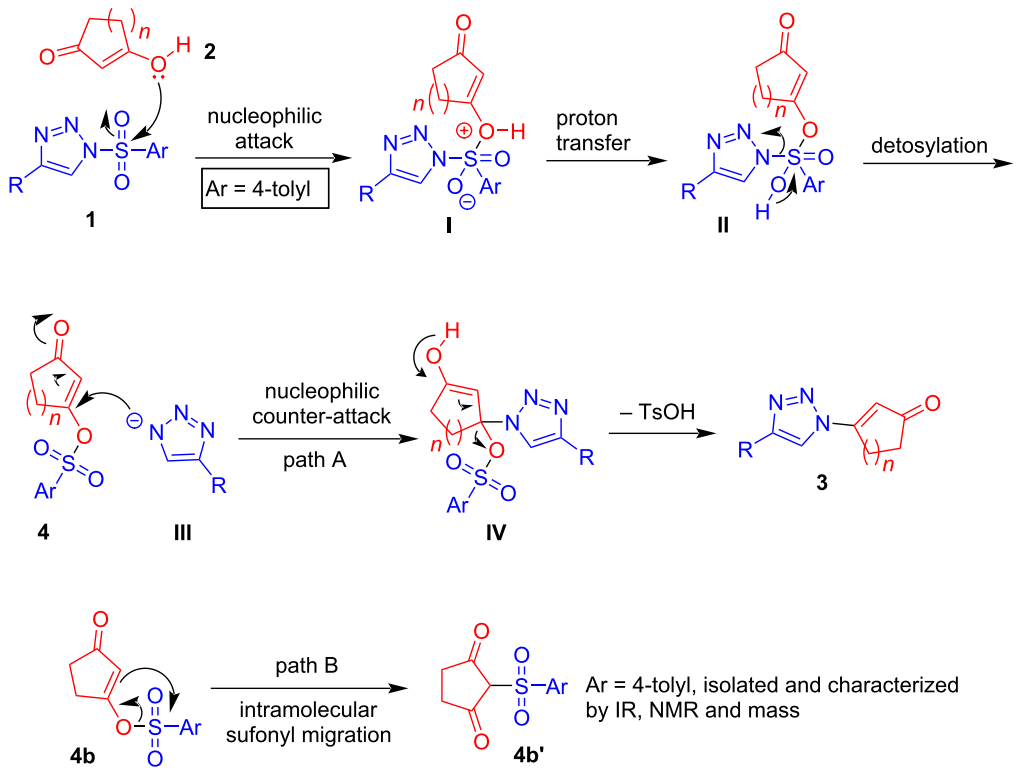

Scheme 4: Mechanistic proposal for the formation of β-triazolylenones.

intermediates. The five membered tosyloxyenone intermediate is a planar molecule and therefore free of any major steric crowding (Figure 1). Hence, the incoming nucleophile can easily attack the β-position without any difficulty. On the other hand, the six membered *o*-tosyl intermediate is likely to exist in twist-boat conformation. When R = H, the pseudoaxial approach of the nucleophile towards the β-position leading to the enolate intermediate **VI** (R = H) bearing pseudoequatorially oriented OTs group or the pseudoequatorial approach of the nucleophile leading to the intermediate **VII** (R = H) bearing pseudoaxially oriented OTs group suffers from only limited steric crowding (1,3-diaxial interaction). In the case of dimedone **2d**, the two bulky methyl groups impart greater steric hindrance (1,3-diaxial interaction) to the incoming nucleophile in the event of pseudoaxial approach leading to intermediate **VI** (R = Me) and to the axial OTs group in the resulting intermediate **VII** (R = Me) in the event of equatorial approach of the nucleophile. Therefore, the reaction proceeds in the case of 1,3-cyclohexanedione (**2a**), but stops at the tosyl/mesyl migration step and does not proceed further in the case of dimedone (**2d**). Unlike cyclic 1,3-dicarbonyls, the acyclic 1,3-dicarbonyls possess intramolecular hydrogen bonding and are in rapid equilibrium with their keto-form. In polar solvents, the stability of the enol form is further decreased and, therefore, the keto-enol equilibrium lies more towards the keto-form [53-56]. Presumably for this reason, the acyclic 1,3-dicarbonyls did not react in the desired way under our experimental conditions.

Conclusion

In conclusion, we have developed a metal-free and catalyst-free approach for the desulfonylative coupling of *N*-tosyl-1,2,3-triazoles with cyclic 1,3-diketones to form various β-triazolylenones. Although the scope of the 1,3-dicarbonyl compound is limited, the protocol is very convenient and useful as it employs very mild reaction conditions. It is also highly regioselective and `affords only N^1-alkylated products in moderate to excellent yields.

Supporting Information

Supporting Information File 1

Experimental details and characterization data of new compounds.
[https://www.beilstein-journals.org/bjoc/content/supplementary/1860-5397-17-66-S1.pdf]

Supporting Information File 2

Copies of NMR spectra.
[https://www.beilstein-journals.org/bjoc/content/supplementary/1860-5397-17-66-S2.pdf]

Supporting Information File 3

Crystallographic data for compound **3e**.
[https://www.beilstein-journals.org/bjoc/content/supplementary/1860-5397-17-66-S3.cif]

Acknowledgements

We thank Dr Deepa Nair, Mr Sudheesh T Sivanandan and Dr Pallabita Basu, Department of Chemistry, Indian Institute of Technology Bombay, for assistance with the X-ray crystallographic analysis.

Funding

ENSJ thanks CNPq, CAPES, Return Fellowship of the Alexander von Humboldt Foundation (AvH) and the Royal Society of Chemistry for the research fund grant (R19-9781). INNN thanks SERB, India for financial support. SP thanks CSIR, India for a senior research fellowship.

ORCID® iDs

Soumyaranjan Pati - https://orcid.org/0000-0003-4552-6076
Renata G. Almeida - https://orcid.org/0000-0003-2896-0487
Eufrânio N. da Silva Júnior - https://orcid.org/0000-0003-1281-5453
Irishi N. N. Namboothiri - https://orcid.org/0000-0002-8945-3932

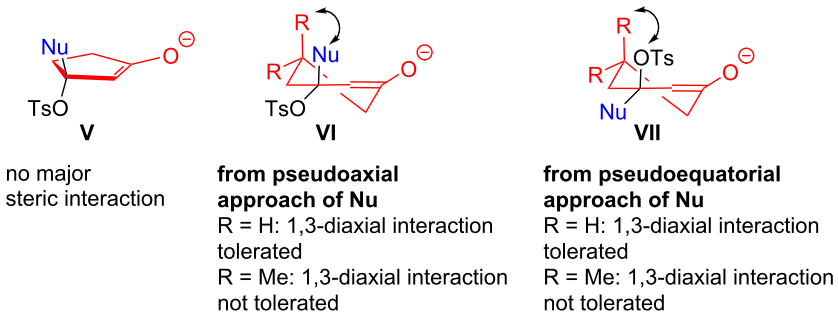

Figure 1: Nucleophilic addition to 5- and 6-membered cyclic tosyloxyenones.

Preprint

A non-peer-reviewed version of this article has been previously published as a preprint: https://doi.org/10.3762/bxiv.2020.134.v1

References

1. Astruc, D.; Liang, L.; Rapakousiou, A.; Ruiz, J. *Acc. Chem. Res.* **2012,** *45,* 630–640. doi:10.1021/ar200235m
2. Chu, C.; Liu, R. *Chem. Soc. Rev.* **2011,** *40,* 2177–2188. doi:10.1039/c0cs00066c
3. Finn, M. G.; Fokin, V. V. *Chem. Soc. Rev.* **2010,** *39,* 1231–1232. doi:10.1039/c003740k
4. Lau, Y. H.; Rutledge, P. J.; Watkinson, M.; Todd, M. H. *Chem. Soc. Rev.* **2011,** *40,* 2848–2866. doi:10.1039/c0cs00143k
5. Muller, T.; Bräse, S. *Angew. Chem., Int. Ed.* **2011,** *50,* 11844–11845. doi:10.1002/anie.201105707
6. Chabre, Y.; Roy, R. *Curr. Top. Med. Chem.* **2008,** *8,* 1237–1285. doi:10.2174/156802608785848987
7. Colombo, M.; Peretto, I. *Drug Discovery Today* **2008,** *13,* 677–684. doi:10.1016/j.drudis.2008.03.007
8. Hanselmann, R.; Job, G. E.; Johnson, G.; Lou, R.; Martynow, J. G.; Reeve, M. M. *Org. Process Res. Dev.* **2010,** *14,* 152–158. doi:10.1021/op900252a
9. Moumné, R.; Larue, V.; Seijo, B.; Lecourt, T.; Micouin, L.; Tisné, C. *Org. Biomol. Chem.* **2010,** *8,* 1154–1159. doi:10.1039/b921232a
10. Clark, P. R.; Williams, G. D.; Hayes, J. F.; Tomkinson, N. C. O. *Angew. Chem., Int. Ed.* **2020,** *59,* 6740–6744. doi:10.1002/anie.201915944
11. Chattopadhyay, B.; Gevorgyan, V. *Angew. Chem., Int. Ed.* **2012,** *51,* 862–872. doi:10.1002/anie.201104807
12. Horneff, T.; Chuprakov, S.; Chernyak, N.; Gevorgyan, V.; Fokin, V. V. *J. Am. Chem. Soc.* **2008,** *130,* 14972–14974. doi:10.1021/ja805079v
13. Davies, H. M. L.; Alford, J. S. *Chem. Soc. Rev.* **2014,** *43,* 5151–5162. doi:10.1039/c4cs00072b
14. Huisgen, R. *Angew. Chem., Int. Ed. Engl.* **1963,** *2,* 565–598. doi:10.1002/anie.196305651
15. Huisgen, R. *Angew. Chem., Int. Ed. Engl.* **1963,** *2,* 633–645. doi:10.1002/anie.196306331
16. Rostovtsev, V. V.; Green, L. G.; Fokin, V. V.; Sharpless, K. B. *Angew. Chem., Int. Ed.* **2002,** *41,* 2596–2599. doi:10.1002/1521-3773(20020715)41:14<2596::aid-anie2596>3.0.co;2-4
17. Tornøe, C. W.; Christensen, C.; Meldal, M. *J. Org. Chem.* **2002,** *67,* 3057–3064. doi:10.1021/jo011148j
18. Zhang, L.; Chen, X.; Xue, P.; Sun, H. H. Y.; Williams, I. D.; Sharpless, K. B.; Fokin, V. V.; Jia, G. *J. Am. Chem. Soc.* **2005,** *127,* 15998–15999. doi:10.1021/ja054114s
19. Johansson, J. R.; Beke-Somfai, T.; Said Stålsmeden, A.; Kann, N. *Chem. Rev.* **2016,** *116,* 14726–14768. doi:10.1021/acs.chemrev.6b00466
20. Sakai, K.; Hida, N.; Kondo, K. *Bull. Chem. Soc. Jpn.* **1986,** *59,* 179–183. doi:10.1246/bcsj.59.179
21. Catalán, J.; Sánchez-Cabezudo, M.; De Paz, J. L. G.; Elguero, J.; Taft, R. W.; Anvia, F. *J. Comput. Chem.* **1989,** *10,* 426–433. doi:10.1002/jcc.540100318
22. Tomas, F.; Abboud, J. L. M.; Laynez, J.; Notario, R.; Santos, L.; Nilsson, S. O.; Catalan, J.; Claramunt, R. M.; Elguero, J. *J. Am. Chem. Soc.* **1989,** *111,* 7348–7353. doi:10.1021/ja00201a011
23. Tomas, F.; Catalan, J.; Perez, P.; Elguero, J. *J. Org. Chem.* **1994,** *59,* 2799–2802. doi:10.1021/jo00089a026
24. Sun, C.; Yuan, X.; Li, Y.; Li, X.; Zhao, Z. *Org. Biomol. Chem.* **2017,** *15,* 2721–2724. doi:10.1039/c7ob00142h
25. Berthold, D.; Breit, B. *Org. Lett.* **2018,** *20,* 598–601. doi:10.1021/acs.orglett.7b03708
26. Ramachary, D. B.; Reddy, G. S.; Peraka, S.; Gujral, J. *ChemCatChem* **2017,** *9,* 263–267. doi:10.1002/cctc.201601317
27. Wei, H.; Hu, Q.; Ma, Y.; Wei, L.; Liu, J.; Shi, M.; Wang, F. *Asian J. Org. Chem.* **2017,** *6,* 662–665. doi:10.1002/ajoc.201700045
28. Bhagat, U. K.; Kamaluddin; Peddinti, R. K. *Tetrahedron Lett.* **2017,** *58,* 298–301. doi:10.1016/j.tetlet.2016.11.125
29. Bhagat, U. K.; Peddinti, R. K. *J. Org. Chem.* **2018,** *83,* 793–804. doi:10.1021/acs.joc.7b02793
30. Roshandel, S.; Lunn, M. J.; Rasul, G.; Muthiah Ravinson, D. S.; Suri, S. C.; Prakash, G. K. S. *Org. Lett.* **2019,** *21,* 6255–6258. doi:10.1021/acs.orglett.9b02140
31. Li, Z.; Wei, Q.; Song, L.; Han, W.; Wu, X.; Zhao, Y.; Xia, F.; Liu, S. *Org. Lett.* **2019,** *21,* 6413–6417. doi:10.1021/acs.orglett.9b02269
32. Harisha, M. B.; Nagaraj, M.; Muthusubramanian, S.; Bhuvanesh, N. *RSC Adv.* **2016,** *6,* 58118–58124. doi:10.1039/c6ra10452e
33. Gu, C.-X.; Bi, Q.-W.; Gao, C.-K.; Wen, J.; Zhao, Z.-G.; Chen, Z. *Org. Biomol. Chem.* **2017,** *15,* 3396–3400. doi:10.1039/c7ob00329c
34. Bonne, D.; Coquerel, Y.; Constantieux, T.; Rodriguez, J. *Tetrahedron: Asymmetry* **2010,** *21,* 1085–1109. doi:10.1016/j.tetasy.2010.04.045
35. Rubinov, D. B.; Rubinova, I. L.; Akhrem, A. A. *Chem. Rev.* **1999,** *99,* 1047–1066. doi:10.1021/cr9600621
36. Govindh, B.; Diwakar, B. S.; Murthy, Y. L. N. *Org. Commun.* **2012,** *5,* 105–119.
37. Ford, A.; Miel, H.; Ring, A.; Slattery, C. N.; Maguire, A. R.; McKervey, M. A. *Chem. Rev.* **2015,** *115,* 9981–10080. doi:10.1021/acs.chemrev.5b00121
38. Zhang, Y.; Wang, J. *Chem. Commun.* **2009,** 5350–5361. doi:10.1039/b908378b
39. Baiju, T. V.; Namboothiri, I. N. N. *Chem. Rec.* **2017,** *17,* 939–955. doi:10.1002/tcr.201600141
40. Garnovskii, A. D.; Vasil'chenko, I. S. *Russ. Chem. Rev.* **2002,** *71,* 943–968. doi:10.1070/rc2002v071n11abeh000759
41. Garnovskii, A. D.; Vasil'chenko, I. S. *Usp. Khim.* **2005,** *74,* 211–234. doi:10.1070/rc2005v074n03abeh001164
42. Skopenko, V. V.; Amirkhanov, V. M.; Sliva, T. Y.; Vasil'chenko, I. S.; Anpilova, E. L.; Garnovskij, A. D. *Usp. Khim.* **2004,** *73,* 737–752. doi:10.1070/rc2004v073n08abeh000909
43. Aromí, G.; Gamez, P.; Reedijk, J. *Coord. Chem. Rev.* **2008,** *252,* 964–989. doi:10.1016/j.ccr.2007.07.008
44. Lal, S.; Chowdhury, A.; Namboothiri, I. N. N. *Tetrahedron* **2017,** *73,* 1297–1305. doi:10.1016/j.tet.2017.01.003
45. Mane, V.; Kumar, T.; Pradhan, S.; Katiyar, S.; Namboothiri, I. N. N. *RSC Adv.* **2015,** *5,* 69990–69999. doi:10.1039/c5ra11471c
46. Ayyagari, N.; Mehta, A.; Gopi, E.; Deb, I.; Mobin, S. M.; Namboothiri, I. N. N. *Tetrahedron* **2013,** *69,* 5973–5980. doi:10.1016/j.tet.2013.04.083
47. Nair, D. K.; Mobin, S. M.; Namboothiri, I. N. N. *Tetrahedron Lett.* **2012,** *53,* 3349–3352. doi:10.1016/j.tetlet.2012.04.084
48. Ayyagari, N.; Namboothiri, I. N. N. *Tetrahedron: Asymmetry* **2012,** *23,* 605–610. doi:10.1016/j.tetasy.2012.04.011
49. Ayyagari, N.; Jose, D.; Mobin, S. M.; Namboothiri, I. N. N. *Tetrahedron Lett.* **2011,** *52,* 258–262. doi:10.1016/j.tetlet.2010.11.017
50. Nair, D. K.; Menna-Barreto, R. F. S.; da Silva Júnior, E. N.; Mobin, S. M.; Namboothiri, I. N. N. *Chem. Commun.* **2014,** *50,* 6973–6976. doi:10.1039/c4cc02279c

51. Kremsmair, A.; Skotnitzki, J.; Knochel, P. *Chem. – Eur. J.* **2020,** *26,* 11971–11973. doi:10.1002/chem.202002297
52. Analogous formation of α-triazolylazine via reaction of an *N*-oxide with *N*-tosyl-1,2,3-triazole has been reported: a) Ref [32]. b) Sontakke, G. S.; Shukla, R. K.; Volla, M. R. *Beilstein J. Org. Chem.* **2021,** *17,* 485–493. doi:10.3762/bjoc.17.42
53. Jana, K.; Ganguly, B. *ACS Omega* **2018,** *3,* 8429–8439. doi:10.1021/acsomega.8b01008
54. Singh, I.; Calvo, C. *Can. J. Chem.* **1975,** *53,* 1046–1050. doi:10.1139/v75-147
55. Hudson, B. S.; Braden, D. A.; Allis, D. G.; Jenkins, T.; Baronov, S.; Middleton, C.; Withnall, R.; Brown, C. M. *J. Phys. Chem. A* **2004,** *108,* 7356–7363. doi:10.1021/jp048613b
56. Ferrari, E.; Saladini, M.; Pignedoli, F.; Spagnolo, F.; Benassi, R. *New J. Chem.* **2011,** *35,* 2840–2847. doi:10.1039/c1nj20576e

License and Terms

BEILSTEIN JOURNAL OF ORGANIC CHEMISTRY

Nitroalkene reduction in deep eutectic solvents promoted by BH_3NH_3

Chiara Faverio, Monica Fiorenza Boselli, Patricia Camarero Gonzalez, Alessandra Puglisi and Maurizio Benaglia*

Letter

Open Access

Address:
Dipartimento di Chimica, Università degli Studi di Milano, Via C. Golgi, 19, I-20133, Milano, Italy

Email:
Maurizio Benaglia* - maurizio.benaglia@unimi.it

* Corresponding author

Keywords:
alternative solvents; atom economy; DES; nitro derivatives; reduction

Beilstein J. Org. Chem. **2021,** *17,* 1041–1047.
https://doi.org/10.3762/bjoc.17.83

Received: 23 December 2020
Accepted: 18 April 2021
Published: 06 May 2021

This article is part of the thematic issue "Green chemistry II".

Associate Editor: L. Vaccaro

Abstract

Deep eutectic solvents (DESs) have gained attention as green and safe as well as economically and environmentally sustainable alternative to the traditional organic solvents. Here, we report the combination of an atom-economic, very convenient and inexpensive reagent, such as BH_3NH_3, with bio-based eutectic mixtures as biorenewable solvents in the synthesis of nitroalkanes, valuable precursors of amines. A variety of nitrostyrenes and alkyl-substituted nitroalkenes, including α- and β-substituted nitroolefins, were chemoselectively reduced to the nitroalkanes, with an atom economy-oriented, simple and convenient experimental procedure. A reliable and easily reproducible protocol to isolate the product without the use of any organic solvent was established, and the recyclability of the DES mixture was successfully investigated.

Introduction

The search for alternative solvents, not derived from oil but from biorenewable resources, is a topic of primary importance in modern chemistry [1,2]. The solvents are the major contributor to the waste generated in chemical industries, and the elimination or replacement of these with more sustainable alternatives is part of the efforts of the whole research community concerned with the concept of a circular economy [3].

In this context, deep eutectic solvents (DESs) have attracted an increasing attention as green, safe, economically and environmentally sustainable alternative to the traditional organic solvents [4]. They are combinations of two or three naturally occurring components, able to engage in reciprocal hydrogen bond interactions to form an eutectic mixture with a melting point lower than that of either of the individual components. DESs feature several favorable properties: they do not need any purification and the physicochemical properties can be easily tuned and designed to meet specific requirements; they also offer the possibility to develop convenient methodologies to isolate the product by extraction or precipitation, and

thus making the reuse of the DES mixture feasible. The large number of biodegradable raw materials that can be used to form eutectic mixtures offers an incredibly high variety of combinations to generate new, safe and biodegradable DESs [5].

Another fundamental principle of green chemistry is the atom economy concept. In this context, ammonia borane (AB) is receiving increasing attention as relatively inexpensive, useful reduction reagent for developing new green synthetic transformations [6-12]. Compared to other bioinspired reagents, such as Hantzsch esters, AB represents a more convenient reagent that generates much less waste [10]. We have recently reported the use of ammonia borane in the chemoselective reduction of a variety of nitrostyrenes and alkyl-substituted nitroalkenes to the corresponding nitroalkanes, without any catalyst or additive [13].

We thought that the combination of an atom economic, very convenient and inexpensive reagent such as BH_3NH_3 in bio-based eutectic mixtures as biorenewable alternative solvents in the synthesis of nitroalkanes, valuable precursors of amines, would represent a significant step towards the development of more sustainable synthetic organic methodologies for the preparation of valuable molecules. In the present communication, we report the results of our explorative studies, aimed to develop a chemoselective nitroalkene reduction in DESs, with the goals to establish a reliable and reproducible protocol to isolate the product without the use of any organic solvent and to assess the recovery and the recyclability of the DES mixture [14].

Results and Discussion

Based on our previous experiences with organocatalytic reactions in alternative, biodegradable solvents [15,16], and following some preliminary investigations on the physicochemical properties of several DES combinations, for this application, we decided to focus our attention on the use of some choline chloride (ChCl)-based eutectic mixtures as reaction media.

The reduction of β-nitrostyrene to afford (2-nitroethyl)benzene was selected as model reaction, and it was performed typically in the presence of 1 molar equiv of ammonia borane for 18 h at 60 °C (see Table 1).

First, the behavior of three eutectic mixtures was investigated in the reduction performed at a 0.5 M substrate concentration (entries 1–3, Table 1). A low yield of product **2** and a significant amount of unreacted starting material were observed for DESs A and C; only with a ChCl/gly mixture, DES B, the product was isolated in 27% yield. For sake of comparison, the reaction was also performed in water, where a negligible amount of the product was detected, and in glycerol, which proved to be a good reaction medium (41% yield) [17]. In order to further speed up the reaction and suppress the byproducts formation [18], the reaction was performed at 60 °C for 18 h on a 0,1 M substrate concentration (entries 6–9, Table 1).

Under those conditions, the product was isolated after chromatographic purification in a higher yield; in DES B, 41% yield was reached, while in glycerol, the reaction gave 61% yield

Table 1: Preliminary studies on AB-mediated nitrostyrene reduction in different solvent systems.

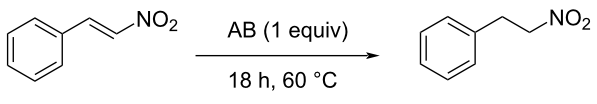

1 **2**

entry	DES	components	substrate *c*, M	yield, %
1	DES A	ChCl/urea 1:2	0.5	7
2	DES B	ChCl/gly 1:2	0.5	27
3	DES C	ChCl/fructose/H_2O 1:1:1	0.5	n.d.
4	glycerol (gly)	gly	0.5	41
5	water	water	0.5	<5
6	DES B	ChCl/gly 1:2	0.1	41
7[a]	DES B	ChCl/gly 1:2	0.1	30
8	gly	gly	0.1	61
9	water	water	0.1	7

[a]Reacton time 4 h.

(entries 6 and 8, Table 1). Therefore, DES mixture B (ChCl/gly 1:2) and glycerol were selected as reaction media of choice to further investigate the reduction of nitroalkenes mediated by ammonia borane. Both solvent systems represent promising alternatives, green solvents for organic reactions; glycerol is a nontoxic, biodegradable and nonflammable solvent for which no special handling or storage precautions are required [19]. Some limits, such as high viscosity and low solubility of highly hydrophobic compounds and possible side reactions due to the presence of hydroxy groups, can be overcome by adding a cosolvent; indeed, glycerol is often used as a component of eutectic mixtures, such as in DES B, as in this work.

In a general procedure, nitroolefin (0.4 mmol) and ammonia borane (0.4 mmol) were added to 4.5 g of freshly prepared DES. After the reaction mixture was heated at 60 °C for 18 h, the reaction was cooled to room temperature, and the product was isolated, either by adding 4 mL of water, which dissolves the DES, and extracting the nitroalkane with AcOEt, or by direct separation of the organic residue from the eutectic mixture (see below for recycling experiments and Supporting Information File 1 for details on the different work-up procedures).

The synthetic applicability was then investigated by studying the reduction of differently substituted aryl- and alkylnitroalkenes. The reaction was successfully performed with different nitrostyrenes (Scheme 1). Electron-rich nitroalkenes were reduced in fair to very good yield (up to 80% yield, see products **4a**–**d** in Scheme 1). The reaction of substrates featuring unprotected hydroxy groups is possible (see product **4a**). The reaction of substrates bearing electron-withdrawing residues with ammonia borane was observed to proceed slower, and the use of two equiv of NH_3BH_3 was necessary to speed up the reaction and obtain the products with good yield after 18 hours (see adducts **4e**–**f**). For those less reactive compounds, glycerol proofed to be a better reaction solvent.

The reduction of either α- or β-substituted nitrostyrenes was successfully accomplished both in glycerol and in DES B, with the eutectic mixture generally performing better than glycerol alone; indeed, α-substituted nitroalkane **4h** was isolated in 75% yield after 18 h of reaction at 60 °C. We further explored other DESs, and in particular, we turned our attention to betaine-containing eutectic mixtures DES D and E, and a ChCl/L-(+)-lactic acid mixture, DES F (Table 2).

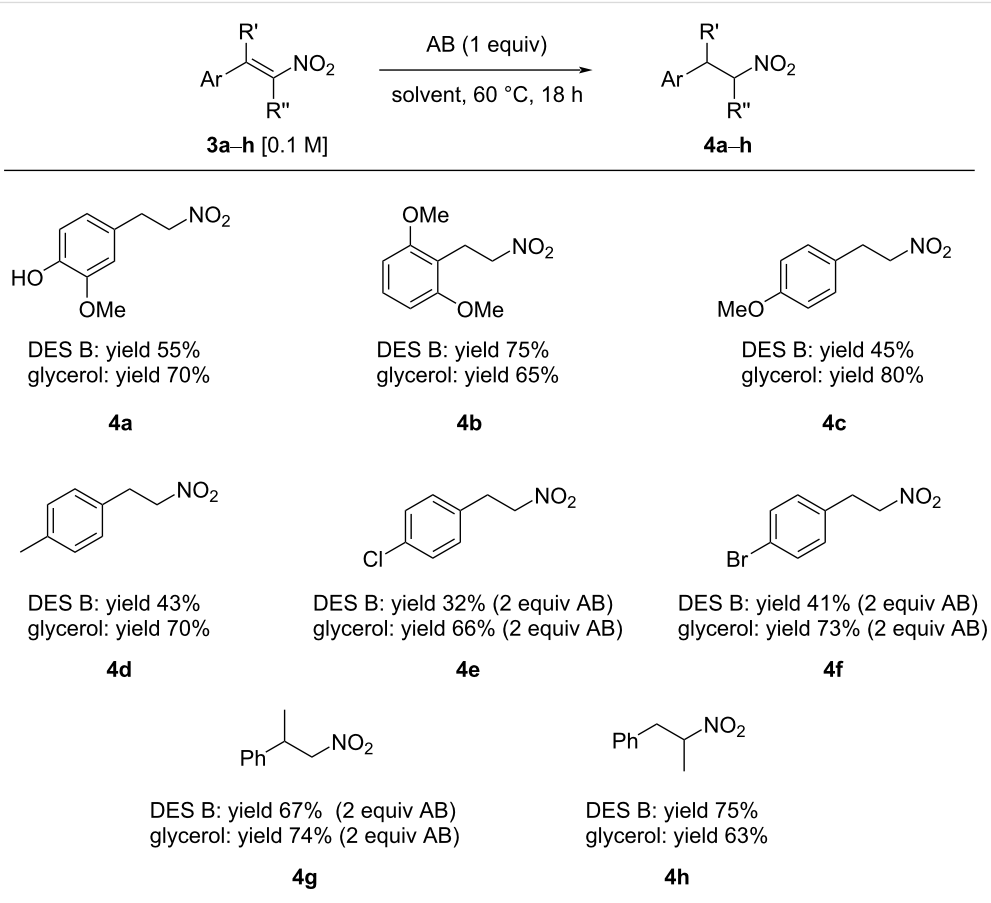

Scheme 1: AB-mediated reductions of nitrostyrenes **3a–h**.

Table 2: Preliminary studies on AB-mediated nitrostyrene reduction in DESs **D**–**F**.

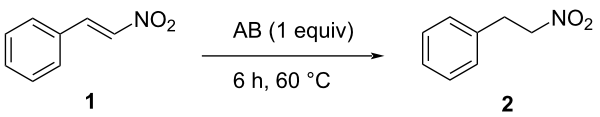

1 **2**

entry	DES	components	substrate *c*, M	yield, %
1	DES D	betaine/glycolic acid 1:2	0.75 M	73
2	DES E	betaine/gly 1:2	0.75 M	n.d.
3	DES F	ChCl/L-(+)-lactic acid 1:3[a]	0.75 M	30

[a]A 90% solution of lactic acid in water, dried on $CaCl_2$ pellets, was used.

The reduction worked in all systems, in low yield with DES E (where it was not possible to separate the product from the DES) and DES F, but it proceeded in very high yield and short reaction time in DES D.

Based on these findings, the reduction of some selected substrates in betaine/glycolic acid mixtures was reinvestigated (Scheme 2). We were pleased to see that after only 6 h of reaction in DES D, the corresponding nitroalkanes were obtained in good to excellent yield as very clean products. Notably, the formation of byproducts was not detected, even in traces. It is also worth mentioning that in DES D, it was possible to perform the reaction at a 0.75 M concentration, while with other deep eutectic mixtures and in glycerol, it was necessary to run the reaction in more diluted solutions (0.1 M) to obtain a better yield.

Ammonia borane also proved to be an efficient reagent for the reduction of both linear and branched aliphatic nitroolefins, affording the expected products in fair to good yield (Scheme 3).

The reduction of (2-nitrovinyl)cyclohexane (**5a**) afforded product **6a** in 60% yield in DES B. Analogously, nitrocyclohexene was reduced in 60% yield in a ChCl/glycerol mixture, while **6c** was obtained in similar yields in glycerol or DES B. Noteworthy, the reduction of nitrobutadiene **5d** produced nitro derivative **6d** in 63% yield in glycerol and 44% in DES B, with complete control of the chemoselectivity. Remarkably, the reduction of nitrodiene **5e**, featuring an ester group, was also accomplished with complete chemoselectivity in 50% yield in DES B and in 60% yield in glycerol. The reduction of the nitro group to an amine, followed by cyclization would afford the unsaturated δ-lactam, a valuable precursor for further synthetic elaborations. Noteworthy, AB was also able to efficiently reduce both isomers of tetrasubstituted nitroacrylate **5d**, which showed poor reactivity in the Hantzsch ester-mediated reduction in toluene, where only a low yield of the product could be obtained. However, in glycerol, the reaction of **5d** with ammonia borane afforded product **6d** in 61% isolated yield as 1:1 mixture of diastereomers (the diastereomeric ratio was not influenced by the reaction time, temperature or concentration). Finally, the possibility to develop a reliable, convenient protocol for the isola-

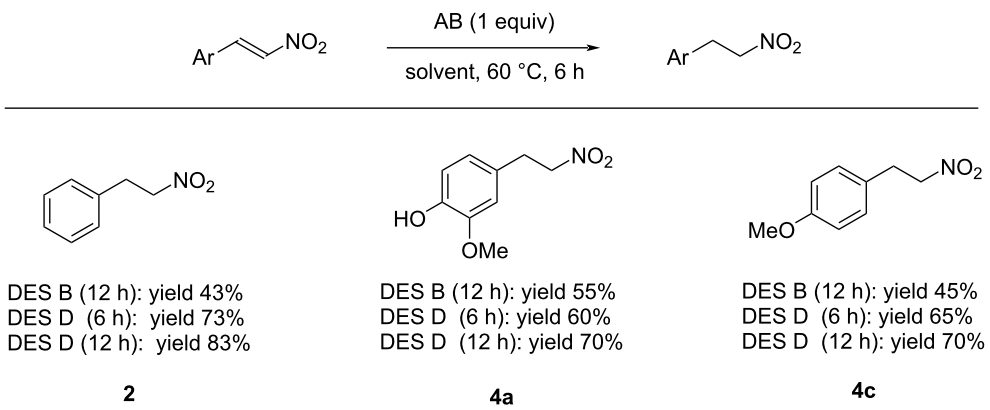

DES B (12 h): yield 43%
DES D (6 h): yield 73%
DES D (12 h): yield 83%

2

DES B (12 h): yield 55%
DES D (6 h): yield 60%
DES D (12 h): yield 70%

4a

DES B (12 h): yield 45%
DES D (6 h): yield 65%
DES D (12 h): yield 70%

4c

Scheme 2: AB-mediated reductions of nitrostyrenes **1**, **3a**, and **3c** using DESs B and D.

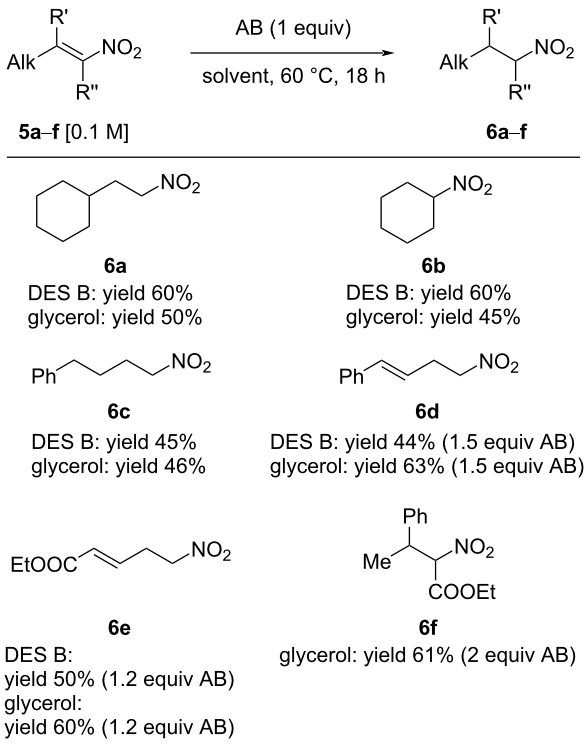

Scheme 3: AB-mediated reductions of nitroalkenes **5a–f**.

tion of the nitroalkane and the recycling of the DES mixture was investigated (Scheme 4).

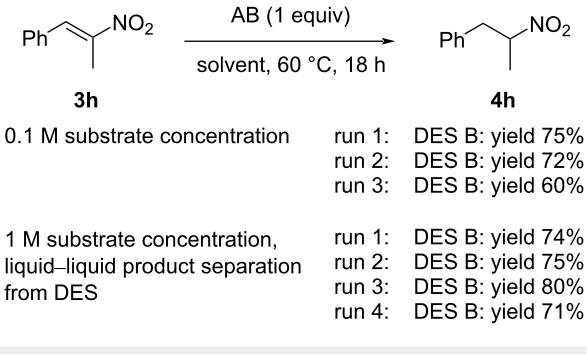

Scheme 4: Recovery and recycling experiments in the AB-mediated reduction of nitrostyrene **3h** to afford nitroalkane **4h**.

The first studies moved from the standard work-up procedure for the reaction performed at 0.1 M substrate concentration, which typically involves the addition of water to dissolve the DES and a small quantity of ethyl acetate to favor the extraction of the product and its separation from the eutectic mixture. However, when the recycling protocol was studied, in order to reuse the DES, at the end of the reaction, water was not added, and the product was extracted by simply adding ethyl acetate and separating the upper, organic phase. The DES phase was then reused as such, without any purification. After the first reaction (75% yield), DES B was reused in a second run that afforded the product in 72% yield; however, in the third run, a decreased yield was observed.

In order to realize a more convenient and more efficient protocol that avoids the use of any organic solvent, the reduction of **3h** was performed with a 1 M substrate concentration and afforded, in DES B, nitroalkane **4h** in 74% yield, which was isolated as pure compound by a simple liquid–liquid biphase separation from the eutectic mixture (see details and pictures in Supporting Information File 1). The DES was reused other three times with no appreciable difference in the yield.

Conclusion

In conclusion, the combination of an atom economically convenient and inexpensive reagent such as ammonia borane with bio-based and biorenewable alternative solvents such as deep eutectic mixtures was efficiently used in the chemoselective reduction of nitroalkenes to afford the corresponding nitroalkanes in fair to good yield. The possibility to isolate the product without the addition of any organic solvent and to recycle the eutectic mixtures at least three times in further reactions was also demonstrated. A wide variety of alkyl- and aryl-substituted nitroalkenes were reduced with high chemoselectivity, including β-substituted nitroolefins, and thus paving the way to the study of innovative, sustainable and stereoselective reductive methods to synthesize enantiopure nitroalkanes, valuable precursors of chiral amines.

Experimental

Experimental procedure for the reduction in glycerol

The desired nitroolefin (0.4 mmol) was suspended in glycerol (4 mL) in a 7 mL vial equipped with a 3.5 cm-long magnetic stir bar. Ammonia borane (12 mg, 0.4 mmol) was added to the suspension at room temperature, and the reaction flask was placed in an oil bath (already heated at 60 °C). After 18 h, the reaction mixture was cooled to room temperature, and it was diluted with 4 mL of water. The product was extracted with ethyl acetate (3 × 4 mL). The combined organic phases were washed with water (2 × 4 mL), dried over Na_2SO_4, filtered, and the solvent was evaporated under reduced pressure. The crude product was purified by column chromatography (silica as stationary phase; eluent: *n*-hexane/ethyl acetate).

Experimental procedure for the reduction in DES

In a 7 mL vial with a 3.5 cm-long magnetic stir bar, 4.5 g of DES were freshly prepared, ChCl and glycerol (1:2 molar ratio)

were mixed, and the mixture was heated at 70 °C for 15 min until it became a colorless liquid. Then, the DES was slowly cooled to room temperature in 15 min. The desired nitroolefin (0.4 mmol) was suspended in the DES, ammonia borane (12 mg, 0.4 mmol) was added to the suspension, and the reaction mixture was heated at 60 °C. After 18 h, the reaction mixture was cooled to room temperature, the DES was dissolved with the addition of 4 mL of water, and the product was extracted with AcOEt (3 × 4 mL). The combined organic phase was washed with water (2 × 4 mL), dried over Na_2SO_4, filtered, and the solvent was evaporated under reduced pressure. The crude product was purified by column chromatography (silica as stationary phase; eluent: *n*-hexane/ethyl acetate).

Recycling experiments with liquid–liquid biphasic separation

In a 7 mL vial with a 3.5 cm-long magnetic stir bar, 2.5 g of DES were freshly prepared, ChCl and glycerol (1:2 molar ratio) were mixed, and the mixture was heated at 70 °C for 15 min until it became a colorless liquid. Then, the DES was slowly cooled to room temperature in 15 min. *trans*-β-Methyl-β-nitrostyrene (326 mg, 2 mmol) was suspended in the DES. Ammonia borane (62 mg, 2 mmol) was added to the suspension, and the reaction mixture was heated at 60 °C. After 18 h, the reaction mixture was cooled to room temperature, centrifuged, and the product was removed by liquid–liquid separation with a Pasteur pipette. The crude product was purified by column chromatography (silica as stationary phase; eluent: *n*-hexane/ethyl acetate).

For the subsequent runs, fresh β-methyl-β-nitrostyrene (326 mg, 2 mmol) was suspended in the DES, and ammonia borane (1 equiv) was added to the mixture. The procedure is analogous to the first run.

Supporting Information

Supporting Information File 1

Experimental setup and general procedures for the reduction reactions as well as product characterization and NMR data.
[https://www.beilstein-journals.org/bjoc/content/supplementary/1860-5397-17-83-S1.pdf]

Funding

M. B. thanks MUR for the project PRIN 2017 "NATURECHEM. M. B. thanks Università degli Studi di Milano for the PSR 2019-financed project "Catalytic strategies for the synthesis of high added-value molecules from bio-based starting material". M. B. and P. C. G. thank the ITN-EID project Marie Skłodowska-Curie Actions Innovative Training Network–TECHNOTRAIN H2020-MSCA-ITN-2018 Grant Agreement 812944. http://www.technotrain-ITN.eu.

ORCID® iDs

Chiara Faverio - https://orcid.org/0000-0002-3260-3944
Monica Fiorenza Boselli - https://orcid.org/0000-0002-5418-2714
Alessandra Puglisi - https://orcid.org/0000-0002-8581-8009
Maurizio Benaglia - https://orcid.org/0000-0002-9568-9642

References

1. Smith, E. L.; Abbott, A. P.; Ryder, K. S. *Chem. Rev.* **2014,** *114,* 11060–11082. doi:10.1021/cr300162p
2. Alonso, D. A.; Baeza, A.; Chinchilla, R.; Guillena, G.; Pastor, I. M.; Ramón, D. J. *Eur. J. Org. Chem.* **2016,** 612–632. doi:10.1002/ejoc.201501197
3. Keijer, T.; Bakker, V.; Slootweg, J. C. *Nat. Chem.* **2019,** *11,* 190–195. doi:10.1038/s41557-019-0226-9
4. Perna, F. M.; Vitale, P.; Capriati, V. *Curr. Opin. Green Sustainable Chem.* **2020,** *21,* 27–33. doi:10.1016/j.cogsc.2019.09.004
5. Ramón, D. J.; Guillena, G., Eds. *Deep Eutectic Solvents: Synthesis, Properties, and Applications,* 1st ed.; Wiley-VCH: Weinheim, Germany, 2019. doi:10.1002/9783527818488
6. Kumar, R.; Karkamkar, A.; Bowden, M.; Autrey, T. *Chem. Soc. Rev.* **2019,** *48,* 5350–5380. doi:10.1039/c9cs00442d
7. Bhunya, S.; Malakar, T.; Ganguly, G.; Paul, A. *ACS Catal.* **2016,** *6,* 7907–7934. doi:10.1021/acscatal.6b01704
8. Han, D.; Anke, F.; Trose, M.; Beweries, T. *Coord. Chem. Rev.* **2019,** *380,* 260–286. doi:10.1016/j.ccr.2018.09.016
9. Colebatch, A. L.; Weller, A. S. *Chem. – Eur. J.* **2019,** *25,* 1379–1390. doi:10.1002/chem.201804592
10. Faverio, C.; Boselli, M. F.; Medici, F.; Benaglia, M. *Org. Biomol. Chem.* **2020,** *18,* 7789–7813. doi:10.1039/d0ob01351j
11. Boom, D. H. A.; Jupp, A. R.; Slootweg, J. C. *Chem. – Eur. J.* **2019,** *25,* 9133–9152. doi:10.1002/chem.201900679
12. Rossin, A.; Peruzzini, M. *Chem. Rev.* **2016,** *116,* 8848–8872. doi:10.1021/acs.chemrev.6b00043
13. Faverio, C.; Boselli, M. F.; Raimondi, L.; Benaglia, M. *SynOpen* **2020,** *4,* 116–122. doi:10.1055/s-0040-1705980
14. Azizi, N.; Batebi, E.; Bagherpour, S.; Ghafuri, H. *RSC Adv.* **2012,** *2,* 2289. doi:10.1039/c2ra01280d
15. Massolo, E.; Palmieri, S.; Benaglia, M.; Capriati, V.; Perna, F. M. *Green Chem.* **2016,** *18,* 792–797. doi:10.1039/c5gc01855b
16. Brenna, D.; Massolo, E.; Puglisi, A.; Rossi, S.; Celentano, G.; Benaglia, M.; Capriati, V. *Beilstein J. Org. Chem.* **2016,** *12,* 2620–2626. doi:10.3762/bjoc.12.258
17. Gu, Y.; Jérôme, F. *Green Chem.* **2010,** *12,* 1127–1138. doi:10.1039/c001628d
18. In the reaction, variable amounts of the dimer product, obtained by the attack of a molecule of reduced nitroalkane to a molecule of unreacted nitroalkene still present in solution, were observed and contributed in some cases to a lower yield of the reduction product **2**.
19. García, J. I.; García-Marín, H.; Pires, E. *Green Chem.* **2014,** *16,* 1007–1033. doi:10.1039/c3gc41857j